10-17-96

WBS: 1.2.2.3
QA: L
SCPB: N/A

Civilian Radioactive Waste Management System
Management and Operating Contractor

DISPOSAL CRITICALITY ANALYSIS METHODOLOGY TECHNICAL REPORT

Document No. B00000000-01717-5705-00020 Revision 00

August 15, 1996

Prepared for:

U. S. Department of Energy
Yucca Mountain Site Characterization Project Office
P.O. Box 98608
Las Vegas, Nevada 89193-8608

Prepared by:

Office of Civilian Radioactive Waste Management System
Management and Operating Contractor
101 Convention Center Drive
Las Vegas, Nevada 89109

Under Contract Number
DE-AC01-91RW00134

Civilian Radioactive Waste Management System
Management and Operating Contractor

DISPOSAL CRITICALITY ANALYSIS METHODOLOGY TECHNICAL REPORT

Document No. B00000000-01717-5705-00020 Revision 00

August 15, 1996

Prepared for:

U. S. Department of Energy
Yucca Mountain Site Characterization Project Office
P.O. Box 98608
Las Vegas, Nevada 89193-8608

Prepared by:

Office of Civilian Radioactive Waste Management System
Management and Operating Contractor
101 Convention Center Drive
Las Vegas, Nevada 89109

Under Contract Number
DE-AC01-91RW00134

Civilian Radioactive Waste Management System
Management & Operating Contractor

DISPOSAL CRITICALITY ANALYSIS METHODOLOGY TECHNICAL REPORT

Document No. B00000000-01717-5705-00020 Revision 00

August 15, 1996

Prepared by: D. A. Thomas 2 Date: 08-14-96
D. A. Thomas, Lead Coordinating Author
Waste Package Development

Authors: Peter Gottlieb, Author, Waste Package Development
J. R. Massari, Author, Waste Package Development
C. W. Mays, Lead Technical Author, Waste Package Development
J. K. McCoy, Author, Waste Package Development
J. A. McNeish, Author, Performance Assessment
M. L. Scott, Author, Licensing
D. A. Thomas, Lead Coordinating Author, Waste Package Development
K. D. Wright, Author, Waste Package Development

Approved by: C W Mays for Date: 8/14/96
H. A. Benton, Manager
Waste Package Development

Approved by: _____ Date: 8/14/96
A. M. Segrest, Manager
Mined Geologic Disposal System

Concurred by: _____ Date: 8/14/96
R. P. Ruth, Manager (Acting)
Quality Assurance Nevada Site

Civilian Radioactive Waste Management System
Management & Operating Contractor

DISPOSAL CRITICALITY ANALYSIS METHODOLOGY TECHNICAL REPORT

Document No. B00000000-01717-5705-00020 Revision 00

August 15, 1996

Approved by: _____ Date: 8-14-96
T. W. Doering, Manager
Waste Package Design

Concurred by: _____ Date: 8/14/96
for M. A. Lugo, Manager (Acting)
Licensing

Concurred by: _____ Date: 8/14/96
R. W. Andrews, Manager
Performance Assessment

Reviewed by:

R. W. Barnard, Performance Assessment
K. M. Crosswait, Waste Management and Integration
C. R. Hastings, Project Engineering
W. R. Hunt, Quality Assurance
R. O. Johnson, Systems Analysis and Integration
T. L. Lotz, Waste Package Development
R. D. Memory, Systems Engineering
M. L. Scott, Licensing (Other than Chapter 2)
David Stahl, Waste Package Materials
J. D. Weaver, Licensing (Chapter 2)

PREFACE

The United States Department of Energy (DOE) is developing a methodology for criticality analysis to support disposal of commercial spent nuclear fuel in a geologic repository. A topical report on the disposal criticality analysis methodology is scheduled to be submitted to the United States Nuclear Regulatory Commission (NRC) for formal review in September 1998. This technical report is being issued to show the status of this development program, as it stands to-date. Although it is structured similarly to the formal topical report, this report is a work-in-progress, and has inconsistencies in level-of-detail and completeness which will be remedied over the next two years.

This report is intended primarily as a vehicle for obtaining feedback from reviewers on the methodology as it has evolved to this point in time. Where available, supporting data is provided to facilitate more detailed review and comment. Areas of the technical report which are incomplete or where additional supporting data is required for completion of the topical report will be identified (i.e., marked To Be Determined (TBD) or To Be Verified (TBV)).

The technical report was prepared in accordance with the Civilian Radioactive Waste Management System Management & Operating (M&O) Contractor Quality Administrative Procedures (QAPs) specified by the QAP-2-0 Activity Evaluation, titled: "Prepare the Disposal Criticality Analysis Methodology Technical Report".[P-1] The activity evaluation determined that the development of this report is subject to the DOE Office of Civilian Radioactive Waste Management (OCRWM) Quality Assurance Requirements and Description (QARD)[P-2] controls. The methodology described in the report is related to the evaluation of the Mined Geologic Disposal System waste package and engineered barrier system; the waste package and engineered barrier system have been identified as Yucca Mountain Site Characterization Project Q-List items important to safety and waste isolation. The waste package is on the Q-List by direct inclusion by the DOE; a QAP-2-3 evaluation has yet to be conducted. There are no determination of importance evaluations developed in accordance with Nevada Line Procedure, NLP-2-0, since this report does not involve any field activity.

Much of the quality affecting information in this report has not been verified under the OCRWM quality assurance program controls in accordance with the QARD. The quality-affecting information presented in this report has been developed using standard nuclear industry quality assurance practices (NQA-1). Therefore, the unverified information presented in the report will be treated as unqualified or unconfirmed and will be marked TBV or TBD, or otherwise clearly identified, and referenced to a source. In addition, Chapter 2 of this report addresses regulatory

topics and issues that are considered as unqualified and unconfirmed by the M&O quality assurance program. The information presented in this report is not design information that can be used to support procurement, fabrication, or construction. The software used in this report's sample evaluation chapter is not quality related, which would require validation in accordance with the M&O QAP computer software controls (QAP-SI series procedures). The correct installation of all scientific and engineering software used to generate results reported in this document has been checked with sample calculations.

The technical report has no interfaces outside the OCRWM program. The technical report does have some interfaces on common topics being developed in different areas of OCRWM, namely burnup credit. The technical report references information also presented in the "Topical Report on Actinide-Only Burnup Credit for PWR Spent Nuclear Fuel Packages" (currently under review by the NRC). Some of the data and methodology used in the "Actinide-Only" burnup credit topical report will be referenced for disposal criticality analyses.

In reviewing this release of the technical report, the reviewer should realize that this is not the final version of the topical report. It is intended to inform the reader of the current methodology for disposal criticality analysis, provide some of the supporting data for the methodology, and to identify the additional data and supporting analyses required.

ABSTRACT

The design and development of criticality control systems is an engineering activity that is frequently performed in the nuclear industry. An approved methodology and experience with the analysis required for criticality control evaluations are important parts of developing criticality control systems. This report describes the methodology that is planned for use in demonstrating criticality control for the potential Yucca Mountain high-level waste repository and demonstrating protection of public health and safety. Experience with using this methodology will be important in establishing an acceptable approach to developing disposal criticality control systems.

This report provides a guide for performing disposal criticality analysis. A risk-based methodology will be used to demonstrate disposal criticality control. The various models contained in the methodology (neutronics, scenario generator, consequence, and total system performance) are described and the validation process for these models presented. The criteria for determining the suitability of waste packages for emplacement in the repository are described along with the physical implementation and control procedures to be followed. A sample evaluation is provided to illustrate the methodology presented in the report. Details of the experiments used to validate the models, sources of information to establish the probabilities of events, and calculational data are provided in appendices. When complete, the methodology will provide a systematic approach for evaluating a waste form/waste package/engineered barrier/repository system combination for disposal criticality control through the entire postclosure period of regulatory concern.

When the development of the methodology described in this technical report is completed, it will be documented in a topical report. The United States Nuclear Regulatory Commission staff will be asked to review the topical report and accept the methodology. The United States Department of Energy will then use the approved methodology in the license application for the potential Yucca Mountain repository to demonstrate acceptability of proposed systems for control of criticality.

INTENTIONALLY LEFT BLANK

TABLE OF CONTENTS

TABLE OF CONTENTS

Chapter - Section **Page**

LIST OF FIGURES

LIST OF TABLES

1.0 INTRODUCTION

The United States Congress assigned the Department of Energy (DOE) the responsibility of managing the geologic disposal of commercial spent nuclear fuel (SNF) and defense high level waste (DHLW) by enactment of the Nuclear Waste Policy Act [1-1] of 1982 and the Amendments Act [1-2] of 1987. Criticality control is an important aspect of geologic disposal and must be evaluated for license applications. This report describes a methodology that is being developed to provide a technical basis for disposal criticality evaluations. The completed methodology will be presented to the Nuclear Regulatory Commission (NRC) in a topical report and will, after acceptance by the NRC, be used in the license application for the potential Yucca Mountain repository to demonstrate acceptability of proposed systems for control of criticality.

1.1 Background

The planned DOE approach for demonstrating postclosure disposal criticality control is risk-based. The risk-based approach is expected to be able to demonstrate, in a licensing proceeding, that the health and safety of the public will be protected against the consequences of potential criticality events. Risk is defined as the product of the probability of a given process or event and its consequences. A risk-based approach may be thought of as a "bottom-line" approach that bases acceptability of a situation or condition on its projected effect on the health and safety of the public. When dealing with radioactivity, the measure of effect on health and safety is radioactive dose projected to be received by the public. The National Academy of Sciences has recommended dose-based environmental standards for Yucca Mountain.

The Yucca Mountain Project planning assumption, to be validated during development of the disposal criticality analysis methodology, is that the risk-based approach to dealing with disposal criticality is not only the best approach, but also that it is the only feasible approach. The reasons for this assumption are discussed in Chapter 2 of this technical report.

The methodology presented in this technical report is not yet mature. It will be fully developed in the future and will be submitted in the form of a topical report to the NRC for acceptance. If accepted by the NRC, it will be used or referenced in a future potential license application to show compliance with the disposal criticality requirements.

The methodology will be used to estimate the probability and nature of potential criticality events. The results of use of the methodology will be projected perturbations to the repository source term and the repository thermal effect. Chapter 3 of this technical report provides additional information on how these results will be input into total system performance assessments to predict the effects of potential disposal criticality on the ability of the repository to protect the health and safety of the public.

1.2 Objective

The objective of this report is to present a methodology that is being developed for performing criticality analyses for long-term disposal in a repository of commercial light water reactor (LWR) SNF. This technical report is intended to describe the methodology at its present state of development. The completed methodology will be documented in a topical report.

The topical report will specifically seek NRC acceptance of the following: (References are to sections of this technical report that provide information on the associated topics.)

1. The methodology for performing criticality analyses for disposal of commercial SNF including the following models supporting this methodology;
   a. The neutronics models (Section 4.1). These include
      i. The SNF isotopic model (Section 4.1.1) for the 14 actinides and 15 fission products (principal isotopes) analyzed
      ii. The criticality calculational model (Section 4.1.2) for determining the subcritical limit for evaluating control systems. The subcritical limit is determined from analysis of experimental criticality data and represents an upper bound for the calculated k_{eff} (effective neutron multiplication factor) of the system being analyzed to ensure subcriticality.

   b. The configuration generation models (Section 4.2). These include
      i. The repository environment model (Section 4.2.1)
      ii. The material degradation model (Section 4.2.2)
      iii. The waste form degradation model (Section 4.2.3)
      iv. The material transport model (Section 4.2.4)
      v. The material precipitation/retardation models (Section 4.2.5)

c. The criticality consequence model (Section 4.3) for determining the potential impact of a criticality event on the radionuclide inventory and thermal effect, should such assessment be determined to be necessary based on the results of criticality analysis.

2. Validation of the SAS2H sequence of the SCALE-4.3 [1-3] code system using the 44 energy group cross section library based on the SNF isotopic model validation methodology (Section 4.1.3)

3. Validation of the MCNP 4A [1-4] code system and its associated ENDF/B-V continuous energy cross section libraries for criticality control analyses for waste disposal in a repository based on the criticality model validation methodology (Section 4.1.3)

1.3 Scope

The technical report is to be used for informational purposes only. This document presents a risk-based disposal criticality analysis methodology for the postclosure period. The scope of the technical report and proposed topical report (to be developed from this technical report) is limited as follows:

- Applies only to spent fuel from commercial nuclear reactors. (Other waste forms, e.g., DHLW and DOE-owned spent fuel, will be discussed in addenda to the planned topical report.)

- Applies to analysis of potential criticality events both inside and outside the waste packages.

- Describes the criticality analysis methodology, validation of that methodology, and uncertainties and conservatisms (To Be Determined (TBD)) in the methodology. Does not describe the design basis or design strategy for providing disposal criticality control. The design basis will be provided or referenced in the license application.

- Describes the isotopics model and validation for that model (TBD).

- Describes the methodology for establishing the probability and process of assembling spent nuclear fuel material into potentially critical configurations.

- Describes the range of applicability of the methodology for criticality analyses in the repository (TBD).

- Describes the approach to be used to provide input to total system performance assessment (TSPA) but does not discuss in detail the TSPA analyses.

[Note: As stated, the proposed methodology in this report is for commercial LWR SNF only. After the acceptance of the base methodology for commercial LWR SNF, amendments or addenda will be made covering any of the other waste forms selected for disposal. Most of the models in the base methodology should cover any of the waste forms (To Be Verified (TBV)). The addenda for the additional waste forms will address any special aspects or differences from the base methodology (e.g., different waste form corrosion model). (TBD)]

1.4 Approach to Disposal Criticality Analysis

The approach used to evaluate the effectiveness of criticality control methods after permanent closure of the repository considers configurations of fissile material for three regions. The three regions are: 1) interior to the waste package, 2) exterior to the waste package in the engineered barrier system (EBS) near-field locations, and 3) exterior to the EBS in the far-field locations. Probabilistic methods, described in this report (Sections 3.2 and 4.2), are used to determine the probability of sequences (or process chains) which lead to potential configurations (for each of the three regions) that may result in criticality. The criticality potential of the configurations identified is evaluated using deterministic methods. The criticality potential is then compared with the appropriate subcritical limit value for that type of configuration identified. The subcritical limit is an upper bound placed on the calculated k_{eff} for configurations evaluated in each of the regions. The subcritical limit values, including their range of applicability, are determined as part of the neutronics model validation (Section 4.1.3 - TBD).

A criticality consequence analysis is performed, as described in this report (Sections 3.4 and 4.3), for those configurations that exceed the subcritical limit. This analysis determines the potential impact of a criticality event on the repository radionuclide inventory and thermal effect. Data

from this analysis is used in a performance assessment to ensure that the overall system performance objectives for the geologic repository after permanent closure are met. Criticality control measures will be augmented, as necessary, to ensure that the performance objectives are met.

Before detailed TSPA analyses are performed, the sensitivity of these analyses to the potential consequence of a criticality (i.e., perturbations in the source term and thermal effects) is determined as described in Section 3.1. The criterion for performing TSPA is established based on the probability of creating a critical assembly in the repository and the magnitude of the consequence of the resulting criticality event.

[Note: Although the approach to disposal criticality control will focus on the risk associated with potential criticality events, these events are viewed as undesirable whatever their consequences might be. Therefore, the criticality control approach will also identify processes, conditions, and events that strongly influence the probabilities of criticality events occurring. The results of these evaluations will be used to identify feasible methods of minimizing the probability of criticality events occurring.]

1.5 Disposal Criticality Control Methods

Criticality control methods are required to ensure compliance with regulatory requirements. An overview of criticality control methods for engineered barrier systems that meet these requirements (TBV) is presented in this section. In addition to these methods, burnup credit (taking credit for fuel depletion and the generation of neutron absorbers in spent nuclear fuel assemblies) may be used to assist in meeting regulatory requirements. Although burnup credit is not a design method that is implemented for criticality control, burnup is an intrinsic property of spent nuclear fuel that may be considered in designing criticality control systems. The disposal criticality analysis methodology must be able to evaluate the effectiveness of burnup credit and the design methods used for controlling criticality. Validation of the methodology used to evaluate the criticality control potential of these methods and the range-of-applicability of this methodology are addressed in Section 4.1.

Criticality control requirements for waste package disposal can be satisfied by using burnup credit and the following control methods, separately or in combination:

1. Geometry restrictions.

2. Limiting the amount of fissile material.

3. Adding neutron absorber material.

4. Limiting the amount of moderator.

Burnup credit and the other control methods used to satisfy requirements are addressed in the following subsections.

1.5.1 Burnup Credit

Burnup credit is the process of accounting for the reduced reactivity of spent nuclear fuel (commercial LWR SNF) as compared to fresh fuel of the same initial enrichment. The approach recognizes that the fuel has been irradiated and accounts for the net depletion of fissile material and for the creation of neutron-absorbing isotopes as a result of fission in an operating reactor. The criticality potential of SNF also varies with cooling time (the time since removal from the reactor core) as radionuclides are created and subsequently decay. Neutronics models used to estimate the criticality potential of SNF show that the reduced reactivity (criticality potential) due to burnup is a valuable contributor to long-term criticality control.

Evaluation, using the burnup credit approach, of an engineered barrier system design requires a reasonable and conservative prediction of the isotopic composition of the SNF and analysis of the system reactivity based on these isotopes. The burnup credit methodology is validated using experimental data. This includes fresh fuel criticality experiments, commercial LWR criticality data, and chemical assay data for commercial spent nuclear fuel. Analysis of this data establishes the biases and uncertainties in the methodology and extends these biases and uncertainties to the range of applicability for long-term waste disposal in a repository. The burnup credit methodology presented in this report is applicable for configurations internal to waste packages. For external configurations, the material separation, transport, and deposition processes are such that credit cannot be taken for some species of neutron absorbers which were formerly present in the SNF (TBV). More discussion on the applicability of burnup credit is provided in Sections 3.1 and 4.1.3.

The methodology described in this report references the data and parts of the methodology presented to the NRC in the "Topical Report on Actinide-Only Burnup Credit for PWR Spent Nuclear Fuel Packages"[1-5].

1.5.2 Basket Design as a Criticality Control Method

Geometry restrictions are implemented in the waste package through the use of a basket, which restricts the arrangement of fuel within the canister or container. The amount of fissile material (number of fuel assemblies) in the waste package is also limited by the basket design. (Limiting the amount of fissile material is the ultimate criticality control method.) The basket design controls the number of fuel assemblies and their arrangement within the waste package, and therefore affects the criticality potential of the system. The degradation of the basket over time (and the potential loss of geometry control) is an important consideration for this methodology.

The disposal criticality analysis methodology, as described, will account for the geometry of materials and amounts of fissile material in systems being analyzed. Validation of this methodology for various amounts and geometric arrangements of fissile materials is described in Section 4.1.3 and Appendix B.2. The material performance aspects of the basket are presented in Section 4.2.2 (TBV).

1.5.3 Neutron Absorber Credit

Neutron absorbers are materials that capture neutrons to prevent them from continuing to add to the fission chain reaction. The use of supplemental neutron absorber materials is an accepted method for criticality control. Neutron absorber credit is routinely used as a criticality control measure in reactors, spent fuel pools, and cask systems.

Neutron absorber materials placed in control panels and control rods provide a significant amount of negative reactivity, thus lowering the system's potential for criticality. The amount of criticality control is dependent upon the type and amount of neutron absorber present. Some of the neutron absorbers used by the nuclear industry are boron, cadmium, gadolinium, hafnium, and silver-indium-cadmium. The neutron absorbers are normally alloyed or mixed in small amounts with carrier materials.

Maintaining criticality control with a neutron absorber depends upon retaining the absorber in the carrier material. Potential mechanisms for loss of the absorber material through physical removal (e.g., leaching or preferential corrosion) must be considered. Material performance and neutron depletion evaluations must be made for the neutron absorber material loaded into a control system (e.g., panel or rod). This will determine the amount of absorber available for criticality control at future times during disposal in the repository. More discussion on neutron absorber credit as it applies to disposal criticality analysis appears in Chapter 4 and in Appendix B. The neutronics aspects are presented in Section 4.1.3 and Appendix B.2, while the material performance aspects are presented in Section 4.2.2 (TBV).

1.5.4 Limiting the Amount of Moderator

The presence of moderator material in a waste package containing commercial LWR SNF increases the reactivity of the package. Since the engineered barrier system is designed to reduce the presence of moderating material, the only source of moderator of concern for criticality control internal to the waste package results from the condition in which water enters the waste package. The inclusion of additional (filler) material to limit the amount of water that can enter the waste package is referred to as moderator displacement. Moderator displacement is an effective criticality control mechanism. Use of a particular filler material for criticality control requires quantification of the amount of the filler material that can be loaded in the package, the reactivity effect of displacing an equivalent amount of moderator, and the impact on waste package mass due to the addition of the filler material. Evaluations and experiments are being performed (TBD) to ensure that the material performance characteristics of the filler will permit it to last over the time period of criticality control during isolation. More discussion on moderator displacement filler material as it applies to disposal criticality analysis appears in Chapter 4. The neutronics aspects are presented in Section 4.1.3, while the material performance aspects are presented in Section 4.2.2 (TBV).

In addition to the specific criticality control requirements for filler material, the following issues concerning degradation must also be considered when using a filler material (TBV):

a. Chemical interactions between the filler and waste must not compromise the function of the waste package,

b. Filler materials with explosive, pyrophoric or chemically reactive characteristics are precluded,

c. Filler materials that are liquid under ambient conditions are precluded,

d. Galvanic interactions between the filler material and other components must not compromise the function of the waste package, and

e. Filler materials or their decomposed components must not accelerate the transport of radionuclides through any of the barriers.

[Note: Other methods exist for limiting moderator (moderator exclusion and rod consolidation), but are not preferred for disposal applications due to material performance issues and impacts on functions other than criticality. The analysis methodology will be able to evaluate the other methods, if they are used for disposal.]

1.6 Overview of the Report

This report presents a methodology for performing criticality analyses for long-term disposal of commercial spent nuclear fuel in a repository. Chapter 1 has presented the objectives and scope of this report, has briefly described the approach used to evaluate the effectiveness of criticality control methods, and has provided an overview of criticality control methods for an engineered barrier system in a repository. It was noted that the methodology presented in this report is a risk-based methodology.

Chapter 2 discusses industry technical standards and regulatory guidance documents used in whole or in part in development of the technical report. This section also addresses the need for risk-based disposal criticality analysis, and it describes the current status of efforts to obtain credit for burnup.

Chapter 3 presents the methodology being developed for evaluating the criticality potential of commercial spent nuclear fuel emplaced in the Yucca Mountain repository. First, an overview of the methodology is given. The flow process for various analyses performed to demonstrate criticality control is presented. This presentation illustrates the risk-based methodology and the

criticality control requirements for waste packages to be considered suitable for disposal. A more detailed description of the various analysis methodologies is then presented.

The methodology discussed in Chapter 3 is based on specific models. These models and their validation are discussed in Chapter 4. The neutronics models for performing disposal criticality analyses, the models for identifying configurations for criticality analyses, and the criticality consequence model. The relevant total system performance models are also briefly described for informational purposes. The neutronics models are used in determining the isotopic concentrations of SNF and performing criticality analyses for various configurations of SNF. The computer code systems, cross section libraries, and measured data used in the model development and validation are described. Included in the configuration generator are models for the repository environment, material and waste form degradation, material transport, and material precipitation/retardation. Some of these models are identical to the total system performance models, since similar processes and events are considered by both functions. The criticality consequence model evaluates the impact of a potential criticality based on the type of criticality event identified. A discussion of the criticality consequence model along with the categories of potential criticality events considered is provided. Measured/experimental data used in model development and validation are included in the appendices.

Chapter 5 presents the waste disposal criticality acceptability criteria for waste shipments received at the repository, along with the physical implementation and administrative controls relating to the loading of waste packages. The required documentation accompanying the shipments is discussed, as well as the verification process.

Chapter 6 provides the results of a sample criticality analysis for a disposal waste package design. A 21 pressurized water reactor (PWR) assembly waste package at the potential Yucca Mountain repository was chosen for the sample evaluation. Only results from these analyses are presented. Probabilistic evaluations performed in determination of configurations for criticality analyses, as well as the criticality analyses are also described in the appendices. [Note: All analyses for Chapter 6, including supporting analyses described in the appendices, are TBV.]

Chapter 7 summarizes the methodology presented in this report and provides conclusions regarding the purpose, potential uses, and limitations on the uses of the report. Finally, the references for this report are provided in Chapter 8 and a listing of the appendices is included in Chapter 9.

2.0 REGULATORY PERSPECTIVE

This Chapter addresses regulatory topics and issues and shall be considered as unqualified and unconfirmed information in accordance with the Civilian Radioactive Waste Management System Management and Operating Contractor (M&O) Quality Assurance Program. This information was developed by the M&O Licensing Department using the Chapter 2.0 references identified in Chapter 8.0. It should be noted that this chapter does not contain design information.

The purpose of the Disposal Criticality Analysis Technical Report is to present a risk-based methodology for criticality analysis that is appropriate for use in analysis of the postclosure period in a potential repository. As discussed in Chapter 1, the technical report describes the methodology at its present, incomplete state of development. Development and refinement of the methodology will continue.

The Disposal Criticality Analysis Methodology Topical Report, whose development will follow completion of this technical report, will provide a methodology for disposal criticality analysis that will be used to demonstrate compliance with applicable NRC regulations. The framework within which the DOE will ensure compliance with regulatory requirements is contained in the Office of Civilian Radioactive Waste Management (OCRWM) technical document hierarchy. Details of this hierarchy are provided in Section 1.2 of the CRWMS Requirement Document.[2-1]

In contrast to the topical report, the technical report is not a regulatory document and has no specific regulatory-related function. However, the methodology described in the technical report (revised and further developed as needed) is proposed for use in the topical report, assuming the methodology is consistent with the NRC disposal criticality regulations in effect when the topical report is submitted. Therefore, the information presented in the technical report may eventually be used to support a regulatory function.

This chapter of the technical report provides information on certain regulatory-related aspects of criticality control and analysis. It describes NRC guidance and industry standards that have been used in development of the technical report and are expected to be used in development of the topical report. It also discusses the need for risk-based criticality analysis methodology. Finally,

it discusses burnup credit, an important aspect of demonstrating compliance with disposal criticality regulations.

2.1 NRC Guidance and Industry Standards

The DOE has used NRC guidance and various applicable industry standards in the development of the technical report, and additional guidance may be used in the development of the topical report.

2.1.1 NUREGs

The DOE, in developing the Disposal Criticality Analysis Methodology Technical Report, has reviewed the information and guidance contained in NUREG/CR-2300[2-2], "PRA Procedures Guide." The Probabilistic Risk Assessment (PRA) Procedures Guide provides methods and information for performing the three levels of analysis for a nuclear power plant risk assessment. In general, much of the information contained within the PRA Procedures Guide is specific to the analysis of nuclear power plants, and is not applicable to disposal criticality analysis. However, the flow of the disposal criticality risk analysis as described in the technical report is consistent with the three levels of PRA discussed in the PRA Procedures Guide. The process entails the following steps: 1) Identifying sequences of events and/or processes leading to criticality and determining the probability of each sequence; 2) estimating the power, duration, and radionuclide inventory increase resulting from each criticality sequence; and 3) estimating the consequences of each criticality sequence on the performance of the repository as part of the Total System Performance Assessment.

The DOE may use other NUREGs in development of the topical report. The topical report will explicitly reference each such document that is used.

2.1.2 Industry Standards

The DOE, in developing the technical report, has used the following industry standards:

- ANSI/ANS-8.1-1983, American National Standard for Nuclear Criticality Safety in Operations with Fissionable Materials Outside Reactors.[2-3] This standard provides guidance

for the prevention of criticality accidents in the handling, storing, processing, and transporting of certain fissionable material, specifically U-233 and -235 and Pu-239. It provides basic criteria and limits for certain simple geometries of fissionable materials. It also states requirements for establishing validity and ranges of applicability of any calculational method used in assessing criticality safety.

The methodology described in the technical report for criticality analyses external to a waste package (both near-field and far-field locations) uses and is consistent with this standard. The guidance in this standard is followed in establishing subcritical limits. Its guidance for establishing bias by correlating the results of criticality experiments with results obtained for these same systems by the method being validated has been used, as has its guidance for using trends in the bias to extend the range of applicability of the calculational method (TBD).

The standard describes use of the double contingency criterion, which states that two unlikely and independent events are required for a criticality to occur. The repository and waste package designs will make use of this criterion to the extent feasible. However, the extremely long period of regulatory concern for disposal criticality makes it very difficult to identify events in the distant future as independent, so its usefulness is expected to be limited.

- ANSI/ANS-8.17-1984 (R1989), Criticality Safety Criteria for the Handling, Storage, and Transportation of LWR Fuel Outside Reactors.[2-4] This standard provides guidance for criticality safety for a specific waste form, light water reactor spent fuel, as opposed to the more general scope of ANSI/ANS-8.1-1983. ANSI/ANS-8.17-1984 (R1989), which is intended to provide supplemental guidance for ANSI/ANS-8.1-1983, allows reliance on neutron absorbers for criticality control. In addition, it allows credit to be taken for burnup through reactivity measurement or through analysis and verification of exposure history. It provides criteria to establish criticality, though it does not require a specific margin to criticality be maintained.

  The methodology used in the technical report for criticality analyses internal to a waste package is consistent with this standard. The standard allows neutron absorber credit, which will be sought as determined appropriate through use of material degradation and transport models. The Yucca Mountain Project planning assumption is that the analysis and verification method will be used for burnup verification. Use of burnup/reactivity measurement is a subject currently under discussion between the DOE and the NRC. Finally,

the standard's guidance is used in establishing the subcritical limit (referred to in the standard as "Criteria to Establish Subcriticality").

The standards discussed above are expected to be used in development of the topical report. Additional standards may be identified as applicable. These standards will be used as appropriate and referenced in the topical report. The following standards are already under consideration for use in the topical report:

- ANSI/ANS-8.10-1983, Criteria for Nuclear Criticality Safety Controls in Operations with Shielding and Confinement.[2-5] This standard, though intended for application to fissionable material process facilities outside of reactors, could be interpreted to apply to the postclosure repository, in which adequate protection (including shielding provided by the rock surrounding the repository) for the public against radiation and release of radioactive materials can be demonstrated. The approach described in ANSI/ANS-8.10 requires designing for one unlikely event rather than for two unlikely events as required by ANSI/ANS-8.1-1983 and ANSI/ANS-8.17-1984 (R1989). The Yucca Mountain Project planning assumption is that the approach described in ANSI/ANS-8.10-1983 is consistent with the methodology for demonstrating disposal criticality control that is presented in this technical report, though the applicability of this standard to postclosure repository conditions must be verified.

- ANSI/ANS-8.15-1981, American National Standard for Nuclear Criticality Control of Special Actinide Elements.[2-6] This standard provides guidance for prevention of criticality accidents in the handling, storage, processing, and transportation of special actinide elements. The document provides guidance for 14 nuclides ranging from Np-237 to Cf-251. This standard is the counterpart of ANSI/ANS-8.1-1983 for materials that, while generally much less abundant than those within the scope of ANSI/ANS-8.1-1983, are nevertheless a potential criticality concern. The appropriate use of this standard for guidance on postclosure disposal criticality analysis has not yet been determined.

2.1.3 Regulatory Guides

Guidance from NRC Regulatory Guides was used in development of the technical report as follows:

- Regulatory Guide 3.4, Nuclear Criticality Safety in Operations with Fissionable Materials at Fuels and Materials Activities.[2-7] This Regulatory Guide endorses use of ANSI/ANS-8.1-1983 for general storage and transport of fissionable materials. As described in the previous subsection, the methodology presented in the technical report is consistent with ANSI/ANS-8.1-1983, and therefore with Regulatory Guide 3.4.

- Regulatory Guide 3.58, Criticality Safety for Handling, Storing, and Transporting LWR Fuel at Fuels and Materials Facilities.[2-8] This Regulatory Guide endorses ANSI/ANS-8.17-1984 (R1989) for storage and transportation of light water reactor spent fuel, though it takes exception to verification of exposure history as an acceptable method to verify burnup in order to take burnup credit. This method is one of two that is presented in the standard.

  As noted in the previous subsection, the methodology presented in the technical report is consistent with ANSI/ANS-8.17-1984 (R1989). With regard to burnup verification, it should be noted that the DOE's "Topical Report on Actinide-Only Burnup Credit for PWR Spent Nuclear Fuel Packages,"[2-9] which has been submitted to the NRC for acceptance, includes the verification of exposure history as a partial verification of burnup. That report, which is discussed in Section 2.4 of the technical report, also includes flux measurements to verify burnup. The extent to which measurements would be needed to verify exposure history is the subject of ongoing DOE and NRC discussion.

The Regulatory Guides discussed above are planned for use in development of the topical report. The DOE may use additional Regulatory Guides; such use will be explicitly described in the topical report.

2.2 The Need for Risk-Based Regulations

The Yucca Mountain Project planning assumption to be validated (and the view of many knowledgeable persons in the scientific community) is that it is unlikely that a nuclear waste repository can be shown to limit the occurrence of a criticality to a probability which is zero, or vanishingly small (i.e., incredible). It is very difficult, for the extremely long period of regulatory concern likely to apply to a geologic repository, to define a credibility standard that is acceptable to all parties in a licensing proceeding. Accepted standards exist in reactor licensing, but the period of regulatory concern is many orders of magnitude smaller than that likely to be

applicable to a geologic repository. For example, should the period of regulatory concern be substantially longer than 10,000 years, an event with a very low probability of occurring in one year could have a high probability of occurring over the much longer period. There is no precedent for establishing a credibility threshold in this type of situation.

In keeping with the recent recommendations of the National Academy of Sciences [2-10], the repository's ability to meet risk-based performance objectives to protect the health and safety of the public is the focus of the methodology presented in this technical report. Risk is defined as the product of probability and consequence of a process or event under consideration. Risk-based repository performance objectives are currently under consideration by the Environmental Protection Agency and the NRC.

Using risk-based criticality analysis, criticality would be evaluated as a potential threat to overall repository performance. The probabilities and consequences of potential criticality events would be input into the overall repository performance assessment, and evaluated along with other potential risks. Redesign would be required if the design, considering criticality and all other analyzed phenomena, were found to not meet the performance objectives. Use of risk-based analysis in regulatory matters is encouraged by the NRC in its recent policy statement entitled "Final Policy Statement on Use of Probabilistic Risk Assessment Methods in Nuclear Regulatory Activities."[2-11]

Criticality events are considered undesirable even if the risks they pose are determined to be small. Therefore, in addition to assessing risks associated with potential criticality events, the probability of the events and the contributing factors to their potential for occurrence would be analyzed. This analysis would attempt to identify processes, conditions, and events most likely to lead to criticality. With this information, the design team would seek feasible approaches to minimizing the probability of occurrence of potential criticality events.

2.3 Burnup Credit

The time dependence of the isotopics of spent fuel is an issue that is an essential part of the methodology for demonstrating control of disposal criticality. The DOE plans to seek burnup credit for disposal criticality as described in section 1.5.1 of this technical report.

The NRC has approved burnup credit for use in PWR spent fuel pools. To date the NRC has not granted burnup credit for transportation. The DOE is working to obtain burnup credit, concentrating on transportation of fissile material, and has submitted to the NRC a topical report on the subject, titled "Topical Report on Actinide-Only Burnup Credit for PWR Spent Fuel Packages."[2-9] The DOE is currently addressing NRC comments with the intent to submit a revised report in the near future. The DOE is also planning to develop topical reports to obtain NRC acceptance of credit for selected fission products in reducing criticality potential during storage and transportation.

The Disposal Criticality Analysis Methodology Topical Report will include or reference information that is expected to be sufficient to allow the NRC to grant burnup credit for selected radionuclides to be used in disposal criticality analysis. Data and other information from the "Topical Report on Actinide-Only Burnup Credit for PWR Spent Nuclear Fuel Packages" and from future topical reports related to burnup credit for storage and transportation will be used in this effort to the extent feasible.

INTENTIONALLY LEFT BLANK

3.0 METHODOLOGY

The methodology for performing disposal criticality analyses of spent nuclear fuel for long-term disposal in a repository is presented in this Chapter. This methodology is applicable for disposal criticality control analysis following permanent closure of the repository. Although the methodology will apply to the entire period of regulatory concern, there will be variations in the application of the individual models as conditions, events of interest, and levels of uncertainties change. Prior to closure of the repository (operations phase) the methodology will be based upon existing criticality analysis techniques. These techniques have been well established through operating experience from other DOE and NRC licensed facilities, and therefore, are not described in this report.

An overview of the postclosure methodology is presented in Figure 3-1. This figure illustrates the methodology for identifying configurations of fissile materials resulting from the degradation of SNF waste packages, evaluating the criticality potential of these configurations, and performing criticality consequence analyses to project perturbations to the repository source term and thermal effect. The results of the criticality consequence analyses provide input for total system performance assessments to evaluate the effects of these projected perturbations on the ability of the repository to protect the health and safety of the public. The optimization of a design to reduce the risk from criticality requires multiple passes through the flow process shown in Figure 3-1. The details of such an optimization are beyond the scope of this document. The design optimization will be part of the supporting analyses presented or referenced in the license application.

The intent of Figure 3-1 is to show the flow process of the various analyses performed and the models used for these analyses. The specific models and their validation will be described in Chapter 4. Some of the models are developed as part of the TSPA process, as indicated in Figure 3-1. The individual steps in the various analyses are applied repeatedly and iteratively to simulate uncertainties in waste package/EBS environmental parameters and material performance.

The process starts with the isotopics model determining the SNF isotopic concentrations in the waste form contained in the waste package/EBS design. For this version of the report, the only waste form considered is commercial LWR SNF. Varying environmental conditions within the

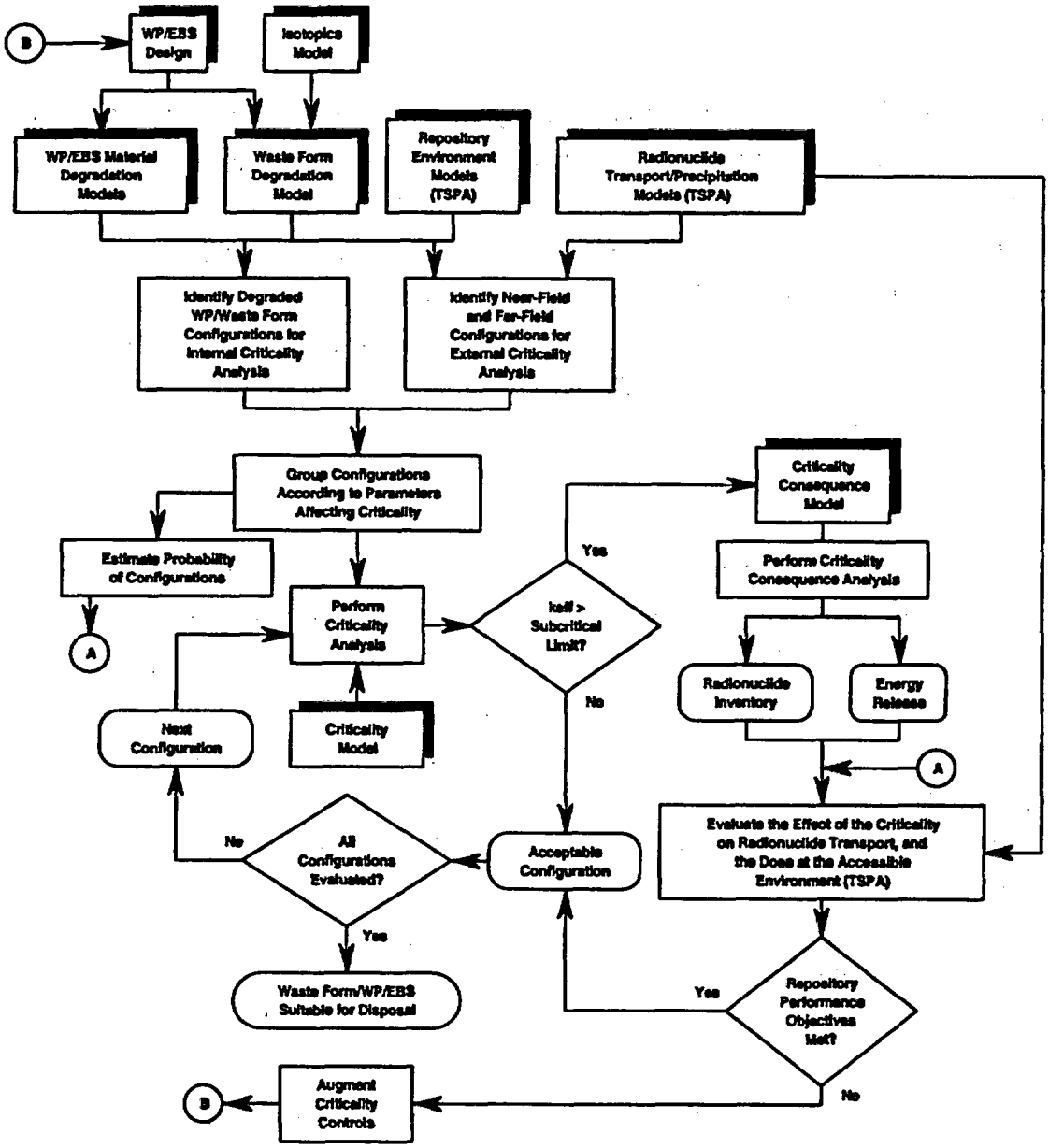

Figure 3-1. Overview of Disposal Criticality Analysis Methodology

repository over the long time periods considered for disposal may result in degradation of the waste package and the waste form. This may lead to changes in the configuration of fissile and other neighboring materials. The configurations to be evaluated are generated by sampling from the probability distributions of individual processes which are combined into sequences or scenarios.

The probability distributions for the individual processes in a sequence are based on models of natural processes and/or material performance. Probability distributions of various processes are used in identifying configurations which are then grouped according to parameters likely to affect criticality. For each configuration generated, the probability of attaining the configuration is estimated for the given time periods.

The criticality potential (k_{eff}) of selected configurations is determined from criticality analysis and compared with the subcritical limit. (The subcritical limit is an upper bound on k_{eff} established by the methodology. The basis for establishing the subcritical limit will be discussed in Section 3.3). If the calculated k_{eff} of the configuration is less than or equal to the subcritical limit, no further analysis of that configuration is required. However, if the k_{eff} value is greater than the subcritical limit, further analyses are performed to determine if additional criticality control is required. Since a risk-based methodology is being used for disposal criticality analysis, exceeding the subcritical limit requires additional analyses be performed to estimate the risk (to public health and safety and the environment) associated with a potential criticality for that configuration. The acceptability of the risk associated with the configuration is determined by meeting the performance objectives.

To estimate the risk when the subcritical limit is exceeded, an evaluation of the impact of the potential criticality on the radionuclide inventory and thermal effect is performed. Data from this analysis is provided as input for a performance assessment evaluation. The performance assessment evaluation will include a multiple step process to evaluate the information provided regarding radionuclide inventory and thermal effect impacts caused by the potential criticality. Depending on the results of the criticality consequence evaluation, additional TSPA may be required. Although the methodology for the TSPA is beyond the scope of this report, common models (and data) are shared by both methodologies as indicated in Figure 3-1. The results of the TSPA, if required, are used to demonstrate that the repository performance objectives are met and to determine if augmentation of criticality controls is required. If additional criticality controls are required, new configurations are identified and the process is repeated. When all of

the configurations have been classified as acceptable configurations (of fissile material, moderator, and neutron absorber), the waste form/waste package/EBS are acceptable for disposal from a standpoint of criticality.

3.1 Approach

The approach followed to demonstrate long-term criticality control after permanent closure of the repository is presented in this section. This approach considers configurations of fissile material for three regions or locations within the repository. The three regions include potential critical configurations interior to the waste package, exterior to the waste package but inside the EBS (near-field), and exterior to the EBS (far-field). For configurations interior to the waste package, burnup credit may be used to reduce the requirements of other control methods. However, for configurations exterior to the waste package (both near-field and far-field) credit may not be taken for neutron absorption by fission products. It cannot be assumed that these isotopes will remain with the actinides during the material separation, transport, and deposition processes (TBV). The amount of credit that can be taken for the actinides (fissile depletion and buildup of absorbers) for external configurations has not yet been determined.

The design-related objective of criticality analysis is to estimate the degree to which the waste package criticality control methods are effective, as a function of time after emplacement and as a function of the changes in repository environment and composition. These changes are characterized by events and processes. The probabilities of occurrence of these events or processes, and the resulting parameter changes, are a function of time. The probabilities and consequence (parameter changes) are used to determine the risk. The effectiveness of the criticality control is ultimately measured by the increased risk of radiation dose due to the increase in radionuclide inventory which can result from a criticality. The increased risk is determined as part of the TSPA process.

The analysis methodology will evaluate criticality potential as an explicit function of time. However, current interpretation of regulatory requirements and analyses thus far indicate that the time dependent behavior will be most conveniently understood in terms of the following time phases:

- Preclosure/operations phase, including the waste emplacement and retrievability period. These operations encompass approximately 100 years.

- The containment phase, lasting from the closure of the repository to approximately 1,000 years after closure. The waste package performance during this phase is measured against the regulatory requirement of, "Substantially Complete Containment."

- The isolation phase, lasting from approximately 1,000 years after closure to the end of the period of regulatory concern (currently undefined but assumed to be 10,000 years after closure as required by the most recent Environmental Protection Agency regulation, which has been remanded).

Because of present uncertainties in the period of regulatory concern, this report defines a fourth phase, the extended isolation phase. The extended isolation phase refers to a time period for which criticality analysis must be performed if the future period of regulatory concern is much longer than 10,000 years. For such a long period of regulatory concern, the approach to criticality analysis may need to vary to deal with the increased uncertainties in the distant future. The points in time at which such variations will be needed have not yet been determined, so the period covered by the extended isolation phase has also not yet been defined.

The period of regulatory concern is expected to be established by the time the topical report is completed. The topical report will then define the approach or approaches to be used for the entire period of regulatory concern.

Analysis thus far shows that during the preclosure and containment phases, the only expected location for a criticality is within the waste package (internal criticality), because there is insufficient time for dissolution of the SNF waste form and removal from the waste package (TBV).[3-1] Since some of the waste packages will not breach for up to 100,000 years, there is even a possibility of internal criticality during the isolation and extended isolation phases, as well. External criticality within the EBS (typically in the invert below the waste package) may occur during the isolation or extended isolation phases. The greatest probability of far-field external criticality occurs in the extended isolation phase.[3-2]

For each of the three potential criticality regimes, an initial performance assessment will be conducted. This analysis will assume that a representative criticality event has occurred,

consistent with the amount of fissile material available to participate in the event, while employing reasonable bounding assumptions relative to material composition/geometric arrangement and the dynamics of the assumed criticality event. If the perturbations to the system (e.g., radionuclides generated by the fissions and thermal effects from the heat generation) are insignificant, then the consequence of the criticality event is insignificant, and the potential criticality need be considered no further. In such cases, a criticality-event perturbation to the TSPA source term will not be included in those analyses.

If the perturbations to the system are significant, then the next step is to consider the scenarios developed in Section 3.2 to identify the processes that can cause a geologically created critical mass. These analyses provide bounds on the probability of occurrence and magnitude of consequences for the creation of a critical configuration in the repository. If it can be shown that there are no reasonable probabilities and consequences for a criticality event, then no further analyses need be done.

If the geologic formation of a critical configuration is credible, then the TSPA source term must include this perturbation. TSPA analyses will then estimate the effects on repository performance (e.g., radionuclide doses or releases) arising from criticality events.

[Note: The quantitative measure of significance or insignificance is TBD. The combining of multiple insignificant consequences into an overall significant consequence is still under consideration. (TBD).]

3.1.1 Waste Package - Internal Criticality

Two basic conditions required for criticality (for commercial LWR SNF) are the introduction of a moderator and the loss or absence of neutron absorber. If the moderator is water, there must be some mechanism for its retention within the waste package. As part of the criticality analysis methodology, a systematic evaluation is performed identifying water, or other moderator sources and mechanisms for loss of the neutron absorber. For purposes of preliminary analysis, the corresponding processes can be approximated by discrete events occurring at (or before) specific times. Therefore, the general techniques of Failure Modes and Effects Analysis (FMEA) are used to identify the sequence of events which could lead to breach of the waste package and failure of the criticality control mechanisms internal to the waste package. A (simplified) event sequence includes the following:

1. Increased water flow through the repository.

2. Concentration of the flow so as to directly impinge upon the waste package (e.g. flowing fractures in the drift directly above the waste package, or flooding of the entire drift) through failure of repository drainage/deflection systems.

3. Breach of the waste package (most likely by corrosion) to permit moderator (water) entry into waste package.

4. Leaching of the neutron absorber materials from the containing matrix (basket criticality control material)

5. Sufficient fissile material remaining in the waste package after all of the above events. This implies a minimal dissolution of the SNF. Preliminary analyses show that the fuel rods and assemblies must retain their structural integrity so that when the water does pond in the waste package it can fit between fuel elements to provide sufficient moderation.

6. Sufficient standing water within a waste package or in the drift.

3.1.2 Engineered Barrier Segment Near-Field

The events analyzed for internal criticality are relevant as precursors of the conditions for external criticality, except that with the increased time they become part of continuous processes with changing (time dependent) probabilities, which can no longer be approximated by discrete events with a fixed probability. For this reason, the analysis process is no longer a simple FMEA. The following additional events/processes are of importance for external criticality:

- Dissolution of the SNF, so that the fissile material can be transported out of the waste package.

- Reconcentration of the fissile material in the near-field/invert (e.g. filtration of Pu or U colloids by the network of narrow fractures).

3.1.3 Far-Field

The slow dissolution rate of the SNF and slow migration of the fissile material to the far-field, puts the earliest expected time for far-field criticality beyond 10,000 years, and into the extended isolation phase (TBV).[3-2] The following processes are necessary for far-field criticality (TBV):

- Dissolution and mobilization of the SNF.
- Transport to the repository far-field saturated zone (sufficient quantities having escaped precipitation in the invert or in any Calico Hills zeolites).
- Existence of a reducing zone, or other formation for concentrating the fissile material, below the water table (in the saturated zone).
- Waste stream flow through the reducing zone.

3.2 Probabilistic Evaluations of Events and Processes

Probabilistic evaluation of waste package criticality is the analysis of waste package performance under the spectrum of possible environmental conditions with probabilistic techniques also applied to the uncertainty regarding waste form and waste package material performance. The FMEA for internal criticality is the first step of the probabilistic evaluation process. In the overall scheme of criticality analysis, probabilistic evaluations have two purposes. (1) The probabilistic results are used to prioritize the configurations for the calculation of k_{eff}. (2) They also constitute the first step of the risk analysis process which expresses the hazards from the repository in terms of the expected dose (or some other risk measure) impacting some population (e.g., humans at the accessible environment). The prioritization of configurations for criticality analysis according to probability may be revised if the overall risk analysis identifies such large consequences with a configuration having a very low probability, that the expected dose to a population turns out to be significant.

The determination of possible configurations requires the evaluation of events and processes affecting the waste packages and engineered barrier system including transport of materials to various locations within the EBS and to far-field locations within the geologic repository. In

evaluating these events and processes, degradation of materials in the waste packages under the influence of adverse environmental conditions in the repository is considered. For the long time periods involved, a great variety of conditions is possible. Probabilistic evaluations are used for an initial prioritization of the sets of conditions according to their probability of occurrence. Criticality analyses are performed for on these configurations, in order of priority.

3.2.1 Probabilistic Evaluations Compared with Traditional PRA

A well known example of probabilistic evaluation in the nuclear industry is the PRA. PRA is widely used by the nuclear power industry for judging the importance of plant systems and components important to radiological safety. Nuclear powerplant PRAs are used for identifying potential vulnerabilities and guiding design change and maintenance decisions towards optimizing plant safety; they are also used to show that risk has been reduced to an acceptable level. While the goal of the probabilistic evaluations discussed in this report remains the same as that for nuclear power plants, differences in conditions require methods which differ from those utilized in traditional PRA. Principal examples of these different conditions are as follows:

1. Analyses must cover a longer period of time. Assumptions of constant failure rates, or even constantly increasing or decreasing failure rates, may not be correct due to potentially fluctuating environmental conditions.

2. Partial component failures must be accounted for, since they may have significant consequences.

3. In many cases, component failures cannot be assumed to be independent. Failures are often dependent on previous component failures or environmental changes.

4. Due to changing isotopics, the time in which a failure or event occurs may also affect the consequences of the event.

By comparison with traditional PRA, the phenomena most significant to criticality analyses can be grouped for illustrative purposes into the following interrelated categories:

1. Environmental conditions: particularly water infiltration/flow, water chemistry, and temperature.

2. Response of the waste package components to the repository environment.

3. Reconfiguration of assemblies, fuel rods, or fuel particles due to corrosion and failure of mechanical structures.

4. Relocation of isotopes via transport by groundwater and re-concentration.

The probability of internal criticality (within the waste package) is dependent on events and processes from the first four of these categories. The probability of external criticality (fissile material transported and concentrated beyond the immediate vicinity of the waste package) is dependent on all five. Variation in the probabilities of events in each of the five categories occurs with the passage of time and as a result of interactions with events in other categories.

3.2.2 Probabilistic Methodology

Although different from the traditional nuclear powerplant PRA, the waste package/repository long term probabilistic evaluation can be represented/summarized by a pseudo-FMEA of the waste package. In this pseudo-FMEA, there is no explicit failure event associated with the waste package, but the continuous degradation processes can be understood by such summary representations as a logic tree or a fault tree. For internal criticality, the goal of this pseudo-FMEA is to identify how waste package component (e.g., barriers, welds, fuel assemblies, basket plates or tubes, fuel rods) degradation events and processes will produce changes in the configuration/geometry of the waste package (barriers and contents). The pseudo-FMEA also considers any prior failures or degradations which are required antecedents for the downstream (in time) degradation of some component. For example, the waste package barriers must be breached, and water must enter the waste package, before the neutron absorbing material can be removed from the waste package basket.

If necessary, component failure events may be grouped into general configuration change categories. These categories are discrete representations of a continuum of parametric values. This discretization approximation is used to reduce the number of configurations to a manageable level. This discretization also provides a better analog of the traditional FMEA concepts of discrete configuration changes.

In the next step, the categories of discrete configuration changes or component failures defined in the FMEA are used to build a waste package configuration logic tree. An example waste package configuration logic tree is shown in Figure 3-2. This logic tree is visually and conceptually similar to the event trees used in nuclear power plant PRAs. There are two principal differences for the present application: (1) For many of the steps, the probabilities are conditioned upon the occurrence of prior events so many events must occur in sequence, and (2) for most of the steps the events represent a continuum of processes, which are represented by probability density functions instead of discrete probabilities. The configuration change categories (or events) are listed across the top of the tree (E_1 thru E_6), and all possible configurations (regardless of likelihood) are listed down the right side.

In Figure 3-2, the prime notation has been used to indicate complement. For example E_2' indicates a configuration where the inner barrier has not been breached. These changes may or may not be dependent on a previous configuration change. For example, the category E_2 indicates a configuration where the inner barrier has been breached. Corrosion breach of the inner barrier cannot occur until breach of the outer barrier exposes it to the external environment.

The probabilities are best expressed by the continuous probability density function (PDF) and the cumulative distribution function (CDF). The PDF, f(t), is defined by:

$$\Pr\{t \le T \le t+dt\} = f(t)dt;$$

the CDF, F(t), is defined by either:

$$F(t) = \int_0^t f(t')dt'$$

or

$$F(t) = \Pr\{T \le t\},$$

which are equivalent.

Uncond. PDF:	$f_1(t)$	$f_2(t)$	$f_3(t)$	$f_4(t)$	$f_5(t)$	$f_6(t)$
Config. PDF[1]:	$f_1(t)$	$f_{12}(t)$	$f_{123}(t)$	$f_{124}(t)$	$f_{125}(t)$	$f_{126}(t)$
Config. CDF[2]:	$F_1(t)$	$F_{12}(t)$	$F_{123}(t)$	$F_{124}(t)$	$F_{125}(t)$	$F_{126}(t)$

Aggressive Environment (Degradation Initiator)	E_1: Outer Barrier Breached	E_2: Inner Barrier Breached	E_3: Basket Structure Collapse	E_4: Fuel Assembly Collapse	E_5: Fuel Rods Breached	E_6: Absorber Removed From WP	Waste Package Configuration Description

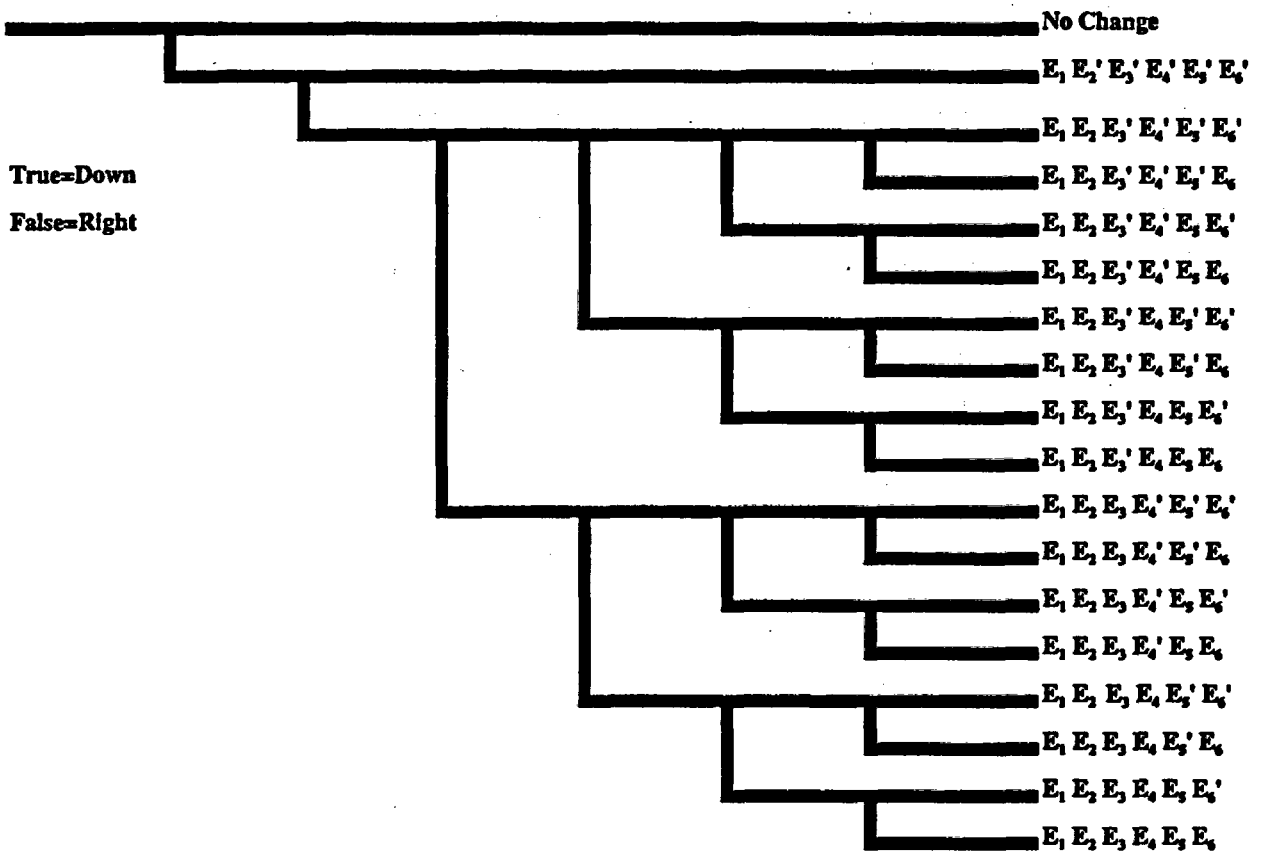

Notes:

1 Multiple subscripts indicate that the PDF is generated by convolution of the indicated unconditional PDFs. For example $f_{12}(t)$ indicates the convolution of the unconditional PDFs $f_1(t)$ and $f_2(t)$.

2 Upper case "F" indicates the CDF obtained through integration of the indicated PDF. For example $F_{12}(t)$ represents the CDF of the convolved PDF $f_{12}(t)$.

Figure 3-2 Example Waste Package Configuration Logic Tree

If $f_1(t)$ represents the PDF for corrosion breach of the outer barrier, and $f_2(t)$ represents the unconditional PDF for corrosion breach of the inner barrier, then the PDF for category E_2 is defined as the convolution of the two PDFs, $f_{12}(t)$, which is given by:

$$f_{12}(t) = \int_0^t f_1(\tau) f_2(t-\tau) d\tau$$

Of course, the dependence of inner barrier corrosion on outer barrier breach is more complex than is represented by this convolution. The inner barrier corrosion or degradation will be proportional to the amount of inner barrier exposed to corroding water, which will, in turn, be proportional to the outer barrier surface area which has been penetrated (for designs with no gap). The more complex dependence is reflected, to some degree, in the barrier corrosion model of TSPA-95, and will be even more refined for TSPA-VA (Viability Assessment) and for the topical report.

The probability that the logic tree category E_2 has occurred by a given time is then represented by the CDF, $F_{12}(t)$, which is obtained by integrating the convolved PDF, $f_{12}(t)$. This particular illustration of the causal relationship is supported as long as the breach is due to corrosion from the outside. The probability that a given configuration (shown to the right of the tree) has occurred by time *t* would generally be determined by taking a multiple convolution over the times of occurrence of each event. Since many of these events (or processes) are independent, the convolution may degenerate into the product of the probabilities that each of the categories has or has not occurred by time *t* (as indicated), which is obtained from the CDF for each category at time *t*.

This logic tree is described here to illustrate the process of considering all relevant configurations. The logic tree cannot actually describe the very many degrees of partial process completion (e.g., partial barrier corrosion) which are significant in the overall waste package degradation. In addition, the logic tree is unable to conveniently handle certain combinations and non-corrosion modes of degradation, such as rockfall on a partially corroded package, and would be unable to support external criticality analyses.

3.2.3 Scenario Generation

The events and processes which make up the postclosure behavior are most conveniently analyzed in terms of the sequence in which they occur. These sequences can be best understood when grouped into scenarios listing the process outcomes. This section provides an overview of the methodology for generating a set of scenarios which represent the range of possibilities. Three typical scenarios leading to the three types of criticality (internal, near-field external, and far-field external) are shown in the three branches of Figure 3-3. These scenarios can be said to be probabilistic in their initiation, because their initiation depends on environmental parameters which are best described by a probability distribution. For the preliminary evaluations, the scenarios are said to be initiated probabilistically and to evolve deterministically. In other words, once the environmental parameters are selected randomly at the beginning of the scenario, they are assumed to be constant throughout the time of evolution of the scenario, so the scenario evolution becomes deterministic. Both the probabilistically determined initial environmental parameters and the subsequent process evolution will be consistent with, and/or derived from, the methodology and results of TSPA-VA.

The implementation of the scenario generation process is provided by a computer code, called the scenario generation tool, which tracks the parameters which characterize configurations with the greatest criticality potential. The algorithms of the scenario generation tool computer code will generally be abstractions of the physical processes elucidated by the physics and chemistry codes used in TSPA.

Construction of the scenario generation tool will consist of the following activities, in approximately the indicated sequence.

- Determination of the species of importance (particularly fissile nuclides and neutron absorbers)

- Definition of the sample space consisting of compartments formed from the discretization of phases and locations of the species of importance. Examples of such compartments are the amount of iron in the basket steel, iron in solution, boron in solution, etc.

- Abstraction of transfer rates between the sample space compartments based on physical and chemical process models as elucidated by TSPA, either through the parameterization of the

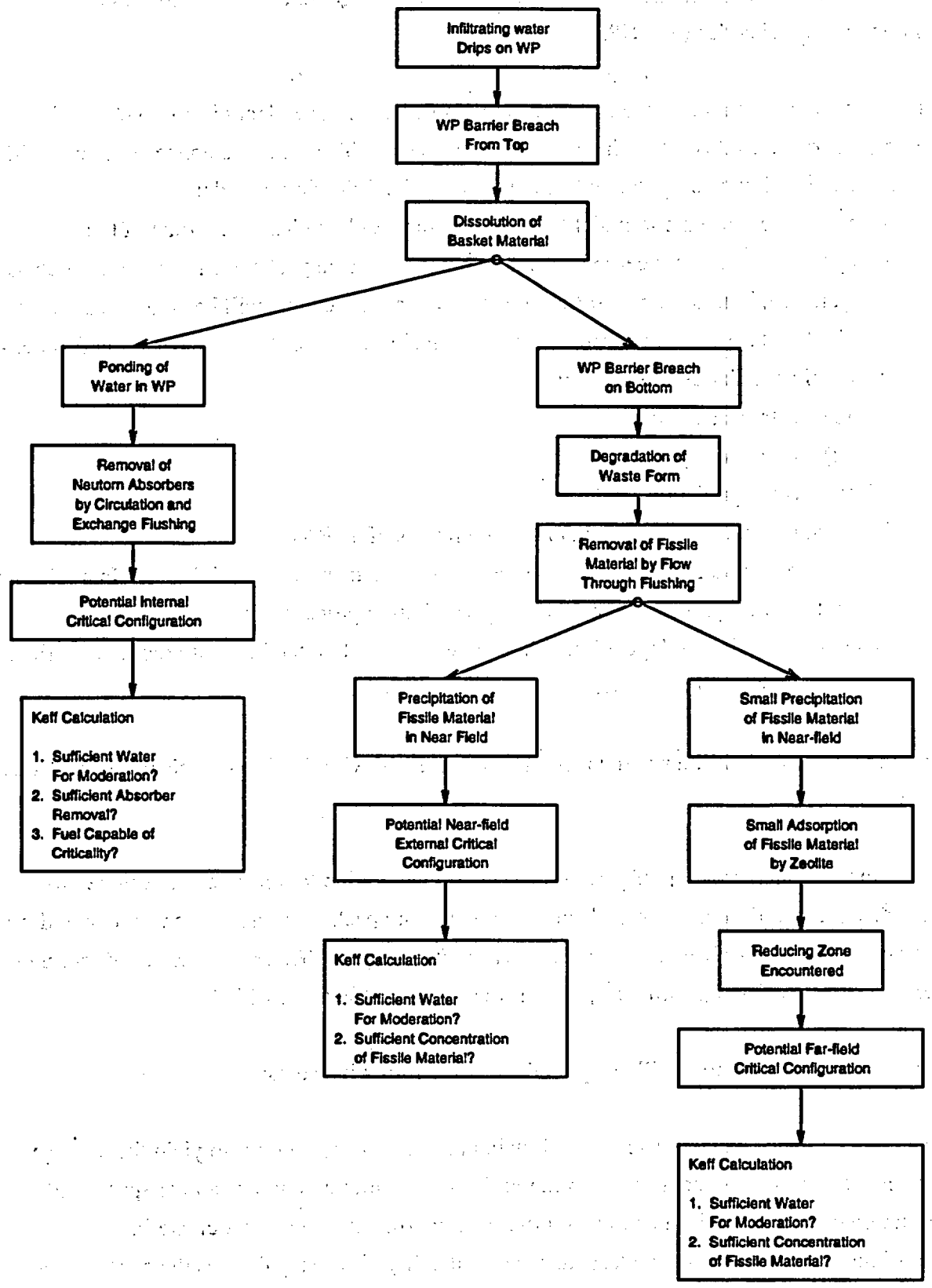

Figure 3-3. Illustration of Scenario Generation Methodology

results of physics and chemistry codes like FEHM and EQ3/6, or through the results of summary model codes like RIP.

- Development of mass balance equations (first order, time dependent differential equations) using the transfer rates determined in the previous step. These mass balance equations will be implemented in a computer code incorporating the following models:
  - Repository environment model (abstracted from results of TSPA). Some of the components will be concerned with the immediate waste package environment, such as temperature, humidity, or infiltration rate. Other components will be concerned with the far-field rock, such as the probability of a reducing zone existing in the saturated zone. - Material degradation models for:
    (1) waste package barriers
    (2) waste package basket
  - Waste form degradation model
  - Material transport model (abstracted from results of TSPA)
  - Material precipitation/retardation model (abstracted from results of TSPA). In addition to straight forward physical adsorption or precipitation processes, chemical changes analogous to mineral deposition will also be evaluated on the basis of recommendations of experts who will also review the resulting analysis.

- Estimation of probabilities and uncertainties connected with the five models of the previous item.

A preliminary implementation of part of the scenario generation tool has been developed to determine concentration of neutron absorbers in the waste package as a function of time and used in the *Second Waste Package Probabilistic Criticality Analysis: Generation and Evaluation of Internal Criticality Configurations*[3-1], which was completed in March 1996.

The scenario generation tool will be applied using the following steps:

- The mass balance equations are solved (using the computer program) to yield the average expected values of concentrations in the various compartments of the sample space, and as a function of time. Emphasis will be on those compartments which participate in configurations having the greatest chance of criticality. This step defines the configurations for evaluation in the subsequent steps.

- Probabilities are estimated for the mean value configurations, using the parameter distributions and uncertainties in the parameters in the models.

- Those external criticality configurations that rely on some specific capability of fissile precipitation or adsorption (e.g. reducing zone) will incorporate the probability of the fissile laden repository effluent encountering such a reducing zone.

3.2.4 Bookkeeping of Configurations

This section describes the process for keeping track of intermediate and end points of scenarios and to apply probabilities to the deterministic parameters of the equations in the scenario generator. This process is implemented in a configuration bookkeeping tool which serves as a completeness and consistency check on the scenario generation.

The complete configuration bookkeeping tool is built by an iterative process. The full capability version of the tool should be ready in 1997, and it will be updated annually to reflect new data from long-term material degradation tests and TSPA on waste package barrier corrosion, waste form degradation, neutron absorber degradation, and transport and precipitation of fissile and neutron absorber nuclides.

A Monte Carlo model is used to follow a waste package (or a full repository of waste packages) through its lifetime, determining when various environmental and configuration changes are likely to occur. The Monte Carlo model will require inputs from several sources. External water flow rates, temperature, humidity, and pathways will be taken from the appropriate TSPA models/results. The flow process for the Monte Carlo iterations and bookkeeping is shown in Figures 3-4A, 3-4B, and 3-4C. Figure 3-4A shows the relationship of the processes involved in degradation and breach of the waste package barriers. Figure 3-4B shows the relationships for degradation of the waste package internals. Figure 3-4C shows the relationships for the criticality-related processes external to the waste package and also shows the process for accumulating the variety of criticality probabilities.

The internal criticality model follows a waste package through its postclosure life and establishes the probabilities of configuration changes, given the probabilities of environmental conditions and non-corrosion failure modes.

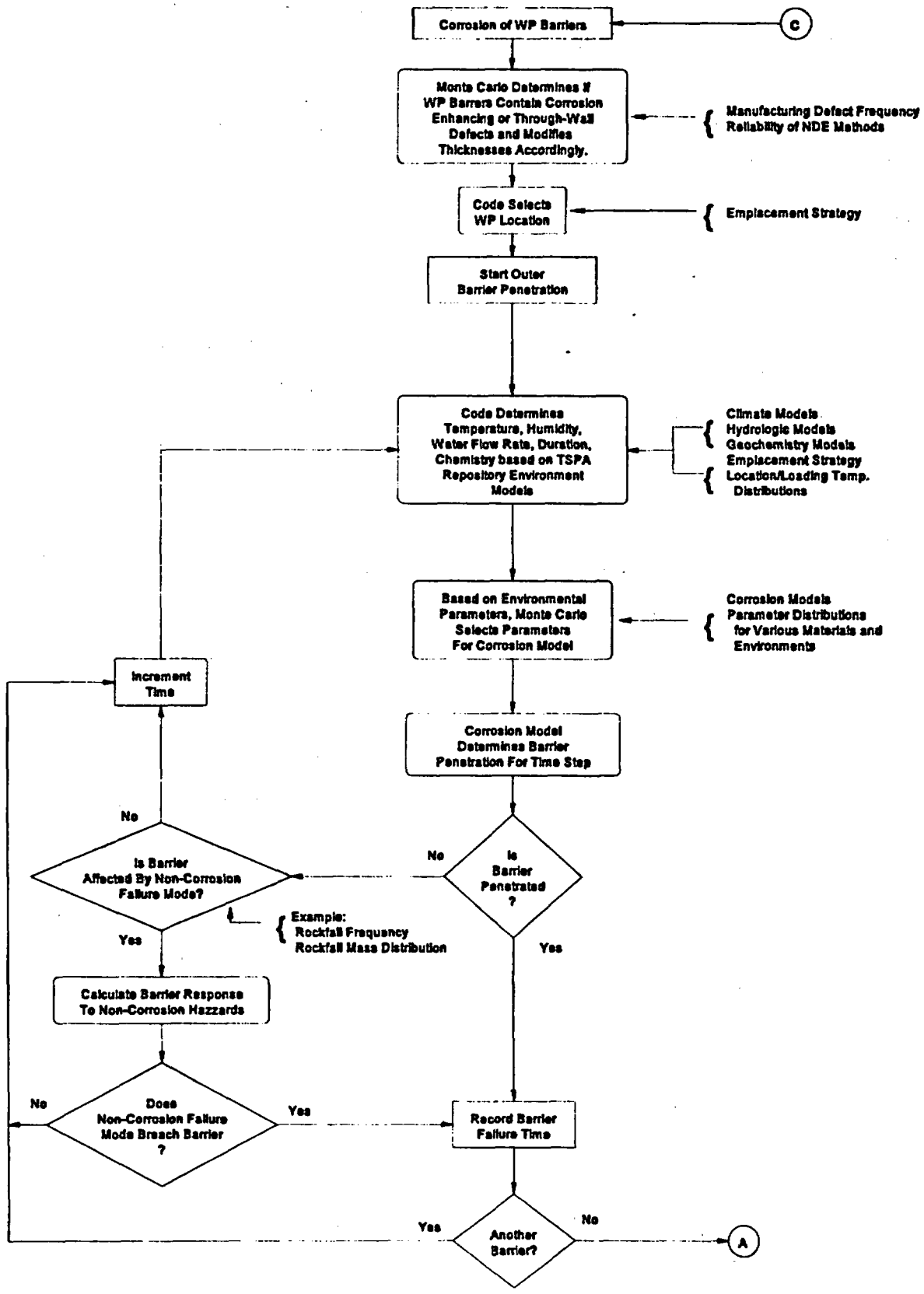

Figure 3-4A. Configuration Bookkeeper - Barrier Penetration Sequences

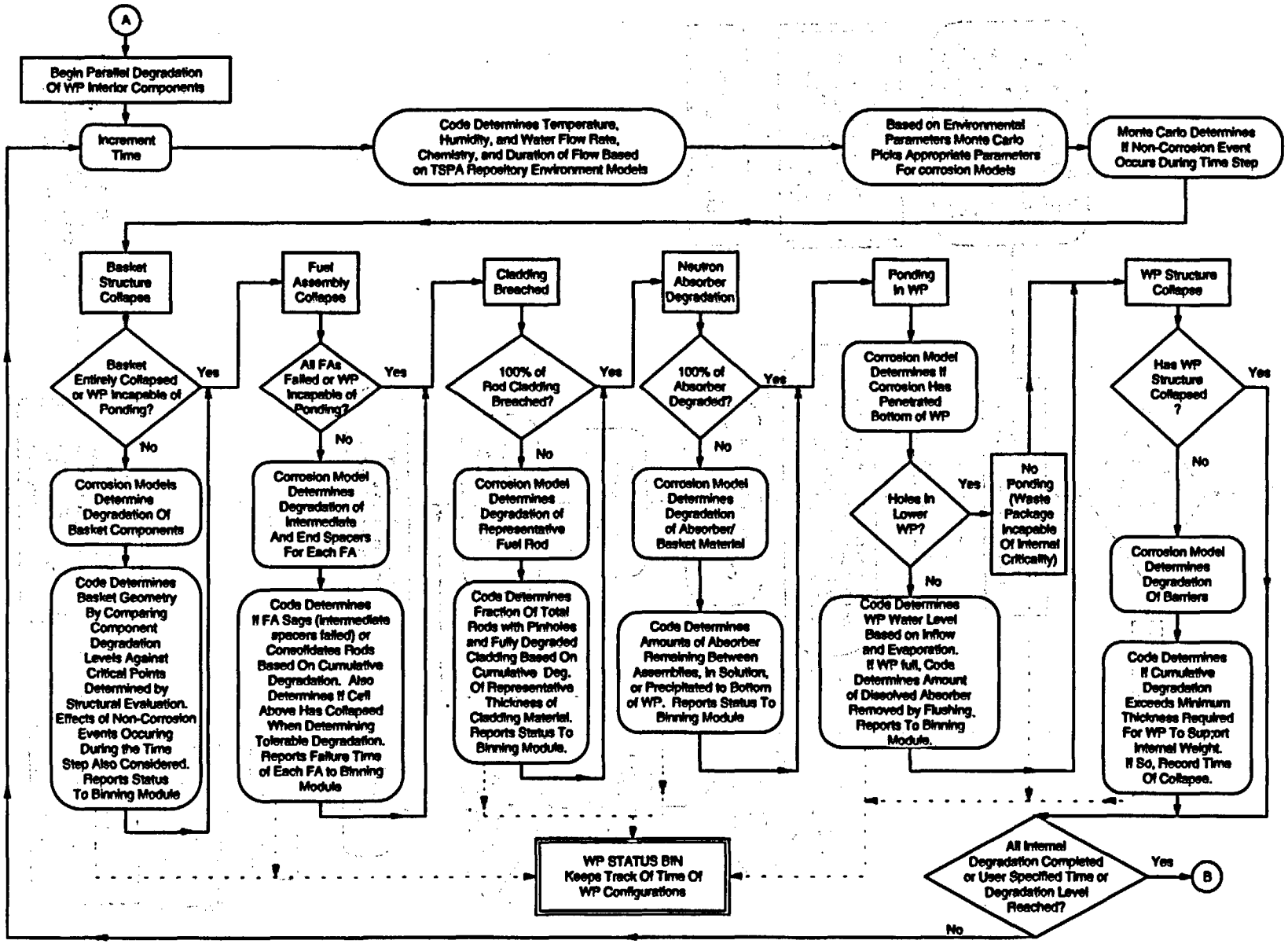

Figure 3-4B. Configuration Bookkeeper - Basket Degradation Sequences

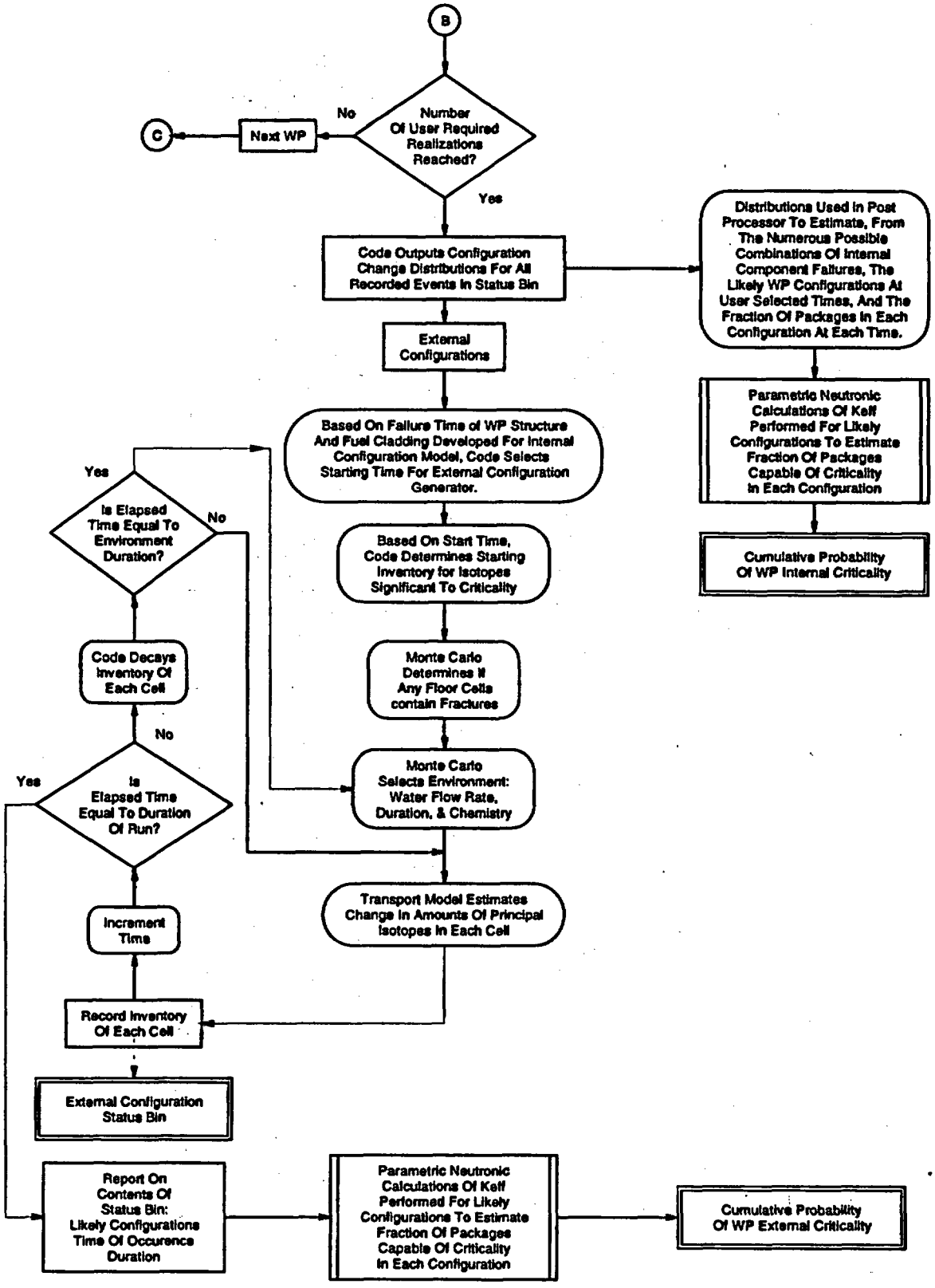

Figure 3-4C. Configuration Bookkeeper - External Process Sequences, Potentially Critical Configurations, and Accumulation of Criticality Probability

Using the probability distributions for cladding breached as a function of time generated by the internal model, the external model selects the starting time for external events and the isotopic inventory for the starting configurations. Initially, the entire inventory is located in one or two cells representing an individual waste package. The model then determines how each isotope is transported down the drift, into the tuff floor, or down a fracture (if one exists nearby) using available transport models. Transport is also dependent on the environment in existence at a given time, which is determined by Monte Carlo methods from existing models. Again, deterministic criticality analyses are performed for the more probable configurations.

3.3 Criticality Analysis

The part of the methodology for evaluating nuclear criticality of fissile material configurations in the potential repository is summarized in this section. Model validation is performed based on criticality analyses using fresh fuel critical experiments and commercial reactor criticality data for spent nuclear fuel. A complete description of the models and the validation process is given in Section 4.1.

Criticality analyses for disposal are performed using a combination of computer codes to calculate the isotopic compositions of fissile material and the reactivity of the geometric configuration. The isotopic compositions are obtained from computer codes contained in the SAS2H sequence of SCALE 4.3[3-3]. Reactivities are calculated with the MCNP[3-4] code which uses the isotopic compositions of the materials and a system of nuclear data libraries (generally termed ENDF - the Evaluated Nuclear Data File system), plus a detailed model of the fissile geometry, to calculate the k_{eff} of the system. A detailed description of the code systems and their associated nuclear data libraries used in criticality analyses for disposal is provided in Section 4.1

Configurations of fissile material are identified for criticality analyses for each of the three repository regions previously described; (1) inside the waste package, (2) outside the waste package in the near-field, and (3) outside the EBS in the far-field. For these analyses, an upper bound is placed on the calculated value of k_{eff} to ensure subcriticality of the configurations analyzed. This upper bound, called the subcritical limit, contains the criticality analysis method bias, the bias uncertainty, and an additional arbitrary margin (consistent with applicable regulatory requirements) to ensure subcriticality. Although the same criticality analysis method is used for each of the three regions, the method bias and uncertainty, and thus, the subcritical

limit values can be expected to be different for each region. The subcritical limit is determined during the validation process for the criticality analysis methodology. The determination of the subcritical limit and its applicability to criticality analyses for the three repository regions is described in Section 4.1 (TBD).

3.4 Criticality Consequence Analysis

Criticality analyses are performed for configurations identified within the waste package, outside the waste package in the near-field, and outside the EBS in the far-field. When the k_{eff} of the configuration analyzed exceeds the subcritical limit (upper bound established by the methodology), a criticality consequence analysis is performed. This analysis determines the impact of a potential criticality event on the radionuclide inventory and on the thermal effect (based on the energy yield) within the repository. Probabilities of criticality events and the results of the criticality consequence analyses provide input for a performance assessment to demonstrate that the repository performance objectives are met.

3.4.1 Type of Criticality Event

The consequence of a criticality event is dependent upon the type of event. The type of criticality event is dependent upon the time to initiate the event (i.e., to assemble the critical mass/configuration), the amount of moderator material present, and the energy yield of the event. The energy yield, which determines the consequence, is dependent upon the amount of fissile material and the positive and negative feedback mechanisms present in the system.

The potential types of criticality events are identified below:

1. Slow assembly, moderated, low yield
2. Slow assembly, moderated, high yield
3. Slow assembly, unmoderated, low yield
4. Slow assembly, unmoderated, high yield
5. Fast assembly, moderated, low yield
6. Fast assembly, moderated, high yield
7. Fast assembly, unmoderated, low yield
8. Fast assembly, unmoderated, high yield

Based on natural processes and conditions anticipated for the repository, the first item on this list is far more likely than the others (see Section 3.4.2)(TBV). The last four items are currently believed to be virtually impossible in the natural environment because there is no known naturally occurring mechanism for fast assembly (TBV). Nevertheless scenarios are continuing to be studied that could conceivably result in fast assembly of a critical mass of fissile material from commercial SNF. [Note: Further discussion of probabilities of the above eight combinations (including credibility) will be provided in the topical report.]

3.4.2 Evaluation of Criticality Event Consequences

The processes which could lead to a criticality event in a mined geologic disposal system (MGDS) are slow geological (water infiltration) and chemical (corrosion) processes. Therefore, slow assembly, low-power criticality events are considered to be the most likely criticality events in a repository (TBV). It is expected that when analyzed in detail, even these events have a very low probability. Verification of these expectations through probabilistic evaluations will be performed. These evaluations will be used to determine the probabilities of obtaining conditions conducive to a criticality event. Based upon preliminary analyses[3-1], it is anticipated that a slow assembly, low-power event would have a low energy release and would affect only a small volume of the repository (a few meters from the event)(TBV). This is based on the assumption that negative feedback mechanisms will shut down the chain reaction soon after criticality is achieved, which must be verified. However, if sufficient negative feedback was not available, a low-power, long time-scale event could result in a high energy yield, yet still be benign with respect to repository performance. The major consequence of a slow assembly, low-power criticality event during the postclosure period is the generation of more radionuclides which would then be available for transport into the accessible environment. An example of determining the radionuclide inventory for a low-power, long time-scale criticality event is presented in Appendix D.

[Note: The methodology for evaluating the consequence of a potential criticality has not been completed at this time. A more detailed discussion will be provided when this methodology is finalized.]

3.5 Risk Analysis

The risk associated with repository criticality is the product of the probability of occurrence multiplied by the consequence and summed over all possible criticality events (or probability-consequence pairs). If the probability distribution is continuous, then the summation becomes an integration. In practice the consequence will be measured by important impact parameters, such as the following:

- Radiation dose to the average nearby population, as a function of time
- Radiation dose to the most affected individual in the nearby population

Radiation doses will be estimated as part of TSPA, and will use, as input, the increased radionuclide inventory and thermal effects estimated by the criticality consequence model (described in Section 3.4).

Section 6.5 provides an illustration of the process for estimating total dose to the affected population as a function of time.

3.6 Total System Performance Consequences

As discussed in Section 3.1, a systematic performance assessment evaluation will be conducted to determine the most significant consequences of the potential criticality events. If the consequences are determined to be insignificant, no additional TSPA will be conducted. If the consequences are determined to be potentially significant, the consequence of significant criticality events will be evaluated as necessary; (1) within the failed waste package, (2) outside the waste package in the near-field, and (3) outside the EBS in the far-field. The approach to the evaluation of the potentially significant consequences for each of these regions is summarized as follows:

- Start with the already identified potential criticality events (Sections 3.2 and 3.3) and associated perturbations to the inventory of radionuclides and thermal effect (temperature at the source as a function of time) (Section 3.4);

- Use the thermal effect to determine timing of return of ambient ground-water flow conditions (if the event causes the removal of ambient ground-water) in the vicinity of the criticality and refine the inventory as necessary;

- Use geochemical models to estimate the release rate of radionuclides from the vicinity of the criticality caused by leaching of the inventory by the ground-water flow (i.e., develop the source term for the inventory produced by the criticality); and

- Use source term and the inventory in a total system performance assessment model to evaluate the dose history at the accessible environment or at other locations as required by regulations.

The total system performance model tracks radionuclides as they are leached from the inventory, and transported through the unsaturated and the saturated zones, and provides the concentration of radionuclides in ground water at the accessible environment. For criticalities that occur within a failed waste package, or in the near-field, the source term is located in the unsaturated zone, but for those that occur in the far-field the source term is likely to be located in the saturated zone (TBV). Over the transport pathway from the source to the accessible environment processes such as retardation, dispersion, and dilution reduce the concentration of radionuclides. Radioactive decay may either reduce or increase the concentration of a particular radionuclide over the transport path (the increase being produced by ingrowth of daughter products). It is assumed that at the accessible environment a person uses the ground water for drinking, or for both drinking and food production. The radionuclide concentration at the accessible environment is converted to dose using a conversion factor that is derived using a dose model and the water use scenario.

The performance assessment model used to evaluate the dose at the accessible environment has the capability of tracking several inventories simultaneously (e.g., defense high-level waste, commercial spent fuel, and release from a criticality). Because of this capability, the dose attributed to the criticality alone can be evaluated and compared to that from the entire repository. This comparison allows the investigator to determine the significance of the criticality in terms of total dose at the accessible environment. The performance assessment model also has the capability of including a distribution of criticalities in time and space to evaluate the long-term effects of multiple cyclic events on the total dose at the accessible environment.

INTENTIONALLY LEFT BLANK

4.0 MODEL DESCRIPTION AND VALIDATION

The methodology for performing disposal criticality analyses for the Yucca Mountain repository was described in Chapter 3.0. This methodology is based on models for performing neutronics calculations, models for generating potential configurations of fissile materials, models for assessing the consequence of potential criticality events, and performance assessment models. This Chapter provides a description of these models along with possible information and data to be used in their validation. The definitive models, and the methodologies to be used to validate the models are currently TBD.

4.1 Neutronics Models

Two types of neutronics models are used in assessing the criticality potential of spent nuclear fuel. The first model utilizes the SAS2H[4-1] computer code to determine the composition of spent nuclear fuel from commercial light water reactors, and the second model uses the MCNP[4-2] code for performing criticality analyses for various configurations of fissile materials. These models are described in this section, followed by a discussion of the model validation strategy. The experimental data and supporting analyses for the validation process are discussed in Appendices B-1 and B-2.

[Note: Additional validation analyses will be performed prior to release of the topical report. The method biases and uncertainties, determined from all validation analyses performed, will then be used in establishing the subcritical limit values for each of the three regions or locations in the repository where criticality analyses are performed.]

4.1.1 Isotopic Model

The isotopic model determines the individual isotopic concentrations of fissile and absorbing isotopes to be used for criticality evaluations. Taking credit for the reduced reactivity associated with the net depletion of fissile isotopes and the creation of neutron absorbing isotopes during the period since nuclear fuel was first inserted into a reactor is referred to as burnup credit. This period includes both the time that the fuel was in a reactor and exposed to a high neutron flux (in a power production mode) and the "cooling time" since it was removed from the reactor. Burnup

is the amount of exposure of a nuclear fuel assembly, in a power production mode, expressed in units of gigawatt days per metric ton of uranium (GWd/MTU) initially loaded into the assembly. Burnup credit accounts for the reduced reactivity potential of a fuel assembly associated with this power production mode and varies with the fuel burnup, cooling time, and the initial enrichment of U-235 in the fuel. Conditions in the reactor core during burnup that affect the neutron spectrum, and therefore the isotopic composition of the fuel at discharge from the reactor, must be quantified if burnup credit is to be appropriately applied. These conditions include reactor power variations (and associated moderator and fuel temperature variations), addition of neutron absorbing materials (e.g., soluble boron, control rods, and burnable poison rods), and alteration of the amount of moderator material (e.g., moderator displacement by non-fuel rods). Investigations of some of these conditions are discussed in Reference 4-3.

[Note: This technical report is written for commercial SNF from light water reactors. Other SNF (e.g., DOE and Naval) and high level waste (HLW)(e.g., DHLW and Pu) when selected for geologic disposal will be addressed in addenda to the Topical Report.]

For the methodology developed in this report, the neutronics model for determining isotopic concentrations of SNF uses the SAS2H sequence of the SCALE-4.3 computer code system with the 44-energy group cross section library.[4-1] SAS2H is the control module for the analytical sequence. The functional modules (or codes) within the sequence are BONAMI-S, NITAWL-S, XSDRNPM-S, COUPLE-S, and ORIGEN-S. SAS2H converts user input data into those required by the functional modules. BONAMI-S and NITAWL-S perform problem-dependent resonance processing of neutron cross sections. XSDRNPM-S is a one-dimensional discrete-ordinates code that produces a weighted cross section library and spectra data. This data is used by COUPLE-S to update an ORIGEN-S data library. ORIGEN-S is a point-depletion/decay code that computes the time-dependent isotopic concentrations using the matrix exponential expansion technique. For short-lived nuclides a form of the Bateman equation is used to ensure better accuracy. ORIGEN-S computes the isotopic concentrations (actinides and fission products) for all required conditions. This includes both power operation and shutdown. ORIGEN-S is also used in calculating radioactive decay and daughter isotope buildup after the fuel is withdrawn from the reactor core. Since ORIGEN-S is a point model, spatial effects are not explicitly modeled. However, spatial effects are incorporated in the model through the one-dimensional spatial weighting of data by XSDRNPM-S.

A fuel assembly is modeled with SAS2H in one-dimensional cylindrical geometry. This modeling is a two step process. First, the fuel is represented as an infinite lattice of fuel pins with XSDRNPM-S, where resonance data is obtained from BONAMI-S and NITAWL-S. Second, cell-weighted cross sections from XSDRNPM-S are then applied to the fuel zone in a larger cell model representing part or all of a fuel assembly within an infinite lattice. Material and volume ratios for the zones must be appropriate for the physical system being represented. Weighted cross section and spectra data from this model are used by COUPLE-S to update the ORIGEN-S data library. ORIGEN-S performs point depletion calculations to provide updated isotopic concentrations that are fed back to the one-dimensional model. The first step is then repeated and new weighted cross section and spectra data are determined for the next depletion calculation. Updating of the ORIGEN-S library for depletion time steps is performed to appropriately represent changes (with depletion) in the neutron energy spectrum within the fuel assembly. A more detailed discussion of the SAS2H modeling is presented in Reference 4-4. Comparisons of SAS2H generated data with data generated by a two-dimensional lattice physics code will be presented in Appendix B.

A subset of the isotopes present in SNF will be used in criticality evaluations of waste packages in a repository. The selection process to determine the isotopes to be included in these evaluations was based on the physical, nuclear, and chemical properties of SNF isotopes. The nuclear properties considered were cross sections and half-lives of the isotopes. The physical properties were concentration (amount present in the SNF) and state (solid, liquid, or gas). The chemical properties included the volatility and solubility of the isotopes. In selecting the isotopes to be included, time effects (during disposal) and relative importance of isotopes for criticality (combination of cross sections and concentrations) were considered. During the selection process no isotopes with significant positive reactivity effects (fissile isotopes) were removed from consideration. The only isotopes removed from consideration were non-fissile absorbers. Thus, the selection process was conservative.

The actinide isotopes selected for the Actinide-Only burnup credit criticality analysis methodology[4-5] are also selected for the disposal criticality analysis methodology. Four additional isotopes have been added to this list. For long disposal times U-233 buildup becomes significant and is added to the list. Np-237 (which decays through Pa-233 to U-233) also increases during the containment phase due to the decay of Am-241 and is added to the list. The isotopes Am-242m (which has a significant fission cross section) and Am-243 (which decays through Np-239 to Pu-239) are also included.

Using this selection process, 14 actinides and 15 fission products (referred to as "Principal Isotopes") were chosen as the SNF isotopes to be used for disposal burnup credit evaluations. A list of these isotopes is presented in Table 4-1. Analyses supporting the selection of these isotopes are presented in *Disposal Needs for Isotopic Data.*[4-6] A measure of the conservatism in the model is obtained from criticality analyses of spent nuclear fuel (commercial reactor criticality data) using the principal isotopes and an expanded set of isotopes. Results from these analyses are reported in Appendix B-1.

Table 4-1. SNF Principal Isotopes for Burnup Credit

^{95}Mo	^{145}Nd	^{151}Eu	^{236}U	^{241}Pu
^{99}Tc	^{147}Sm	^{153}Eu	^{238}U	^{242}Pu
^{101}Ru	^{149}Sm	^{155}Gd	^{237}Np	^{241}Am
^{103}Rh	^{150}Sm	^{233}U	^{238}Pu	^{242m}Am
^{109}Ag	^{151}Sm	^{234}U	^{239}Pu	^{243}Am
^{143}Nd	^{152}Sm	^{235}U	^{240}Pu	

[Note: The completed topical report will include guidelines for selecting conservative input parameters in the isotopics model. (TBD)]

4.1.2 Criticality Model

The methodology for validation of criticality models for assessing nuclear criticality control in waste packages for disposal in a repository is presented in this section. The various computer codes and associated cross section data used for model development and validation are described. Model validation is performed based on criticality analyses using fresh fuel critical experiments and commercial reactor criticality data for spent nuclear fuel. A procedure is described for using the results of the criticality evaluations to determine a subcritical limit, which places an upper bound on the calculated k_{eff} of systems analyzed to ensure subcriticality (TBD). A more detailed description of the experimental data and validation analyses is given in Appendix B.

4.1.2.1 Criticality Model Description

For the methodology developed in this report, the neutronics model for disposal criticality analysis uses the MCNP 4A computer code system to calculate nuclear reactivity (or chain reaction potential) of fissile systems. MCNP is a general-purpose Monte Carlo N-Particle code that can be used for neutron, photon, electron, or coupled neutron/photon/electron transport, including the capability to calculate eigenvalues for critical systems. The composition of the SNF materials, obtained from SAS2H (or ORIGEN-S), are input to the MCNP code. Nuclear cross section data are obtained by MCNP from the ENDF libraries in a compressed ENDF (ACE) format provided by Los Alamos National Laboratory (LANL). The neutron cross sections in the ACE libraries are not collapsed into energy groups (as is done for the KENO code variants); but instead, cross sections are provided at energies ranging from very low energies through 20 MeV in sufficient detail that the original voluminous ENDF data can be accurately reproduced by linear interpolation.

MCNP uses pointwise cross section data, which tabulate the cross section for each different type of possible nuclear interaction as a function of energy. For neutrons, all interactions given in a particular cross section evaluation (such as ENDF/B-V) are accounted for. Neutrons in the thermal energy range are described by both the free gas and $S(\alpha,\beta)$ models. The cross section representation used by MCNP is thus very complete.

MCNP allows explicit geometry modeling of fissile systems through a system of geometric representations that permit geometric forms to be assembled into any arbitrary structure. The code treats arbitrary three-dimensional configurations of materials in geometric cells bounded by first-degree and second-degree surfaces and fourth-degree elliptical tori.

4.1.2.1.1 The Monte Carlo Method

The Monte Carlo method is a method of simulating and recording the behavior of individual particles within a system. The behavior of the simulated particles is extrapolated to describe the average behavior of all of the particles within the system. The Monte Carlo method as applied to neutrons in an MCNP criticality calculation is based upon following a number of individual neutrons through their various transport experiences such as scattering, fission, absorption, or leakage. The fission process is regarded as the birth event that separates generations of neutrons. A generation is the lifetime of a neutron from birth by fission to death by either escape, parasitic

capture, or absorption leading to fission. The average behavior of the sample set of neutrons is used to describe the average behavior of the system with regard to the number of neutrons in successive generations (i.e., effective neutron multiplication factor, k_{eff}).

4.1.2.1.2 MCNP's Critical Multiplication Factor (k_{eff})

MCNP 4A calculates three k_{eff} estimates for each cycle in a given problem. These are:

1. the collision estimate,
2. the absorption estimate, and
3. the track length estimate.

A detailed description of the three k_{eff} estimates may be found in Chapter 2, Section VIII, Part B, of the MCNP Manual.[4-2] The k_{eff} estimate used in the criticality analyses for this report is a statistical combination of all three k_{eff} estimates. As described by statisticians at the Los Alamos National Laboratory[4-2], "the three-combined k_{eff} is the best final estimate from an MCNP calculation.... The confidence interval based on the three statistically combined k_{eff} estimate is the recommended result to use for all final k_{eff} confidence interval quotations because all of the available information has been used in the final result."

4.1.2.1.3 Assessing the Validity of a Criticality Calculation

Before an MCNP k_{eff} result can be considered acceptable, the validity of the calculation must be determined. Two minimum requirements for assessing the validity of an MCNP criticality calculation include:

1. all cells containing fissionable material should be adequately sampled, and

2. the fundamental spatial mode should be achieved before commencing the accumulation of data for calculation of the mean k_{eff}.

MCNP provides several features which help in assessing the validity of a k_{eff} calculation. To satisfy the first requirement, "MCNP verifies that at least one fission source point was generated in each cell containing fissionable material."[4-2]

To satisfy the second requirement, MCNP provides several checks to determine if the fundamental spatial mode was achieved prior to the completion of the I_C cycles (I_C is the number of source cycles that are skipped before data accumulation begins in an MCNP calculation). One check is the comparison of the estimated three-combined k_{eff} and its standard deviation for the first and second half of the active k_{eff} cycles. If the difference between the average k_{eff} values for the two halves does not appear to be zero or if the ratio of the two standard deviations is larger than expected, a "WARNING" message is provided in the output. MCNP determines the number of cycles which must be skipped to produce the minimum standard deviation for the three-combined k_{eff} estimate. If this result is larger than I_C it may be indicative that more cycles should be skipped before accumulating k_{eff} data. MCNP checks each k_{eff} estimate's cycle data to assure normality at the 95% and 99% confidence levels. If a k_{eff} estimate is not normally distributed with respect to the mean k_{eff} at the 99% confidence level a "WARNING" message is provided in the output. "Unless there is a high positive correlation among the three estimates, it is expected to be rare that all three k_{eff} estimates will not appear normally distributed at the 99% confidence level when the normal spatial mode has been achieved and maintained."[4-2] Finally, MCNP tests for a monotonic trend of the three-combined k_{eff} estimate's results over the last ten active cycles. If the spatial mode is well converged and maintained, there should not be a monotonic trend within the last ten active cycles. A "WARNING" message is provided in the output if a monotonic trend is detected.

Compliance with the two minimum requirements addressed above should be verified for each criticality calculation using the checks provided by the MCNP code. If either of the two requirements appear to be violated, the k_{eff} results for the calculation should be evaluated further.

4.1.2.1.4 Cross Section Data

Utilizing the appropriate material cross section data in an MCNP criticality calculation is essential to obtaining credible results. The cross sections for the various neutron interactions are used to determine the flow of the criticality calculation at each interaction site. The MCNP neutron interaction tables are processed from evaluated data in the ENDF/B-V format.

The MCNP neutron interaction tables provide the following data:

1. all available cross section data,
2. angular distribution data for scattered neutrons,
3. energy distribution data for inelastically scattered neutrons,
4. data about secondary photon production,
5. Q-value data for each reaction, and
6. the average number of neutrons per fission data for fissionable isotopes.

A description of the MCNP cross section data used for the validation analyses presented in this report is given in Appendix B-2.

4.1.2.1.5 S(α,β) Thermal Treatment

The S(α,β) thermal treatment accounts for binding effects in molecules and crystalline solids. The S(α,β) thermal scattering treatment is a necessary requirement in a highly moderating medium where low-energy scattering may be dominant. S(α,β) thermal treatment tables are available for a limited number of materials. In the analyses performed for this report the thermal treatment is consistently applied to the materials having available data. The materials using the S(α,β) treatment in the critical benchmarks in this report include light water, polyethylene, and graphite.

4.1.3 Neutronics Model Validation

The definitive neutronics models and model validation methods are currently TBD. This section outlines the overall strategy currently being developed to validate the isotopic and criticality models and the associated SAS2H and MCNP codes. The overall validation strategy consists of three phases, which are described in more detail in the following sections. The first phase validates the isotopic and criticality models together by comparing commercial reactor criticality data to reactivity values calculated by MCNP, with SAS2H-generated isotopic data used as input to the MCNP calculations. The second phase provides further confirmation of the SAS2H-based isotopics model by comparing SAS2H-generated isotopic data to radiochemical assay experimental data. The third phase provides a further confirmation of the MCNP-based criticality model by comparing MCNP-based reactivity data to a wide range of fresh fuel criticality experiment results. The DOE will ensure that the validation approach used will be applicable to the expected commercial SNF waste stream.

4.1.3.1 Phase 1 Validation - Use of Commercial Reactor Criticality Data

During Phase 1 validation, the isotopic and criticality models are validated together, using data from commercial nuclear reactor restarts. Prior to restarting a commercial nuclear reactor from a shutdown, subcritical condition, the NRC requires that a prediction be made as to the point at which criticality will occur during the restart. For a PWR, criticality is determined by the reactivity of the fuel in the core, the control rod positions, and the soluble boron concentration in the primary coolant (water). Accurate isotopic data on the fuel, together with an accurate reactivity analysis model are required to predict the critical rod positions/boron concentration for a reactor restart. Therefore, data from reactor restarts, coupled with data generated from licensed core reload analysis codes, can be used to validate the isotopic and reactivity models to be used for disposal criticality analyses.

Two types of reactor criticality data can potentially be used for this validation method: 1) data from restarts performed with All Rods Out (ARO), during which reactivity control is provided exclusively by varying the boron concentration, and; 2) data from restarts/recoveries performed with rods partially inserted, during which both rod position and boron concentration is used to control reactivity. Although the restarts performed ARO are somewhat simpler to analyze, these restarts are typically performed infrequently, typically after long-duration shutdowns when boron is added to provide more of a shutdown margin. Restarts/recoveries with rods partially inserted occur after shorter-duration maintenance, and hence can be more frequent than ARO restarts. Hence, although using data from restarts/recoveries with rods inserted adds to the analysis effort, it also provides a substantially larger database than use of ARO restart data exclusively. To avoid unnecessary complexity caused by post-shutdown xenon transients, data from restarts/recoveries which occur less than two days after shutdown are not used in this validation method.

The overall validation strategy for phase one consists of the following steps: 1) obtaining data on the core critical configuration using reactor core data and data from a reload analysis code: 2) generating core fuel isotopics with SAS2H using this data, and; 3) inputting the SAS2H isotopics data and core critical configuration data into an MCNP-based reactivity model to calculate the reactivity of the core. The MCNP k_{eff} result should, ideally, be equal to 1.0 for a critical core. Differences from the ideal result may then be analyzed for biases and trends to determine a model which conservatively bounds the criticality analysis model. (The methodology for determining the biases, trends, and bounding model is currently under development. (TBD))

Table 4-2 shows the types of data needed to perform the SAS2H and MCNP analyses of the reactor restarts, as well as where the data originates. As this table shows, a number of data categories needed by both SAS2H and MCNP models come from the reload analysis code. For the purposes of this methodology the CASMO[4-7]/NEMO[4-8] code system will be used.

The CASMO/NEMO code system has been accepted by the NRC for use in commercial reactor reload licensing analyses. CASMO is a multigroup, two-dimensional transport theory code for performing burnup calculations for PWR and boiling water reactor (BWR) fuel assemblies. The code models cylindrical fuel rods of varying composition in a square-pitch array with allowances for fuel rods loaded with gadolinium, burnable absorber rods, cluster control rods, in-core instrument channels, water gaps, boron steel curtains, and cruciform control rods. The CASMO output provides few-group cross sections and reaction rates for any region of the assembly for use in overall reactor calculations. NEMO is a two-group, three-dimensional diffusion theory code for calculating power distributions and performing reactivity analyses for pressurized water reactors. The nodal expansion method is used in solving the two-group, multidimensional neutron diffusion equations. NEMO uses cross section data from CASMO for the diffusion theory and burnup calculations. Isotopic concentrations are calculated for 13 of the 14 actinide principal isotopes (NEMO does not consider U-233) and 1 of the 15 fission product principal isotopes (Sm-149). Isotopic concentrations are also calculated for I-135, Xe-135, Pm-147, Pm-148, Pm-148m, and Pm-149. The remaining fission products are treated as a single "lumped-fission-product". NEMO also accounts for thermal-hydraulic feedback effects in the reactor.

The reactor cases selected for evaluation include first cores (all fresh fuel), beginning-of-cycle reload cores, and reactor restarts (mid- to end-of-cycle) defining a range of burnup and cool-time (time since reactor shutdown) conditions. All of these cases are for zero power conditions. The neutron energy spectrum for the cases selected shifts with increasing burnup from one dominated by U-235 (for first cores) to one that is more balanced between U-235 and the plutonium isotopes for the reactor restarts. The range of neutron energy spectra characterized by these reactors is representative of the range anticipated for criticality evaluations for configurations inside a disposal waste package.

Table 4-2. Neutronics Model Data Needs

Data Category	Data Sources			Data Needed By	
	Reactor Design/Records Data	Reload Analysis Code Data	SAS2H Depletion Calculation Results	SAS2H Model	MCNP Model
AROCBC (see Note 1)	X (rod positions, CBC)	X (AROCBC if rods partially inserted)			X
Fuel Assembly, BPRA, and Core Geometry and Material Descriptions	X			X	X
Nodal Moderator Specific Volumes & Nodal Fuel Temperatures for Depletion Calculations	X (core operations data) X (core operations data)	X (nodal burnup weighted moderator specific volume) X (nodal burnup weighted fuel temperature)		X X	
Moderator Temperature & Fuel Temperature for Statepoint Restart	X (reactor startup report) X (reactor startup report)				X X
Nodal BOC Burnup History	X (core operations data)	X (3-dimensional burnup of each assembly)		X	
Nodal Fuel Isotopic Compositions at Statepoint Startup			X (single- or multi-axial node depletion calculations)		X
Nodal Burnable Poison Isotopic Compositions at Statepoint Startup			X (single- or multi-axial node depletion calculations)		X

Note 1: AROCBC = All Rods Out Critical Boron Concentration. For restarts/recoveries completed with rods partially inserted, the reload analysis code is used to calculate the effective AROCBC. This is then used in the SAS2H/MCNP models.

A wide range of SNF data is represented by the reactor cases selected. These include 10 first core cases (all fresh fuel), 26 beginning-of-cycle (BOC) reload core cases, and 49 reactor restarts (mid- to end-of-cycle). Both B&W and Westinghouse reactors are included in this data base. Important characteristics of the fuel in these reactors relative to burnup credit are as follows:

- Individual fuel assembly burnup range 0 - 50 GWd/MTU
- Core average burnup range 0 - 30 GWd/MTU
- Initial enrichment range 1.9 - 4.97 wt. % U-235
- Individual fuel assembly cooling time range 2 days - 15 years
- Core average cooling time range 2 days - 2.7 years

The initial analyses are being performed for the Crystal River Unit 3 reactor. A total of 10 BOC reload cases and 23 reactor restarts have been identified for analyses. Some preliminary results of the validation analyses performed for Crystal River Unit 3 are presented in Appendix B-1. These include SAS2H-MCNP criticality evaluations for cycles 7 and 9. For the cycle 7 evaluation the reactor was restarted at 260.6 effective-full-power-days (EFPD) into the cycle following an 18 day shutdown. Two cases were analyzed for cycle 9. The first was at 158.6 EFPD following a two day shutdown. For this case a small amount of Xe-135 was still present in the core due to the short shutdown time. However, the small amount present had minimum impact on the criticality calculation. The second case for cycle 9 was at 219.4 EFPD following a 32 day shutdown. The equivalent core-averaged burnups for these cases are as follows:

- Cycle 7, 260.6 EFPD = 18.098 GWd/MTU
- Cycle 9, 158.6 EFPD = 19.099 GWd/MTU
- Cycle 9, 219.4 EFPD = 20.984 GWd/MTU

4.1.3.2 Phase 2 Validation - Use of Radiochemical Assay Data

This validation phase augments the use of commercial reactor criticality data by comparing SAS2H-generated isotopic data to radiochemical assay experimental data. The second validation phase thereby provides further confirmation of the SAS2H-based isotopics model (TBV).

Values for the isotopic concentrations of the actinides and fission products used in establishing burnup credit are determined from radiochemical assays of SNF. These data will be used for validating the methodology for calculating isotopic concentrations in SNF assemblies. One source of these data is the Materials Characterization Center (MCC) at the Pacific Northwest Laboratories (PNL). A second source is data from the German Obrigheim reactor.

[Note: Additional data will be obtained from the CERES International Collaborative Program and other source(s) to-be-determined (TBD)].

The fuel assemblies analyzed at the MCC were from two PWR cores[4-9,4-10,4-11,4-12] and one BWR core.[4-13] The PWR assemblies analyzed consisted of three 14×14 Combustion Engineering (CE) fuel assemblies from the Calvert Cliffs Unit 1 reactor and one 15×15 Westinghouse (W) assembly from the H. B. Robinson reactor. For the BWR core two 7×7 General Electric (GE) fuel assemblies from the Cooper Nuclear Power Plant were analyzed. A single fuel pin was chosen from each assembly for study. Individual fuel pellets were selected from three axial locations for the fuel pins from the Calvert Cliffs and Cooper assemblies. Fuel pellets were selected from four axial locations for the chosen fuel pins from the H. B. Robinson assembly. Thus, the MCC measurements provided assays for a total of 19 different samples. The fuel burnup for these samples ranged from 17.84 to 46.46 GWd/MTU. The initial enrichments ranged from 2.45 to 3.04 weight percent U-235. Not all of the isotopes listed in Table 4-1 were measured for these 19 samples. Only three samples were analyzed for most of the fission products. These were analyzed by three different laboratories.

The assay data from MCC was pellet-specific data. For the Obrigheim[4-14,4-15] fuel the assay data provided "assembly-averaged" isotopic values. Samples of the Obrigheim fuel were prepared by dividing a fuel assembly into two 12-foot half-sections. Each half-section was then dissolved and assayed. A total of 6 samples were prepared and independently evaluated at four different European laboratories.

Data from these experiments are used to support the validation of the SNF isotopic model. Results from analysis of this data will be used in conjunction with the results from analysis of the commercial reactor criticality data in identifying trends in the modeling of isotopic concentrations. The validated model may then be used in determining isotopic concentrations for criticality analysis with burnup credit.

[Note: Analysis of the radiochemical assay measurements with SCALE 4.3 will be completed for the release of the topical report. An additional section (or sections) describing the analysis of this data will then be provided.]

4.1.3.3 Phase 3 Validation - Fresh Fuel Critical Experiments

This validation phase augments the use of commercial reactor criticality data by comparing MCNP-based reactivity calculations to a wide range of fresh fuel criticality experiment results. The third validation phase thereby provides further confirmation of the MCNP-based criticality model.

Disposal criticality analyses must be performed for various types of fissile materials, both internal and external to the waste package. The complex variety of material types and geometric configurations may be simplified into three general categories for the purpose of validation of MCNP. In specific cases, a more detailed breakdown might be desirable, so subcategories are also provided. The general categories are: PWR and BWR fuel, high enrichment research reactor and naval fuel, and uranium/plutonium systems which result from degraded waste forms both internal and external to the waste package.

The fresh fuel critical experiment library is currently composed of 289 critical experiments which are classified according to fuel, geometry, and moderating or reflecting characteristics. Twenty fresh fuel classifications currently exist within the library to accommodate the various experimental configuration characteristics. The current classifications and number of critical experiments in each are shown in Table 4-3. For final model validation, these experiments will be grouped according to applicability for potential LWR SNF configurations for disposal criticality analyses.

It is important to note that some of the critical benchmark experiments discussed here are exponential approach to critical experiments that never obtained a measured critical condition.

The MCNP calculated k_{eff} for these exponential critical experiments is based on the nominal critical configuration determined by extrapolation from measured k_{eff} data. However, the majority of experiments in the current critical experiment library are true criticals which reached the critical condition with a measured k_{eff} of unity.

A description is provided in Appendix B-2 of each of the experiments listed in Table 4-3 along with discussions of validation analyses performed. The validation analyses included a preliminary determination of the method bias and uncertainty. The bias and uncertainty in both the critical experiments and the calculations used to analyze the critical experiments contribute to the overall bias and uncertainty in the calculational method. Preliminary results from the

Table 4-3. Fresh Fuel Critical Experiment Library Classifications

Classification			Number of Experiments
Fissile Metal Fuel	Cylinder Arrays	Unmoderated	29
	Slab Lattice Geometries	Moderated	22
	Single Unit Cylinders	Bare	7
		Reflected	14
	Single Unit Spheres	Bare	6
		Reflected	6
	Single Unit Annuli	Bare	2
		Reflected	32
	Unique Geometries		4
Fissile Oxide Fuel	Cylinder Arrays	Unmoderated	3
		Moderated	7
	Lattice Geometries	Moderated	41
Fissile Solution Fuel	Cylinder Arrays	Bare	6
		Reflected	41
	Single Unit Cylinders	Bare	15
		Reflected	37
	Single Unit Spheres	Bare	10
		Reflected	3
	Single Unit Parallelepipeds	Bare	2
		Reflected	2
Total Number of Fresh Fuel Critical Experiments in Library:			289

analyses are reported in this appendix. Preliminary trending analyses were also performed (and reported in Appendix B-2) for the 41 experiments classified as "fissile oxide fuel / lattice geometries / moderated", a complete trending analysis for all experiments has not been performed. The preliminary results in Appendix B-2 are presented for illustrative purposes only.

The goal of the final analysis of these experiments is to determine the subcritical limit, as a function of the appropriate trend parameter, that will be applicable to the types of configurations in each of the three regions (inside waste package, external near-field, and external far-field) where disposal criticality analyses will be performed. Results from the analysis of the 41 fissile oxide/lattice geometry fresh fuel experiments will be combined with results from the analysis of the commercial reactor criticality data. The combined data will then be used to determine the subcritical limit to be applied for intact fuel criticality analyses employing burnup credit. The remaining experiments will be grouped according to applicability for potential degraded fuel and external configurations. Data from these experiments will be used to determine subcritical limit values to be applied for external near-field and external far-field criticality analyses. The determination of the subcritical limit values will complete the validation process for the MCNP criticality analysis model. The subcritical limit values and the validation process will be presented in the topical report.

4.1.3.4 Applicability of Critical Experiments to Disposal

The critical experiments for spent nuclear fuel and high enrichment fuels are directly applicable to disposal when the waste forms are intact. Degraded waste forms within the Waste Package are also well represented by the critical experiments because the isotopic compositions are not changed, although the geometric and chemical forms of the degraded mass may be different (TBV).

The experimental data set addresses several types and forms of neutron-absorbing materials. The methodology presented here also allows the use of moderator displacement filler material for reactivity control. The range of the water-to-fuel volume ratios (H/X) is adequate for validating the capability of the criticality model to predict the reactivity associated with the moderator displacement effect (TBV).

The results (isotopic bias and uncertainty) from the analysis of chemical assay data for commercial SNF are applied in the analysis of commercial reactor criticals to establish burnup

credit. These experiments cover a broad range of initial fuel enrichments and burnups. The chemical assay and reactor criticality data analyzed also represent a range of cooling times for commercial spent nuclear fuel. The range of cooling times represented in the commercial reactor criticals and isotopic assay data is short compared to the time period for disposal. However, the data is sufficient to establish and validate an isotopics concentration model which is applicable to criticality analyses for long-term disposal (TBV).

For the isolation and extended isolation phases, when material and waste form degradation may be great and isotopic transport and redeposition may have occurred, potential critical systems may have an energy spectrum significantly different from that of the fuel pin lattices analyzed for the operations and containment phases. The criticality experiments in the benchmark set were therefore selected to include a broad neutron energy spectrum range.

Internal and external criticality of degraded waste packages are reasonably well represented by the solution critical experiments since fission products will be excluded from external configuration analyses (for reasons described in Section 3.1 - TBV), and the solution systems also do not contain fission product neutron absorbers other than trace amounts. The fissile material in solution critical experiments is distributed uniformly throughout the solution, as opposed to precisely localized as in nuclear fuel assemblies. The moderator present in external degraded material systems may be water, tuff, or a combination of water and tuff. The range of water contents is reasonably well represented by the range of uranyl nitrate and plutonium nitrate concentrations in the solution experiments (TBV), but tuff is not contained in any of the critical experiments. Either additional experiments containing similar silicon-based materials such as tuff will be required or bounding neutron cross section data must be justified and applied (TBV).

4.2 Scenario Generation and Configuration Bookkeeping

Scenario generation will be implemented by a computer code called the scenario generation tool. The algorithms of this code will consist of five sub-models. These sub-models are mostly derived from the abstraction of TSPA code results. The first sub-model (repository environment) provides input parameters to the other four. The other four sub-models provide the mass balance equations which determine the expected values of species concentrations in the various sample space compartments. Alternative scenarios will be generated as a function of the input parameters which are determined from appropriate probability distributions. The evolution of the

scenarios is described in terms of the environmental parameters and the location and concentrations of isotopic species which are major determinants of criticality (neutron absorbers and fissile material).

To obtain practical and quantitative descriptions of the scenarios in terms of these parameters, a set of bins, or compartments, is defined with each bin to encompass a discrete range of values for the parameters. To keep track of the probability distribution among these bins, as a function of the probability distribution of the input environmental parameters and as a function of the changing parameters in the deterministic scenario equations, a configuration bookkeeping tool is developed. This tool is implemented by a computer code using Monte Carlo simulations to populate the bins, or compartments, according to the outcomes of the events and processes.

The following subsections describe the sub-models which drive the deterministic evolution of the scenario generation tool. As indicated in Section 3.2.3, these models consist primarily of mass balance equations (first order, time dependent differential equations) using the transfer rates determined by the detailed process analysis preceding their implementation in the computer code. This detailed process analysis is also described in the following sections.

As part of the scenario generation tool, these models are ultimately incorporated into the configuration bookkeeping tool.

4.2.1 Repository Environment Model

The repository environment sub-model provides the distribution of parameters to be used as input to the other 4 sub-models. All the algorithms and parameter values of this sub-model are derived directly from, are abstracted from the results of, or are in agreement with, corresponding sub-models of the TSPA model. Furthermore, the use of these sub-models will be consistent with their use in TSPA-95 and TSPA-VA.

4.2.1.1 Fundamental Environmental Parameters

The hydraulic properties of the repository rock are determined by measurements taken primarily from surface drilling and from sampling in the Exploratory Studies Facility (ESF). These parameters will be updated as part of the Scientific Investigations and TSPA processes. Examples of the parameters are porosity, matrix permeability, and fracture permeability. In

general, higher permeability will increase the probability of internal criticality by increasing the initial flow rate, thereby increasing the rate at which the neutron absorber can be leached from the criticality control structures in which it is embedded (e.g. waste package basket, or disposal control rods). For external criticality, the spatial variations of fracture permeability will significantly affect the probability of re-concentration to a critical mass (TBV).

Other parameters will change under the influence of the heat from emplaced waste packages. Some typical parameters of this type are infiltration rate, initial water pH, and dissolved oxygen. The modeling of processes which change these parameters from their initial values is described in Section 4.2.1.2.

4.2.1.2 Environmental Parameters Derived from Modeling Waste Package - Environment Interactions

Many environmental parameters will be changed significantly by the presence of the repository, particularly from the thermal load from the emplaced waste packages. The change in these parameters (with respect to their measured initial values) is estimated, as part of the TSPA process, from recognized computer codes which model the fundamental heat and mass transfer processes.

Starting with typical initial measurements as inputs, temperature, humidity, and infiltration rate are determined as a function of time using a hydrothermal code with the following principal inputs: heat generation (by the waste packages), heat transfer (by mass transport, diffusion, radiation, and convection), and hydrologic permeability.

Water chemistry parameters (pH and principal ion concentration) are determined as a function of time by using a chemical thermodynamics code, such as EQ3/6, with input parameter values from rock sample measurements. Certain basic reaction rates are in the code database, and others are developed from the degradation models of waste package materials and the waste forms, described below.

These fundamental physical process codes will generally be run only a limited number of times as part of the TSPA process, and this will only be for the purpose of establishing a parameterization which will then be incorporated into the simple mass-balance equations of the scenario generation code. In fact, maximum use will be made of cases already run by

performance assessment, for representative repository parameter values. Any probabilistic implications of the results of these fundamental process codes will be incorporated in the configuration bookkeeper.

4.2.1.3 Environmental Parameters Derived from Modeling of Prior Geologic Processes

Certain environmental parameters cannot be measured directly, and their values must be estimated from models of geologic processes which could have taken place at some time in the past and would have left the geologic environment unchanged since then. An illustration of such a modeling process is given in Appendix C; this model estimates the probability of occurrence of a reducing zone at the lower boundary of the tuff at Yucca Mountain. In particular, the estimate is based on the probability of the occurrence of organic deposits of sufficient size and density to accumulate a critical mass of low enriched uranium from a groundwater stream flowing through the deposit. Further description of the model is given in Appendix C. This appendix also shows how the probability of occurrence is incorporated in a stand-alone analysis of this type of criticality. The probability will be incorporated into the configuration bookkeeper when it becomes available.

The model illustrated in Appendix C was developed in consultation with, and the product is reviewed by, geologists expert in the uranium and other mineral deposits. Refinements of this model, and other models of this type, will also be developed in consultation with and reviewed by geologists and geochemists with appropriate expertise.

4.2.1.4 Validation of Environment Model

The repository environmental models used in the scenario generation tool are mostly derived from performance assessment models, as indicated in Section 4.2.1. Therefore, the validation of the these parts of the scenario generation tool is accomplished indirectly by the validation of the TSPA models from which the scenario generation sub-models are derived. The validation of the TSPA models is part of the TSPA process and is described in the appropriate planning documents.

Thermal Conditions and Groundwater Hydrology Model

These scenario generation tool models will be developed from the abstraction of corresponding hydrothermal performance assessment code results, particularly those used for TSPA. These codes have been extensively verified and validated. For this project, the final validation is expected to be against data from the ESF heater tests.

Groundwater Chemistry

These scenario generation tool models will be developed from the abstraction of corresponding chemical/thermodynamics performance assessment code results, particularly those used for TSPA. These codes have been extensively verified and validated. For this project, the final validation is expected to be against the results of various tests being conducted on dissolution rates of waste package materials and waste forms.

Models of Prior Geologic Processes

These models, illustrated by the reducing zone formation model described in Appendix C, deal with phenomena which are not directly measurable. At present there are no corresponding or antecedent models in the TSPA process. It is expected that these validations will be accomplished by peer review.

4.2.2 Material Degradation Model

This section discusses materials for disposal container components, mechanisms for degradation of these materials, models for such degradation, and methods of validating such models.

4.2.2.1 Materials for Disposal Container Components

Waste packages for high-level radioactive waste will include several components. *Waste forms* and *canistered waste forms* are placed into *disposal containers*. Together, the two form a *waste container*. The waste container differs from a *waste package*, as defined in 10 CFR 60, in that materials surrounding the individual waste containers are excluded. The disposal container may include a *basket*, which supports the waste and may perform other functions such as stiffening and strengthening the containment barriers, absorbing neutrons, and conducting heat to the

containment barriers. Although they are not present in current designs, control rods and filler material have been considered for inclusion in the waste package. For PWR fuel, *control rods* would be inserted into SNF assemblies to absorb neutrons. A *filler material* would be placed in void spaces to absorb neutrons or displace moderator; filler material would possibly be added in granular form. Outside the waste package, a *waste package support* may be placed under the containment barriers to hold the waste package in place during seismic events, aid heat removal from the bottom of the waste package, and separate the containment barriers from potentially corrosive materials in the invert. Degradation of the basket material could lead to removal of the neutron absorber from the waste package, which would increase the probability of internal criticality. Scenarios of greatest interest include breach of the containment barriers, which could allow water to fill the waste package and act as a moderator, and dissolution of neutron-absorbing isotopes from control rods or neutron-absorbing panels in the basket.

Materials that have been proposed for use in disposal containers are listed in Table 4-4.[4-20, 4-39, 4-40, 4-41] Waste package supports have not received significant attention to date, so no material is listed as being under consideration for this purpose. Table 4-5 lists the current materials selection for major components of the waste package.[4-20] These are the materials that, in light of current knowledge, are expected to provide the best overall cost and performance. Research on other materials is continuing, however, because of the possibility that current understanding of the near-field environment and waste package degradation is incorrect. ASTM A 516 is a low-carbon steel. ASTM B 443 is a nickel-base alloy (Alloy 625). Neutronit A978 is a proprietary grade of stainless steel with boron; its composition is based on that of Type 316. For PWR fuel, the fuel basket includes not only neutron-absorbing plates but also tubes that promote conduction of heat from the fuel to the containment barriers.

Table 4-4. Materials Proposed for Use in Disposal Containers

Material	Proposed uses
Carbon steel Low alloy steel	Corrosion-allowance containment barrier Filler material Heat-conducting material for basket Basket guides Canister guide
Austenitic stainless steel	Moderately corrosion-resistant containment barrier Internal structural material, structural material for basket
High-nickel alloys Nickel-base superalloys	Corrosion-resistant containment barrier
Copper-base alloys Copper-nickel alloys	Moderately corrosion-resistant containment barrier
Titanium alloys	Corrosion-resistant containment barrier
Ceramic coatings	Corrosion-resistant containment barrier
Aluminum-boron alloys and composites	Neutron-absorbing material for basket
Aluminum alloys without boron	Heat-conducting material for basket
Austenitic stainless steel with boron	Structural and neutron-absorbing material for basket Neutron-absorbing material for control rods
Zirconium-hafnium alloys	Neutron-absorbing material for control rods

Table 4-5. Current Waste Package Materials Selection

Component	Material
Corrosion allowance barrier for SNF waste forms	ASTM A 516
Corrosion resistant barrier for SNF waste forms	ASTM B 443
Fuel basket tubes for SNF waste forms (PWR only)	ASTM A 516
Fuel basket plates for SNF waste forms	Neutronit A978
Waste container fill gas for SNF waste forms	Helium
Basket guides for SNF waste forms	ASTM A 516
Corrosion allowance barrier for HLW glass	ASTM A 516
Corrosion resistant barrier for HLW glass	ASTM B 443
Canister guide for HLW glass	ASTM A 516

4.2.2.2 Degradation Mechanisms for Disposal Container Components

Because of the wide variety of materials under consideration and uncertainty about the repository environment, many forms of degradation are possible. For the metallic components, possible forms of corrosion include atmospheric and aqueous general corrosion, dry oxidation, pitting, crevice corrosion, galvanic corrosion, stress corrosion cracking, and microbiologically influenced corrosion. For some of the proposed containment barrier materials, some of these corrosion forms occur in liquid water or in humid air; others require liquid water.

The ceramic materials that have been considered, notably spinel, mullite, and alumina, are not subject to the electrochemical forms of corrosion but are subject to dissolution if they are contacted by liquid water. The rate of dissolution will depend on the water chemistry, with pH being particularly important.

Environmental attack on the waste package supports and the outermost containment barrier may begin immediately upon emplacement. Inner barriers and any internal structure will be protected by the outer barrier until the outer barrier is breached; it is expected that an inert environment will be provided inside the waste package.[4-16,4-17,4-18]

4.2.2.3 Models for Material Degradation

Because of the importance of corrosion control to industry, there is a substantial body of information on corrosion rates and mechanisms under various conditions. Unfortunately, 1) industrial conditions are normally different from (and often much more aggressive than) expected repository conditions, 2) repository time scales are much longer than industrial time scales, and 3) many corrosion measurements are not sufficiently sensitive to detect corrosion rates that would be significant to repository performance. As a result, most corrosion predictions must be extrapolated from tests under conditions that are more severe than those expected in a repository.

Dry oxidation of metallic materials is not expected to be significant under postulated repository conditions. Calculations for expected repository temperatures and humidities indicate that the penetration depths for dry oxidation will be much smaller than those for corrosion in humid air.[4-19, 4-21]

The current level of understanding varies for different mechanisms of corrosion. At present, models for dry oxidation and atmospheric and aqueous general corrosion have been developed. These models are discussed briefly below. Other models will be discussed when they become available.

For corrosion-allowance materials, the most important degradation mechanism is expected to be general corrosion. Stahl[4-19] has presented a model, with coefficients, for corrosion depth as a function of time and temperature for exposure to water under constant conditions. Two extensions of this model have been proposed[4-21, 4-31]; both of these that give corrosion rate for atmospheric corrosion in humid air as a function of temperature and humidity. In the limiting case of 100% relative humidity and constant temperature, they reduce to Stahl's model.

The rate of galvanic corrosion depends on (among other things) the galvanic potential difference between the two coupled materials, the surface areas of the materials, and water chemistry. Quantitative prediction normally requires measurement. Galvanic corrosion can be mitigated by proper waste package design. For example, the current design uses two barriers and puts the more active material on the outside, so that after breach any remaining metal from the outer barrier would provide cathodic protection to the inner barrier. Similarly, the basket guides and basket tubes are more active than the basket plates and will corrode sacrificially to protect the plates, which must provide long term criticality control.

For corrosion-resistant materials, the most important degradation mechanisms are expected to be various forms of localized corrosion. Localized corrosion (pitting, stress corrosion cracking, and crevice corrosion) is strongly dependent on water chemistry, and microbiologically influenced corrosion is strongly dependent on humidity or the presence of liquid water and on the presence of suitable nutrients. Microbiologically influenced corrosion is poorly understood. Since it is difficult to control the repository conditions, if these forms of corrosion are significant, they must be controlled by material selection. It is possible that for many waste packages the near-field environment will be so benign that none of the forms of localized corrosion will be significant. Under such conditions, the containment barrier will remain intact for an extremely long time.

More information on and better models for materials degradation will be produced by the ongoing materials research effort. These will be used when available and as applicable.

4.2.2.4 Validation of Models

For times up to a few years, integrated corrosion tests in a laboratory are expected to provide the best tests of the applicability of these models. Long-term (at least five-year) corrosion tests under expected and postulated repository conditions are scheduled to begin during the 1996 fiscal year.[4-22] Because of the extremely long times over which repository materials must perform, however, complete validation of models by laboratory experiments is not practical. Laboratory results may be supplemented by data for natural or historical analogs, but analogs are not expected to be available for all materials. It appears that the best approach to validation of performance under repository conditions is to predict performance by using conservative bounding models backed by adequate experimental data (such as those provided by the long-term (at least five-year) tests), then conduct a performance confirmation program in an operating repository. Such a program could have a duration that is an order of magnitude longer than what is practical for laboratory experiments. Predictions of long-term performance must ultimately rely on models that will allow extrapolation from shorter-term data.

4.2.3 Waste Form Degradation Model

This section discusses materials for waste form components, mechanisms for degradation of these components, models for such degradation, and methods of validating such models.

4.2.3.1 Waste Form Components

Expected waste forms include commercial spent nuclear fuel and defense high level waste glass. Other types of waste forms that may arrive include highly enriched Naval fuel, DOE fuel from production reactors, and waste forms for surplus fissile materials. The scope of this report is limited to commercial spent nuclear fuel. Other waste forms will be treated in an addendum.

Components of commercial spent nuclear fuel that significantly affect criticality include the cladding, the spacer grids and end plates, and the oxide (fuel pellet fragments). Since commercial fuel is slightly under moderated, collapse of a fuel assembly will tend to reduce reactivity. Spacer grids and end plates are made of corrosion-resistant materials, typically nickel-base superalloys or austenitic stainless steel. Fuel cladding is normally made of a zirconium-base alloy, though some older fuels have a stainless steel cladding, and some newer fuels will have zirconium alloyed with niobium rather than tin. The fuel pellets, which are typically fragmented when discharged from the reactor, are uranium dioxide (UO_2) with a mixture of activation and fission products.

4.2.3.2 Degradation Mechanisms for Waste Form Components

Metallic components of commercial spent nuclear fuel are made of corrosion-resistant and heat-resistant materials. Because of the limited amounts of available reactive species, no significant degradation due to oxidation or corrosion can occur in an intact disposal container.[4-16]

Since the spacer grids and end plates are made of corrosion-resistant material, their degradation is expected to be slow even if the waste package is flooded. Localized corrosion is the most likely form of degradation since these materials resist general corrosion.

The zirconium-base alloys used for fuel cladding are also quite corrosion resistant. However, some degradation of these materials can occur even in an intact disposal container. Substantial research efforts have been made in this area.[4-23,4-24,4-25] Degradation mechanisms that have received significant attention include creep rupture, iodine stress corrosion cracking, various forms of hydrogen degradation, and oxidation.

The fuel pellet fragments are also subject to degradation. At sufficiently high temperatures in an oxidizing environment, the fragments will oxidize, from UO_2 to U_4O_9 and from U_4O_9 to U_3O_8.[4-26]

The first step results in a slight reduction in volume and opening of grain boundaries. The second step results in a large increase in volume and reduction of the fragments to powder. The increase in volume could result in splitting of the cladding. The oxides are also subject to dissolution. Oxidation (particularly oxidation to U_3O_8) and dissolution are coupled effects. By splitting the cladding, the formation of U_3O_8 will increase exposure of the fuel to water, and by breaking the fuel fragments into powder, it will greatly increase the surface area and dissolution rate. Oxidation can be controlled by providing an inert environment for the fuel while the temperature is high.

4.2.3.3 Models for Material Degradation

Models for corrosion of corrosion-resistant metals, such as those that are used in spacer grids, end plates, and cladding, are described in Section 4.2.2.3 above.

Iodine stress corrosion cracking of zirconium-base alloys has been considered and rejected as a significant cause of cladding failure[4-23] because in typical spent nuclear fuel neither the concentration of free iodine in spent nuclear fuel nor the stress intensity factor is high enough to cause stress corrosion cracking.

Failure of cladding by creep rupture has been considered by several authors.[4-25,4-27,4-28] A significant result of this work is that cladding failures by creep rupture will tend to produce small perforations in the cladding rather than gross ruptures.[4-24] Upon such a failure, the fuel rod pressurization gas (helium) will escape, and the driving force for further damage by creep rupture will be eliminated. It is possible that even cladding that has been perforated by creep rupture will act as a significant barrier to release of radionuclides from the waste form.

Various forms of hydrogen damage to cladding have been discussed and generally dismissed as a concern for dry storage.[4-23] Since conditions in an intact disposal container are similar to those for dry storage, significant hydrogen damage is not expected under these conditions.[4-16] Even after failure of the disposal container, significant hydrogen damage is not expected because of the modest temperatures and low water pressures.

Fuel oxidation has been investigated by Einziger[4-26] and the results have been applied to model degradation under expected repository conditions.[4-21] It was concluded that failure by fuel oxidation will not be significant because the requirements for protection by the disposal container

are modest. The time for which protection is required will depend on repository design but is typically a few tens to a few hundreds of years. It has also been found that the fuel becomes cool enough that oxidation is negligible before the surface of the disposal container cools to the boiling point of water. While the disposal container is hot, aqueous corrosion is not possible, so there is great confidence that the container will be protective.

Although its dissolution is slow, oxide fuel is subject to dissolution. Experiments[4-29] indicate that dissolution involves the formation of a complicated series of mineral phases. The overall process, however, might be approximated by congruent dissolution. Because of the relatively low solubility of uranium oxides, significant fuel dissolution requires that material be removed from the waste package. Accordingly, dissolution does not increase criticality potential inside the waste package, but it may need to be considered as contributing to critical configurations outside the waste package.

4.2.3.4 Validation of Models

For spent nuclear fuel, the processes that could result in significant changes in reactivity are corrosion of the metal components of the fuel assemblies, oxidation of the UO_2 fuel pellet fragments, and dissolution of the UO_2 fuel. Experimental work is planned or underway on all of these processes.[4-30] Particular attention is being paid to choosing conditions that are relevant to disposal. The data from these experiments will be used as the basis for validating the models of waste form material degradation.

A systems study is underway to determine what measures should be taken in an operating repository to monitor the degradation of emplaced waste packages. Such efforts will provide data on degradation under actual repository conditions, and they will allow measurements over time scales that are impractically long for laboratory experiments, but such results will not be available until long after license application.

4.2.4 Material Transport Model

The material transport (aqueous) sub-model will follow the TSPA methodology. For the unsaturated zone models ranging from the simplified methodology of RIP (Repository Integration Program)(one dimensional with bulk permeability properties only) to the very comprehensive TOUGH2 (including explicit representation of fracture flow) have been applied.

The sophisticated techniques are also available for the saturated zone, but a simple plume dispersion model is often adequate. An illustration of the plume dispersion model applied to the possible combination of fissile bearing streams from several waste packages is given in Appendix C.

The material transport model will be validated with respect to the underlying TSPA models (TBV).

4.2.5 Material Retardation/Precipitation Models

The retardation sub-model will follow the TSPA methodology, which presently models the simple equilibrium sorption reaction using the standard differential material-balance equations, incorporating a sorption (or distribution) coefficient, K_d, which is defined as the moles of radionuclide per gram of solid phase divided by the moles of radionuclide per milliliter of aqueous phase. The result of the mass-balance analysis can usually be expressed as a reduction of the nominal groundwater velocity (Darcy velocity) by a factor known as the retardation coefficient

$$R_d = 1 + \rho_{bd} K_d / (\phi S_w),$$

where ρ_{bd} is the dry bulk density, ϕ is the porosity of the rock, and S_w is water saturation in the porespace.

The mechanism for precipitation or sorption is the same as for retardation; the volumetric slowing of flow is equal to the material sorbed onto the solid, and is also measured by K_d. Sorption will be strongest in minerals known as zeolites, which account for over 50% of the rock in the Calico Hills (CH) rock layer, which lies below the emplacement horizon (in the Topopah Spring (TS) rock layer) at the potential Yucca Mountain repository.

Retardation/precipitation of fissile material is important in the determination of time at which a critical mass can be accumulated and the size of the rock region over which the material is distributed. The region over which the precipitated fissile material is distributed is inversely related to the maximum concentration.

Appendix C provides an illustration of the calculation of the maximum possible sorption of UO_2 in zeolite which shows that for commercial SNF the maximum possible density will be far less than is necessary for criticality. Since the calculation in Appendix C was concerned only with the maximum sorptive capacity of the zeolite, there was no use of the transport model.

The material retardation and precipitation models will be validated with respect to the underlying TSPA models (TBV). It should be noted that the prior geologic processes models mentioned in Section 4.2.1.3 and illustrated in Appendix C, also have some effect on the material retardation and precipitation parameters.

4.3 Criticality Consequence Model

[Note: The criticality consequence model has not been completed at this time. A more detailed discussion will be provided when this methodology is finalized in the topical report.]

A criticality consequence analysis is performed when the calculated k_{eff} of the system (or configuration) analyzed exceeds the subcritical limit. The purpose of this analysis is to determine the impact of the event on the radionuclide inventory and repository conditions in the vicinity of the event. The impact of the event is dependent upon the location where the event occurs, the time to initiate the event, and the feedback mechanism present to either sustain or terminate the criticality. These, in turn, will affect the energy yield resulting from the event. The energy yield is time dependent and is controlled by the feedback mechanisms present. The thermal effect is determined from the energy yield.

Several approaches to criticality consequence analyses are under consideration. The approach (or method) used for analysis is dependent upon the type of criticality event being considered (as noted in Section 3.4). The processes leading to a criticality event in a geologic disposal system are slow geological (water infiltration) and chemical (corrosion) processes. For commercial reactor SNF, it is believed that slow assembly, low-power, criticality events are the only credible events possible (TBV). Quasi-static models may be used for these types of events. An example of this type of analysis method is provided in Appendix D. For other types of events it may be necessary to use more elaborate dynamics models. The degree of sophistication required in criticality consequence modeling will be partially determined by results from the scenario generator.

4.4 Total System Performance Models

If the initial performance assessment evaluation indicates the need to conduct detailed TSPA calculations using the perturbed radionuclide inventory, several models are required. Prior to using a total system performance assessment model, the source term for the criticality (i.e., the rate of release of radionuclides over time from the vicinity of the criticality) will be determined. This will be conducted to evaluate the solubility/alteration of the inventory produced by the criticality. The EQ3/6 code package is used to evaluate geochemical models of the criticality produced inventories. The result will be an estimate of the dissolved concentrations of radionuclides. The release rate over time as a function of groundwater flow and temperature, and the total inventory of radionuclides are then used in the total system performance assessment model.

The current approach to TSPA of a potential radioactive waste repository makes use of the computer program RIP in conjunction with detailed process-level models. The proposed methodology for this report is to use the same codes unless preferable alternatives are developed for TSPA prior to the time at which analyses are required. This RIP, and the detailed process models are described in TSPA 1995[4-31]. The RIP was specifically developed by Golder Associates Inc. in order to evaluate the performance of a potential radioactive waste disposal facility at Yucca Mountain[4-32,4-38] and has subsequently been applied to a wide variety of proposed radioactive waste disposal facilities both in the U.S. and abroad. Most recently, the RIP has been applied to the WIPP site in New Mexico[4-33,4-35] and has been used to evaluate alternative disposal options for low-level waste for the State of New York[4-36]. The RIP is fully documented in a Theory Manual and User's Guide[4-34] and has a context-sensitive help package. The program has recently been formally verified consistent with ASME NQA-1 and ISO-9000 standards[4-37].

The major features of the four component models of RIP (see Figure 4-1) that comprise the performance assessment model are; (1) waste package behavior and radionuclide release component model, (2) radionuclide transport pathways component model, (3) disruptive events model, and (4) biosphere dose/risk model. These models are summarized briefly below. For evaluation of the consequences of a criticality, the waste package component model could be modified or replaced by the source term for the criticality that is supplied to the TSPA.

The *waste package behavior and radionuclide release component model* input requirements are descriptions of the radionuclide inventories in the waste packages, a description of near-field environmental conditions (which may be defined as temporally and spatially variable), and subjective estimates of high-level parameters describing container failure, matrix alteration/dissolution, and radionuclide mass transfer. The waste package component model can simulate two layers of containment (e.g., outer package and zircaloy cladding). Waste package failure rates, along with matrix alteration/dissolution rates, are used to compute the rate at which radionuclides are *exposed*. Once the radionuclides are exposed, RIP computes the rate of *mass transfer* out of, and away from, the waste package (or the vicinity of the criticality). Parameters describing waste package failure and radionuclide exposure and mass transfer can be functions of near-field environmental conditions. The output from this component (for each system realization) consists of time histories of release for each radionuclide from the waste packages (or from the vicinity of a criticality), and acts as the input for the transport pathways component.

The *radionuclide transport pathways component* model simulates radionuclide transport through the near and far field in a probabilistic mode. The RIP model uses a phenomenological approach that attempts to describe rather than explain the transport system. The resulting transport algorithm is based on a network of user defined *pathways*. The geosphere and biocell pathways reflect the major features of the hydrologic system and the biosphere, and are conduits through which transport occurs. The pathways may be used for both flow balance and radionuclide transport purposes, and may account for either gas or liquid transport. The purpose of a pathway is to represent large-scale heterogeneity of the hydrologic system, such as geologic structures and formation-scale hydrostratigraphy.

Geosphere pathways may be subdivided into *flow modes*, which address heterogeneity at the local scale (e.g., flow in rock matrix, flow in fractures). The flow modes are primarily distinguished from one another based on flow velocity, although retardation parameters may also differ between flow modes.

The transport of radionuclides along a geosphere pathway is based on a *breakthrough curve*, which is calculated as a cumulative probability distribution for radionuclide travel times along the pathway. The breakthrough curve combines the effects of all flow modes and retardation on the radionuclide travel time, and determines the expected proportion of mass that has traversed the pathway by any specified time. The breakthrough curve is computed based on a Markov process algorithm for exchange between different flow modes.

The third performance assessment component model represents *disruptive events*. Disruptive events are defined as discrete occurrences that have some quantifiable effect on the processes described by the other two component models. Examples of disruptive events include volcanism, faulting, and human intrusion. The user first identifies all significant events (i.e., events that are both credible and consequential). Having done so, each event is assigned a rate of occurrence and, if desired, one or more descriptor parameters, which define the characteristics and magnitude of the event (e.g., length of a volcanic dike). Descriptor parameters may be represented stochastically. Event occurrences are simulated as Poisson processes.

The user defines probability distributions for the event consequences (which may be functions of event descriptors). A consequence may take the form of a number of discrete responses (e.g., disrupting a number of waste packages, moving radionuclides from some waste packages directly to the accessible environment). It is also possible for an event to directly modify parameters defined in the other two component models. This capability can be used to specify long-term consequences (e.g., raising the water table or opening a new pathway).

The fourth performance assessment component model describes the fate and effect of radionuclides in the biosphere. The *biosphere dose/risk model* allows the user to define *dose receptors* in the system. Receptors receive radiation doses from specified geosphere (e.g., a water supply aquifer) or biosphere (e.g., a pond, or flora and fauna) pathways. Concentrations in these pathways are converted to radiation doses (or cancer risks) based on user-defined conversion factors.

Figure 4-1. Components of the Repository Integration Program which is Used for Total System Performance Assessment.

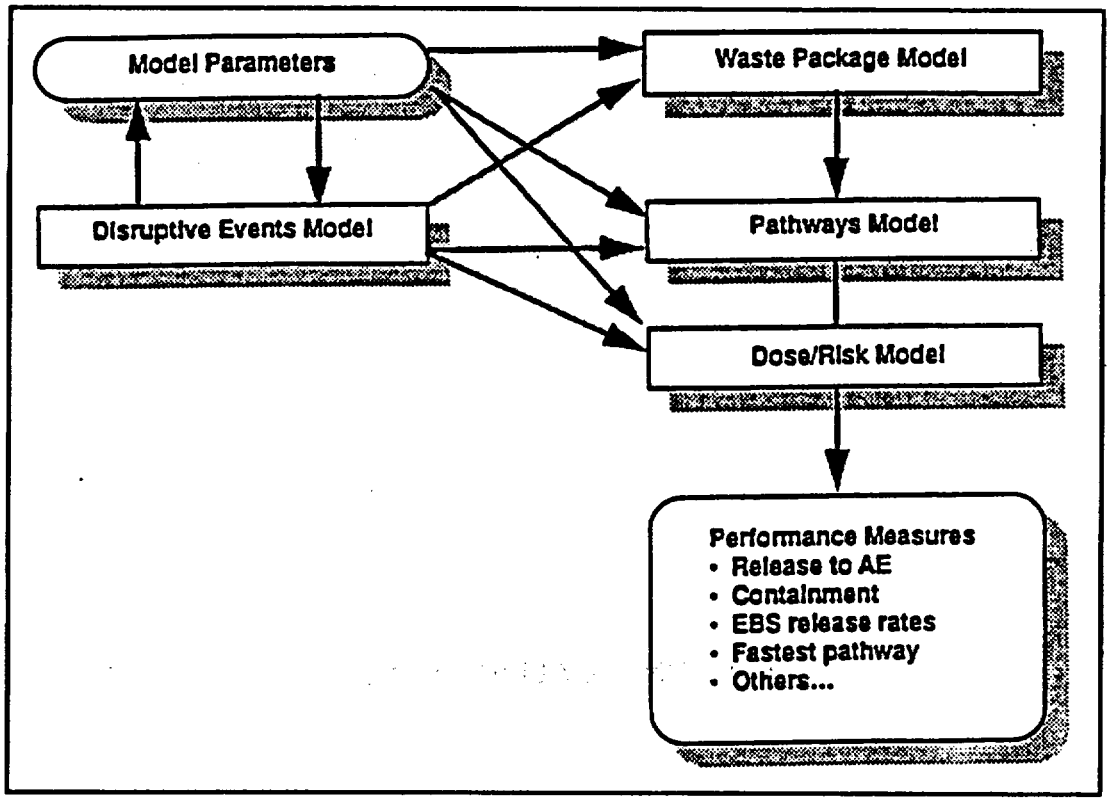

INTENTIONALLY LEFT BLANK

5.0 WASTE DISPOSAL CRITICALITY ACCEPTABILITY CRITERIA

[Note: This chapter of the technical report provides only a general description of the disposal criticality acceptability criteria. The chapter will be expanded in the topical report to address the establishment of the detailed disposal criticality acceptability criteria and the physical implementations and administrative controls for loading waste packages.]

Prior to emplacement of nuclear waste containing fissile material in a deep geologic repository, it must be demonstrated with reasonable assurance that criticality control of the waste will be maintained in accordance with the governing regulations. This Chapter presents the approach to determining the criticality acceptability criteria for emplacement of waste at the repository and to determining the physical implementation and control requirements that will ensure the criteria are met. The waste disposal criticality acceptability criteria are not the same as the waste acceptance criteria applied to waste received by the DOE OCRWM from waste owners/generators. The waste disposal criticality acceptability criteria are related to the Waste Receipt Criteria for acceptance of waste at the repository. Waste disposal criticality acceptability criteria are the criteria for ensuring the waste as emplaced in a repository is in a configuration suitable for disposal, from a standpoint of criticality.

The basic criterion for geologic disposal of SNF waste packages as part of the repository EBS is that the established limits on the release of radionuclides to the accessible environment (or other limits established in future regulations) shall not be exceeded through the period of regulatory concern. The waste package/EBS criticality acceptability criteria must support this basic criterion for geologic disposal plus any additional criteria established for control of criticality events. The overall basis and details for the criteria are discussed in Chapter 2. This Chapter will discuss more of the details of addressing the criteria with limits on the waste form characteristics and waste package/EBS designs.

5.1 Waste Package/EBS Criticality Acceptability Criteria

The criticality acceptability criteria are based on the results of the evaluations performed using the methodology from Chapter 3. Loading criteria are determined for the waste form characteristics a given design can accept and still meet the criticality acceptability criteria.

Loading criteria are established for a category of waste (PWR SNF or BWR SNF) to be sealed in a given waste package design for emplacement in a given underground repository EBS design. The combination of waste form, waste package design, EBS design, and repository site must meet the criticality acceptance criteria for the waste to be acceptable for disposal. If the criticality acceptance criteria are not met, the designs must be modified or the amount of waste must be reduced until the criteria are met.

Evaluations must be performed to establish the loading criteria for each category of waste to be loaded into the specific waste package/EBS design. Once the loading criteria are established for each design, confirmation is then required that the waste packages are loaded according to the loading criteria determined by the evaluations.

5.2 Physical Implementation and Controls

The physical implementation and administrative controls relating to the loading of a disposal waste package are to be addressed in this section. Procedures are developed to ensure that the SNF intended to be loaded into a specific waste package is loaded in that waste package, and that any requirements imposed relative to criticality control of the waste package (e.g., enrichment, burnup, fissile content, etc.) are met. The implementation of the procedures for controlling the loading of waste packages depends upon documentation of the waste form characteristics, identification of the waste forms, and verification of the information.

5.2.1 Fuel Assembly Records

Part of the requirements for determining suitability for emplacement of SNF shipments received at a repository is the receipt of supporting documentation. The supporting documentation will include all the records determined to be necessary to document criticality related information. The specific records needed for the criticality acceptability criteria considerations, and the mechanism by which such records will be obtained, are currently TBD.

Records are maintained for every commercial nuclear fuel assembly. The reactor records track each assembly from the time it is received at the reactor site until it is shipped off site. The record for each assembly includes its initial properties, its operating history in the reactor core, and any modifications made to it. The initial fuel assembly properties in the reactor record

includes the assembly design type (components, dimensions, and masses) and the initial enrichments. The operating history records include individual assembly burnup information. The records will also contain documentation of any modifications performed on a fuel assembly for Special Nuclear Material Control and Accounting purposes.

For tracking purposes, a unique identification number is stamped on each fuel assembly. Part of the Waste Disposal Receipt Criteria for bare SNF shipments includes checking the fuel assembly identification numbers against the numbers listed in the accompanying documentation.

[Note: Similar records and identification numbers will accompany shipments of DHLW pour canisters. A similar verification will be performed by checking the identification number on the canister against the accompanying records.(TBD)]

5.2.2 Burnup/Fissile Content Verification

The records accompanying the commercial SNF assemblies shipped to a repository will include a record of each fuel assembly's initial enrichment and burnup. These pieces of information are key to criticality evaluations. No special verification beyond checking the fuel assembly records is expected to be required for fuel enrichment information. It is expected that additional verification will be required for fuel assembly burnup information.

Burnup measurement systems are expected to provide the required additional verification of the records. Fuel assemblies shipped in burnup credit transportation casks and as canistered fuel (CF) are expected to have the burnup verification measurement performed prior to shipment to the repository. Fuel assemblies shipped in non-burnup credit casks and dual-purpose canisters may need to be measured at the repository surface facility prior to loading into a waste package. The final details of the burnup measurement system necessity are still being determined.

[Note: The DHLW shipments will be accompanied by records documenting the fissile isotope contents of each canister. The fissile isotope content is controlled during the manufacturing process within limits. The verified records of this controlled process will accompany the shipment.]

5.2.3 Waste Package Loading Procedure

The waste package loading procedure will ensure that the fuel assemblies to be loaded in a disposal waste package are properly identified prior to emplacement. The waste package loading procedure will use the limits established in the loading criteria as a basis for what fuel assemblies are acceptable for disposal in which waste package design.

Independent double verification of the identification numbers of the fuel assemblies received and the loading of these fuel assemblies into the specified disposal waste package shall be performed. Independent double verification is also required for the incorporation of any additional control material (i.e., loaded according to specifications). Similarly for CF, independent double verification of the CF identification numbers received and the loading of the canisters containing commercial SNF into the specified disposal waste package shall be performed.

[Note: For DHLW, each unit will be identified according to identification number and fissile content. These units will then be loaded into a disposal waste package as specified and the entire process from identification to emplacement shall be independently double verified.]

6.0 SAMPLE EVALUATION

This Chapter provides a sample case of a disposal criticality analysis evaluation for a waste package/EBS design in a repository. The sample system to be evaluated is presented in Section 6.1. Each of the methodology steps discussed earlier in the report (Sections 3.2 through 3.6) will be performed in the sample evaluation.

[Note: The Sample Evaluation Chapter will become an Appendix for the topical report.]

6.1 System Description

The sample evaluation is performed for PWR SNF assemblies with the design basis characteristics, in a 21 PWR waste package design. The waste packages are located in an EBS (subsurface) design at the sample repository. The sample repository site is the potential Yucca Mountain Site in Nevada.

6.1.1 Waste Form

The waste form used in the sample evaluations are B&W 15×15 Mark B4 PWR SNF assemblies. The mechanical parameters of the B&W 15×15 fuel assembly used for the sample evaluation are listed in Table 6-1. The fuel characteristics used in the sample evaluation are the design basis fuel characteristics, 3.00 weight percent initial enrichment U-235 and 20 GWd/MTU burnup, from the MGDS Advanced Conceptual Design Report.[6-1] The mechanical parameters and design basis fuel characteristics are used by SAS2H[6-2] and MCNP 4A[6-3] to generate the SNF isotopic concentrations and to calculate the reactivity of configurations containing the fissile material. A graphical representation of a fuel assembly is provided in Figure 6-1.

Figure 6-1 shows a B&W 15×15 fuel assembly, with a cut-away center to show the rods from a control rod assembly (CRA) (labeled "Rod control cluster"). The assemblies used in the sample evaluation did not include CRAs. Figure 6-1 also shows a cross section cut of a fuel rod (labeled "Fuel element") with a blow up of a section showing the fuel cladding, the pellet-clad gap (labeled "Annulus"), and the fuel pellet.

Table 6-1 Mechanical Parameters of B&W 15x15 Fuel Assembly

Parameter	Value	Units	Metric	Units	Radius (cm)	Ref
Fuel rods	208	/assembly	-	-	-	6-4
Fuel rod array	15x15	-	-	-	-	6-4
Guide tubes	16	/assembly	-	-	-	6-4
Instrumentation tubes	1	/assembly	-	-	-	6-4
Clad/tube material	Zircaloy-4	-	-	-	-	6-4
Fuel pellet OD	0.3686	inches	0.9362	cm	0.4681	6-4
Fuel Stack height	141.8	inches	360.2	cm	-	6-4
Mass of U	1023	lb	464	kgm	-	6-5
Mass of UO_2	1160.64	lb	526.38	kgm	-	6-4
Percent of Theoretical Density	95	%	-	-	-	6-4
Fuel clad OD	0.430	inches	1.092	cm	0.546	6-4
Clad thickness	0.0265	inches	0.0673	cm	-	6-4
Fuel clad ID*	0.377	inches	0.957	cm	0.479	-
Fuel rod pitch	0.568	inches	1.443	cm	-	6-4
Guide tube OD	0.530	inches	1.346	cm	0.673	6-4
Guide tube thickness	0.016	inches	0.041	cm	-	6-4
Guide tube ID*	0.498	inches	1.264	cm	0.632	-
Instrumentation tube OD	0.493	inches	1.252	cm	0.626	6-4
Instrumentation tube thickness	0.016	inches	0.041	cm	-	-
Instrumentation tube ID*	0.461	inches	1.170	cm	0.585	-
Fuel assembly envelope	8.536	inches	21.681	cm	-	6-4

* The inside diameters (IDs) above are calculated by subtracting 2x thickness from the outside diameter (OD).
(Reference 6-4, Table 2.5) (Reference 6-5, Table 2A-8)

Figure 6-1: B&W 15x15 Fuel Assembly

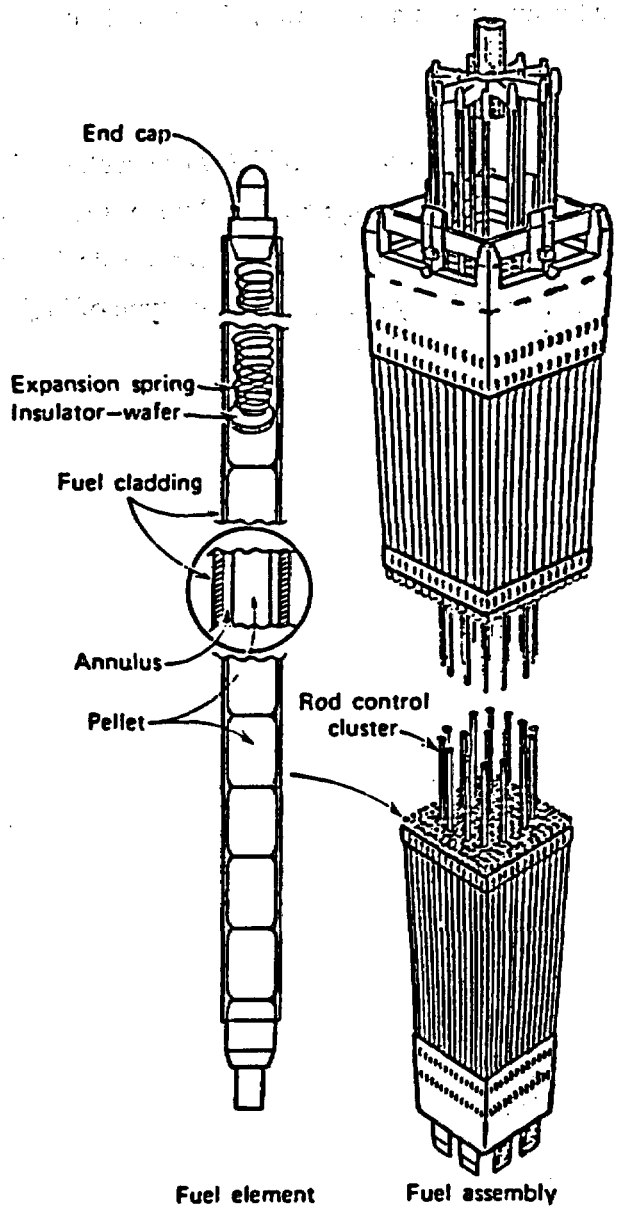

6.1.2 Waste Package Design

The waste package design used in the sample evaluation is the 21 PWR Advanced Uncanistered Fuel (AUCF) waste package design. Figure 6-2 provides a graphical description of the AUCF design. The design relies on burnup credit and neutron absorbers to provide disposal criticality control.

Figure 6-2 identifies the major components of the AUCF waste package design. The material call outs for the components in the waste package are listed under the components (A516, 316B6A, and Alloy 625). The A516 refers the type of the carbon steel, the 316B6A refers to the type of borated stainless steel, and the Alloy 625 refers to the type of high nickel alloy.

Figure 6-2: 21 PWR AUCF Waste Container

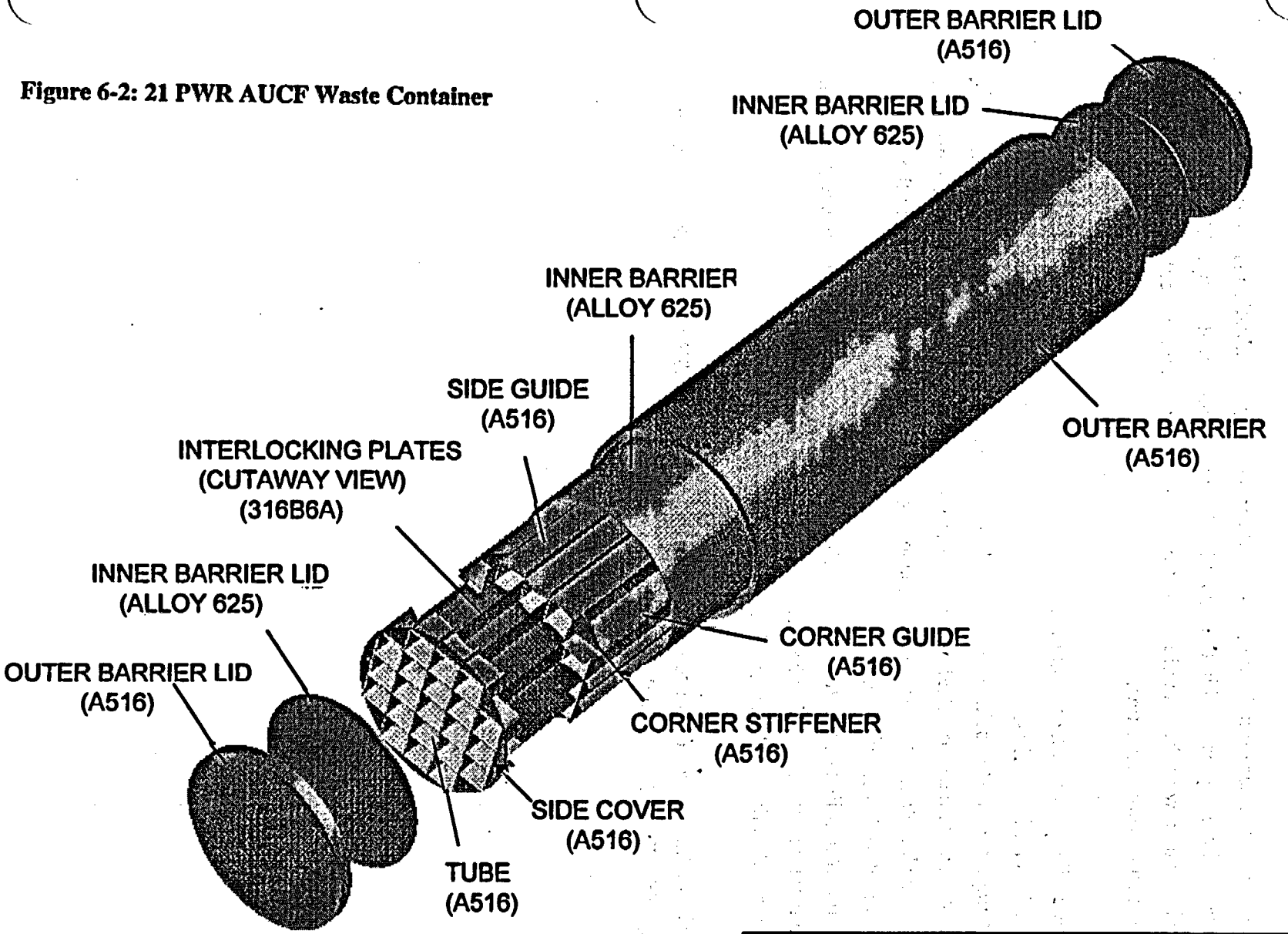

LENGTH = 5.336 M
DIAMETER = 1.650 M
TARE WEIGHT = 31,413 KG
LOADED WEIGHT = 47,797 KG

Waste Package Development

21 PWR AUCF Waste Container

6.1.3 Engineered Barrier System Design

The EBS design (the underground structures) used for the sample evaluation is a modified EBS design similar to the one presented in the MGDS Advanced Conceptual Design (ACD) Report[6-1]. Figure 6-3 shows a view of the sample evaluation engineered barrier segment design. The EBS design has the following properties:

- 5 meter diameter emplacement drifts,
- ~ 2000 meter long drifts,
- Pier emplaced waste packages (instead of rail cars as used in the MGDS ACD Report[6-1]),
- Piers consist of a carbon steel bar anchored to the steel sets with crushed tuff underneath,
- Waste package pedestal supports are made of carbon steel and are attached to the piers,
- Invert material is crushed tuff,
- 19.5 meter nominal center-to-center spacing between emplaced 21 PWR waste packages,
- 22.5 meters nominal spacing between emplacement drifts, and
- No backfill in the emplacement drifts.

Figure 6-3 shows three types of waste packages in the drift. The PWR waste package was the only type specifically addressed in the sample evaluation.

Figure 6-3: Engineered Barreri Segment

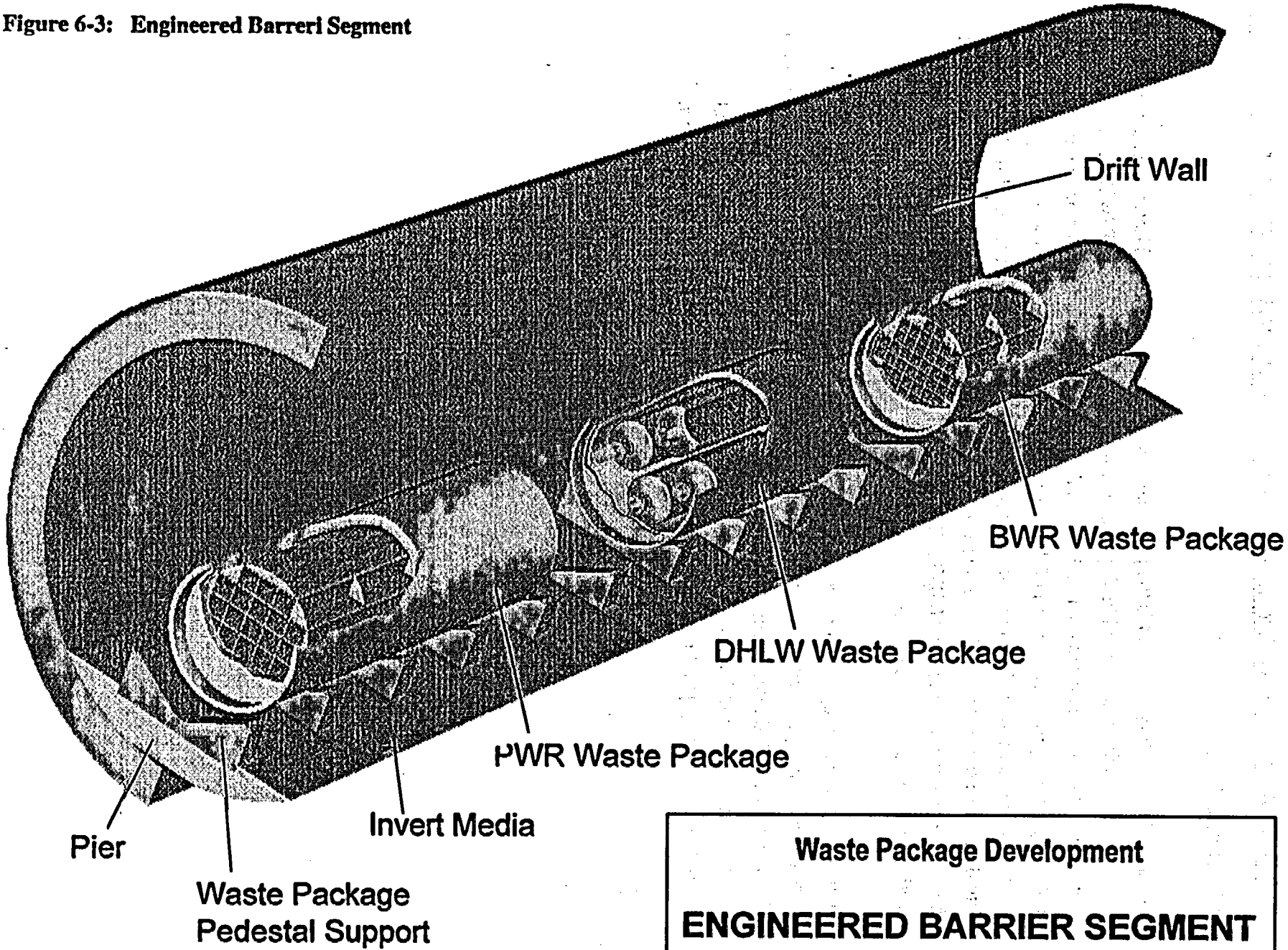

6.1.4 Repository

The sample repository site used is the potential Yucca Mountain Site in Nevada. The repository emplacement horizon is situated in Topopah Springs welded Unit 2 tuff (TSw2). The emplacement horizon is more than 300 meters from both the ground surface and above the water table. Figure 6-4 provides a sketch of the Waste Package (WP) Emplacemet Concept used for the sample evaluation, including a cut away pillar showing the different types of rock layers found between the surface and water table at the Yucca Mountain site. A detailed description of the rock layers can be found in MGDS ACD Report.[6-1] The pillar in Figure 6-4 shows only a portion of a single emplacement drift.

Figure 6-5 provides a graphical representation of a sample repository layout for the potential Yucca Mountain repository. The ramps, emplacement blocks, Yucca Mountain ridge, and water table are all identified in the figure. The parallel lines shown in the areas identified as emplacement blocks are the drifts where waste packages would be emplaced. A detailed description of the conceptual repository layouts for can be found in MGDS ACD Report.[6-1]

Figure 6-4:

WP Emplacement Concept

Including Rock Layers from Surface to Water Table

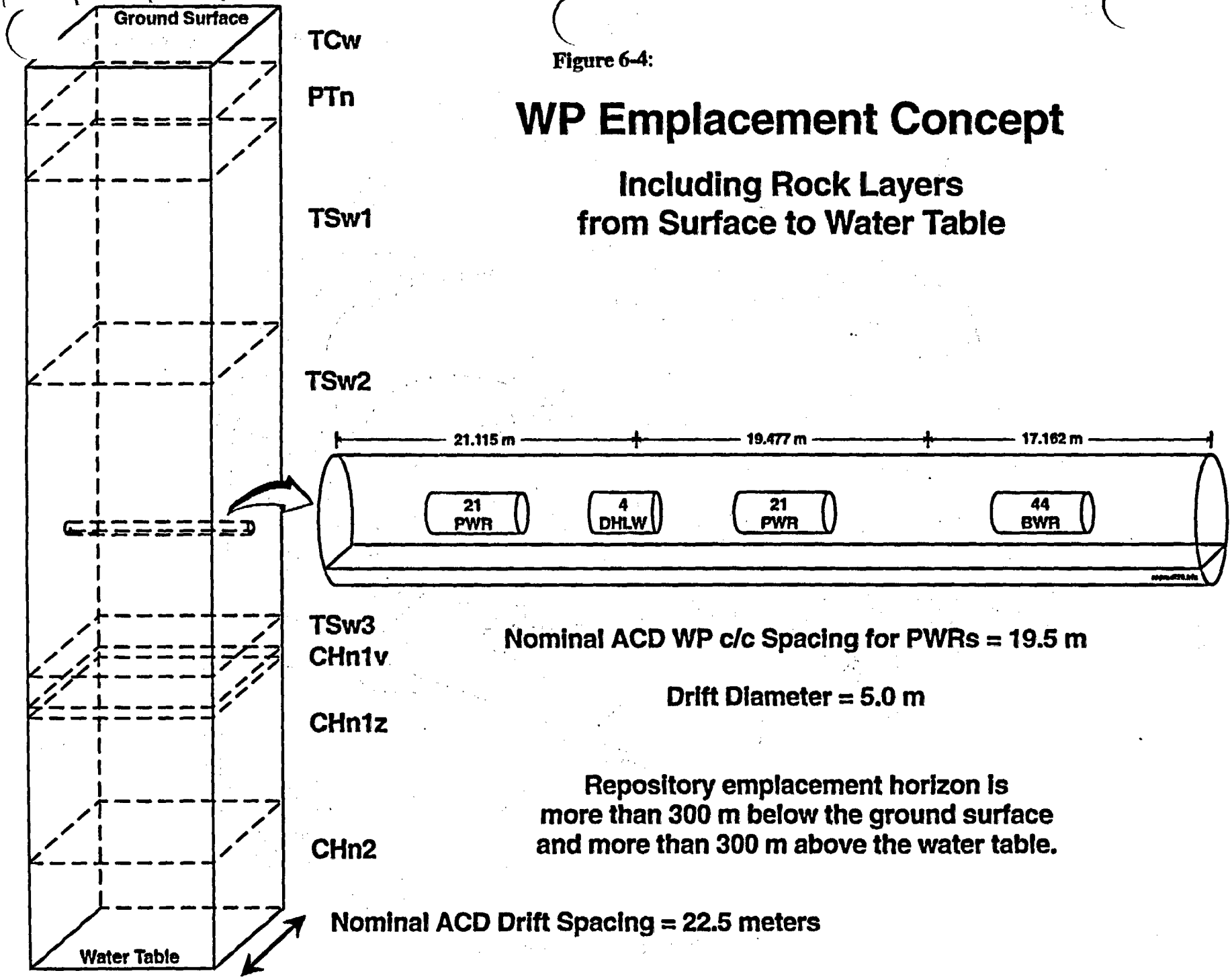

Nominal ACD WP c/c Spacing for PWRs = 19.5 m

Drift Diameter = 5.0 m

Repository emplacement horizon is more than 300 m below the ground surface and more than 300 m above the water table.

Nominal ACD Drift Spacing = 22.5 meters

Figure 6-5: Sample Repository Layout

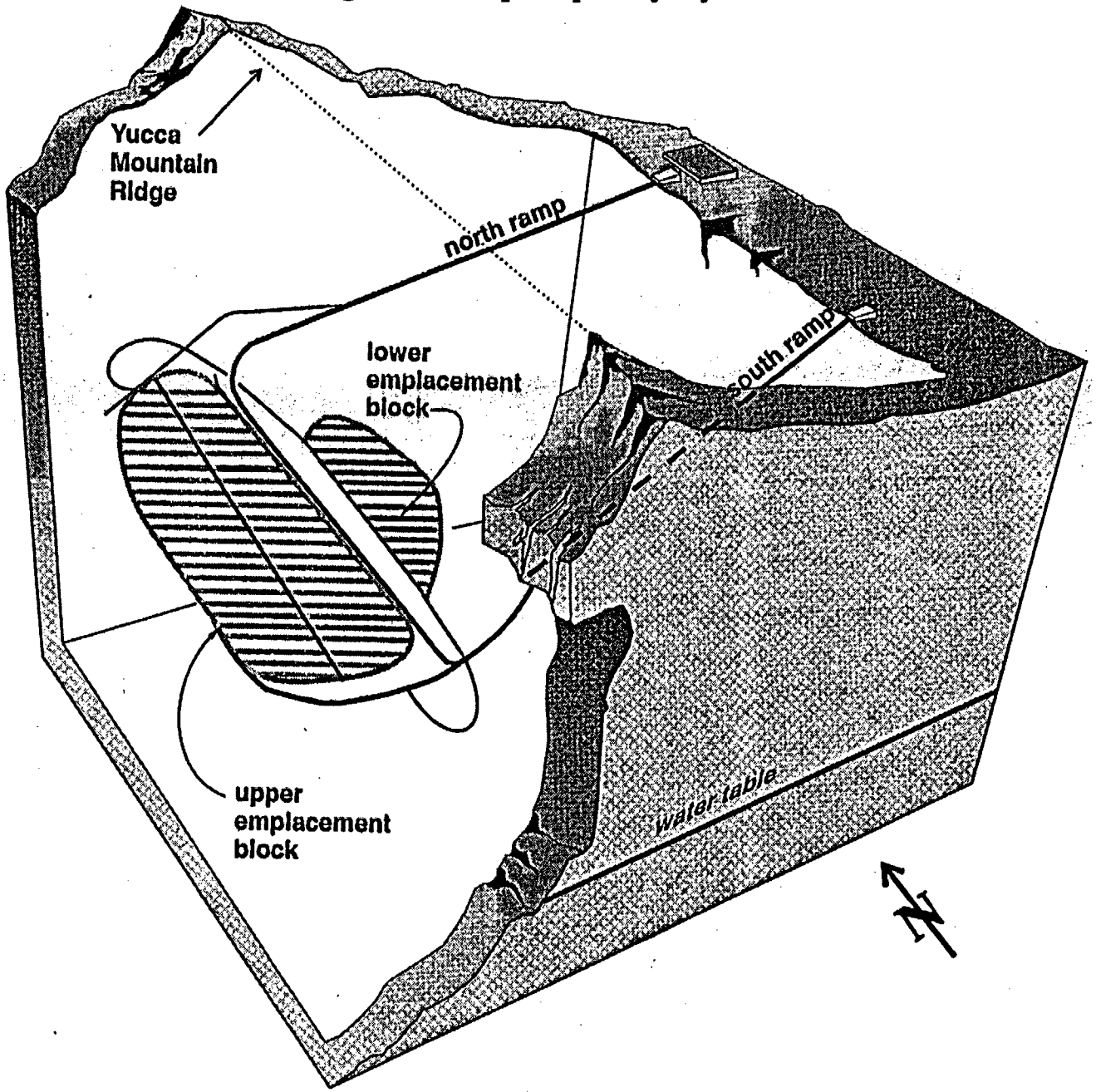

6.2 Sample Determination of Potentially Critical Configurations

The range of potential criticality configurations for the sample AUCF waste package/EBS design at the potential Yucca Mountain repository site are determined using the configuration generator model described in Section 4.2. The generation of these configurations follow the methodology described in Section 3.2. The details of this work are provided in Appendix C (TBD).

6.2.1 Sample Internal Waste Package Configurations

The following is a summary of the configurations which have been examined to date for internal criticality. These configurations were evaluated in the *Second Waste Package Probabilistic Criticality Analysis.*[6-6]

(1) The carbon steel tubes and guides have completely oxidized. The basket structure has collapsed, however, the fuel assemblies are still separated by the borated stainless steel plates between them. The borated stainless steel has partially corroded, with most of the boron from the corroded portions dissolved. Table 6-2 provides the results of k_{eff} calculations for variations of this degraded configuration using the Monte Carlo neutronics code MCNP.

Table 6-2. Progressive Degradation of Borated Stainless Steel Control Panels

% SS-B Plate Thickness Remaining	% of WP Void Space Filled With Fe_2O_3	k_{eff} (at 10,000 year peak)
80	0	0.894
50	0	0.917
50	10	0.851
25	20	0.857
25	15	0.880
10	25	0.887
10	20	0.908
10	10	0.944

(2) The borated stainless steel is fully corroded, with large amounts of iron oxide still remaining from corrosion of the carbon steel tubes and guides, and the stainless steel

plates. With the complete degradation of the stainless steel plates separating them, the fuel assemblies have settled through the oxides and are now touching. Only small amounts of boron remain trapped within the mass of oxides or in solution. Table 6-3 provides the results of k_{eff} calculations for variations of this degraded configuration using the Monte Carlo neutronics code MCNP.

Table 6-3. Basket Structure Gone, Uniform Iron Oxide and Boron Concentration

% of WP Void Filled With Fe_2O_3	% of Original B-10 Remaining In WP	k_{eff} (at 10,000 year peak)
0	0	1.093
30	0	0.928
30	2	0.913
30	5	0.890
20	0	0.979
20	5	0.941
20	10	0.902
20	15	0.872
20	25	0.812
20	100	0.572
10	10	0.947
10	15	0.909
10	20	0.879

6.2.2 Sample EBS Near-Field Configurations

The sample configurations of degraded commercial SNF in the Engineered Barrier System Near-Field are listed below:

- Fissile material left as a residue from evaporating water, with subsequent re-saturation to provide moderator.

- Fissile material adsorbed by an ion-exchange process (e.g. on a zeolite)

6.2.3 Sample Far-Field Configurations

Although far-field external criticality appears to have a very low probability, the following configurations appear to be among the most likely [6-7]:

- Uranium adsorbed in a reducing mineral deposit, most likely of fossil organic origin.
- Fissile material adsorbed in a zeolite material
- Fissile material (uranium or plutonium) precipitated on the walls of fractures

The first two have been analyzed in the *Probabilistic External Criticality Evaluation* [6-7], in which it was shown that there is very small probability of accumulating a critical mass with commercial SNF (TBV). It was also shown that the second configuration could not possibly produce a critical mass with commercial SNF. The third configuration will be analyzed in the near future.

[Note: Analysis of these far-field configurations with highly enriched uranium waste forms is expected to show larger probability of accumulation of a critical mass. The highly enriched uranium waste forms requires less mass, and therefore less material transport, to form critical masses. The larger probability of these far-field configurations with highly enriched waste forms may still be insignificant. (TBV)]

6.3 Sample Criticality Evaluations

The sample criticality evaluation performed for each of the configurations in the three different regions are discussed in this section. The MCNP 4A [6-3] computer code with point-wise continuous energy spectrum cross sections is the criticality model being used to calculate reactivity (k_{eff}) for the configurations. The subcritical limit values used for the criticality analysis were determined by analyzing the various benchmark cases specified in Section 4.1.2. From the benchmark analyses, the subcritical limits for the different ranges of configuration were determined for the MCNP code system. The results and details of this work are provided in Appendix B. A summary of the sample results are presented in Table 6-4.

Table 6-4: Sample Subcritical Limits for Potential Configurations (TBD)

Configurations	Subcritical Limit
Moderated intact fuel lattice inside waste package, intact to degraded waste package basket array	0.93 (TBD)
Moderated degrade fuel (non lattice) inside waste package, degraded waste package basket	0.92 (TBD)
Moderated fissile actinides outside waste package in the near-field	0.92 (TBD
Moderated fissile actinides outside waste package in the far-field	0.92 (TBD)

6.3.1 Sample Waste Package Criticality Evaluations

The following steps were performed for the sample waste package criticality evaluation:

1. The configurations internal to the waste package determined in Section 6.2.1 were modeled with the criticality model (MCNP 4A).

2. SNF isotope concentrations from the SNF isotopics model (ORIGEN-S/SCALE 4.3) at the appropriate cooling times (modified according to the applicable degradation and transport models) were entered into the criticality models.

3. Criticality analyses of the configurations were performed and the appropriate subcritical limits were applied to the results. The results are listed in Tables 6-2 and 6-3 (TBD). The details of the calculations are listed in Appendix C (TBV).

4. For the current model, the percentages of materials remaining for the k_{eff} data sets from each of the two configurations discussed above were converted into masses of boron and iron remaining in the flooded waste package. A linear regression was then performed with the data sets for each configuration to develop equations describing k_{eff} as a function of the mass of boron and iron remaining. The purpose of this model is to facilitate the screening of the multitude of configurations (i.e.,

remove configurations with k_{eff} less than the subcritical limit from further consideration). The regression lines for the two configurations are given by the following equations (where Fe is in metric tons and B is in kilograms):

(1) Partial basket:
$k_{eff} = 1.026 - 0.0242*Fe - 0.00645*B$, $R^2=0.91$

(2) Assemblies touching:
$k_{eff} = 1.068 - 0.0221*Fe - 0.0236*B$, $R^2=0.99$

Pooled data sets:
$k_{eff} = 0.989 - 0.0132*Fe - 0.00679*B$, $R^2=0.54$.
(Where R^2 is the fraction of the variation explained by the regression.)

The complete calculations are described in Appendix C. It should be noted that the partial basket regression implicitly incorporates the effect of decreasing basket thickness, which is generally proportional to the explicitly decreasing amounts of boron and iron. The fact that the pooled data set has such a small R^2 indicates that the two sets represent somewhat different physical processes, which is consistent with the fact that the partial basket variation incorporates the effect of varying assembly spacing, while the assemblies touching case does not. This distinction will be reflected in further criticality analyses by switching from the partial basket model to the assemblies touching model when the simplified configuration bookkeeper (discussed in Appendix C) indicates that the stainless steel plates have completely degraded. Currently, these models also assume the configuration occurs at the time of peak postclosure k_{eff} (at approximately 10,000 years)[6-6]. Future versions of these k_{eff} models will incorporate the effects of time, once sufficient MCNP runs have been performed to characterize this effect for each configuration.

5. The final step is to combine the configuration dependent k_{eff} models with the configuration bookkeeper to provide an estimate of the flooded and degraded waste package k_{eff} as a function of time. In the configuration bookkeeper, the boron and iron concentrations are decreased at each time step to reflect the corrosion and removal process. A simple deterministic example of this process is provided in Appendix C. In this example, five basic parameters affecting the corrosion of basket materials and the

removal of boron and iron from the waste package are varied between high and low values. The minimum amount of time required to remove sufficient boron and iron such that the flooded waste package k_{eff} exceeds 0.91 (the deliminator or subcritical limit used for the analysis [6-6]) is estimated for various combinations of these parameters. Future versions of the configuration bookkeeper will have probability distributions assigned to these parameters so that the probability of exceeding the defined criticality limit as a function of time can be estimated.

6.3.2 Sample EBS Near-Field Criticality Evaluations

Analysis of the configurations identified in Section 6.2.2 has not yet been completed. The following steps will be performed for the sample EBS near-field criticality evaluation:

1. The configurations in the EBS near-field determined in Section 6.2.2 will be modeled with the criticality model (MCNP 4A).

2. SNF isotope concentrations from the validated SNF isotopics model (ORIGEN-S/SCALE 4.3) at the appropriate cooling times will be modified by the appropriate degradation, transport, and precipitation/retardation models. The modified isotopic concentrations will be entered into the criticality models.

3 Criticality analyses of the configurations will be performed and the appropriate subcritical limits will be applied to the results.

4. The system configurations where the calculated k_{eff} does not exceed the subcritical limit, will be dropped from further consideration.

[Note: As part of the design process (which is outside the scope of this document) any system configuration where k_{eff} does exceed the subcritical limit will be evaluated for low impact fixes (redesigns or augment control measures).]

6.3.3 Sample Far-Field Criticality Evaluations

A set of 10 uranium/water concentrations in tuff was evaluated to determine the minimum critical mass/radius spheres. This set represented 3 SNF types, chosen to represent the 2%, 4%,

and 13% most stressing fuel with respect to k_∞. For each of these fuel types, the analysis was a two step process. First the most critical volume % of UO_2 (highest k_∞) was determined for a family of water concentrations, using MCNP to calculated k_∞, for a range of UO_2 volume %. The k_∞ values for one fuel type (PWR, 3.00% initial enrichment, 20 GWd/MTU) are shown in Appendix C.

The second step was to calculate k_{eff} using MCNP, for a range of radii, and interpolate to determine the critical radius, at which the value of k_{eff} is equal to the criticality threshold[6-7]. The most appropriate value of criticality threshold k_{eff} was 1 minus (bias and uncertainty of the computational process) minus (twice standard deviation of the specific Monte Carlo calculation). [Note: The criticality threshold will be replaced by the subcritical limit in future evaluations.] For these cases, a fresh fuel bias and uncertainty was used because only the long lived uranium isotopes (and Np-237) were included in the configurations. The conservative assumption was made that none of the fission products and shorter lived actinides from the SNF, are in the uranium-bearing groundwater from the repository (TBV). The other isotopes either decayed, or were removed from the SNF matrix much earlier than the uranium, or remained in the matrix after removal of the uranium. This process is illustrated in Appendix C for the UO_2 concentration giving the highest peak k_∞ for a range of water concentrations.

The critical masses calculated according to this method are then compared against information on the grade (concentration) of natural ore deposits and their frequency of occurrence to determine the probability that reducing zones capable of concentrating a critical mass will occur in the specific repository environment. This comparison is also presented in Appendix C.

6.4 Sample Criticality Consequence Evaluations

This section discusses the results of a sample criticality consequence evaluation. The scenarios evaluated are based upon the configurations identified in Section 6.3. The consequence of criticality events was evaluated for systems where k_{eff} exceeded the subcritical. The base results of these consequence evaluations are perturbations in the radionuclide inventory (TBV). The detailed results are shown in Appendix D (TBV).

The internal criticality scenarios evaluated thus far simulate a flooded waste package that is gradually approaching a critical condition (k_{eff}=1) as a result of positive reactivity insertions

caused by a slow loss of boron and iron from the package interior. Once a waste package reaches a k_{eff} of 1, continued small positive reactivity insertions will cause the power output of the waste package to begin to slowly rise (i.e., a long reactor period). If the power exceeds a certain limit, the rate at which water is consequentially removed from the waste package will exceed the rate of input, and the resulting water level drop will provide a negative reactivity insertion driving the waste package back towards a subcritical condition. Conversely, if insufficient power is produced, the water level will be maintained and the exchange process discussed previously will continue to remove dissolved boron, thus providing a continued source of positive reactivity insertions until the point of equilibrium is achieved. The maximum steady state power can then be estimated by determining the power required to maintain the bulk waste package water temperature at the point where water is removed at the same rate that it drips into the waste package. The waste package must produce sufficient power to raise the temperature of the incoming water to this equilibrium value, as well as account for heat losses to the environment by radiation and/or conduction. Preliminary calculations, which are provided in detail in Appendix D, have shown that at a water temperature of 57.4°C, the evaporation rate will match the maximum TSPA-95 rate at which water drips into a WP located beneath a flowing fracture. The thermal power required to raise the water temperature to 57.4°C, while at the same time compensating for heat losses to the environment is 2.18 kW.

To evaluate the effects of a criticality on the radionuclide inventory of a waste package, the computer code ORIGEN-S was run using the PWR criticality design basis fuel[6-1], and the steady state power of 2.18 kW discussed above. The criticality was assumed to occur after the fuel had aged/decayed for 15,000 years and was maintained at the above mentioned power for three durations: 1,000, 5,000 and 10,000 years. The maximum duration of 10,000 years is based on the assumption that it is the upper bound for the conditions supporting criticality (high infiltration, integrity of the lower part of the barrier, sufficient fissile material and void space remaining). The output of these runs was the radionuclide inventory, in curies, at the times corresponding to the end of each criticality, and at fuel ages (time since reactor discharge) of 45,000 and 65,000 years. In addition a fourth, decay-only case was run to determine the radionuclide inventories at the above times for fuel which did not experience a criticality event. The percentage increase in the inventories of 36 of the isotopes examined in TSPA-95 is provided in Appendix D. The overall effect of the criticality can be summarized by the percentage increase in the total curies, over that of the decay only case, for the 36 TSPA-95 isotopes. Table 6-5 shows this comparison. The explicitly stated times are measured from emplacement. Figure 6-6 graphically shows that even the 10,000 year duration criticality does

not increase the inventory of the 36 isotopes above that at the time the criticality began. In addition, the criticality appears to have no significant long-term effect on the inventory of these isotopes. Within 25,000 years the total inventory of these 36 isotopes in fuel assemblies which experienced a criticality can barely be distinguished from the inventory in fuel assemblies which did not experience a criticality.

Table 6-5. Percentage Increase in Total Curies of the 36 TSPA-95 Isotopes

Duration of Criticality	Percent Increase at End of Criticality	Percent Increase at 45,000 years	Percent Increase at 65,000 years
1,000 years	8.5% (16k years)	0.73%	0.73%
5,000 years	15% (20k years)	4.2%	3.7%
10,000 years	24% (25k years)	9.9%	8.5%

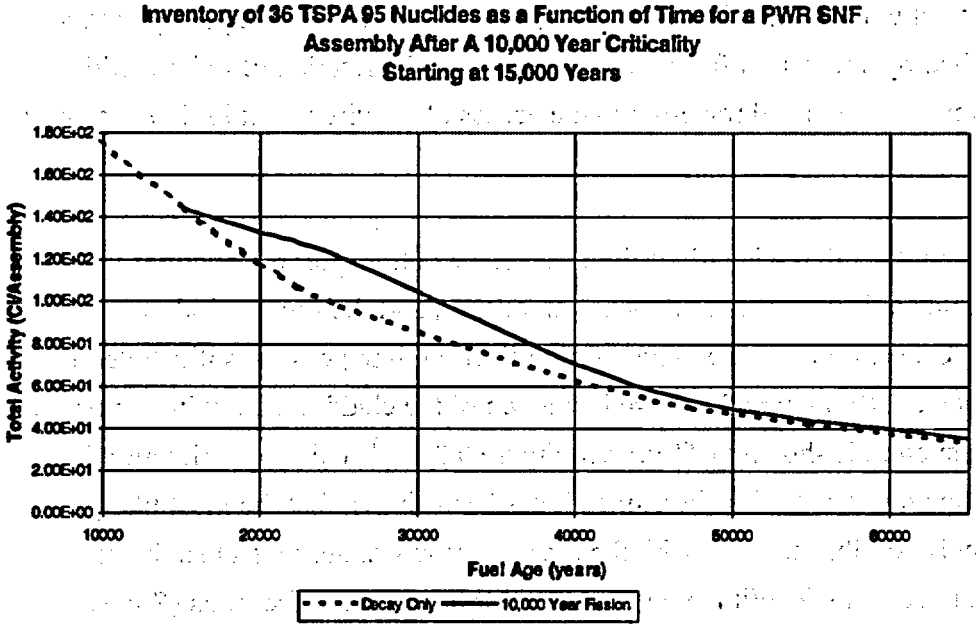

Figure 6-6.

6.5 Sample Risk Evaluation

This section discusses the results of a sample Risk Evaluation performed for the potential critical events identified in Section 6.3. The probability of the potential critical configuration occurring (from Section 6.2) and the consequence of the resulting criticality (from Section 6.4) are combined into a risk of violating the performance objectives of the facility.

The following examples illustrate the criticality risk calculation in terms of dose at the accessible environment. When the risk-based criticality methodology is finally used in the licensing process, the expected dose rate will be computed by taking the source term from the radionuclide increase resulting from a criticality and applying the TSPA Monte Carlo analysis of the groundwater transport of this increased inventory to the accessible environment. This process must be summed over all times of occurrence of the criticality weighted by the probability of the occurrence of the criticality at that time. For purposes of this illustration, the result of the comprehensive methodology can be represented by a convolution operation which sums the product of the expected number of criticalities which occur in some time interval, $d\tau$, about a time τ, multiplied by the increase in radionuclide inventory caused by each criticality (which is generally a function of τ but will be considered to be independent of time for simplicity in this illustration), and multiplied by a transport factor which represents the fraction of radionuclide inventory mobilized from the source and traveling to the accessible environment in time $t-\tau$, over τ from 0 to t.

The transport factor represents both the length of time necessary to transport the nuclides from the source to the accessible environment once they are mobilized, and the time period over which they will be mobilizing. One extreme of the range of mobilization time periods is illustrated by the mobilization from intact SNF (assumed to have lost much of the cladding, but with the oxide matrix relatively intact), such as is shown in TSPA-95, Figure 9.3-5.[6-9] This approximation is also appropriate following an internal criticality, since it has been shown that the most likely internal criticality (if any is possible at all) is with the assemblies reasonably intact so that the criticality can obtain the maximum benefit from the moderator between the fuel rods (*Second Waste Package Probabilistic Criticality Analysis*[6-6]). In this case the dose rate increases with time up to 200,000 years, after which it remains relatively constant for up to 1,000,000 years, due to the long half-life of the isotopes being considered, and the slow dissolution of the SNF. At some later time the dose would decrease significantly due to the depletion of the source. For

illustration of the relatively intact, slow dissolution case the process prior to the depletion of the source will be represented by the transport factor:

$$1-e^{-\alpha(t-\tau)}$$

where α represents the reciprocal of the minimum transport time to the accessible environment, and an illustrative value is $\alpha = 0.75$ per 100,000 years.

It should be noted that the asymptotic value of the transport factor is normalized to 1 to represent the conservative assumption that all the nuclides will eventually reach the accessible environment; furthermore the cutoff time, after which the source depletion would diminish the dose rate, is being neglected. This approximation is probably appropriate for a criticality internal to the waste package in which the SNF remains relatively intact and will dissolve slowly.

An illustrative PDF for the time of occurrence of the criticality is:

$$\text{pdf}(\tau) = \beta^2 \tau e^{-\beta\tau}$$

where β represents the reciprocal of the time duration over which there is a significant probability of criticality occurrence, and an illustrative value is $\beta = 1.2$ per 100,000 years.

This function peaks at 83,000 years, representing two effects: (1) the conservative estimate in the *Initial Waste Package Probabilistic Criticality Analysis*[6-8], which showed that it took nearly 100,000 years to reach an expected number of criticalities, and (2) the fact that sometime before 500,000 years the probability of internal criticality will decrease significantly because most of the waste packages can no longer contain sufficient water to provide the moderation necessary for criticality. Forming the convolution by multiplying the PDF by the transport factor and integrating over τ from 0 to t gives the normalized (as explained below) expected dose due to a single criticality:

$$1 - e^{-\beta t} - t\beta\, e^{-\beta t} - \beta^2\, e^{-\alpha t}\left((1-e^{-(\beta-\alpha)t})/(\alpha-\beta)^2 + t\, e^{-(\beta-\alpha)t}/(\alpha-\beta)\right)$$

This normalized expected dose is plotted in Figure 6-7, along with the PDF used to generate it. To complete the risk calculation the normalized expected dose must be multiplied by: (1) the fractional increase in radionuclide inventory, (2) the fraction of waste packages achieving

criticality, and (3) by the peak dose rate given in TSPA-95, Figure 9.3-5.[6-9] The *Second Waste Package Probabilistic Criticality Analysis*[6-6] shows the fractional increase in radionuclide inventory for the longest lived isotopes, due to a single waste package criticality, to be as follows: ^{99}Tc 4.1%, ^{237}Np 2.1%, ^{129}I 4.1%. As discussed in connection with the PDF above, the expected number of criticalities in 100,000 years is only 1, while the TSPA-95 results represent the independent contributions of the number of waste packages which would have been breached in the Monte Carlo simulation of that more comprehensive methodology. Hence there is a reduction by an additional factor of up to 10,000 (the approximate total number of SNF waste packages). Since the present TSPA-95 analysis does not give this number directly, and in view of the illustrative purpose of this calculation, the explicit result of applying these factors is not presented here.

It should be noted that these fractional increases are different from the increases in total curies given in Section 6.4, above, because the focus here is on long lived isotopes. It is this focus on long lived isotopes which makes the fractional increase applicable to the total dose rates given in TSPA-1995, Figure 9.3-5.[6-9]

Following an external criticality (if one could occur) the resulting increased radionuclide inventory would be much more readily mobilized (than would the relatively intact SNF in the case considered above). Therefore, the comprehensive TSPA methodology would produce a time dependent dose reflecting a transport function which peaked and declined over a time period much shorter than 1,000,000 years. Since this situation has not yet been analyzed by the TSPA methodology, the form of the transport function must be hypothesized. For this purpose a probability density function is used:

$$pdf_1(t-\tau) = \alpha^2 t e^{-\alpha(t-\tau)}, \text{ where } \alpha = 0.75 \text{ per } 100{,}000 \text{ years,}$$

which has the same rising behavior as the transport function, but is normalized so that its integral is 1. The functional form for the PDF of the external criticality occurrence time is the same as for the internal criticality, but the peak is broader and occurs at 400,000 years.

$$pdf_2(t)=\beta^2 t e^{-\beta t}, \text{ where } \beta = 0.25 \text{ per } 100{,}000 \text{ years}$$

In this illustration of external criticality α and β have approximately the same meaning as for the internal criticality illustration described above. The convolution of the criticality occurrence and the subsequent transport to the accessible environment is then represented by the integral:

$$pdf_c(t) = \int_0^t pdf_2(\tau) pdf_1(t-\tau) d\tau$$

which can be evaluated analytically to give:

$$pdf_c(t) = \alpha^2\beta^2 e^{-\alpha t}\left[-\frac{t^2 e^{-(\beta-\alpha)t}}{\beta-\alpha} + \frac{t(1-e^{-(\beta-\alpha)t})}{(\beta-\alpha)^2} + \frac{t^2 e^{-(\beta-\alpha)t}}{\beta-\alpha} + \frac{2te^{-(\beta-\alpha)t}}{(\beta-\alpha)^2} + \frac{2(1-e^{-(\beta-\alpha)t})}{(\beta-\alpha)^3}\right]$$

A graph of this normalized expected dose is given in Figure 6-8, together with the $pdf_2(t)$. It should be noted that the normalization of this expected dose is different from that shown in Figure 6-7 for the internal criticality. Correction factors for fractional nuclide increase and fraction of total inventory reaching criticality would be applied, but they would be different from the internal criticality case. More importantly, these correction factors would have to be applied to the short dissolution time analog of TSPA-1995 Figure 9.3-5.[6-9]

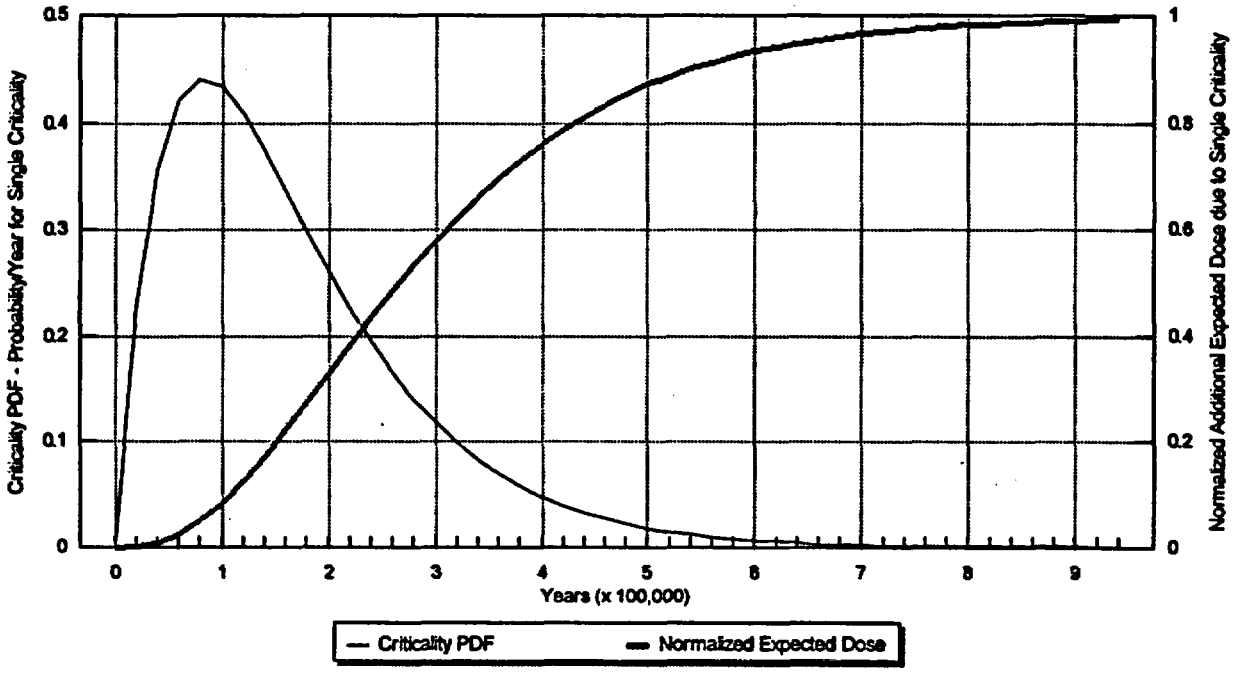

Figure 6-7. Normalized Additional Dose Due to a Single Internal Criticality Event

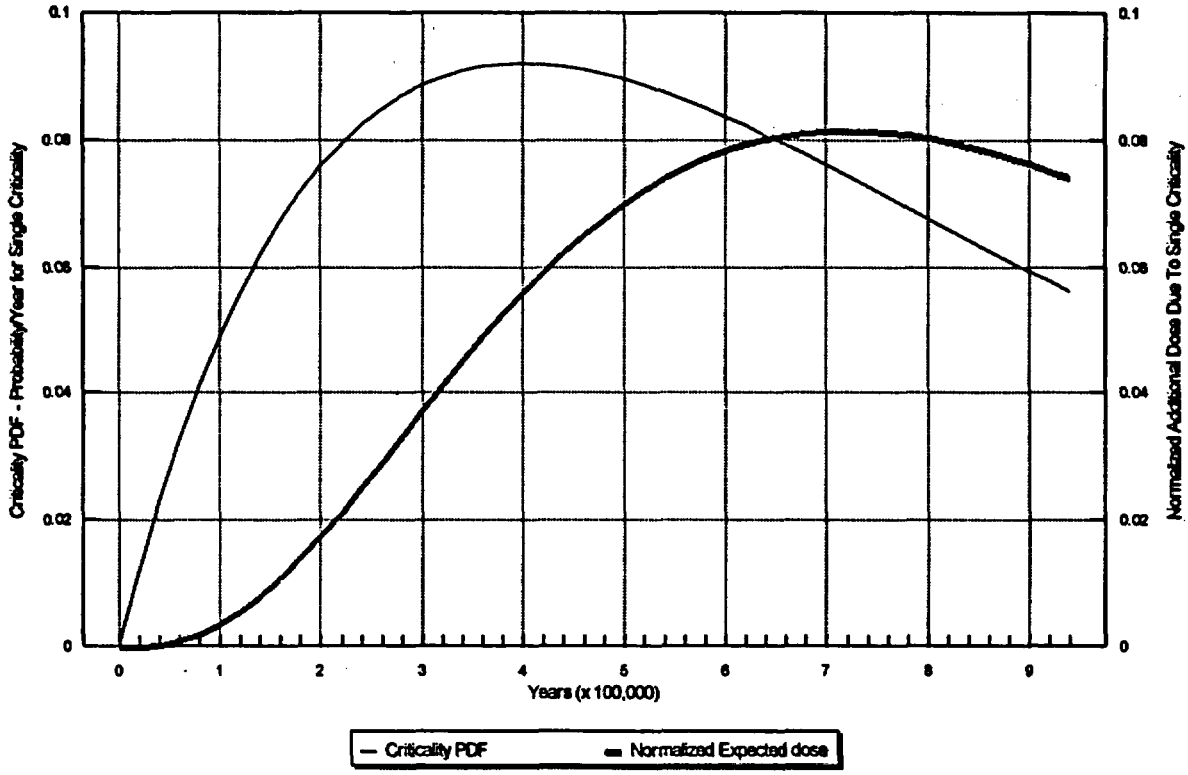

Figure 6-8. Additional Normalized Dose Due to Single External Criticality Event.

6.6 Sample Total System Performance Consequence Evaluation

As previously discussed in Section 3.1, a performance assessment evaluation will be conducted prior to a detailed TSPA analysis that uses a perturbed source term. If the consequence is determined to be insignificant upon evaluation of the perturbed source term, no criticality perturbations to TSPA analyses will be conducted. However, if detailed TSPA calculations are warranted, the approach described in Section 3.1 and using the models described in Section 4.4 will be implemented.

An example calculation was conducted for this report using a perturbed source term from an internal waste package criticality event theorized in the an earlier evaluation.[6-6] The results of the example evaluation indicate that, for the example potential critical events, there was no significant adverse effect to the repository Total System Performance. The dose to the public was not significantly increased by the inclusion of the potential criticality events identified as part of the example evaluations. The summary of results from this evaluation are listed in Table 6-6 (TBD).

Three criticality events were defined in *Second Waste Package Probabilistic Criticality Analysis*.[6-6] The three criticality events were:

1) 1,000 year criticality occurring after 15,000 years,
2) 5,000 year criticality occurring after 15,000 years, and
3) 10,000 year criticality occurring after 15,000 years.

The inventory created by the criticality event for these three cases were presented in Tables 7.5-1, 7.5-2, and 7.5-3 in the *Second Waste Package Probabilistic Criticality Analysis*.[6-6] The percent difference due to the criticality was also presented in these tables and gives an indication of the increase or decrease of the particular isotope inventory.

A quantitative total system performance assessment using the perturbed radionuclide inventory is given below. The key isotopes contributing to release and dose to man were determined in TSPA-1995[6-9] to be ^{129}I, ^{237}Np, and ^{99}Tc. ^{129}I and ^{99}Tc provided peak release to and doses at the accessible environment at early times and ^{237}Np provided peak, and generally, highest release at later times in the simulations conducted for TSPA-1995. The percent increase from the original inventory of each of the key radionuclides for each of the criticality events was reviewed and is

presented in Table 6-6. These data indicate that the greatest increase in source term inventory occurs for the longest criticality event (10,000 year event). However, the change is only approximately a 4 percent increase in inventory. Assuming an addition of 4 percent to the inventory of the key radionuclides as determined by TSPA-1995, the criticality would potentially produce a maximum of 4 percent increase in the simulated release or dose to man. However, the actual increase in release or dose to man is expected to be lower because the total 4 percent increase is not expected to reach the accessible environment due to dissolution rate limitations of the new source term. This increase in release is not expected to be significant to total performance.

Table 6-6. Criticality Effect on Radionuclides Determined to Be Important to Total Performance

Radionuclide	% Increase for 1,000 Yr Criticality	% Increase for 5,000 Yr Criticality	% Increase for 10,000 Yr Criticality
^{129}I	0.45	2.0	4.1
^{99}Tc	0.53	2.2	4.1
^{237}Np	0.26	1.0	2.1

The case with a criticality event lasting 10,000 years occurring 15,000 years after closure is considered. The TSPA-1995 case of 83 MTU/acre, backfill, high infiltration, and drips on the waste package was the base case for the analyses. The criticality event was assumed to occur within a single waste package and the waste package failure was assumed to be the most conservative for the case under analysis. Dissolution rate of the source term was assumed to be the same as the initial waste form itself, since the criticality event was assumed to occur within the cladding. The inventory of the criticality source term was assumed to be increased or decreased according to the analyses presented in Table 7.5-3 of the *Second Waste Package Probabilistic Criticality Analysis.*[6-6]

Figure 6-9 shows the base case dose history at the accessible environment for the three radionuclides contributing the most to the total dose. The addition of the criticality event source term (one waste package with an inventory greater than the original inventory according to the *Second Waste Package Probabilistic Criticality Analysis*[6-6]) does not change the results of this

figure due to the relatively small inventory in the single waste package compared to the overall waste inventory in the potential repository.

Figure 6-10 shows the dose history at the accessible environment for the same three radionuclides that results from the criticality event. The doses are generally several orders of magnitude below the base case and are inconsequential to performance of the repository.

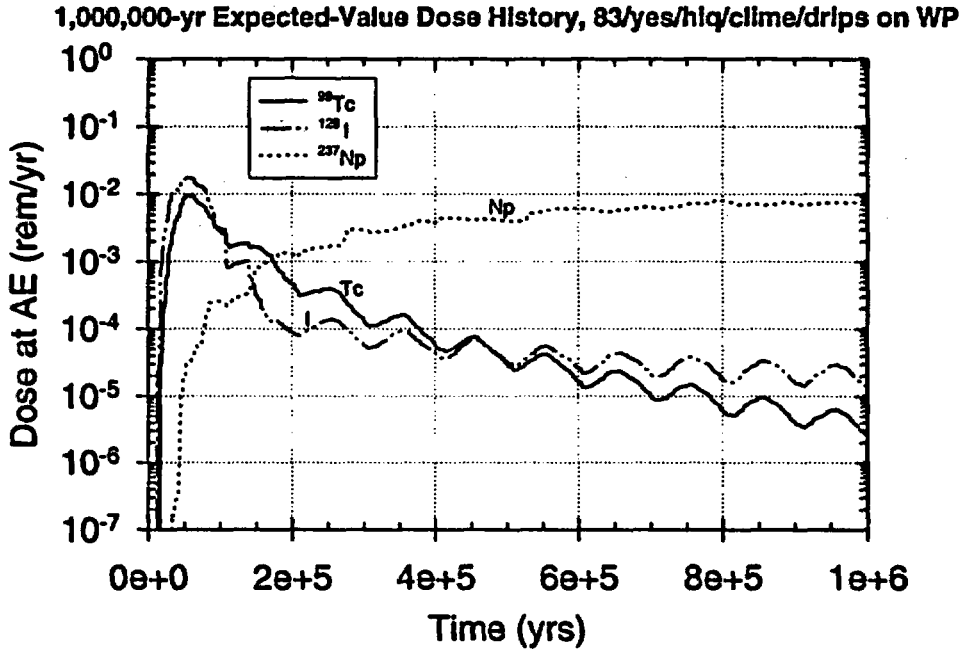

Expected-Value dose history at accessible environment including criticality inventory.

Figure 6-9

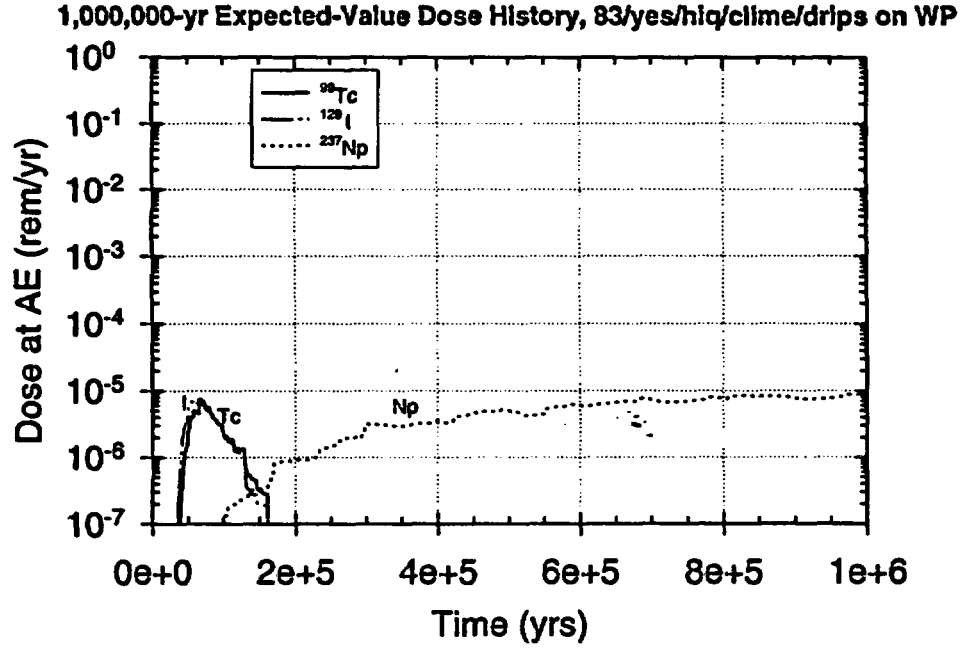

Expected-Value dose history at accessible environment only from criticality inventory.

Figure 6-10

7.0 SUMMARY AND CONCLUSIONS

A methodology for assessing nuclear criticality control in waste packages for disposal in the potential repository at Yucca Mountain is presented in this report. Criticality evaluations are performed for three regions or locations within the repository; internal (to waste package), near-field external, and far-field external. The methodology evaluates criticality potential as an explicit function of time. The time period of concern starts with the containment phase (the period from permanent closure to 1,000 years after closure) and proceeds through the isolation phase (the period from the end of the containment phase to the end of the period of regulatory concern, currently undefined but assumed to be 10,000 years in the most recent EPA regulation, which has been remanded). This report has defined an additional phase, the extended isolation phase. This is a phase, discussed in Chapter 3, that may require variations in the approach to criticality analysis if the period of regulatory concern is much longer than 10,000 years.

The methodology relies on probabilistic evaluations for identifying configurations with potential for criticality. The criticality potential (k_{eff}) of selected configurations is determined and compared with the appropriate subcritical limit. When the subcritical limit is exceeded, a criticality consequence analysis is performed to evaluate the impact of the potential criticality event on the radionuclide inventory and thermal effects in the vicinity of the event. The results of this analysis are provided as input for a total system performance assessment. The results of the TSPA (risk associated with potential criticality event) are used to demonstrate compliance with the repository performance objectives and to determine if augmentation of criticality controls is required. Thus, a risk-based methodology is used for evaluating criticality potential of waste package designs.

Burnup credit and four methods for disposal criticality control are presented. The criticality control methods include imposing geometry restrictions, limiting the amount of fissile material, adding neutron absorber material, and limiting the amount of moderator. These methods, along with burnup credit, will reduce the k_{eff} values determined during the criticality evaluations of disposal waste packages. A total of 14 actinide and 15 fission product isotopes (principal isotopes) are identified for the burnup credit methodology. Commercial reactor criticality data is used in validating the neutronics model. Chemical assay data is used to augment the validation of the SNF isotopic model, and fresh fuel criticality experiments are used to augment validation of the criticality analysis model used for evaluating the criticality potential of intact waste packages

and configurations of fissile material representing various degraded states. The data library consists of 289 fresh fuel criticality experiments. The subcritical limit values, for the three regions in the repository where criticality evaluations are performed, is established based on evaluations of the measured criticality data.

A sample evaluation is provided to illustrate the methodology presented in the report. A description of the experiments and analyses performed supporting the development and validation of the various models presented in this report are presented in the appendices.

As indicated in this report, the development and validation of the models supporting the disposal criticality analysis methodology is an ongoing process that has not been completed. Therefore, it is premature to draw specific conclusions concerning these models. Over the next two years this effort will be completed and documented in the final topical report. The topical report will then present specific conclusions relative to the accuracy and applicability of the models for disposal criticality evaluations.

In Chapter 1, the Yucca Mountain Project planning assumption was presented. This assumption states that the risk-based approach to dealing with disposal criticality is not only the best approach, but also that it is the only feasible approach. This assumption will be validated during the completion of the development of the disposal criticality analysis methodology. Conclusions relative to this risk-based approach will be presented in the topical report.

8.0 REFERENCES

The References in this report have been developed from both Q and Non-Q sources, and include regulatory documents, Codes and Standards, computer code manuals, and correspondences. The References are segregated below to clearly identify their associated category and Q status.

The following References are legal and regulatory documents, so a Q classification does not apply to them:
1-1, 1-2, 2-2, 2-7, 2-8, 2-11

The following References are OCRWM Requirement Documents and QA (Quality Assurance) implementing documents so are treated as Q data:
P-1, P-2, 2-1, 4-18

The following References are computer code manuals that have not been incorporated into an approved QA Program and so are treated as non-Q data:
1-3, 3-3, 4-1, 4-7, 4-8, 4-14, 6-2

The following References are computer code manuals that have been incorporated into an approved QA Program and so are treated as Q data:
1-4, 3-4, 4-2, 6-3

The following References are Codes and Standards and so are treated as Q data:
2-3, 2-4, 2-5, 2-6

The following References are reports and analyses performed at DOE national labs or by the M&O, following their respective QA programs. The information from these References will be treated as Q information.
3-1, 3-2, 4-3, 4-4, 4-9, 4-10, 4-11, 4-12, 4-13, 4-15, 4-16, 4-17, 4-23, 4-24, 6-1, 6-4, 6-5, 6-7, 6-8

The following References contain non-Q information:
4-6, 4-19, 4-20, 4-21, 4-22, 4-30

The following References are information accepted by the scientific and engineering community as established fact and will be treated as Q information:
4-25, 4-26, 4-27

The following References contain unverified information which will be treated as non-Q:
1-5, 2-9, 2-10, 3-4, 4-5, 4-28, 4-29, 4-31, 4-32, 4-33, 4-34, 4-35, 4-36, 4-37, 4-38, 6-9

The References listed below are identified as they appear in this report by Chapter.

Preface

P-1. Activity Evaluation: *"Prepare the Disposal Criticality Analysis Methodology Technical Report"*, DI Number: BB0000000-01717-2200-00032 REV 02, CRWMS, M&O

P-2. *Quality Assurance Requirements and Description*, DOE/RW-0333P REV 5, DOE, October 31, 1995

Chapter 1

1-1. *Nuclear Waste Policy Act of 1982, Public Law 97-425.* January 7, 1983.

1-2. *Nuclear Waste Policy Amendments Act of 1987, Public Law 100-23.* December, 1987.

1-3. *SAS2H: A Coupled One-Dimensional Depletion and Shielding Analysis Code*, Draft - NUREG/CR-0200, Vol. 1, Sect. S2, Rev. 5, O.W. Hermann and C.V. Parks, Oak Ridge National Laboratory (ORNL), Oak Ridge, TN, September 1995.

1-4. *MCNP: A General Monte Carlo N-Particle Transport Code, Version 4A*, La-12625-M, J.F. Briesmeister, Ed., Los Alamos, NM, LANL, November 1993.

1-5. *Topical Report on Actinide-Only Burnup Credit for PWR Spent Nuclear Fuel Packages*, DOE/RW-0472, DOE OCRWM, Washington, D.C., May 1995.

Chapter 2

2-1. *Civilian Radioactive Waste Management System Managing and Operation Contractor Requirement Document*, DI Number: A00000000-00811-1708-00003 REV 02, CRWMS M&O.

2-2. *PRA Procedures Guide*, NUREG/CR-2300, NRC.

2-3. *American National Standard for Nuclear Criticality Safety in Operations with Fissionable Materials Outside Reactors*, ANSI/ANS-8.1-1983, American Nuclear Society (ANS), La Grange Park, IL, October 1983.

2-4. *Criticality Safety Criteria for the Handling, Storage, and Transportation of LWR Fuel Outside Reactors*, ANSI/ANS-8.17-1984 (R1989), ANS, La Grange Park, IL, January 1984 (Revised 1989).

2-5. *Criteria for Nuclear Criticality Safety Controls in Operations with Shielding and Confinement*, ANSI/ANS-8.10-1983, ANS, La Grange Park, IL, 1983.

2-6. *American National Standard for Nuclear Criticality Control of Special Actinide Elements*, ANSI/ANS-8.15-1981, ANS, La Grange Park, IL, November 1981.

2-7. *Nuclear Criticality Safety in Operations with Fissionable Materials at Fuels and Materials Facilities*, Regulatory Guide 3.4, Revision 2, NRC, March 1986.

2-8. *Criticality Safety for Handling, Storing, and Transporting LWR Fuel at Fuels and Materials Facilities*, Regulatory Guide 3.58, NRC, October 1986.

2-9. *Topical Report on Actinide-Only Burnup Credit for PWR Spent Nuclear Fuel Packages*, DOE/RW-0472, DOE OCRWM, Washington, D.C., May 1995.

2-10. *Technical Bases for Yucca Mountain Standards*, National Academy of Sciences, Washington, D.C., August 1995.

2-11. *Use of Probabilistic Risk Assessment Methods in Nuclear Regulatory Activities; Final Policy Statement*, 60 FR 42622, NRC, August 1995.

Chapter 3

3-1. *Second Waste Package Probabilistic Criticality Analysis: Generation and Evaluation of Internal Criticality Configurations*, DI Number: BBA000000-01717-2200-00005, Rev. 00, P. Gottlieb and J. Massari, CRWMS M&O, Las Vegas, Nevada, March 1996.

3-2 *Probabilistic External Criticality Evaluation*, DI Number: BB0000000-01717-2200-00037, Rev. 00, P. Gottlieb and J. Massari, CRWMS M&O, Las Vegas, Nevada, May 1996.

3-3. *SAS2H: A Coupled One-Dimensional Depletion and Shielding Analysis Code*, Draft - NUREG/CR-0200, Vol. 1, Sect. S2, Rev. 5, O.W. Hermann and C.V. Parks, ORNL, Oak Ridge, TN, September 1995.

3-4. *MCNP: A General Monte Carlo N-Particle Transport Code, Version 4A*, La-12625-M, J.F. Briesmeister, Ed., Los Alamos, NM, LANL, November 1993.

Chapter 4

4-1. *SAS2H: A Coupled One-Dimensional Depletion and Shielding Analysis Code*, Draft - NUREG/CR-0200, Vol. 1, Sect. S2, Rev. 5, O.W. Hermann and C.V. Parks, ORNL, Oak Ridge, TN, September 1995.

4-2. *MCNP: A General Monte Carlo N-Particle Transport Code, Version 4A*, La-12625-M, J.F. Briesmeister, Ed., Los Alamos, NM, LANL, November 1993.

4-3. *Sensitivity and Parametric Evaluations of Significant Aspects of Burnup Credit for PWR Spent Fuel Packages*, ORNL/TM-12973, M.D. DeHart, ORNL, ORNL, Oak Ridge, TN, June 1995.

4-4. *Validation of the SCALE System for PWR Spent Fuel Isotopic Composition Analysis*, ORNL/TM-120667, O.W. Hermann, S. M. Bowman, M. C. Brady, and C.V. Parks, ORNL, Oak Ridge, TN.

4-5. *Topical Report on Actinide-Only Burnup Credit for PWR Spent Nuclear Fuel Packages*, DOE/RW-0472, DOE OCRWM, Washington, D.C., May 1995.

4-6. *Disposal Needs for Isotopic Data*, DI Number: BBA000000-01717-4200-00013 Rev. 00, CRWMS M&O, Las Vegas, Nevada, March 15, 1995.

4-7. *CASMO-3 - A Fuel Assembly Burnup Program*, STUCSVIK/NFA-89/3, M. Edenius, et al., Nykoping, Sweden, Studsvik AB , November 1989.

4-8. *NEMO - Nodal Expansion Method Optimized: A Code to Calculate Reactivity and Power Distributions for a Pressurized Water Reactor*, BAW-10180-a, Rev. 1, G.H. Hobson, et al., B&W Fuel Company, Lynchburg, VA, March 1993.

4-9. *Characterization of Spent Fuel Approved Testing Material --ATM-101*, PNL-5109-101, R.J. Guenther, et al., Battelle Pacific Northwest Laboratory (PNL).

4-10. *Characterization of Spent Fuel Approved Testing Material --ATM-103*, PNL-5109-103, R.J. Guenther, et al., PNL, April 1988.

4-11. *Characterization of Spent Fuel Approved Testing Material --ATM-104*, PNL-5109-104, R.J. Guenther, et al., PNL , December 1991.

4-12. *Characterization of Spent Fuel Approved Testing Material --ATM-106*, PNL-5109-106, R.J. Guenther, et al., PNL, October 1988.

4-13. *Characterization of Spent Fuel Approved Testing Material --ATM-105*, PNL-5109-105, R.J. Guenther, et al., PNL , December 1991.

4-14. *Improved and Consistent Determination of the Nuclear Inventory of Spent PWR Fuel on the Basis of Cell Burnup Methods Using KORIGEN*, (ORNL-TR-5043) KFK 3014, U. Fisher and H.W. Wiese, Karlsruhe Nuclear Research Center, January 1983.

4-15. *Verification of the OREST (HAMMER-ORIGEN) Depletion Program System Using Post-Irradiation Analyses of Fuel Assemblies 168, 170, 171, and 176 from the Obrigheim Reactor*, (ORNL-TR-8820). GRS-a-962, U. Hesse, Gesellschaft fur Reaktorscherheit (GRS) mbH, 1984.

4-16. *Analysis of Degradation Due to Water and Gases in MPC*, DI Number: BB0000000-01717-0200-00005 REV 01, CRWMS M&O, Las Vegas, Nevada, September 29, 1995.

4-17. *Evaluation of Cover Gas Impurities and Their Effects on the Dry Storage of LWR Spent Fuel*, PNL-6365, R. W. Knoll and E. R. Gilbert, PNL, November 1987.

4-18. *Yucca Mountain Site Characterization Project, Engineered Barrier Design Requirements Document*, YMP/CM-0024, Rev.0, ICN 1, DOE OCRWMS, September 21, 1994.

4-19. "Waste Package Corrosion Inputs", IOC LV.WP.DS.06/93-107, from D. Stahl to R. Memory and S. Saterlie, CRWMS M&O, June 21, 1993

4-20. *Waste Package Materials Selection Analysis*, DI Number: BBA000000-01717-0200-00020, Rev. 00, J. K McCoy, CRWMS M&O, Las Vegas, Nevada , August 1, 1996.

4-21. *Update Report on RIP/YMIM Analysis of Designs*, DI Number: BBA000000-01717-5705-00002, REV02, CRWMS M&O, Las Vegas, Nevada, July 13, 1995.

4-22. *Scientific Investigation Plan for Metal Barrier Selection and Testing*, SIP-CM-01, CRWMS M&O, Las Vegas, Nevada, June 20, 1996.

4-23. *Control of Degradation of Spent LWR Fuel During Dry Storage in an Inert Atmosphere*, PNL-6364, M. E. Cunningham, E. P. Simonen, R. T. Alleman, I. S. Levy, R. F. Hazelton, and E. R. Gilbert, PNL, October 1987.

4-24. *Zircaloy Cladding Performance Under Spent Fuel Disposal Conditions*, BNL 52235, C. Pescatore, M. G. Cowgill, and T. M. Sullivan, Brookhaven National Laboratory (BNL), April 1990.

4-25. *Temperature Limit Determination for the Inert Dry Storage of Spent Nuclear Fuel*, EPRI TR-103949, C. Pescatore, M. Cowgill, Electric Power Research Institute (EPRI), May 1994.

4-26. *Oxidation of Spent Fuel at Between 250 and 360 °C*, EPRI NP-4524, R. E. Einziger, EPRI, April 1986.

4-27. Robert E. Einziger and Rajiv Kohli, "Low-Temperature Rupture Behavior of Zircaloy-Clad Pressurized Water Reactor Spent Fuel Rods Under Dry Storage Conditions", *Nuclear Technology*, 67, 107–123 (1984).

4-28. J. K. McCoy and T. W. Doering, "Prediction of Cladding Life in Waste Package Environments", in *High Level Radioactive Waste Management: Proceedings of the Fifth International Conference*, (ANS, La Grange Park, IL, and American Society of Civil Engineers, New York, 1994), pp. 565–572.

4-29. *Interim Report: Unsaturated Dissolution Release Testing*, MOL.209, attachment to letter LV.WP.DS.09/25.328, September 27, 1995, from A. M. Segrest to R. L. Craun.

4-30. *Scientific Investigation Plan for YMP WBS Element 1.2.2.3.1.1: YMP Spent Fuel Waste Form Testing*, SIP-WF-01, Rev. 1.0, CRWMS M&O, Las Vegas, Nevada, December, 1992.

4-31. *Total System Performance Assessment - 1995: An Evaluation of the Potential Yucca Mountain Repository*, DI Number: B00000000-01717-2200-00136, Rev. 01, R. W. Andrews, J. E. Atkins, J. O. Duguid, B. E. Dunlap, J. E. Houseworth, L. R. Kennedy, J. H. Lee, S. Lingineni, J. A. McNeish, S. Mishra, M. Reeves, D. C. Sassani, S. D. Sevougian, F. Tsai, V. Vallikat, Q. L. Wang, and Y. Xiang, CRWMS, M&O, Las Vegas, Nevada, November, 1995.

4-32. *Application of the RIP (Repository Integration Program) to the Proposed Repository at Yucca Mountain: Conceptual Model and Input Data Set*, Golder Associates, Redmond, Washington, 1993.

4-33. *Alternative Conceptualizations for WIPP Performance Assessment Modeling*, Golder Associates, Inc., prepared for the WIPP Technical Assistance Contractor (WTAC), DOE., November, 1995.

4-34. *RIP Performance Assessment and Strategy Evaluation Model: Theory Manual and User's Guide, Version 3.20*, Golder Associates, Redmond, WA , 1994.

4-35. *Implementation of the SPM-2 Data Set Within RIP*, Golder Associates, Inc., Draft Report prepared for the WTAC, DOE August 1995.

4-36. *Long-Term Performance Assessment of New York Low-Level Radioactive Waste Disposal Methods*, Golder Associates, Inc., Draft Report prepared for New York State Low-Level Radioactive Waste Siting Commission, 923-D006.003 , June 1995.

4-37. *Verification Report for the Repository Integration Program (RIP)*, Golder Associates, Inc., prepared for the WTAC, DOE, August 1995.

4-38. Miller, I., R. Kossik, and M. Cunnane, "A New Methodology for Repository Site Suitability Evaluation," *Proceedings of the Third International Conference for High Level Radioactive Waste Management*, Las Vegas, Nevada, April 12-16, 1992.

4-39. IOC LV.WP.TLL.07/96-161, "Current WP Designs", from T. L. Lotz to J. K. McCoy, CRWMS M&O, Las Vegas, Nevada, July 5, 1996.

4-40. *Waste Package Design Implications of the Survey of Nonmetalic Barrier Processing*, DI Number: BBA000000-01717-5705-00004 REV 00, CRWMS M&O, Las Vegas, Nevada, July 5, 1994.

4-41. *Mined Geologic Disposal System Advanced Conceptual Design Report*, DI Number: B00000000-01717-5705-00027 REV 00, Volumes I - IV, CRWMS M&O, Las Vegas, Nevada, March 1996.

Chapter 5

None.

Chapter 6

6-1. *Mined Geologic Disposal System Advanced Conceptual Design Report*, DI Number: B00000000-01717-5705-00027 REV 00, Volumes I - IV, CRWMS M&O, Las Vegas, Nevada, March 1996.

6-2. *SAS2H: A Coupled One-Dimensional Depletion and Shielding Analysis Code*, Draft - NUREG/CR-0200, Vol. 1, Sect. S2, Rev. 5, O.W. Hermann and C.V. Parks, ORNL, Oak Ridge, TN, September 1995.

6-3. *MCNP: A General Monte Carlo N-Particle Transport Code, Version 4A*, La-12625-M, J.F. Briesmeister, Ed., Los Alamos, NM, LANL, November 1993.

6-4 *Preliminary Waste Form Characteristics Report, Version 1.0*, R. B. Stout. and H. Leider, UCRL-ID-108314 Rev. 1, Lawerence Livermore National Laboratory, December 1994.

6-5 *Characteristics of Potential Repository Wastes*, DOE/RW-0184-R1, Volume 1, DOE OCRWM, July, 1992.

6-6 *Second Waste Package Probabilistic Criticality Analysis: Generation and Evaluation of Internal Criticality Configurations*, DI Number: BBA000000-01717-2200-00005, Rev. 00, P. Gottlieb and J. Massari, CRWMS M&O, Las Vegas, Nevada, March 1996.

6-7 *Probabilistic External Criticality Evaluation*, DI Number: BB0000000-01717-2200-00037, Rev. 00, P. Gottlieb and J. Massari, CRWMS M&O, Las Vegas, Nevada, May 1996.

6-8 *Initial Waste Package Probabilistic Criticality Analysis: Uncanisterized Fuel*, DI Number: BBA000000-01717-2200-00079, Rev. 01, P. Gottlieb and J. Massari, CRWMS M&O, Las Vegas, Nevada, 1995.

6-9 *Total System Performance Assessment - 1995: An Evaluation of the Potential Yucca Mountain Repository*, DI Number: B00000000-01717-2200-00136, Rev. 01, R. W. Andrews, J. E. Atkins, J. O. Duguid, B. E. Dunlap, J. E. Houseworth, L. R. Kennedy, J. H. Lee, S. Lingineni, J. A. McNeish, S. Mishra, M. Reeves, D. C. Sassani, S. D. Sevougian, F. Tsai, V. Vallikat, Q. L. Wang, and Y. Xiang, CRWMS, M&O, Las Vegas, Nevada, November, 1995.

Chapter 7

None

9.0 LIST OF APPENDICES

The following is a list of the appendices which are the detailed supporting data, technical documents, reports, and studies whose information was used in the technical report [all TBD].

A. Acronyms and Glossary
   - A.1 List of Acronyms and Abbreviations (4 pages)
   - A.2 Glossary of Terms (7 pages)

B. Neutronics Supporting Information
   - B.1 Commercial Reactor Critical Studies (59 pages)
   - B.2 Comparison Between MCNP and Critical Experiments (98 pages)

C. Criticality Scenario Generation
   - C.1 Repository Environment (9 pages)
   - C.2 Waste Package Degradation Mode Analysis (12 pages)
   - C.3 Simple Internal Configuration Bookkeeper (10 pages)
   - C.4 Waste Package Criticality Analyses (4 pages)
   - C.5 Earliest Time to Internal Waste Package Criticality (7 pages)
   - C.6 External Criticality Scenario Generation (3 pages)
   - C.7 Far Field Criticality Analysis (3 pages)
   - C.8 Probability of Assembling a Far Field Critical Mass (9 pages)
   - C.9 References (4 pages)

D. Criticality Event Consequence Analysis Supporting Information
   - D.1 Estimated Power and Duration of an Internal Criticality (4 pages)
   - D.2 Effect of an Internal Criticality on the Radionuclide Inventory of the Waste Package (8 pages)
   - D.3 Not Used (Increase in Radionuclide Inventory from an External Criticality(TBD))
   - D.4 References (1 page)

[Note: The information presented in appendices B, C, and D is preliminary and is provided to illustrate the current status of the methodology. This information will be updated as the methodology is finalized and will be presented in separate technical documents. The topical report will reference these technical documents.]

INTENTIONALLY LEFT BLANK

APPENDIX A

ACRONYMS AND GLOSSARY

INTENTIONALLY LEFT BLANK

Appendix A.1: List of Acronyms and Abbreviations

ACD	Advanced Conceptual Design
ACE	Type of nuclear data library used in the MCNP computer program
Ag	Silver
Am	Americium
ANS	American Nuclear Society
ANSI	American National Standards Institute, Inc.
ARO	All Rods Out
AROCBC	All Rods Out Critical Boron Concentration
ASME	American Society of Mechanical Engineers
ASTM	American Society for Testing and Materials
ATM	Approved Test Material
AUCF	Advanced Uncanistered Fuel waste package design
AVEL	Average lethargy of the neutron causing fission
B	Boron
B&W	Babcock and Wilcox or B&W Fuel Company
BNL	Brookhaven National Laboratory
BOC	Beginning of Cycle
BONAMI-S	Name of a computer program, part of SCALE
BPR	Burnable Poison Rod
BPRA	Burnable Poison Rod Assembly
BWR	Boiling Water Reactor
C	Carbon
°C	Degrees Centigrade
CASMO	Name of a computer program
CDF	Cumulative Distribution Function
CE	Combustion Engineering
CERES	Name of an International Collaborative Program
Cf	Californium
CF	Canistered Fuel
CFR	Code of Federal Regulations
CH	Calico Hills
CHn1v	Calico Hills nonwelded unit 1 vitric
CHn1z	Calico Hills nonwelded unit 1 zeolitized
Cm	Curium
COUPLE-S	Name of a computer program, part of SCALE
CRA	Control Rod Assembly
CRC	Commercial Reactor Critical
CRWMS	Civilian Radioactive Waste Management System
Cs	Cesium
CSAS	Name of a computer program sequence, part of SCALE
DHLW	Defense High-Level Waste
DI	Document Identifier
DOE	U. S. Department of Energy
EBS	Engineered Barrier System or Segment

Appendix A.1: List of Acronyms and Abbreviations

EFPD	Effective Full Power Days
ENDF	Name of a nuclear cross section library set (Evaluated Nuclear Data File)
EOC	End of Cycle
EPA	U. S. Environmental Protection Agency
EPRI	Electric Power Research Institute
EQ3/6	Name of a computer program
ESF	Exploratories Studies Facility
Eu	Europium
Fe	Iron
Fe_nO_m	Iron oxide (n and m numbers)
FEHM	Name of a computer program
FMEA	Failure Modes and Effects Analysis
Gd	Gadolinium
GE	General Electric
GROA	Geologic Repository Operations Area
GWd/MTU	Gigawatt-Day per Metric Ton of Uranium
HFP	Hot Full Power
HLW	High-level Waste
H/X	Water-to-fuel volume ratio
HZP	Hot Zero Power
I	Iodine
I_C	Number of source cycles that are skipped before data accumulation begins in an MCNP calculation
ID	Inside Diameter
IOC	Interoffice Correspondence
ISO-9000	Name of the International Standards Office's Quality Assurance Program
K_d	Sorption (or distribution) coefficient
k_{eff}	Effective neutron multiplication factor
k_∞	Infinite neutron multiplication factor
KENO	Name of a computer program
kW	Kilowatt
LA	License Application
LANL	Los Alamos National Laboratory
LBL	Lawrence Berkeley Laboratory
LLNL	Lawrence Livermore National Laboratory
LWR	Light Water Reactor
MCC	Material Characterization Center
MCNP	Name of a computer program (Monte Carlo N-Particle)
M&O	Management and Operating Contractor
MeV	Million Electron Volts
MGDS	Mined Geologic Disposal System
Mo	Molybdenum
MOX	Mixed Oxide
MPa	Megapascals

Appendix A.1: List of Acronyms and Abbreviations

MPC	Multi-Purpose Canister
MTU	Metric Tons of Uranium
MWd	Megawatt Days
Nd	Neodymium
NEMO	Name of a computer program
NLP	Nevada Site Administrative Line Procedure
NITAWL-S	Name of a computer program, part of SCALE
Np	Neptunium
NQA-1	Nuclear Quality Assurance
NRC	U.S. Nuclear Regulatory Commission
NUREG	Nuclear Regulation
O	Oxygen
OCRWM	Office of Civilian Radioactive Waste Management
OD	Outside Diameter
ORIGEN-S	Name of a computer program, part of SCALE
ORNL	Oak Ridge National Laboratory
Pa	Protactinium
PDF	Probability Density Function
Pm	Promethium
PNL	Pacific Northwest Laboratory
PRA	Probabilistic Risk Analysis
PTn	Paintbrush Tuff Non-welded
Pu	Plutonium
PWR	Pressurized Water Reactor
Q	Quality Affecting (A classification of information)
QA	Quality Assurance
QAP	Quality Administrative Procedure
QARD	Quality Assurance Requirements and Description
R^2	The fraction of the variation explained by the regression
REV	Revision
Rh	Rhodium
RIP	Name of a computer program (Repository Integration Program)
RSIC	Radiation Shielding Information Center
Ru	Ruthenium
RW	Radioactive Waste (referring to DOE/RW)
SAS2H	Name of a computer code sequence, part of SCALE
SCALE	Name of a computer program (Standardized Computer Analysis for Licensing Evaluations)
SIP	Scientific Investigation Plan
SL	Subcritical Limit
Sm	Samarium
SNF	Spent Nuclear Fuel
SNL	Sandia National Laboratories
SRP	Savannah River Plant

Appendix A.1: List of Acronyms and Abbreviations

SRS	Savannah River Site
SS-B	Stainless Steel Boron
S_w	Water saturation in the porespace
t	Time
TBD	To Be Determined
TBR	To Be Resolved
TBV	To Be Verified
Tc	Technetium
TCw	Tiva Canyon welded
TOUGH2	Name of a computer program (Transport of Unsaturated Groundwater and Heat)
TS	Topopah Spring
TSPA	Total System Performance Assessment
VA	Viability Assessment
TSw	Topopah Spring welded
TSw2	Topopah Spring welded unit 2
TSw3	Topopah Spring welded unit 3 (Vitrophyre tuff)
TUFF	Name of a computer program
U	Uranium
U_nO_m	Uranium Oxide (n and m are numbers)
UCF	Uncanistered Fuel
UCRL	University of California Research Laboratory
UNS	Unified Numbering System for Metals and Alloys
USL	Upper Safety Limit
W	Westinghouse
WIPP	Waste Isolation Pilot Plant
WP	Waste Package
WTAL	WIPP Technical Assistance Contractor
wt. %	Weight Percent
Xe	Xenon
XSDRNPM-S	Name of a computer program, part of SCALE
YMP	Yucca Mountain Site Characterization Project
ZAID	Name of a isotope identifier for cross section libraries
α	Reciprocal of the minimum transport time to the accessible environment
β	Bias or the reciprocal of the time duration over which there is a significant probability of criticality occurrence
ϕ	Porosity of the rock
ρ_{bd}	Dry bulk density
τ	Time, primarily as variable of integration ($d\tau$)

Appendix A.2: Glossary of Terms

This glossary contains the meaning of the specialized terms used in the report. The references in square brackets at the end of a definition are the highest level document which contains that definition verbatim.

Accessible environment means: (1) The atmosphere, (2) the land surface, (3) surface water, (4) oceans, and (5) the portion of the lithosphere that is outside the controlled area. [10 CFR 60.2]

Anticipated processes and events are those natural processes and events that are reasonably likely to occur during the period the intended performance objective must be achieved. To the extent reasonable in the light of the geologic record, it shall be assumed that those processes operating in the geologic setting during the Quaternary Period continue to operate, but with the perturbation caused by the presence of emplaced radioactive waste superimposed thereon. [10 CFR 60.2]

As low as is reasonably achievable means making every reasonable effort to maintain exposures to radiation as far below the dose limits in 10 CFR 20 as is practical consistent with the purpose for which the licensed activity is undertaken, taking into account the state of technology, the economics of improvements in relation to state of technology, the economics of improvements in relation to benefits to the public health and safety, and other societal and socioeconomic considerations, and in relation to utilization of nuclear energy and licensed materials in the public interest. [10 CFR 20.1003]

Backfill is a material used to fill the space previously created by excavation or drilling, such as in a shaft or borehole.

Barrier is any material or structure that prevents or substantially delays movement of water or radionuclides. [10 CFR 60.2]

Burnup credit is an approach used in criticality control evaluations which accounts for the reduction in criticality potential associated with spent nuclear fuel relative to that of fresh fuel. Burnup credit reflects the net depletion of fissile material and the creation of neutron absorbing isotopes during the fission reaction. Burnup credit is one of the licensing issues which will be addressed in the Topical Reports submitted to the U.S. Nuclear Regulatory Commission.

Canister is a metal receptacle with the following purpose: (1) for solidified high-level radioactive waste, its purpose is a pour mold, and (2) for spent fuel, it may provide structural support for loose rods, nonfuel components, or confinement of radionuclides during preclosure operations.

Cask is a container for shipping or storing spent nuclear fuel and/or high-level waste that meets all applicable regulatory requirements.

Canistered Fuel Disposal Container, CI BBAAB0000. The Canistered Fuel Disposal Container Subsystem Element includes all items that form a disposal container for a canistered SNF waste form which is a small CF or a large CF. This subsystem element includes the small CF disposal container

component and the large CF disposal container component. The CF disposal container includes but is not limited to multiple containment barriers including multiple closure lids.

Civilian Radioactive Waste Management System is the composite of the sites, and all facilities, systems, equipment, materials, information, activities, and the personnel required to perform those activities necessary to manage radioactive waste disposal.

Cladding is the metal cylinder that surrounds the uranium pellets.

Container is the component of the waste package that is placed around the waste form or the canistered waste form to perform the function of containing radionuclides.

Containment is the confinement of radioactive waste within a designated boundary. [10 CFR 60.2]

Criticality control is the suite of measures taken to maintain nuclear fuel, including spent fuel, in a subcritical condition during storage, transportation and disposal, so that no self-sustaining nuclear chain reaction can occur. Subcriticality is assured by loading spent fuel that meets certain requirements related to fuel age, enrichment, and reduction in nuclear fuel reactivity through burnup.

DHLW Disposal Container, CI BBAAC0000. The Defense High-Level Waste (DHLW) Disposal Container Subsystem Element includes all items which form a disposal container for high-level process waste forms packaged in waste canisters originating from Savannah River, Hanford, Idaho National Engineering Laboratory, West Valley, and any other designated locations supplying process waste for disposal. The DHLW disposal container includes but is not limited to multiple containment barriers including multiple closure lids, and internal structure.

Disposal is the isolation of radioactive wastes from the accessible environment. [10 CFR 60.2] Disposal means the emplacement in a repository of high-level radioactive waste, spent nuclear fuel, or other highly radioactive material with no foreseeable intent of recovery, whether or not such emplacement permits the recovery of such waste. [10 CFR 961.11][NWPA Section 2(9)]

Disposal container is a vessel consisting of the barrier materials and internal components designed to meet disposal requirements, into which the uncanistered or canistered waste form will be placed.

Disposal system is any combination of engineered and natural barriers that isolate spent nuclear fuel or radioactive waste after disposal. [40 CFR 191.12(a)]

Drift is a nearly horizontal mine passageway driven on or parallel to the course of a vein or rock stratum or a small crosscut in a mine.

Emplacement Drift Backfill Materials Subsystem Element includes all backfill materials placed in the waste emplacement drifts as an engineered barrier for the purpose of containing and isolating the waste from the accessible environment. Backfill will be used to retard the migration of

radionuclides from the waste package to the geologic setting. It may also be placed in peaked layers to provide a barrier which prevents water from contacting the waste package.

Emplacement Drift Invert Subsystem Element consists of the material or inverted arch placed at the bottom of the emplacement drift to provide a floor with a flat surface. The Invert includes the invert materials placed in the waste emplacement drifts as an engineered barrier for the purpose of containing and isolating the waste from the accessible environment. The invert will retard the migration of radionuclides from the waste package to the geologic setting.

Engineered Barrier Segment, CI BB0000000. The Engineered Barrier Segment includes the Waste Package Subsystem and the Underground Facility Subsystem. The major components of the Engineered Barrier Segment shall contribute to the assigned function, Isolate Waste, by containing waste in the waste packages during the prescribed containment period, and then by limiting the release of radionuclides during the post-containment period.

The Waste Package Subsystem includes the uncanistered fuel, canistered fuel, and defense high-level waste disposal containers, filler materials, shielding, packing and absorbent materials, and waste package support subsystem elements. The Underground Facility Subsystem includes the emplacement drift openings, emplacement drift backfill materials, and emplacement drift invert subsystem elements.

Engineered barrier system (EBS) is the waste packages and the underground facility. [10 CFR 60.2]

EBS Near-Field. For purposes of disposal criticality analyses the EBS near-field encompasses the underground facility (the Engineered Barrier System excluding the waste package). The near-field is considered to extend approximately 2 meter into the rock surrounding all the emplacement drifts.

Far-Field. For purposes of disposal criticality analyses the far-field is considered as all areas starting from outside the near vicinity of the emplacement drifts (the near-field), out to the accessible environment.

Filler Materials, CI BBAAD0000. The Filler Materials Subsystem Element includes all filler materials used to fill the free space remaining in disposal containers after loading the high-level nuclear waste. Filler materials may used for neutron absorption, moderator displacement, chemical buffering, or radionuclide retardation. The most likely application would be the addition of filler material to selected SNF waste package disposal containers, i.e., UCF, CF, or dual purpose canisters, for the purpose of moderator displacement to aid in criticality control. Filler material may also be added to DHLW waste package disposal containers. Filler materials, if used, will be added to the waste packages disposal containers only at the repository.

Geologic repository is a system which is intended to be used for, or may be used for, the disposal of radioactive wastes in excavated geologic media. A geologic repository includes (1) the geologic

repository operations area, and (2) the portion of the geologic setting that provides isolation of the radioactive waste. [10 CFR 60.2]

Geologic repository operations area (GROA) is a high-level radioactive waste facility that is part of a geologic repository, including both surface and subsurface areas, where waste handling activities are conducted. [10 CFR 60.2]

High-level radioactive waste (HLW) means (1) the highly radioactive material resulting from the reprocessing of spent nuclear fuel, including liquid waste produced directly in reprocessing and any solid material derived from such liquid waste that contains fission products in sufficient concentrations; and (2) other highly radioactive material that the Nuclear Regulatory Commission, consistent with existing law, determines by rule requires permanent isolation. The CRWMS will only accept solidified HLW. For the purposes of this document, HLW is vitrified borosilicate glass cast in a stainless steel canister. [NWPA Section 2(12)] [10 CFR 72.3] [10 CFR 960.2] [10 CFR 961.11] [MGDS-RD]

(Items) Important to Waste Isolation means the natural and engineered barriers that are relied on for achieving the postclosure performance objectives in 10 CFR 60 Subpart E.

Institutional Barrier System consists of the active and passive institutional controls.

Active institutional controls include (1) controlling access to the MGDS by any means other than passive institutional controls, (2) performing maintenance operations or remedial actions at a site, (3) controlling or cleaning up releases from a site, or (4) Monitoring parameters related to disposal system performance.

Passive institutional controls include (1) permanent markers placed at a disposal site, (2) public records and archives, (3) government ownership and regulations regarding land or resource use, and (4) other means of preserving knowledge about the location, design, and contents of a disposal system. (TBR) [40 CFR 191.02]

Isolation is inhibiting the transport of radioactive material so that amounts and concentrations of this material entering the accessible environment will be kept within prescribed limits. [10 CFR 60.2]

k_{eff} is the effective neutron multiplication factor for a system. It is a measure of the reactivity or criticality potential of a system.

k_{∞} is the infinite neutron multiplication factor.

Multi-purpose canister refers to a sealed, metallic container maintaining multiple spent nuclear fuel assemblies in a dry, inert environment and overpacked separately and uniquely for the various system elements of storage, transportation, and disposal. (See definition of waste form.)

Off-normal are abnormal or unplanned events or conditions that adversely affect, potentially affect, or are indicative of degradation in, the safety, security, environmental or health protection performance or operation of a facility.

Package means the packaging together with its radioactive contents as presented for transport. [10 CFR 71.4]

Packaging means the assembly of components necessary to ensure compliance with the packaging requirements of 10 CFR 71. It may consist of one or more receptacles, absorbent materials, spacing structures, thermal insulation, radiation shielding, and devices for cooling or absorbing mechanical shocks. The vehicle, tie-down system, and auxiliary equipment may be designated as part of the packaging. [10 CFR 71.4]

Packing and Absorbent Materials, CI BBAD00000. The Packing and Absorbent Materials Subsystem Element includes any items or materials immediately surrounding an individual waste container that inhibit the release of radionuclides to the accessible environment.

Performance assessment means any analysis that predicts the behavior of a system or a component of a system under a given set of constant or transient conditions.

Permanent closure is final backfilling of the underground facility and the sealing of shafts and boreholes. [10 CFR 60.2]

Postclosure means the period of time after the permanent closure of the geologic repository.

Preclosure means the period of time before and during the permanent closure of the geologic repository.

Radioactive waste or waste is HLW and other radioactive materials other than HLW that are received for emplacement in a geologic repository. [10 CFR 60.2]

Repository is any system licensed by the Commission that is intended to be used for, or may be used for, the permanent deep geologic disposal of high-level radioactive waste and spent nuclear fuel, whether or not such system is designed to permit the recovery, for a limited period during initial operation, of any materials placed in such system. Such term includes both surface and subsurface areas at which high-level radioactive waste and spent nuclear fuel handling activities are conducted. [NWPA]

Retrieval is the act of intentionally removing radioactive waste from the underground location at which the waste had been previously emplaced for disposal. [10 CFR 60.2]

Shielding, CI BBAC00000. The Shielding Subsystem Element includes any material that provides radiation protection, beyond the limited shielding inherently provided by the disposal container, which will be disposed of as part of the waste package. This configuration item excludes any

shielding that is not an integral part of the waste package (i.e., overpacks necessary for transport or for use within containment buildings where waste containers are handled or stored).

Spent nuclear fuel (SNF) is fuel which has been withdrawn from a nuclear reactor following irradiation, the constituent elements of which have not separated by reprocessing. [Specifically in this document, SNF includes (1) intact, non-defective fuel assemblies; (2) failed fuel assemblies in canisters; (3) fuel assemblies in canisters; (4) consolidated fuel rods in canisters; (5) non-fuel assembly hardware inserted in PWR fuel assemblies, including, but not limited to, control rod assemblies, burnable poison assemblies, thimble plug assemblies, neutron source assemblies, instrumentation assemblies; (6) fuel channels attached to boiling water reactor fuel assemblies; and (7) non-fuel assembly hardware and structural parts of assemblies resulting from consolidation in canisters.] [NWPA Section 2(23)][10 CFR 961.11]

Subcritical Limit is the value that the calculated k_{eff} for a system/configuration of fissile material must be shown to be below to be considered subcritical. The subcritical limit is dependant upon the computer system being used to calculate k_{eff}, the configuration being evaluated, and the regulatory margins specified for the application.

Unanticipated processes and events mean those processes and events affecting the geologic setting that are judged not to be reasonably likely to occur during the period the intended performance objective must be achieved, but which are nevertheless sufficiently credible to warrant consideration. Unanticipated processes and events may be either natural processes or events or processes and events initiated by human activities other than those activities licensed under this part. Processes and events may be either natural processes or events or processes and events initiated by human activities other than those activities licensed under this part. Processes and events initiated by human activities may only be found to be sufficiently credible to warrant consideration if it is assumed that (1) the monuments provided by this part are sufficiently permanent to serve their intended purpose; (2) the value to future generations of potential resources within the site can be assessed adequately under the applicable provisions of this part; (3) an understanding of the nature of radioactivity, and an appreciation of its hazards, have been retained in some functioning institutions; (4) institutions are able to assess risk and to take remedial action at a level of social organization and technological competence equivalent to, or superior to, that which was applied in initiating the processes or events concerned; and (5) relevant records are preserved, and remain accessible, for several hundred years after permanent closure. [10 CFR 60.2]

UCF Disposal Container with Basket, CI BBAAA0000. The Uncanistered Fuel (UCF) Disposal Container with Basket Subsystem Element is a disposal container containing a fuel basket. The UCF disposal container is employed only at the repository for the disposal of uncanistered (bare) commercial PWR and BWR spent nuclear fuel assemblies. Such assemblies would originate from either SNF sent to the repository in bare fuel transportation casks, or the contents of any dual purpose canisters which are determined to be unsuitable for disposal. The UCF disposal container includes but is not limited to multiple containment barriers including multiple closure lids, basket members, optional neutron absorber material, optional thermal shunts, and internal supports for the basket. The containment barriers consist of corrosion-allowance and/or corrosion-resistant materials.

Criticality control alternatives include but are not limited to neutron absorber material alloyed with the basket material, addition of neutron absorbing panels or control rods, and/or addition of filler material for moderator displacement to aid in criticality control.

Underground facility is the underground structure, including openings and backfill materials, but excluding shafts, boreholes, and their seals. [10 CFR 60.2]

Underground Facility, CI BBD000000. The Underground Facility Subsystem is that portion of the Engineered Barrier Segment that has been allocated the primary function of limiting radionuclide transport.

The Underground Facility Subsystem includes the following Subsystem Elements: Emplacement Drift Openings, Emplacement Drift Backfill Materials, and Emplacement Drift Invert.

Unrestricted area means any area, access to which is not controlled by the licensee for purposes of protection of individuals from exposure to radiation and radioactive materials, and any area used for residential quarters.

Waste container is a sealed disposal container with the uncanistered or canistered waste form (and possibly filler material) placed therein.

Waste form is the radioactive waste materials and any encapsulating or stabilizing matrix. [10 CFR 60.2] A loaded multi-purpose canister is a canistered waste form. [MGDS-RD]

Waste package means the waste form and any containers, shielding, packing and other absorbent materials immediately surrounding an individual waste container. [10 CFR 60.2]

Waste Package, CI BBA000000. The Waste Package Subsystem includes any waste form containers, shielding, and packing and absorbent materials immediately surrounding an individual disposal container. The multibarrier disposal containers will be used for geologic disposal of high-level radioactive waste forms, limited to intact irradiated reactor fuel assemblies from pressurized water reactors, boiling water reactors, and vitrified glass or other solid process high-level waste forms in canisters. The multibarrier disposal containers will consist of multiple layers of corrosion-allowance and/or corrosion-resistant materials.

The Waste Package Subsystem includes the following Subsystem Elements: UCF Disposal Container and Basket, Canistered Fuel Disposal Container, DHLW Disposal Container, Filler Materials, Shielding, Packing and Absorbent Materials, and Waste Package Support.

Waste Package Support, CI BBAB00000. The Waste Package Support Subsystem Element includes the components necessary to support and stabilize the waste container when emplaced in the repository. These components are those items which (1) are in immediate contact with the emplaced disposal container (or shield, if included), and (2) will remain permanently emplaced in the drift with the waste package. The items in this subsystem include but are not limited to cradles

used to support the disposal container/shield and any associated items to restrain movement of the disposal container/shield.

APPENDIX B

Neutronics Supporting Information

INTENTIONALLY LEFT BLANK

APPENDIX B.1

Commercial Reactor Critical Studies

INTENTIONALLY LEFT BLANK

Table of Contents

[The information presented in this appendix is preliminary and should not be used for direct support of any procurement, fabrication, or construction activities.]

1. Introduction

The validation of criticality analyses performed on configurations containing spent nuclear fuel (SNF) requires both a validation of the SNF composition calculations and a validation of the relevant criticality calculations. This paper presents an overview of the methodology development for calculating SNF compositions and integral reactivity worth for actual commercial light-water reactor configurations at intra-cycle statepoints. The methodology and results presented in this paper are applicable to calculations performed using a combination of the Modular Code System for Performing Standardized Computer Analyses for Licensing Evaluation (SCALE) (Ref. 10.1) and the Monte-Carlo N-Particle Transport Code System (MCNP) (Ref. 10.2).

In the commercial reactor critical (CRC) evaluations, the SAS2H control module of the SCALE modular code system is used to perform fuel depletion and decay calculations to obtain spent fuel isotopic compositions. The MCNP code system is then used to perform criticality calculations on configurations containing the SCALE-generated SNF isotopic compositions. The CRC results obtained by utilizing the methodology presented in this paper define a basis for the validation of both the SNF isotopic composition calculations and the MCNP criticality calculations for systems containing SNF.

The SAS2H/MCNP critical multiplication factor (k_{eff}) results for the CRCs are compared to the k_{eff} results for equivalent core-follow calculations performed using the CASMO/NEMO codes of Framatome Cogema Fuels. The fuel temperature, moderator specific volume, and burnup data utilized in producing the SAS2H and MCNP calculational models were obtained from the CASMO/NEMO core-follow calculations. A comparison between SAS2H/MCNP and CASMO/NEMO serves to demonstrate the performance of the SAS2H/MCNP combination in predicting SNF compositions and reactivity worth.

The CRC evaluations summarized in this paper were performed for both single-node and multi-node axial representations of the reactor cores. The multi-node axial representation of the core was composed of 18 axial nodes. Additionally, criticality calculations were performed using fuel isotopic sets of various size. The fuel isotopic set variations ranged from 84 isotopes containing actinides and fission products to 10 isotopes containing only actinides. The sensitivity in integral reactivity worth with respect to axial parameter variations and fuel isotopic compositions provide insight into the potential for developing a simplified criticality calculational methodology for SNF that retains conservatism without sacrificing realism.

2. Applicability

All information presented in this study is preliminary and shall be treated as unqualified. This information will require subsequent qualification. This paper does not directly support any construction, fabrication, or procurement activity. Any data from this study used for input into documents supporting construction, fabrication, or procurement must be documented and

controlled in accordance with the appropriate Quality Assurance Requirements and Description (QARD) (Ref. 10.3) controls.

3. Computer Software

The calculation of SNF isotopic compositions and their associated integral reactivity worth is performed using a combination of the SCALE and MCNP code systems. The SAS2H control module of the SCALE modular code system is used to perform the fuel depletion and decay calculations for a commercial light-water reactor configuration at a specified intra-cycle statepoint to obtain the SNF isotopic composition data for use in a subsequent MCNP criticality calculation.

The SCALE 4.3 code system (Ref. 10.1) obtained from the Radiation Shielding Information Center (RSIC) was utilized in the analyses contained within this paper. SCALE 4.3 is produced and maintained by Oak Ridge National Laboratory.

The MCNP 4A code system (Ref. 10.2) obtained from RSIC was utilized in the analyses contained within this paper. MCNP 4A is produced and maintained by Los Alamos National Laboratory.

The SCALE 4.3 and MCNP 4A calculations pertaining to this study were performed on Hewlett Packard Apollo 9000, Series 735 Workstations.

3.1 SCALE 4.3

The SCALE system was developed for the Nuclear Regulatory Commission to satisfy a need for a standardized method of analysis for the evaluation of nuclear fuel facility and package designs. In its present form, the system has the capability to perform criticality, shielding, and heat transfer analyses using well-established functional modules tailored to the SCALE system. Spent fuel characteristics for these analyses can be obtained from a module that performs a depletion calculation. (Ref. 10.1, pg. iii)

The SCALE system consists of analytical sequences which are automated to perform the necessary data processing and manipulation of well-established computer codes required by the sequence. The user is able to select an analytical sequence characterized by the type of analysis (criticality, shielding, or heat transfer) to be performed and the geometric complexity of the system being analyzed. The user then prepares a single set of input for the control module corresponding to this analytical sequence. The control module input is in terms of easily visualized engineering parameters specified in a simplified, free-form format. The control modules use this information to derive additional parameters and prepare the input for each of the functional modules in the analytical sequence. (Ref. 10.1, pgs. iii-iv)

3.1.1 SAS2H

The description of the SAS2H control module and the associated calculational modules presented in this paper is a summary of the discussion presented in the SCALE 4.3 users manual (Ref. 10.1).

In the CRC analysis procedure, the SAS2H control module of the SCALE modular code system is used to perform a sequence of fuel depletion and decay calculations required to obtain spent fuel isotopic compositions. The objectives of SAS2H with respect to CRC analyses include the following--

1) predict spent fuel characteristics for spent fuel assemblies having a specified reactor history;
2) apply standard analytical models that represent the physics of the system being analyzed (within the 1-D transport limits of the problem);
3) apply acceptable and documented data bases that can be updated in the future;
4) automate the use of known methods of calculating some of the input parameters and the selection of appropriate control options for the various codes applied in the analysis.

SAS2H calculates the time-dependent fuel composition of a reactor fuel assembly by sequencing five independently tasked calculational modules of the SCALE code system. The sequence implemented by SAS2H results in an iterative burnup calculational procedure in which two separate lattice-cell calculations are performed for each iteration to determine the appropriate neutron spectrum and associated nuclide cross-sections. At specified times during the burnup, the cross-sections are updated using resonance processing codes and 1-D transport analyses. These updated cross-sections are used in point depletion calculations that produce the time-dependent fuel compositions required for the next cross-section update. This procedure is repeated numerous times over the operating history of the reactor to obtain the desired burnup of the fuel composition.

The 1-D transport analyses required to obtain the relevant neutron flux distribution necessary for cross-section weighting is performed on two separate lattice-cells to approximate 2-D effects that are introduced in fuel assemblies containing guide tubes and burnable poison rods (BPRs). A general description of the two-part neutron flux distribution calculation is provided in Section 3.1.4. The axial variation in the neutron flux is not considered in the SAS2H sequence. A multi-dimensional representation of the fuel assembly must be incorporated to account for axial variations in the neutron flux. To account for axial variations in the neutron flux, the CRC analyses incorporate an 18 axial node model in which a separate SAS2H sequence calculation is performed for each node of each assembly in a symmetric one-eighth core geometric configuration.

The SAS2H control module reads a set of well defined user input. The user input is converted by the SAS2H control module into the data required by each calculational module to perform the necessary calculations relevant to fuel depletion and decay. The basic user input required by the SAS2H control sequence includes the following--

1) the material zone dimensions of the fuel-pin cell and the larger unit cell representation of the fuel assembly used to incorporate 2-D effects;
2) the material densities of the fresh fuel assembly;
3) the material temperatures;
4) the specific power, exposure time and shutdown time of the fuel assembly in each appropriate cycle of the reactor history;
5) the various control parameters used to select libraries, the optional parameters preferred over the defaults for each calculational module, the level of output printout, and the modifications to the transport computations (e.g. the fineness of mesh intervals or the problem convergence criteria).

The SCALE system driver invokes the execution of the various calculational modules in the SAS2H control sequence and returns control to the SAS2H sequence. The pertinent results obtained from a calculational module are processed by SAS2H and used to generate the input data for subsequent calculational modules. Passes through the functional modules are repeated until the case in completed.

3.1.2 Overview of Calculational Modules

The SAS2H control sequence accesses five calculational modules of the SCALE code system for performing fuel depletion and decay calculations. The five calculational modules include BONAMI, NITAWL-II, XSDRNPM, COUPLE, and ORIGEN-S. Each of the calculational modules have a specific purpose in the sequence to perform the fuel depletion and decay calculations.

The BONAMI calculational module applies the Bondarenko method of resonance self-shielding to nuclides for which Bondarenko data is available.

The NITAWL-II calculational module performs Nordheim resonance self-shielding corrections for nuclides that have resonance parameter data available.

The XSDRNPM calculational module performs a 1-D neutron transport calculation on a specified geometry to facilitate production of cell-weighted cross-sections for fuel depletion calculations.

The COUPLE calculational module updates all cross-section constants included on an ORIGEN-S nuclear data library with data from the cell-weighted cross-section library obtained from the XSDRNPM calculation. Additionally, the weighting spectrum produced by XSDRNPM is applied to update all nuclides in the ORIGEN-S library which were not included in the XSDRNPM calculation.

The ORIGEN-S calculational module performs a zero dimensional nuclide generation and depletion calculation for a specified reactor fuel history. A decay calculation is also performed by ORIGEN-S for prescribed downtimes during the reactor history.

3.1.3 General Description of Method

The method applied by SAS2H starts with the data describing a fuel assembly or node of a fuel assembly as it is initially loaded into a particular reactor. The composition, temperatures, geometry, and time-dependent specific power of the fuel assembly are required inputs to SAS2H. For each time-dependent fuel composition, the new SAS2H sequence performs a 1-D neutron transport analysis using XSDRNPM and a two-part procedure incorporating two separate lattice-cell models. The first model is a unit fuel-pin cell from which cell-weighted cross-sections are obtained. The second model represents a larger unit cell within an infinite lattice. The material zones of the larger unit cell can be structured for different types of light-water reactor fuel assemblies containing water holes, burnable absorber rods, gadolinium fuel rods, etc. Problem-dependent resonance self-shielding of the cross-sections is performed using the BONAMI and NITAWL-II calculational modules. (Ref. 10.1, pg. S2.2.2)

The neutron flux spectrum obtained from the larger unit cell model is used to determine the appropriate nuclide cross-sections for the specified burnup-dependent fuel composition. The cross-sections derived from a transport analysis at each time step are used in an ORIGEN-S point-depletion calculation that produces the burnup-dependent fuel compositions to be used in the next spectrum calculation. This sequence is repeated over the prescribed operating history of the reactor. Ultimately, the nuclide inventory (actinides, fission products, and light elements) is computed at the burnup corresponding to the discharge of the assembly from the reactor. The buildup and decay of the nuclides in the fuel assembly are computed by ORIGEN-S for the downtimes relevant to reactor operation. For the CRC analyses, the ORIGEN-S buildup and decay calculations are performed for both the downtimes between cycles of insertion for an assembly and the downtime prior to the intra-cycle restart statepoint. (Ref. 10.1, pg. S2.2.2)

3.1.4 Preparation of Fuel Cross-Sections

The preparation of fuel cross-sections employs a two-part calculational procedure that utilizes two separate 1-D neutron transport calculations performed on different models to account for 2-D variations in fuel assembly design. The calculational flow path invoked by SAS2H is illustrated in Figure 3.1.4-1 (Ref. 10.1, pg. S2.2.4).

Figure 3.1.4-1 Calculational Flow Path Invoked by SAS2H

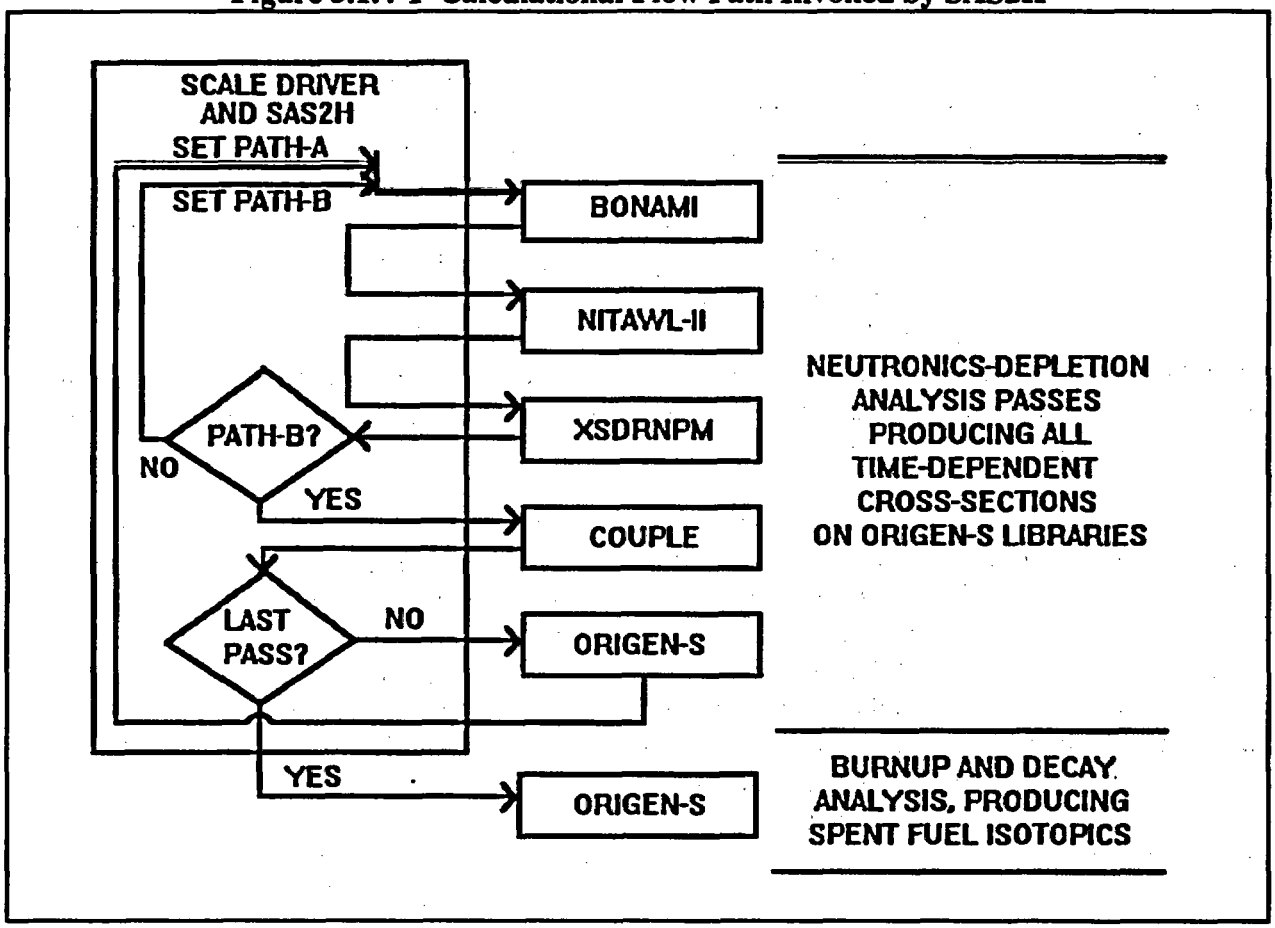

The upper part of Figure 3.1.4-1 shows the flow path for the neutronics-depletion analysis "passes" that create a cross-section library at specified burnup intervals. First, in path A, BONAMI, NITAWL-II, and XSDRNPM are invoked to produce the cell-weighted cross-sections of the fuel zone. The second return to the driver for path B of the reactor pass invokes all five calculational modules. The compositions for the first reactor pass are simply the nuclide mixtures of the new, or freshly loaded, fuel assembly. After completion of the path A and path B computations, execution continues with COUPLE updating an ORIGEN-S working library with data on the XSDRNPM weighted working library. The ORIGEN-S calculational module is invoked to compute the time-dependent densities of the nuclides in the fuel and burnable poison for the specified power and exposure times. SAS2H is then invoked for the next control function in the sequence.

The path A and path B models both utilize the same calculational modules (BONAMI, NITAWL-II, and XSDRNPM), but the models themselves are quite different. The path A model is simply a one-dimensional representation of an assembly unit cell containing a fuel rod. The fuel rod is modeled explicitly with the square unit cell perimeter converted to a circular perimeter maintaining the same total unit cell area. A reflective boundary condition is applied to the perimeter of the path A unit cell to simulate an infinite array of unit cells. The resonance self-shielding calculations and a 1-D neutron transport calculation are then performed on the path A model to obtain the neutron flux and cell-weighted cross-sections for the fuel region. The cell-

weighted cross-sections from the path A model are then applied to the fuel region in the path B model.

The path B model is a larger unit cell representation of all or part of the fuel assembly in an infinite lattice. The path B model is used to calculate an "assembly-averaged" fuel region flux that considers the effects due to the path A model, the assembly lattice locations containing different types of rods or water holes, and the moderator present in assembly-to-assembly spacings. The use of cell-weighted cross-sections from the path A model in the 1-D neutron transport calculation of the path B model is an approximate method for simulating 2-D effects present in fuel assemblies containing guide tubes and burnable poison rods. An example of a typical path B larger unit cell model for a PWR assembly containing guide tubes is presented in Figure 3.1.4-2.

Figure 3.1.4-2 Typical Path B Model for PWR Control Rod Assembly

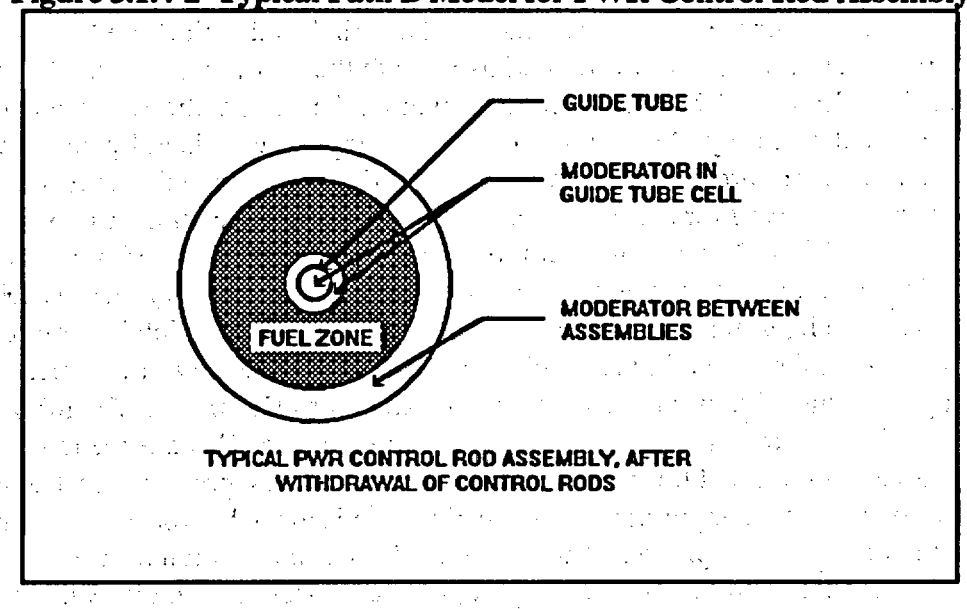

The essential rule in deriving the zone radii is to maintain the relative volumes for all zones in the actual assembly. The central region of the larger cell can be modeled as an assembly guide tube, a burnable poison rod containing no fuel, an orifice rod, an axial peaking rod, a fuel rod containing a burnable poison, or almost any other pin-cell type rod. The moderator of the central region in the path B model is the moderator associated with the assembly unit cell modeled in the central region. A fuel region surrounds the central unit cell moderator. The radius of the fuel region is determined such that the volume ratio of fuel to moderator in the assembly is maintained in the path B model. The region surrounding the fuel in the path B model may be composed of assembly housing material (for BWRs) or moderator between assemblies by conserving volumes. Fuel assemblies which are radically non-symmetric (i.e. not all of the guide tubes contain burnable poison rods) may be modeled by conserving material mass rather than volume. The assembly spacer grids and other hardware are typically ignored due to their limited effect on the neutron flux and associated energy spectrum.

There are certain approximations made in developing the path B model. Two important approximations relevant to CRC analyses include--

1) the path B model assumes that the spacings of the non-fuel pin-cell locations are equidistantly spaced;
2) the path B model allows placement of the assembly-to-assembly moderator around the fuel region even though the path B model may only represent a portion of the entire fuel assembly.

The significance of these approximations appear to be less for the path B larger unit cell than if the additional zones representing the guide tubes or burnable poison rods were placed directly around the fuel rod unit cell (path A model).

The isotopic compositions for the various materials in the path A and path B models are prepared by the Material Information Processor of SCALE using both the user input and the SCALE Standard Composition Library. The user is required to input the compositions of the materials as defined in the fresh fuel assembly. Materials in the SAS2H input are defined by mixture numbers. The first three mixture numbers are reserved for the materials in the path A model. Mixture number one is reserved for the fresh fuel composition. Mixture number two is reserved for the cladding composition. Mixture number three is reserved for the borated moderator composition. Additional mixture numbers may then be defined to represent other materials (i.e. burnable absorber). The input mixtures define the "input mixing table" which is composed of the nuclide identification number, the mixture number, and the number density of the nuclide in the mixture. The input mixing table is combined with trace amounts (1E-20 atoms/b-cm) of nuclides present in the specified neutron cross-section library used in the SAS2H sequence to produce a "master mixing table". Additional trace amounts of selected nuclides, presented in Table 3.1.4-1, are also included to ensure that appropriate cross-section data is available for important nuclides that build up in the fuel during depletion. The user may also define additional trace nuclides in mixture one of the SAS2H input to ensure that appropriate cross-section data is available.

Table 3.1.4-1 Selected Nuclides Automatically Added by SAS2H for Neutronics Processing

Xe-135	Cs-133	U-234	U-235
U-236	U-238	Np-237	Pu-238
Pu-239	Pu-240	Pu-241	Pu-242
Am-241	Am-242m	Am-243	Cm-242
Cm-243	Cm-244	1/v-absorbers	

After the neutronics code interfaces are completed, SAS2H generates interface files for codes that couple burnup-dependent densities into the model for producing time-dependent cross-sections. First, an interface data set is produced for COUPLE, which updates cross-section constants on libraries input to ORIGEN-S. Finally, an input data set for ORIGEN-S is developed to execute a depletion case in which computed densities of the fuel are saved in a data set at prescribed time intervals.

3.1.5 Time-Dependent Depletion and Decay Calculation

During the irradiation of fuel in a reactor, nuclide densities vary as a function of the neutron flux and its associated energy spectrum. SAS2H performs the neutronics depletion calculations previously described in Section 3.1.4 at a number of irradiation intervals to account for the variations in neutron flux and its associated energy spectrum that effect the fuel isotopic composition as a function of time. The irradiation intervals defined by the user are called "passes". The SAS2H sequence performs a number of passes prescribed by the user to adequately simulate the reactor history so that the resulting fuel isotopic composition for the assembly or node of the assembly may be determined. Referring to Figure 3.1.4-1, each pass through the procedure involves the following five steps--

1) preparation of new data interfaces by SAS2H;
2) return of control to the SCALE driver for execution of the three codes required in the path A model;
3) preparation of the data interfaces for the path B model by SAS2H;
4) return of control to the SCALE driver for execution of the five codes required in the path B model;
5) return to SAS2H.

The user inputs the number of irradiation steps requested, the number of cross-section libraries to make per step, the specific power of the assembly or assembly node at each step, the total operation time (calendar days) of each step, and the downtime following each step. The irradiation steps are determined based on the reactor history and the detail required by the user. A single irradiation step or multiple irradiation steps may be specified to represent each reactor cycle. The irradiation-time associated with each cross-section library is derived from the input.

The moderator density does not change from the initial material specification (mixture 3) unless requested by the user. The soluble boron fraction in the moderator varies with reactor operation time. To account for this the SAS2H sequence applies a default linear interpolation that specifies a boron concentration in the initial irradiation step which is 1.9 times the boron concentration specified on the mixture 3 material specification card. The boron concentration in the final irradiation step is 0.1 times the mixture 3 specified concentration. As an alternative to the default linear boron letdown scheme the user may specify a fraction of the mixture 3 boron concentration for each irradiation step in the depletion calculation. The boron concentration does not change as a function of time over each irradiation step. The specified boron concentration at each irradiation step should be the average boron concentration over the duration of the irradiation

step. The CRC analyses employ the method of specifying boron fractions at each irradiation step so that the actual boron letdown curves for the reactor may be followed more accurately.

With the exception of the fresh fuel library, each cross-section library is based on the number densities obtained for the midpoint of the irradiation-time interval. The midpoint number densities for an irradiation interval are computed from an ORIGEN-S case that uses the cross-section library from the previous irradiation interval. This procedure is graphically illustrated in Figure 3.1.5-1 for a two-step case where two libraries are requested per step. (Ref. 10.1, pg. S2.2.8)

Figure 3.1.5-1 Schematic of Successive ORIGEN-S Cases Used to Produce the Burnup-Dependent Number Densities

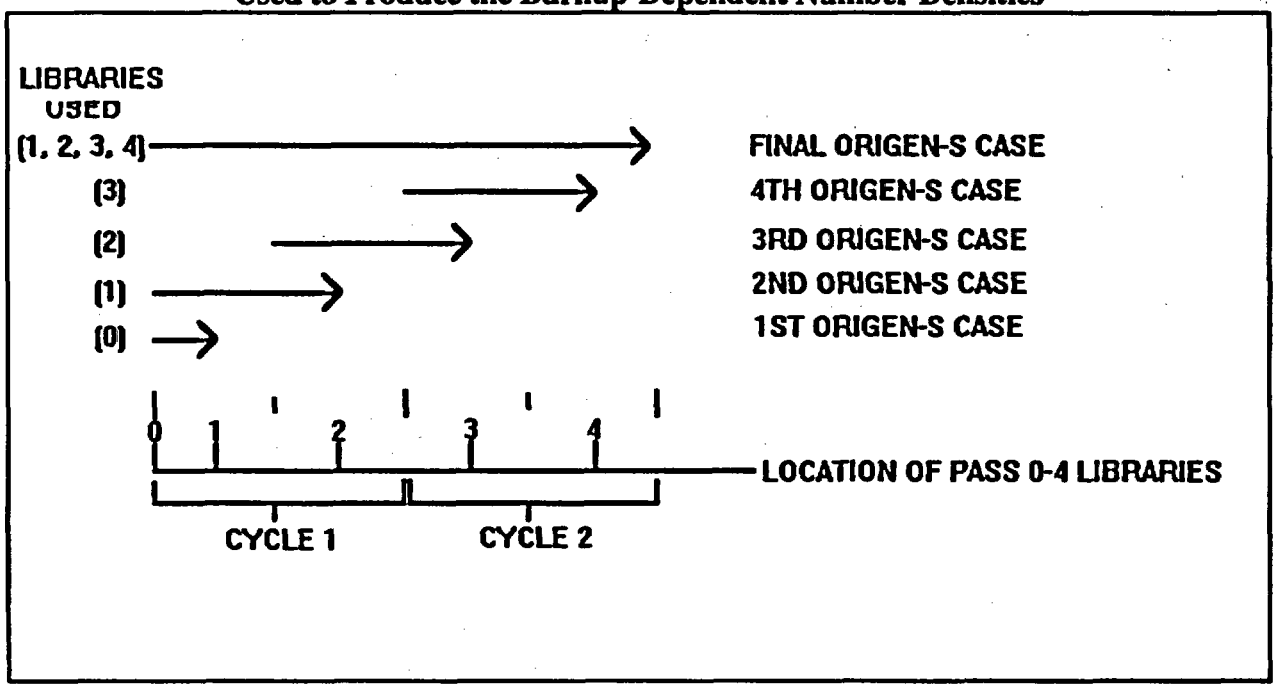

In reference to Figure 3.1.5-1, the first step is to produce the "PASS 0" library prepared using the fresh-fuel isotopics. This initial library is used in the first ORIGEN-S case to generate number densities at the midpoint of the first irradiation interval. Next, the SAS2H module--

1) computes density-dependent parameters for the resonance calculations;
2) increments the required data set unit numbers;
3) adds "PASS 1" to the ORIGEN-S library title;
4) updates the ORIGEN-S input for the second case to save number densities for the starting point and the midpoint of the second irradiation interval;
5) rewrites all code interfaces using the new data.

Then the "PASS 1" library is produced by invoking execution of the five codes in both path A and path B a second time with the new input interfaces. Each additional pass applies the same procedure as used for "PASS 1". The midpoint densities are applied to the neutronics analysis to produce a new library. The depletion computation applies this library and the densities calculated for the start of the pass. A decay computation with zero power is applied for reactor downtime, if specified for the end of a cycle, before deriving densities for the next pass. All ORIGEN-S libraries are saved, starting with the "PASS 1" library. The last pass is the only one in which there is a major difference in the procedure. After the completion of COUPLE in the final pass, the required libraries have been produced. The final ORIGEN-S case corresponding to the last pass uses all the libraries and runs through the entire reactor history input to the SAS2H module. All the cross-section libraries produced during all previous passes are combined into the final multi-burnup-dependent ORIGEN-S binary library made for the case.

The final ORIGEN-S case utilizes all previously determined cross-section libraries for each step to deplete the fuel from its fresh fuel state to its discharge state. The final ORIGEN-S case includes all nuclides (over 1600) in the ORIGEN-S binary library. Cross-section constants are either updated directly from previous XSDRNPM output, or for those nuclides not included in the pin-cell analysis, from broad-group flux weight factors.

In the example shown in Figure 3.1.5-1, the final ORIGEN-S case begins with the nuclide generation and depletion calculation performed using the cross-section library, power, and time interval for "PASS 1". Four equal-size time steps are used during the irradiation time, followed by a single downtime interval. If no downtime was specified, a zero-time interval is applied. Next, a similar computation is performed using the compositions determined at the end of the "PASS 1" calculation and the cross-section data on the "PASS 2" library. The analysis proceeds with each succeeding library and corresponding assembly power and time interval. Ultimately, the discharge composition of the fuel assembly is determined. Finally, a decay-only subcase using six equal-size time steps is performed for the final requested downtime.

3.1.6 SAS2H Results Relative to CRC Analyses

The number densities for the heavy nuclides of the fuel, together with their activation products and fission products, are all computed by ORIGEN-S. In addition, ORIGEN-S calculates the depletion of most light elements, including the burnable poisons (boron, gadolinium, and cadmium), and most isotopes of the specified structural materials. However, the densities of alloys or elements in the clad, moderator, or structural materials, and oxygen in the fuel remain constant. (Ref. 10.1, pg. S2.2.9)

The fuel and burnable poison isotopic compositions are extracted from the final ORIGEN-S output for use in a subsequent MCNP criticality calculation. The fuel and burnable poison compositions are provided from ORIGEN-S in grams per assembly and must be converted to atoms/b-cm based on the MCNP normalization which is based on the actual fuel volume in the assembly.

3.2 MCNP Code System

The Monte Carlo N-Particle Transport Code System (MCNP), Version 4A (Ref. 10.2) is used in this study. The MCNP 4A criticality calculations documented in this study were performed on Hewlett Packard Apollo 9000, Series 735 Workstations. An associated continuous energy cross-section set based on ENDF/B-V is used by MCNP. This library provides much more detail than multi-group cross-section sets.

The MCNP 4A code system is appropriate for the application of determining the k_{eff} values of configurations or systems containing fissionable material. This study provides supplementary evidential support for the validation of MCNP 4A as an appropriate tool to be utilized in k_{eff} calculations.

3.2.1 MCNP General Description

A full description of the MCNP 4A computer code is provided in the MCNP user manual. The following excerpts will provide a general description.

> "MCNP is a general-purpose Monte Carlo N-Particle code that can be used for neutron, photon, electron, or coupled neutron/photon/electron transport, including the capability to calculate eigenvalues for critical systems. The code treats arbitrary three-dimensional configurations of materials in geometric cells bounded by first-degree and second-degree surfaces and fourth-degree elliptical tori."
>
> "Pointwise cross-section data are used. For neutrons, all reactions given in a particular cross-section evaluation (such as ENDF/B-V) are accounted for. Thermal neutrons are described by both the free gas and $S(\alpha,\beta)$ models."
>
> "Important standard features that make MCNP very versatile and easy to use include a powerful general source, criticality source, and surface source; both geometry and output tally plotters; a rich collection of variance reduction techniques; a flexible tally structure; and an extensive collection of cross-section data." (Ref. 10.2, pg. ix)

3.2.2 Monte Carlo Method

The Monte Carlo method is a method of simulating and recording the behavior of individual particles within a system. The behavior of the simulated particles is extrapolated to describe the average behavior of all of the particles within the system. The Monte Carlo method as applied to neutrons in an MCNP criticality calculation is based upon following a number of individual neutrons through their various transport experiences such as scattering, fission, absorption, or leakage. The fission process is regarded as the birth event that separates generations of neutrons. A generation is the lifetime of a neutron from birth by fission to death by either escape, parasitic capture, or absorption leading to fission. The average behavior of the sample set of neutrons is

used to describe the average behavior of the system with regard to the number of neutrons in successive generations (i.e. critical multiplication factor, k_{eff}).

3.2.3 MCNP's Critical Multiplication Factor (k_{eff}) Results

MCNP 4A calculates three k_{eff} estimates for each cycle in a given problem--

1) the collision estimate,
2) the absorption estimate, and
3) the track length estimate.

A detailed description of the three k_{eff} estimates may be found in Chapter 2, Section VIII, Part B, of the MCNP User Manual (Ref. 10.2). The k_{eff} estimate used in the criticality analyses and in the bias value determination of this study is the statistical combination of all three k_{eff} estimates. According to statisticians at the Los Alamos National Laboratory, "the three-combined k_{eff} estimator is the best final estimate from an MCNP calculation." (Ref. 10.2, pg. 2-146) "The confidence interval based on the three statistically combined k_{eff} estimate is the recommended result to use for all final k_{eff} confidence interval quotations because all of the available information has been used in the final result." (Ref. 10.2, pg. 2-149)

3.2.4 Assessing the Validity of a Criticality Calculation

Before an MCNP k_{eff} result can be considered acceptable the validity of the calculation must be determined. Two minimum requirements for assessing the validity of an MCNP criticality calculation include--

1) all cells containing fissionable material should be adequately sampled, and
2) the fundamental spatial mode should be achieved before commencing the accumulation of data for calculation of the mean k_{eff}.

MCNP provides several features which help in assessing the validity of a k_{eff} calculation. To satisfy the first requirement, "MCNP verifies that at least one fission source point was generated in each cell containing fissionable material." (Ref. 10.2, pg. 2-150)

To satisfy the second requirement, MCNP provides several checks to determine if the fundamental spatial mode was achieved prior to the completion of the I_c cycles (I_C is the number of source cycles that are skipped before k_{eff} data accumulation begins). One check is the comparison of the estimated three-combined k_{eff} and its standard deviation for the first and second half of the active k_{eff} cycles. If the difference between the average k_{eff} values for the two halves does not appear to be zero or if the ratio of the two standard deviations is larger than expected a "WARNING" message is provided in the output. MCNP determines the number of cycles which must be skipped to produce the minimum standard deviation for the three-combined k_{eff} estimate. If this result is larger than I_c it may be indicative that more cycles should be skipped before accumulating k_{eff} data. MCNP checks each k_{eff} estimate's cycle data to assure

normality at the 95% and 99% confidence levels. If a k_{eff} estimate is not normally distributed with respect to the mean k_{eff} at the 99% confidence level a "WARNING" message is provided in the output. "Unless there is a high positive correlation among the three estimates, it is expected to be rare that all three k_{eff} estimates will not appear normally distributed at the 99% confidence level when the normal spatial mode has been achieved and maintained." (Ref. 10.2, pg. 2-150) Finally, MCNP tests for a monotonic trend of the three-combined k_{eff} estimate's results over the last ten active cycles. If the spatial mode is well converged and maintained, there should not be a monotonic trend within the last ten active cycles. A "WARNING" message is provided in the output if a monotonic trend is detected.

Compliance with the two minimum requirements addressed above should be verified for each criticality calculation using the checks provided by the MCNP code. If either of the two requirements appear to be violated, the k_{eff} results for the calculation should be evaluated further.

3.2.5 Cross-Sections

Utilizing the appropriate material cross-sections in an MCNP criticality calculation is essential to obtaining credible results. The cross-sections for the various neutron interactions are used to determine the flow of the criticality calculation at each interaction site. The MCNP neutron interaction tables are processed from evaluated data in the ENDF/B-V format.

The MCNP neutron interaction tables provide the following data--

1) all available cross-section data,
2) angular distribution data for scattered neutrons,
3) energy distribution data for inelastically scattered neutrons,
4) data about secondary photon production,
5) Q-value data for each reaction, and
6) the average number of neutrons per fission data for fissionable isotopes.

"For a particular table, the cross-sections for each reaction are given on one energy grid that is sufficiently dense that linear-linear interpolation between points reproduces the evaluated cross-sections within a specified tolerance that is generally within 1% or less" of the evaluated data (Ref. 10.2, pg. 2-18). A "thinned" neutron interaction table is available for some nuclides. The "thinned" tables have a significantly reduced size with a tolerance that is greater than 1%. The "thinned" tables are not recommended for use in calculations involving transport through the resonance region (Ref. 10.2, pg. 2-18).

Neutron interaction table designations are included as part of the material composition input to MCNP. Each material composition is composed of one or more elements or isotopes designated by a ZAID identifier. The ZAID identifier takes the form "ZZZAAA.nnC" where "ZZZ" represents the atomic number of the element ("ZZZ" may be one or two digits), "AAA" represents the elemental isotope ("AAA" must be three digits incorporating leading zeros), and "nn" represents the neutron interaction table designation.

Several neutron interaction tables are available to meet different user needs. The ".50C" and ".51C" series of data tables are both derived from the ENDF/B-V evaluated data. "The ".50C" series is the most faithful reproduction of the evaluated data (Ref. 10.2, pg. 2-20)." "The ".51C" series, also called the "thinned" series, has been processed with a less rigid tolerance than the ".50C" series." (Ref. 10.2, pg. 2-20) The ".35C" series data tables are produced by the Physical Data Group at Lawrence Livermore National Laboratory. The Livermore evaluations "manifest a philosophy of reproducing the data with the fewest number of points." (Ref. 10.2, pg. 2-20) The ".55C" series is the most recent evaluation produced by the Applied Nuclear Science Group T-2 at Los Alamos National Laboratory. "Generally, these evaluations (".55C") are the most complex because they are the most thorough." (Ref. 10.2, pg. 2-20)

Calculations involving transport through the resonance region should use the most detailed neutron interaction tables available unless there is a valid reason to do otherwise, such as the availability of more appropriate temperature dependent cross-sections. An MCNP k_{eff} calculation result is uniquely defined by the neutron interaction tables it utilizes. Table 3.2.5-1 contains a listing of elements and isotopes with their ZAIDs which may be utilized in criticality analyses. The cross-section tables for the elements and isotopes of the CRC analyses summarized in this study are obtained from the set displayed in Table 3.2.5-1.

Table 3.2.5-1
Preferred ZAIDs for Various Elements and Isotopes

Element	Symbol	Isotope	ZAID	Filename	Source
1 Hydrogen	H	H-1	1001.50C	rmccs	ENDF/B-V
	D	H-2	1002.55C	rmccs	GROUP T-2
	T	H-3	1003.50C	rmccs	ENDF/B-V
2 Helium	He	He-3	2003.50C	rmccs	ENDF/B-V
	He	He-4	2004.50C	rmccs	ENDF/B-V
3 Lithium	Li	Li-6	3006.50C	rmccs	ENDF/B-V
	Li	Li-7	3007.55C	rmccs	GROUP T-2
4 Beryllium	Be	Be-9	4009.50C	rmccs	ENDF/B-V
5 Boron	B	B-10	5010.50C	rmccs	ENDF/B-V
	B	B-11	5011.56C	newxs	GROUP T-2
6 Carbon	C	nat.	6000.50C	rmccs	ENDF/B-V
	C	C-12	6012.50C	rmccs	ENDF/B-V
7 Nitrogen	N	N-14	7014.50C	rmccs	ENDF/B-V
8 Oxygen	O	O-16	8016.50C	rmccs	ENDF/B-V
9 Fluorine	F	F-19	9019.50C	endf5p	ENDF/B-V

Element	Symbol	Isotope	ZAID	Filename	Source
11 Sodium	Na	Na-23	11023.50C	endf5p	ENDF/B-V
12 Magnesium	Mg	nat.	12000.50C	endf5u	ENDF/B-V
13 Aluminum	Al	Al-27	13027.50C	rmccs	ENDF/B-V
14 Silicon	Si	nat.	14000.50C	endf5p	ENDF/B-V
15 Phosphorus	P	P-31	15031.50C	endf5u	ENDF/B-V
16 Sulfur	S	S-32	16032.50C	endf5u	ENDF/B-V
17 Chlorine	Cl	nat.	17000.50C	endf5p	ENDF/B-V
19 Potassium	K	nat.	19000.50C	endf5u	ENDF/B-V
20 Calcium	Ca	nat.	20000.50C	endf5u	ENDF/B-V
22 Titanium	Ti	nat.	22000.50C	endf5u	ENDF/B-V
23 Vanadium	V	nat.	23000.50C	endf5u	ENDF/B-V
24 Chromium	Cr	nat.	24000.50C	rmccs	ENDF/B-V
25 Manganese	Mn	Mn-55	25055.50C	endf5u	ENDF/B-V
26 Iron	Fe	nat.	26000.55C	rmccs	GROUP T-2
27 Cobalt	Co	Co-59	27059.50C	endf5u	ENDF/B-V
28 Nickel	Ni	nat.	28000.50C	rmccs	ENDF/B-V
29 Copper	Cu	nat.	29000.50C	rmccs	ENDF/B-V
33 Arsenic	As	As-75	33075.35C	rmccsa	ENDL-85
36 Krypton	Kr	Kr-83	36083.50C	rmccsa	ENDF/B-V
40 Zirconium	Zr	nat.	40000.50C	endf5p	ENDF/B-V
	Zr	Zr-93	40093.50C	kidman	ENDF/B-V
41 Niobium	Nb	Nb-93	41093.50C	endf5p	ENDF/B-V
42 Molybdenum	Mo	nat.	42000.50C	endf5u	ENDF/B-V
	Mo	Mo-95	42095.50C	kidman	ENDF/B-V
43 Technetium	Tc	Tc-99	43099.50C	kidman	ENDF/B-V
44 Ruthenium	Ru	Ru-101	44101.50C	kidman	ENDF/B-V
	Ru	Ru-103	44103.50C	rmccsa	ENDF/B-V
45 Rhodium	Rh	Rh-103	45103.50C	kidman	ENDF/B-V
	Rh	Rh-105	45105.50C	kidman	ENDF/B-V
46 Palladium	Pd	Pd-105	46105.50C	kidman	ENDF/B-V

Element	Symbol	Isotope	ZAID	Filename	Source
	Pd	Pd-108	46108.50C	kidman	ENDF/B-V
47 Silver	Ag	Ag-109	47109.50C	rmccsa	ENDF/B-V
48 Cadmium	Cd	nat.	48000.50C	endf5u	ENDF/B-V
50 Tin	Sn	nat.	50000.35C	endl85	ENDL-85
53 Iodine	I	I-135	53135.50C	kidman	ENDF/B-V
54 Xenon	Xe	Xe-131	54131.50C	kidman	ENDF/B-V
	Xe	Xe-135	54135.50C	eprixs	ENDF/B-V
55 Cesium	Cs	Cs-133	55133.50C	kidman	ENDF/B-V
	Cs	Cs-135	55135.50C	kidman	ENDF/B-V
56 Barium	Ba	Ba-138	56138.50C	rmccs	ENDF/B-V
59 Praseodymium	Pr	Pr-141	59141.50C	kidman	ENDF/B-V
60 Neodymium	Nd	Nd-143	60143.50C	kidman	ENDF/B-V
	Nd	Nd-145	60145.50C	kidman	ENDF/B-V
	Nd	Nd-147	60147.50C	kidman	ENDF/B-V
	Nd	Nd-148	60148.50C	kidman	ENDF/B-V
61 Promethium	Pm	Pm-147	61147.50C	kidman	ENDF/B-V
	Pm	Pm-148	61148.50C	kidman	ENDF/B-V
	Pm	Pm-149	61149.50C	kidman	ENDF/B-V
62 Samarium	Sm	Sm-147	62147.50C	kidman	ENDF/B-V
	Sm	Sm-149	62149.50C	endf5u	ENDF/B-V
	Sm	Sm-150	62150.50C	kidman	ENDF/B-V
	Sm	Sm-151	62151.50C	kidman	ENDF/B-V
	Sm	Sm-152	62152.50C	kidman	ENDF/B-V
63 Europium	Eu	Eu-151	63151.55C	newxs	GROUP T-2
	Eu	Eu-153	63153.55C	newxs	GROUP T-2
	Eu	Eu-154	63154.50C	endf5u	ENDF/B-V
	Eu	Eu-155	63155.50C	kidman	ENDF/B-V
64 Gadolinium	Gd	nat.	64000.35C	rmccsa	ENDL-85
	Gd	Gd-155	64155.50C	endf5u	ENDF/B-V
	Gd	Gd-157	64157.50C	endf5u	ENDF/B-V

Element	Symbol	Isotope	ZAID	Filename	Source
72 Hafnium	Hf	nat.	72000.50C	newxs	ENDF/B-V
73 Tantalum	Ta	Ta-181	73181.50C	endf5u	ENDF/B-V
74 Tungsten	W	nat.	74000.55C	rmccs	GROUP T-2
82 Lead	Pb	nat.	82000.50C	rmccs	ENDF/B-V
92 Uranium	U	U-233	92233.50C	rmccs	ENDF/B-V
	U	U-234	92234.50C	endf5p	ENDF/B-V
	U	U-235	92235.50C	rmccs	ENDF/B-V
	U	U-235 @ (600K)	92235.53C	eprixs	ENDF/B-V
	U	U-236	92236.50C	endf5p	ENDF/B-V
	U	U-238	92238.50C	rmccs	ENDF/B-V
	U	U-238 @ (600K)	92238.53C	eprixs	ENDF/B-V
93 Neptunium	Np	Np-237	93237.55C	rmccsa	GROUP T-2
94 Plutonium	Pu	Pu-238	94238.50C	endf5p	ENDF/B-V
	Pu	Pu-239	94239.55C	rmccs	GROUP T-2
	Pu	Pu-240	94240.50C	rmccs	ENDF/B-V
	Pu	Pu-241	94241.50C	endf5p	ENDF/B-V
	Pu	Pu-242	94242.50C	endf5p	ENDF/B-V
	Pu	Pu-243	94243.35C	endl85	ENDL-85
95 Americium	Am	Am-241	95241.50C	endf5u	ENDF/B-V
	Am	Am-242m	95242.50C	endf5u	ENDF/B-V
	Am	Am-243	95243.50C	endf5u	ENDF/B-V
96 Curium	Cm	Cm-243	96243.35C	endl85	ENDL-85
	Cm	Cm-244	96244.50C	endf5u	ENDF/B-V
	Cm	Cm-245	96245.35C	endl85	ENDL-85
	Cm	Cm-248	96248.35C	endl85	ENDL-85

3.2.6 S(α,β) Thermal Treatment

The S(α,β) thermal treatment accounts for binding effects in molecules and crystalline solids. The S(α,β) thermal scattering treatment is a necessary requirement in a highly moderating medium where low-energy scattering may be dominant. S(α,β) thermal treatment tables are available for a limited number of materials. In the CRC analyses, the thermal treatment is consistently applied to the borated moderator.

4. CRC Analysis Description

The CRC analyses summarized in this paper were performed on the Crystal River, Unit 3, pressurized water reactor. Three CRC analyses have been performed on the Crystal River, Unit 3 core at various intra-cycle statepoints. The three statepoints which have been analyzed include--

1) Cycle 7, 260.6 EFPD = 18.098 GWd/MTU core average burnup,
2) Cycle 9, 158.6 EFPD = 19.099 GWd/MTU core average burnup,
3) Cycle 9, 219.4 EFPD = 20.984 GWd/MTU core average burnup.

The Crystal River, Unit 3 core is composed of 177 fuel assemblies. A symmetric one-eighth core geometry is evaluated in the CRC analyses. The one-eighth core geometry consists of 29 assemblies. Figure 4-1 shows the general one-eighth core configuration and the assembly numbering sequence utilized in the CRC analyses.

Figure 4-1 Crystal River, Unit 3 One-Eighth Core Symmetry Configuration

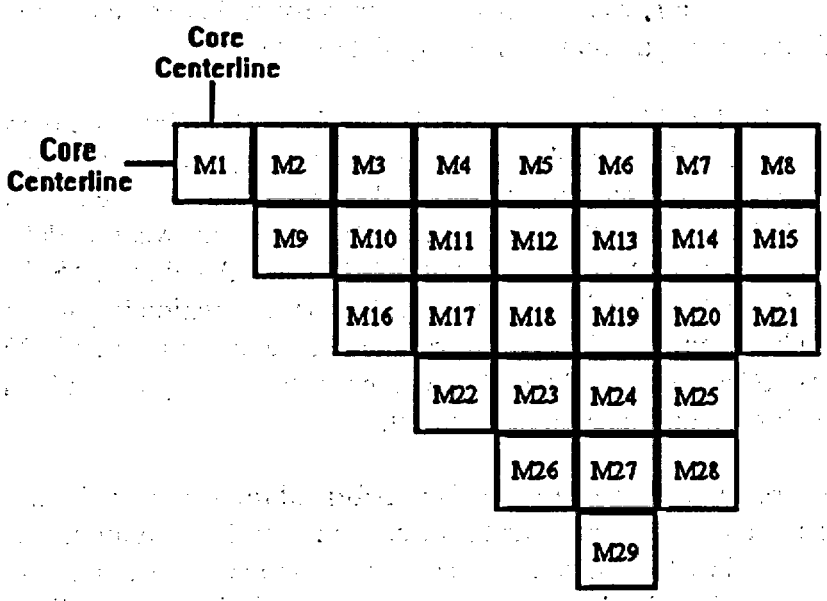

Due to the proprietary nature of the input data required to perform the CRC analyses on the Crystal River, Unit 3 reactor core, the actual numerical data describing the core configurations and fuel assembly configurations are not presented in this paper. Rather, general descriptions of the methods employed in performing the calculations are presented. Data presented in this paper is not sufficient for reproduction of the calculations.

To perform a CRC analysis for a specific statepoint in a reactor's history, all information for each fuel assembly in the reactor at the statepoint of interest must be utilized. The assembly information required to perform the appropriate fuel depletion and decay calculations include the following--

1) the assembly configuration (number and position of the fuel rods, the guide tubes, the burnable poison rods, and the instrument tube), dimensions, and material compositions;
2) the assembly initial fuel enrichment;
3) the complete irradiation history of the cycle (previous cycles and relative one-eighth core positions, BPRAs and enrichments);
4) exposure weighted fuel temperatures at the statepoint of interest for each node of the assembly being analyzed;
5) exposure weighted moderator density and temperatures for each node of the assembly being analyzed;
6) burnups for each node of the assembly being analyzed at the beginning-of-cycle (BOC) and end-of-cycle (EOC) for every cycle that the assembly was irradiated;
7) burnup for each node of the assembly being analyzed at the statepoint of interest.

Additional general input information required to perform the fuel depletion calculations include--

1) the boron letdown curve for every cycle pertaining to an assembly's irradiation history;
2) the cycle lengths and downtimes between cycles for every cycle relevant to an assembly in the one-eighth core configuration at the statepoint of interest.

The CRC analyses summarized in this paper were performed for an 18 axial-node representation of the reactor core. Therefore, each assembly in the one-eighth core geometry was divided into 18 axial-nodes. The top axial-node was modeled as 17.78 cm in height, and the bottom axial-node was modeled as 22.352 cm in height. The intermediate axial-nodes were modeled as 20.0025 cm in height resulting in a total core height of 360.172 cm. A unique SAS2H calculation was required for each node of each assembly due to the variation in parameters as a function of axial position between assemblies. This resulted in the performance of 522 unique SAS2H calculations per CRC analysis to obtain the required isotopic composition input for the MCNP criticality calculations at the statepoint of interest.

The CRC analyses summarized in this paper were also performed for a single axial-node representation of the reactor core to demonstrate the effect on integral reactivity due to axial effects which may be obscured by the utilization of assembly average parameters. For the single axial-node CRCs one unique SAS2H calculation was required per fuel assembly. Therefore, a total of 29 SAS2H calculations were required to produce the isotopic compositions necessary to perform the MCNP criticality calculation.

The MCNP calculations for the CRC analyses consist of modeling the reactor core and evaluating the critical multiplication factor at the startup statepoint of interest. The fuel and burnable poison isotopic compositions obtained from the SAS2H calculations are utilized in the MCNP criticality calculations. The MCNP criticality calculations for each CRC described in this paper were performed with seven different sets of fuel isotopic compositions to demonstrate the integral reactivity worth associated with certain sets of isotopes utilizing the MCNP cross-sections.

For the three CRC statepoint analyses summarized in this paper, a total of 1,653 unique SAS2H calculations and 42 unique MCNP calculations were performed. The input data for the SAS2H and MCNP calculations was obtained from the Crystal River, Unit 3, core operations reports, cycle reload reports, fuel redepletion calculations, CASMO/NEMO core follow calculations, and various drawings for the fuel rods, fuel assemblies, guide tubes, instrument tubes, burnable poison rods, reactor thermal shield, core baffle, core barrel, and reactor vessel. The applicability of the various references listed above is described in subsequent sections presenting the general SAS2H and MCNP modeling techniques.

5. SAS2H Model Development for CRC Analyses

The SAS2H model development described in this section is a general description of the methods employed in producing the various input decks required to perform fuel depletion and decay calculations relevant to the CRC analyses. The level of information presented in this section assumes that the reader has a working knowledge of the SAS2H control sequence of the SCALE modular code system.

5.1 Cross-Section Library

The SAS2H fuel depletion and decay calculations performed for the CRC analyses utilized the 44-group collapsed cross-section library available with the SCALE modular code system. The 44-group library was collapsed from the 238-group ENDF/B-V library using a flux spectrum calculation based on a 17×17 pressurized water reactor (PWR) fuel pin cell calculation performed with the XSDRNPM calculational module of the SCALE code system. A discrepancy in the 44-group library was reported in the July 1996 issue of the SCALE Newsletter which was pre-released in May 1996 (Ref. 10.4). The discrepancy reported was that the 44-group library which had been previously distributed by the RSIC had been collapsed from the 238-group library using an unmoderated aluminum/U-235 flux spectrum rather than the reported light water reactor fuel pin-cell flux spectrum. However, the 44-group library utilized in the SAS2H calculations relevant to the CRC analyses summarized within this report was collapsed using the correct neutron flux spectrum.

5.2 Initial Fuel Composition and Temperatures

The UO_2 fuel composition provided in the SAS2H input decks for the various assemblies is based on the actual fuel batch parameters listed in the core reload reports for cycles 7 and 9. The core reload reports for cycles 3 through 9 are listed in references 5 through 11. To account for fuel volume loss to the pellet chamfers, the density of the fuel provided in the SAS2H input is

based on the mass of uranium per assembly and the fuel pellet stack volume using the specified active fuel length. The initial enrichment of the fuel was used to calculate the weight percent of each uranium isotope using the following empirical relationships (Ref. 10.12)--

$$w_{234} = 0.007731(w_{235})^{1.0837}$$
$$w_{236} = 0.0046(w_{235})$$
$$w_{238} = 100 - w_{234} - w_{235} - w_{236}$$

where w represents the weight percent of a given isotope.

The fuel temperatures provided in the SAS2H input decks were the exposure-weighted average fuel temperatures for the assembly node of interest. For the single axial-node calculations, the fuel temperatures were the exposure-weighted average fuel temperatures for the entire assembly. These exposure-weighted average fuel temperatures were obtained from the CASMO/NEMO core follow calculations. The exposure-weighted fuel temperatures are acceptable representations of the actual fuel temperatures in the core due to the fact that CASMO/NEMO accounts for the time-dependent behavior of core parameters (i.e. flux redistribution).

The density and enrichment of freshly loaded PWR fuel typically does not vary in the axial direction. Therefore, the uranium loading and fuel volume for the entire assembly is used to determine the fuel density for each axial node without regard to axial variation. The exposure-weighted fuel temperature does vary in the axial direction. Therefore, unique CASMO/NEMO fuel temperature data was utilized for each node in the multi-node CRC analyses. The single axial-node CRC analyses employ the same methodology, but require only 1/18 of the multi axial-node fuel temperature input data.

Trace amounts (1E-21 atoms/b-cm) of various fission product isotopes were included in the initial fuel mixture to ensure the availability of cross-section data for subsequent fuel depletion calculations. The 42 nuclides for which trace concentrations were provided are listed in Table 5.2-1. The same listing of trace nuclides were consistently applied in all SAS2H input decks.

Table 5.2-1 Trace Nuclides Listed in CRC SAS2H Calculations

Kr-83	Kr-85	Sr-90	Y-89
Mo-95	Zr-93	Zr-94	Zr-95
Nb-94	Tc-99	Rh-103	Rh-105
Ru-101	Ru-106	Pd-105	Pd-108
Ag-109	Sb-124	Xe-131	Xe-132
Xe-135	Xe-136	Cs-134	Cs-135
Cs-137	Ba-136	La-139	Ce-144
Nd-143	Nd-145	Pm-147	Pm-148
Nd-147	Sm-147	Sm-149	Sm-150
Sm-151	Sm-152	Gd-155	Eu-153
Eu-154	Eu-155		

5.3 Cladding Material Description

The fuel rod cladding material utilized in the CRC analyses for Crystal River, Unit 3, was Zircaloy-4 (zirc-4). The material composition for zirc-4 was explicitly modeled using a density of 6.56 g/cc and the following material composition (Ref. 10.13)--

Oxygen:	0.12 wt%	Chromium:	0.10 wt%	Iron:	0.20 wt%
Tin:	1.40 wt%	Zirconium:	98.18 wt%.		

A cladding temperature of 694 K was consistently applied to all mixture 2 compositions in the SAS2H input decks. The sensitivity of the resulting isotopic compositions to cladding temperature is null due the absence of resonances in zirc-4 and the relative transparency of zirc-4 to neutrons with respect to scattering.

5.4 Borated Moderator Material Description

The borated moderator was defined using the "h2o" standard material composition in the SCALE Standard Composition Library. An arbitrary material specification with the moderator mixture number (3) was used to specify the boron concentration in the moderator. The boron concentration specified in the base moderator material composition was always the average boron concentration for the first irradiation step of the depletion sequence. The boron concentration in the subsequent irradiation steps of the depletion sequence were defined by specifying fractions of the initial irradiation step boron fraction such that the actual boron letdown curves from the core operations reports were accurately followed. The core operations reports applicable to the CRCs summarized in this paper are listed in references 14 through 24.

The soluble boron concentration does not vary axially in the reactor. Therefore, the same boron letdown scheme is applied to all fuel assembly nodes in a given reactor cycle.

The moderator temperature and density for each node of the assembly were calculated using CASMO/NEMO generated moderator specific volumes. The system pressure of 2200 psia was used in conjunction with the compressed water density vs pressure vs temperature table provided in the SCALE users manual (Ref. 10.1, pg. S2.5.12) to obtain the appropriate moderator temperature based on the specific volume provided by CASMO/NEMO.

The axial variation in moderator temperature and density is very important to obtaining the correct neutron flux spectrum in cross-section processing for fuel depletion calculations. The specific volumes provided by CASMO/NEMO are considered to be excellent due to the fact that time-dependent variations in the axial flux distribution are considered in performing the CASMO/NEMO core follow calculations.

5.5 Assembly Lattice Specifications

The fuel rod pitch, fuel rod outer diameter, fuel rod inner diameter, and fuel pellet diameter were provided in each SAS2H input deck as specified in the reference drawings (Refs. 24 and 25). The assembly configuration was obtained from reference drawings (Refs. 26 through 28). The fuel length was specified as the appropriate node height in the multi-axial-node CRC analyses. The fuel length in the single-axial-node CRC analyses was specified as the entire active fuel length (Ref. 10.29).

5.6 Path A and Path B Unit Cell Models

The path A unit cell model for all CRC analyses is composed of a fuel rod surrounded by the unit cell moderator. The unit cell perimeter is converted from a square to a circle by conserving area (i.e. square unit cell area = π * (unit cell radius)^2).

Three path B unit cell models are used for the CRC analyses summarized in this paper. Each larger unit cell model is composed of a central region, a fuel region, and an outer region. The various path B larger unit cells models are developed to approximate 2-D effects present in the Crystal River, Unit 3, B&W 15x15 fuel assemblies.

The first path B larger unit cell model, designated "path B guide tube model", is shown graphically in Figure 5.6-1. The path B guide tube model contains a central region composed of a guide tube unit pin-cell converted to radial dimensions as previously described for the path A model. The fuel region area surrounding the guide tube unit pin-cell is determined such that the assembly fuel-to-moderator material volume ratio is conserved. An outer moderator region surrounds the fuel region. The outer moderator region represents the moderator present in the assembly-to-assembly spacing. The area of this region is determined such that the ratio of the assembly spacing volume to actual assembly volume is maintained. The following is a general description of the calculations performed in deriving the path B guide tube larger unit cell model dimensions--

The subscripts refer to the zones depicted in Figure 5.6-1. The "r" variables refer to the radii of each zone in the larger unit cell model. The term area as used in this description is actually volume per unit length.

Nomenclature:

AUC = Area of an assembly unit pin-cell
FR Pitch = Fuel rod pitch
Fuel Locs = Number of fuel rod locations
NF Locs = Number of non-fuel pin-cell locations
FtoNF Ratio = Ratio of the fuel pin-cell area to non-fuel pin cell area
ASSY Pitch = Assembly-to-assembly pitch
MAA = Moderator area surrounding the fuel assembly

Step 1: r_1 = guide tube inner radius
Step 2: r_2 = guide tube outer radius
Step 3: AUC = (FR Pitch)^2 = $\pi * r_3^2$
Step 4: FtoNF Ratio = Fuel Locs / NF Locs
Zone 4 area = $\pi * (r_4^2 - r_3^2)$ = AUC * FtoNF Ratio
Step 5: Assembly area = (Fuel Locs + NF Locs) * (FR Pitch)^2
Number of pin-cells represented by larger unit cell = 1 Guide Tube + FtoNF Ratio
[Note: This model assumes the instrument tube and guide tube are identical. This assumption is negligible with respect to fuel depletion calculations.]
MAA = (ASSY Pitch)^2 - Assembly area
Zone 5 area = $\pi * (r_5^2 - r_4^2)$ = (Number of pin-cells represented by larger unit cell) * (MAA / (Fuel Locs + NF Locs))

Figure 5.6-1 Path B Guide Tube Larger Unit Cell Model

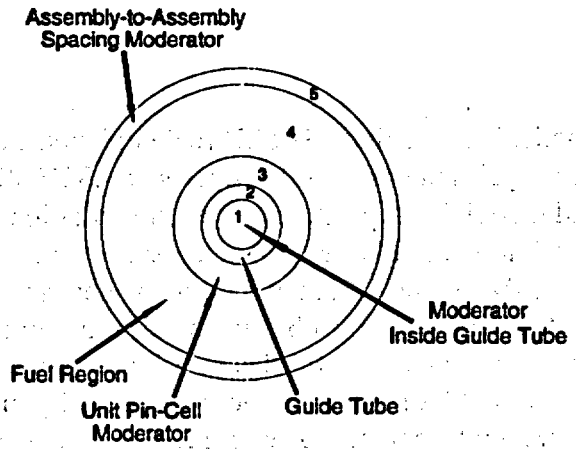

Path B Guide Tube Model

The second path B larger unit cell model, designated "path B BPRA model", is shown graphically in Figure 5.6-2. The path B BPRA model contains a central region composed of a BPR centered inside a guide tube unit pin-cell which has been converted to radial dimensions as previously described for the path A model. The fuel region area surrounding the guide tube unit pin-cell is determined such that the assembly fuel-to-moderator material volume ratio is conserved. An outer moderator region surrounds the fuel region. The outer moderator region represents the moderator present in the assembly-to-assembly spacing. The area of this region is determined such that the ratio of the assembly spacing volume to actual assembly volume is maintained. The zone radii for the fuel and outer moderator regions of the path B BPRA model are determined in the same manner as previously described for the path B guide tube model. The radii for zones 1 through 5 depicted in Figure 5.6-2 are the actual dimensions of the BPR and guide tube. The radii for zones 6, 7, and 8 in Figure 5.6-2 are the same as those for zones 3, 4, and 5, respectively, in the path B guide tube model.

Figure 5.6-2 Path B BPRA Larger Unit Cell Model

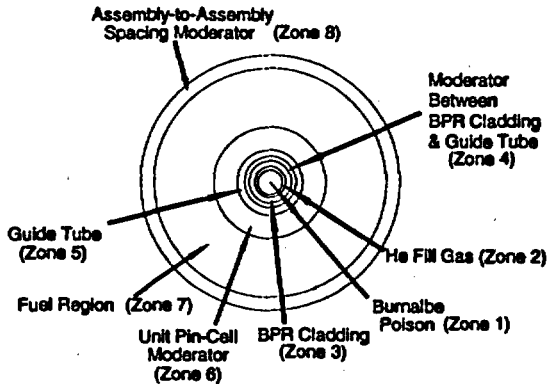

Path B BPRA Model

The purpose of the third model is to facilitate SAS2H fuel depletion calculations for assemblies that contain BPRA's in some cycles but not in other cycles. SAS2H allows new definitions of the larger unit cell radii and material compositions for each irradiation step in the depletion sequence. However, the total number of larger unit cell zones may only be set once. Therefore, if an assembly contained a BPRA in one cycle but did not in subsequent cycles, a larger unit cell representing the path B guide tube model must be available for use with the same number of zones as defined for all larger unit cells. The third path B larger unit cell model, designated "path B guide tube for use with BPRA model", is shown graphically in Figure 5.6-3. The path B guide tube for use with BPRA model contains a central region composed of a guide tube unit pin-cell which has been converted to radial dimensions as previously described for the path A model. The fuel region area surrounding the guide tube unit pin-cell is determined such that the assembly fuel-to-moderator material volume ratio is conserved. An outer moderator region surrounds the fuel region. The outer moderator region represents the moderator present in the assembly-to-assembly spacing. The area of this region is determined such that the ratio of the

assembly spacing volume to actual assembly volume is maintained. The zone radii for the fuel and outer moderator regions of the path B guide tube for use with BPRA model are determined in the same manner as previously described for the path B guide tube model. The radii for zones 1 through 5 depicted in Figure 5.6-3 are the same as those define for the path B BPRA model. The radii for zones 6, 7, and 8 in Figure 5.6-2 are the same as those for zones 3, 4, and 5, respectively, in the path B guide tube model.

Figure 5.6-3 Path B Guide Tube Larger Unit Cell Model for Use in Conjunction with the Path B BPRA Larger Unit Cell Model

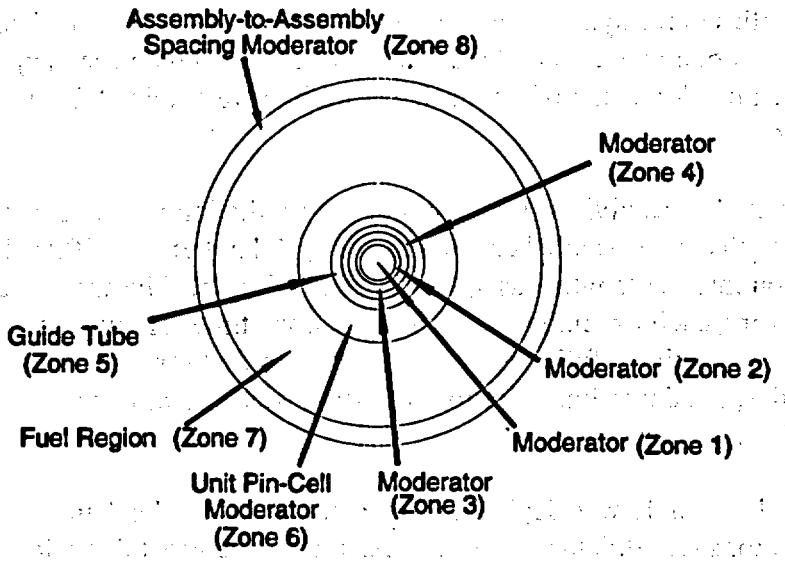

Path B Guide Tube For Use With BPRA Model

The path B larger unit cell descriptions are provided explicitly for each irradiation step in the SAS2H input decks for assemblies that contain a BPRA in one cycle but not in another by setting the "mxrepeats" card to 0. The path B larger unit cell description is provided once in the SAS2H input for assemblies that never contain a BPRA throughout their irradiation history. SAS2H automatically applies the same larger unit cell description to all irradiation intervals if instructed to do so by setting the "mxrepeats" card to 1.

5.7 SAS2H Irradiation History Modeling for CRC Analyses

Applying an accurate irradiation history model in the SAS2H sequence for performing fuel depletion calculations relevant to CRC analyses is important to obtaining correct isotopic compositions. The SAS2H fuel depletion calculation is divided into a number of user defined

irradiation steps. At each step the user specifies the power in megawatts of the assembly or assembly node, the irradiation step duration in calendar days, the zero power decay downtime to follow the irradiation step, and the fraction of the initially specified soluble boron in the moderator representing the average boron concentration during the irradiation step interval.

In the CRC analyses, the assembly nodal power or assembly average power for each reactor cycle was determined by obtaining three parameters-- the average relevant assembly nodal burnup over the reactor cycle, the reactor cycle length in calendar days, and the mass of uranium in the assembly node. The assembly average nodal burnup was divided by the reactor cycle length in calendar days and multiplied by the mass of uranium in the assembly node to obtain the average power of the assembly node over the cycle of interest. Nodal average assembly powers were consistently applied to all irradiation intervals representing each reactor cycle.

Each of the 29 assemblies in the symmetric one-eighth core geometry was tracked back through its irradiation history to obtain the required parameters to establish the necessary irradiation history. The cycle burnups for each node of each assembly were obtained from CASMO/NEMO core-follow calculations.

Each relevant reactor cycle was divided into a number of irradiation intervals of equal size. The irradiation interval lengths were established such that they did not exceed 100 calendar days. The average irradiation interval length was approximately 80 days. The cross-section libraries were updated once during each irradiation interval. The downtime following each set of irradiation intervals representing a full reactor cycle was specified for a zero decay calculation. For re-insert assemblies, the downtime prior to reinsertion was determined using data obtained from the core operations reports.

Each node of each fuel assembly was depleted using a unique SAS2H calculation. The actual relevant reactor operations report data was used to establish the correct depletion sequences for each assembly. The single-axial-node fuel depletion calculation for an assembly utilized the same irradiation step sequence as the corresponding multiple axial-node calculations with the exception that one calculation was performed per assembly and the total assembly average powers were utilized rather than the nodal assembly powers.

The detail utilized in the SAS2H calculations for the CRC analyses provides confidence that the resulting isotopic concentrations represent a realistic prediction based on real core physics parameters. This fact facilitates narrowing the source of resulting isotopic uncertainties and variations to sources in the cross-sections and intrinsic code performance.

6. MCNP Model Development for CRC Analyses

The MCNP criticality calculations are performed for reactor startup conditions at each of the intra-cycle statepoints of interest. The MCNP model development for the CRC analyses is based on actual characteristics of the reactor core under consideration. Reference drawings for the core and fuel assemblies were obtained to create the MCNP models relevant to the CRC analyses summarized in this paper. The reference drawings are currently considered proprietary information; therefore, no numerical data or detailed material composition data is presented in this paper. [Note: These drawings will be reviewed and non-proprietary tables containing data required for CRC analyses will be constructed and presented in the topical report.]

6.1 General Core Arrangement in MCNP

The Crystal River, Unit 3, reactor core was modeled in MCNP using a symmetric one-quarter core representation and reflective surfaces. An MCNP generated plot showing the x-y plane cross-sectional view of the reactor configuration as modeled in MCNP is presented in Figure 6.1-1. The reactor vessel, core barrel, thermal shield, and core baffle were all explicitly modeled. The fuel assembly lattice configuration was modeled with depleted BPR assemblies inserted in appropriate places. The fuel regions in the fuel rods of the multi-axial-node MCNP models were divided into 18 axial zones. The depleted fuel compositions obtained from the SAS2H sequence represent 522 unique material compositions in the MCNP models. The depleted BPR compositions obtained from the SAS2H sequence represent 160 unique material compositions in the MCNP models. Effects of varying the fuel isotopic composition were examined by excluding certain sets of isotopes and performing MCNP criticality calculations on each set. More detailed descriptions of the MCNP model development are presented in the following section.

Crystal River, Unit 3, Cycle 7
260.6 EFPD Statepoint

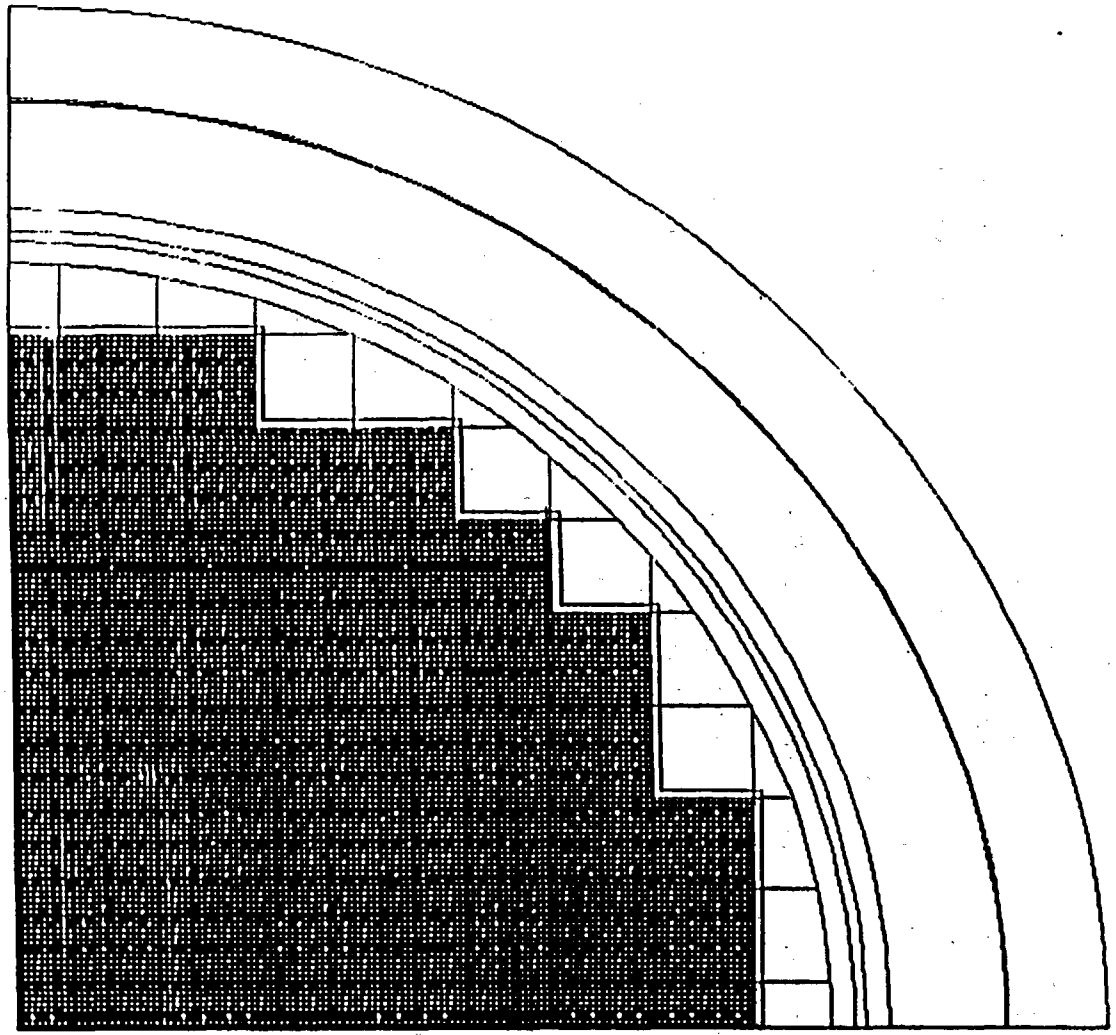

Figure 6.1-1: MCNP Plot: x-y cross-sectional view of the Crystal River, Unit 3, MCNP geometric modeling

6.2 Reactor Vessel, Core Thermal Shield, Core Barrel, and Core Baffle

The Crystal River, Unit 3, reactor vessel was modeled in MCNP using dimensions from actual design drawings (Ref. 10.30). The material composition of the reactor vessel was modeled as grade 55 A516 carbon steel.

The core thermal shield, core barrel, and core baffle were all modeled using dimensions from actual design drawings (Ref. 10.31 through 10.35). The material compositions of the core thermal shield, core barrel, and core baffle were all modeled as stainless steel 304.

6.3 Top and Bottom Reflector

The top and bottom core reflectors were modeled as a 50 percent borated moderator and 50 percent stainless steel 304 homogeneous mixture. This approximation was used to avoid explicit modeling of end fitting and plenum details that are irrelevant to criticality calculations. An MCNP plot of the core's axial geometric representation is presented in Figure 6.3-1.

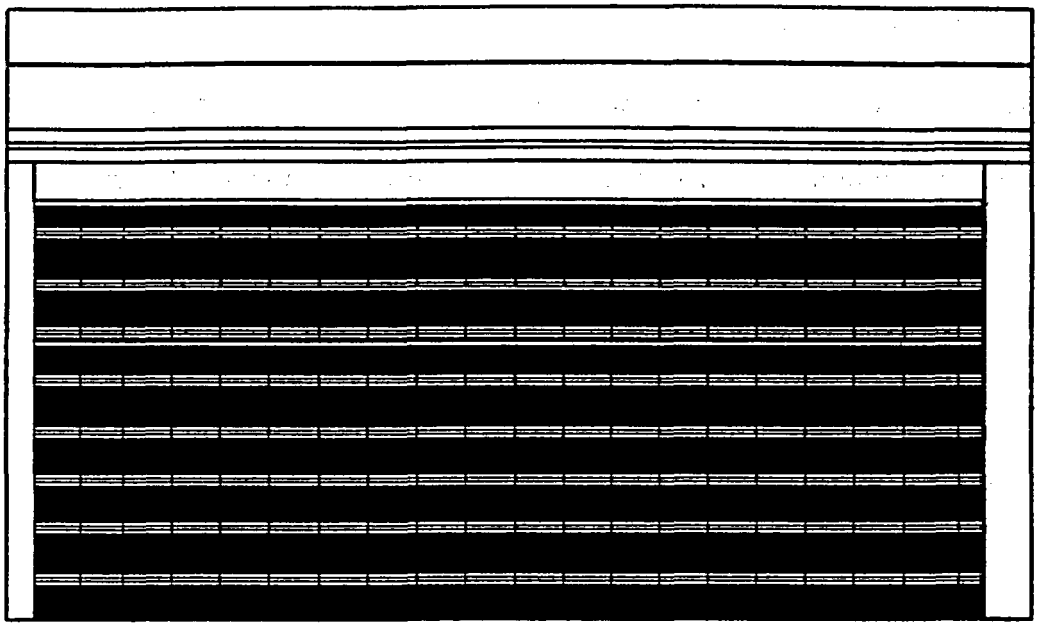

Crystal River, Unit 3, Cycle 7
260.6 EFPD Statepoint

Figure 6.3-1 MCNP Plot: x-z cross-section of the Crystal River, Unit 3, MCNP geometric modeling

6.4 Fuel Rod, Guide Tube, and Instrument Tube Modeling

For the multi axial-node models, the fuel rods were modeled in MCNP as having 18 axial fuel locations. The height of each axial-node was the same as that previously modeled in SAS2H. A different fuel material composition was calculated for each axial-node. Each fuel composition also had a unique density dependent of the composition. For the single axial-node models, the fuel was modeled as one region extending the length of the fuel rod. The fuel rod cladding was modeled as zirc-4. The gap between the fuel and cladding was explicitly modeled as void. The fuel rods were modeled with a height equal to the active fuel height. The dimensions used in modeling the fuel rods were obtained from actual design drawings (Refs. 24, 25, and 29). The top and bottom reflector mixture bounds the top and bottom of the fuel rods. A cross-sectional view of the MCNP geometric modeling for the fuel rods is shown in Figure 6.4-1.

The guide tubes were modeled explicitly in the MCNP geometry. The dimensions of the guide tubes were obtained from actual design drawings (Ref. 10.36). The instrument tubes were also modeled explicitly in the MCNP geometry. The dimensions of the instrument tube were obtained from actual design drawings (Ref. 10.37).

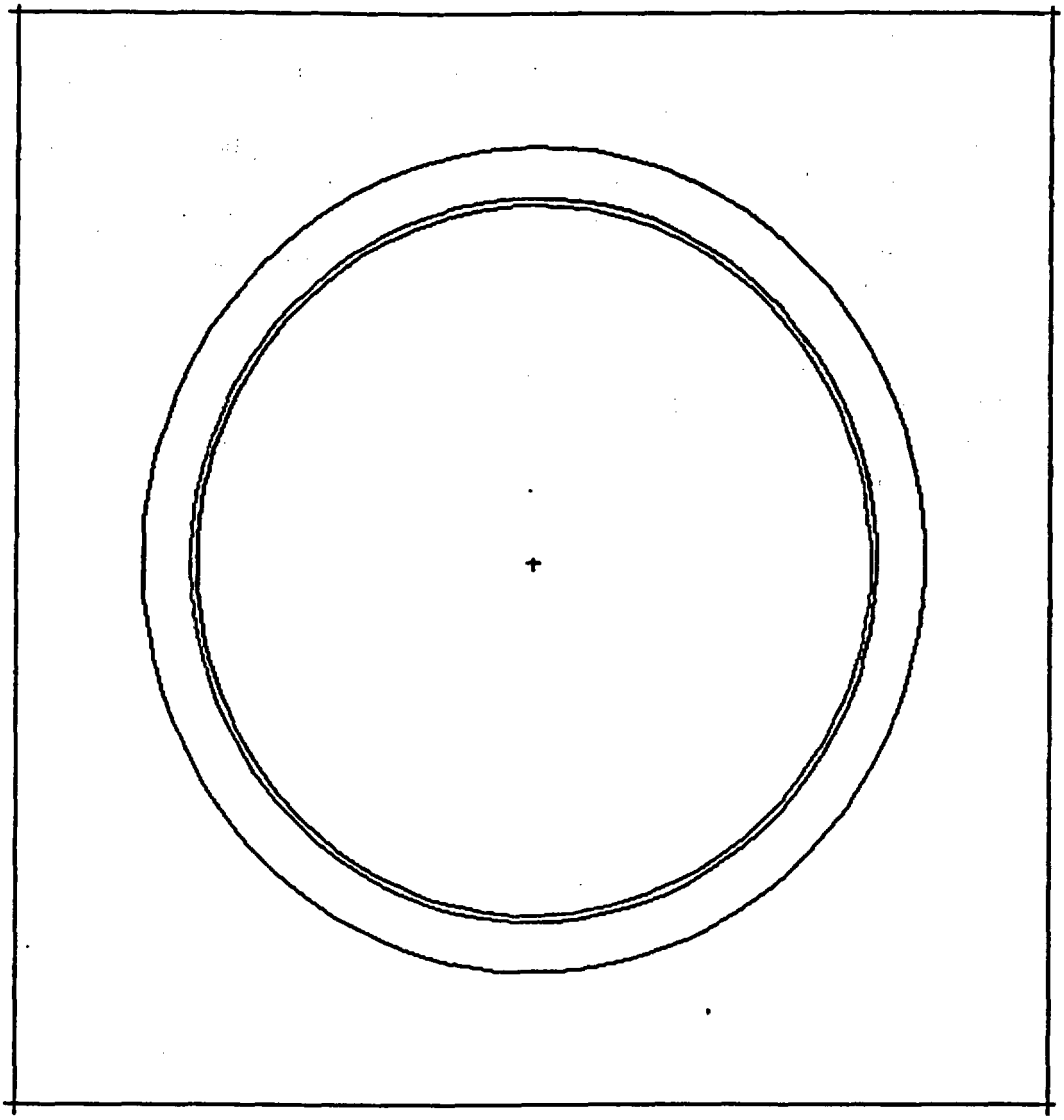

Crystal River, Unit 3, Cycle 7
260.6 EFPD Statepoint

Figure 6.4-1 MCNP Plot: x-y cross-section of the Crystal River, Unit 3, MCNP fuel rod geometric modeling

6.5 BPR Modeling

The BPRs were modeled in MCNP using characteristics obtained from actual design drawings (Refs. 38 and 39) and pellet specification references (Ref. 10.40). The burnable poison was divided into 16 axial nodes corresponding to the node descriptions applied in SAS2H to appropriately deplete the burnable poison material. The top and bottom nodes of the axial fuel representation do not have corresponding BPRs. This detail was also applied in the SAS2H depletion calculations. The burnable poison compositions obtained from the SAS2H depletion calculations were utilized as the material composition descriptions in MCNP. Each BPR node has a unique material composition and corresponding density. The single axial-node models use an assembly average burnable poison composition obtained from the single-node SAS2H calculations. The burnable poison in the single-node MCNP models extend the length of the active fuel due to the restrictions imposed by a single-node model. The MCNP plot of the BPR rod cross-section is presented in Figure 6.5-1.

Crystal River, Unit 3, Cycle 7
260.6 EFPD Statepoint

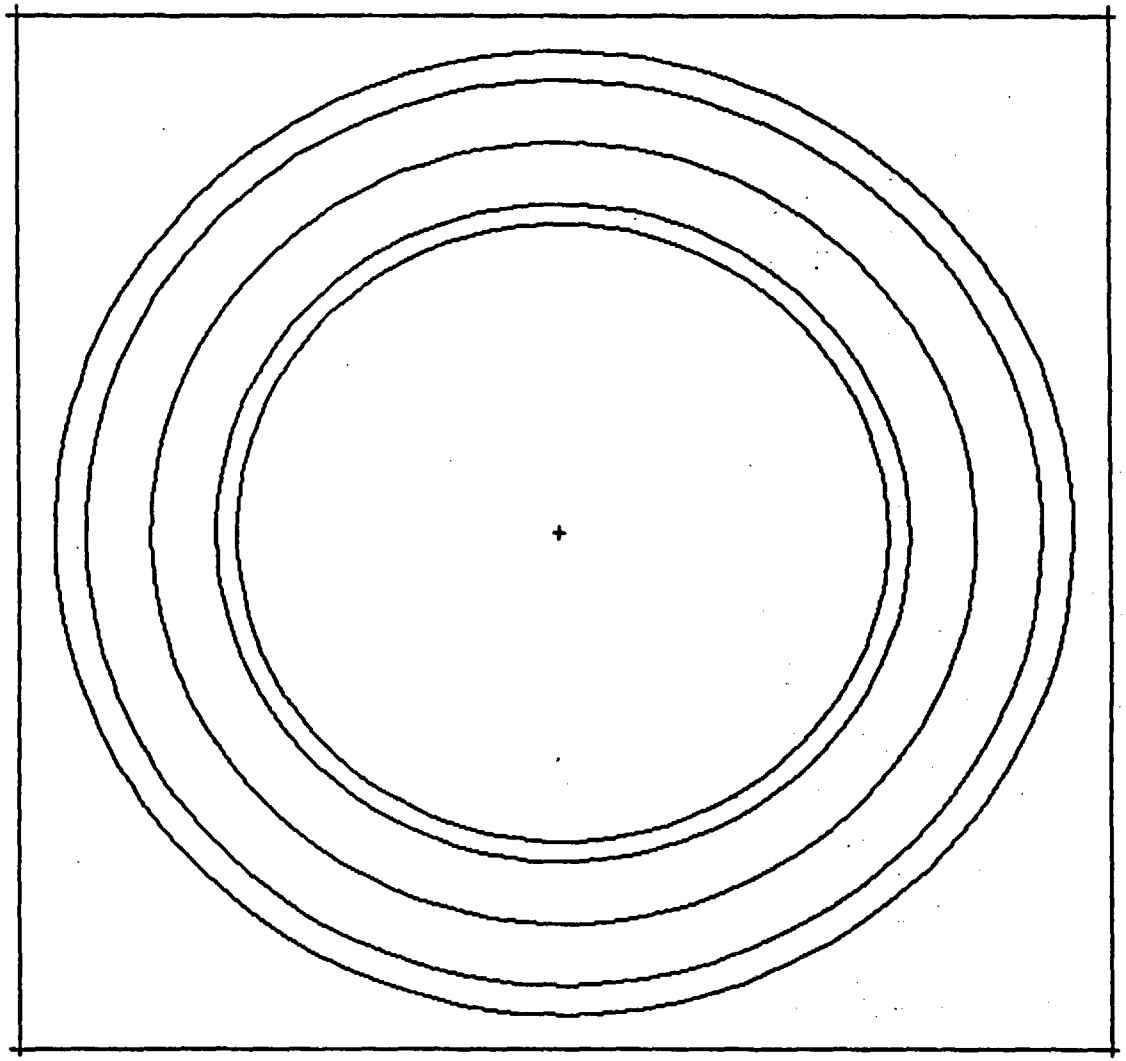

Figure 6.5-1 MCNP Plot: x-y cross-section of the Crystal River, Unit 3, MCNP BPR geometric modeling

6.6 Fuel Assembly Modeling

The fuel assemblies were explicitly modeled in MCNP using arrays filled with fuel rods, guide tubes, instrument tubes, and burnable poison rods as appropriate. The fuel assembly dimensions were obtained from actual design drawings (Refs. 26, 27, and 28). The inter-rod spacing contained borated moderator. The boron concentration used in the MCNP models was the all-rods-out critical boron concentration (AROCBC) calculated by CASMO/NEMO.

6.7 Fuel Isotopic Variations

The fuel isotopic compositions were varied to examine the effect on integral reactivity of certain sets of isotopes. Each fuel isotopic variation represents a different MCNP criticality calculation. A total of five sets of different fuel isotopic compositions were examined. The following is a listing of the five sets with a brief description of each. The oxygen-16 isotope is always included in each set. Therefore, oxygen is not explicitly listed in the delineation of the various isotope sets.

1) 84 Isotope Set: This fuel isotopic composition set is composed of 84 isotopes. This set represents all of the isotopes obtained from ORIGEN-S that had MCNP cross-section data tables available. A listing of the isotopes contained in this set is provided in Table 6.7-1.

2) Principal Isotope Set: This is a subset of 29 isotopes from the 84 isotope set which contain both actinides and fission products. A listing of the isotopes contained in this set is provided in Table 6.7-2.

3) Principal Actinide Set: This set is composed of 14 actinides. A listing of the isotopes contained in this set is provided in Table 6.7-3.

4) Actinide-Only Set: This set is composed of 10 actinides. A listing of the isotopes contained in this set is provided in Table 6.7-4.

5) Actinide-Only Set with f_{buc} factors applied: This set is composed of the 10 isotopes in the Actinide-Only Set with the exception that conservative multipliers were applied to the isotopic concentrations. This set was examined to demonstrate the gross conservatism introduced into the integral reactivity worth of a real system by applying the f_{buc} method presented in the *Topical Report on Actinide-Only Burnup Credit for PWR Spent Nuclear Fuel Packages* (Ref. 10.41). The f_{buc} multiplier factors for the 10 isotopes are listed in Table 6.75.

Table 6.7-1 84 Isotope Set

Cm-248	He-4	Th-232	U-233	U-234	U-235
U-236	U-238	Np-236	Np-237	Pu-237	Pu-238
Pu-239	Pu-240	Pu-241	Pu-242	Am-241	Am-242m
Am-243	Cm-242	Cm-243	Cm-244	Cm-245	Cm-246
Cm-247	H-1	Li-6	As-75	Kr-80	Kr-82
Kr-83	Kr-84	Kr-86	Y-89	Zr-93	Mo-95
Tc-99	Ru-101	Ru-103	Rh-103	Pd-105	Pd-108
Ag-109	Xe-131	Xe-134	Xe-135	Cs-133	Cs-135
Ba-138	Pr-141	Nd-143	Nd-145	Nd-147	Nd-148
Pm-147	Pm-148	Sm-147	Sm-149	Sm-150	Sm-151
Sm-152	Eu-151	Eu-152	Eu-153	Eu-154	Eu-155
Gd-152	Gd-154	Gd-155	Gd-156	Gd-157	Gd-158
Gd-160	Ho-165	H-3	Li-7	Be-9	Nb-93
Rh-105	Ag-107	Pm-149	Pa-233	Np-235	Np-238

Table 6.7-2 Principal Isotope Set

Mo-95	Tc-99	Ru-101	Rh-103	Ag-109	Nd-143
Nd-145	Sm-147	Sm-149	Sm-150	Sm-151	Sm-152
Eu-151	Eu-153	Gd-155	U-233	U-234	U-235
U-236	U-238	Np-237	Pu-238	Pu-239	Pu-240
Pu-241	Pu-242	Am-241	Am-242m	Am-243	

Table 6.7-3 Principal Actinide Set

U-233	U-234	U-235	U-236	U-238	Np-237
Pu-238	Pu-239	Pu-240	Pu-241	Pu-242	Am-241
Am-242m	Am-243				

Table 6.7-4 Actinide-Only Set

U-234	U-235	U-236	U-238	Pu-238	Pu-239
Pu-240	Pu-241	Pu-242	Am-241		

Table 6.7-5 Actinide-Only f_{buc} Multiplication Factors

Isotope	f_{buc}
U-234	0.509
U-235	1.115
U-236	0.955
U-238	0.990
Pu-238	0.829
Pu-239	1.033
Pu-240	1.000
Pu-241	1.016
Pu-242	1.000
Am-241	0.583

6.8 Monte Carlo Parameters and Initial Source Distribution

A total of 325 neutron generation cycles were performed for each MCNP calculation. Each cycle tracked 2500 individual neutrons. The first 25 neutron generation cycles were excluded from the data contributing to the average k_{eff} of the system. The initial k_{eff} guess for each system was unity.

The initial source distribution used in each MCNP calculation consisted of 882 neutrons distributed both radially and axially throughout the core.

7. CRC k_{eff} Results

MCNP CRC calculations were performed for the three statepoints from Crystal River, Unit 3 described in Section 4. The five fuel isotopic sets described in Section 6.7 were used in these calculations.

NEMO criticality calculations were also performed for the three statepoints. The NEMO k_{eff} results for the three statepoints are presented in Table 7-1. Results for both multi-axial-node and single-axial-node configurations are given. The data in this table is representative of NEMO core-follow criticality calculations for other reactors.

Table 7-1
Crystal River, Unit 3 CRC Analysis for Three Statepoints
NEMO Criticality Calculations

Statepoint	Multi-axial-node k_{eff}	Single-axial-node k_{eff}	% Difference in k_{eff}
Cycle 7, 260.6 EFPD	0.9989	1.0034	0.45
Cycle 9, 158.6 EFPD	0.9971	1.0025	0.54
Cycle 9, 219.4 EFPD	0.9981	1.0029	0.48

A total of 30 MCNP CRC calculations are summarized in this appendix. For each of the three statepoints from Crystal River, Unit 3, a total of 10 criticality calculations were performed. A criticality calculation using each of the five fuel isotopic sets described in Section 6.7 was performed for both the multi-axial-node and the single-axial-node configurations. Tables 7-2 through 7-7 contain the k_{eff} results for each CRC criticality analysis.

Table 7-2
Crystal River, Unit 3 CRC Analysis k_{eff} Results for Cycle 7, 260.6 EFPD
SAS2H Based Multi-Node Calculations

Case Description	Case Input / Output	k_{eff}	σ
84 Isotope Set	c7mn2 / c7mn2.O	1.00112	0.00073
Principal Isotope Set	c7mn3 / c7mn3.O	1.02244	0.00073
Principal Actinide Set	c7mn5 / c7mn5.O	1.06578	0.00079
Actinide-Only Set	c7mn6 / c7mn6.O	1.06779	0.00079
Actinide-Only Set (with f_{burn}'s applied)	c7mn7 / c7mn7.O	1.09209	0.00078

Table 7-3
Crystal River, Unit 3 CRC Analysis k_{eff} Results for Cycle 7, 260.6 EFPD
SAS2H Based Single-Node Calculations

Case Description	Case Input / Output	k_{eff}	σ
84 Isotope Set	c7sn2 / c7sn2.O	1.00515	0.00080
Principal Isotope Set	c7sn3 / c7sn3.O	1.03042	0.00074
Principal Actinide Set	c7sn5 / c7sn5.O	1.06905	0.00077
Actinide-Only Set	c7sn6 / c7sn6.O	1.07283	0.00084
Actinide-Only Set (with f_{bnc}'s applied)	c7sn7 / c7sn7.O	1.09925	0.00076

Table 7-4
Crystal River, Unit 3 CRC Analysis k_{eff} Results for Cycle 9, 158.6 EFPD
SAS2H Based Multi-Node Calculations

Case Description	Case Input / Output	k_{eff}	σ
84 Isotope Set	9amn2 / 9amn2.O	0.99805	0.00072
Principal Isotope Set	9amn3 / 9amn3.O	1.02612	0.00075
Principal Actinide Set	9amn5 / 9amn5.O	1.05859	0.00078
Actinide-Only Set	9amn6 / 9amn6.O	1.06252	0.00078
Actinide-Only Set (with f_{bnc}'s applied)	9amn7 / 9amn7.O	1.08732	0.00079

Table 7-5
Crystal River, Unit 3 CRC Analysis k_{eff} Results for Cycle 9, 158.6 EFPD
SAS2H Based Single-Node Calculations

Case Description	Case Input / Output	k_{eff}	σ
84 Isotope Set	9asn2 / 9asn2.O	1.00498	0.00077
Principal Isotope Set	9asn3 / 9asn3.O	1.02816	0.00073
Principal Actinide Set	9asn5 / 9asn5.O	1.06192	0.00081
Actinide-Only Set	9asn6 / 9asn6.O	1.06533	0.00073
Actinide-Only Set (with f_{bnc}'s applied)	9asn7 / 9asn7.O	1.09266	0.00076

Table 7-6
Crystal River, Unit 3 CRC Analysis k_{eff} Results for Cycle 9, 219.4 EFPD
SAS2H Based Multi-Node Calculations

Case Description	Case Input / Output	k_{eff}	σ
84 Isotope Set	9bmn2 / 9bmn2.O	0.99771	0.00079
Principal Isotope Set	9bmn3 / 9bmn3.O	1.01989	0.00083
Principal Actinide Set	9bmn5 / 9bmn5.O	1.06232	0.00077
Actinide-Only Set	9bmn6 / 9bmn6.O	1.06686	0.00077
Actinide-Only Set (with f_{burn}'s applied)	9bmn7 / 9bmn7.O	1.09165	0.00075

Table 7-7
Crystal River, Unit 3 CRC Analysis k_{eff} Results for Cycle 9, 219.4 EFPD
SAS2H Based Single-Node Calculations

Case Description	Case Input / Output	k_{eff}	σ
84 Isotope Set	9bmn2 / 9bmn2.O	1.00440	0.00074
Principal Isotope Set	9bmn3 / 9bmn3.O	1.02704	0.00075
Principal Actinide Set	9bmn5 / 9bmn5.O	1.06646	0.00074
Actinide-Only Set	9bmn6 / 9bmn6.O	1.06938	0.00077
Actinide-Only Set (with f_{burn}'s applied)	9bmn7 / 9bmn7.O	1.09552	0.00077

In the development of an acceptable criticality evaluation methodology which accounts for generation and depletion of isotopes in the fuel, it is important to know how the integral reactivity worth of the fuel composition changes with the exclusion of certain isotopes. The comparison of the k_{eff} results for the various fuel isotopic cases provides information on the reactivity worth of various sets of isotopes. Tables 7-8 through 7-16 contain percent differences in reactivity between the various cases analyzed. The percent difference values presented in these tables are calculated relative to the largest isotope set in each comparison.

Table 7-8 Percent Differences in k_{eff} Between Cases within the SAS2H Based Multi-Node Calculations for Cycle 7 at 260.6 EFPD

Comparison Description	% Difference in k_{eff}
84 Isotope Set vs Principal Isotope Set	2.13
84 Isotope Set vs Principal Actinide Set	6.46
84 Isotope Set vs Actinide-Only Set	6.66
84 Isotope Set vs Actinide-Only Set with f_{buc}'s	9.09
Principal Isotope Set vs Principal Actinide Set	4.24
Principal Isotope Set vs Actinide-Only Set	4.44
Principal Isotope Set vs Actinide-Only Set with f_{buc}'s	6.81
Principal Actinide Set vs Actinide-Only Set	0.19
Principal Actinide Set vs Actinide-Only Set with f_{buc}'s	2.47
Actinide-Only Set vs Actinide-Only Set with f_{buc}'s	2.28

Table 7-9 Percent Differences in k_{eff} Between Cases within the SAS2H Based Single-Node Calculations for Cycle 7 at 260.6 EFPD

Comparison Description	% Difference in k_{eff}
84 Isotope Set vs Principal Isotope Set	2.51
84 Isotope Set vs Principal Actinide Set	6.36
84 Isotope Set vs Actinide-Only Set	6.73
84 Isotope Set vs Actinide-Only Set with f_{buc}'s	9.36
Principal Isotope Set vs Principal Actinide Set	3.75
Principal Isotope Set vs Actinide-Only Set	4.12
Principal Isotope Set vs Actinide-Only Set with f_{buc}'s	6.68
Principal Actinide Set vs Actinide-Only Set	0.35
Principal Actinide Set vs Actinide-Only Set with f_{buc}'s	2.82
Actinide-Only Set vs Actinide-Only Set with f_{buc}'s	2.46

Table 7-10 Percent Differences in k_{eff} Between the SAS2H Based Single-Node and Multi-Node Calculations for Cycle 7 at 260.6 EFPD

Comparison Description	% Difference in k_{eff}
84 Isotope Set	0.40
Principal Isotope Set	0.78
Principal Actinide Set	0.31
Actinide-Only Set	0.47
Actinide-Only Set with f_{buc}'s	0.66

Table 7-11 Percent Differences in k_{eff} Between Cases within the SAS2H Based Multi-Node Calculations for Cycle 9 at 158.6 EFPD

Comparison Description	% Difference in k_{eff}
84 Isotope Set vs Principal Isotope Set	2.81
84 Isotope Set vs Principal Actinide Set	6.07
84 Isotope Set vs Actinide-Only Set	6.46
84 Isotope Set vs Actinide-Only Set with f_{buc}'s	8.94
Principal Isotope Set vs Principal Actinide Set	3.16
Principal Isotope Set vs Actinide-Only Set	3.55
Principal Isotope Set vs Actinide-Only Set with f_{buc}'s	5.96
Principal Actinide Set vs Actinide-Only Set	0.37
Principal Actinide Set vs Actinide-Only Set with f_{buc}'s	2.71
Actinide-Only Set vs Actinide-Only Set with f_{buc}'s	2.33

Table 7-12 Percent Differences in k_{eff} Between Cases within the SAS2H Based Single-Node Calculations for Cycle 9, 158.6 EFPD

Comparison Description	% Difference in k_{eff}
84 Isotope Set vs Principal Isotope Set	2.31
84 Isotope Set vs Principal Actinide Set	5.67
84 Isotope Set vs Actinide-Only Set	6.01
84 Isotope Set vs Actinide-Only Set with f_{buc}'s	8.72
Principal Isotope Set vs Principal Actinide Set	3.28
Principal Isotope Set vs Actinide-Only Set	3.62
Principal Isotope Set vs Actinide-Only Set with f_{buc}'s	6.27
Principal Actinide Set vs Actinide-Only Set	0.32
Principal Actinide Set vs Actinide-Only Set with f_{buc}'s	2.89
Actinide-Only Set vs Actinide-Only Set with f_{buc}'s	2.57

Table 7-13 Percent Differences in k_{eff} Between the SAS2H Based Single-Node and Multi-Node Calculations for Cycle 9 at 158.6 EFPD

Comparison Description	% Difference in k_{eff}
84 Isotope Set	0.69
Principal Isotope Set	0.20
Principal Actinide Set	0.31
Actinide-Only Set	0.26
Actinide-Only Set with f_{buc}'s	0.49

Table 7-14 Percent Differences in k_{eff} Between Cases within the SAS2H Based Multi-Node Calculations for Cycle 9 at 219.4 EFPD

Comparison Description	% Difference in k_{eff}
84 Isotope Set vs Principal Isotope Set	2.22
84 Isotope Set vs Principal Actinide Set	6.48
84 Isotope Set vs Actinide-Only Set	6.93
84 Isotope Set vs Actinide-Only Set with f_{buc}'s	9.42
Principal Isotope Set vs Principal Actinide Set	4.16
Principal Isotope Set vs Actinide-Only Set	4.61
Principal Isotope Set vs Actinide-Only Set with f_{buc}'s	7.04
Principal Actinide Set vs Actinide-Only Set	0.43
Principal Actinide Set vs Actinide-Only Set with f_{buc}'s	2.76
Actinide-Only Set vs Actinide-Only Set with f_{buc}'s	2.32

Table 7-15 Percent Differences in k_{eff} Between Cases within the SAS2H Based Single-Node Calculations for Cycle 9 at 219.4 EFPD

Comparison Description	% Difference in k_{eff}
84 Isotope Set vs Principal Isotope Set	2.25
84 Isotope Set vs Principal Actinide Set	6.18
84 Isotope Set vs Actinide-Only Set	6.47
84 Isotope Set vs Actinide-Only Set with f_{buc}'s	9.07
Principal Isotope Set vs Principal Actinide Set	3.84
Principal Isotope Set vs Actinide-Only Set	4.12
Principal Isotope Set vs Actinide-Only Set with f_{buc}'s	6.67
Principal Actinide Set vs Actinide-Only Set	0.27
Principal Actinide Set vs Actinide-Only Set with f_{buc}'s	2.72
Actinide-Only Set vs Actinide-Only Set with f_{buc}'s	2.44

Table 7-16 Percent Differences in k_{eff} Between the SAS2H Based Single-Node and Multi-Node Calculations for Cycle 9 at 219.4 EFPD

Comparison Description	% Difference in k_{eff}
84 Isotope Set	0.67
Principal Isotope Set	0.70
Principal Actinide Set	0.39
Actinide-Only Set	0.24
Actinide-Only Set with f_{buc}'s	0.35

8. Sample of CRC Isotopic Results

A tremendous amount of isotopic data is generated in each CRC analysis. Each node of the multi-axial-node CRC analyses has a specific fuel composition that is a function of several key parameters. Some of the more important physical parameters influencing the fuel isotopic compositions for a node of a given assembly include--

1) burnup
2) fuel temperature
3) moderator temperature and density
4) relative power distributions
5) neutron energy spectral shifts.

The code performance in predicting the spent fuel isotopic compositions are dependent not only on the parameters identified above, but also on the cross-section libraries and code calculational methods. The CASMO/NEMO code system has been used successfully to design and analyze nuclear reactor cores. The Crystal River, Unit 3, core is one such reactor. The CRC analyses summarized in this paper utilized input parameters for the various burnups, fuel temperatures, and moderator densities which were obtained from the CASMO/NEMO code system. The exposure weighted fuel temperatures and moderator specific volumes utilized in the SAS2H fuel depletion calculations were determined by CASMO/NEMO such that the effects of the time-dependent neutron flux spectral shifts and redistribution were appropriately included in the resulting averaged values. Therefore, a comparison of the isotopic results obtained from the SAS2H and CASMO/NEMO calculations serves to demonstrate SAS2H's ability to predict fuel isotopics with respect to a well-established commercial nuclear design and analysis code.

A sample of the various isotopic profiles obtained from the CRC analyses are presented in this summary to provide an example of the calculational detail represented in the CRC analyses. Isotopic comparisons between SAS2H and CASMO/NEMO are presented in this summary to demonstrate preliminary data which will be evaluated to quantify the ability of the SAS2H sequence to accurately predict fuel isotopic compositions with respect to a licensed commercial nuclear design code.

Figures 8-1 through 8-4 contain SAS2H and CASMO/NEMO axial isotopic profile comparisons for U-235 in four different fuel assemblies from the Crystal River, Unit 3, 260.6 EFPD statepoint CRC analysis. The four fuel assemblies were chosen to cover a broad range of burnup characteristics. None of the four assemblies had BPRAs inserted during their irradiation histories. The following is a listing of the average burnups and initial enrichments for the four assemblies--

(Refer to Figure 4-1)

Assembly 8: 6.27 GWd/MTU, 3.84 wt% U-235 initial enrichment
Assembly 29: 15.61 GWd/MTU, 2.62 wt% U-235 initial enrichment
Assembly 1: 24.83 GWd/MTU, 2.64 wt% U-235 initial enrichment
Assembly 9: 31.36 GWd/MTU, 3.29 wt% U-235 initial enrichment.

Tables 8-1 through 8-4 presents the same U-235 data in a different form for the four fuel assemblies. In these tables the ratio of CASMO/NEMO to SAS2H isotopic concentrations of U-235 are given at each axial node in the four assemblies. In addition, values are provided at each axial node for burnup, burnup weighted fuel temperatures, and burnup weighted moderator densities. These burnup weighted values were obtained from the core-follow analyses of Crystal River Unit 3.

Since CASMO/NEMO utilizes a lumped fission product, individual isotopic profile comparisons can not be performed for isotopes other than the primary actinides and fission products which CASMO/NEMO explicitly models. However, the excellent results presented in Section 7 for the integral reactivity worth of the 84 isotope set with respect to the measured k_{eff} of unity suggests that the individual fission product isotopics calculated by SAS2H are either quite accurate or there are some very fortunate cancellation of errors occurring in the isotopic concentrations to yield k_{eff} results between 0.10 and 0.22 percent of the measured value for three separate calculations. Investigation of the independently calculated SAS2H fission product distributions will provide insight into the performance of SAS2H with respect to fission product production in fuel depletion calculations.

The data presented in this CRC summary is all preliminary and currently under evaluation. The isotopic results are being evaluated to determine the performance characteristic of SAS2H in predicting spent fuel isotopic compositions. Therefore, discussion and conclusions concerning the preliminary data presented in this summary is not provided. Once the proprietary issues regarding the input required to perform the CRC evaluations are settled, the complete CRC calculation descriptions, isotopic results, data evaluation and conclusions regarding the performance of SAS2H will be presented.

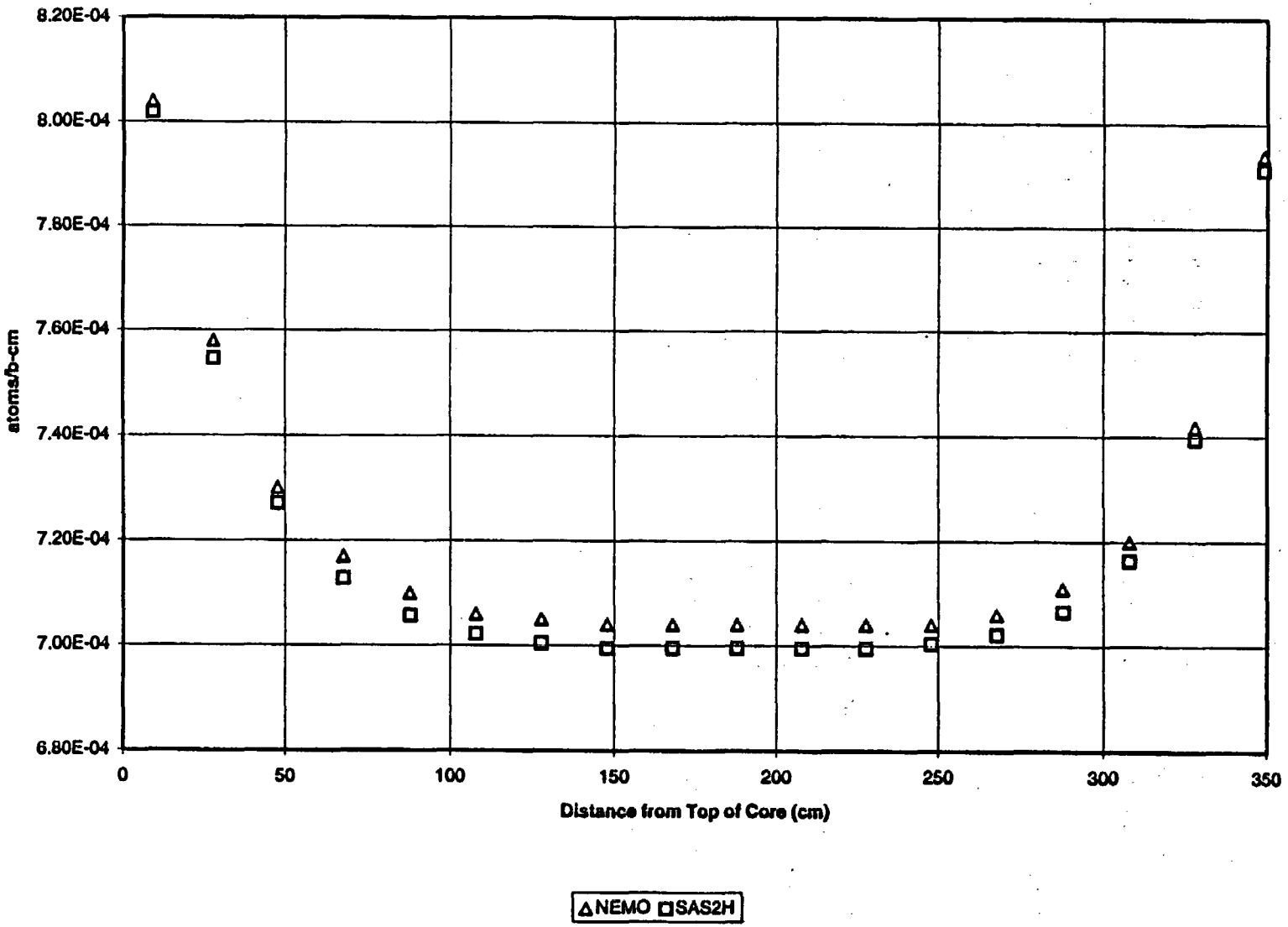

Figure 8-1 Axial Isotopic Profile Comparison Between SAS2H and CASMO/NEMO

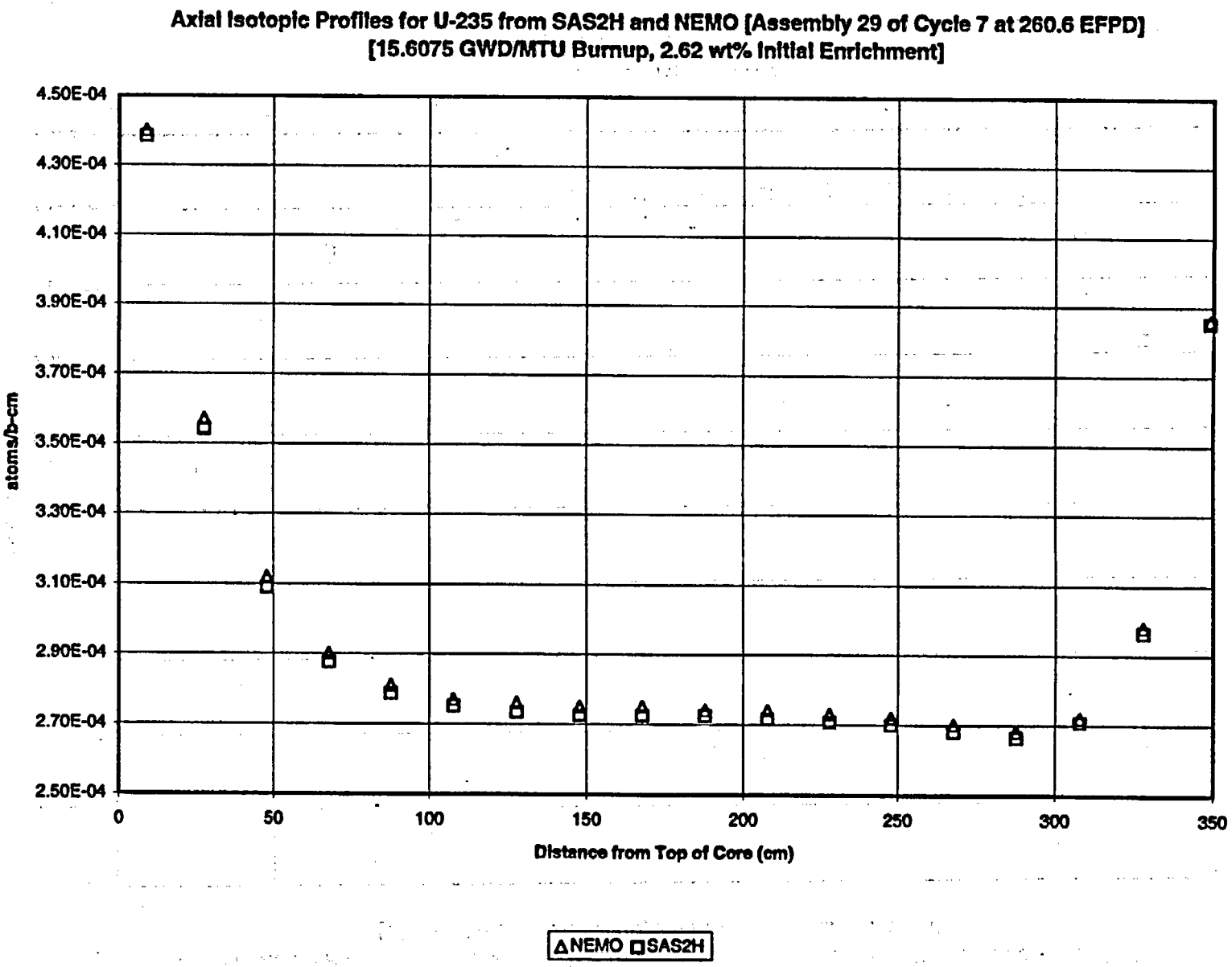

Figure 8-2 Axial Isotopic Profile Comparison Between SAS2H and CASMO/NEMO

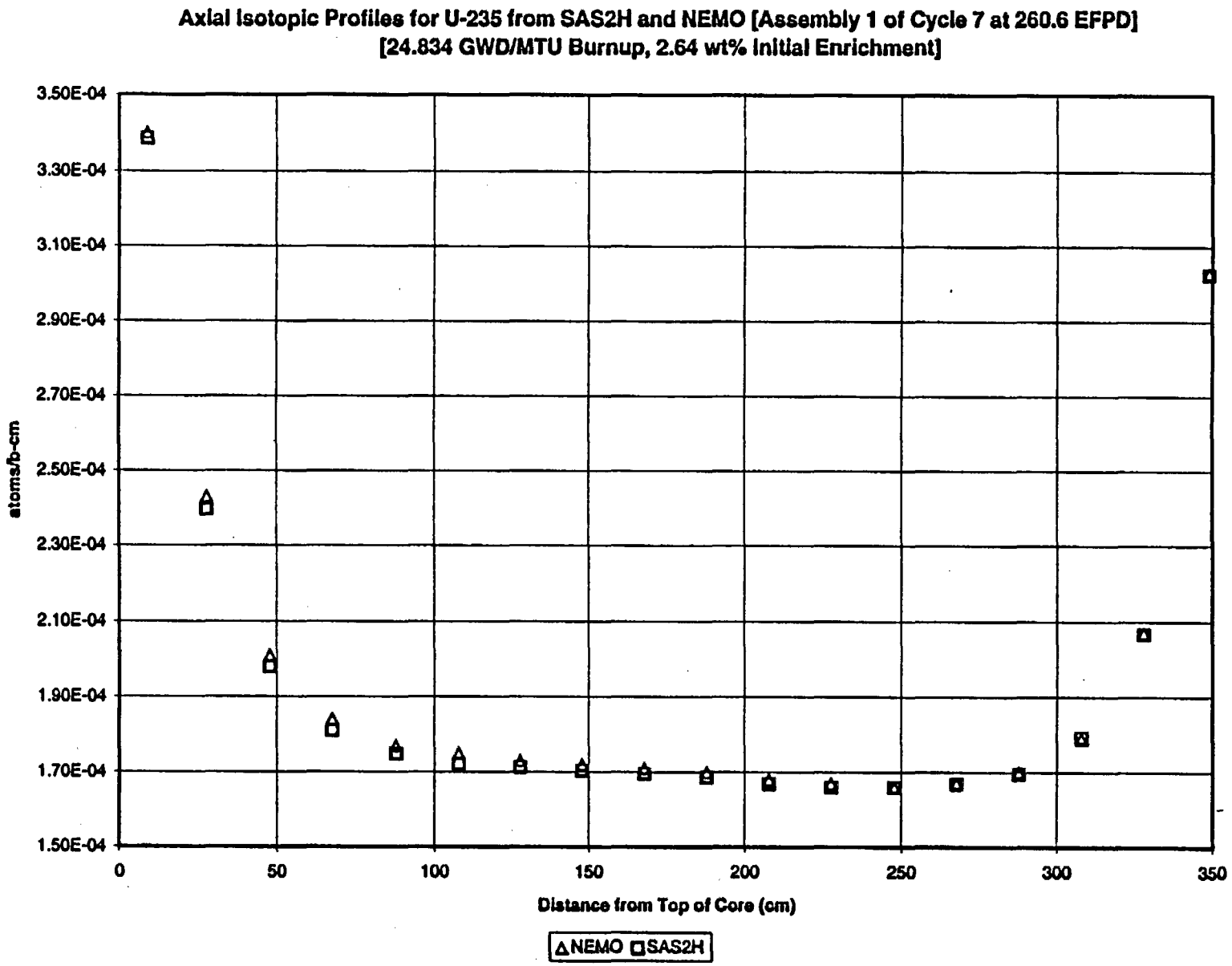

Figure 8-3 Axial Isotopic Profile Comparison Between SAS2H and CASMO/NEMO

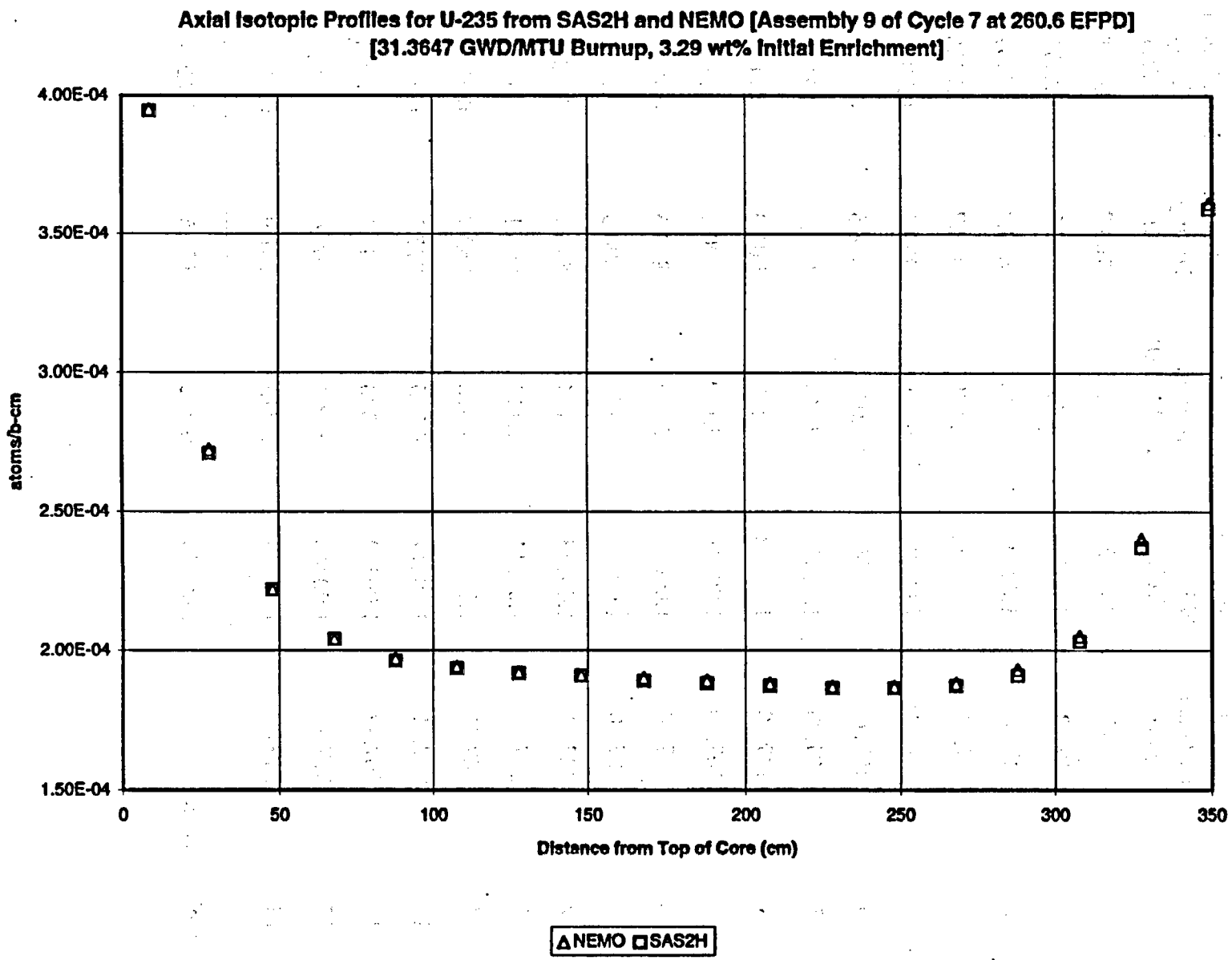

Figure 8-4 Axial Isotopic Profile Comparison Between SAS2H and CASMO/NEMO

Table 8-1 Crystal River Unit 3 Assembly A08 3.84 wt% U-235 @ 6.27 GWd/MTU U-235 NEMO/SAS2H Isotopic Ratio

Node	Axial Distance (cm)	Ratio of NEMO to SAS2H	Nodal Burnup (GWd/MTU)	Fuel Temp. History (K)	Mod. Density History (g/cc)
1	8.89	1.00255	2.816	703.3	0.6958
2	27.78	1.00454	4.769	792.2	0.6972
3	47.78	1.00405	5.961	849.3	0.6997
4	67.79	1.00582	6.570	878.7	0.7026
5	87.79	1.00602	6.880	892.7	0.7057
6	107.79	1.00541	7.034	898.5	0.7090
7	127.79	1.00653	7.107	901.0	0.7120
8	147.80	1.00638	7.139	901.3	0.7153
9	167.80	1.00638	7.150	900.5	0.7187
10	187.80	1.00638	7.154	899.6	0.7219
11	207.80	1.00638	7.153	898.5	0.7250
12	227.81	1.00638	7.144	896.7	0.7282
13	247.81	1.00511	7.112	894.1	0.7313
14	267.81	1.00541	7.026	888.7	0.7344
15	287.81	1.00617	6.825	877.3	0.7373
16	307.82	1.00502	6.380	854.1	0.7402
17	327.82	1.00340	5.402	807.0	0.7425
18	349.00	1.00348	3.243	701.9	0.7444
Assembly Average:		1.00526	6.272	857.5	0.7204

Table 8-2 Crystal River Unit 3 Assembly A29 2.62 wt% U-235 @ 15.61 GWd/MTU U-235 NEMO/SAS2H Isotopic Ratio

Node	Axial Distance (cm)	Ratio of NEMO to SAS2H	Nodal Burnup (GWd/MTU)	Fuel Temp. History (K)	Mod. Density History (g/cc)
1	8.89	1.00358	6.930	748.3	0.7143
2	27.78	1.00789	11.600	783.2	0.7149
3	47.78	1.00993	14.552	805.4	0.7159
4	67.79	1.00825	16.060	817.2	0.7171
5	87.79	1.00808	16.735	821.7	0.7182
6	107.79	1.00655	17.008	822.9	0.7194
7	127.79	1.00943	17.111	823.0	0.7208
8	147.80	1.00904	17.144	822.7	0.7219
9	167.80	1.00904	17.160	822.4	0.7232
10	187.80	1.00538	17.183	822.4	0.7243
11	207.80	1.00866	17.225	822.6	0.7255
12	227.81	1.00828	17.282	823.0	0.7266
13	247.81	1.00789	17.346	823.0	0.7278
14	267.81	1.00710	17.437	822.8	0.7289
15	287.81	1.00630	17.555	821.7	0.7298
16	307.82	1.00458	17.254	818.4	0.7307
17	327.82	1.00505	15.340	805.6	0.7318
18	349.00	1.00183	9.738	764.0	0.7331
Assembly Average:		1.00684	15.608	810.7	0.7237

Table 8-3 Crystal River Unit 3 Assembly A01 2.64 wt% U-235 @ 24.83 GWd/MTU U-235 NEMO/SAS2H Isotopic Ratio

Node	Axial Distance (cm)	Ratio of NEMO to SAS2H	Nodal Burnup (GWd/MTU)	Fuel Temp. History (K)	Mod. Density History (g/cc)
1	8.89	1.00425	12.907	860.4	0.7028
2	27.78	1.01382	20.306	899.0	0.7043
3	47.78	1.01533	24.265	916.6	0.7060
4	67.79	1.01602	25.975	923.3	0.7075
5	87.79	1.01210	26.669	925.4	0.7091
6	107.79	1.01614	26.935	926.2	0.7105
7	127.79	1.00973	27.037	926.3	0.7119
8	147.80	1.00912	27.092	925.8	0.7134
9	167.80	1.00851	27.161	925.0	0.7149
10	187.80	1.00789	27.277	923.8	0.7162
11	207.80	1.00663	27.418	922.4	0.7176
12	227.81	1.00599	27.526	920.5	0.7188
13	247.81	0.99996	27.549	918.5	0.7199
14	267.81	1.00064	27.435	916.5	0.7211
15	287.81	1.00261	27.042	913.8	0.7222
16	307.82	0.99820	25.952	908.9	0.7231
17	327.82	1.00076	23.085	898.7	0.7242
18	349.00	1.00107	15.187	864.3	0.7253
Assembly Average:		1.00692	24.834	912.0	0.7151

Table 8-4 Crystal River Unit 3 Assembly A09 3.29 wt% U-235 @ 31.36 GWd/MTU U-235 NEMO/SAS2H Isotopic Ratio

Node	Axial Distance (cm)	Ratio of NEMO to SAS2H	Nodal Burnup (GWd/MTU)	Fuel Temp. History (K)	Mod. Density History (g/cc)
1	8.89	1.00130	17.224	727.1	0.6858
2	27.78	1.00458	26.475	821.2	0.6876
3	47.78	1.00030	31.133	871.3	0.6905
4	67.79	0.99912	33.022	892.5	0.6939
5	87.79	1.00413	33.764	900.1	0.6977
6	107.79	1.00245	34.059	901.8	0.7012
7	127.79	1.00130	34.182	901.4	0.7050
8	147.80	1.00072	34.242	900.1	0.7088
9	167.80	1.00482	34.289	898.1	0.7128
10	187.80	1.00425	34.346	896.8	0.7164
11	207.80	1.00367	34.406	896.3	0.7201
12	227.81	1.00309	34.446	896.3	0.7236
13	247.81	1.00309	34.417	896.3	0.7275
14	267.81	1.00367	34.227	894.6	0.7311
15	287.81	1.01120	33.688	888.6	0.7345
16	307.82	1.00841	32.340	872.7	0.7378
17	327.82	1.01255	28.890	834.8	0.7409
18	349.00	1.00535	19.264	728.3	0.7433
Assembly Average:		1.00414	31.365	867.6	0.7147

9. Summary

The CRC analyses provide a means for validating computed SNF compositions and their associated reactivity worth calculations. A comparison between calculated and measured integral reactivity worth for systems containing SNF facilitates the performance evaluation of the SAS2H sequence of the SCALE modular code system for predicting spent fuel isotopics. Comparison of the SAS2H calculated SNF isotopic compositions with fuel isotopics determined using the commercial nuclear reactor design and analysis code combination of CASMO/NEMO provides confidence in the accuracy of the SNF isotopic compositions. The purpose of the CRC evaluations are to demonstrate and quantify the level of confidence that should be attributed to SNF compositions and associated reactivity calculations relevant to disposal of high-level radioactive materials.

The CRC summary provided in this paper presents the methods utilized in performing fuel depletion and decay calculations using the SAS2H sequence of the SCALE modular code system to provide material composition input for an MCNP criticality evaluation of the system under consideration. The three Crystal River, Unit 3, CRC analyses which have been performed were briefly described. The description and results presented in this paper were intended to convey a sense of the magnitude of information available from the CRC analyses and also demonstrate the accuracy of the calculations performed in each CRC analysis.

The CRC analyses provide detailed isotopic information and associated reactivity worth necessary to quantify the accuracy of the code systems being evaluated. A comparison of the reactivity worth calculated using the SAS2H and MCNP codes to the corresponding measured reactivity worth of the various commercial nuclear reactor configurations demonstrates the ability of the code systems to work in tandem and produce accurate results. The cross-comparison of SAS2H generated isotopic compositions with NEMO generated isotopic compositions will provide insight into the performance of the SAS2H code system on an individual nuclide basis for the major actinide contributors and certain fission product isotopes such as Sm-149. Data for other fission product isotopes is available from the SAS2H sequence to assist in evaluating the presence of potential cancellations of error in the isotopic concentrations that may allow misleading production of accurate reactivity worth results. The CRC evaluations are the key to determining the accuracy of calculated SNF compositions and their associated reactivity worth. Detailed descriptions of the CRC analyses described in this paper will be subsequently released upon settlement of proprietary issues related to the detailed reactor information utilized in performing the CRC evaluations.

10. References

10.1 O. W. Hermann and C. V. Parks. *SAS2H: A Coupled One-Dimensional Depletion and Shielding Analysis Module*, NUREG/CR-0200 Rev. 5, Oak Ridge National Laboratory, September 1995.

10.2 J. F. Briesmeister, Ed. *MCNP--A General Monte Carlo N-Particle Transport Code, Version 4A*, LA-12625-M, Los Alamos National Laboratory, November 1993.

10.3 *Quality Assurance Requirements and Description*, DOE/RW-0333P Rev. 5, U.S. Department of Energy (DOE).

10.4 *SCALE Newsletter*, Computational Physics and Engineering Division, Nuclear Engineering Applications Section, Oak Ridge National Laboratory, Number 14, July 1996.

10.5 *Crystal River Unit 3--Cycle 3 Reload Report*, BAW-1607 Rev. 1, Babcock & Wilcox, April 1980.

10.6 *Crystal River Unit 3--Cycle 4 Reload Report*, BAW-1684, Babcock & Wilcox, June 1981.

10.7 *Crystal River Unit 3--Cycle 5 Reload Report*, BAW-1767, Babcock & Wilcox, March 1983.

10.8 *Crystal River Unit 3--Cycle 6 Reload Report*, BAW-1860, Babcock & Wilcox, April 1985.

10.9 *Crystal River Unit 3--Cycle 7 Reload Report*, BAW-1988, Babcock & Wilcox, February 1987.

10.10 *Crystal River Unit 3--Cycle 8 Reload Report*, BAW-2102 Rev. 1, Babcock & Wilcox, June 1990.

10.11 *Crystal River Unit 3--Cycle 9 Reload Report*, BAW-2158 Rev. 1, Babcock & Wilcox, June 1992.

10.12 G. W. Morey. *The Properties of Glass*, 2nd ed., Reinhold, New York, 1954.

10.13 *Material Compositions and Number Densities for Neutronics Calculations*: BBA000000-01717-0200-00002 Rev. 0, Civilian Radioactive Waste Management System (CRWMS) Management & Operating Contractor (M&O).

10.14 *Core Operation Report, Crystal River Unit 3, Cycle 1 Operation, January 14, 1977 to March 3, 1978*, BAW-1545, Babcock & Wilcox, March 1979.

10.15 *Core Operation Report, Crystal River Unit 3, Cycle 1 Operation, September 15, 1978 to April 23, 1979*, BAW-1555, Babcock & Wilcox, June 1979.

10.16 *Core Operation Report, Crystal River Unit 3, Cycle 2 Operation, July 29, 1979 to February 26, 1980.*

10.17 *Core Operation Report, Crystal River Unit 3, Cycle 3 Operation, August 8, 1980 (Initial Criticality) to September 28, 1981 (EOC)*, BAW-1764, Babcock & Wilcox, November 1982.

10.18 *Core Operation Report, Crystal River Unit 3, Cycle 4 Operation, December 10, 1981 (Initial Criticality) to March 19, 1983 (EOC)*, BAW-1785, Babcock & Wilcox, May 1983.

10.19 *Core Operation Report, Crystal River Unit 3, Cycle 5 Operation, July 24, 1983 (Initial Criticality) to March 8, 1985 (EOC)*, BAW-1876, Babcock & Wilcox, June 1985.

10.20 *Core Operation Report, CR-3, Cycle 6, August 18, 1985 (Initial Criticality) to September 18, 1987 (EOC)*, BAW-2013, Babcock & Wilcox, December 1987.

10.21 *Core Operation Report, CR-3, Cycle 7, January 8, 1988 (Initial Criticality) to March 14, 1990 (EOC)*, BAW-2112, Babcock & Wilcox, October 1990.

10.22 *Core Operation Report, Crystal River Unit 3, Cycle 8, June 21, 1990 (Initial Criticality) to April 30, 1992 (EOC)*, BAW-2179, Babcock & Wilcox, December 1992.

10.23 *Core Operation Report, CR-3, Cycle 9, July 14, 1992 (Initial Criticality) to April 7, 1994 (EOC)*, BAW-2225, Babcock & Wilcox, July 1994.

10.24 *Fuel Rod Cladding, Mark-B Drawing.* Drawing Number (DN): 170346C Rev 0, Babcock & Wilcox, February 25, 1975.

10.25 *UO_2 Fuel Pellet, Mark-B Drawing.* DN: 1004892C Rev 3, Babcock & Wilcox, November 1, 1978.

10.26 *Mark-B4 Fuel Assembly General Arrangement Drawing.* DN: 32958F Rev 9, Babcock & Wilcox, March 1, 1973.

10.27 *Mark B4-Z Fuel Assembly Drawing.* DN: 1163550F Rev 1, Babcock & Wilcox, May 22, 1986.

10.28 *Mark-B9 Fuel Assembly General Arrangement Drawing.* DN: 1207221F Rev 1, Babcock & Wilcox, February 19, 1991.

10.29 *Pressurized Fuel Rod Assembly, Mark-B Drawing.* DN: 130289D Rev 6, Babcock & Wilcox, February 14, 1975.

10.30 *Arrangement of Reactor Vessel Longitudinal Section Drawing*. DN: 126951E Rev 8, Babcock & Wilcox, April 4, 1967.

10.31 *Thermal Shield Machining Details Sheet 1 Drawing*. DN: 142915E Rev 6, Babcock & Wilcox, September 23, 1967.

10.32 *Core Barrel Cylinder Assembly Machining Details Drawing*. DN: 142907E Rev 7, Babcock & Wilcox, July 17, 1969.

10.33 *Core Barrel Assembly Drawing*. DN: 27061F Rev 6, Babcock & Wilcox, July 18, 1969.

10.34 *Core Barrel Details Sheet-3 Drawing*. DN: 142901E Rev 2, Babcock & Wilcox, April 3, 1969.

10.35 *Core Barrel Details Sheet-1 Drawing*. DN: 142908E Rev 3, Babcock & Wilcox, April 3, 1969.

10.36 *Guide Tube Recrystallized Drawing*. DN: 1155390C Rev 0, Babcock & Wilcox, January 9, 1985.

10.37 *Instrument Tube, Mark-B Drawing*. DN: 170340C Rev 1, Babcock & Wilcox, February 25, 1975.

10.38 *Mark-B Burnable Poison Pellet Drawing*. DN: 1004934C Rev 0, Babcock & Wilcox, November 27, 1978.

10.39 *Burnable Poison Rod Drawing*. DN: 115701D Rev 7, Babcock & Wilcox, December 2, 1971.

10.40 *Al2O3-B4C Pellet Specification Revision*. BWNT Document No.: 32-1240838-00, B&W Nuclear Technologies, December 20, 1995.

10.41 *Technical Report on Actinide-Only Burnup Credit for PWR Spent Nuclear Fuel Packages*, DOE/RW-0472 Rev 0, DOE.

INTENTIONALLY LEFT BLANK

Disposal Criticality Analysis Methodology Technical Report

APPENDIX B.2

Comparison Between MCNP and Critical Experiments

INTENTIONALLY LEFT BLANK

Table of Contents

[The information presented in this study is preliminary and should not be used for direct support of any procurement, fabrication, or construction activities.]

1. Introduction

The calculational method for determining the critical multiplication factor (k_{eff}) of the waste package during the design process relies upon the use of a computer code. The code being utilized by the Waste Package Development Department of the Mined Geologic Disposal System (MGDS) of the Yucca Mountain Site Characterization Project to determine the k_{eff} for the waste package and the repository (external to the waste package) is the Monte Carlo N-Particle Transport Code System (MCNP) developed by Los Alamos National Laboratory (LANL) (Ref. 9.1).

The purpose of this study is to quantify the MCNP code system's ability to accurately calculate the critical multiplication factor (k_{eff}) for various configurations in support of the development of the disposal criticality methodology. This study quantifies the effectiveness of the MCNP criticality calculation over numerous ranges of potential configurations anticipated during long-term deep geologic disposal. This study verifies the applicability of the MCNP code system to the calculation of k_{eff} values for both intact and degraded configurations.

The calculation of bias values and enhanced subcritical margins as described in Section 7.5 is based on the results of numerous critical benchmark evaluations performed using the MCNP code system provides a means for quantifying the effectiveness of the MCNP criticality calculation. Potential correlations between k_{eff} and certain characterization parameters are also examined to identify the presence of trends in the bias. The bias value calculations and trending analyses use standard small-sample statistical methods. A detailed description of the applicable small-sample statistical methods are presented in Sections 7.5 and 7.6 of this study. To assure compliance with the bias value requirements set forth in ANSI/ANS-8.17 (Ref. 9.2) and 10 CFR 60.131(b)(7) (Ref. 9.3), the bias value results determined in this study may serve as preliminary bias values to be applied in subsequent criticality calculations relevant to the disposal criticality control methodology.

2. Scope

All information (excluding regulations and standards) presented in this study is preliminary and shall be treated as unqualified. This information will require subsequent qualification. This paper does not directly support any construction, fabrication, or procurement activity. Any data from this study used for input into documents supporting construction, fabrication, or procurement must be documented and controlled in accordance with the appropriate Quality Assurance Requirements and Description (QARD) (Ref. 9.6) controls.

3. Regulations and Standards

This study provides a description of the database and the methodology for determining calculational bias and uncertainty values for disposal criticality analyses. The bias and uncertainty values are required per the following regulations and standards.

Regulations-- Title 10 Code of Federal Regulations, Part 60-- Disposal of High-Level Radioactive Wastes in Geologic Repositories, 1995. [10 CFR 60.131(b)(7)] (Ref. 9.3)

Standards-- American National Standard Criticality Safety Criteria for the Handling, Storage, and Transportation of LWR Fuel Outside Reactors, January 13, 1984. [ANSI/ANS-8.17-1984] (Ref. 9.2)

4. MCNP Code System

The Monte Carlo N-Particle Transport Code System (MCNP), Version 4A (Ref. 9.1) is used in this study. The MCNP 4A criticality calculations documented in this study were performed on Hewlett Packard Apollo 9000, Series 735 Workstations. An associated continuous energy cross-section set based on ENDF/B-V is used by MCNP. This library provides much more detail than multi-group cross-section sets.

The MCNP 4A code system is appropriate for the application of determining the k_{eff} values of configurations or systems containing fissionable material. This study provides supplementary evidential support for the validation of MCNP 4A as an appropriate tool to be utilized in k_{eff} calculations.

4.1 MCNP General Description

A full description of the MCNP4A computer code is provided in the MCNP user manual. The following excerpts will provided a general description.

> "MCNP is a general-purpose Monte Carlo N-Particle code that can be used for neutron, photon, electron, or coupled neutron/photon/electron transport, including the capability to calculate eigenvalues for critical systems. The code treats arbitrary three-dimensional configurations of materials in geometric cells bounded by first-degree and second-degree surfaces and fourth-degree elliptical tori.
>
> "Pointwise cross-section data are used. For neutrons, all reactions given in a particular cross-section evaluation (such as ENDF/B-V) are accounted for. Thermal neutrons are described by both the free gas and $S(\alpha,\beta)$ models.
>
> "Important standard features that make MCNP very versatile and easy to use include a powerful general source, criticality source, and surface source; both geometry and output tally plotters; a rich collection of variance reduction techniques; a flexible tally structure; and an extensive collection of cross-section data." (Ref. 9.1, Pg ix)

4.2 Monte Carlo Method

The Monte Carlo method is a method of simulating and recording the behavior of individual particles within a system. The behavior of the simulated particles is extrapolated to describe the average behavior of all of the particles within the system. The Monte Carlo method as applied to neutrons in an MCNP criticality calculation is based upon following a number of individual neutrons through their various transport experiences such as scattering, fission, absorption, or leakage. The fission process is regarded as the birth event that separates generations of neutrons. A generation is the lifetime of a neutron from birth by fission to death by either escape, parasitic capture, or absorption leading to fission. The average behavior of the sample set of neutrons is used to describe the average behavior of the system with regard to the number of neutrons in successive generations (i.e. critical multiplication factor, k_{eff}).

4.3 MCNP's Critical Multiplication Factor (k_{eff}) Results

MCNP 4A calculates three k_{eff} estimates for each cycle in a given problem--

1) the collision estimate,
2) the absorption estimate, and
3) the track length estimate.

A detailed description of the three k_{eff} estimates may be found in Chapter 2, Section VIII, Part B, of the MCNP User Manual (Ref. 9.1). The k_{eff} estimate used in the criticality analyses and in the bias value determination of this study is the statistical combination of all three k_{eff} estimates. According to statisticians at the Los Alamos National Laboratory, "the three-combined k_{eff} estimator is the best final estimate from an MCNP calculation." (Ref. 9.1, Pg 2-146) "The confidence interval based on the three statistically combined k_{eff} estimate is the recommended result to use for all final k_{eff} confidence interval quotations because all of the available information has been used in the final result." (Ref. 9.1, Pg 2-149)

4.4 Assessing the Validity of a Criticality Calculation

Before an MCNP k_{eff} result can be considered acceptable the validity of the calculation must be determined. Two minimum requirements for assessing the validity of an MCNP criticality calculation include--

1) all cells containing fissionable material should be adequately sampled, and
2) the fundamental spatial mode should be achieved before commencing the accumulation of data for calculation of the mean k_{eff}.

MCNP provides several features which help in assessing the validity of a k_{eff} calculation. To satisfy the first requirement, "MCNP verifies that at least one fission source point was generated in each cell containing fissionable material." (Ref. 9.1, Pg 2-150)

To satisfy the second requirement, MCNP provides several checks to determine if the fundamental spatial mode was achieved prior to the completion of the I_c cycles (I_C is the number

of source cycles that are skipped before k_{eff} data accumulation begins). One check is the comparison of the estimated three-combined k_{eff} and its standard deviation for the first and second half of the active k_{eff} cycles. If the difference between the average k_{eff} values for the two halves does not appear to be zero or if the ratio of the two standard deviations is larger than expected a "WARNING" message is provided in the output. MCNP determines the number of cycles which must be skipped to produce the minimum standard deviation for the three-combined k_{eff} estimate. If this result is larger than I_c it may be indicative that more cycles should be skipped before accumulating k_{eff} data. MCNP checks each k_{eff} estimate's cycle data to assure normality at the 95% and 99% confidence levels. If a k_{eff} estimate is not normally distributed with respect to the mean k_{eff} at the 99% confidence level a "WARNING" message is provided in the output. "Unless there is a high positive correlation among the three estimates, it is expected to be rare that all three k_{eff} estimates will not appear normally distributed at the 99% confidence level when the normal spatial mode has been achieved and maintained." (Ref. 9.1, Pg 2-150) Finally, MCNP tests for a monotonic trend of the three-combined k_{eff} estimate's results over the last ten active cycles. If the spatial mode is well converged and maintained, there should not be a monotonic trend within the last ten active cycles. A "WARNING" message is provided in the output if a monotonic trend is detected.

Compliance with the two minimum requirements addressed above should be verified for each criticality calculation using the checks provided by the MCNP code. If either of the two requirements appear to be violated, the k_{eff} results for the calculation should be evaluated further.

4.5 Cross-Sections

Utilizing the appropriate material cross-sections in an MCNP criticality calculation is essential to obtaining credible results. The cross-sections for the various neutron interactions are used to determine the flow of the criticality calculation at each interaction site. The MCNP neutron interaction tables are processed from evaluated data in the ENDF/B-V format.

The MCNP neutron interaction tables provide the following data--

1) all available cross-section data,
2) angular distribution data for scattered neutrons,
3) energy distribution data for inelastically scattered neutrons,
4) data about secondary photon production,
5) Q-value data for each reaction, and
6) the average number of neutrons per fission data for fissionable isotopes.

"For a particular table, the cross-sections for each reaction are given on one energy grid that is sufficiently dense that linear-linear interpolation between points reproduces the evaluated cross-sections within a specified tolerance that is generally within 1% or less" of the evaluated data (Ref. 9.1). A "thinned" neutron interaction table is available for some nuclides. The "thinned" tables have a significantly reduced size with a tolerance that is greater than 1%. The "thinned" tables are not recommended for use in calculations involving transport through the resonance region (Ref. 9.1).

Neutron interaction table designations are included as part of the material composition input to MCNP. Each material composition is composed of one or more elements or isotopes designated by a ZAID identifier. The ZAID identifier takes the form "ZZZAAA.nnC" where "ZZZ" represents the atomic number of the element ("ZZZ" may be one or two digits), "AAA" represents the elemental isotope ("AAA" must be three digits incorporating leading zeros), and "nn" represents the neutron interaction table designation.

Several neutron interaction tables are available to meet different user needs. The ".50C" and ".51C" series of data tables are both derived from the ENDF/B-V evaluated data. "The ".50C" series is the most faithful reproduction of the evaluated data (Ref. 9.1)." "The ".51C" series, also called the "thinned" series, has been processed with a less rigid tolerance than the ".50C" series." (Ref. 9.1) The ".35C" series data tables are produced by the Physical Data Group at Lawrence Livermore National Laboratory. The Livermore evaluations "manifest a philosophy of reproducing the data with the fewest number of points." (Ref. 9.1) The ".55C" series is the most recent evaluation produced by the Applied Nuclear Science Group T-2 at Los Alamos National Laboratory. "Generally, these evaluations (".55C") are the most complex because they are the most thorough ." (Ref. 9.1)

Calculations involving transport through the resonance region should use the most detailed neutron interaction tables available unless there is a valid reason to do otherwise, such as the availability of more appropriate temperature dependent cross-sections. An MCNP k_{eff} calculation result is uniquely defined by the neutron interaction tables it utilizes. Table 4.1.5-1 contains a listing of elements and isotopes with their ZAIDs which may be utilized in criticality analyses for which the enhanced subcritical margins and maximum allowable k_{eff} values determined in this study are applicable. The cross-section tables for the elements and isotopes of the critical configuration simulations contained in this analysis are obtained from the set displayed in Table 4.1.5-1. The waste package criticality analyses must apply ZAIDs from the listing in Table 4.1.5-1 to maintain the validity of the bias values determined in this study.

Table 4.1.5-1
Preferred ZAIDs for Various Elements and Isotopes

Element	Symbol	Isotope	ZAID	Filename	Source
1 Hydrogen	H	H-1	1001.50C	rmccs	ENDF/B-V
	D	H-2	1002.55C	rmccs	GROUP T-2
	T	H-3	1003.50C	rmccs	ENDF/B-V
2 Helium	He	He-3	2003.50C	rmccs	ENDF/B-V
	He	He-4	2004.50C	rmccs	ENDF/B-V
3 Lithium	Li	Li-6	3006.50C	rmccs	ENDF/B-V
	Li	Li-7	3007.55C	rmccs	GROUP T-2
4 Beryllium	Be	Be-9	4009.50C	rmccs	ENDF/B-V
5 Boron	B	B-10	5010.50C	rmccs	ENDF/B-V
	B	B-11	5011.56C	newxs	GROUP T-2

Element	Symbol	Isotope	ZAID	Filename	Source
6 Carbon	C	nat.	6000.50C	rmccs	ENDF/B-V
	C	C-12	6012.50C	rmccs	ENDF/B-V
7 Nitrogen	N	N-14	7014.50C	rmccs	ENDF/B-V
8 Oxygen	O	O-16	8016.50C	rmccs	ENDF/B-V
9 Fluorine	F	F-19	9019.50C	endf5p	ENDF/B-V
11 Sodium	Na	Na-23	11023.50C	endf5p	ENDF/B-V
12 Magnesium	Mg	nat.	12000.50C	endf5u	ENDF/B-V
13 Aluminum	Al	Al-27	13027.50C	rmccs	ENDF/B-V
14 Silicon	Si	nat.	14000.50C	endf5p	ENDF/B-V
15 Phosphorus	P	P-31	15031.50C	endf5u	ENDF/B-V
16 Sulfur	S	S-32	16032.50C	endf5u	ENDF/B-V
17 Chlorine	Cl	nat.	17000.50C	endf5p	ENDF/B-V
19 Potassium	K	nat.	19000.50C	endf5u	ENDF/B-V
20 Calcium	Ca	nat.	20000.50C	endf5u	ENDF/B-V
22 Titanium	Ti	nat.	22000.50C	endf5u	ENDF/B-V
23 Vanadium	V	nat.	23000.50C	endf5u	ENDF/B-V
24 Chromium	Cr	nat.	24000.50C	rmccs	ENDF/B-V
25 Manganese	Mn	Mn-55	25055.50C	endf5u	ENDF/B-V
26 Iron	Fe	nat.	26000.55C	rmccs	GROUP T-2
27 Cobalt	Co	Co-59	27059.50C	endf5u	ENDF/B-V
28 Nickel	Ni	nat.	28000.50C	rmccs	ENDF/B-V
29 Copper	Cu	nat.	29000.50C	rmccs	ENDF/B-V
33 Arsenic	As	As-75	33075.35C	rmccsa	ENDL-85
36 Krypton	Kr	Kr-83	36083.50C	rmccsa	ENDF/B-V
40 Zirconium	Zr	nat.	40000.50C	endf5p	ENDF/B-V
	Zr	Zr-93	40093.50C	kidman	ENDF/B-V
41 Niobium	Nb	Nb-93	41093.50C	endf5p	ENDF/B-V
42 Molybdenum	Mo	nat.	42000.50C	endf5u	ENDF/B-V
	Mo	Mo-95	42095.50C	kidman	ENDF/B-V
43 Technetium	Tc	Tc-99	43099.50C	kidman	ENDF/B-V
44 Ruthenium	Ru	Ru-101	44101.50C	kidman	ENDF/B-V
	Ru	Ru-103	44103.50C	rmccsa	ENDF/B-V
45 Rhodium	Rh	Rh-103	45103.50C	kidman	ENDF/B-V

Element	Symbol	Isotope	ZAID	Filename	Source
	Rh	Rh-105	45105.50C	kidman	ENDF/B-V
46 Palladium	Pd	Pd-105	46105.50C	kidman	ENDF/B-V
	Pd	Pd-108	46108.50C	kidman	ENDF/B-V
47 Silver	Ag	Ag-109	47109.50C	rmccsa	ENDF/B-V
48 Cadmium	Cd	nat.	48000.50C	endf5u	ENDF/B-V
50 Tin	Sn	nat.	50000.35C	endl85	ENDL-85
53 Iodine	I	I-135	53135.50C	kidman	ENDF/B-V
54 Xenon	Xe	Xe-131	54131.50C	kidman	ENDF/B-V
	Xe	Xe-135	54135.50C	eprixs	ENDF/B-V
55 Cesium	Cs	Cs-133	55133.50C	kidman	ENDF/B-V
	Cs	Cs-135	55135.50C	kidman	ENDF/B-V
56 Barium	Ba	Ba-138	56138.50C	rmccs	ENDF/B-V
59 Praseodymium	Pr	Pr-141	59141.50C	kidman	ENDF/B-V
60 Neodymium	Nd	Nd-143	60143.50C	kidman	ENDF/B-V
	Nd	Nd-145	60145.50C	kidman	ENDF/B-V
	Nd	Nd-147	60147.50C	kidman	ENDF/B-V
	Nd	Nd-148	60148.50C	kidman	ENDF/B-V
61 Promethium	Pm	Pm-147	61147.50C	kidman	ENDF/B-V
	Pm	Pm-148	61148.50C	kidman	ENDF/B-V
	Pm	Pm-149	61149.50C	kidman	ENDF/B-V
62 Samarium	Sm	Sm-147	62147.50C	kidman	ENDF/B-V
	Sm	Sm-149	62149.50C	endf5u	ENDF/B-V
	Sm	Sm-150	62150.50C	kidman	ENDF/B-V
	Sm	Sm-151	62151.50C	kidman	ENDF/B-V
	Sm	Sm-152	62152.50C	kidman	ENDF/B-V
63 Europium	Eu	Eu-151	63151.55C	newxs	GROUP T-2
	Eu	Eu-153	63153.55C	newxs	GROUP T-2
	Eu	Eu-154	63154.50C	endf5u	ENDF/B-V
	Eu	Eu-155	63155.50C	kidman	ENDF/B-V
64 Gadolinium	Gd	nat.	64000.35C	rmccsa	ENDL-85
	Gd	Gd-155	64155.50C	endf5u	ENDF/B-V
	Gd	Gd-157	64157.50C	endf5u	ENDF/B-V
72 Hafnium	Hf	nat.	72000.50C	newxs	ENDF/B-V

Element	Symbol	Isotope	ZAID	Filename	Source
73 Tantalum	Ta	Ta-181	73181.50C	endf5u	ENDF/B-V
74 Tungsten	W	nat.	74000.55C	rmccs	GROUP T-2
82 Lead	Pb	nat.	82000.50C	rmccs	ENDF/B-V
92 Uranium	U	U-233	92233.50C	rmccs	ENDF/B-V
	U	U-234	92234.50C	endf5p	ENDF/B-V
	U	U-235	92235.50C	rmccs	ENDF/B-V
	U	U-235 @ (600K)	92235.53C	eprixs	ENDF/B-V
	U	U-236	92236.50C	endf5p	ENDF/B-V
	U	U-238	92238.50C	rmccs	ENDF/B-V
	U	U-238 @ (600K)	92238.53C	eprixs	ENDF/B-V
93 Neptunium	Np	Np-237	93237.55C	rmccsa	GROUP T-2
94 Plutonium	Pu	Pu-238	94238.50C	endf5p	ENDF/B-V
	Pu	Pu-239	94239.55C	rmccs	GROUP T-2
	Pu	Pu-240	94240.50C	rmccs	ENDF/B-V
	Pu	Pu-241	94241.50C	endf5p	ENDF/B-V
	Pu	Pu-242	94242.50C	endf5p	ENDF/B-V
	Pu	Pu-243	94243.35C	endl85	ENDL-85
95 Americium	Am	Am-241	95241.50C	endf5u	ENDF/B-V
	Am	Am-242m	95242.50C	endf5u	ENDF/B-V
	Am	Am-243	95243.50C	endf5u	ENDF/B-V
96 Curium	Cm	Cm-243	96243.35C	endl85	ENDL-85
	Cm	Cm-244	96244.50C	endf5u	ENDF/B-V
	Cm	Cm-245	96245.35C	endl85	ENDL-85
	Cm	Cm-248	96248.35C	endl85	ENDL-85

4.6 S(α,β) Thermal Treatment

The S(α,β) thermal treatment accounts for binding effects in molecules and crystalline solids. The S(α,β) thermal scattering treatment is a necessary requirement in a highly moderating medium where low-energy scattering may be dominant. S(α,β) thermal treatment tables are available for a limited number of materials. In this study the thermal treatment is consistently applied to the materials having available data. The materials using the S(α,β) treatment in the critical benchmarks of this study include light-water, polyethylene, and graphite.

5. Assumptions

The assumptions listed in this section are applicable to this study as described.

5.1 The use of published MCNP k_{eff} results in Section 7, which are obtained from documents generated by several national laboratories, are acceptable for use in the determination of preliminary bias values and enhanced subcritical margins. The MCNP 4A code system was used to performed 65 of the fresh fuel criticality evaluations contained in the critical experiment library. The demonstrated agreement in Section 7.4, between the study calculated k_{eff} results and the published k_{eff} results provide justification for this assumption.

5.2 The exclusion of the critical experiment bias and uncertainty values, including their associated uncertainties, is acceptable for the preliminary determination of the enhanced subcritical margins in Section 7.5.2. The justification for this assumption is provided by the fact that the enhanced subcritical margins and maximum allowable k_{eff}'s (subcritical limits (SL)) reported for each classification in Section 7.5.3, are treated as preliminary results. Additionally, these preliminary results are not expected to significantly change after further evaluation due to compensating conservatism in the statistical methodology, such as setting the partial derivatives of the mean calculated benchmark k_{eff} with respect to bias and uncertainty in both the critical experiments and the calculations equal to one, as described in Section 7.5.2.

6. Objectives

This study involves the use of the MCNP code system to perform criticality analyses on various critical benchmark configurations to determine their critical multiplication factors (k_{eff}'s). Each analyzed critical configuration represents a critical experiment whose k_{eff} value has been experimentally evaluated. The k_{eff} result obtained from the MCNP computer simulation of each critical experiment is compared to the experiment's empirical value to quantify the effectiveness of the MCNP criticality calculation.

The objectives of this study include the following–

1) Create a table of preliminary enhanced subcritical margins and maximum allowable k_{eff} (subcritical limit) values representative of the MCNP code system's ability to accurately predict k_{eff} for classifications of experiments containing physically and neutronically similar configurations.

2) Investigate the use of a trending analysis methodology for determining the applicability of a classification's bias value to a particular configuration's k_{eff} result. The bias values for the experiments within each classification may be correlated to certain physical and neutronic characterization parameters. A correlation between the MCNP-based bias values and the characterization parameters may assist in calculating an appropriate bias value applicable to the

particular configuration being analyzed. The trending analysis investigations in this study are limited to the examination of correlations between k_{eff} and the average lethargy of the neutron causing fission (AVEL) and between k_{eff} and the moderator to fuel atom ratio (H/X ratio). Trending analysis investigations are limited to the classification of experiments representative of the intact waste package configuration (i.e. "Fissile Oxide Fuel / Lattice Geometries / Moderated").

3) Provide a general description of the critical experiment library, including MCNP simulation k_{eff} results for each experiment, which will serve as the initial database for the determination of appropriate enhanced subcritical margins applicable to MCNP criticality calculations. The critical experiment library is subdivided into a number of distinct experiment classifications. Each experiment classification represents a group of critical experiments having similar fuel type, geometry, and moderation or reflection characteristics. The current classifications contained in the critical experiment library were developed to encompass the set of critical experiments readily available for inclusion in this study such that a broad range of physical and neutronic system characteristics were sampled. The final critical experiment library will contain specific experiment classifications that are based upon credible, potential degradation sequences (to be determined) for which criticality analyses will need to be performed.

This study verifies the applicability of the MCNP code system in the calculation of k_{eff}. To assure compliance with the bias value requirements set forth in ANSI/ANS-8.17 (Ref. 9.2) and 10 CFR 60.131(b)(7) (Ref. 9.3), the enhanced subcritical margin results corresponding to the various critical configuration classifications included in the critical experiment library may serve as *preliminary* results for calculating maximum allowable k_{eff} values to be applied in subsequent criticality calculations relevant to disposal criticality scenarios.

7. Study Description and Results

It is necessary to have a *quantified* level of confidence that the MCNP code system is capable of accurately predicting the k_{eff} of fissile material containing waste during disposal regardless of the configuration. The *quantified* level of confidence to be attributed to the MCNP code system's k_{eff} results may be obtained by evaluating the performance of the MCNP code system in simulating critical benchmark experiments whose material and neutronic characteristics are similar to those of disposal configurations. Demonstrating that the MCNP code system is applicable to the determination of k_{eff} values for the range of probable configurations requires the evaluation of code performance in simulating a broad range of critical benchmark experiments whose characteristics are representative of the potential configurations.

7.1 Critical Experiment Library

The requirements pertaining to criticality control in ANSI/ANS-8.17 (Ref. 9.2) and 10 CFR 60.131(b)(7) (Ref. 9.3) state that appropriate bias values for criticality calculations must be

derived from a database of critical benchmarks having physical and neutronic characteristics similar to those of the configurations to which the bias value will be applied. To establish the database from which appropriate bias values will be determined, a literature search was performed to obtain a set of 289 critical benchmark experiments. The current set of readily available critical experiments was chosen because they potentially represent the range of waste characteristics for disposal. However, this set of experiments is not defined to be inclusive. A large number of documented critical experiments exist outside of those currently included in the library. Additional experiments may be added in the future to extend the range of bias value applicability as more abstract configurations become of interest.

The critical experiment library is currently composed of 289 critical experiments which are classified according to fuel, geometry, and moderating or reflecting characteristics. Twenty fresh fuel classifications currently exist within the library to accommodate the various experimental configuration characteristics. The current classifications and number of critical experiments in each are shown in Table 7.1-1. Sections 7.2.1 through 7.2.20 contain summary general descriptions of each experiment in the twenty classifications.

It is important to note that some of the critical benchmark experiments included in the current critical experiment library are exponential approach to critical experiments that never obtained a measured critical condition. The MCNP calculated k_{eff} for these exponential critical experiments is based on the nominal critical configuration determined by extrapolation from measured k_{eff} data. However, the majority of experiments in the current critical experiment library are true criticals which reached the critical condition with a measured k_{eff} of unity.

Table 7.1-1
Fresh Fuel Critical Experiment Library Classifications

Classification			Number of Experiments
Fissile Metal Fuel	Cylinder Arrays	Unmoderated	29
	Slab Lattice Geometries	Moderated	22
	Single Unit Cylinders	Bare	7
		Reflected	14
	Single Unit Spheres	Bare	6
		Reflected	6
	Single Unit Annuli	Bare	2
		Reflected	32
	Unique Geometries		4
Fissile Oxide Fuel	Cylinder Arrays	Unmoderated	3
		Moderated	7
	Lattice Geometries	Moderated	41
Fissile Solution Fuel	Cylinder Arrays	Bare	6
		Reflected	41
	Single Unit Cylinders	Bare	15
		Reflected	37
	Single Unit Spheres	Bare	10
		Reflected	3
	Single Unit Parallelepipeds	Bare	2
		Reflected	2
Total Number of Fresh Fuel Critical Experiments in Library:			289

7.2 Fresh Fuel Critical Experiments

The fresh fuel critical benchmark descriptions presented in this section are organized according to fuel (i.e. fissile metals, fissile oxides, fissile solutions), geometry (i.e. lattices, cylinders, spheres, parallelepipeds, annuli, etc.), moderation, and reflection. The critical configurations which have been analyzed with the MCNP 4A code system are identified as such in the description of each experiment classification. Additional reported MCNP results were obtained from the various critical benchmark references. An experiment identifier representing each configuration is provided for subsequent referencing in this study. The references from which the critical benchmark information was obtained are identified in a table at the beginning of each section corresponding to a critical experiment library classification. Some of the reference documents for configurations in the preliminary critical experiment library are intermediate documents which summarize a group of critical benchmark reports. Original references were used for MCNP modeling when available.

7.2.1 Fissile Metal Fuel / Cylinder Arrays / Unmoderated

This classification currently consists of twenty-nine critical experiments including one experiment with plutonium fuel. The critical configurations in this section are characterized as having a fast neutron energy spectrum. The bias obtained from this classification may be applicable to potential severely degraded waste package internal criticality evaluation scenarios or repository external criticality evaluation scenarios involving interacting units of highly enriched fissionable material in non-thermalizing environments. Four of the experiments have been simulated with the MCNP 4A code system and are identified as such in their descriptions. The k_{eff} and standard deviations presented for the other experiments are the published values obtained from various references. Table 7.2.1-1 contains a listing of this classification's experiments including the k_{eff} result and the reference identifiers corresponding to each experimental description.

Table 7.2.1-1
Classification: Fissile Metal Fuel / Cylinder Arrays / Unmoderated

Experiment ID	k_{eff} (MCNP)	sigma (MCNP)	Reference
prob1	0.9999*1	0.0009	9.11, 9.12
prob7	1.0002*1	0.0008	9.11, 9.12
Pu 3X3 *2	1.0000	0.0019	9.13, 9.14
A15	0.9957	0.0022	9.12, 9.15
A21	0.9925	0.0020	9.12, 9.15
A41	0.9947	0.0022	9.12, 9.15
A51	0.9946	0.0020	9.12, 9.15
A61	0.9851	0.0024	9.12, 9.15
ARRAY.2	0.9982	0.0020	9.12, 9.15
prob3	0.9961*1	0.0011	9.11, 9.12
prob5	0.9995	0.0027	9.11, 9.12
A11	1.0029	0.0019	9.12, 9.15
A12	1.0085	0.0028	9.12, 9.15
A13	1.0070	0.0024	9.12, 9.15
A14	1.0006	0.0025	9.12, 9.15
A22	0.9976	0.0022	9.12, 9.15
A23	1.0035	0.0024	9.12, 9.15
A24	1.0029	0.0024	9.12, 9.15
A25	0.9979	0.0022	9.12, 9.15
A32	0.9996	0.0021	9.12, 9.15
A33	1.0070	0.0024	9.12, 9.15
A34	1.0065	0.0025	9.12, 9.15
A35	0.9991	0.0027	9.12, 9.15

Experiment ID	k_{eff} (MCNP)	sigma (MCNP)	Reference
A42	0.9968	0.0021	9.12, 9.15
A43	1.0020	0.0028	9.12, 9.15
A44	0.9997	0.0027	9.12, 9.15
A45	0.9944	0.0029	9.12, 9.15
A62	0.9977*1	0.0024	9.12, 9.15
ARRAY.5	1.0028	0.0029	9.12, 9.15

*1 These k_{eff} results are obtained from the MCNP 4A code system.

*2 This critical experiment contains plutonium fuel.

The following listing contains a brief description for each experiment identifier presented in Table 7.2.1-1. These descriptions are general statements whose purpose is to only identify the type of critical configuration. A complete detailed description for each experiment is provided in the references listed in Table 7.2.1-1.

prob1: unreflected 2x2x2 array of 93.2 wt% enriched uranium cylinders

prob7: unreflected 2x2x2 array of 93.2 wt% enriched uranium cylinders based upon applying specular reflecting boundary conditions to a unit cell containing one cylinder

Pu 3x3: a 3x3 array of fuel rods each containing three stacked cylinders of plutonium metal

A15: a 2x2x4 array of 9.767 kg U-235/unit cylinders of diameter 11.506 cm and of height 5.382 cm

A21: a 3x3x3 array of 9.771 kg U-235/unit cylinders of diameter 11.509 cm and of height 5.382 cm

A41: a 3x3x3 array of 9.776 kg U-235/unit cylinders of diameter 9.116 cm and of height 8.641 cm

A51: a 3x3x5 array of 9.747 kg U-235/unit cylinders of diameter 11.494 cm and of height 5.382 cm

A61: a 4x4x4 array of 9.724 kg U-235/unit cylinders of diameter 11.481 cm and of height 5.382 cm

ARRAY.2: a 2x2x2 array of 19.535 kg U-235/unit cylinders of diameter 11.506 cm and of height 10.765 cm

prob3: a 2x2x2 array of 93.2 wt% enriched uranium cylinders enclosed in a 15.24 cm paraffin reflector

prob5: a 2x2x2 array of 93.2 wt% enriched uranium cylinders enclosed in a 30.48 cm paraffin reflector

A11: a 2x2x2 array of 9.767 kg U-235/unit cylinders of diameter 11.506 cm and of height 5.382 cm

A12: a 2x2x2 array of 9.767 kg U-235/unit cylinders of diameter 11.506 cm and of height 5.382 cm

A13:	a 2x2x2 array of 9.767 kg U-235/unit cylinders of diameter 11.506 cm and of height 5.382 cm
A14:	a 2x2x2 array of 9.767 kg U-235/unit cylinders of diameter 11.506 cm and of height 5.382 cm
A22:	a 3x3x3 array of 9.771 kg U-235/unit cylinders of diameter 11.509 cm and of height 5.382 cm
A23:	a 3x3x3 array of 9.771 kg U-235/unit cylinders of diameter 11.509 cm and of height 5.382 cm
A24:	a 3x3x3 array of 9.771 kg U-235/unit cylinders of diameter 11.509 cm and of height 5.382 cm
A25:	a 3x3x3 array of 9.771 kg U-235/unit cylinders of diameter 11.509 cm and of height 5.382 cm
A32:	a 2x2x2 array of 9.792 kg U-235/unit cylinders of diameter 9.116 cm and of height 8.641 cm
A33:	a 2x2x2 array of 9.792 kg U-235/unit cylinders of diameter 9.116 cm and of height 8.641 cm
A34:	a 2x2x2 array of 9.792 kg U-235/unit cylinders of diameter 9.116 cm and of height 8.641 cm
A35:	a 2x2x2 array of 9.792 kg U-235/unit cylinders of diameter 9.116 cm and of height 8.641 cm
A42:	a 3x3x3 array of 9.776 kg U-235/unit cylinders of diameter 9.116 cm and of height 8.641 cm
A43:	a 3x3x3 array of 9.776 kg U-235/unit cylinders of diameter 9.116 cm and of height 8.641 cm
A44:	a 3x3x3 array of 9.776 kg U-235/unit cylinders of diameter 9.116 cm and of height 8.641 cm
A45:	a 3x3x3 array of 9.776 kg U-235/unit cylinders of diameter 9.116 cm and of height 8.641 cm
A62:	a 4x4x4 array of 9.724 kg U-235/unit cylinders of diameter 11.481 cm and of height 5.382 cm
ARRAY.5:	a 2x2x2 array of 19.535 kg U-235/unit cylinders of diameter 11.506 cm and of height 10.765 cm

7.2.2 Fissile Metal Fuel / Slab Lattice Geometries / Moderated

This classification currently consists of twenty-two critical experiments. The critical configurations in this section are characterized as having thermal to epithermal neutron energy spectrums. All twenty-two of the experiments contain SPERT-D fuel which is an alloy of uranium and aluminum. These experiments are representative of research reactor fuel which will be disposed of in specialized waste packages. The experiments in this configuration may also represent certain neutronic and physical characteristics of potential waste package degradation scenarios. The k_{eff} and standard deviations presented for the experiments are the published values obtained from reference documentation. Table 7.2.2-1 contains a listing of this classification's experiments including the k_{eff} result and the reference identifier corresponding to each experimental description.

Table 7.2.2-1
Classification: Fissile Metal Fuel / Slab Lattice Geometries / Moderated

Experiment ID	k_{eff} (MCNP)	sigma (MCNP)	Reference
SPERT-D.1	1.0033	0.0028	9.16, 9.17
SPERT-D.2	1.0121	0.0028	9.16, 9.17
SPERT-D.3	1.0104	0.0026	9.16, 9.17
SPERT-D.4	1.0052	0.0024	9.16, 9.17
SPERT-D.5	0.9959	0.0025	9.16, 9.17
SPERT-D.6	0.9965	0.0025	9.16, 9.17
SPERT-D.7	0.9898	0.0024	9.16, 9.17
SPERT-D.8	0.9918	0.0023	9.16, 9.17
SPERT-D.9	1.0151	0.0027	9.16, 9.17
SPERT-D.10	1.0005	0.0026	9.16, 9.17
SPERT-D.11	0.9990	0.0027	9.16, 9.17
SPERT-D.12	1.0015	0.0031	9.16, 9.17
SPERT-D.13	1.0021	0.0024	9.16, 9.17
SPERT-D.14	1.0265	0.0031	9.16, 9.17
SPERT-D.15	0.9919	0.0026	9.16, 9.17
SPERT-D.16	0.9933	0.0026	9.16, 9.17
SPERT-D.17	1.0046	0.0028	9.16, 9.17
SPERT-D.18	0.9960	0.0024	9.16, 9.17
SPERT-D.19	1.0032	0.0027	9.16, 9.17
SPERT-D.20	1.0058	0.0027	9.16, 9.17
SPERT-D.21	1.0030	0.0026	9.16, 9.17
SPERT-D.22	0.9993	0.0029	9.16, 9.17

The following listing contains a brief description for each experiment identifier presented in Table 7.2.2-1. These descriptions are general statements whose purpose is to only identify the type of critical configuration. A complete detailed description for each experiment is provided in the references listed in Table 7.2.2-1.

SPERT-D.1: a 4x3.77 array of SPERT-D fuel assemblies with an assembly-to-assembly spacing of 0.0 cm

SPERT-D.2: a 4x3.16 array of SPERT-D fuel assemblies with an assembly-to-assembly spacing of 0.635 cm

SPERT-D.3: a 4x3.09 array of SPERT-D fuel assemblies with an assembly-to-assembly spacing of 1.270 cm

SPERT-D.4: a 4x3.16 array of SPERT-D fuel assemblies with an assembly-to-assembly spacing of 1.905 cm

SPERT-D.5: a 4x3.70 array of SPERT-D fuel assemblies with an assembly-to-assembly spacing of 2.540 cm

SPERT-D.6: a 5x4.03 array of SPERT-D fuel assemblies with an assembly-to-assembly spacing of 3.175 cm

SPERT-D.7: a 6x5.34 array of SPERT-D fuel assemblies with an assembly-to-assembly spacing of 3.810 cm

SPERT-D.8: a 7x6.68 array of SPERT-D fuel assemblies with an assembly-to-assembly spacing of 4.064 cm

SPERT-D.9: a 4x3.20x3 array of SPERT-D fuel assemblies with an assembly-to-assembly spacing of 0.0 cm

SPERT-D.10: a 3x3.36x3 array of SPERT-D fuel assemblies with an assembly-to-assembly spacing of 1.270 cm

SPERT-D.11: a 4x4x3 array of SPERT-D fuel assemblies with an assembly-to-assembly spacing of 3.175 cm

SPERT-D.12: a 4x7.04 array of SPERT-D fuel assemblies with a horizontal spacing of 0.0 cm and a vertical spacing of 1.905 cm; two cadmium sheets are positioned between the top two and bottom two rows of assemblies

SPERT-D.13: a 4x504 array of SPERT-D fuel assemblies with a horizontal spacing of 0.0 cm and a vertical spacing of 1.905 cm; one cadmium sheet is positioned between the middle two rows of assemblies

SPERT-D.14: a 16x2.32 array of SPERT-D fuel assemblies with a horizontal and vertical assembly spacing of 0.0 cm

SPERT-D.15: a 16x3 array of SPERT-D fuel assemblies with a horizontal spacing of 1.270 cm and a vertical spacing of 5.5626 cm

SPERT-D.16: a 16x4 array of SPERT-D fuel assemblies with a horizontal spacing of 1.270 cm and a vertical spacing of 6.5024 cm

SPERT-D.17: two 16x2 arrays of SPERT-D fuel assemblies each having a horizontal assembly spacing of 1.270 cm and a vertical assembly spacing of 1.270 cm; a lateral 16.18 cm gap exists between the two arrays

SPERT-D.18: a 3x3.09 array of SPERT-D fuel assemblies with 0.000 g Boron/liter in the moderator

SPERT-D.19: a 4x4.20 array of SPERT-D fuel assemblies with 0.389 g Boron/liter in the moderator

SPERT-D.20: a 5x4.41 array of SPERT-D fuel assemblies with 0.579 g Boron/liter in the moderator

SPERT-D.21: a 6x4.96 array of SPERT-D fuel assemblies with 0.773 g Boron/liter in the moderator

SPERT-D.22: a 6x5.55 array of SPERT-D fuel assemblies with 0.871 g Boron/liter in the moderator

7.2.3 Fissile Metal Fuel / Single Unit Cylinders / Bare

This classification currently consists of seven critical experiments. The critical configurations in this section are characterized as having fast neutron energy spectrums. The enhanced subcritical margin and maximum allowable k_{eff} obtained from this classification may be applicable to potential severely degraded waste package internal or repository external criticality scenarios involving single units of highly enriched fissionable material in non-thermalizing environments.

The k_{eff} and standard deviations presented for the experiments are the published values obtained from various references. Table 7.2.3-1 contains a listing of this classification's experiments including the k_{eff} result and the reference identifier corresponding to each experimental description.

Table 7.2.3-1
Classification: Fissile Metal Fuel / Cylindrical Geometries / Bare

Experiment ID	k_{eff} (MCNP)	sigma (MCNP)	Reference
10.9% U-CYL	1.0024	0.0013	9.13
14.11% U-CYL	1.0003	0.0014	9.13
SIMP.9	0.9964	0.0019	9.15
SIMP.10	0.9966	0.0019	9.15
SIMP.11	0.9938	0.0021	9.15
SIMP.12	0.9953	0.0020	9.15
SIMP.13	0.9971	0.0019	9.15

The following listing contains a brief description for each experiment identifier presented in Table 7.2.3-1. These descriptions are general statements whose purpose is to only identify the type of critical configuration. A complete detailed description for each experiment is provided in the references listed in Table 7.2.3-1.

10.9% U-CYL: a 10.9 wt% enriched bare uranium cylinder with radius 26.65 cm and height 119.392 cm

14.11% U-CYL: a 14.11 wt% enriched bare uranium cylinder with radius 26.65 cm and height 44.239 cm

SIMP.9: an unreflected 54.7 kg U-235 cylinder with a diameter of 17.771 cm and a height of 12.629 cm

SIMP.10: an unreflected 69.7 kg U-235 cylinder with a diameter of 22.85 cm and a height of 9.748 cm

SIMP.11: an unreflected 92.3 kg U-235 cylinder with a diameter of 27.931 cm and a height of 8.642 cm

SIMP.12: an unreflected 120.5 kg U-235 cylinder with a diameter of 33.01 cm and a height of 8.08 cm

SIMP.13: an unreflected 153.0 kg U-235 cylinder with a diameter of 38.086 cm and a height of 7.708 cm

7.2.4 Fissile Metal Fuel / Single Unit Cylinders / Reflected

This classification currently consists of fourteen critical experiments. The critical configurations in this section are characterized as having fast neutron energy spectrums. The enhanced subcritical margin and maximum allowable k_{eff} obtained from this classification may be applicable to potential severely degraded waste package internal or repository external criticality scenarios involving single units of highly enriched fissionable material in highly reflecting

environments. The k_{eff} and standard deviations presented for the experiments are the published values obtained from various references. Table 7.2.4-1 contains a listing of this classification's experiments including the k_{eff} result and the reference identifier corresponding to each experimental description.

Table 7.2.4-1
Classification: Fissile Metal Fuel / Single Unit Cylinders / Reflected

Experiment ID	k_{eff} (MCNP)	sigma (MCNP)	Reference
SIMP.14	0.9996	0.0026	9.15
SIMP.15	0.9680	0.0023	9.15
SIMP.16	0.9496	0.0025	9.15
SIMP.17	0.9953	0.0023	9.15
MIH16	0.9846	0.0024	9.15, 9.18
MIH17	0.9895	0.0025	9.15, 9.18
MIH18	0.9874	0.0024	9.15, 9.18
MIH19	0.9935	0.0024	9.15, 9.18
MIH20	0.9927	0.0023	9.15, 9.18
MIH21	0.9974	0.0026	9.15, 9.18
MIH22	1.0002	0.0024	9.15, 9.18
MIH23	0.9933	0.0027	9.15, 9.18
MIH24	0.9938	0.0024	9.15, 9.18
MIH25	0.9952	0.0027	9.15, 9.18

The following listing contains a brief description for each experiment identifier presented in Table 7.2.4-1. These descriptions are general statements whose purpose is to only identify the type of critical configuration. A complete detailed description for each experiment is provided in the references listed in Table 7.2.4-1.

SIMP.14: a water reflected 93.18 kg U-235 cylinder of diameter 8.23 cm and height 100.33 cm

SIMP.15: a graphite reflected 37.92 kg U-235 cylinder of diameter 8.23 cm and height 40.894 cm

SIMP.16: a graphite reflected 51.99 kg U-235 cylinder of diameter 38.1 cm and height 2.7686 cm

SIMP.17: a water reflected 59.03 kg U-235 cylinder of diameter 38.1 cm and height 3.1242 cm

MIH16: a polyethylene reflected 101.08 kg U-235 cylinder of diameter 38.09 cm and height 5.1714 cm

MIH17: a polyethylene reflected 83.04 kg U-235 cylinder of diameter 33.01 cm and height 5.6515 cm

MIH18: a polyethylene reflected 66.21 kg U-235 cylinder of diameter 27.93 cm and height 6.2382 cm

MIH19: a polyethylene reflected 52.28 kg U-235 cylinder of diameter 22.85 cm and height 7.3863 cm

MIH20: a polyethylene reflected 44.03 kg U-235 cylinder of diameter 17.77 cm and height 10.2489 cm

MIH21: a polyethylene reflected 56.89 kg U-235 cylinder of diameter 38.08 cm and height 2.8677 cm

MIH22: a polyethylene reflected 47.48 kg U-235 cylinder of diameter 33.01 cm and height 3.1572 cm

MIH23: a polyethylene reflected 38.59 kg U-235 cylinder of diameter 27.93 cm and height 3.6246 cm

MIH24: a polyethylene reflected 30.997 kg U-235 cylinder of diameter 22.85 cm and height 4.3459 cm

MIH25: a polyethylene reflected 15.74 kg U-235 cylinder of diameter 17.77 cm and height 5.7810 cm

7.2.5 Fissile Metal Fuel / Single Unit Spheres / Bare

This classification currently consists of six critical experiments including three experiments with plutonium fuel. The critical configurations in this section are characterized as having fast neutron energy spectrums. The enhanced subcritical margin obtained from this classification may be applicable to potential severely degraded waste package internal or repository external criticality scenarios involving single units of highly enriched fissionable material in non-thermalizing environments. Two of the experiments have been simulated with the MCNP 4A code system. The k_{eff} and standard deviations presented for the remaining experiments are the published values obtained from various references. Table 7.2.5-1 contains a listing of this classification's experiments including the k_{eff} result and the reference identifier corresponding to each experimental description.

Table 7.2.5-1
Classification: Fissile Metal Fuel / Single Unit Spheres / Bare

Experiment ID	k_{eff} (MCNP)	sigma (MCNP)	Reference
GE GODIVA	0.9983*1	0.0011	9.19, 9.20
LANL GODIVA	0.9976	0.0011	9.13, 9.20
GE JEZEBEL *2	0.9965*1	0.0010	9.19, 9.20
99.5 wt% LANL JEZEBEL *2	0.9986	0.0021	9.13
80.0 wt% LANL JEZEBEL *2	1.0075	0.0012	9.13
SIMP.1	0.9779	0.0020	9.15

*1 These k_{eff} results are from the MCNP 4A code system.

*2 These critical experiments contain plutonium fuel.

The following listing contains a brief description for each experiment identifier presented in Table 7.2.5-1. These descriptions are general statements whose purpose is to only identify the type of critical configuration. A complete detailed description for each experiment is provided in the references listed in Table 7.2.5-1.

GE GODIVA:	a metallic uranium sphere of radius 8.741 cm
LANL GODIVA:	a metallic 93.71 wt% enriched uranium sphere of radius 8.741 cm and weight 52.42 kg
GE JEZEBEL:	a metallic plutonium sphere of radius 6.385 cm
95.5 wt% LANL JEZEBEL:	a 95.5 wt% enriched plutonium sphere of radius 6.385 cm and weight 17.02 kg
80.0 wt% LANL JEZEBEL:	an 80 wt% enriched plutonium sphere of radius 6.660 cm and weight 19.46 kg
SIMP.1:	an unreflected 49.12 kg sphere of U-235 with a radius of 17.11 cm

7.2.6 Fissile Metal Fuel / Single Unit Spheres / Reflected

This classification currently consists of six critical experiments. The critical configurations in this section are characterized as having fast neutron energy spectrums. The enhanced subcritical margin and maximum allowable k_{eff} obtained from this classification may be applicable to potential severely degraded waste package internal or repository external criticality scenarios involving single units of highly enriched fissionable material in highly reflecting environments. The k_{eff} and standard deviations presented for the experiments are the published values obtained from various references. Table 7.2.6-1 contains a listing of this classification's experiments including the k_{eff} result and the reference identifier corresponding to each experimental description.

Table 7.2.6-1
Classification: Fissile Metal Fuel / Single Unit Spheres / Reflected

Experiment ID	k_{eff} (MCNP)	sigma (MCNP)	Reference
GRPH U-SPH	0.9981	0.0010	9.13
REF U-SPH	0.9956	0.0011	9.13
SIMP.2	0.9980	0.0024	9.15
SIMP.3	1.0013	0.0024	9.15
SIMP.18	0.9800	0.0024	9.15
BYE1	0.9918	0.0026	9.15

The following listing contains a brief description for each experiment identifier presented in Table 7.2.6-1. These descriptions are general statements whose purpose is to only identify the type of critical configuration. A complete detailed description for each experiment is provided in the references listed in Table 7.2.6-1.

GRPH U-SPH: a 93.5 wt% uranium sphere of radius 7.39840 cm reflected by a uniform 5.1 cm thick layer of graphite

REF U-SPH: a 97.67 wt% enriched uranium sphere of radius 6.5537 cm submerged in a cylindrical tank of water with radius 30 cm and height 70 cm

SIMP.2: a water reflected uranium sphere of diameter 13.525 cm containing 22.8 kg U-235

SIMP.3: a graphite reflected uranium sphere of diameter 13.796 cm containing 24.2 kg U-235

SIMP.18: a water reflected uranium sphere of diameter 13.38 cm containing 23.2 kg U-235

BYE1: a water reflected uranium sphere of diameter 13.107 cm containing 21.643 kg U-235

7.2.7 Fissile Metal Fuel / Single Unit Annuli / Bare

This classification currently consists of two critical experiments. The critical configurations in this section are characterized as having fast neutron energy spectrums. The enhanced subcritical margin and maximum allowable k_{eff} obtained from this classification may be applicable to potential severely degraded waste package internal or repository external criticality scenarios involving single units of highly enriched fissionable material in non-thermalizing environments. The k_{eff} and standard deviations presented for the experiments are the published values obtained from various references. Table 7.2.7-1 contains a listing of this classification's experiments including the k_{eff} result and the reference identifier corresponding to each experimental description.

Table 7.2.7-1
Classification: Fissile Metal Fuel / Single Unit Annuli / Bare

Experiment ID	k_{eff} (MCNP)	sigma (MCNP)	Reference
SIMP.4	0.9933	0.0018	9.15
SIMP.7	0.9905	0.0022	9.15, 9.21

The following listing contains a brief description for each experiment identifier presented in Table 7.2.7-1. These descriptions are general statements whose purpose is to only identify the type of critical configuration. A complete detailed description for each experiment is provided in the references listed in Table 7.2.7-1.

SIMP.4: an unreflected uranium annulus containing 167 kg U-235 with an inner diameter of 17.8 cm, an outer diameter of 38.1 cm, and a height of 10.7 cm

SIMP.7: an unreflected uranium annulus containing 154.34 kg U-235 with an inner diameter of 17.8 cm, an outer diameter of 33.02 cm, and a height of 14.5796 cm

7.2.8 Fissile Metal Fuel / Single Unit Annuli / Reflected

This classification currently consists of thirty-two critical experiments. The critical configurations in this section are characterized as having fast neutron energy spectrums. The enhanced subcritical margin and maximum allowable k_{eff} obtained from this classification may be applicable to potential severely degraded waste package internal or repository external criticality scenarios involving single units of highly enriched fissionable material in highly reflecting environments. The k_{eff} and standard deviations presented for the experiments are the published values obtained from various references. Table 7.2.8-1 contains a listing of this classification's experiments including the k_{eff} result and the reference identifier corresponding to each experimental description.

Table 7.2.8-1
Classification: Fissile Metal Fuel / Single Unit Annuli / Reflected

Experiment ID	k_{eff} (MCNP)	sigma (MCNP)	Reference
SIMP.5	0.9933	0.0018	9.15
SIMP.6	1.0002	0.0025	9.15
MIH1	0.9985	0.0021	9.15, 9.18
MIH2	0.9960	0.0020	9.15, 9.18
MIH3	0.9984	0.0021	9.15, 9.18
MIH4	0.9962	0.0025	9.15, 9.18
MIH5	0.9926	0.0025	9.15, 9.18
MIH6	0.9937	0.0025	9.15, 9.18
MIH7	0.9971	0.0026	9.15, 9.18
MIH8	0.9982	0.0012	9.15, 9.18
MIH9	0.9963	0.0025	9.15, 9.18
MIH10	0.9927	0.0028	9.15, 9.18
MIH11	0.9928	0.0022	9.15, 9.18
MIH12	0.9976	0.0028	9.15, 9.18
MIH13	0.9933	0.0025	9.15, 9.18
MIH14	0.9945	0.0025	9.15, 9.18
MIH15	0.9910	0.0028	9.15, 9.18
MIH51	0.9985	0.0021	9.15, 9.18
MIH52	0.9934	0.0021	9.15, 9.18
MIH53	1.0001	0.0022	9.15, 9.18
MIH54	0.9947	0.0022	9.15, 9.18
MIH55	1.0006	0.0026	9.15, 9.18
MIH56	1.0024	0.0027	9.15, 9.18
MIH57	1.0003	0.0026	9.15, 9.18

Experiment ID	k_{eff} (MCNP)	sigma (MCNP)	Reference
MIH58	1.0029	0.0028	9.15, 9.18
MIH59	0.9996	0.0026	9.15, 9.18
MIH60	0.9872	0.0020	9.15, 9.18
MIH61	0.9978	0.0023	9.15, 9.18
MIH62	0.9957	0.0024	9.15, 9.18
MIH63	0.9958	0.0025	9.15, 9.18
MIH64	0.9987	0.0026	9.15, 9.18
MIH65	1.0002	0.0023	9.15, 9.18

The following listing contains a brief description for each experiment identifier presented in Table 7.2.8-1. These descriptions are general statements whose purpose is to only identify the type of critical configuration. A complete detailed description for each experiment is provided in the references listed in Table 7.2.8-1.

SIMP.5: a water reflected uranium annulus containing 29.7 kg U-235 with an inner diameter of 9.8 cm, an outer diameter of 15.6 cm, and a height of 14.6 cm

SIMP.6: a graphite reflected uranium annulus containing 57 kg U-235 with an inner diameter of 33.02 cm, an outer diameter of 38.08 cm, and a height of 11.5468 cm

MIH1: a polyethylene reflected uranium annulus containing 164.93 kg U-235 with an inner diameter of 22.87 cm, an outer diameter of 38.09 cm, and a height of 12.9413 cm

MIH2: a polyethylene reflected uranium annulus containing 158.06 kg U-235 with an inner diameter of 17.79 cm, an outer diameter of 38.09 cm, and a height of 10.1879 cm

MIH3: a polyethylene reflected uranium annulus containing 134.27 kg U-235 with an inner diameter of 17.79 cm, an outer diameter of 33.01 cm, and a height of 12.6162 cm

MIH4: a polyethylene reflected uranium annulus containing 75.108 kg U-235 with an inner diameter of 27.95 cm, an outer diameter of 38.09 cm, and a height of 8.1559 cm

MIH5: a polyethylene reflected uranium annulus containing 85.38 kg U-235 with an inner diameter of 27.95 cm, an outer diameter of 38.09 cm, and a height of 9.2532 cm

MIH6: a polyethylene reflected uranium annulus containing 68.66 kg U-235 with an inner diameter of 22.86 cm, an outer diameter of 38.08 cm, and a height of 5.4 cm

MIH7: a polyethylene reflected uranium annulus containing 76.75 kg U-235 with an inner diameter of 22.87 cm, an outer diameter of 33.08 cm, and a height of 6.0198 cm

MIH8: a polyethylene reflected uranium annulus containing 65.54 kg U-235 with an inner diameter of 17.79 cm, an outer diameter of 38.09 cm, and a height of 4.1961 cm

MIH9: a polyethylene reflected uranium annulus containing 71.10 kg U-235 with an inner diameter of 17.79 cm, an outer diameter of 38.09 cm, and a height of 4.5568 cm

MIH10: a polyethylene reflected uranium annulus containing 62.43 kg U-235 with an inner diameter of 22.86 cm, an outer diameter of 33.01 cm, and a height of 8.0329 cm

MIH11: a polyethylene reflected uranium annulus containing 70.45 kg U-235 with an inner diameter of 22.86 cm, an outer diameter of 33.01 cm, and a height of 9.0373 cm

MIH12: a polyethylene reflected uranium annulus containing 56.40 kg U-235 with an inner diameter of 17.79 cm, an outer diameter of 33.01 cm, and a height of 5.3010 cm

MIH13: a polyethylene reflected uranium annulus containing 62.35 kg U-235 with an inner diameter of 17.79 cm, an outer diameter of 33.01 cm, and a height of 5.8395 cm

MIH14: a polyethylene reflected uranium annulus containing 51.02 kg U-235 with an inner diameter of 17.79 cm, an outer diameter of 27.93 cm, and a height of 8.0010 cm

MIH15: a polyethylene reflected uranium annulus containing 55.07 kg U-235 with an inner diameter of 17.79 cm, an outer diameter of 27.93 cm, and a height of 8.6716 cm

MIH51: a graphite reflected uranium annulus containing 127.99 kg U-235 with an inner diameter of 22.87 cm, an outer diameter of 38.09 cm, and a height of 13.5877 cm

MIH52: a graphite reflected uranium annulus containing 161.74 kg U-235 with an inner diameter of 17.79 cm, an outer diameter of 38.09 cm, and a height of 10.4212 cm

MIH53: a graphite reflected uranium annulus containing 141.53 kg U-235 with an inner diameter of 17.79 cm, an outer diameter of 33.01 cm, and a height of 13.3587 cm

MIH54: a graphite reflected uranium annulus containing 51.15 kg U-235 with an inner diameter of 27.95 cm, an outer diameter of 38.09 cm, and a height of 5.5728 cm

MIH55: a graphite reflected uranium annulus containing 50.44 kg U-235 with an inner diameter of 27.95 cm, an outer diameter of 38.09 cm, and a height of 5.4889 cm

MIH56: a graphite reflected uranium annulus containing 48.66 kg U-235 with an inner diameter of 22.87 cm, an outer diameter of 38.09 cm, and a height of 3.8329 cm

MIH57: a graphite reflected uranium annulus containing 48.67 kg U-235 with an inner diameter of 22.87 cm, an outer diameter of 38.08 cm, and a height of 3.8278 cm

MIH58: a graphite reflected uranium annulus containing 47.66 kg U-235 with an inner diameter of 17.79 cm, an outer diameter of 38.09 cm, and a height of 3.0709 cm

MIH59: a graphite reflected uranium annulus containing 47.66 kg U-235 with an inner diameter of 17.79 cm, an outer diameter of 38.09 cm, and a height of 3.0658 cm

MIH60: a graphite reflected uranium annulus containing 72.28 kg U-235 with an inner diameter of 22.87 cm, an outer diameter of 33.01 cm, and a height of 9.2583 cm

MIH61: a graphite reflected uranium annulus containing 69.2 kg U-235 with an inner diameter of 22.87 cm, an outer diameter of 33.01 cm, and a height of 8.9027 cm

MIH62: a graphite reflected uranium annulus containing 46.11 kg U-235 with an inner diameter of 17.79 cm, an outer diameter of 33.01 cm, and a height of 4.3485 cm

MIH63: a graphite reflected uranium annulus containing 46.11 kg U-235 with an inner diameter of 17.79 cm, an outer diameter of 33.01 cm, and a height of 4.3485 cm

MIH64: a graphite reflected uranium annulus containing 39.38 kg U-235 with an inner diameter of 17.79 cm, an outer diameter of 27.93 cm, and a height of 6.2128 cm

MIH65: a graphite reflected uranium annulus containing 38.9 kg U-235 with an inner diameter of 17.79 cm, an outer diameter of 27.93 cm, and a height of 6.1163 cm

7.2.9 Fissile Metal Fuel / Unique Geometries

This classification currently consists of four critical experiments. All four of the the experiments have been simulated with the MCNP 4A code system. The k_{eff} and standard deviations presented are the values calculated with the MCNP 4A code system. Table 7.2.9-1 contains a listing of this classification's experiments including the k_{eff} result and the reference identifier corresponding to each experimental description.

Table 7.2.9-1
Classification: Fissile Metal Fuel / Unique Geometries

Experiment ID	k_{eff} (MCNP)	sigma (MCNP)	Reference
prob12	0.9985[*1]	0.0012	9.11, 9.12
prob13	0.9949[*1]	0.0008	9.11
prob14	0.9985[*1]	0.0008	9.11
prob15	1.0016[*1]	0.0010	9.11

[*1] These k_{eff} results are from the MCNP 4A code system.

The following listing contains a brief description for each experiment identifier presented in Table 7.2.9-1. These descriptions are general statements whose purpose is to only identify the type of critical configuration. A complete detailed description for each experiment is provided in the references listed in Table 7.2.9-1.

prob12: a 2x2x2 array of four 93.2 wt% enriched uranium metal cylinders and four plexiglass cylinders containing 93.2 wt% enriched uranium nitrate solution; similar cylinders are positioned above one another in the 2x2x2 array

prob13: two 93.2 wt% enriched uranium metal cuboids of different size positioned inside a uranium annulus of the same enrichment; the cuboids are positioned such that the bottom of the smaller cuboid is flush with the bottom of the annulus; the larger cuboid sits atop the smaller with its upper surface extending beyond the top surface of the annulus; the two cuboids are offset in opposite directions toward the inner surface of the annulus while maintaining a parallel relationship to one another

prob14: a 93.2 wt% enriched uranium metal cylinder positioned inside a uranium annulus of the same enrichment; the cylinder and annulus have the same height, and the cylinder is offset inside the annulus such that the outer surface of the cylinder is tangent to the inner surface of the annulus

prob15: a 97.6 wt% enriched uranium metal sphere supported on a plexiglass doughnut in the center of a cylinder of water; the uranium sphere has a diameter of 13.1074 cm and extends down through the doughnut; the water cylinder is 44.1844 cm in height and 65.94 cm in diameter

7.2.10 Fissile Oxide Fuel / Cylinder Arrays / Unmoderated

This classification currently consists of three critical experiments. The critical configurations in this section are characterized as having fast neutron energy spectrums. The enhanced subcritical margin and maximum allowable k_{eff} obtained from this classification may be applicable to potential severely degraded waste package internal or repository external criticality scenarios involving interacting units of highly enriched fissionable material in non-thermalizing, highly reflecting environments. The k_{eff} and standard deviations presented for the experiments are the published values obtained from various references. Table 7.2.10-1 contains a listing of this classification's experiments including the k_{eff} result and the reference identifier corresponding to each experimental description.

Table 7.2.10-1
Classification: Fissile Oxide Fuel / Cylinder Arrays / Unmoderated

Experiment ID	k_{eff} (MCNP)	sigma (MCNP)	Reference
MAG.2	1.0050	0.0023	9.22, 9.23
MAG.3	0.9945	0.0025	9.22, 9.23
MAG.4	0.9943	0.0025	9.22, 9.23

The following listing contains a brief description for each experiment identifier presented in Table 7.2.10-1. These descriptions are general statements whose purpose is to only identify the type of critical configuration. A complete detailed description for each experiment is provided in the references listed in Table 7.2.10-1.

MAG.2: a polyethylene reflected 4x4x1 array of stainless steel cans each containing 20 kg of 93.15 wt% enriched UO2

MAG.3: a polyethylene reflected 3x2x2 array of stainless steel cans each containing 20 kg of 93.15 wt% enriched UO2

MAG.4: a polyethylene reflected 3x3x2 array of stainless steel cans each containing 20 kg of 93.15 wt% enriched UO2

7.2.11 Fissile Oxide Fuel / Cylinder Arrays / Moderated

This classification currently consists of seven critical experiments. The critical configurations in this section are characterized as having thermal to epithermal neutron energy spectrums. The enhanced subcritical margin and maximum allowable k_{eff} obtained from this classification may be applicable to potential severely degraded waste package internal or repository external criticality scenarios involving interacting units of highly enriched fissionable material in moderating environments. All seven of the the experiments have been simulated with the MCNP 4A code system. The k_{eff} and standard deviations presented are the values obtained from MCNP 4A. Table 7.2.11-1 contains a listing of this classification's experiments including the k_{eff} result and the reference identifier corresponding to each experimental description.

Table 7.2.11-1[*1]
Classification: Fissile Oxide Fuel / Cylinder Arrays / Moderated

Experiment ID	k_{eff} (MCNP)	sigma (MCNP)	Reference
MAG.1	1.0318	0.0031	9.22, 9.23
MAG.5	0.9977	0.0028	9.22, 9.23
MAG.7	0.9994	0.0028	9.22, 9.23
MAG.13	0.9970	0.0027	9.22, 9.23
MAG.15	1.0020	0.0028	9.22, 9.23
MAG.17	0.9997	0.0029	9.22, 9.23
MAG.20	1.0030	0.0030	9.22, 9.23

[*1] All k_{eff} results are from the MCNP 4A code system.

The following listing contains a brief description for each experiment identifier presented in Table 7.2.11-1. These descriptions are general statements whose purpose is to only identify the type of critical configuration. A complete detailed description for each experiment is provided in the references listed in Table 7.2.11-1.

MAG.1: a polyethylene reflected, plexiglass moderated 7x7x4 array of stainless steel cans each containing 0.421 kg of 93.15 wt% enriched UO2

MAG.5: a polyethylene reflected, plexiglass moderated 3x3x2 array of stainless steel cans each containing 20 kg of 93.15 wt% enriched UO2

MAG.7: a polyethylene reflected, plexiglass moderated partially filled 3x3x2 array of stainless steel cans each containing 20 kg of 93.15 wt% enriched UO2

MAG.13: a polyethylene reflected, alcohol moderated 2x2x1 array of stainless steel cans each containing 17 kg of 93.15 wt% enriched UO2 with alcohol

MAG.15: a polyethylene reflected, alcohol moderated 2x3x1 array of stainless steel cans each containing 17 kg of 93.15 wt% enriched UO2 with alcohol

MAG.17: a polyethylene reflected, alcohol moderated 2x4x1 array of stainless steel cans each containing 17 kg of 93.15 wt% enriched UO2 with alcohol

MAG.20: a polyethylene reflected, alcohol moderated 3x3x1 array of stainless steel cans each containing 17 kg of 93.15 wt% enriched UO2 with alcohol

7.2.12 Fissile Oxide Fuel / Lattice Geometries / Moderated

This classification currently consists of forty-one critical experiments including thirteen experiments that utilize PuO2/UO2 (mixed oxide) fuel. The critical experiments in this classification represent all intact and moderately degraded commercial spent nuclear fuel waste package scenarios. These experiments are characterized as having thermal neutron energy spectrums and moderator-to-fuel atom ratios similar to those found in light-water reactors. All forty-one of the the experiments have been simulated with the MCNP 4A code system. The k_{eff} and standard deviations presented are the values obtained from MCNP 4A. Table 7.2.12-1 contains a listing of this classification's experiments including the k_{eff} result and the reference identifier corresponding to each experimental description.

Table 7.2.12-1
Classification: Fissile Oxide Fuel / Lattice Geometries / Moderated

Experiment ID	k_{eff} (MCNP)	sigma (MCNP)	Reference
SCPC	1.0004	0.0015	9.19
SCNOPC	0.9975	0.0013	9.19
BA3GD4	1.0004	0.0017	9.19
BA5GD4	0.9934	0.0016	9.19
BA3GD16	0.9984	0.0014	9.19
BORAX-V.2	1.0259	0.0023	9.16, 9.24-9.29
BORAX-V.3	1.0123	0.0023	9.16, 9.24-9.29
EXP1	0.9991	0.0013	9.30, 9.31
EXP2	1.0005	0.0013	9.30, 9.31
EXP3	1.0003	0.0013	9.30, 9.31
EXP4	1.0019	0.0014	9.30, 9.31
EXP5	0.9969	0.0015	9.30, 9.32

Experiment ID	k_{eff} (MCNP)	sigma (MCNP)	Reference
EXP6	1.0038	0.0015	9.30, 9.32
EXP7	0.9965	0.0016	9.30, 9.33
EXP8	1.0082	0.0015	9.30
EXP9	1.0050	0.0015	9.30
EXP10	1.0046	0.0015	9.30
EXP11	1.0004	0.0015	9.30
EXP12	1.0044	0.0016	9.30
EXP13	0.9998	0.0016	9.30
EXP14	1.0012	0.0014	9.30
EXP15	1.0011	0.0012	9.30
EXP16	0.9981	0.0014	9.30
EXP17	0.9886	0.0015	9.30
EXP18	1.0097	0.0014	9.30
EXP19	0.9955	0.0013	9.30
EXP20	0.9951	0.0013	9.30
EXP21	0.9985	0.0013	9.30
EXP22 *2	0.9966	0.0015	9.30
EXP23 *2	0.9990	0.0015	9.30
EXP24 *2	1.0060	0.0014	9.30
EXP25 *2	1.0087	0.0015	9.30
EXP26 *2	1.0088	0.0014	9.30
EXP27 *2	1.0090	0.0015	9.30
EXP28 *2	0.9998	0.0017	9.30
EXP29 *2	1.0032	0.0017	9.30
EXP30 *2	0.9985	0.0017	9.30
EXP31 *2	1.0034	0.0016	9.30
EXP32 *2	1.0038	0.0017	9.30
EXP33 *2	1.0098	0.0016	9.30
EXP34 *2	0.9874	0.0015	9.30, 9.34

*2 These critical experiments contain mixed oxide fuel (PuO2/UO2).

The following listing contains a brief description for each experiment identifier presented in Table 7.2.12-1. These descriptions are general statements whose purpose is to only identify the type of critical configuration. A complete detailed description for each experiment is provided in the references listed in Table 7.2.12-1.

SCPC: a water moderated 4x4 core of fuel bundles; each bundle is a 7x7 array of Zircaloy-2 clad UO2 fuel rods contained in an aluminum channel; three uranium enrichments 1.19, 1.67, and 2.42 wt% are distributed in each bundle; the central four bundles are surrounded by borated stainless steel curtains

SCNOPC: identical to the SCPC experiment previously described with the one exception that the borated stainless steel poison curtains are removed from the configuration

BA3GD4: a borated water moderated 4x4 core of fuel bundles; each bundle is an 8x8 array of Zircaloy-2 clad UO2 fuel rods contained in a Zircaloy-2 channel; four uranium enrichments of 1.409, 2.086, 2.813, and 3.074 wt% are used along with Gd2O3 burnable poison rods; the central four bundles each contain three burnable poison rods (BPR), and the perimeter bundles contain no BPRs

BA5GD4: a borated water moderated 4x4 core of fuel bundles; each bundle is an 8x8 array of Zircaloy-2 clad UO2 fuel rods contained in a Zircaloy-2 channel; four uranium enrichments of 1.409, 2.086, 2.813, and 3.074 wt% are used along with Gd2O3 burnable poison rods; the central four bundles each contain five BPRs, and the perimeter bundles contain no BPRs

BA3GD16: a borated water moderated 4x4 core of fuel bundles; each bundle is an 8x8 array of Zircaloy-2 clad UO2 fuel rods contained in a Zircaloy-2 channel; four uranium enrichments of 1.409, 2.086, 2.813, and 3.074 wt% are used along with Gd2O3 burnable poison rods; each bundle in the core contains three BPRs

BORAX-V.2: four boiling fuel assemblies containing two poison rods are grouped within an aluminum shroud; five cruciform and four "T"-shaped control rods are used; the configurations moderated and reflected with water within the cylindrical reactor vessel

BORAX-V.3: a configuration consisting of 16 superheater assemblies each of which contains five subassemblies of four fuel plates enclosed in a stainless steel box; each plate contains a fuel meat of highly enriched UO2 stainless steel cermet that is clad with stainless steel

EXP1: a configuration of three 20x16 fuel rod clusters of 2.35 wt% U-235 enriched UO2 rods; rod square pitch of 2.032 cm; cluster spacing of 8.39 cm between outer rods; water moderated and reflected

EXP2: a configuration of one 20x16 and two 22x16 fuel rod clusters of 2.35 wt% U-235 enriched UO2 rods; rod square pitch of 2.032 cm; cluster spacing of 5.05 cm between outer rods; water moderated and reflected; 0.713 cm thick Boral absorber plates between fuel clusters

EXP3: a configuration of three 20x16 fuel rod clusters of 2.35 wt% U-235 enriched UO2 rods; rod- square pitch of 2.032 cm; cluster spacing of 8.67 cm between outer rods; water moderated and reflected; 0.625 cm thick aluminum absorber plates between fuel clusters

EXP4: a configuration of three 20x16 fuel rod clusters of 2.35 wt% U-235 enriched UO2 rods; rod square pitch of 2.032 cm; cluster spacing of 6.88 cm between outer rods; water moderated and reflected; 0.485 cm thick steel absorber plates between fuel clusters

EXP5: a configuration of three 12x16 fuel rod clusters of 4.31 wt% U-235 enriched UO2 rods; rod square pitch of 1.892 cm; cluster spacing of 19.24 cm between outer rods; water moderated and reflected; uranium reflecting walls (7.65x152.3x121.9 cm) along length of cluster configuration

EXP6: a configuration of three 12x16 fuel rod clusters of 4.31 wt% U-235 enriched UO2 rods; rod square pitch of 1.892 cm; cluster spacing of 18.18 cm between outer rods; water moderated and reflected; lead reflecting walls (10.2x164.0x123.4 cm) along length of cluster configuration

EXP7: a configuration of three 12x16 fuel rod clusters of 4.31 wt% U-235 enriched UO2 rods; rod square pitch of 1.892 cm; cluster spacing of 15.84 cm between outer rods; water moderated and reflected; steel reflecting walls (17.85x147.3x121.9 cm) along length of cluster configuration

EXP8: 40x8.92 array of 4.31 wt% U-235 enriched UO2 rods (357 total rods); rod square pitch of 1.890 cm; water moderated and reflected; no soluble boron

EXP9: 40x30.92 array of 4.31 wt% U-235 enriched UO2 rods (1237 total rods); rod square pitch of 1.890 cm; water moderated and reflected; soluble boron concentration of 2.55 g/liter

EXP10: 40x11.57 array of 4.31 wt% U-235 enriched UO2 rods (509 total rods); rod square pitch of 1.715 cm; water moderated and reflected; no soluble boron

EXP11: 44x27.09 array of 4.31 wt% U-235 enriched UO2 rods (1192 total rods); rod square pitch of 1.715 cm; water moderated and reflected; soluble boron concentration of 2.55 g/liter

EXP12: water moderated and reflected 2x2 array of 16x15 fuel rod clusters with Boral flux trap between clusters; fuel clusters contain 4.31 wt% U-235 enriched UO2 fuel rods with 1.891 cm square pitch

EXP13: water moderated and reflected 2x2 array of three 14x15 and one 15x15 fuel rod clusters with Boral flux trap between clusters; three 0.63 cm aluminum absorber plates are equally spaced in the flux trap; fuel clusters contain 4.31 wt% U-235 enriched UO2 fuel rods with 1.891 cm square pitch

EXP14: array of 708 fuel rods containing 2.35 wt% U-235 enriched UO2; rod pitch is 1.562 cm; a 0.9525 thick lead shield covers the fuel; water moderated and reflected with no soluble boron

EXP15: array of 342 fuel rods containing 2.35 wt% U-235 enriched UO2; rod pitch is 2.210 cm; a 0.9525 thick lead shield covers the fuel; water moderated and reflected with no soluble boron

EXP16: a full core containing 2.46 and 4.02 wt% U-235 enriched UO2 rods; this core is radially and bottom reflected by water; the critical condition of the configuration is controlled by the soluble boron concentration; there are no Gd2O3 rods in this configuration; the boron concentration is 1899.3 ppm; there are 3920, 2.46 wt% rods and 888, 4.02 wt% rods; there are 153 water rods in the configuration

EXP17: a 19x19 array of UO2 (5.742 wt% U-235) fuel rods; rod pitch of 1.422 cm; water moderated and reflected with no soluble boron; critical height of water is 83.71 cm

EXP18: a 13x14 array of UO2 (5.742 wt% U-235) fuel rods; rod pitch of 2.012 cm; water moderated and reflected with no soluble boron; critical height of water is 90.60 cm

EXP19: a 3x3 array of 14x14 fuel clusters; the fuel clusters are separated by a gap of one pitch thickness; 84 B4C rods are positioned in the gap between the clusters; the fuel is 2.46 wt% U-235 enriched UO2; critical water height is 145.68 cm; 30 cm radial water reflector

EXP20: full core containing 1.94, 2.46, and 4.02 wt% U-235 enriched UO2 fuel rods; core is radially and bottom reflected by water; critical condition of the configuration is controlled by the soluble boron concentration; the boron concentration is 1653.8 ppm; the configuration contains 28 Gd2O3 rods with 1.94 wt% UO2; 3920, 2.46 wt% rods; 860, 4.02 wt% rods; 153 water rods

EXP21: full core containing 1.94, 2.46, and 4.02 wt% U-235 enriched UO2 fuel rods; core is radially and bottom reflected by water; critical condition of the configuration is controlled by the soluble boron concentration; the boron concentration is 1579.4 ppm; the configuration contains 36 Gd2O3 rods with 1.94 wt% UO2; 3920, 2.46 wt% rods; 852, 4.02 wt% rods; 153 water rods

EXP22: a water moderated and reflected core of 469 PuO2-UO2 fuel rods; core lattice square pitch of 1.778 cm; a 0.9525 lead shield covers the core at the top of the fuel rods

EXP23: a water moderated and reflected core of 761 PuO2-UO2 fuel rods; core lattice square pitch of 1.778 cm; a 0.9525 cm lead shield covers the core at the top of the fuel rods; soluble boron concentration of 681 ppm

EXP24: a water moderated and reflected core of 195 PuO2-UO2 fuel rods; core lattice square pitch of 2.210 cm; a 0.9525 cm lead shield covers the core at the top of the fuel rods

EXP25: a water moderated and reflected core of 761 PuO2-UO2 fuel rods; core lattice square pitch of 2.210 cm; a 0.9525 cm lead shield covers the core at the top of the fuel rods; soluble boron concentration of 1090 ppm

EXP26: a water moderated and reflected core of 160 PuO2-UO2 fuel rods; core lattice square pitch of 2.515 cm; a 0.9525 cm lead shield covers the core at the top of the fuel rods

EXP27: a water moderated and reflected core of 689 PuO2-UO2 fuel rods; core lattice square pitch of 2.515 cm; a 0.9525 cm lead shield covers the core at the top of the fuel rods; soluble boron concentration of 767 ppm

EXP28: a 22x23 array of PuO2-UO2 (6.6 wt% PuO2) fuel rods; array has a square pitch of 1.321 cm; the critical water height is 84.56 cm; no soluble boron; fuel array is completely reflected by water

EXP29: a 19x19 array of PuO2-UO2 (6.6 wt% PuO2) fuel rods; array has a square pitch of 1.422 cm; the critical water height is 82.96 cm; no soluble boron; fuel array is completely reflected by water

EXP30: a 21x21 array of PuO2-UO2 (6.6 wt% PuO2) fuel rods; array has a square pitch of 1.422 cm; the critical water height is 89.70 cm; the boron concentration is 337 ppm; fuel array is completely reflected by water

EXP31: a 13x13 array of PuO2-UO2 (6.6 wt% PuO2) fuel rods; array has a square pitch of 1.867 cm; the critical water height is 70.11 cm; no soluble boron; fuel array is completely reflected by water

EXP32: a 12x12 array of PuO2-UO2 (6.6 wt% PuO2) fuel rods; array has a square pitch of 2.012 cm; the critical height of the water is 78.43 cm; no soluble boron; fuel array is completely reflected by water

EXP33: a 11x11 array of PuO2-UO2 (6.6 wt% PuO2) fuel rods; array has a square pitch of 2.642 cm; the critical height of the water is 81.17 cm; no soluble boron; fuel array is completely reflected by water

EXP34: a core of 1174 UO2 rods of 4.31 wt% U-235 enriched UO2 and 583 PuO2-UO2 rods of 2 wt% natural UO2; core is a triangular lattice with a pitch of 1.598 cm; core is loaded such that each PuO2-UO2 rod is by six UO2 rods; core is water moderated and reflected

7.2.13 Fissile Solution Fuel / Cylinder Arrays / Bare

This classification currently consists of six critical experiments. The critical experiments in this section are characterized as having thermal to epithermal neutron energy spectrums. The enhanced subcritical margin and maximum allowable k_{eff} obtained from this classification may be applicable to potential severely degraded waste package internal or repository external criticality scenarios involving interacting volumes of highly enriched fissionable solution suspended in a generally non-thermalizing, non-reflective environment. Table 7.2.13-1 contains a listing of this classification's experiments including the k_{eff} result and the reference identifier corresponding to each experimental description.

Table 7.2.13-1
Classification: Fissile Solution Fuel / Cylinder Arrays / Bare

Experiment ID	k_{eff} (MCNP)	sigma (MCNP)	Reference
THO1	0.9968	0.0033	9.35, 9.36
THO7	0.9846	0.0032	9.35, 9.36
THO12	0.9715	0.0032	9.35, 9.36
THO13	0.9724	0.0031	9.35, 9.36
prob20	0.9971*1	0.0013	9.11
THREE U-CYL	0.9991	0.0011	9.13, 9.37

*1 This k_{eff} result was obtained from the MCNP 4A code system.

The following listing contains a brief description for each experiment identifier presented in Table 7.2.13-1. These descriptions are general statements whose purpose is to only identify the type of critical configuration. A complete detailed description for each experiment is provided in the references listed in Table 7.2.13-1.

THO1:	an unreflected 2x2x2 array of plexiglass cylinders containing 415.0 gU/l uranyl nitrate solution
THO7:	an unreflected 3x3x3 array of plexiglass cylinders containing 415.0 gU/l uranyl nitrate solution
THO12:	an unreflected 4x4x4 array of plexiglass cylinders containing 415.0 gU/l uranyl nitrate solution
THO13:	an unreflected 5x5x5 array of plexiglass cylinders containing 415.0 gU/l uranyl nitrate solution
prob20:	a triangular pitched array of seven uncapped aluminum cylinders containing 93.2 wt% enriched uranyl nitrate solution
THREE U-CYL:	three unreflected aluminum cylinders containing 93.2 wt% enriched UO2F2 water solution positioned in an equilateral configuration with a surface separation of 0.38 cm

7.2.14 Fissile Solution Fuel / Cylinder Arrays / Reflected

This classification currently consists of forty-one critical experiments. The critical experiments in this section are characterized as having thermal to epithermal neutron energy spectrums. The enhanced subcritical margin and maximum allowable k_{eff} obtained from this classification may be applicable to potential severely degraded waste package internal or repository external criticality scenarios involving interacting volumes of highly enriched fissionable solution suspended in a reflective environment. The k_{eff} and standard deviations presented for the experiments are the published values obtained from various references. Table 7.2.14-1 contains a listing of this classification's experiments including the k_{eff} result and the reference identifier corresponding to each experimental description.

Table 7.2.14-1
Classification: Fissile Solution Fuel / Cylinder Arrays / Reflected

Experiment ID	k_{eff} (MCNP)	sigma (MCNP)	Reference
ROT50	1.0128	0.0028	9.35, 9.38
ROT51	1.0029	0.0030	9.35, 9.38
ROT52	1.0113	0.0027	9.35, 9.38
ROT53	1.0013	0.0029	9.35, 9.38
ROT54	1.0104	0.0027	9.35, 9.38
ROT55	1.0042	0.0032	9.35, 9.38
ROT56	1.0082	0.0030	9.35, 9.38
ROT57	1.0139	0.0032	9.35, 9.38
ROT58	1.0020	0.0031	9.35, 9.38
ROT59	1.0011	0.0032	9.35, 9.38
ROT60	0.9910	0.0040	9.35, 9.38
ROT61	1.0058	0.0032	9.35, 9.38
ROT62	1.0060	0.0026	9.35, 9.38

Experiment ID	k_{eff} (MCNP)	sigma (MCNP)	Reference
ROT63	1.0083	0.0035	9.35, 9.38
ROT64	1.0056	0.0031	9.35, 9.38
ROT65	1.0072	0.0032	9.35, 9.38
ROT66	1.0115	0.0034	9.35, 9.38
ROT67	1.0024	0.0028	9.35, 9.38
ROT68	1.0018	0.0026	9.35, 9.38
ROT69	0.9984	0.0028	9.35, 9.38
ROT70	0.9963	0.0028	9.35, 9.38
ROT71	1.0010	0.0024	9.35, 9.38
ROT72	0.9996	0.0027	9.35, 9.38
ROT73	1.0101	0.0036	9.35, 9.38
ROT74	1.0020	0.0031	9.35, 9.38
ROT75	1.0098	0.0033	9.35, 9.38
ROT76	1.0097	0.0035	9.35, 9.38
ROT77	1.0071	0.0032	9.35, 9.38
ROT78	1.0084	0.0030	9.35, 9.38
ROT79	1.0058	0.0031	9.35, 9.38
ROT80	1.0029	0.0030	9.35, 9.38
THO2	1.0071	0.0035	9.35, 9.36
THO3	1.0248	0.0035	9.35, 9.36
THO4	1.0339	0.0028	9.35, 9.36
THO5	1.0221	0.0033	9.35, 9.36
THO6	0.9950	0.0033	9.35, 9.36
THO8	1.0039	0.0024	9.35, 9.36
THO9	1.0316	0.0032	9.35, 9.36
THO10	1.0259	0.0032	9.35, 9.36
THO11	0.9902	0.0032	9.35, 9.36
prob18	1.0294*1	0.0012	9.11, 9.36

*1 This k_{eff} results was obtained from the MCNP 4A code system.

The following listing contains a brief description for each experiment identifier presented in Table 7.2.14-1. These descriptions are general statements whose purpose is to only identify the type of critical configuration. A complete detailed description for each experiment is provided in the references listed in Table 7.2.14-1.

ROT50: a reflected 4x4x1 array of stainless steel sleeved aluminum cylinders containing uranyl nitrate solution

ROT51: a reflected 2x2x1 array of stainless steel sleeved aluminum cylinders containing uranyl nitrate solution

ROT52: a reflected 4x4x1 array of stainless steel sleeved aluminum cylinders containing uranyl nitrate solution

ROT53: a reflected 4x4x1 array of aluminum cylinders containing uranyl nitrate solution

ROT54: a reflected 2x2x1 array of aluminum cylinders containing uranyl nitrate solution

ROT55: a reflected 2x2x1 array of aluminum cylinders containing uranyl nitrate solution

ROT56: a reflected 4x4x1 array of aluminum cylinders containing uranyl nitrate solution

ROT57: a reflected 4x4x1 array of stainless steel sleeved aluminum cylinders containing uranyl nitrate solution

ROT58: a reflected 4x4x1 array of aluminum cylinders containing uranyl nitrate solution

ROT59: a reflected 2x2x1 array of stainless steel sleeved aluminum cylinders containing uranyl nitrate solution

ROT60: a reflected 2x2x1 array of aluminum cylinders containing uranyl nitrate solution

ROT61: a reflected 4x4x1 array of stainless steel sleeved aluminum cylinders containing uranyl nitrate solution

ROT62: a reflected 4x4x1 array of aluminum cylinders containing uranyl nitrate solution

ROT63: a reflected 2x4x1 array of aluminum cylinders containing uranyl nitrate solution

ROT64: a reflected 2x3x1 array of aluminum cylinders containing uranyl nitrate solution

ROT65: a reflected 2x2x1 array of stainless steel sleeved aluminum cylinders containing uranyl nitrate solution

ROT66: a reflected 2x2x1 array of aluminum cylinders containing uranyl nitrate solution

ROT67: a reflected 4x4x1 array of stainless steel sleeved aluminum cylinders containing uranyl nitrate solution

ROT68: a reflected 4x4x1 array of aluminum cylinders containing uranyl nitrate solution

ROT69: a reflected 2x2x1 array of stainless steel sleeved aluminum cylinders containing uranyl nitrate solution

ROT70: a reflected 2x2x1 array of aluminum cylinders containing uranyl nitrate solution

ROT71: a reflected 4x4x1 array of stainless steel sleeved aluminum cylinders containing uranyl nitrate solution

ROT72: a reflected 4x4x1 array of aluminum cylinders containing uranyl nitrate solution

ROT73: a reflected 4x4x1 array of stainless steel sleeved aluminum cylinders containing uranyl nitrate solution

ROT74: a reflected 4x4x1 array of aluminum cylinders containing uranyl nitrate solution

ROT75: a reflected 2x2x1 array of stainless steel sleeved aluminum cylinders containing uranyl nitrate solution

ROT76: a reflected 2x2x1 array of aluminum cylinders containing uranyl nitrate solution

ROT77: a reflected 4x4x1 array of stainless steel sleeved aluminum cylinders containing uranyl nitrate solution

ROT78: a reflected 4x4x1 array of aluminum cylinders containing uranyl nitrate solution

ROT79: a reflected 3x2x1 array of stainless steel sleeved aluminum cylinders containing uranyl nitrate solution

ROT80: a reflected 3x2x1 array of aluminum cylinders containing uranyl nitrate solution

THO2: a reflected 2x2x2 array of plexiglass cylinders containing uranyl nitrate solution

THO3: a reflected 2x2x2 array of plexiglass cylinders containing uranyl nitrate solution

THO4: a reflected 2x2x2 array of plexiglass cylinders containing uranyl nitrate solution

THO5: a reflected 2x2x2 array of plexiglass cylinders containing uranyl nitrate solution

THO6: a reflected 2x2x2 array of plexiglass cylinders containing uranyl nitrate solution

THO8: a reflected 3x3x3 array of plexiglass cylinders containing uranyl nitrate solution

THO9: a reflected 3x3x3 array of plexiglass cylinders containing uranyl nitrate solution

THO10: a reflected 3x3x3 array of plexiglass cylinders containing uranyl nitrate solution

THO11: a reflected 3x3x3 array of plexiglass cylinders containing uranyl nitrate solution

prob18: a paraffin reflected 3X3X3 array of plexiglass bottles containing 92.6 wt% enriched uranyl nitrate solution

7.2.15 Fissile Solution Fuel / Single Unit Cylinders / Bare

This classification currently consists of fifteen critical experiments. The critical experiments in this section are characterized as having thermal to epithermal neutron energy spectrums. The enhanced subcritical margin and maximum allowable k_{eff} obtained from this classification may be applicable to potential severely degraded waste package internal or repository external criticality scenarios involving an isolated volume of highly enriched fissionable solution in a non-thermalizing environment. The k_{eff} and standard deviations presented for the experiments are the published values obtained from various references. Table 7.2.15-1 contains a listing of

this classification's experiments including the k_{eff} result and the reference identifier corresponding to each experimental description.

Table 7.2.15-1
Classification: Fissile Solution Fuel / Single Unit Cylinders / Bare

Experiment	k_{eff} (MCNP)	sigma (MCNP)	Reference
ROT1	1.0053	0.0031	9.35, 9.38
ROT6	0.9989	0.0036	9.35, 9.38
ROT11	1.0184	0.0038	9.35, 9.38
ROT16	1.0064	0.0034	9.35, 9.38
ROT21	1.0032	0.0037	9.35, 9.38
ROT26	0.9937	0.0033	9.35, 9.38
ROT40	1.0038	0.0030	9.35, 9.38
ROT41	1.0083	0.0031	9.35, 9.38
ROT42	0.9970	0.0034	9.35, 9.38
ROT43	0.9943	0.0031	9.35, 9.38
GWI5	1.0053	0.0015	9.35, 9.38
GWI6	1.0090	0.0017	9.35, 9.38
GWI7	1.0032	0.0014	9.35, 9.38
GWI8	1.0045	0.0013	9.35, 9.38
GWI9	0.9956	0.0011	9.35, 9.38

The following listing contains a brief description for each experiment identifier presented in Table 7.2.15-1. These descriptions are general statements whose purpose is to only identify the type of critical configuration. A complete detailed description for each experiment is provided in the references listed in Table 7.2.15-1.

ROT1: an open top stainless steel cylinder partially filled with a 145.68 gU/l uranyl nitrate solution

ROT6: an open top stainless steel cylinder partially filled with a 346.73 gU/l uranyl nitrate solution

ROT11: an open top aluminum cylinder partially filled with a 142.92 gU/l uranyl nitrate solution

ROT16: an open top aluminum cylinder partially filled with a 357.71 gU/l uranyl nitrate solution

ROT21: an open top aluminum cylinder partially filled with a 145.68 gU/l uranyl nitrate solution

ROT26: an open top aluminum cylinder partially filled with a 357.71 gU/l uranyl nitrate solution

ROT40: an open top aluminum cylinder partially filled with a 59.63 gU/l uranyl nitrate solution

ROT41: an open top aluminum cylinder partially filled with a 54.89 gU/l uranyl nitrate solution

ROT42: an open top aluminum cylinder partially filled with a 137.40 gU/l uranyl nitrate solution

ROT43: an open top aluminum cylinder partially filled with a 63.95 gU/l uranyl nitrate solution

GWI5: a closed carbon steel cylinder partially filled with 17.31 gU/l uranyl nitrate solution

GWI6: a closed carbon steel cylinder partially filled with 17.02 gU/l uranyl nitrate solution

GWI7: a closed carbon steel cylinder partially filled with 15.27 gU/l uranyl nitrate solution

GWI8: a closed carbon steel cylinder partially filled with 14.60 gU/l uranyl nitrate solution

GWI9: a closed carbon steel cylinder partially filled with 14.06 gU/l uranyl nitrate solution

7.2.16 Fissile Solution Fuel / Single Unit Cylinders / Reflected

This classification currently consists of thirty-seven critical experiments. The critical experiments in this section are characterized as having thermal to epithermal neutron energy spectrums. The enhanced subcritical margin and maximum allowable k_{eff} obtained from this classification may be applicable to potential severely degraded waste package internal or repository external criticality scenarios involving an isolated volume of highly enriched fissionable solution suspended in a reflective environment. The k_{eff} and standard deviations presented for the experiments are the published values obtained from various references. Table 7.2.16-1 contains a listing of this classification's experiments including the k_{eff} result and the reference identifier corresponding to each experimental description.

Table 7.2.16-1
Classification: Fissile Solution Fuel / Single Unit Cylinders / Reflected

Experiment	k_{eff} (MCNP)	sigma (MCNP)	Reference
ROT2	1.0094	0.0035	9.35, 9.38
ROT3	1.0066	0.0033	9.35, 9.38
ROT4	1.0114	0.0034	9.35, 9.38
ROT5	1.0070	0.0034	9.35, 9.38
ROT7	1.0085	0.0040	9.35, 9.38
ROT8	1.0046	0.0031	9.35, 9.38
ROT9	1.0063	0.0034	9.35, 9.38
ROT10	1.0078	0.0030	9.35, 9.38
ROT12	1.0103	0.0035	9.35, 9.38
ROT13	1.0120	0.0032	9.35, 9.38
ROT14	1.0089[*1]	0.0034	9.35, 9.38

Experiment	k_{eff} (MCNP)	sigma (MCNP)	Reference
ROT15	1.0114	0.0035	9.35, 9.38
ROT17	1.0033	0.0032	9.35, 9.38
ROT18	1.0049	0.0036	9.35, 9.38
ROT19	0.9995	0.0036	9.35, 9.38
ROT20	1.0088	0.0032	9.35, 9.38
ROT22	1.0025	0.0033	9.35, 9.38
ROT23	1.0162	0.0034	9.35, 9.38
ROT24	1.0080	0.0032	9.35, 9.38
ROT25	1.0092	0.0033	9.35, 9.38
ROT27	1.0029	0.0034	9.35, 9.38
ROT28	1.0128	0.0032	9.35, 9.38
ROT29	0.9971	0.0030	9.35, 9.38
ROT30	1.0176	0.0034	9.35, 9.38
ROT31	1.0083	0.0029	9.35, 9.38
ROT32	0.9985	0.0030	9.35, 9.38
ROT33	1.0122	0.0025	9.35, 9.38
ROT34	1.0072	0.0032	9.35, 9.38
ROT35	1.0005	0.0028	9.35, 9.38
ROT36	1.0140	0.0029	9.35, 9.38
ROT37	0.9978	0.0032	9.35, 9.38
ROT38	1.0286	0.0035	9.35, 9.38
ROT39	1.0118	0.0026	9.35, 9.38
FOX9	0.9980	0.0032	9.35
FOX10	1.0036	0.0032	9.35
FOX11	0.9757	0.0030	9.35
FOX12	0.9595	0.0033	9.35

*1 This k_{eff} result was obtained from the MCNP 4A code system.

The following listing contains a brief description for each experiment identifier presented in Table 7.2.16-1. These descriptions are general statements whose purpose is to only identify the type of critical configuration. A complete detailed description for each experiment is provided in the references listed in Table 7.2.16-1.

ROT2: a stainless steel cylinder partially filled with 144.38 gU/l uranyl nitrate
ROT3: stainless steel cylinder partially filled with 144.38 gU/l uranyl nitrate
ROT4: stainless steel cylinder partially filled with 147.66 gU/l uranyl nitrate

ROT5: stainless steel cylinder partially filled with 147.66 gU/l uranyl nitrate
ROT7: a stainless steel cylinder partially filled with 334.77 gU/l uranyl nitrate
ROT8: a stainless steel cylinder partially filled with 334.77 gU/l uranyl nitrate
ROT9: a stainless steel cylinder partially filled with 345.33 gU/l uranyl nitrate
ROT10: a stainless steel cylinder partially filled with 345.33 gU/l uranyl nitrate
ROT12: an aluminum cylinder partially filled with 144.38 gU/l uranyl nitrate
ROT13: an aluminum cylinder partially filled with 144.38 gU/l uranyl nitrate
ROT14: an aluminum cylinder partially filled with 147.66 gU/l uranyl nitrate
ROT15: an aluminum cylinder partially filled with 147.66 gU/l uranyl nitrate
ROT17: an aluminum cylinder partially filled with 334.77 gU/l uranyl nitrate
ROT18: an aluminum cylinder partially filled with 334.77 gU/l uranyl nitrate
ROT19: an aluminum cylinder partially filled with 345.33 gU/l uranyl nitrate
ROT20: an aluminum cylinder partially filled with 345.33 gU/l uranyl nitrate
ROT22: an aluminum cylinder partially filled with 144.38 gU/l uranyl nitrate
ROT23: an aluminum cylinder partially filled with 144.38 gU/l uranyl nitrate
ROT24: an aluminum cylinder partially filled with 147.66 gU/l uranyl nitrate
ROT25: an aluminum cylinder partially filled with 147.66 gU/l uranyl nitrate
ROT27: an aluminum cylinder partially filled with 334.77 gU/l uranyl nitrate
ROT28: an aluminum cylinder partially filled with 334.77 gU/l uranyl nitrate
ROT29: an aluminum cylinder partially filled with 345.33 gU/l uranyl nitrate
ROT30: an aluminum cylinder partially filled with 345.33 gU/l uranyl nitrate
ROT31: a stainless steel cylinder partially filled with 60.32 gU/l uranyl nitrate
ROT32: a stainless steel cylinder partially filled with 60.32 gU/l uranyl nitrate
ROT33: an aluminum cylinder partially filled with 60.32 gU/l uranyl nitrate
ROT34: an aluminum cylinder partially filled with 60.32 gU/l uranyl nitrate
ROT35: an aluminum cylinder partially filled with 60.32 gU/l uranyl nitrate
ROT36: an aluminum cylinder partially filled with 60.32 gU/l uranyl nitrate
ROT37: an aluminum cylinder partially filled with 66.33 gU/l uranyl nitrate
ROT38: an aluminum cylinder partially filled with 59.65 gU/l uranyl nitrate
ROT39: an aluminum cylinder partially filled with 59.65 gU/l uranyl nitrate
FOX9: a 0.1524 cm thick aluminum cylinder of height 89.6048 cm and inner diameter 15.24 cm; the aluminum cylinder is filled with a solution of uranyl fluoride containing 889.46 gU/l
FOX10: a 0.1524 cm thick aluminum cylinder of height 39.0048 cm and inner diameter 16.51 cm; the aluminum cylinder is filled with a solution of uranyl fluoride containing 576.95 gU/l
FOX11: a 0.1524 cm thick aluminum cylinder of height 12.7048 cm and inner diameter 25.4 cm; the aluminum cylinder is filled with a solution of uranyl fluoride containing 889.46 gU/l
FOX12: a 0.1524 cm thick aluminum cylinder of height 8.0048 cm and inner diameter 38.1 cm; the aluminum cylinder is filled with a solution of uranyl fluoride containing 889.46 gU/l

7.2.17 Fissile Solution Fuel / Single Unit Spheres / Bare

This classification currently consists of ten critical experiments. The critical experiments in this section are characterized as having thermal to epithermal neutron energy spectrums. The

enhanced subcritical margin and maximum allowable k_{eff} obtained from this classification may be applicable to potential severely degraded waste package internal or repository external criticality scenarios involving an isolated volume of highly enriched fissionable solution suspended in a non-reflective environment. Four of the experiments have been simulated with the MCNP 4A code system. The k_{eff} and standard deviations presented for the other experiments are the published values obtained from various references. Table 7.2.17-1 contains a listing of this classification's experiments including the k_{eff} result and the reference identifier corresponding to each experimental description.

Table 7.2.17-1
Classification: Fissile Solution Fuel / Single Unit Spheres / Bare

Experiment ID	k_{eff} (MCNP)	sigma (MCNP)	Reference
ORNL1	0.9994*1	0.0012	9.19
ORNL2	0.9986*1	0.0013	9.19
PNL1	1.0116*1	0.0013	9.19
PNL2	1.0069*1	0.0015	9.19
prob21	0.9962	0.0008	9.11
GWI1	0.9981	0.0020	9.35
GWI2	0.9910	0.0019	9.35
GWI3	0.9859	0.0018	9.35
GWI4	0.9878	0.0023	9.35
FOX5	1.0027	0.0017	9.35

*1 These k_{eff} results are from the MCNP 4A code system.

The following listing contains a brief description for each experiment identifier presented in Table 7.2.17-1. These descriptions are general statements whose purpose is to only identify the type of critical configuration. A complete detailed description for each experiment is provided in the references listed in Table 7.2.17-1.

ORNL1: an unreflected sphere of radius 34.6 cm of 93 wt% enriched uranyl nitrate solution without boron

ORNL2: an unreflected sphere of radius 34.6 cm of 93 wt% enriched uranyl nitrate solution with boron

PNL1: an unreflected sphere of radius 19.5085 cm of plutonium nitrate solution with an H/Pu atomic ratio of 668

PNL2: an unreflected sphere of radius 19.5085 cm of plutonium nitrate solution with an H/Pu atomic ratio of 125

prob21: an unreflected aluminum spherical container of thickness 0.0159 cm and inside diameter of 69.2 cm which is 98% filled with uranyl fluoride; the uranyl fluoride enrichment is 4.98% with an H/U-235 atomic ratio of 1099

GWI1: an unreflected aluminum sphere filled with a 20.12 gU/l uranyl nitrate

GWI2: an unreflected, boron poisoned aluminum sphere filled with a 23.53 gU/l uranyl nitrate solution

GWI3: an unreflected, boron poisoned aluminum sphere filled with a 26.77 gU/l uranyl nitrate solution

GWI4: an unreflected, boron poisoned aluminum sphere filled with a 28.45 gU/l uranyl nitrate solution

FOX5: an unreflected aluminum sphere filled with 19.992 gU/l uranyl fluoride

7.2.18 Fissile Solution Fuel / Single Unit Spheres / Reflected

This classification currently consists of three critical experiments. The critical experiments in this section are characterized as having thermal to epithermal neutron energy spectrums. The enhanced subcritical margin and maximum allowable k_{eff} obtained from this classification may be applicable to potential severely degraded waste package internal or repository external criticality scenarios involving an isolated volume of highly enriched fissionable solution suspended in a highly reflective environment. Table 7.2.18-1 contains a listing of this classification's experiments including the k_{eff} result and the reference identifier corresponding to each experimental description.

Table 7.2.18-1
Classification: Fissile Solution Fuel / Single Unit Spheres / Reflected

Experiment ID	k_{eff} (MCNP)	sigma (MCNP)	Reference
FOX6	1.0034	0.0032	9.35
FOX7	0.9980	0.0029	9.35
FOX8	1.0004	0.0017	9.35

The following listing contains a brief description for each experiment identifier presented in Table 7.2.18-1. These descriptions are general statements whose purpose is to only identify the type of critical configuration. A complete detailed description for each experiment is provided in the references listed in Table 7.2.18-1.

FOX6: a 0.16 cm thick aluminum sphere of 23.0353 cm inner diameter filled with a solution of uranyl fluoride containing 348.6 gU/l

FOX7: a 0.16 cm thick aluminum sphere of 23.68846 cm inner diameter filled with a solution of uranyl fluoride containing 213.28 gU/l

FOX8: a 0.2 cm thick aluminum sphere of 55.82644 cm inner diameter filled with a solution of uranyl fluoride containing 22.042 gU/l

7.2.19 Fissile Solution Fuel / Single Unit Parallelepipeds / Bare

This classification currently consists of two critical experiments. The critical experiments in this section are characterized as having thermal to epithermal neutron energy spectrums. The enhanced subcritical margin and maximum allowable k_{eff} obtained from this classification may be applicable to potential severely degraded waste package internal or repository external

criticality scenarios involving an isolated volume of highly enriched fissionable solution suspended in a non-reflective environment. Table 7.2.19-1 contains a listing of this classification's experiments including the k_{eff} result and the reference identifier corresponding to each experimental description.

Table 7.2.19-1
Classification: Fissile Solution Fuel / Single Unit Parallelepipeds / Bare

Experiment ID	k_{eff} (MCNP)	sigma (MCNP)	Reference
FOX1	0.9996	0.0031	9.35
FOX3	0.9932	0.0035	9.35

The following listing contains a brief description for each experiment identifier presented in Table 7.2.19-1. These descriptions are general statements whose purpose is to only identify the type of critical configuration. A complete detailed description for each experiment is provided in the references listed in Table 7.2.19-1.

FOX1: an unreflected aluminum cuboid containing 94.18 gU/l uranyl fluoride solution

FOX3: two unreflected aluminum cuboids containing 94.18 gU/l uranyl fluoride solution; the cuboids are positioned on a common plane parallel to one another with a surface separation of 15.24 cm

7.2.20 Fissile Solution Fuel / Single Unit Parallelepipeds / Reflected

This classification currently consists of two critical experiments. The critical experiments in this section are characterized as having thermal to epithermal neutron energy spectrums. The enhanced subcritical margin and maximum allowable k_{eff} obtained from this classification may be applicable to potential severely degraded waste package internal or repository external criticality scenarios involving an isolated volume of highly enriched fissionable solution suspended in a highly reflective environment. Table 7.2.20-1 contains a listing of this classification's experiments including the k_{eff} result and the reference identifier corresponding to each experimental description.

Table 7.2.20-1
Classification: Fissile Solution Fuel / Single Unit Parallelepipeds / Reflected

Experiment ID	k_{eff} (MCNP)	sigma (MCNP)	Reference
FOX2	1.0019	0.0032	9.35
FOX4	1.0057	0.0031	9.35

The following listing contains a brief description for each experiment identifier presented in Table 7.2.20-1. These descriptions are general statements whose purpose is to only identify the type of critical configuration. A complete detailed description for each experiment is provided in the references listed in Table 7.2.20-1.

FOX2: a water reflected aluminum cuboid partially filled with 94.18 gU/l uranyl fluoride solution

FOX4: two unreflected aluminum cuboids containing 94.18 gU/l uranyl fluoride solution; the cuboids are positioned on a common plane parallel to one another with a surface separation of 15.2398 cm

7.3 Comparison Between MCNP 4A Results and KENO V.a Results

The comparison between MCNP k_{eff} results and previously published KENO V.a k_{eff} results for a number of critical configurations demonstrates the MCNP code system's ability to consistently calculate k_{eff} values comparable to those obtained from a previously accepted calculational tool applicable to licensing analyses.

The KENO V.a code is a three-dimensional, multi-group, Monte Carlo criticality calculation module of the SCALE modular code system. The KENO V.a code has been used in the past as a calculational tool for the licensing of various system's with the Nuclear Regulatory Commission. The KENO V.a code has proven to be excellent for the criticality evaluation of light-water moderated lattice geometries. KENO V.a implements a grouped cross-section structure. The KENO V.a geometry specification implements a combinatorial approach of nesting certain geometric units (spheres, hemispheres, cylinders, hemicylinders, cubes, or cuboids) within one another while following a restricted set of guidelines to compose a three-dimensional model for the configuration of interest. The lower-level unit volumes displace the higher-level unit volumes in the geometric nesting methodology. Hole specifications are also used to place one unit within another unit. One important restriction in the KENO V.a geometric modeling methodology is that units or holes must be completely enclosed within other units or holes assuring that no unit or hole surfaces intersect. The flexibility of the geometry specification methodology utilized by the KENO V.a code is restrictive when applied to complex configurations.

The MCNP code system is a three-dimensional, continuous-energy, Monte Carlo photon and neutron transport code. MCNP is capable of performing tallies to obtain a wide variety of parameters (i.e. fluxes or dose rates within a volume, currents across a surface, fission rates within a given volume, etc.). MCNP is also capable of performing criticality calculations, which are of interest in this study. The MCNP 4A code system utilizes a continuous-energy cross-section structure derived from ENDF-V data. MCNP is capable of analyzing complex geometrical configurations. MCNP accomplishes this by implementing a robust geometrical description methodology based on the specification of user-defined materials in cells bounded by first and second-degree surfaces. This section contains a criticality calculation performance comparison between the MCNP 4A code and the KENO V.a code. This comparison serves to further qualify the effectiveness of the MCNP criticality calculation. Table 7.3-1 contains the MCNP 4A and the KENO V.a k_{eff} results for the critical configurations contained within the current critical experiment library that were analyzed with both codes. Figure 7.3-1 shows the comparison between the MCNP 4A and the KENO V.a k_{eff} results.

Table 7.3-1
k_{eff} Result Comparison Between MCNP 4A and KENO V.a

Experiment ID (Description)	MCNP 4A k_{eff}	MCNP 4A sigma	KENO V.a k_{eff}	KENO V.a sigma	% Diff. MCNP vs KENO
prob1 (Metal, Unmoderated)	0.9999	0.0009	0.9996	0.0011	0.0270
prob7 (Metal, Unmoderated)	1.0002	0.0004	0.9984	0.0011	0.1823
prob3 (Metal, Unmoderated)	0.9961	0.0011	1.0009	0.0013	-0.4776
A62 (Metal, Unmoderated)	0.9977	0.0024	1.0095	0.0039	-1.1689
prob12 (Metal, Unique)	0.9985	0.0012	1.0055	0.0013	-0.6952
prob13 (Metal, Unique)	0.9898	0.0009	1.0026	0.0012	-1.2777
prob14 (Metal, Unique)	0.9985	0.0008	1.0011	0.0010	-0.2607
prob15 (Metal, Unique)	1.0016	0.0010	1.0012	0.0020	0.0360
MAG.1 (Oxide, Moderated)	1.0318	0.0031	1.0117	0.0032	1.9868
MAG.5 (Oxide, Moderated)	0.9977	0.0028	1.0031	0.0034	-0.5383
MAG.7 (Oxide, Moderated)	0.9994	0.0028	0.9990	0.0035	0.0400
MAG.13 (Oxide, Moderated)	0.9970	0.0027	1.0192	0.0034	-2.1782
MAG.15 (Oxide, Moderated)	1.0020	0.0028	1.0157	0.0035	-1.3488
MAG.17 (Oxide, Moderated)	0.9997	0.0029	1.0118	0.0035	-1.1959
MAG.20 (Oxide, Moderated)	1.0030	0.0030	1.0131	0.0035	-0.9969
BORAX-V2 (Oxide, Lattice)	1.0259	0.0023	1.0192	0.0024	0.6554

Experiment ID (Description)	MCNP 4A k_{eff}	MCNP 4A sigma	KENO V.a k_{eff}	KENO V.a sigma	% Diff. MCNP vs KENO
BORAX-V3 (Oxide, Lattice)	1.0129	0.0021	1.0129	0.0021	-0.0592
EXP1 (Oxide, Lattice)	0.9991	0.0013	0.9912	0.0014	0.7970
EXP2 (Oxide, Lattice)	1.0005	0.0013	0.9927	0.0010	0.7857
EXP3 (Oxide, Lattice)	1.0003	0.0013	0.9924	0.0013	0.7960
EXP4 (Oxide, Lattice)	1.0019	0.0014	0.9921	0.0014	0.9878
EXP5 (Oxide, Lattice)	0.9966	0.0015	0.9994	0.0014	-0.2502
EXP6 (Oxide, Lattice)	1.0039	0.0015	1.0000	0.0015	0.3800
EXP7 (Oxide, Lattice)	0.9965	0.0016	0.9970	0.0016	-0.0502
EXP8 (Oxide, Lattice)	1.0082	0.0015	0.9952	0.0011	1.3063
EXP9 (Oxide, Lattice)	1.0050	0.0015	0.9991	0.0012	0.5905
EXP10 (Oxide, Lattice)	1.0046	0.0015	0.9940	0.0011	1.0664
EXP11 (Oxide, Lattice)	1.0004	0.0015	0.9904	0.0013	1.0097
EXP12 (Oxide, Lattice)	1.0044	0.0016	0.9971	0.0016	0.7321
EXP13 (Oxide, Lattice)	0.9998	0.0016	0.9924	0.0011	0.7457
EXP14 (Oxide, Lattice)	1.0012	0.0014	0.9904	0.0014	1.0905
EXP15 (Oxide, Lattice)	1.0011	0.0012	0.9946	0.0013	0.6535
EXP16 (Oxide, Lattice)	0.9981	0.0014	0.9953	0.0011	0.2813

Experiment ID (Description)	MCNP 4A k_{eff}	MCNP 4A sigma	KENO V.a k_{eff}	KENO V.a sigma	% Diff. MCNP vs KENO
EXP17 (Oxide, Lattice)	0.9886	0.0015	0.9861	0.0016	0.2535
EXP18 (Oxide, Lattice)	1.0097	0.0014	0.9972	0.0011	1.2535
EXP19 (Oxide, Lattice)	0.9955	0.0013	0.9912	0.0010	0.4338
EXP20 (Oxide, Lattice)	0.9951	0.0013	0.9919	0.0010	0.3226
EXP21 (Oxide, Lattice)	0.9985	0.0013	0.9949	0.0010	0.3618
EXP22 (MOX, Lattice)	0.9966	0.0015	0.9956	0.0013	0.1004
EXP23 (MOX, Lattice)	0.9990	0.0015	0.9955	0.0014	0.3516
EXP24 (MOX, Lattice)	1.0060	0.0014	1.0037	0.0010	0.2292
EXP25 (MOX, Lattice)	1.0087	0.0015	1.0071	0.0012	0.1589
EXP26 (MOX, Lattice)	1.0088	0.0014	1.0077	0.0015	0.1092
EXP27 (MOX, Lattice)	1.0090	0.0015	1.0072	0.0009	0.1787
EXP28 (MOX, Lattice)	0.9998	0.0017	1.0015	0.0012	-0.1697
EXP29 (MOX, Lattice)	1.0032	0.0017	1.0014	0.0018	0.1797
EXP30 (MOX, Lattice)	0.9985	0.0017	1.0027	0.0015	-0.4189
EXP31 (MOX, Lattice)	1.0034	0.0016	1.0031	0.0017	0.0299
EXP32 (MOX, Lattice)	1.0038	0.0017	1.0040	0.0018	-0.0199
EXP33 (MOX, Lattice)	1.0098	0.0016	1.0057	0.0022	0.4077

Experiment ID (Description)	MCNP 4A k_{eff}	MCNP 4A sigma	KENO V.a k_{eff}	KENO V.a sigma	% Diff. MCNP vs KENO
EXP34 (MOX, Lattice)	0.9874	0.0015	0.9869	0.0012	0.0507
prob20 (Solution, Bare)	0.9971	0.0013	0.9791	0.0014	1.8354
prob18 (Solution, Reflected)	1.0294	0.0012	1.0088	0.0015	2.0381
ROT14 (Solution, Reflected)	1.0089	0.0034	1.0122	0.0039	-0.3300
prob21 (Solution, Bare)	0.9962	0.0008	1.0012	0.0009	-0.4994

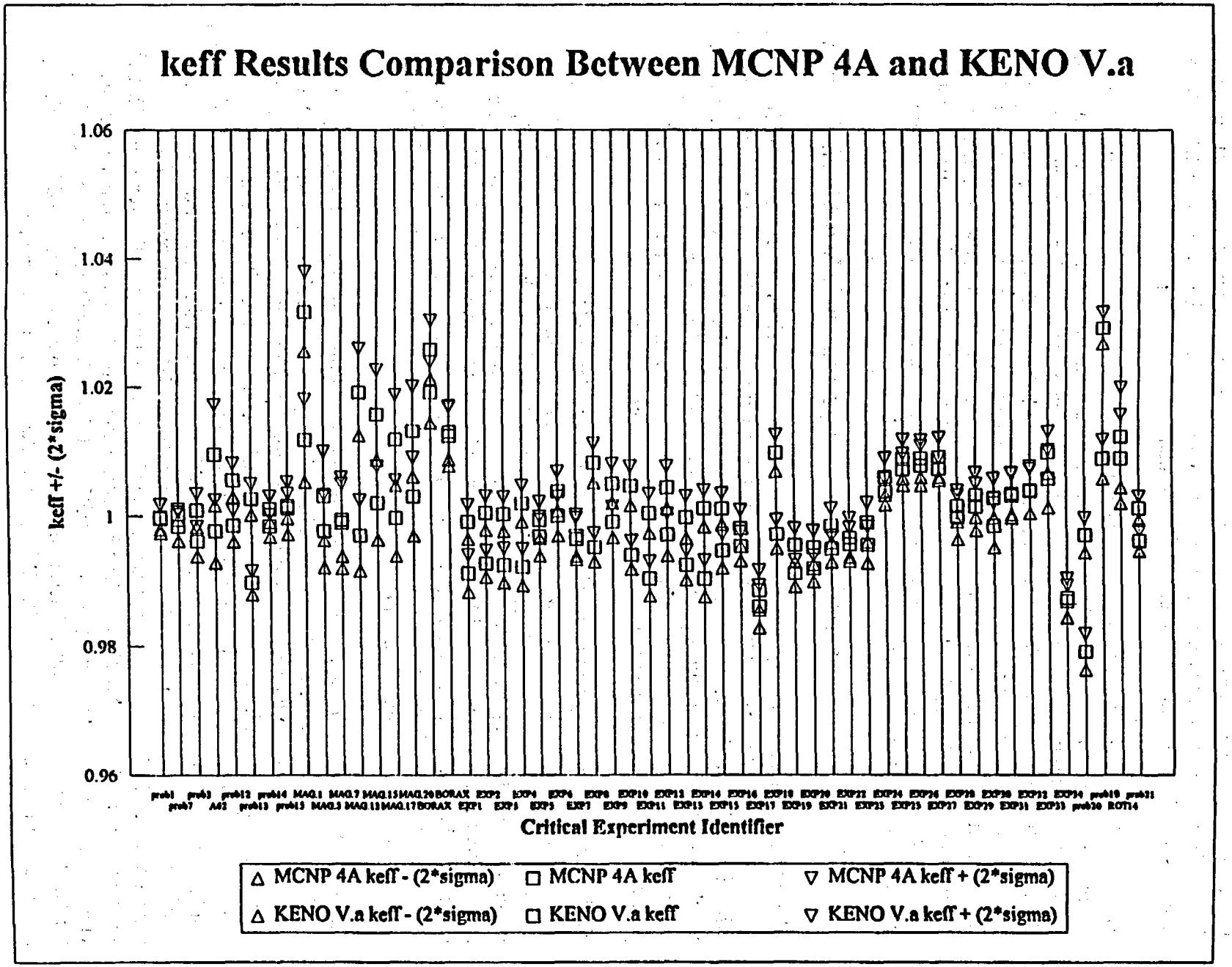

Figure 7.3-1 Comparison Between MCNP 4A and KENO V.a k_{eff} Results

The comparison between MCNP 4A and KENO V.a shows relatively good agreement between the two code systems in terms of k_{eff}. The two code systems use different cross-section formats. MCNP 4A uses a continuous energy cross-section format as described in Section 4.1.5. KENO V.a uses a collapsed multigroup cross-section format.

The general descriptions of each case are provided in Table 7.3-1 to assist in identifying any interesting trends in k_{eff} versus system characteristics between the two codes. Examination of the percent differences between MCNP 4A and KENO V.a in terms of k_{eff} for the various system characteristics does not identify any significant trending behavior. Both positive and negative percent differences exist for each group of system characteristics. The MCNP k_{eff} calculations for the uranium dioxide moderated lattices appear to demonstrate a slightly more conservative behavior in predicting k_{eff} than the KENO V.a calculations. However, this statement is not conclusive. Generally, MCNP 4A's and KENO V.a's k_{eff} predictions are the same within the statistical error of the calculations.

7.4 Comparison Between MCNP 4A Results and Published MCNP Results

The enhanced subcritical margin and maximum allowable k_{eff} values describing the MCNP code system's k_{eff} calculational ability as presented in this paper are dependent on the k_{eff} results in the critical experiment library. Many of the k_{eff} results reported in the library were obtained from a number of sources which utilize previous versions of the MCNP code system. The k_{eff} results obtained by using previous versions of MCNP are considered equally valid for bias value determination as long as the cross-section data remains consistent.

To demonstrate the acceptability of using the previously calculated k_{eff} results from various references, a comparative analysis was performed to show that the previous versions of MCNP and MCNP 4A provide the same k_{eff} results within a 95% confidence interval. If a sample of k_{eff} results obtained from a previous version of MCNP is compared to the corresponding set of k_{eff} results obtained from the MCNP 4A code system and shown to have overlapping 95% confidence intervals, the complete set of k_{eff} results published using the previous versions of MCNP are considered acceptable for use in preliminary bias value determination as long as the cross-section data remains consistent.

The MCNP 4A results are reported where available in the critical experiment library. Currently 65 of the 289 critical experiments contained in the library have been simulated with the MCNP 4A code system. Of the 65 MCNP 4A simulated critical experiments, 31 were experiments previously analyzed with earlier versions of the MCNP code system. These 31 critical experiments are used as the sample set to demonstrate the acceptability of using the additional k_{eff} results contained in the various references from which they were taken, thus providing justification for assumption 5.1. Table 7.4-1, and Figure 7.4-1, show the results of the comparative analysis between the published k_{eff} values obtained using earlier versions of MCNP and those obtained using MCNP 4A. The 31 critical experiment k_{eff} results from the various sampled references are the same (within the 95% confidence interval) as their corresponding MCNP 4A calculated k_{eff} results. Therefore, it is acceptable to use the published k_{eff} results obtained from earlier versions of MCNP for *preliminary* bias value determination.

Table 7.4-1
Comparison Between Published MCNP Results and the MCNP 4A Results

Experiment ID [Reference]	Published k_{eff} [MCNP Version]	Published sigma	Calculated k_{eff} [MCNP 4A]	Calculated sigma	Difference Between Published k_{eff} & Calculated k_{eff}
prob1 [5.11, 5.12]	0.9999 [MCNP 4.2]	0.0009	0.9999	0.0009	0.0000
prob7 [5.11, 5.12]	0.9993 [MCNP 4.2]	0.0009	1.0002	0.0004	-0.0009
prob3 [5.13, 5.14]	0.9990 [MCNP 4.2]	0.0011	0.9961	0.0011	0.0029
A62 [5.12, 5.15]	0.9969 [MCNP 4.0]	0.0021	0.9977	0.0024	0.0008
GE GODIVA [5.19, 5.20]	0.9981 [MCNP 3B][1]	0.0011	0.9983	0.0011	-0.0002
GE JEZEBEL [5.19, 5.20]	1.0007 [MCNP 3B][1]	0.0011	0.9965	0.0010	0.0042
prob12 [5.11, 5.12]	0.9997 [MCNP 4.2]	0.0012	0.9985	0.0012	0.0012
prob13 [5.11]	0.9942 [MCNP 4.2]	0.0009	0.9949	0.0008	-0.0007
prob14 [5.11]	0.9991 [MCNP 4.2]	0.0009	0.9985	0.0008	0.0006
prob15 [5.11]	1.0016 [MCNP 4.2]	0.0011	1.0016	0.0010	0.0000
SCPC [5.19]	1.0024 [MCNP 3B][1]	0.0015	1.0004	0.0015	0.0020
SCNOPC [5.19]	0.9977 [MCNP 3B][1]	0.0015	0.9975	0.0013	0.0002
BA3GD4[2] [5.19]	0.9992 [MCNP 3B][1]	0.0016	1.0004	0.0017	-0.1110
BA5GD4[2] [5.19]	0.9963 [MCNP 3B][1]	0.0015	0.9934	0.0016	0.0029
BA3GD16[2] [5.19]	0.9996 [MCNP 3B][1]	0.0015	0.9984	0.0014	0.1202
MAG.1 [5.22, 5.23]	1.0319 [MCNP 4.0]	0.0026	1.0318	0.0031	0.0001
MAG.5 [5.22, 5.23]	0.9900 [MCNP 4.0]	0.0031	0.9977	0.0028	-0.0077
MAG.7 [5.22, 5.23]	0.9957 [MCNP 4.0]	0.0026	0.9994	0.0028	-0.0037
MAG.13 [5.22, 5.23]	1.0045 [MCNP 4.0]	0.0026	0.9970	0.0027	0.0075
MAG.15 [5.22, 5.23]	0.9961 [MCNP 4.0]	0.0027	1.0020	0.0028	-0.0059
MAG.17 [5.22, 5.23]	0.9946 [MCNP 4.0]	0.0023	0.9997	0.0029	-0.0051
MAG.20 [5.22, 5.23]	1.0000 [MCNP 4.0]	0.0027	1.0030	0.0030	-0.0030
BORAX-V.2 [5.16, 5.24-5.29]	1.0192 [MCNP 4.0]	0.0024	1.0259	0.0023	-0.0067
BORAX-V.3 [5.16, 5.24-5.29]	1.0129 [MCNP 4.0]	0.0021	1.0123	0.0023	0.0006
prob20 [5.11]	0.9960 [MCNP 4.2]	0.0012	0.9971	0.0013	-0.0011
prob18 [5.11, 5.36]	1.0302 [MCNP 4.2]	0.0013	1.0294	0.0012	0.0008

Experiment ID [Reference]	Published k_{eff} [MCNP Version]	Published sigma	Calculated k_{eff} [MCNP 4A]	Calculated sigma	Difference Between Published k_{eff} & Calculated k_{eff}
ROT14 [5.35, 5.38]	1.0073 [MCNP 4.0]	0.0034	1.0089	0.0034	-0.0015
ORNL1 [5.19]	1.0003 [MCNP 3B]	0.0013	0.9994	0.0012	0.0009
ORNL2 [5.19]	0.9984 [MCNP 3B]	0.0013	0.9986	0.0013	-0.0002
PNL1 [5.19]	1.0157 [MCNP 3B]	0.0015	1.0116	0.0013	0.0041
PNL2 [5.19]	1.0115 [MCNP 3B]	0.0017	1.0069	0.0015	0.0046

1 The specific version of MCNP is not clearly indicated in NEDO-32028. However, the other results contained within the reference indicate using MCNP, Version 3B. The referenced manual in NEDO-32028 for these experiments indicate that they may be from MCNP, Versions 3A, 3B, or 4.0. Regardless of the previous version used the results agree well with MCNP 4A.

2 The published results for these cases are from GE Nuclear Energy MCNP calculations which utilize proprietary GE cross-sections. Therefore, a true comparison cannot be made between MCNP 4A and the previous version of MCNP used to calculate the published results. However, it is informative to see how well the preferred MCNP ENDF/B-V based cross-sections correspond to the proprietary GE cross-sections.

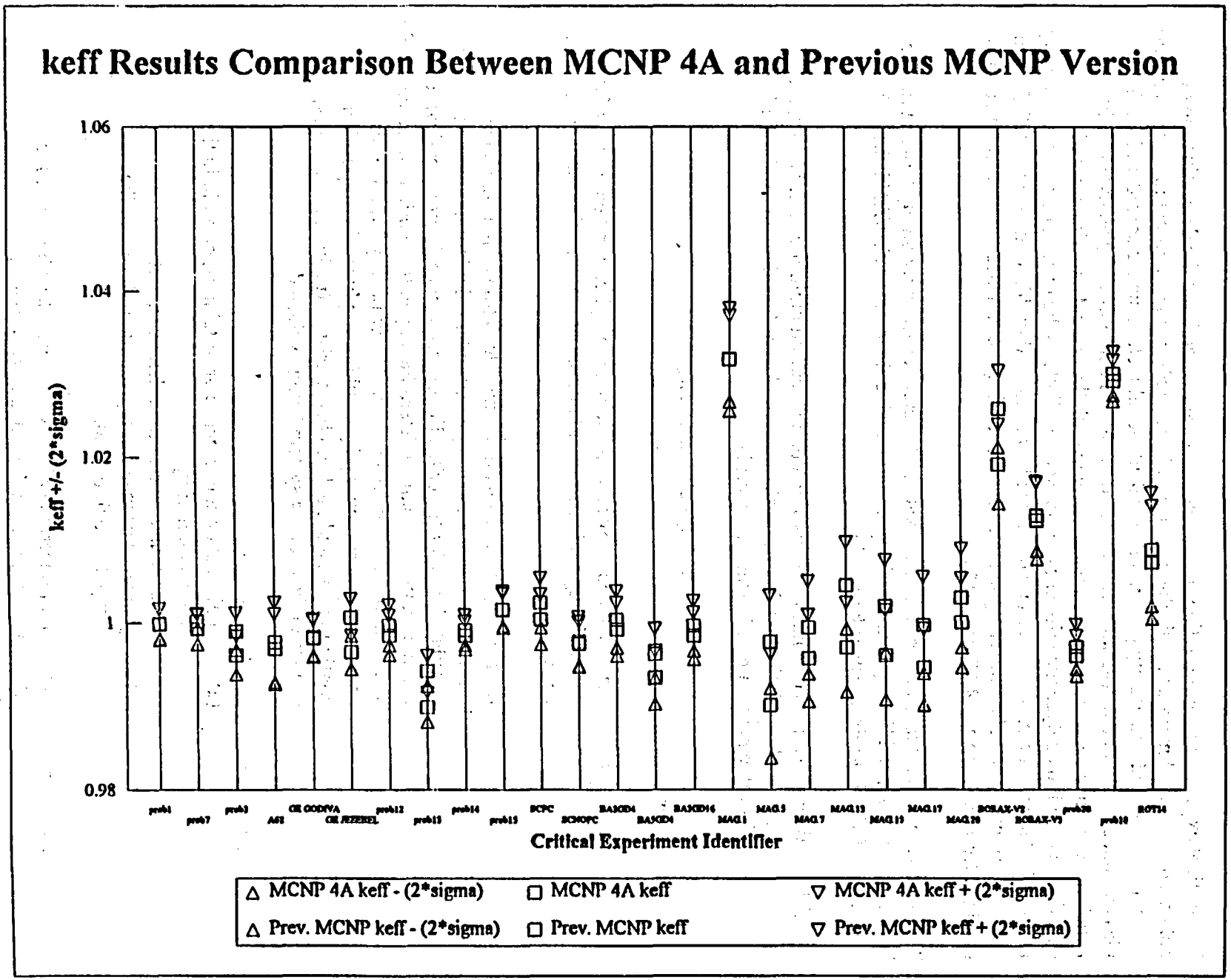

Figure 7.4-1 Comparison Between Previously Published MCNP k_{eff} Results and Calculated MCNP 4A k_{eff} Results

7.5 Enhanced Subcritical Margin

The critical experiment configurations contained in this study facilitate the determination of enhanced subcritical margins applicable for disposal. The enhanced subcritical margin takes into account the bias and uncertainty present in the calculational method under consideration. The bias and uncertainty in the criticality calculational method is determined by analyzing critical benchmark experiments. The bias and uncertainty in both the critical experiments and calculations used to analyze the critical experiments contribute to the overall bias and uncertainty in the calculational method. The calculational method examined in this study is the MCNP code system's criticality calculation. The guidance for determining the enhanced subcritical margin is obtained from ANSI/ANS-8.17 (Ref. 9.2).

The following excerpt is from the American National Standard Criticality Safety Criteria for the Handling, Storage, and Transportation of LWR Fuel Outside Reactors, ANSI/ANS-8.17(5)--

"5. Criteria to Establish Subcriticality

5.1 Where methods of analysis are used to predict neutron multiplication factors, the calculated multiplication factor, k_s, shall be equal to or less than an established allowable neutron multiplication factor; i.e.

$$k_s \leq k_c - \Delta k_s - \Delta k_c - \Delta k_m$$

where,

k_s = the calculated allowable maximum multiplication factor, k_{eff}, of the system being evaluated for all normal or credible abnormal conditions or events.

k_c = the mean k_{eff} that results from the calculation of the benchmark criticality experiments using a particular calculational method. If the calculated k_{eff}s for the criticality experiments exhibit a trend with a parameter, then k_c shall be determined by extrapolation on the basis of a best fit to the calculated values. The criticality experiments used as benchmarks in computing k_c should have physical compositions, configurations, and nuclear characteristics (including reflectors) similar to those of the system being evaluated.

Δk_s = an allowance for
(a) statistical or convergence uncertainties, or both, in the computation of k_s,
(b) material and fabrication tolerances, and
(c) geometric or material representations used in the computational method.

Δk_c = a margin for uncertainty in k_c which includes allowance for
(a) uncertainties in the critical experiments,
(b) statistical or convergence uncertainties, or both, in the computation of k_c,

(c) uncertainties due to extrapolation of k_c outside the range of experimental data, and

(d) uncertainties due to limitations in the geometrical of material representations used in the computational method.

Δk_m = an arbitrary margin to ensure the subcriticality of k_s.

The various uncertainties may be combined statistically if they are independent. Correlated uncertainties should be combined additively."

Starting with the formulation from ANSI/ANS-8.17(5.1):

$$k_s \leq k_c - \Delta k_s - \Delta k_c - \Delta k_m \qquad \text{Equation 7.5-1.}$$

Let,

$$\text{Bias Value} = \beta = 1 - k_c \qquad \text{Equation 7.5-2.}$$

and,

$$\text{Uncertainty in Bias Value} = \Delta\beta = \Delta k_c \qquad \text{Equation 7.5-3.}$$

Substituting Equations 2 and 3 into Equation 1 yields,

$$k_s + \Delta k_s \leq 1.0 - \beta - \Delta\beta - \Delta k_m \qquad \text{Equation 7.5-4.}$$

According to ANSI/ANS-8.17, it is appropriate to use a bias value based on the mean k_{eff} (k_c) for a classification of critical benchmarks whose characteristics determine the range of applicability of the bias value. This range of applicability for the bias value is determined by the similarities between the critical configurations within the classification used to obtain the k_c term and the configuration being analyzed. The similarities between the critical configurations and the waste configuration should be based on the neutronic characteristics and physical compositions of the two systems.

The k_s term as related to ANSI/ANS-8.17(5.1) is the maximum allowable calculated value of k_{eff} for any waste package configuration. For this study the Δk_s term represents the statistical uncertainty and modelling uncertainty in the MCNP simulation of the waste configuration.

The requirements set forth in 10 CFR 60.131(b)(7) (Ref. 9.3) require $k_s + \Delta k_s$ not to exceed a value of 0.95 (Δk_m) for all systems involved in processing, transporting, handling, storing, retrieving, emplacing, and isolating radioactive waste. Therefore, the subcritical margin according to 10 CFR 60.131(b)(7) is 0.05. The enhanced subcritical margin is obtained by following the guidance set forth in ANSI/ANS-8.17(5.1). According to ANSI/ANS-8.17(5.1), in addition to the 0.05 subcritical margin established in 10 CFR 60.131(b)(7) an additional margin for safety accounting for bias and uncertainty in the calculational method should be employed. The inclusion of factors accounting for bias and uncertainty in the calculational method introduces the enhanced subcritical margin.

The enhanced subcritical margin is defined as--

$$\beta + \Delta\beta + \Delta k_m \qquad \text{Equation 7.5-5}$$

where,

$\beta = (1 - k_c)$ = bias value for the applicable critical experiment classification
$\Delta\beta = \Delta k_c$ = uncertainty in the bias value
$\Delta k_m = 0.05$.

7.5.1 Treatment of Bias and Uncertainty

The definitions of bias and uncertainty are fundamental to this discussion. The bias represents the systematic error present in any evaluation, and the uncertainty represents the random error present in any evaluation. Each experimental and calculated k_{eff} in this study has an associated bias and uncertainty. The k_{eff} value for an individual experiment or calculation may be presented in the following manner--

$$k_{eff_i} = 1 + bias_i + uncertainty_i$$

Equation 7.5.1-1.

The bias and uncertainty terms have different constituents depending on whether they represent an experimentally or calculationally determined k_{eff}.

The bias value for a calculationally determined k_{eff} includes bias due to systematic errors in the calculation. Systematic errors in the calculation may at a minimum be comprised of the following--

1) errors in k_{eff} due to cross-section anomalies,
2) errors in k_{eff} due to calculation procedures such as an inadequate initial source distribution such that the fundamental mode is not obtained before collecting neutron multiplication data,
3) errors in k_{eff} due to material or geometric modelling assumptions.

The bias value for the experimentally determined k_{eff} is due to systematic errors present in the critical experiments themselves. Systematic errors in the critical experiments may at a minimum be comprised of the following--

1) overestimation of the fissile content in the system,
2) use of poor counting statistics in the detector systems,
3) unknown trends in fabrication methods (i.e. unknown voids in casting operations, unknown bias in material composition analyses, impurities in material compositions, etc.).

The uncertainty value for a calculationally determined k_{eff} is dependent on the calculational method employed. In the case of using a Monte-Carlo calculational method, the uncertainty in the calculation is a statistical uncertainty. The statistical uncertainty in the context of a Monte-Carlo calculation is a function of several parameters. Two of the more important parameters include the number of neutron histories tracked per generation and the number of generations followed. The MCNP code system's Monte-Carlo criticality evaluation quantifies the statistical uncertainty of the calculation in terms of a standard deviation about the mean k_{eff}.

The uncertainty value for the experimentally determined k_{eff} is dependent primarily upon the characteristics of the experimental equipment. Examples of sources contributing to the experimental uncertainty include tolerances in the machining of equipment or tolerances in the positioning of materials.

The bias and uncertainty present in both the experimentally determined k_{eff} values and the calculated k_{eff} values are integral components in the calculation of an overall bias and uncertainty representative of the calculational method's ability to accurately predict the neutron multiplication factor of a system. The following discussion describes how the various biases and uncertainties should be dealt with statistically to satisfy the requirements set forth in ANSI/ANS-8.17(5.1).

The k_c term in Section 7.5 represents the average calculated k_{eff} for a set of critical benchmarks used to establish the enhanced subcritical margin required for a particular computational method. In accordance with the previous discussion, the k_c term may be presented as:

$$k_c = \overline{k_{eff_{BENCH}}} = \frac{\sum_i (k_{eff_{BENCH_i}})}{N} = \frac{\sum_i (1 + bias_i + uncertainty_i)}{N}$$

Equation 7.5.1-2.

i = a critical experiment benchmark calculation,
bias = the bias in the critical benchmark calculation,
uncertainty = the uncertainty in the critical benchmark calculation,
N = the number of critical benchmark calculations contributing to k_c

The bias as defined in Equation 7.5.2 is the deviation of the average k_{eff} for the set of critical benchmarks from unity. Using the Equation 7.5.1-2, the bias may be presented as:

$$\beta = 1 - k_c = \frac{\sum_i (bias_i)}{N} + \frac{\sum_i (uncertainty_i)}{N}$$

Equation 7.5.1-3.

From Equation 7.5.1-3, it is shown that the bias (β) is the sum of the average bias and average uncertainty for all critical benchmark evaluations used to determine k_c.

The uncertainty in the bias as described in Equation 7.5-3 and ANSI/ANS-8.17 is a complex term due to the number of constituents of which it is composed. The uncertainty in the bias may be presented as:

$$\Delta\beta = \Delta k_c = \overline{unc}_{BENCH} + \sigma_{\overline{k}_{effBENCH}}$$

Equation 7.5.1-4.

The two components of $\Delta\beta$ include the uncertainty in the benchmark evaluations and the standard deviation of the mean k_{eff} for the population of critical benchmark evaluations.

The uncertainty in the benchmark evaluations includes the uncertainty in the calculation of the benchmarks and the uncertainty in the benchmark experiments themselves. The uncertainty in the calculation of the benchmarks using the MCNP code system's criticality calculation is quantified as the average of the standard deviations in k_{eff} for the set of critical benchmark calculations. The uncertainty in the critical experiments in terms of reactivity is a function of the tolerances in the experimental equipment and experimental procedures.

The standard deviation of the mean k_{eff} for the population of critical benchmark evaluations may be expressed as:

$$\sigma_{\overline{k}_{effBENCH}} \leq s_{\overline{k}_{effBENCH}} * c_{95/95}$$

Equation 7.5.1-5.

The $c_{95/95}$ value is the one-sided, non-central student-t value applicable to the set of (N) critical benchmarks contributing to $s^2_{keff,BENCH}$. The $s^2_{keff,BENCH}$ term represents the variance in experimental and calculational bias and uncertainty for the sample set of critical benchmark evaluations used to determine the bias (β). The average k_{eff} of the critical benchmark simulations is a function of both the critical experiments and the computational evaluation of the critical experiments. The critical experiments and the computational evaluation of the critical experiments are independent, though. Using the propagation of errors formulation, the constituents of $s^2_{keff,BENCH}$ are presented as:

$$s_{\overline{keff}_{BENCH}}^2 = \left(\frac{\partial \overline{k}_{effBENCH}}{\partial\, bias_{CALC}}\right)^2 s_{bias_{CALC}}^2 + \left(\frac{\partial \overline{k}_{effBENCH}}{\partial\, uncertainty_{CALC}}\right)^2 s_{uncertainty_{CALC}}^2 + \left(\frac{\partial \overline{k}_{effBENCH}}{\partial\, bias_{EXP}}\right)^2 s_{bias_{EXP}}^2 + \left(\frac{\partial \overline{k}_{effBENCH}}{\partial\, uncertainty_{EXP}}\right)^2 s_{uncertainty_{EXP}}^2$$

Equation 7.5.1-6.

The partial derivatives of the average k_{eff} value for the set of critical benchmark evaluations with respect to bias and uncertainty in either the experiments or the calculations is a small fraction of the average k_{eff} value (i.e. less than 1.0). Therefore, to assure conservatism and simplify the

statistical analysis, the partial derivatives of the average k_{eff} will be set to one. Equation 7.5.1-6, then simplifies to:

$$s_{\overline{keff}_{BENCH}}^2 = s_{bias_{CALC}}^2 + s_{uncertainty_{CALC}}^2 + s_{bias_{EXP}}^2 + s_{uncertainty_{EXP}}^2$$

Equation 7.5.1-7.

The calculation of each term on the right side in Equation 7.5.1-7, utilizes the following definition of the variance--

$$s(x)^2 = \left(\frac{1}{N-1}\right) \sum_{i}^{N} (x_i - \bar{x})^2$$

Equation 7.5.1-8

N	=	the size of the sample set,
x	=	the value of a member of the sample set
$\bar{x}$	=	the mean of the sample set
$s(x)^2$	=	the average variance of the sample set about the mean of the sample set.

The variances in the calculational bias and uncertainty are quantified in this study and contribute to the variance in the benchmark evaluations as indicated in Equation 7.5.1-7.

7.5.2 Calculation of the Bias and the Uncertainty in Bias

The calculation of the bias and the uncertainty in the bias is performed for each classification in the critical experiment library following the methodology described in Section 7.5.1. The experimental bias and uncertainty as well as the variances in the experimental bias and uncertainty have not been quantified in this study. The exclusion of the experimental bias and uncertainty should not affect the enhanced subcritical margin results for the classifications containing true critical experiments. Some classifications in the study contain exponential approach to critical experiments whose bias and uncertainty may be significant. However, due to the expected insignificant effect of the experimental bias and uncertainties as compared to the calculational bias and uncertainties, the enhanced subcritical margin for the classifications containing these exponential criticals remains representative of the applicable margin. Additionally, the effect of excluding the variance in the experimental bias and uncertainty is compensated to a degree by the fact that the partial derivatives of the mean k_{eff} with respect to the calculational bias and uncertainty were set equal to one in Equation 7.5.1-6.

Tables 7.5.2-1 through 7.5.2-20 contain the calculational results for the bias and uncertainty in the bias for each experimental classification in the critical experiment library. The enhanced subcritical margin and resulting maximum allowable k_{eff} for analyses bounded by the characteristics of each classification are also presented.

Table 7.5.2-1

Classification: Fissile Metal Fuel / Cylinder Arrays / Unmoderated						
Case Identifier	keff	sigma	(keff-ave.keff)	(keff-av.keff)^2	(sigma-ave.sigma)	(sigma-ave.sigma)^2
prob1	0.9999	0.0009	0.0004	1.9990E-07	-1.2812E-03	1.6415E-06
prob7	1.0002	0.0004	0.0008	6.3537E-07	-1.7962E-03	3.2264E-06
Pu 3X3	1.0000	0.0019	0.0006	3.3305E-07	-3.1121E-04	9.6850E-08
A15	0.9957	0.0022	-0.0037	1.3912E-05	-1.1207E-05	1.2559E-10
A21	0.9925	0.0020	-0.0069	4.8232E-05	-2.1121E-04	4.4608E-08
A41	0.9947	0.0022	-0.0047	2.1939E-05	-1.1207E-05	1.2559E-10
A51	0.9946	0.0020	-0.0048	2.3039E-05	-2.1121E-04	4.4608E-08
A61	0.9851	0.0024	-0.0143	2.0489E-04	1.3879E-04	1.9264E-08
ARRAY.2	0.9982	0.0020	-0.0012	1.5151E-06	-2.1121E-04	4.4608E-08
prob3	0.9961	0.0011	-0.0033	1.0909E-05	-1.0712E-03	1.1475E-06
prob5	0.9995	0.0027	0.0001	5.9449E-09	4.8879E-04	2.3892E-07
A11	1.0029	0.0019	0.0035	1.1938E-05	-3.1121E-04	9.6850E-08
A12	1.0085	0.0028	0.0091	8.3122E-05	5.8879E-04	3.4668E-07
A13	1.0070	0.0024	0.0076	5.7367E-05	1.8879E-04	3.5643E-08
A14	1.0006	0.0025	0.0012	1.4984E-06	2.8879E-04	8.3401E-08
A22	0.9976	0.0022	-0.0018	3.2577E-06	-1.1207E-05	1.2559E-10
A23	1.0035	0.0024	0.0040	1.6314E-05	1.8879E-04	3.5643E-08
A24	1.0029	0.0024	0.0035	1.2426E-05	1.8879E-04	3.5643E-08
A25	0.9979	0.0022	-0.0015	2.1871E-06	-1.1207E-05	1.2559E-10
A32	0.9998	0.0021	0.0001	1.7717E-08	-1.1121E-04	1.2367E-08
A33	1.0070	0.0024	0.0076	5.8081E-05	1.8879E-04	3.5643E-08
A34	1.0065	0.0025	0.0071	5.0440E-05	2.8879E-04	8.3401E-08
A35	0.9991	0.0027	-0.0003	1.0817E-07	4.8879E-04	2.3892E-07
A42	0.9968	0.0021	-0.0027	7.0538E-06	-1.1121E-04	1.2367E-08
A43	1.0020	0.0028	0.0026	6.7709E-06	5.8879E-04	3.4668E-07
A44	0.9997	0.0027	0.0003	1.0440E-07	4.8879E-04	2.3892E-07
A45	0.9944	0.0029	-0.0050	2.5411E-05	6.8879E-04	4.7444E-07
A62	0.9977	0.0024	-0.0017	2.9684E-06	1.7879E-04	3.1967E-08
ARRAY.5	1.0028	0.0029	0.0034	1.1724E-05	6.8879E-04	4.7444E-07
AVERAGE:	0.9994	0.0022	SUM:	6.7640E-04	SUM:	9.0877E-06
Bias:	0.0006		VARIANCES:			
			calc. bias:	2.4157E-05	calc. unc.:	3.2456E-07
One-Sided, Non-Central Student-t (95/95):				2.2320E+00		
			Uncertainty in the Bias:	1.3255E-02		
Robust Subcritical Margin:			0.0638			
Maximum Allowable keff:			0.9362			

Table 7.5.2-2

Classification: Fissile Metal Fuel / Slab Lattice Geometries / Moderated						
					(sigma-	(sigma-
Case Identifier	keff	sigma	(keff-ave.keff)	(keff-av.keff)^2	ave.sigma)	ave.sigma)^2
SPERT-D.1	1.0033	0.0028	0.0011	1.2982E-06	1.5455E-04	2.3884E-08
SPERT-D.2	1.0121	0.0028	0.0100	1.0001E-04	1.5455E-04	2.3884E-08
SPERT-D.3	1.0104	0.0026	0.0083	6.8482E-05	-4.5455E-05	2.0661E-09
SPERT-D.4	1.0052	0.0024	0.0031	9.3844E-06	-2.4545E-04	6.0248E-08
SPERT-D.5	0.9959	0.0025	-0.0062	3.8958E-05	-1.4545E-04	2.1157E-08
SPERT-D.6	0.9965	0.0025	-0.0057	3.2065E-05	-1.4545E-04	2.1157E-08
SPERT-D.7	0.9898	0.0024	-0.0124	1.5256E-04	-2.4545E-04	6.0248E-08
SPERT-D.8	0.9918	0.0023	-0.0103	1.0598E-04	-3.4545E-04	1.1934E-07
SPERT-D.9	1.0151	0.0027	0.0130	1.6935E-04	5.4545E-05	2.9752E-09
SPERT-D.10	1.0005	0.0026	-0.0016	2.6850E-06	-4.5455E-05	2.0661E-09
SPERT-D.11	0.9990	0.0027	-0.0031	9.4962E-06	5.4545E-05	2.9752E-09
SPERT-D.12	1.0015	0.0031	-0.0006	4.1938E-07	4.5455E-04	2.0661E-07
SPERT-D.13	1.0021	0.0024	0.0000	9.2073E-11	-2.4545E-04	6.0248E-08
SPERT-D.14	1.0265	0.0031	0.0244	5.9436E-04	4.5455E-04	2.0661E-07
SPERT-D.15	0.9919	0.0026	-0.0102	1.0405E-04	-4.5455E-05	2.0661E-09
SPERT-D.16	0.9933	0.0026	-0.0089	7.8705E-05	-4.5455E-05	2.0661E-09
SPERT-D.17	1.0046	0.0028	0.0025	6.3474E-06	1.5455E-04	2.3884E-08
SPERT-D.18	0.9960	0.0024	-0.0061	3.7071E-05	-2.4545E-04	6.0248E-08
SPERT-D.19	1.0032	0.0027	0.0010	1.0453E-06	5.4545E-05	2.9752E-09
SPERT-D.20	1.0058	0.0027	0.0037	1.3406E-05	5.4545E-05	2.9752E-09
SPERT-D.21	1.0030	0.0026	0.0008	7.2149E-07	-4.5455E-05	2.0661E-09
SPERT-D.22	0.9993	0.0029	-0.0028	8.0400E-06	2.5455E-04	6.4793E-08
AVERAGE:	1.0021	0.0026	SUM:	1.5344E-03	SUM:	9.7455E-07
Bias:	-0.0021		VARIANCES:			
			calc. bias:	7.3068E-05	calc. unc.:	4.6407E-08
One-Sided, Non-Central Student-t (95/95):				2.3490E+00		
		Uncertainty in the Bias:		2.2731E-02		
Robust Subcritical Margin:			0.0706			
Maximum Allowable keff:			0.9294			

Table 7.5.2-3

Classification: Fissile Metal Fuel / Single Unit Cylinders / Bare						
Case Identifier	keff	sigma	(keff-ave.keff)	(keff-av.keff)^2	(sigma-ave.sigma)	(sigma-ave.sigma)^2
10.9% U-CYL	1.0024	0.0013	0.0050	2.4866E-05	-4.8571E-04	2.3592E-07
14.11% U-CYL	1.0003	0.0014	0.0029	8.3323E-06	-3.8571E-04	1.4878E-07
SIMP.9	0.9964	0.0019	-0.0010	1.0887E-06	1.1429E-04	1.3061E-08
SIMP.10	0.9966	0.0019	-0.0008	7.2153E-07	1.1429E-04	1.3061E-08
SIMP.11	0.9938	0.0021	-0.0036	1.3202E-05	3.1429E-04	9.8776E-08
SIMP.12	0.9953	0.0020	-0.0021	4.3240E-06	2.1429E-04	4.5918E-08
SIMP.13	0.9971	0.0019	-0.0003	7.1518E-08	1.1429E-04	1.3061E-08
AVERAGE:	0.9974	0.0018	SUM:	5.2606E-05	SUM:	5.6857E-07
Bias:	0.0026		VARIANCES:			
			calc. bias:	8.7676E-06	calc. unc.:	9.4762E-08
One-Sided, Non-Central Student-t (95/95):				3.3990E+00		
			Uncertainty in the Bias:	1.1904E-02		
Robust Subcritical Margin:			0.0645			
Maximum Allowable keff:			0.9355			

Table 7.5.2-4

Classification: Fissile Metal Fuel / Single Unit Cylinders / Reflected						
Case Identifier	keff	sigma	(keff-ave.keff)	(keff-av.keff)^2	(sigma-ave.sigma)	(sigma-ave.sigma)^2
SIMP.14	0.9996	0.0026	0.0110	1.2201E-04	1.3571E-04	1.8418E-08
SIMP.15	0.9680	0.0023	-0.0206	4.2445E-04	-1.6429E-04	2.6990E-08
SIMP.16	0.9496	0.0025	-0.0390	1.5226E-03	3.5714E-05	1.2755E-09
SIMP.17	0.9953	0.0023	0.0067	4.4794E-05	-1.6429E-04	2.6990E-08
MIH16	0.9846	0.0024	-0.0040	1.5921E-05	-6.4286E-05	4.1327E-09
MIH17	0.9895	0.0025	0.0010	9.4062E-07	3.5714E-05	1.2755E-09
MIH18	0.9874	0.0024	-0.0012	1.4236E-06	-6.4286E-05	4.1327E-09
MIH19	0.9935	0.0024	0.0049	2.4432E-05	-6.4286E-05	4.1327E-09
MIH20	0.9927	0.0023	0.0042	1.7346E-05	-1.6429E-04	2.6990E-08
MIH21	0.9974	0.0026	0.0088	7.7790E-05	1.3571E-04	1.8418E-08
MIH22	1.0002	0.0024	0.0116	1.3497E-04	-6.4286E-05	4.1327E-09
MIH23	0.9933	0.0027	0.0047	2.2220E-05	2.3571E-04	5.5561E-08
MIH24	0.9938	0.0024	0.0052	2.7320E-05	-6.4286E-05	4.1327E-09
MIH25	0.9952	0.0027	0.0068	4.3703E-05	2.3571E-04	5.5561E-08
AVERAGE:	0.9886	0.0025	SUM:	2.4799E-03	SUM:	2.5214E-07
Bias:	0.0114		VARIANCES:			
			calc. bias:	1.9076E-04	calc. unc.:	1.9396E-08
One-Sided, Non-Central Student-t (95/95):				2.6140E+00		
			Uncertainty in the Bias:	3.8570E-02		
Robust Subcritical Margin:			0.1000			
Maximum Allowable keff:			0.9000			

Table 7.5.2-5

Classification: Fissile Metal Fuel / Single Unit Spheres / Bare						
Case Identifier	keff	sigma	(keff-ave.keff)	(keff-av.keff)^2	(sigma-ave.sigma)	(sigma-ave.sigma)^2
GE GODIVA	0.9983	0.0011	0.0022	4.8642E-06	-3.3167E-04	1.1000E-07
LANL GODIVA	0.9976	0.0011	0.0015	2.3578E-06	-3.1167E-04	9.7136E-08
GE JEZEBEL	0.9965	0.0010	0.0005	2.0748E-07	-3.7167E-04	1.3814E-07
95.5 LANL JEZ	0.9986	0.0021	0.0025	6.4288E-06	6.8833E-04	4.7380E-07
80.0 LANL JEZ	1.0075	0.0012	0.0114	1.3077E-04	-2.1167E-04	4.4803E-08
SIMP.1	0.9779	0.0020	-0.0182	3.3006E-04	5.3833E-04	2.8980E-07
AVERAGE:	0.9961	0.0014	SUM:	4.7469E-04	SUM:	1.1537E-06
Bias:	0.0039		VARIANCES:			
			calc. bias:	9.4937E-05	calc. unc.:	2.3074E-07
One-Sided, Non-Central Student-t (95/95):				3.7080E+00		
		Uncertainty in the Bias:		3.7585E-02		
Robust Subcritical Margin:			0.0915			
Maximum Allowable keff:			0.9085			

Table 7.5.2-6

Classification: Fissile Metal Fuel / Single Unit Spheres / Reflected						
Case Identifier	keff	sigma	(keff-ave.keff)	(keff-av.keff)^2	(sigma-ave.sigma)	(sigma-ave.sigma)^2
GRPH U-SPH	0.9981	0.0010	0.0040	1.5705E-05	-9.8333E-04	9.6694E-07
REF U-SPH	0.9956	0.0011	0.0015	2.1404E-06	-8.8333E-04	7.8028E-07
SIMP.2	0.9980	0.0024	0.0039	1.4930E-05	4.1667E-04	1.7361E-07
SIMP.3	1.0013	0.0024	0.0072	5.1552E-05	4.1667E-04	1.7361E-07
SIMP.18	0.9800	0.0024	-0.0141	1.9850E-04	4.1667E-04	1.7361E-07
BYE1	0.9918	0.0026	-0.0024	5.6692E-06	6.1667E-04	3.8028E-07
AVERAGE:	0.9941	0.0020	SUM:	2.8850E-04	SUM:	2.6483E-06
Bias:	0.0059		VARIANCES:			
			calc. bias:	5.7700E-05	calc. unc.:	5.2967E-07
One-Sided, Non-Central Student-t (95/95):				3.7080E+00		
		Uncertainty in the Bias:		3.0278E-02		
Robust Subcritical Margin:			**0.0861**			
Maximum Allowable keff:			**0.9139**			

Table 7.5.2-7

Classification: Fissile Metal Fuel / Single Unit Annuli / Bare						
Case Identifier	keff	sigma	(keff-ave.keff)	(keff-av.keff)^2	(sigma-ave.sigma)	(sigma-ave.sigma)^2
SIMP.4	0.9933	0.0018	0.0014	1.8824E-06	-2.0000E-04	4.0000E-08
SIMP.7	0.9905	0.0022	-0.0014	1.8824E-06	2.0000E-04	4.0000E-08
AVERAGE:	0.9919	0.0020	SUM:	3.7648E-06	SUM:	8.0000E-08
Bias:	0.0081		VARIANCES:			
			calc. bias:	3.7648E-06	calc. unc.:	8.0000E-08
One-Sided, Non-Central Student-t (95/95):				2.6260E+01		
		Uncertainty in the Bias:		5.3491E-02		
Robust Subcritical Margin:			**0.1116**			
Maximum Allowable keff:			**0.8884**			

Table 7.5.2-8

Classification: Fissile Metal Fuel / Single Unit Annuli / Reflected						
Case Identifier	keff	sigma	(keff-ave.keff)	(keff-av.keff)^2	(sigma-ave.sigma)	(sigma-ave.sigma)^2
SMP.5	0.9933	0.0018	-0.0033	1.0751E-05	-5.7187E-04	3.2704E-07
SMP.6	1.0002	0.0025	0.0037	1.3492E-05	1.2813E-04	1.6416E-08
MIH1	0.9985	0.0021	0.0019	3.6144E-06	-2.7188E-04	7.3916E-08
MIH2	0.9960	0.0020	-0.0006	3.6101E-07	-3.7187E-04	1.3829E-07
MIH3	0.9984	0.0021	0.0018	3.1904E-06	-2.7188E-04	7.3916E-08
MIH4	0.9962	0.0025	-0.0004	1.5988E-07	1.2813E-04	1.6416E-08
MIH5	0.9926	0.0025	-0.0040	1.5839E-05	1.2813E-04	1.6416E-08
MIH6	0.9937	0.0025	-0.0029	8.4497E-06	1.2813E-04	1.6416E-08
MIH7	0.9971	0.0026	0.0005	2.8107E-07	2.2813E-04	5.2041E-08
MIH8	0.9982	0.0012	0.0016	2.6803E-06	-1.1719E-03	1.3733E-06
MIH9	0.9963	0.0025	-0.0003	9.6003E-08	1.2813E-04	1.6416E-08
MIH10	0.9927	0.0028	-0.0038	1.4645E-05	4.2813E-04	1.8329E-07
MIH11	0.9928	0.0022	-0.0037	1.3971E-05	-1.7187E-04	2.9541E-08
MIH12	0.9976	0.0028	0.0010	1.0757E-06	4.2813E-04	1.8329E-07
MIH13	0.9933	0.0025	-0.0033	1.0594E-05	1.2813E-04	1.6416E-08
MIH14	0.9945	0.0025	-0.0021	4.2718E-06	1.2813E-04	1.6416E-08
MIH15	0.9910	0.0028	-0.0056	3.1146E-05	4.2813E-04	1.8329E-07
MIH51	0.9985	0.0021	0.0019	3.5500E-06	-2.7188E-04	7.3916E-08
MIH52	0.9934	0.0021	-0.0032	1.0118E-05	-2.7188E-04	7.3916E-08
MIH53	1.0001	0.0022	0.0035	1.2209E-05	-1.7187E-04	2.9541E-08
MIH54	0.9947	0.0022	-0.0018	3.3593E-06	-1.7187E-04	2.9541E-08
MIH55	1.0006	0.0026	0.0040	1.6146E-05	2.2813E-04	5.2041E-08
MIH56	1.0024	0.0027	0.0059	3.4541E-05	3.2813E-04	1.0767E-07
MIH57	1.0003	0.0026	0.0037	1.3728E-05	2.2813E-04	5.2041E-08
MIH58	1.0029	0.0028	0.0064	4.0502E-05	4.2813E-04	1.8329E-07
MIH59	0.9996	0.0026	0.0030	8.9470E-06	2.2813E-04	5.2041E-08
MIH60	0.9872	0.0020	-0.0094	8.7869E-05	-3.7187E-04	1.3829E-07
MIH61	0.9978	0.0023	0.0013	1.5754E-06	-7.1875E-05	5.1660E-09
MIH62	0.9957	0.0024	-0.0009	7.9182E-07	2.8125E-05	7.9102E-10
MIH63	0.9958	0.0025	-0.0007	5.5927E-07	1.2813E-04	1.6416E-08
MIH64	0.9987	0.0026	0.0022	4.6620E-06	2.2813E-04	5.2041E-08
MIH65	1.0002	0.0023	0.0037	1.3360E-05	-7.1875E-05	5.1660E-09
AVERAGE:	0.9966	0.0024	SUM:	3.8654E-04	SUM:	3.6047E-06
Bias:	0.0034		VARIANCES:			
			calc. bias:	1.2469E-05	calc. unc.:	1.1628E-07
One-Sided, Non-Central Student-t (95/95):				2.1970E+00		
		Uncertainty in the Bias:		1.0166E-02		
Robust Subcritical Margin:			0.0636			
Maximum Allowable keff:			0.9364			

Table 7.5.2-9

Classification: Fissile Metal Fuel / Unique Geometries						
Case Identifier	keff	sigma	(keff-ave.keff)	(keff-av.keff)^2	(sigma-ave.sigma)	(sigma-ave.sigma)^2
prob12	0.9985	0.0012	0.0014	2.0164E-06	2.1500E-04	4.6225E-08
prob13	0.9898	0.0009	-0.0073	5.3144E-05	-7.5000E-05	5.6250E-09
prob14	0.9985	0.0008	0.0014	1.9600E-06	-1.3500E-04	1.8225E-08
prob15	1.0016	0.0010	0.0045	1.9981E-05	-5.0000E-06	2.5000E-11
AVERAGE:	0.9971	0.0010	SUM:	7.7101E-05	SUM:	7.0100E-08
Bias:	0.0029		VARIANCES:			
			calc. bias:	2.5700E-05	calc. unc.:	2.3367E-08
One-Sided, Non-Central Student-t (95/95):				5.1440E+00		
		Uncertainty in the Bias:		2.7065E-02		
Robust Subcritical Margin:			0.0800			
Maximum Allowable keff:			0.9200			

Table 7.5.2-10

Classification: Fissile Oxide Fuel / Cylinder Arrays / Unmoderated						
Case Identifier	keff	sigma	(keff-ave.keff)	(keff-av.keff)^2	(sigma-ave.sigma)	(sigma-ave.sigma)^2
MAG.2	1.0050	0.0023	0.0071	5.0438E-05	-1.3333E-04	1.7778E-08
MAG.3	0.9945	0.0025	-0.0035	1.1972E-05	6.6667E-05	4.4444E-09
MAG.4	0.9943	0.0025	-0.0036	1.3264E-05	6.6667E-05	4.4444E-09
AVERAGE:	0.9979	0.0024	SUM:	7.5674E-05	SUM:	2.6667E-08
Bias:	0.0021		VARIANCES:			
			calc. bias:	3.7837E-05	calc. unc.:	1.3333E-08
One-Sided, Non-Central Student-t (95/95):				7.6560E+00		
		Uncertainty in the Bias:		4.9535E-02		
Robust Subcritical Margin:			0.1016			
Maximum Allowable keff:			0.8984			

Table 7.5.2-11

Classification: Fissile Oxide Fuel / Lattice Geometries / Moderated						
					(sigma-ave.sigma)	(sigma-ave.sigma)^2
Case Identifier	keff	sigma	(keff-ave.keff)	(keff-av.keff)^2		
SCPC	1.0004	0.0015	-0.0013	1.7406E-06	-4.2683E-05	1.8216E-09
SCNOPC	0.9975	0.0013	-0.0042	1.8057E-05	-2.6268E-04	6.9002E-08
BA3GD4	1.0004	0.0017	-0.0014	1.8477E-06	1.8732E-04	3.5088E-08
BA5GD4	0.9934	0.0016	-0.0084	6.9878E-05	8.7317E-05	7.6243E-09
BA3GD16	0.9984	0.0014	-0.0034	1.1285E-05	-1.1268E-04	1.2697E-08
BORAX-V.2	1.0259	0.0023	0.0241	5.8181E-04	7.8732E-04	6.1987E-07
BORAX-V.3	1.0129	0.0021	0.0111	1.2416E-04	5.8732E-04	3.4494E-07
EXP1	0.9991	0.0013	-0.0027	7.0720E-06	-2.1268E-04	4.5234E-08
EXP2	1.0005	0.0013	-0.0013	1.5859E-06	-2.1268E-04	4.5234E-08
EXP3	1.0003	0.0013	-0.0015	2.1296E-06	-2.1268E-04	4.5234E-08
EXP4	1.0019	0.0014	0.0001	1.9792E-08	-1.1268E-04	1.2697E-08
EXP5	0.9969	0.0015	-0.0049	2.3613E-05	-1.2683E-05	1.6086E-10
EXP6	1.0038	0.0015	0.0020	4.1644E-06	-1.2683E-05	1.6086E-10
EXP7	0.9965	0.0016	-0.0053	2.7660E-05	8.7317E-05	7.6243E-09
EXP8	1.0082	0.0015	0.0064	4.1482E-05	-1.2683E-05	1.6086E-10
EXP9	1.0050	0.0015	0.0032	1.0502E-05	-1.2683E-05	1.6086E-10
EXP10	1.0046	0.0015	0.0028	8.0695E-06	-1.2683E-05	1.6086E-10
EXP11	1.0004	0.0015	-0.0014	1.8477E-06	-1.2683E-05	1.6086E-10
EXP12	1.0044	0.0016	0.0026	6.9732E-06	8.7317E-05	7.6243E-09
EXP13	0.9998	0.0016	-0.0020	3.8389E-06	8.7317E-05	7.6243E-09
EXP14	1.0012	0.0014	-0.0006	3.1284E-07	-1.1268E-04	1.2697E-08
EXP15	1.0011	0.0012	-0.0007	4.3470E-07	-3.1268E-04	9.7771E-08
EXP16	0.9981	0.0014	-0.0037	1.3391E-05	-1.1268E-04	1.2697E-08
EXP17	0.9886	0.0015	-0.0132	1.7317E-04	-1.2683E-05	1.6086E-10
EXP18	1.0097	0.0014	0.0079	6.3054E-05	-1.1268E-04	1.2697E-08
EXP19	0.9955	0.0013	-0.0063	3.9179E-05	-2.1268E-04	4.5234E-08
EXP20	0.9951	0.0013	-0.0067	4.4347E-05	-2.1268E-04	4.5234E-08
EXP21	0.9985	0.0013	-0.0033	1.0623E-05	-2.1268E-04	4.5234E-08
EXP22	0.9966	0.0015	-0.0052	2.6619E-05	-1.2683E-05	1.6086E-10
EXP23	0.9990	0.0015	-0.0028	7.6138E-06	-1.2683E-05	1.6086E-10
EXP24	1.0060	0.0014	0.0042	1.7983E-05	-1.1268E-04	1.2697E-08
EXP25	1.0087	0.0015	0.0069	4.8173E-05	-1.2683E-05	1.6086E-10
EXP26	1.0088	0.0014	0.0070	4.9571E-05	-1.1268E-04	1.2697E-08
EXP27	1.0090	0.0015	0.0072	5.2427E-05	-1.2683E-05	1.6086E-10
EXP28	0.9998	0.0017	-0.0020	3.8389E-06	1.8732E-04	3.5088E-08
EXP29	1.0032	0.0017	0.0014	2.0756E-06	1.8732E-04	3.5088E-08
EXP30	0.9985	0.0017	-0.0033	1.0623E-05	1.8732E-04	3.5088E-08
EXP31	1.0034	0.0016	0.0016	2.6918E-06	8.7317E-05	7.6243E-09
EXP32	1.0038	0.0017	0.0020	4.1644E-06	1.8732E-04	3.5088E-08
EXP33	1.0098	0.0016	0.0080	6.4653E-05	8.7317E-05	7.6243E-09
EXP34	0.9874	0.0015	-0.0144	2.0619E-04	-1.2683E-05	1.6086E-10
AVERAGE:	1.0018	0.0015	SUM:	1.7889E-03	SUM:	1.7168E-06
Bias:	-0.0018		VARIANCES:			
			calc. bias:	4.4722E-05	calc. unc.:	4.2920E-08
One-Sided, Non-Central Student-t (95/95):				2.1180E+00		
		Uncertainty in the Bias:		1.5683E-02		
Robust Subcritical Margin:			0.0639			
Maximum Allowable keff:			0.9361			

Table 7.5.2-12

Classification: Fissile Oxide Fuel / Cylinder Arrays / Moderated						
Case Identifier	keff	sigma	(keff-ave.keff)	(keff-av.keff)^2	(sigma-ave.sigma)	(sigma-ave.sigma)^2
MAG.1	1.0319	0.0027	0.0301	9.0549E-04	2.8571E-05	8.1633E-10
MAG.5	0.9900	0.0031	-0.0118	1.4013E-04	4.2857E-04	1.8367E-07
MAG.7	0.9957	0.0026	-0.0061	3.7316E-05	-7.1429E-05	5.1020E-09
MAG.13	1.0045	0.0026	0.0027	7.0771E-06	-7.1429E-05	5.1020E-09
MAG.15	0.9961	0.0027	-0.0057	3.2749E-05	2.8571E-05	8.1633E-10
MAG.17	0.9948	0.0023	-0.0072	5.2269E-05	-3.7143E-04	1.3796E-07
MAG.20	1.0000	0.0027	-0.0019	3.4326E-06	2.8571E-05	8.1633E-10
AVERAGE:	1.0018	0.0027	SUM:	1.1785E-03	SUM:	3.3429E-07
Bias:	-0.0018		VARIANCES:			
			calc. bias:	1.9641E-04	calc. unc.:	5.5714E-08
One-Sided, Non-Central Student-t (95/95):				3.3990E+00		
		Uncertainty in the Bias:		5.0314E-02		
Robust Subcritical Margin:			0.0985			
Maximum Allowable keff:			0.9015			

Table 7.5.2-13

Classification: Fissile Solution Fuel / Cylinder Arrays / Bare						
Case Identifier	keff	sigma	(keff-ave.keff)	(keff-av.keff)^2	(sigma-ave.sigma)	(sigma-ave.sigma)^2
THO1	0.9968	0.0033	0.0099	9.8122E-05	7.6167E-04	5.8014E-07
THO7	0.9846	0.0032	-0.0024	5.5476E-06	6.6167E-04	4.3780E-07
THO12	0.9715	0.0032	-0.0154	2.3631E-04	6.6167E-04	4.3780E-07
THO13	0.9724	0.0031	-0.0145	2.1099E-04	5.6167E-04	3.1547E-07
prob20	0.9971	0.0013	0.0102	1.0320E-04	-1.2083E-03	1.4601E-06
THREE U-CYL	0.9991	0.0011	0.0122	1.4856E-04	-1.4383E-03	2.0688E-06
AVERAGE:	0.9869	0.0025	SUM:	8.0273E-04	SUM:	5.3001E-06
Bias:	0.0131		VARIANCES:			
			calc. bias:	1.6055E-04	calc. unc.:	1.0600E-06
One-Sided, Non-Central Student-t (95/95):				3.7080E+00		
		Uncertainty in the Bias:		4.9676E-02		
Robust Subcritical Margin:			0.1128			
Maximum Allowable keff:			0.8872			

Table 7.5.2-14

Classification: Fissile Solution Fuel / Cylinder Arrays / Reflected						
Case Identifier	keff	sigma	(keff-ave.keff)	(keff-ave.keff)^2	(sigma-ave.sigma)	(sigma-ave.sigma)^2
ROT50	1.0128	0.0028	0.0049	2.4471E-05	-2.3244E-04	5.4028E-08
ROT51	1.0029	0.0030	-0.0050	2.4624E-05	-3.2439E-05	1.0523E-09
ROT52	1.0113	0.0027	0.0034	1.1825E-05	-3.3244E-04	1.1052E-07
ROT53	1.0013	0.0029	-0.0066	4.2918E-05	-1.3244E-04	1.7540E-08
ROT54	1.0104	0.0027	0.0025	6.3141E-06	-3.3244E-04	1.1052E-07
ROT55	1.0042	0.0032	-0.0037	1.3699E-05	1.6756E-04	2.8077E-08
ROT56	1.0082	0.0030	0.0003	9.9087E-08	-3.2439E-05	1.0523E-09
ROT57	1.0139	0.0032	0.0061	3.6709E-05	1.6756E-04	2.8077E-08
ROT58	1.0020	0.0031	-0.0058	3.3910E-05	6.7561E-05	4.5645E-09
ROT59	1.0011	0.0032	-0.0067	4.5323E-05	1.6756E-04	2.8077E-08
ROT60	0.9910	0.0040	-0.0169	2.8599E-04	9.6756E-04	9.3617E-07
ROT61	1.0058	0.0032	-0.0021	4.3523E-06	1.6756E-04	2.8077E-08
ROT62	1.0060	0.0026	-0.0019	3.6719E-06	-4.3244E-04	1.8700E-07
ROT63	1.0083	0.0035	0.0004	1.5903E-07	4.6756E-04	2.1861E-07
ROT64	1.0056	0.0031	-0.0022	5.0410E-06	6.7561E-05	4.5645E-09
ROT65	1.0072	0.0032	-0.0007	4.4119E-07	1.6756E-04	2.8077E-08
ROT66	1.0115	0.0034	0.0036	1.3125E-05	3.6756E-04	1.3510E-07
ROT67	1.0024	0.0028	-0.0055	2.9912E-05	-2.3244E-04	5.4028E-08
ROT68	1.0018	0.0026	-0.0061	3.6933E-05	-4.3244E-04	1.8700E-07
ROT69	0.9984	0.0028	-0.0095	8.9856E-05	-2.3244E-04	5.4028E-08
ROT70	0.9963	0.0028	-0.0116	1.3491E-04	-2.3244E-04	5.4028E-08
ROT71	1.0010	0.0024	-0.0069	4.7710E-05	-6.3244E-04	3.9998E-07
ROT72	0.9996	0.0027	-0.0082	6.7737E-05	-3.3244E-04	1.1052E-07
ROT73	1.0101	0.0036	0.0022	4.9808E-06	5.6756E-04	3.2213E-07
ROT74	1.0020	0.0031	-0.0059	3.4272E-05	6.7561E-05	4.5645E-09
ROT75	1.0098	0.0033	0.0019	3.6016E-06	2.6756E-04	7.1589E-08
ROT76	1.0097	0.0035	0.0018	3.4217E-06	4.6756E-04	2.1861E-07
ROT77	1.0071	0.0032	-0.0008	6.3397E-07	1.6756E-04	2.8077E-08
ROT78	1.0084	0.0030	0.0006	3.3037E-07	-3.2439E-05	1.0523E-09
ROT79	1.0058	0.0031	-0.0020	4.1666E-06	6.7561E-05	4.5645E-09
ROT80	1.0029	0.0030	-0.0050	2.5213E-05	-3.2439E-05	1.0523E-09
THO2	1.0071	0.0035	-0.0007	5.5238E-07	4.6756E-04	2.1861E-07
THO3	1.0248	0.0035	0.0169	2.8723E-04	4.6756E-04	2.1861E-07
THO4	1.0339	0.0028	0.0260	6.7677E-04	-2.3244E-04	5.4028E-08
THO5	1.0221	0.0033	0.0143	2.0331E-04	2.6756E-04	7.1589E-08
THO6	0.9950	0.0033	-0.0129	1.6665E-04	2.6756E-04	7.1589E-08
THO8	1.0039	0.0024	-0.0039	1.5581E-05	-6.3244E-04	3.9998E-07
THO9	1.0316	0.0032	0.0238	5.6524E-04	1.6756E-04	2.8077E-08
THO10	1.0259	0.0032	0.0180	3.2579E-04	1.6756E-04	2.8077E-08
THO11	0.9902	0.0032	-0.0177	3.1323E-04	1.6756E-04	2.8077E-08
prob18	1.0294	0.0012	0.0215	4.6177E-04	-1.8024E-03	3.2488E-06
AVERAGE:	1.0079	0.0030	SUM:	4.0525E-03	SUM:	7.7998E-06
Bias:	-0.0079		VARIANCES:			
			calc. bias:	1.0131E-04	calc. unc.:	1.9499E-07
One-Sided, Non-Central Student-t (95/95):				2.1180E+00		
			Uncertainty in the Bias:	2.4371E-02		
Robust Subcritical Margin:			0.0665			
Maximum Allowable keff:			0.9335			

Table 7.5.2-15

Classification: Fissile Solution Fuel / Single Unit Cylinders / Bare						
					(sigma-	(sigma-
Case Identifier	keff	sigma	(keff-ave.keff)	(keff-av.keff)^2	ave.sigma)	ave.sigma)^2
ROT1	1.0053	0.0031	0.0021	4.5403E-06	4.0000E-04	1.6000E-07
ROT6	0.9989	0.0036	-0.0042	1.7734E-05	9.0000E-04	8.1000E-07
ROT11	1.0184	0.0038	0.0153	2.3329E-04	1.1000E-03	1.2100E-06
ROT16	1.0064	0.0034	0.0033	1.0777E-05	7.0000E-04	4.9000E-07
ROT21	1.0032	0.0037	0.0000	1.1424E-09	1.0000E-03	1.0000E-06
ROT26	0.9937	0.0033	-0.0094	8.8251E-05	6.0000E-04	3.6000E-07
ROT40	1.0038	0.0030	0.0007	4.5941E-07	3.0000E-04	9.0000E-08
ROT41	1.0083	0.0031	0.0052	2.6727E-05	4.0000E-04	1.6000E-07
ROT42	0.9970	0.0034	-0.0062	3.7825E-05	7.0000E-04	4.9000E-07
ROT43	0.9943	0.0031	-0.0088	7.7232E-05	4.0000E-04	1.6000E-07
GWI5	1.0053	0.0015	0.0022	4.8921E-06	-1.2000E-03	1.4400E-06
GWI6	1.0090	0.0017	0.0058	3.4185E-05	-1.0000E-03	1.0000E-06
GWI7	1.0032	0.0014	0.0001	6.8558E-09	-1.3000E-03	1.6900E-06
GWI8	1.0045	0.0013	0.0014	1.8654E-06	-1.4000E-03	1.9600E-06
GWI9	0.9956	0.0011	-0.0075	5.6734E-05	-1.6000E-03	2.5600E-06
AVERAGE:	1.0031	0.0027	SUM:	5.9452E-04	SUM:	1.3580E-05
Bias:	-0.0031		VARIANCES:			
			calc. bias:	4.2466E-05	calc. unc.:	9.7000E-07
			One-Sided, Non-Central Student-t (95/95):	2.5660E+00		
			Uncertainty in the Bias:	1.9611E-02		
		Robust Subcritical Margin:	0.0665			
		Maximum Allowable keff:	0.9335			

Table 7.5.2-16

Classification: Fissile Solution Fuel / Single Unit Cylinders / Reflected						
					(sigma-ave.sigma)	(sigma-ave.sigma)^2
Case Identifier	keff	sigma	(keff-ave.keff)	(keff-av.keff)^2		
ROT2	1.0094	0.0035	0.0039	1.5073E-05	2.6108E-04	6.8163E-08
ROT3	1.0066	0.0033	0.0012	1.3723E-06	6.1081E-05	3.7309E-09
ROT4	1.0114	0.0034	0.0059	3.5337E-05	1.6108E-04	2.5947E-08
ROT5	1.0070	0.0034	0.0016	2.4132E-06	1.6108E-04	2.5947E-08
ROT7	1.0085	0.0040	0.0030	9.0508E-06	7.6108E-04	5.7924E-07
ROT8	1.0046	0.0031	-0.0009	7.5089E-07	-1.3892E-04	1.9298E-08
ROT9	1.0063	0.0034	0.0008	6.0289E-07	1.6108E-04	2.5947E-08
ROT10	1.0078	0.0030	0.0023	5.4264E-06	-2.3892E-04	5.7082E-08
ROT12	1.0103	0.0035	0.0048	2.2958E-05	2.6108E-04	6.8163E-08
ROT13	1.0120	0.0032	0.0065	4.2334E-05	-3.8919E-05	1.5147E-09
ROT14	1.0089	0.0034	0.0034	1.1461E-05	2.0108E-04	4.0434E-08
ROT15	1.0114	0.0035	0.0059	3.4568E-05	2.6108E-04	6.8163E-08
ROT17	1.0033	0.0032	-0.0021	4.5349E-06	-3.8919E-05	1.5147E-09
ROT18	1.0049	0.0036	-0.0006	3.7889E-07	3.6108E-04	1.3038E-07
ROT19	0.9995	0.0036	-0.0060	3.5552E-05	3.6108E-04	1.3038E-07
ROT20	1.0088	0.0032	0.0033	1.1025E-05	-3.8919E-05	1.5147E-09
ROT22	1.0025	0.0033	-0.0029	8.5939E-06	6.1081E-05	3.7309E-09
ROT23	1.0162	0.0034	0.0107	1.1461E-04	1.6108E-04	2.5947E-08
ROT24	1.0080	0.0032	0.0025	6.4134E-06	-3.8919E-05	1.5147E-09
ROT25	1.0092	0.0033	0.0037	1.3969E-05	6.1081E-05	3.7309E-09
ROT27	1.0029	0.0034	-0.0026	6.7368E-06	1.6108E-04	2.5947E-08
ROT28	1.0128	0.0032	0.0073	5.3750E-05	-3.8919E-05	1.5147E-09
ROT29	0.9971	0.0030	-0.0084	7.0368E-05	-2.3892E-04	5.7082E-08
ROT30	1.0176	0.0034	0.0121	1.4635E-04	1.6108E-04	2.5947E-08
ROT31	1.0083	0.0029	0.0028	8.0966E-06	-3.3892E-04	1.1487E-07
ROT32	0.9985	0.0030	-0.0069	4.8213E-05	-2.3892E-04	5.7082E-08
ROT33	1.0122	0.0025	0.0067	4.5353E-05	-7.3892E-04	5.4600E-07
ROT34	1.0072	0.0032	0.0017	2.9807E-06	-3.8919E-05	1.5147E-09
ROT35	1.0005	0.0028	-0.0049	2.4439E-05	-4.3892E-04	1.9265E-07
ROT36	1.0140	0.0029	0.0085	7.2343E-05	-3.3892E-04	1.1487E-07
ROT37	0.9978	0.0032	-0.0077	5.9283E-05	-3.8919E-05	1.5147E-09
ROT38	1.0286	0.0035	0.0231	5.3317E-04	2.6108E-04	6.8163E-08
ROT39	1.0118	0.0026	0.0064	4.0583E-05	-6.3892E-04	4.0822E-07
FOX9	0.9980	0.0032	-0.0075	5.5794E-05	-3.8919E-05	1.5147E-09
FOX10	1.0036	0.0032	-0.0019	3.5364E-06	-3.8919E-05	1.5147E-09
FOX11	0.9757	0.0030	-0.0298	8.8938E-04	-2.3892E-04	5.7082E-08
FOX12	0.9595	0.0033	-0.0460	2.1139E-03	6.1081E-05	3.7309E-09
AVERAGE:	1.0055	0.0032	SUM:	4.5507E-03	SUM:	2.9616E-06
Bias:	-0.0055		VARIANCES:			
			calc. bias:	1.2641E-04	calc. unc.:	8.2265E-08
One-Sided, Non-Central Student-t (95/95):				2.1490E+00		
		Uncertainty in the Bias:		2.7408E-02		
Robust Subcritical Margin:			0.0719			
Maximum Allowable keff:			0.9281			

Table 7.5.2-17

Classification: Fissile Solution Fuel / Single Unit Spheres / Bare						
Case Identifier	keff	sigma	(keff-ave.keff)	(keff-av.keff)^2	(sigma-ave.sigma)	(sigma-ave.sigma)^2
ORNL1	0.9994	0.0012	0.0015	2.4006E-06	-3.5700E-04	1.2745E-07
ORNL2	0.9986	0.0013	0.0008	6.3904E-07	-3.1700E-04	1.0049E-07
PNL1	1.0116	0.0013	0.0138	1.8960E-04	-3.1700E-04	1.0049E-07
PNL2	1.0069	0.0015	0.0091	8.2799E-05	-4.7000E-05	2.2090E-09
prob21	0.9962	0.0008	-0.0016	2.6263E-06	-7.7700E-04	6.0373E-07
GWI1	0.9981	0.0020	0.0003	9.2659E-08	4.2300E-04	1.7893E-07
GWI2	0.9910	0.0019	-0.0068	4.6807E-05	3.2300E-04	1.0433E-07
GWI3	0.9859	0.0018	-0.0119	1.4260E-04	2.2300E-04	4.9729E-08
GWI4	0.9878	0.0023	-0.0100	1.0039E-04	7.2300E-04	5.2273E-07
FOX5	1.0027	0.0017	0.0049	2.4024E-05	1.2300E-04	1.5129E-08
AVERAGE:	0.9978	0.0016	SUM:	5.9198E-04	SUM:	1.8052E-06
Bias:	0.0022		VARIANCES:			
			calc. bias:	6.5776E-05	calc. unc.:	2.0058E-07
One-Sided, Non-Central Student-t (95/95):				2.9110E+00		
		Uncertainty in the Bias:		2.5222E-02		
Robust Subcritical Margin:			0.0774			
Maximum Allowable keff:			0.9226			

Table 7.5.2-18

Classification: Fissile Solution Fuel / Single Unit Spheres / Reflected						
Case Identifier	keff	sigma	(keff-ave.keff)	(keff-av.keff)^2	(sigma-ave.sigma)	(sigma-ave.sigma)^2
FOX6	1.0034	0.0032	0.0028	7.7006E-06	6.0000E-04	3.6000E-07
FOX7	0.9980	0.0029	-0.0026	6.6874E-06	3.0000E-04	9.0000E-08
FOX8	1.0004	0.0017	-0.0002	3.5721E-08	-9.0000E-04	8.1000E-07
AVERAGE:	1.0006	0.0026	SUM:	1.4424E-05	SUM:	1.2600E-06
Bias:	-0.0006		VARIANCES:			
			calc. bias:	7.2119E-06	calc. unc.:	6.3000E-07
One-Sided, Non-Central Student-t (95/95):				7.6560E+00		
		Uncertainty in the Bias:		2.4039E-02		
Robust Subcritical Margin:			0.0734			
Maximum Allowable keff:			0.9266			

Table 7.5.2-19

Classification: Fissile Solution Fuel / Single Unit Parallelepipeds / Bare						
					(sigma-	(sigma-
Case Identifier	keff	sigma	(keff-ave.keff)	(keff-av.keff)^2	ave.sigma)	ave.sigma)^2
FOX1	0.9996	0.0031	0.0032	1.0275E-05	-2.0000E-04	4.0000E-08
FOX3	0.9932	0.0035	-0.0032	1.0275E-05	2.0000E-04	4.0000E-08
AVERAGE:	0.9964	0.0033	SUM:	2.0550E-05	SUM:	8.0000E-08
Bias:	0.0036		VARIANCES:			
			calc. bias:	2.0550E-05	calc. unc.:	8.0000E-08
One-Sided, Non-Central Student-t (95/95):				2.6260E+01		
		Uncertainty in the Bias:		1.2257E-01		
Robust Subcritical Margin:			0.1762			
Maximum Allowable keff:			0.8238			

Table 7.5.2-20

Classification: Fissile Solution Fuel / Single Unit Parallelepipeds / Reflected						
					(sigma-	(sigma-
Case Identifier	keff	sigma	(keff-ave.keff)	(keff-av.keff)^2	ave.sigma)	ave.sigma)^2
FOX2	1.0019	0.0032	-0.0019	3.5664E-06	5.0000E-05	2.5000E-09
FOX4	1.0057	0.0031	0.0019	3.5664E-06	-5.0000E-05	2.5000E-09
AVERAGE:	1.0038	0.0032	SUM:	7.1329E-06	SUM:	5.0000E-09
Bias:	-0.0038		VARIANCES:			
			calc. bias:	7.1329E-06	calc. unc.:	5.0000E-09
One-Sided, Non-Central Student-t (95/95):				2.6260E+01		
		Uncertainty in the Bias:		7.3308E-02		
Robust Subcritical Margin:			0.1195			
Maximum Allowable keff:			0.8805			

7.5.3 Summary of the Enhanced Subcritical Margin Calculations

Table 7.5.3-1 summarizes the results for the bias and uncertainty in the bias as calculated in Section 7.5.2. The resulting enhanced subcritical margin and subcritical limit (SL) results are also included. The SL or maximum allowable k_{eff} represents the maximum allowable value of the quantity $k_s + \Delta k_s$ as identified in ANSI/ANS-8.17(5.1) and described in Sections 7.5 and 7.5.2.

Table 7.5.3-1

Library Classification	β	Δβ	Enhanced Subcritical Margin	Subcritical Limit
Fissile Metal Fuel / Cylinder Arrays / Unmoderated	0.0006	1.3255E-2	0.0638	0.9362
Fissile Metal Fuel / Slab Lattice Geometries / Moderated	-0.0021	2.2731E-2	0.0706	0.9294
Fissile Metal Fuel / Single Unit Cylinders / Bare	0.0026	1.1904E-2	0.0645	0.9355
Fissile Metal Fuel / Single Unit Cylinders / Reflected	0.0114	3.8570E-2	0.1000	0.9000
Fissile Metal Fuel / Single Unit Spheres / Bare	0.0039	3.7585E-2	0.0915	0.9085
Fissile Metal Fuel / Single Unit Spheres / Reflected	0.0059	3.0278E-2	0.0861	0.9139
Fissile Metal Fuel / Single Unit Annuli / Bare	0.0081	5.3491E-2	0.1116	0.8884
Fissile Metal Fuel / Single Unit Annuli / Reflected	0.0034	1.0166E-2	0.0636	0.9364
Fissile Metal Fuel / Unique Geometries	0.0029	2.7065E-2	0.0800	0.9200
Fissile Oxide Fuel / Cylinder Arrays / Unmoderated	0.0021	4.9535E-2	0.1016	0.8984
Fissile Oxide Fuel / Cylinder Arrays / Moderated	-0.0018	5.0314E-2	0.0985	0.9015

Library Classification	β	Δβ	Enhanced Subcritical Margin	Subcritical Limit
Fissile Oxide Fuel / Lattice Geometries / Moderated	-0.0018	1.5683E-2	0.0639	0.9361
Fissile Solution Fuel / Cylinder Arrays / Bare	0.0131	4.9676E-2	0.1128	0.8872
Fissile Solution Fuel / Cylinder Arrays / Reflected	-0.0079	2.4371E-2	0.0665	0.9335
Fissile Solution Fuel / Single Unit Cylinders / Bare	-0.0031	1.9611E-2	0.0665	0.9335
Fissile Solution Fuel / Single Unit Cylinders / Reflected	-0.0055	2.7408E-2	0.0719	0.9281
Fissile Solution Fuel / Single Unit Spheres / Bare	0.0022	2.5222E-2	0.0774	0.9226
Fissile Solution Fuel / Single Unit Spheres / Reflected	-0.0006	2.4039E-2	0.0734	0.9266
Fissile Solution Fuel / Single Unit Parallelepipeds / Bare	0.0036	1.2257E-1	0.1762	0.8238
Fissile Solution Fuel/ Single Unit Parallelepipeds / Reflected	-0.0038	7.3308E-2	0.1195	0.8805

7.6 Trending Analysis Technique

The k_{eff} values for the critical benchmark experiments within a classification may exhibit trends with certain physical or neutronic parameters such as the average lethargy of the neutron causing fission (AVEL) or the moderator to fuel atom ratio (H/X Ratio). If it is found that a correlation exists between k_{eff} and a parameter, the bias value for the classification may be determined based upon an extrapolation from a best-fit plot of the critical benchmark k_{eff} values as a function of the parameter of interest.

A lower-tolerance band technique is suggested for performing trending analyses to determine a bias value which is a function of a single characterization parameter. "This approach is a single-sided, uniform width, closed-interval statistical method for the determination of an Upper Safety

Limit (USL) based on the statistical analysis of a number of critical systems." (Ref. 9.41, Pg 3-11) The USL is analogous to the SL or maximum allowable k_{eff} described in Section 7.5. A waste configuration will be considered acceptably subcritical if the sum of the calculated k_{eff} and the calculational uncertainty is less than or equal to the SL (i.e., $k_s + \Delta k_s \leq SL$). Utilizing Equation 7.5-4, the SL is defined as,

$$SL \leq 1.0 - \beta - \Delta\beta - \Delta k_m \qquad \text{Equation 7.6-1.}$$

where the SL is a function of the same parameter as β and $\Delta\beta$.

To conceptually illustrate the lower-tolerance band technique the following description including Figure 7.6-1, are presented exactly as in the "Topical Report on Actinide-Only Burnup Credit for PWR Spent Nuclear Fuel Packages." (Ref. 9.41)

> "Because both β and $\Delta\beta$ can vary with a given parameter, the USL is typically expressed as a function of the parameter, within an appropriate range of applicability derived from the parameter bounds. This approach is conceptually illustrated in Figure 7.6-1. In this figure, the upper line [$k_c(x)$] represents a linear regression fit of a set of benchmark experiment calculation results plotted as a function of the trended parameter, x. The difference between the linear regression fit and k_{eff}=1.0 is the calculational bias. The middle line [$k_c(x)$-W] represents the lower-tolerance band (LTB) for a single additional calculation; e.g., the user can be 95% confident ($1-\gamma_1$=0.95) that the next calculated value of k_{eff} will be greater than [$k_c(x)$-W]. The width of the band between the linear regression fit $k_c(x)$ and the LTB lines is defined by the confidence band parameter, W. The confidence band is determined statistically based on the existing data and a specified level of confidence; the greater the standard deviation in the data or the larger the confidence desired, the larger the band width will be. The confidence band, accounts for uncertainties in the experiments, calculational approach, and calculational data (e.g., neutron cross sections), and is therefore a statistical basis for $\Delta\beta$, the uncertainty in the value of the bias, β. The bottom line in Figure 7.6-1, represents the upper safety limit for subcriticality, based on an additional margin of subcriticality. This safety margin provides further assurance of subcriticality and represents the quantity Δk_m defined earlier.
>
> Based on Equation 7.6-1, and the definitions provided above, the limiting USL condition is defined as:
>
> $$USL(x) = 1.0 - \beta(x) - W - \Delta k_m \qquad \text{Equation 7.6-2.}$$
>
> The bias, β, is treated as a function of the trended parameter x in Equation 7.6-2. As indicated in Figure 7.6-1, $\beta(x) = 1.0 - k_c(x)$, where $k_c(x)$ is determined from a linear regression fit to the data. The bias can now be written in terms of a simple linear expression of the form $\beta = a_0 + a_1 x$. Next, the confidence band for an additional calculation, W, may be determined. W is defined as a function of the trended parameter x, w(x), which is calculated based on a confidence level of ($1-\gamma_1$) using the relationship:

$$w(x) = t_{\gamma_1}\, s_p \left[1 + \frac{1}{n} + \frac{(x-\bar{x})^2}{\sum_{i=1,n}(x_i-\bar{x})^2}\right]^{1/2}$$

Equation 7.6-3.

where,

n = the number of critical experiments used in establishing $k_c(x)$

$t_{\gamma 1}$ = the Student-t value for γ_1 and n-2 degrees of freedom

$\bar{x}$ = the mean value of parameter x in the set of calculations

s_p = the pooled standard deviation for the set of criticality calculations.

The relationship expresses the parameter w(x) as a second-order polynomial. For simplicity, it is desirable to obtain a constant width margin. Hence, for conservatism, the constant lower confidence band width W is defined as the maximum of $(w(x_{min}), w(x_{max}))$, where x_{min} and x_{max} are the minimum and maximum values of the independent trending parameter x, respectively. Typically, W is determined at a 95% confidence level. The pooled standard deviation is obtained from the pooled variance, s_p^2. Pooled variance is given by:

$$s_p^2 = s_{k(x)}^2 + s_w^2$$

Equation 7.6-4.

where $s_{k(x)}^2$ is the variance (or mean square error) of the regression fit, and is given by:

$$s_{k(x)}^2 = \frac{1}{(n-2)}\left[\sum_{i=1,n}(k_i - \bar{k})^2 - \frac{\left[\sum_{i=1,n}(x_i - \bar{x})(k_i - \bar{k})\right]^2}{\sum_{i=1,n}(x_i - \bar{x})^2}\right]$$

Equation 7.6-5.

and s_w^2 is the within-variance of the data:

$$s_w^2 = \frac{1}{n}\sum_{i=1,n}\sigma_i^2$$

Equation 7.6-6.

The term σ_i in Equation 7.6-6, is the standard deviation associated with k_i for a Monte Carlo calculation. For deterministic codes, which do not have a standard deviation associated with a computed value of k, the standard deviation is zero.

Having determined the constant W and substituting for $\beta(x)$ in Equation 7.6-2, an expression for the upper safety limit may be written as:

$$USL(x) = 1.0 - a_0 - a_1x - W - \Delta k_m \qquad \text{Equation 7.6-7.}$$

The administrative safety margin, Δk_m, is typically assigned a value of 0.05 in safety analyses.

The function in Equation 7.6-7, is represented by the lowermost line of Figure 7.6-1. As previously discussed, this line represents an upper bound to ensure subcriticality for a given configuration when the calculated k_{eff} plus uncertainty for the configuration is less than the USL. USL's may be calculated for a number of independent parameters for a given system.

Besides providing a statistically valid methodology to establish criticality calculational method bias and bias uncertainty over a defined range of experimental conditions, the lower-tolerance band technique provides a mechanism to justify extending the range of applicability. ANSI/ANS-8.1 allows the range of applicability to be extended beyond this range by extrapolating the trends established for the bias. However, no precise guidelines are specified for the limits of extrapolation.

It is possible to determine a set of USL's based on various parameters. The subcritical limit is the minimum of all USL's computed for the specific parameters of the system that is representative of the experimental conditions."

As described in Section 7.5, the k_s term as related to ANSI/ANS-8.17(5.1) is the calculated value of k_{eff} for any configuration containing fissile materials, and the Δk_s term is the statistical uncertainty and modelling uncertainty present in the calculation of k_{eff} for the configuration. The final expression used to demonstrate a correlation-based acceptable level of subcriticality for the waste configuration is:

$$k_s + \Delta k_s \leq SL(x) \qquad \text{Equation 7.6-8.}$$

The trending analysis technique utilizes standard linear regression methods to fit the set of critical benchmark calculation k_{eff} values to the trended parameter. Using linear regression, the equation of a line is given by:

$$\hat{y} = b_0 + b_1x$$

Equation 7.6-9

where the slope of the least-squares line is:

$$b_1 = \frac{\sum_i (x_i - \bar{x})(y_i - \bar{y})}{\sum_i (x_i - \bar{x})^2}$$

Equation 7.6-10

and the intercept of the least-squares line is:

$$b_0 = \bar{y} - b_1 \bar{x}$$

Equation 7.6-11.

A detailed description of the linear regression method is provided in Ref. 9.42. The trending analysis described in this section is applied to the "Fissile Oxide Fuel / Lattice Geometries / Moderated" critical experiment library classification in Sections 7.7 and 7.8.

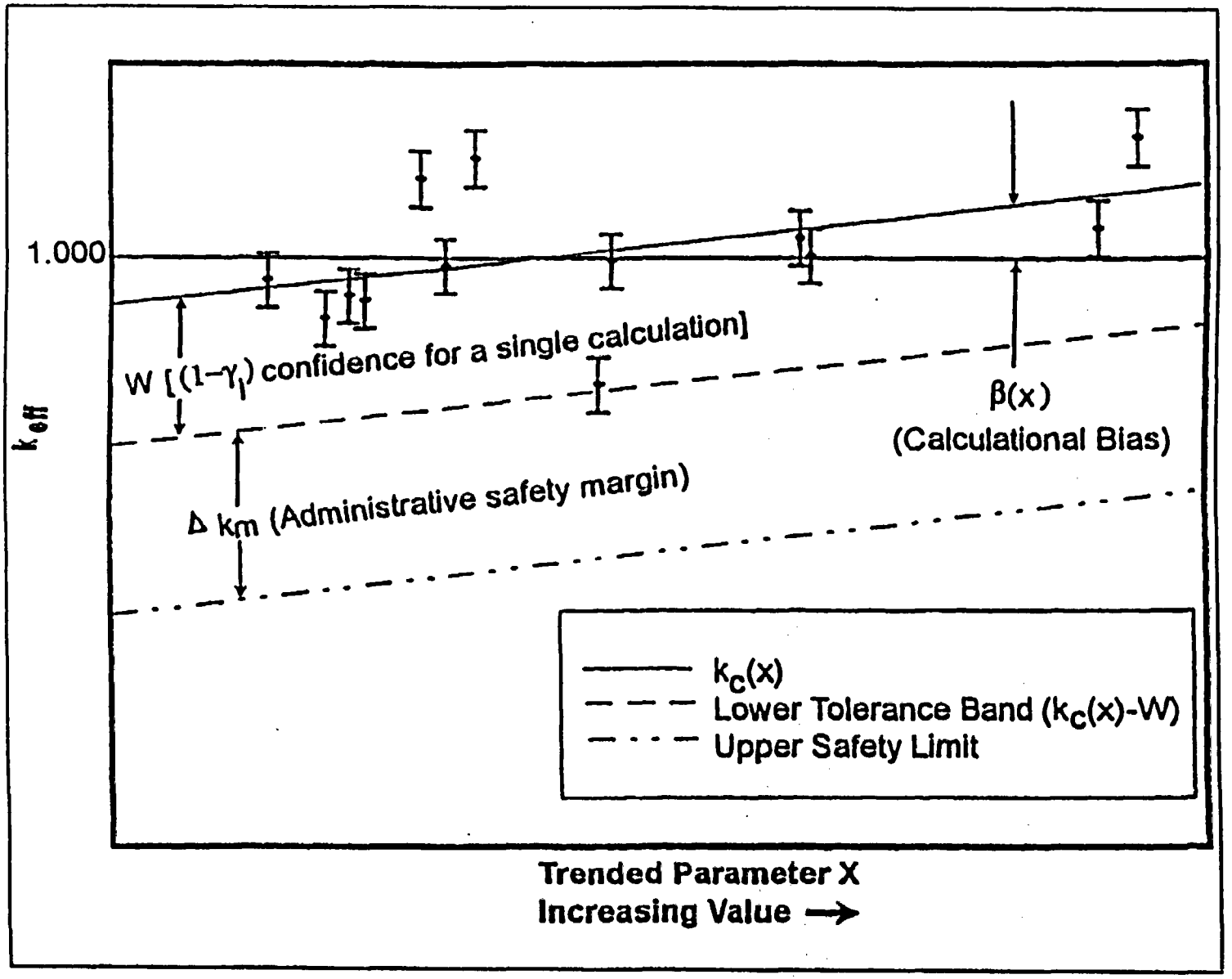

Figure 7.6-1 Illustration of the Lower-Tolerance-Bane Technique for the Determination of an Upper Safety Limit (USL) (Ref. 9.41)

7.7 Average Lethargy of the Neutron Causing Fission Trending Analysis

The average lethargy of the neutron causing fission (AVEL) is calculated using the energy loss to fission and weight loss to fission values provided in the MCNP 4A output. An example of the MCNP output table containing the average energy loss to fission and the average weight loss to fission is shown in Figure 7.7-1. The energy loss to fission is divided by the weight loss to fission to give the average energy of the neutron causing fission. The average lethargy of the neutron is then calculated by taking the natural logarithm of the ratio of the maximum neutron energy attainable to the actual neutron energy. The maximum neutron energy attainable in the MCNP calculation is 20 MeV.

The k_{eff} results for the critical experiment classification "Fissile Oxide Fuel / Lattice Geometries / Moderated" were analyzed to determine if a significant correlation exists between k_{eff} and AVEL. This classification containing 41 unique critical experiments was chosen for the initial trending analysis due to its significance in the waste package development design process. The critical experiments composing this classification share similar physical and neutronic characteristics in the sense that they are all fuel rod lattice geometries with a thermal neutron energy spectrum.

As previously mentioned in Section 7.6, a lower-tolerance band technique is employed in performing trending analysis to determine a bias value which is a function of a single characterization parameter such as AVEL. The statistical procedure for performing trending analysis as presented in this report was applied to the data of the "Fissile Oxide Fuel / Lattice Geometries / Moderated" classification to determine the Subcritical Limit (SL) and its feasibility for use in subsequent criticality calculations related to waste package development. Table 7.7-1, shows the results for the various parameters used in the SL calculation based upon k_{eff} versus AVEL. The AVEL data and other statistical data necessary to perform this trending analysis are presented in Tables 7.7-2 and 7.7-3. The following nomenclature is used in Table 7.7-3, to describe the values shown in each column--

xi:	the average lethargy of the neutron causing fission in system "i",
xave:	the average of the average lethargies of the neutron causing fission in each system,
yi:	the MCNP calculated k_{eff} for system "i",
yave:	the average of the MCNP calculated k_{eff}'s for each system,
yi(regr):	the linear regression k_{eff} for system "i",
sigma:	the standard deviation for the MCNP calculated k_{eff} of system "i".

Figure 7.7-2, shows the results of the k_{eff} versus AVEL trending analysis. A slight positive correlation exists between k_{eff} and AVEL. Since neutron energy and neutron lethargy are inversely related, a slight negative linear correlation exists between k_{eff} and average energy of the neutron causing fission. The significance of the correlation is quantified by the correlation coefficient (r). The correlation coefficient for a linear regression is calculated in the following manner--

$$r = \frac{1}{N-1} \Sigma \left(\frac{x-\bar{x}}{s_x}\right)\left(\frac{y-\bar{y}}{s_y}\right)$$

Equation 7.7-1.

The term s_x and s_y in Equation 7.7-1, are the sample standard deviations of the explanatory and response variables. In this case, "x" represents the AVEL value, and "y" represents the k_{eff} value. The r value for the k_{eff} versus AVEL trending analysis was found to be 0.0033. The positive sense of r confirms the positive correlation between k_{eff} and AVEL. The magnitude of r identifies the strength of the correlation. An r value of -1 or +1 indicates a perfect negative or positive linear correlation, respectively. An r value of 0 indicates a completely nonlinear relationship between two parameters. The r value of 0.0033 for this analysis indicates a weak linear correlation between k_{eff} and AVEL.

The square of the correlation coefficient (r^2) provides additional insight into the strength of the linear correlation between two parameters. The r^2 value represents the fraction of the variation in the response variable that is explained by the least squares regression of the response variable on the explanatory variable. The r^2 value for the k_{eff} versus AVEL analysis was found to be 1.1E-05. This value indicates that the linear regression of k_{eff} on AVEL explains 0.0011 percent of the variation in k_{eff}. This quantity also testifies to the weakness of the linear correlation between k_{eff} and AVEL for this classification.

The motivation for performing the statistical evaluation to determine the SL was to evaluate the potential for obtaining a statistically valid maximum allowable k_{eff} based upon a correlation between k_{eff} and a characteristic parameter of the system such as AVEL. The SL function for this classification indicates a maximum allowable k_{eff} that is greater than the 0.95 value established in 10 CFR 60.131(b)(7) for average neutron causing fission lethargies above 6.7. The SL function results for AVEL values above 6.7 demonstrate the adequacy of the subcritical margin of 0.05 established in 10 CFR 60.131(b)(7). The enhanced subcritical margin for this classification was calculated as 0.0639 in Section 7.5.2. This enhanced subcritical margin provides a maximum allowable k_{eff} of 0.9361. The 0.9361 k_{eff} value is conservative with respect to the SL as a function of AVEL over 90 percent of the evaluated AVEL range. The weakness in the linear correlation between k_{eff} and AVEL suggests that the existing correlation may be easily influenced by the introduction of additional data. The upper (>5.3) end of the AVEL range contains the fewest data points. Therefore, additional data should be evaluated for the upper AVEL range to determine the effect on the correlation. The subjective nature of the k_{eff} vs AVEL correlation suggests that the maximum allowable k_{eff} of 0.9361 based on the enhanced subcritical margin evaluation in Section 7.5.2, is the most appropriate for use in criticality analyses of configurations bounded by the characteristics of the "Fissile Oxide Fuel / Lattice Geometries / Moderated" classification.

Table 7.7-1
Parameters Used in the SL Calculation of k_{eff} vs AVEL

Classification: Fissile Oxide Fuel / Lattice Geometries / Moderated	
Parameter	**Value**
Number of Experiments in Classification (n)	41
Linear Regression Fit, k_{eff}(AVEL)	k_{eff} = 0.96908 + 6.7990E-3(AVEL) for (4.0 ≤ AVEL ≤ 5.3)
Correlation Coefficient, (r)	0.0033
Bias, β(AVEL)	β = 0.03092 - 6.7990E-3(AVEL) for (4.0 ≤ AVEL ≤ 5.3)
Minimum AVEL, (x_{min})	3.9575
Maximum AVEL, (x_{max})	7.1284
Bias at Minimum AVEL, β(x_{min})	0.0040
Bias at Maximum AVEL, β(x_{max})	-0.0175
Average AVEL, ($\bar{x}$)	4.8028
Average k_{eff}, ($\bar{k}$)	1.0018
Variance of Fit, $s_{k(x)}^2$	2.8595E-5
Within-data Variance, s_w^2	2.0029E-6
Pooled Variance, s_p^2	3.0598E-5
Pooled Standard Deviation, s_p	0.0055
One-Sided, Non-Central Student-t (95/95) Value @ (n-2) Degrees of Freedom	2.125
$W_{95\%}$, [Maximum of w(x_{min}) and w(x_{max})]	0.0147
Subcriticalty Limit (SL)	SL = 0.90438 + 6.7990E-3(AVEL) for (4.0 ≤ AVEL ≤ 5.3)

1problem summary

run terminated when 325 kcode cycles were done.

CRYSTAL RIVER, UNIT 3, CYCLE 7, 260.6 EFPD STATEPOINT

06/12/96 15:31:14
probid = 06/12/96 10:10:17

0

neutron creation	tracks	weight (per source)	energy particle)
source	811933	1.0007E+00	2.0573E+00
weight window	0	0.	0.
cell importance	0	0.	0.
weight cutoff	0	3.6091E-02	6.2973E-06
energy importance	0	0.	0.
dxtran	0	0.	0.
forced collisions	0	0.	0.
exp. transform	0	0.	0.
upscattering	0	0.	9.6259E-08
(n,xn)	3229	3.1231E-03	2.4982E-03
fission	0	0.	0.
total	815162	1.0399E+00	2.0598E+00

neutron loss	tracks	weight (per source)	energy particle)
escape	22	2.2208E-05	3.9702E-05
energy cutoff	0	0.	0.
time cutoff	0	0.	0.
weight window	0	0.	0.
cell importance	0	0.	0.
weight cutoff	813529	3.5594E-02	1.1371E-05
energy importance	0	0.	0.
dxtran	0	0.	0.
forced collisions	0	0.	0.
exp. transform	0	0.	0.
downscattering	0	0.	1.9164E+00
capture	0	6.2199E-01	3.1312E-02
loss to (n,xn)	1611	1.5582E-03	1.3256E-02
loss to fission	0	3.8075E-01	9.8796E-02
total	815162	1.0399E+00	2.0598E+00

number of neutrons banked	1618		
neutron tracks per source particle	1.0040E+00		
neutron collisions per source particle	3.5097E+01		
total neutron collisions	28496182		
net multiplication	1.0016E+00	.0000	

average lifetime, shakes		cutoffs	
escape	1.5687E+02	tco	1.0000E+34
capture	1.6498E+03	eco	.0000E+00
capture or escape	1.6497E+03	wc1	-5.0000E-01
any termination	1.6428E+03	wc2	-2.5000E-01

computer time so far in this run 319.91 minutes
computer time in mcrun 316.87 minutes
source particles per minute 2.5623E+03
random numbers generated 418446088

maximum number ever in bank 2
bank overflows to backup file 0
field length 0
most random numbers used was 15191 in history 45577

range of sampled source weights = 9.1274E-01 to 1.0767E+00

Figure 7.7-1 MCNP Table Containing the Average Neutron Energy Loss to Fission and the Average Neutron Weight Loss to Fission

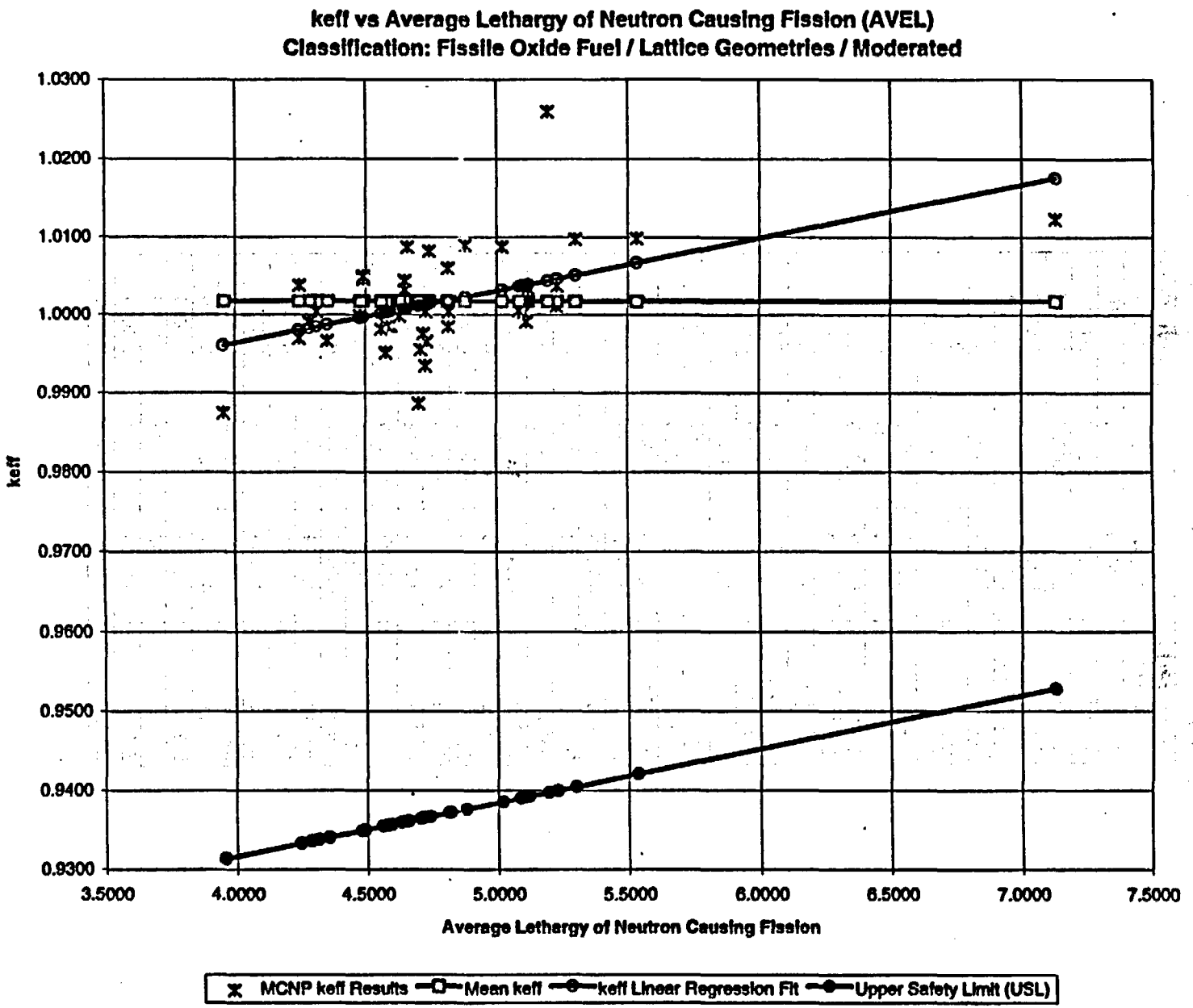

Figure 7.7-2 k_{eff} vs AVEL Trending Analysis Results

Table 7.7-2
Data for the k_{eff} vs AVEL Trending Analysis
Classification: Fissile Oxide Fuel / Lattice Geometries / Moderated

Experiment ID	AVEL	keff (MCNP)	sigma (MCNP)
BORAX-V.3	7.1284	1.0123	0.0023
EXP33	5.5340	1.0098	0.0016
EXP18	5.3003	1.0097	0.0014
EXP32	5.2297	1.0038	0.0017
EXP15	5.2288	1.0011	0.0012
BORAX-V.2	5.1949	1.0259	0.0023
EXP31	5.1210	1.0034	0.0016
EXP1	5.1143	0.9991	0.0013
EXP3	5.1060	1.0003	0.0013
EXP4	5.0986	1.0019	0.0014
EXP2	5.0864	1.0005	0.0013
EXP26	5.0199	1.0088	0.0014
EXP27	4.8799	1.0090	0.0015
BA3GD4	4.8202	1.0004	0.0017
BA3GD16	4.8177	0.9984	0.0014
EXP24a	4.8140	1.0060	0.0014
EXP8	4.7427	1.0082	0.0015
EXP7	4.7347	0.9965	0.0016
SCPC	4.7313	1.0004	0.0015
BA5GD4	4.7296	0.9934	0.0016
SCNOPC	4.7217	0.9975	0.0013
EXP19	4.7116	0.9955	0.0013
EXP17	4.7039	0.9886	0.0015
EXP25	4.6591	1.0087	0.0015
EXP29	4.6491	1.0032	0.0017
EXP12	4.6486	1.0044	0.0016
EXP13	4.6305	0.9998	0.0016
EXP30	4.5957	0.9985	0.0017
EXP14	4.5844	1.0012	0.0014
EXP21	4.5829	0.9985	0.0013
EXP20	4.5778	0.9951	0.0013
EXP16	4.5592	0.9981	0.0014
EXP10	4.4909	1.0046	0.0015
EXP9	4.4896	1.0050	0.0015
EXP28	4.4803	0.9998	0.0017
EXP22	4.3532	0.9968	0.0015
EXP11	4.3121	1.0004	0.0015
EXP23	4.2842	0.9990	0.0015
EXP5	4.2457	0.9969	0.0015
EXP6	4.2444	1.0038	0.0015
EXP34	3.9575	0.9874	0.0015

Table 7.7-3
Data for the k_{eff} vs AVEL Trending Analysis
Classification: Fissile Oxide Fuel / Lattice Geometries / Moderated

Experiment ID	xi-xave	yi-yave	(xi-xave)^2	(yi-yave)^2	(xi-xave)*(yi-yave)	(yi-yi(regr))^2	sigma^2
BORAX-V.3	2.33E+00	1.06E-02	5.41E+00	1.12E-04	2.46E-02	2.75E-05	5.38E-06
EXP33	7.31E-01	8.07E-03	5.35E-01	6.52E-05	5.90E-03	9.63E-06	2.50E-06
EXP18	4.98E-01	7.97E-03	2.48E-01	6.36E-05	3.97E-03	2.11E-05	2.02E-06
EXP32	4.27E-01	2.01E-03	1.82E-01	4.06E-06	8.60E-04	7.89E-07	2.76E-06
EXP15	4.26E-01	-6.66E-04	1.81E-01	4.43E-07	-2.84E-04	1.27E-05	1.49E-06
BORAX-V.2	3.92E-01	2.41E-02	1.54E-01	5.83E-04	9.47E-03	4.61E-04	5.29E-06
EXP31	3.18E-01	1.64E-03	1.01E-01	2.70E-06	5.23E-04	2.70E-07	2.56E-06
EXP1	3.12E-01	-2.67E-03	9.70E-02	7.11E-06	-8.30E-04	2.29E-05	1.61E-06
EXP3	3.03E-01	-1.48E-03	9.20E-02	2.18E-06	-4.48E-04	1.25E-05	1.61E-06
EXP4	2.96E-01	1.54E-04	8.75E-02	2.38E-08	4.56E-05	3.45E-06	1.82E-06
EXP2	2.84E-01	-1.22E-03	8.04E-02	1.48E-06	-3.45E-04	9.89E-06	1.69E-06
EXP26	2.17E-01	7.01E-03	4.71E-02	4.92E-05	1.52E-03	3.07E-05	2.04E-06
EXP27	7.71E-02	7.21E-03	5.95E-03	5.20E-05	5.56E-04	4.48E-05	2.31E-06
BA3GD4	1.74E-02	-1.34E-03	3.03E-04	1.78E-06	-2.33E-05	2.11E-06	2.04E-06
BA3GD16	1.49E-02	-3.34E-03	2.23E-04	1.11E-05	-4.98E-05	1.18E-05	2.50E-06
EXP24a	1.12E-02	4.26E-03	1.26E-04	1.82E-05	4.79E-05	1.75E-05	1.96E-06
EXP8	-6.01E-02	6.46E-03	3.61E-03	4.18E-05	-3.88E-04	4.72E-05	2.43E-06
EXP7	-6.81E-02	-5.24E-03	4.64E-03	2.74E-05	3.57E-04	2.28E-05	2.16E-06
SCPC	-7.15E-02	-1.34E-03	5.11E-03	1.78E-06	9.55E-05	7.22E-07	1.56E-06
BA5GD4	-7.32E-02	-8.34E-03	5.36E-03	6.95E-05	6.10E-04	6.14E-05	2.89E-06
SCNOPC	-8.11E-02	-4.24E-03	6.58E-03	1.79E-05	3.44E-04	1.36E-05	1.69E-06
EXP19	-9.12E-02	-6.24E-03	8.31E-03	3.89E-05	5.69E-04	3.15E-05	2.25E-06
EXP17	-9.89E-02	-1.31E-02	9.79E-03	1.73E-04	1.30E-03	1.55E-04	2.31E-06
EXP25	-1.44E-01	6.96E-03	2.07E-02	4.85E-05	-1.00E-03	6.31E-05	2.31E-06
EXP29	-1.54E-01	1.49E-03	2.36E-02	2.23E-06	-2.30E-04	6.45E-06	2.82E-06
EXP12	-1.54E-01	2.66E-03	2.38E-02	7.10E-06	-4.11E-04	1.38E-05	2.59E-06
EXP13	-1.72E-01	-1.94E-03	2.97E-02	3.75E-06	3.34E-04	5.84E-07	2.66E-06
EXP30	-2.07E-01	-3.25E-03	4.29E-02	1.05E-05	6.72E-04	3.38E-06	2.72E-06
EXP14	-2.18E-01	-5.76E-04	4.77E-02	3.32E-07	1.26E-04	8.27E-07	1.93E-06
EXP21	-2.20E-01	-3.27E-03	4.84E-02	1.07E-05	7.18E-04	3.14E-06	1.80E-06
EXP20	-2.25E-01	-6.69E-03	5.07E-02	4.47E-05	1.51E-03	2.66E-05	1.66E-06
EXP16	-2.44E-01	-3.64E-03	5.93E-02	1.32E-05	8.86E-04	3.92E-06	1.82E-06
EXP10	-3.12E-01	2.86E-03	9.73E-02	8.20E-06	-8.93E-04	2.48E-05	2.22E-06
EXP9	-3.13E-01	3.26E-03	9.81E-02	1.07E-05	-1.02E-03	2.91E-05	2.25E-06
EXP28	-3.23E-01	-1.90E-03	1.04E-01	3.59E-06	6.11E-04	8.81E-08	2.79E-06
EXP22	-4.50E-01	-5.16E-03	2.02E-01	2.66E-05	2.32E-03	4.41E-06	2.25E-06
EXP11	-4.91E-01	-1.34E-03	2.41E-01	1.78E-06	6.55E-04	4.00E-06	2.25E-06
EXP23	-5.19E-01	-2.74E-03	2.69E-01	7.48E-06	1.42E-03	6.25E-07	2.37E-06
EXP5	-5.57E-01	-4.84E-03	3.10E-01	2.34E-05	2.69E-03	1.10E-06	2.25E-06
EXP6	-5.58E-01	2.06E-03	3.12E-01	4.26E-06	-1.15E-03	3.44E-05	2.31E-06
EXP34	-8.45E-01	-1.43E-02	7.14E-01	2.05E-04	1.21E-02	7.36E-05	2.25E-06
SUMS:	3.82E-14	3.33E-16	9.96E+00	1.78E-03	6.77E-02	1.32E-03	9.61E-05

7.8 H/X Ratio Trending Analysis

The moderator to fuel atom ratio (H/X ratio) is a system parameter containing both physical and neutronic information. A higher H/X ratio is usually indicative of a more thermal neutron energy spectrum. A higher H/X ratio is also more indicative of either a smaller fuel rod diameter or a larger rod-to-rod pitch in a lattice geometry. In more complex systems the H/X ratio may be calculated in a number of different ways. The guidelines used to calculate the H/X ratio are as follow--

1) use a cross-sectional cut of the fuel/moderator area when appropriate;
2) avoid including reflector material in the calculation;
3) analyze an individual unit in systems composed of repeated structures.

The k_{eff} results for the critical experiment classification "Fissile Oxide Fuel / Lattice Geometries / Moderated" were analyzed to determine if a correlation exists between k_{eff} and the H/X ratios of the experiments.

The lower-tolerance band technique is applied in the k_{eff} versus H/X ratio trending analysis to determine a bias value that is a function of the H/X ratio characterization parameter. The k_{eff} versus H/X ratio SL for the classification was determined in accordance with the statistical procedure described in Section 7.6. Table 7.8-1, shows the results for the various parameters used in the SL calculation for k_{eff} versus H/X ratio. The H/X ratio data and other statistical data necessary to perform this trending analysis are presented in Tables 7.8-2 and 7.8-3. The following nomenclature is used in Table 7.8-3, to describe the values shown in each column--

xi:	the H/X ratio of the system "i",
xave:	the average of the H/X ratios in the systems under evaluation,
yi:	the MCNP calculated k_{eff} for system "i",
yave:	the average of the MCNP calculated k_{eff}'s for each system,
yi(regr):	the linear regression k_{eff} for system "i",
sigma:	the standard deviation for the MCNP calculated k_{eff} of system "i".

Figure 7.8-1, shows the results of the k_{eff} versus H/X ratio trending analysis. A slight positive linear correlation exists between k_{eff} and H/X ratio for the classification of critical experiments analyzed. The significance of the correlation is quantified by the correlation coefficient (r) as previously described in the AVEL trending analysis discussion in Section 7.7. The r value for the k_{eff} versus H/X ratio trending analysis was found to be 0.1676. The positive sense of r confirms the positive correlation between k_{eff} and H/X ratio. The r magnitude indicates a weak linear correlation between k_{eff} and H/X ratio. The r^2 value was found to be 0.0281. This value indicates that the linear regression of k_{eff} on H/X ratio explains 2.81 percent of the variation in k_{eff}. This quantity testifies to the weakness of the linear correlation between k_{eff} and H/X ratio for this classification.

The maximum allowable k_{eff} determined by the enhanced subcritical margin for this classification (0.9361) is more conservative than the SL as a function of H/X ratio over more than 90 percent of the evaluated H/X ratio range. The weakness in the linear correlation between k_{eff} and H/X ratio suggests that the existing correlation may be easily influenced by the introduction of

additional data. The upper H/X ratio range (>300) contains the fewest data points. Therefore, additional data should be evaluated for the upper H/X ratio range to determine the effect on the correlation. The subjective nature of the k_{eff} vs H/X ratio correlation suggests that the maximum allowable k_{eff} of 0.9361 based on the enhanced subcritical margin evaluation in Section 7.5.2, is the most appropriate for use in criticality analyses of configurations bounded by the characteristics of the "Fissile Oxide Fuel / Lattice Geometries / Moderated" classification.

Table 7.8-1
Parameters Used in the SL Calculation of k_{eff} vs H/X Ratio

Classification: Fissile Oxide Fuel / Lattice Geometries / Moderated	
Parameter	**Value**
Number of Experiments in Classification (n)	41
Linear Regression Fit, k_{eff}(H/X ratio)	$k_{eff} = 0.99995 + 7.5292E\text{-}6(H/X\ ratio)$ for $(72 \le H/X\ ratio \le 540)$
Correlation Coefficient, (r)	0.1676
Bias, β(H/X ratio)	$\beta = 0.00005 - 7.5292E\text{-}6(H/X\ ratio)$ for $(72 \le H/X\ ratio \le 540)$
Minimum H/X ratio, (x_{min})	38.330
Maximum H/X ratio, (x_{max})	668.130
Bias at Minimum H/X ratio, $\beta(x_{min})$	0.0007
Bias at Maximum H/X ratio, $\beta(x_{max})$	-0.0060
Average H/X ratio, ($\bar{x}$)	237.685
Average k_{eff}, ($\bar{k}$)	1.0018
Variance of Fit, $s_{k(x)}^2$	3.7488E-5
Within-data Variance, s_w^2	2.0015E-6
Pooled Variance, s_p^2	3.9489E-5
Pooled Standard Deviation, s_p	0.0063
One-Sided, Non-Central Student-t (95/95) Value @ (n-2) Degrees of Freedom	2.125
$W_{95\%}$, [Maximum of $w(x_{min})$ and $w(x_{max})$]	0.014819
Subcritical Limit (SL)	$SL = 0.93513 + 7.5292E\text{-}6(H/X\ ratio)$ for $(72 \le H/X\ ratio \le 540)$

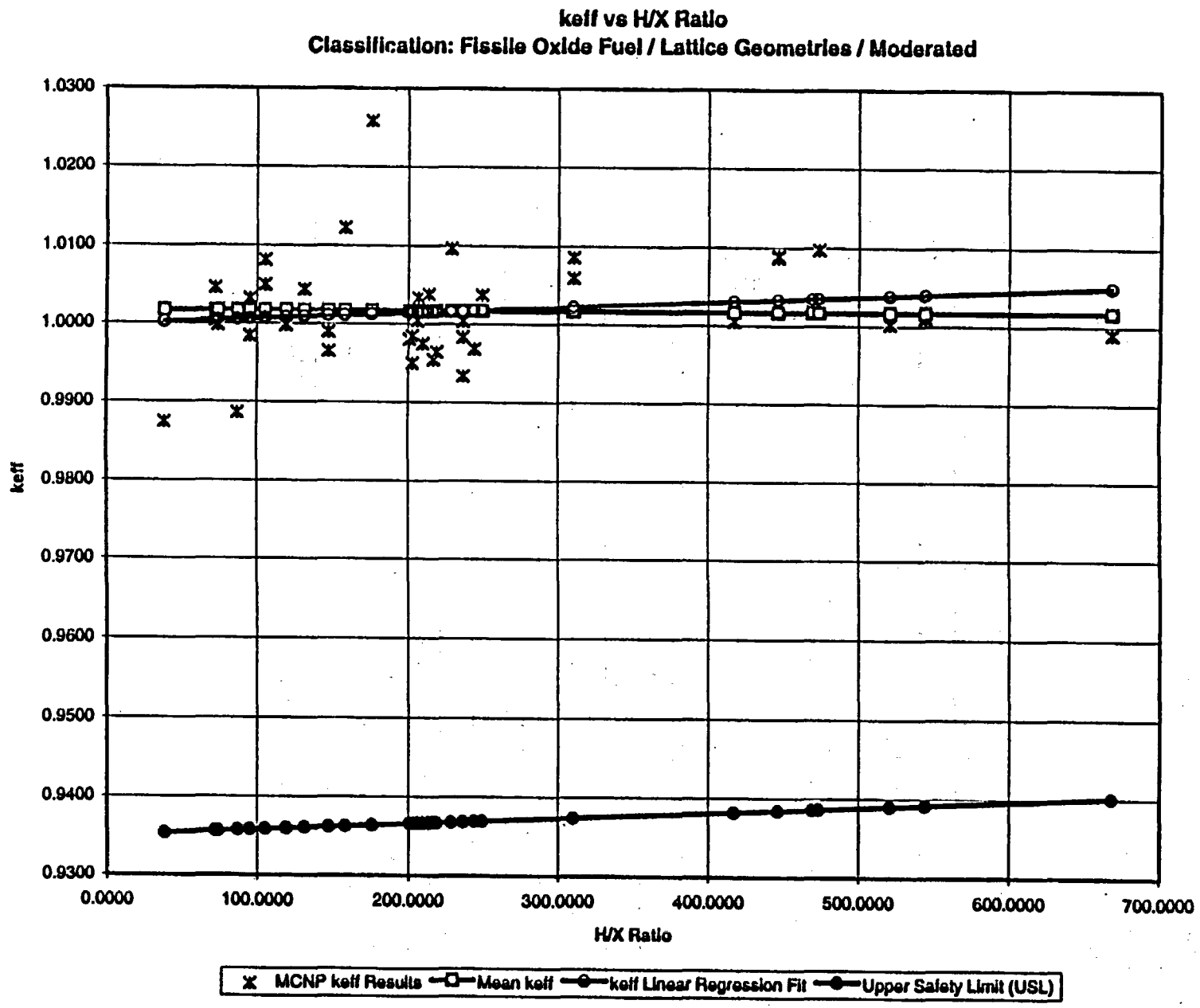

Figure 7.8-1 k_{eff} vs H/X Ratio Trending Analysis Results

Table 7.8-2
Data for the k_{eff} vs H/X Ratio Trending Analysis
Classification: Fissile Oxide Fuel / Lattice Geometries / Moderated

Experiment ID	H/X RATIO	keff (MCNP)	sigma (MCNP)
EXP34	38.3300	0.9874	0.0015
EXP10	72.1140	1.0046	0.0015
EXP11	72.1140	1.0004	0.0015
EXP28	73.9700	0.9998	0.0017
EXP17	87.1200	0.9886	0.0015
EXP29	95.1000	1.0032	0.0017
EXP30	95.1000	0.9985	0.0017
EXP8	105.2800	1.0082	0.0015
EXP9	105.3000	1.0050	0.0015
EXP13	119.2700	0.9998	0.0016
EXP12	131.2100	1.0044	0.0016
EXP22	147.1300	0.9966	0.0015
EXP23	147.1300	0.9990	0.0015
BORAX-V.3	157.9100	1.0123	0.0023
BORAX-V.2	175.7900	1.0259	0.0023
EXP16	200.8100	0.9981	0.0014
EXP20	202.5900	0.9951	0.0013
EXP21	202.7900	0.9985	0.0013
EXP14	203.7200	1.0012	0.0014
SCPC	206.2900	1.0004	0.0015
EXP31	206.9400	1.0034	0.0016
SCNOPC	209.6900	0.9975	0.0013
EXP6	213.6800	1.0038	0.0015
EXP19	216.7500	0.9955	0.0013
EXP7	219.1000	0.9965	0.0016
EXP18	228.8700	1.0097	0.0014
BA3GD16	236.8400	0.9984	0.0014
BA5GD4	236.9500	0.9934	0.0016
BA3GD4	236.9600	1.0004	0.0017
EXP5	244.5800	0.9969	0.0015
EXP32	249.6500	1.0038	0.0017
EXP24a	310.1900	1.0060	0.0014
EXP25	310.1900	1.0087	0.0015
EXP2	417.3000	1.0005	0.0013
EXP26	446.2800	1.0088	0.0014
EXP27	446.2800	1.0090	0.0015
EXP4	469.1700	1.0019	0.0014
EXP33	473.3200	1.0098	0.0016
EXP3	520.7400	1.0003	0.0013
EXP15	544.4200	1.0011	0.0012
EXP1	668.1300	0.9991	0.0013

Table 7.8-3
Data for the k_{eff} vs H/X Ratio Trending Analysis
Classification: Fissile Oxide Fuel / Lattice Geometries / Moderated

Experiment ID	xi-xave	yi-yave	(xi-xave)^2	(yi-yave)^2	(xi-xave)* (yi-yave)	(yi-yi(regr))^2	sigma^2
EXP34	-1.99E+02	-1.43E-02	3.97E+04	2.05E-04	2.86E+00	1.65E-04	2.25E-06
EXP10	-1.66E+02	2.86E-03	2.74E+04	8.20E-06	-4.74E-01	1.69E-05	2.25E-06
EXP11	-1.66E+02	-1.34E-03	2.74E+04	1.79E-06	2.21E-01	8.18E-09	2.25E-06
EXP28	-1.64E+02	-1.90E-03	2.68E+04	3.60E-06	3.11E-01	4.41E-07	2.79E-06
EXP17	-1.51E+02	-1.31E-02	2.27E+04	1.72E-04	1.97E+00	1.44E-04	2.31E-06
EXP29	-1.43E+02	1.49E-03	2.03E+04	2.23E-06	-2.13E-01	6.59E-06	2.82E-06
EXP30	-1.43E+02	-3.25E-03	2.03E+04	1.05E-05	4.63E-01	4.72E-06	2.72E-06
EXP8	-1.32E+02	6.46E-03	1.75E+04	4.18E-05	-8.56E-01	5.56E-05	2.25E-06
EXP9	-1.32E+02	3.26E-03	1.75E+04	1.06E-05	-4.32E-01	1.81E-05	2.25E-06
EXP13	-1.18E+02	-1.94E-03	1.40E+04	3.75E-06	2.29E-01	1.09E-06	2.56E-06
EXP12	-1.06E+02	2.66E-03	1.13E+04	7.09E-06	-2.84E-01	1.20E-05	2.59E-06
EXP22	-9.06E+01	-5.16E-03	8.20E+03	2.66E-05	4.67E-01	2.00E-05	2.25E-06
EXP23	-9.06E+01	-2.72E-03	8.20E+03	7.38E-06	2.46E-01	4.14E-06	2.25E-06
BORAX-V.3	-7.98E+01	1.06E-02	6.36E+03	1.12E-04	-8.43E-01	1.25E-04	5.38E-06
BORAX-V.2	-6.19E+01	2.41E-02	3.83E+03	5.83E-04	-1.49E+00	6.06E-04	5.29E-06
EXP16	-3.69E+01	-3.64E-03	1.36E+03	1.32E-05	1.34E-01	1.13E-05	1.82E-06
EXP20	-3.51E+01	-6.69E-03	1.23E+03	4.47E-05	2.35E-01	4.13E-05	1.66E-06
EXP21	-3.49E+01	-3.27E-03	1.22E+03	1.07E-05	1.14E-01	9.03E-06	1.80E-06
EXP14	-3.40E+01	-5.77E-04	1.15E+03	3.33E-07	1.96E-02	1.03E-07	1.93E-06
SCPC	-3.14E+01	-1.30E-03	9.86E+02	1.68E-06	4.07E-02	1.13E-06	2.16E-06
EXP31	-3.07E+01	1.64E-03	9.45E+02	2.70E-06	-5.05E-02	3.51E-06	2.56E-06
SCNOPC	-2.80E+01	-4.23E-03	7.84E+02	1.79E-05	1.18E-01	1.61E-05	1.56E-06
EXP6	-2.40E+01	2.06E-03	5.76E+02	4.26E-06	-4.95E-02	5.03E-06	2.31E-06
EXP19	-2.09E+01	-6.24E-03	4.38E+02	3.89E-05	1.31E-01	3.70E-05	1.69E-06
EXP7	-1.86E+01	-5.28E-03	3.45E+02	2.78E-05	9.81E-02	2.64E-05	2.43E-06
EXP18	-8.82E+00	7.97E-03	7.77E+01	6.36E-05	-7.03E-02	6.46E-05	2.02E-06
BA3GD16	-8.45E-01	-3.34E-03	7.15E-01	1.11E-05	2.82E-03	1.11E-05	1.96E-06
BA5GD4	-7.35E-01	-8.31E-03	5.41E-01	6.90E-05	6.11E-03	6.89E-05	2.50E-06
BA3GD4	-7.25E-01	-1.34E-03	5.26E-01	1.79E-06	9.70E-04	1.77E-06	2.89E-06
EXP5	6.89E+00	-4.84E-03	4.75E+01	2.34E-05	-3.34E-02	2.39E-05	2.37E-06
EXP32	1.20E+01	2.01E-03	1.43E+02	4.05E-06	2.41E-02	3.70E-06	2.76E-06
EXP24a	7.25E+01	4.28E-03	5.26E+03	1.83E-05	3.11E-01	1.40E-05	2.04E-06
EXP25	7.25E+01	6.91E-03	5.26E+03	4.78E-05	5.01E-01	4.05E-05	2.31E-06
EXP2	1.80E+02	-1.22E-03	3.23E+04	1.48E-06	-2.19E-01	6.60E-06	1.69E-06
EXP26	2.09E+02	7.01E-03	4.35E+04	4.92E-05	1.46E+00	2.96E-05	2.04E-06
EXP27	2.09E+02	7.21E-03	4.35E+04	5.20E-05	1.50E+00	3.18E-05	2.31E-06
EXP4	2.31E+02	1.53E-04	5.36E+04	2.34E-08	3.54E-02	2.53E-06	1.82E-06
EXP33	2.36E+02	8.07E-03	5.55E+04	6.52E-05	1.90E+00	3.97E-05	2.50E-06
EXP3	2.83E+02	-1.48E-03	8.01E+04	2.18E-06	-4.18E-01	1.30E-05	1.61E-06
EXP15	3.07E+02	-6.67E-04	9.41E+04	4.45E-07	-2.05E-01	8.86E-06	1.49E-06
EXP1	4.30E+02	-2.67E-03	1.85E+05	7.11E-06	-1.15E+00	3.49E-05	1.61E-06
SUMS:	3.64E-12	-3.89E-15	8.79E+05	1.77E-03	6.62E+00	1.72E-03	9.61E-05

8. Summary

The critical experiment library presented in this study provides the foundation upon which the preliminary bias values, the enhanced subcritical margin values, and the maximum allowable k_{eff} values are determined. The library encompasses a broad range of critical system physical and neutronic characteristics which may be representative of the range of potential criticality scenarios. The library's twenty critical experiment classifications serve to assist in selecting the appropriate maximum allowable k_{eff} to be used in criticality analyses related to waste package development. The classifications of the library encompass the physical and neutronic characteristics of both the near-field and far-field repository systems. An applicable maximum allowable k_{eff} from Table 7.5.3-1 may be selected for criticality analyses based on the similarities between the physical and neutronic characteristics of the system being analyzed and the library classifications.

The methodology presented in this study for determining an enhanced subcritical margin based on a classification of critical benchmark experiments was developed in accordance with the requirements set forth in 10 CFR 60.131(b)(7) (Ref. 9.3) and the standards set forth in ANSI/ANS-8.17 (Ref. 9.2). The maximum allowable k_{eff}'s developed in this study are treated as preliminary values acceptable for use in calculations relevant to waste package development. The exclusion of the experimental bias and uncertainty associated with the actual critical experiments in the calculations for the preliminary maximum allowable k_{eff} values in this study should not have a significant impact on the final magnitude of the results. This conclusion is based on the use of conservative methods in the development of the maximum allowable k_{eff} values, as described in Section 7.5.1, as well as the expected small magnitude of the experimental bias and uncertainty.

This study examined the use of an subcritical limit (SL) approach for determining maximum allowable k_{eff} values based upon trends between k_{eff} and physical or neutronic characteristics of the critical benchmark system's. The correlation between k_{eff} and the average lethargy of the neutron causing fission (AVEL) was examined for the critical experiment library classification representative of moderated rodded lattices of fissile oxide fuel. There were no significant correlations between k_{eff} and AVEL for this classification. The enhanced subcritical margin and associated maximum allowable k_{eff} for this classification was shown to be more conservative than the SL over 90 percent of the examined AVEL range. A similar examination was performed on the same classification of critical experiments for k_{eff} versus the moderator to fuel atom ratio (H/X ratio). Again, there were no significant trends present between k_{eff} and H/X ratio. The enhanced subcritical margin and associated maximum allowable k_{eff} was also shown to be more conservative than the SL over 90 percent of the examined H/X ratio range.

The results of this study provide quantification of the confidence associated with the MCNP code system for performing criticality evaluations. The flexibility of the geometric modelling and the detail of the continuous energy cross-section sets available with the MCNP code system combine to make it one of the most useful tools available for predicting the k_{eff} value of a system.

9. References

9.1 J. F. Briesmeister, Ed. *MCNP--A General Monte Carlo N-Particle Transport Code, Version 4A*, LA-12625-M, Los Alamos National Laboratory (LANL), November 1993.

9.2 *American National Standard--Criticality Safety Criteria for the Handling, Storage, and Transportation of LWR Fuel Outside Reactors*, ANSI/ANS-8.17-1984, American Nuclear Society Standards Committee Work Group ANS-8.17, January 13, 1984.

9.3 Title 10 Code of Federal Regulations, Part 60, 1995. *Disposal of High-Level Radioactive Wastes in Geologic Repositories*, Washington, D.C.: U.S. Nuclear Regulatory Commission.

9.4 This Reference Left Intentionally Blank

9.5 This Reference Left Intentionally Blank

9.6 *Quality Assurance Requirements and Description*, DOE/RW-0333P REV 05, DOE (U.S. Department of Energy).

9.7 This Reference Left Intentionally Blank

9.8 This Reference Left Intentionally Blank

9.9 This Reference Left Intentionally Blank

9.10 This Reference Left Intentionally Blank

9.11 J. C. Wagner, J. E. Sisolak, and G. W. McKinney. *MCNP: Criticality Safety Benchmark Problems*, LA-12415, LANL, October 1992.

9.12 J. T. Thomas. *Critical Three-Dimensional Arrays of Neutron-Interacting Units, Part II-U(93.2) Metal*, ORNL-TM-868, Oak Ridge National Laboratory (ORNL), July 1964.

9.13 D. J. Whalen, D. A. Cardon, J. L. Uhle, and J. S. Hendricks. *MCNP: Neutron Benchmark Problems*, LA-12212, LANL, November 1991.

9.14 H. F. Finn, N. L. Pruvost, O. C. Kolar, and G. A. Pierce. *Summary of Experimentally Determined Plutonium Array Critical Configurations*, UCRL-51041, Lawrence Livermore National Laboratory (LLNL), May 1971.

9.15 C. Crawford and B. M. Palmer. *Validation of MCNP, A Comparison with SCALE Part 2: Highly Enriched Uranium Metal Systems*, WINCO-1110, Westinghouse Idaho Nuclear Company, Inc. (WINCO), October 1992.

9.16 C. Crawford and B. M. Palmer. *Validation of MCNP: SPERT-D and BORAX-V Fuel*, WINCO-1112, WINCO, November 1992.

9.17 E. B. Johnson and R. K. Reedy, Jr. *Critical Experiments with SPERT-D Fuel Elements*, ORNL-TM-1207, ORNL, July, 1965.

9.18 J. T. Mihalczo. *Graphite and Polyethylene Reflected Uranium-Metal Cylinders and Annuli*, Y-DR-81, Union Carbide Nuclear Division Oak Ridge Y-12 Plant, April 1972.

9.19 S. Sitaraman. *MCNP: Light Water Reactor Critical Benchmarks*, NEDO-32028, General Electric (GE) Nuclear Energy, March 1992.

9.20 G. E. Hansen and H. C. Paxton. *Reevaluated Critical Specifications of Some Los Alamos Fast-Neutron Systems*, LA-4208, LANL, September 1969.

9.21 J. T. Milhalczo. *Criticality Experiments and Calculations with Annular Cylinders of U(93.2) Metal*, Neutron Physics Division Annual Progress Report, ORNL-3499, Vol. 1, ORNL, December 1963.

9.22 C. Crawford and B. M. Palmer. *Validation of MCNP, A Comparison with SCALE Part 3: Highly Enriched Uranium Oxide Systems*, WINCO-1111, WINCO, October 1992.

9.23 D. W. Magnuson. *Critical Experiments with Enriched Uranium Dioxide*, Y-DR-120, Union Carbide Corporation, Nuclear Division, Oak Ridge Y-12 Plant, November 1973.

9.24 BORAX-V Project Staff, Idaho Division. *Experiments with Central Superheater Core CSH-1*, ANL-6961, Argonne National Laboratory (ANL), January 1965.

9.25 J. T. Hagen and R. W. Goin. *BORAX-V Neutronics*, ANL-6964, ANL, December 1965.

9.26 BORAX-V Project Staff. *Design and Hazards Summary Report Boiling Reactor Experiment V (BORAX V)*, ANL-6302, ANL, May 1961.

9.27 BORAX-V Project Staff. *Zero-Power Experiments with Boiling Core B-1, BORAX-V Superheat*, ANL-6689, ANL, June 1963.

9.28 W. C. Kramer and C. H. Bean. *Fabrication of UO_2 -Stainless Steel Dispersion Fuel for BORAX-V Nuclear Superheat*, ANL-6649, ANL, December 1963.

9.29 K. E. Plumlee, Q. L. Baird, G. S. Stanford, and P. I. Amundson. *Critical Experiment with BORAX-V Internal Superheater*, ANL-6691, ANL, November 1963.

9.30 S. M. Bowman and O. W. Hermann. *Reference Problem Set to Benchmark Analysis Methods for Burnup Credit Applications (DRAFT)*, ORNL/TM-12295, Computing Applications Division ORNL, Manuscript Date: November 19, 1993.

9.31 S. R. Bierman, E. D. Clayton, and B. M. Durst. *Critical Separation Between Subcritical Clusters of 2.35 Wt% ^{235}U Enriched UO_2 Rods in Water with Fixed Neutron Poisons*, PNL-2438, Battelle Pacific Northwest Laboratories (PNL), October 1977.

9.32 S. R. Bierman, B. M. Durst, and E. D. Clayton. *Criticality Experiments with Subcritical Clusters of 2.35 Wt% and 4.31 Wt% ^{235}U Enriched UO_2 Rods in Water with Uranium or Lead Reflecting Walls*, PNL-3926, PNL, December 1981.

9.33 S. R. Bierman and E. D. Clayton. *Criticality Experiments with Subcritical Clusters of 2.35 Wt% and 4.31 Wt% ^{235}U Enriched UO_2 Rods in Water with Steel Reflecting Walls*, PNL-3602, PNL, April 1981.

9.34 S. R. Bierman, E. S. Murphy, E. D. Clayton, and R. T. Keay. *Criticality Experiments with Low Enriched UO_2 Fuel Rods in Water Containing Dissolved Gadolinium*, PNL-4976, PNL, February 1984.

9.35 C. Crawford and B. M. Palmer. *Validation of MCNP, A Comparison with SCALE Part 1: Highly Enriched Uranium Solutions*, WINCO-1109, WINCO, October 1992.

9.36 J. T. Thomas. *Critical Three-Dimensional Arrays of Neutron-Interacting Units*, ORNL-TM-719, ORNL, October 1963.

9.37 J. K. Fox, L. W. Gilley, and E. R. Rohrer. *Critical Mass Studies, Part VIII, Aqueous Solutions of U^{233}*, ORNL-2143, ORNL, 1958.

9.38 R. E. Rothe and I. Oh. *Benchmark Critical Experiments on High-Enriched Uranyl Nitrate Solution Systems*, NUREG/CR-0041, Rockwell International Atomics International Division, Rocky Flats Plant, April 1978.

9.39 S. M. Bowman and O. W. Hermann. *SCALE-4 Analysis of Pressurized Water Reactor Critical Configurations: Volume 2-Sequoyah Unit 2, Cycle 3*, ORNL/TM-12294/V2, ORNL, March 1995.

9.40 S. M. Bowman and O. W. Hermann. *SCALE-4 Analysis of Pressurized Water Reactor Critical Configurations: Volume 3-Surry Unit 1, Cycle 2*, ORNL/TM-12294/V3, ORNL, March 1995.

9.41 *Topical Report on Actinide-Only Burnup Credit for PWR Spent Nuclear Fuel Packages*, DOE/RW-0472 REV 0, DOE.

9.42 D. S. Moore and G. P. McCabe. *Introduction to the Practice of Statistics*, W. H. Freeman and Company, New York, 1989.

APPENDIX C

Criticality Scenario Generation

INTENTIONALLY LEFT BLANK

Table of Contents

Introduction

This appendix summarizes the work which has been done to date in support of the probabilistic methodology discussed in the body of the report. Further detail on the subjects discussed in this section can be found in the following documents: *Emplaced Waste Package Structural Capability Through Time Report* (Ref. C.9-1), *Second Waste Package Probabilistic Criticality Analysis: Generation and Evaluation of Internal Criticality Configurations,* and the *Probabilistic External Criticality Evaluation* (Ref. C.9-6).

INTENTIONALLY LEFT BLANK

1. Repository Environment

Knowledge of the expected range of WP environments is essential for any analysis of post-closure criticality performance. This section details those aspects of the enviroment which were considered in the analyses to date.

1.1. WP Surface Temperature and Humidity

Estimates of the waste package surface temperature and relative humidity as a function of time are necessary for implementation of WP barrier and basket corrosion models, and estimates of water evaporation rates. For the current analyses, the temperature and relative humidity curves for the 83 MTU/acre low infiltration cases from TSPA-95 (Ref. C.9-2) have been utilized. Figure C.1 below shows relative as a function of time for the backfill and no-backfill cases. Similarly, Figure C.2 shows waste package surface temperature as a function of time for the backfill and no-backfill cases.

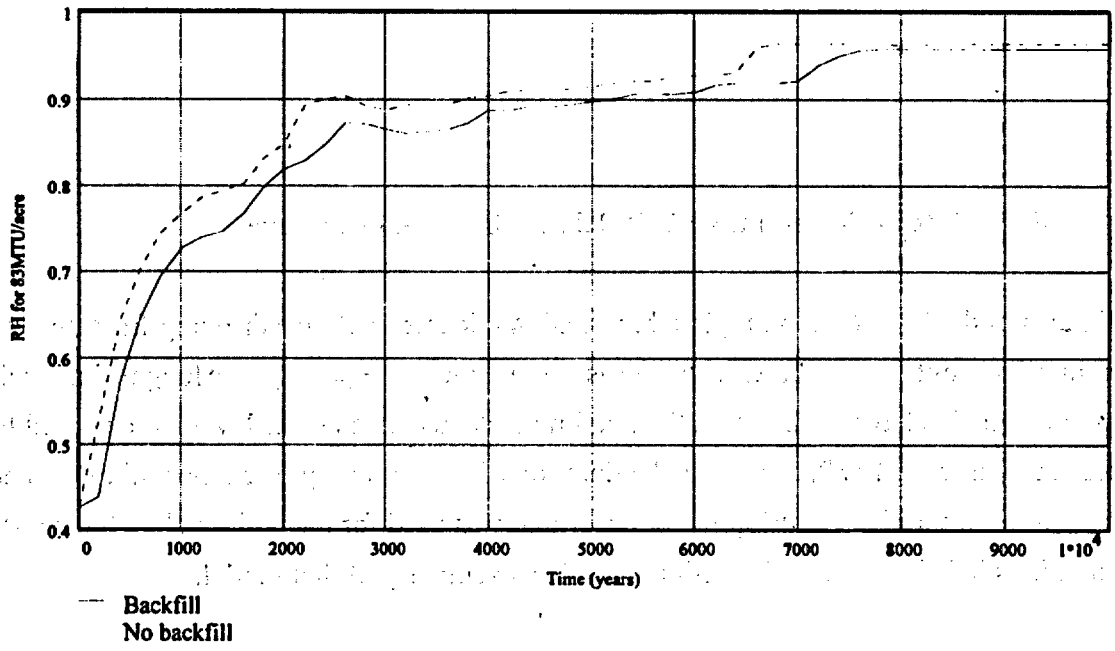

Figure 1-1.TSPA-95 WP Relative Humidty as a Function of Time for 83 MTU/acre case

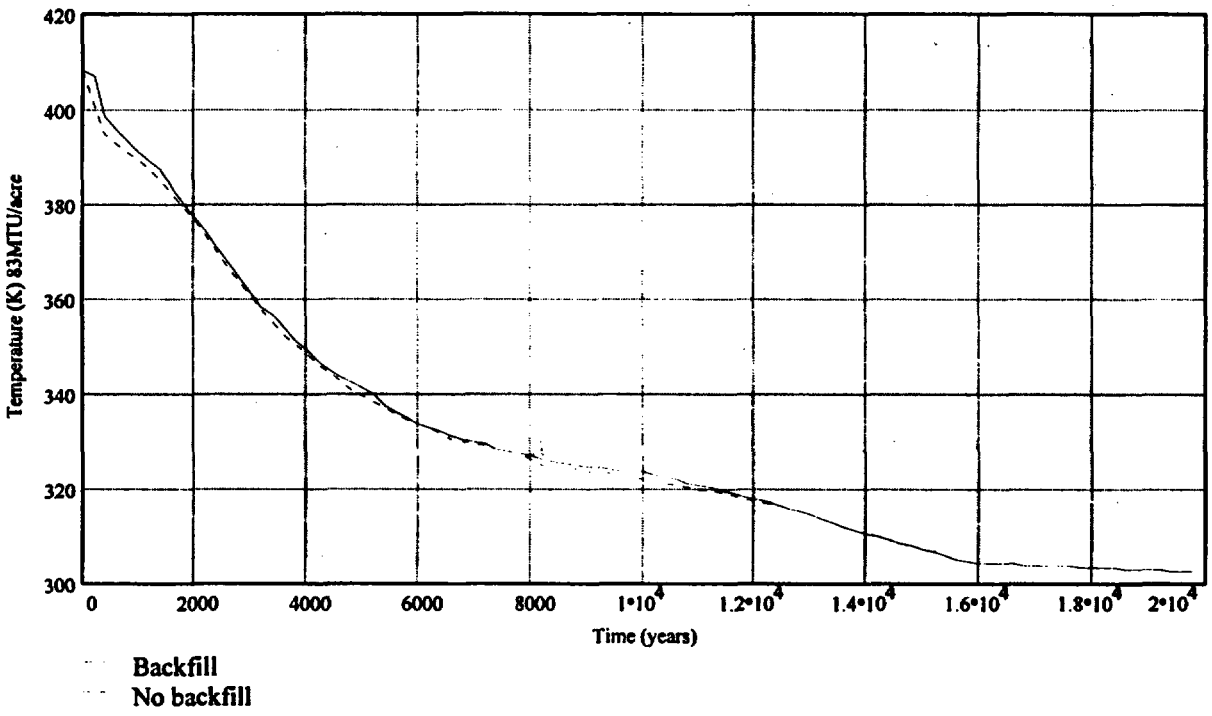

Figure 1-2.TSPA-95 WP Surface Temperature as a Function of Time for 83 MTU/acre case

1.2. Flow Rate of Water onto a WP Below a Dripping Fracture

Estimates of the level of ponding in a breached WP located below a dripping fracture require information about the rate at which water is dripping into the package. Along a similar line, the drip rate will also have an affect on the maximum steady state power level which could be achieved by a critical WP, as well as the duration of the criticality (see Appendix D). The current analyses utilize the dripping model which was used for the radionuclide transport calculations in TSPA-95. This section provides a summary of that model.

1.2.1 Infiltration Rate

The primary influence on the rate at which water drips on a WP located below a dripping fracture is the rate of water infiltration into Yucca Mountain. The simple model for change in infiltration rate as a function of time due to climate cycles is the same as that that detailed in Chapter 7 of TSPA-95 (Ref. C.9-2). For the TSPA-95 model, there are three parameters which must be defined, the cycle period, the minimum infiltration rate (I_{min}) for the cycle (rate at time zero), and the maximum infiltration rate for the cycle which is a multiple of I_{min}. For TSPA-95, this multiplier was uniformly distributed between 1 and 5. These distribution parameters were selected because of information indicating that during the last glacial maximum the annual precipitation rate was 2.5 times that of the present. The cycle period for TSPA-95 was fixed at 100,000 years (peak infiltration occurs at 50,000 years).

For determining the minimum infiltration rate, TSPA-95 had two scenarios: a low infiltration scenario where I_{min} was uniformly distributed between 0.01 and 0.05 mm/yr, and a high infiltration scenario where I_{min} was uniformly distributed between 0.5 and 2 mm/yr. The former (low infiltration) values bound the current day average infiltration rate of 0.02 mm/yr for the rock units immediately above and in the area surrounding the repository. The basic assumption for the low infiltration scenario is that percolation flow occurs predominantly in the vertical direction. The high infiltration scenario assumes that there is some lateral flow due to the sloping nature of the rock units, and factors in the average higher infiltration rate of 1 mm/yr for the Paintbrush tuff outcropping immediately to the north of the repository block.

1.2.2 WP Drip Rate as a Function of Infiltration Rate

The drip rate of water onto a waste package beneath a flowing fracture is taken to be a function of the infiltration rate, as given in TSPA-95 figures 7.3-7 and 7.3-8 for low and high infiltration respectively. This simple relationship was developed for use with the RIP code in TSPA-95 and is based on thermo-hydrologic process-level model simulations conducted using the FEHM code. For the FEHM model, some amount of dripping flow occured if the saturated matrix conductivity was less than the infiltration flux. The relationship between infiltration and drip rates abstracted from the FEHM model is summarized in Figure 1-3 below.

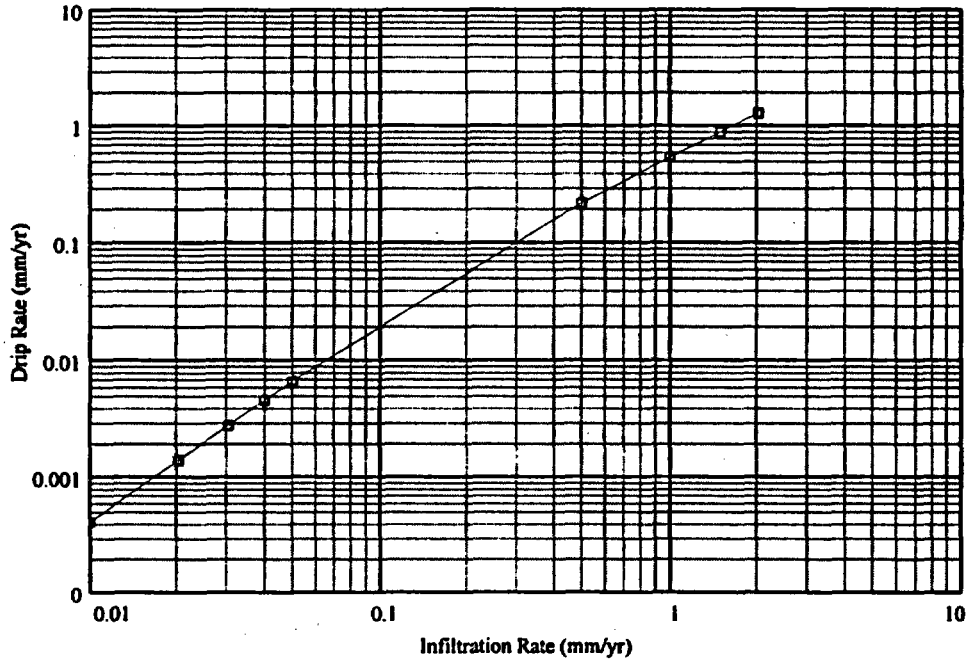

Figure 1-3. Relationship between drip rate and infiltration rate

The TSPA-95 corrosion models did not incorporate a "weeps" type model of fracture flow onto a WP. Instead, aqueous conditions were assumed once drift relative humidity reached the 85-95% range. However, the radionuclide transport part of TSPA-95 did incorporate the above dripping relationship shown in Figure 1-3. The transport model assumed that infiltrating water is focused onto a point over the WP by a fracture network covering a specified collection area. The collection area is defined as a multiple of the physical cross-sectional area of the emplaced WP interior as viewed from above (6.634 m^2). For TSPA-95 the "concentration factor" was taken to be 4, and this value has been used here as well. The flow rate of water onto a WP located below a dripping fracture is then simply 26.54 m^2 times the drip rate. Table 2-1 below shows the range of peak dripping flow rates for the TSPA-95 low and high infiltration scenarios.

Table 1-1. TSPA-95 Peak Dripping Flow Rates Onto A WP

TSPA-95 Scenario	Peak Dripping Flow Rate (liters/year)		
	Minimum	Mean	Maximum
Low Infiltration	1.1E-2	0.7	2.7
High Infiltration	5.8	68.1	190.8

1.3. Potential Far-Field Environments Relevent to Uranium Concentration

This section describes relevant uranium occurrences in tuff that is analogous to the rock at Yucca Mountain and in sedimentary rocks, which provide much higher grade ores. Section C.8 describes how this information is used to build a model for the upper bound of the probability of the existence of reducing zones beneath Yucca Mountain. This upper bound is based on the assumption that the natural environments that accumulated uranium in the past will have the greatest probability of accumulating uranium in the future.

1.3.1 Types of uranium deposits

The United States has approximately 30% of the world uranium reserves (J.W.Brinck, Ref. C.9-7, pg 22), and most is near the Four Corners area of the Colorado Plateau and in Wyoming. Brinck has also estimated the United States total of 259,000 metric tons consists of individual deposits averaging 2300 metric tons at an average ore grade is 0.195% (Ref C.9-7, pg 23). A higher average ore grade has only been reported for one country, South Africa, 0.29% (Ref C.9-8, p. 463), but that the size of those deposits is only 10% of the US.

The largest and richest uranium deposits worldwide are associated with organic material in sedimentary rock. This organic material provides a reducing substrate to convert the soluble hexavalent uranium to the insoluble quadrivalent form, particularly the mineral uraninite (pure UO_2). The groundwater solution which flowed through the rock is generally assumed to have been enriched in hexavalent uranium (uranyl) from some upstream source rock of higher uranium concentration. The deposition substrate is either the organic material itself or H_2S (or some form of organic sulfur) generated by bacterial decay of the organic material. These deposits are found

only in sedimentary rock, generally sandstone, but sometimes limestone. In one deposit (Oklo) the maximum ore grade of a small portion of the total deposit has been found as high as 60%; otherwise the local peak ore concentration has never been above 20% (Ref. C.9-9, p. 20). Of course, individual uraninite nuggets would have uranium concentrations as high as 88%, but these are so small in dimension as to not even be recorded in the general literature.

Another major mechanism for uranium concentration is by deposition on fracture surfaces from hydrothermal (hypogenic) fluids which could have derived their uranium content directly from volcanic magma or from leaching of some nearby source rock. The precipitation from the hydrothermal fluid could be induced by cooling, by encountering an organic reducing zone, or by increased concentrations of inorganic ions (Ca or silicate) which can displace the uranyl from solution. This is the principal type of uranium concentration observed in tuff. Secondary enrichment can occur as uranium is mobilized in the weathering environment.

A third mechanism for uranium concentration is adsorption in zeolites. These are cage-like minerals which have structural channels that can exchange ions with aqueous solutions. Although this is a relatively rare type of uranium deposit, it is relevant to Yucca Mountain, because such a concentration has been observed in clinoptilolite (a common zeolite) that is a major constituent of a tuff similar to that found at Yucca Mountain (Ref. 5.46), and because similar zeolites in tuff (not containing uranium) are fairly common at Yucca Mountain, with many of the drill holes showing zeolite deposits several meters thick and constituting 50 to 70% of the local rock (Ref. C.9-10).

These general mechanisms are limited by available surface area for chemical-physical reaction between solution and host rock. For the organic-reduction mechanism the large surface area is provided by either microfractures in the bulk organic material itself (e.g. a log) or the fine interstices of sedimentary rock containing a more refined organic material with little internal surface area. For the hydrothermal mechanism the surface area is provided by extensive fracturing, which may be provided by the same hydrothermal process as provides the fluid or may have been pre-existing. For the zeolite exchange process, the effective surface area is provided by the cage structure of the zeolite itself.

1.3.2 Maximum uranium concentrations from non-organic reducing zones, hydrothermal and zeolite deposition process

The Pena Blanca uranium district, located 50 km north of Chihuahua City contains some of the richest uranium ore reported for tuff. The peak concentration of 9% uranium was found in a 13 cm diameter, very highly fractured breccia for a total uranium content of less than 3 kg UO_2. This particularly rich breccia sample is one of several characterized by P.C.Goodell (Ref. C.9-11, Table 3, with the size information from a private communication with the author), as part of the Nopal 1 deposit, which is a pipe like body 100 meters high with a 20 meter by 40 meter cross-section, and an average uranium concentration of .11%, as reported by George-Aniel et.al. (Ref. C.9-12, p. 238). The lower grades dominate the rest of the deposit; in fact, the latter reference does not even mention the 3 kg, 9% sample. The source rock for the lower grade deposits is believed to be rhyolites, which range from 10 to 35 ppm U_3O_8.

In the Pena Blanca district, only the peak 9% sample is believed to contain quadrivalent uranium (specifically uraninite, UO_2, Ref. C.9-11, p. 286, uraninite being identified with this peak sample as "in the breccia"),. Although even this high a grade is insufficient for criticality of commercial SNF, it is evidence of some strong organic type reduction from the hexavalent solution which would be necessary to precipitate the higher concentrations required for criticality. The remainder of the district in general, and the Nopal 1 deposit in particular, is the result of a deposition process which does not reduce the hexavalent ions, but only incorporates this hexavalent uranium into carbonate, silicate, and oxide minerals, particularly uranophane $[Ca(UO_2)_2(SiO_3)_2(OH)_2]$(Ref. C.9-11, p. 286). Similar low grade uranium deposits in tuff are found in Oregon (Ref. C.9-13, p. 55) and in Nevada (Ref. C.9-14, p. 104).

It is, therefore, concluded that there is very little likelihood of finding high organic concentrations in tuff, and those rare exceptions are likely to be small, like the 3 kg sample from Pena Blanca. However, there is a possibility of log-type organic deposits in basal pyroclastic deposits, as is discussed in Section C.6, below.

A review of the best known uranium deposit in zeolite, the Tono mine in Japan, has been given by Katayama et.al. (Ref. C.9-15). The maximum uranium concentration reported in this reference is .9%. This observed concentration is consistent with the maximum uranium concentration achieved in a laboratory experiment also reported by Ref. C.9-15, p.448. In this experiment the uranium concentration in the zeolite was found to increase linearly with uranium

concentration in the contacting water, corresponding to a partition coefficient of 700, and to saturate at just under 1% uranium in the zeolite for uranium concentration in the water above 100 ppm. The applicability of this mechanism to Yucca Mountain is discussed in Section C.6, below.

1.3.3 Maximum uranium concentrations resulting from reduction zones of organic origin

The highest recorded grade of uranium ore, 60% was recorded at Oklo, Gabon. The original deposition of the uranium (over 2 billion years ago) is believed to have been due to the reduction of highly concentrated organic material, but the original organic material is no longer distinguishable as such, (Smellie, Ref. C.9-9, p. 19). On the other hand, the United States deposits with the highest concentrations of uranium ore generally contain organic material (or its fossilized remains) which is still identifiable.

Tabular deposits are of two types, peneconcordant (or true bulk) and roll-front (Ref. 5.9, p. 145. The former occupies a larger volume, but the latter is of higher concentration. This difference reflects the nature of the organic deposit responsible, either directly or indirectly, for the reducing zone which caused the uranium precipitiation, the roll-front having been more concentrated than the peneconcordant. Neither of these types of tabular deposits has concentrations as high as the log type deposits, in which the boundaries of the organic material are still recognizable.

The summary of uranium deposits resulting from concentrated organic reducing zones has been given by Breger (Ref. C.9-16); he reports a 64 element sample of mineral concentrations in logs primarily from the Colorado Plateau and Wyoming, with an average of 1.88% uranium (Ref. C.9-16, pp. 102-105). The maximum concentration among these samples is 16.5%. Other reports of maximum concentration near 20% have been given by Hess (Ref. C.9-17, p. 467) and Chenoweth (Ref. C.9-18, p. 168).

The mechanism responsible for the strong deposition capability of organic matter is demonstrated by measurements of the partition coefficient between organic matter (humic material in the form of peat and lignite) and U bearing groundwater, with values as high as 10^4, as reported in studies cited in Ref. C.9-19, p. 44; subsequent experiments, identified in the same reference, also indicate that it is the organic surfaces and not the humic acid in porespaces which cause the adsorption.

Detailed chemical and X-ray diffraction examination of uranium log samples shows both crystalline and and non-crystalline material (the latter of which may be either colloidal material or amorphous solids (Breger, Ref C.9-16, p. 106). It should be noted that the crystallized mineralization usually only extends over a small fraction of the volume of the log. Furthermore, the uranium concentrations can vary by 2 orders of magnitude from one side of a log to the other, particularly if the logs were oriented perpendicular to the direction of groundwater flow during mineralization.

INTENTIONALLY LEFT BLANK

2. WP Degradation Mode Analysis

The purpose of this section is to identify the modes of degradation which may affect the waste package subcomponents (e.g., barriers, fuel assemblies, basket guides, tubes, absorber plates, and fuel rods) and their effect on the configuration/geometry of the waste package. The results of structural analyses of the basket and barrier components will be combined with preliminary, models of the WP environment (see Section C.1), and preliminary corrosion models and rates from TSPA-95, and other sources, to provide an initial estimate of the order and timeframe over which these changes will occur. This information will be utilized, along with that provided by the configuration bookkeeper discussed in Section C.3, to guide waste package criticality analyses. An exploded view of the 21 PWR Advanced Uncanistered Fuel (AUCF) waste package is provided for reference purposes in Figure 2-4.

2.1. Basket Components

This section discusses the three primary basket components responsible for maining the initial configuration of the WP, and the anticipated changes in the WP configuration which will occur as a result of their degradation. These are the side and corner guides, the neutron absorber plates, and the fuel cell tubes.

2.1.1 Side Guides

The AUCF WP side guides are fabricated from 10 mm thick carbon steel plates. Prior to WP breach, the interior of the WP is inerted with a He/Ar fill gas, and no degradation of the side guides and other intenal component would be expected. To estimate the thickness of the side guides as a function of time following WP breach, the carbon steel general corrosion models from TSPA-95 will be used here. The TSPA-95 model for humid-air general corrosion of carbon steel (Ref. C.9-2, p. 5-25) is given by:

$$D_g(t,RH,T) = \exp\left[16.984 + 0.6113 \ln(t) - \frac{893.55}{RH} - \frac{833.27}{T}\right], \quad (1)$$

where D_g is the general corrosion depth (μm), t is the exposure time (years), RH is the relative humidity (%), and T is the temperature (K). The TSPA-95 model for aqueous general corrosion (Ref. C.9-2, p.5-26) is given by:

$$D_g(t,T) = \exp[111.5 + 0.5320 \ln(t) - \frac{23300}{T} - 3.193E\text{-}4\ T^2],$$

(2)

where the variable definitions are the same as for Equation (1). For this estimate, the WP surface temperature and humidity curves for the TSPA-95 83 MTU/acre, low infiltration cases with and without backfill (Ref. C.9-2, Fig. 4.2-8) were used. Side guide temperatures were assumed to be the same as the WP surface temperature.

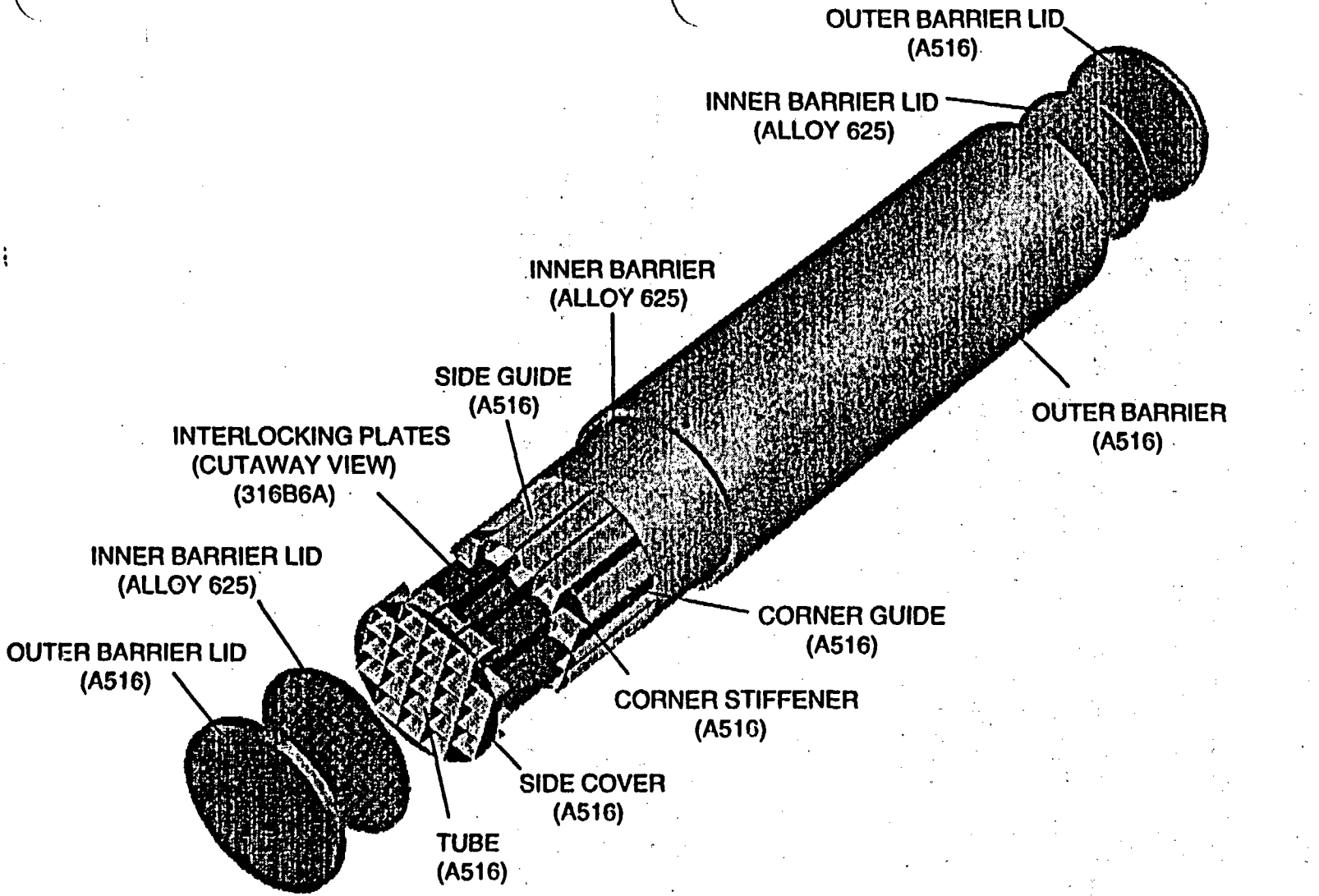

Figure 2-4. Exploded View of 21 PWR Advanced UCF Waste Package

Humid-air corrosion was assumed to initiate when the relative humidity was greater than 70% (middle of the TSPA-95 range of 65-75%, Ref. C.9-2, p. 5-23), and aqueous corrosion was assumed to initiate when the relative humidity was greater then 90% (middle of the TSPA-95 range of 85-95%, Ref. C.9-2, p. 5-23) and the temperature was greater than 100°C.

Side guide degradation was initiated at the time of WP breach. For each case five WP breach times were used. These times were read off of Ref. C.9-2, Fig. 5.7-3a for the no-backfill case, and Ref. C.9-2, Figure 5.7-5a for the backfill case, and correspond to the time of first WP breach, the median WP breach time, and the times when 70%, 80%, and 90% of the WPs had breached. For the backfill case, the WP failure distribution did not reach 90% before 100,000 years, so 50,000 years was assumed for the purpose of determing the side guide failure time in late failing WPs because the temperature and relative humidity appear to have stabilized by this time. The side guide thickness at times following WP breach was determined in half-year timesteps using Mathcad+ v5.0. At timestep t_i, the side guide thickness remaining is given by the following equation,

$$L_i = L_{i-1} - 2\frac{dD_g(t_i - t_0, RH_i, T_i)}{dt}(t_i - t_{i-1}) \qquad (3)$$

where i indicates the timestep, L is the side guide thickness (μm), t is the time since emplacement (years), t_0 is the time of initial exposure, RH is the average relative humidity for the timestep, T is the average temperature for the timestep, and D_g is either Eq. 1 or 2 as indicated by the relative humidity and temperature rules discussed above. The rate is multiplied by two because the both sides of the side guide are exposed. The results are presented in Tables 2-1 and 2-2 below.

Table 2-1. Side guide thickness as a function of WP breach time and time since WP breach for the TSPA-95 83MTU/acre, low infiltration, no-backfill case

WP breach at 2200 years (.003% WPs failed)		WP breach at 3200 years (50% WPs failed)		WP breach at 4000 years (70% WPs failed)		WP breach at 4600 years (80% WPs failed)		WP breach at 10000 years (90% WPs failed)	
Years Since WP Breach	Side Guide thickness (mm)	Years Since WP Breach	Side Guide thickness (mm)	Years Since WP Breach	Side Guide thickness (mm)	Years Since WP Breach	Side Guide thickness (mm)	Years Since WP Breach	Side Guide thickness (mm)
0	10	0	10	0	10	0	10	0	10
100	6.202	100	6.617	25	6.425	25	5.892	25	5.793
200	4.113	200	4.805	50	4.677	50	3.889	50	3.754
300	2.401	300	3.384	75	3.299	75	2.317	75	2.162
400	1.195	400	2.138	100	2.117	100	0.971	100	0.806
500	0.211	500	1.006	125	1.062	125	0	125	0
600	0	600	0	150	0.093	150	0	150	0

Table 2-2. Side guide thickness as a function of WP breach time and time since WP breach for the TSPA-95 83MTU/acre, low infiltration, backfill case

WP breach at 2300 years (.003% WPs failed)		WP breach at 4000 years (50% WPs failed)		WP breach at 5700 years (70% WPs failed)		WP breach at 12000 years (80% WPs failed)		WP breach at 50000 years (>80% WPs failed)	
Years Since WP Breach	Side Guide thickness (mm)	Years Since WP Breach	Side Guide thickness (mm)	Years Since WP Breach	Side Guide thickness (mm)	Years Since WP Breach	Side Guide thickness (mm)	Years Since WP Breach	Side Guide thickness (mm)
0.00	10	0.00	10	0.00	10	0.00	10	0.00	10
100	8	100	7.082	25	5.471	25	6.185	100	6.478
200	6.686	200	5.504	50	3.271	50	4.338	200	4.842
300	5.459	300	4.203	75	1.549	75	2.898	300	3.564
400	4.367	400	3.056	100	0.078	100	1.672	400	2.476
500	3..414	500	2.017	125	0.00	125	0.585	500	1.51
600	2.572	600	1.056	150	0.00	150	0.00	600	0.631

As calculated in Reference C.9-1, the side guide will fail by bending at a thickness of 2.9 mm if there is no backfill, and at a thickness of 3.8 mm if there is backfill present and loading the basket. Table 2-3. indicates the times at which these failure points will be reached for the backfill and no backfill cases. The shorter side guide failure times at higher barrier breach times are a result of the switch from humid air to aqueous corrosion when the relative humidity exceeds 90% and the surface temperature is still high. Longer failure times (> 100 years) are achieved again for side guides in WPs which breach after 20,000 years, when the temperatures are below 30°C.

Table 2-3. Times to WP Side Guide Failure

83 MTU/acre, Low Infiltration, No-Backfill		83 MTU/acre, Low Infiltration, Backfill	
WP Breach Time in Years (Fraction WPs Breached)	Time (years) After WP Breach to Side Guide Failure	WP Breach Time in Years (Fraction WPs Breached)	Time (years) After WP Breach to Side Guide Failure
2200 (0.003)	270	2300 (0.003)	460
3200 (0.5)	340	4000 (0.5)	330
4000 (0.7)	84	5700 (0.7)	44
4600 (0.8)	66	12000 (0.8)	59
10000 (0.9)	63	50000 (> 0.8)	280

Failure of the side guides will cause the bottom row of fuel assemblies to shift downward to touch the inside of the inner barrier. As the criticality control assemblies also rest on the top of the side guides, the entire basket structure should also shift downward. As the corner guides are under less loading, their failure should occur shortly after failure of the side guides. Failure of the corner guides will result in the assemblies on the end of the second row from the bottom to shift downward to touch the inside of the inner barrier. The assemblies above them should remain in place until sufficient degradation of the neutron absorber plates which support them has occured.

2.1.2 Neutron Absorber Plates

The AUCF WP neutron absorber plates are fabricated from 7 mm thick borated Type 316L stainless steel plates. Since long-term corrosion testing of this material in repository type environments is just beginning, specific corrosion models are not yet available. However, a

preliminary evaluation can be made by using previous data collected for 316 stainless steels (Ref. C.9-4), and scoping corrosion tests which compared borated and unborated stainless steels (Ref. C.9-3). For J-13 well water in the temperature range expected after WP breach for the 83 MTU/acre cases, Reference 4 found that the general corrosion rate of 316L stainless steel ranged from 0.037 μm/yr at 100°C to 0.154 μm/yr at 50°C. Scoping corrosion tests (Ref. C.9-3) of borated and unborated Type 304L stainless steels in an extremely aggressive environment (pH = 3.8) found that the borated stainless steel had a corrosion rate that was approximately 4 times higher than that of the unborated stainless steel. Using the above 316L rates, multiplied by an adjustment factor of 4, suggests that it will take 2,000 to 8,500 years following breach of the WP for general corrosion of both sides of the neutron absorber plates to remove the 2.5 mm of material that would be required (Ref. C.9-1) for bending to occur. It will take 4,000 to 17,000 years following breach of the WP for general corrosion of both sides of the neutron absorber plates to remove the 5.05 mm of material that would be required for buckling of the vertical plates to occur if backfill is loading the basket, and 4,300 to 18,000 years to remove the 5.36 mm of material that would be required if backfill is not loading the basket. This information is summarized in Table 2-4 below.

Table 2-4. Times to Neutron Absorber Plate Colapse

Failure Mode	Critical Corrosion Depth	Time After WP Breach To Corrode To Critical Depth
Buckling without Backfill	5.36 mm	4,300-18,000 years
Buckling with Backfill	5.05 mm	4,000-17,000 years
Bending	2.5 mm	2,000-8,500 years

It should be noted that the above failure times assume that the localized corrosion mechanisms, such as pitting or stress corrosion cracking, do not severely affect the structural capability of the absorber plates. This assumption is expected to be valid because the faster localized penetration which can result from pitting typically affects only a small fraction of the overall surface area of stainless steels due the high aspect ratio of the pits. Stress corrosion cracking typically requires tensile stresses in excess of one-half yield, an aggressive environment, and a sensitized material (chromium carbides precipitated at grain boundaries). The criticality control panel assemblies will be fabricated by interlocking borated stainless steel plates. Structural calculations have shown that stresses in the plates due to the static load of the fuel are below one-half yield. In

addition, these plates will not be welded nor exposed to sensitizing temperatures at any time, so sensitization is not expected. However, in some cases (BWR environments), increased susceptibility to stress corrosion cracking has been associated with exposure to high neutron fluences (> 10^{20} n/cm^2). Such fluence levels could not be achieved in the plates under exposure to spent fuel before other mechanism would cause their failure.

2.1.3 Fuel Cell Tubes

The fuel cell tubes are fabricated from carbon steel and have a wall thickness of 5 mm. The tubes will fully degrade before the failure of the side guides or the criticality control plates. In analyzing the criticality control plates, it was determined that the plates could maintain the basket and SNF assembly configuration without structural support from the tubes. Failure of the tubes will, therefore, not cause collapse of the basket, so no specific analysis was performed for the tubes. However, the remaining corrosion products occupy a greater volume than the original tubes and are fairly insoluable. Thus there presence may have some impact on WP internal criticality. This will be discussed further in Sections C.2.2.1, C.3, and C.4.

2.2. Fuel Assembly Response to Loadings

2.2.1 Effect of Degradation Products on Fuel Assemblies

The effect of degradation products on the fuel assemblies is determined in this section of the report. The fuel assembly array of Westinghouse 17x17 is considered for this analysis. The analyses of yield for the side drop and buckling are performed for various sizes of fuel assemblies in Reference C.9-20. The results show that allowable *g* loads calculated for each case in this document are lowest for the 17x17 array. Therefore, the limiting fuel assembly is the 17x17 according to these structural evaluations and it is evaluated here for any potential effect of degradation products on the fuel rods. The analysis results given in Sections C.2.2.1 and C.2.2.2 are taken from Reference C.9-21.

The expansion of the tubes and the plates results in the degradation products moving into void spaces in the fuel assembly. Therefore, the calculations are performed in two parts. First, the volume of expansion due to degradation is determined in the tube and plate structure. Then, the volume of the fuel assembly is calculated based on the cladding dimensions. Since there is a clearance between the fuel assembly and the tubes, this volume is also considered to be filled by

degradation products. If the available space in the tubes after degradation is larger than the volume of the fuel assembly, the fuel assembly does not experience a load due to expansion in the tubes. On the other hand, an available space smaller than the fuel assembly volume causes a compressive load on the fuel assemblies.

The amount of oxidation in the carbon steel is selected as the maximum value for iron and its common degradation products. The ratio of the specific volume per mole of $Fe(OH)_2$ to the iron (Fe) is determined as 3.713 (Ref. C.9-22). This value is used as a factor of volume expansion during degradation of the basket components.

The WP basket assembly structure expands in all directions. Therefore, the outer surface expansion of carbon steel tubes causes both surfaces of the SS-B plates to experience compressive stress. Since the plates also expand, the resulting effect of degradation is an increase in the volume of carbon steel tubes toward the center of each tube. Initial volume per unit length of the tube plus plate structure is, therefore, multiplied by the factor of 3.713 in order to calculate the final inner dimension of the initial materials plus degradation products. Thus, available space in each tube is also obtained using this dimension.

The dimensions of the fuel rod, guide tubes, and instrument tube are used to determine the volume per unit length of the fuel assembly. The calculations showed that the available volume is larger than the total volume of the fuel assembly in the tubes. Therefore, it is concluded that degradation products do not cause any load on the fuel assemblies.

2.2.2 Static Load on Fuel Assemblies Due to Complete Degradation of WP

This calculation is performed to determine the effect of a static load on the fuel assemblies when the WP is completely degraded. A conservative approach is taken by selecting the fuel assembly at the bottom on the symmetry axis to analyze the maximum effect of the static load. The vertical load on one fuel rod is equal to the summation of the total weight of the WP components and fuel assemblies above the bottom fuel assembly, weight of the bottom fuel assembly itself, and the backfill load, divided by the total number of fuel rods in a 17x17 array. The calculations of the *Dynamic Impact Effects on Spent Fuel Assemblies* (Ref. C.9-20) show that the static load on a fuel assembly is taken equally by each fuel rod in the assembly. The same approach is taken for the analysis of static load on the fuel assemblies (Ref. C.9-21).

Having the mass of all the components of the WP (tubes, plates, side guide, inner barrier, and outer barrier), the fuel assemblies, and the backfill calculated, a total mass of approximately 7,602 kg (16,760 lb) is determined to be resting on the bottom fuel assembly on the WP symmetry plane. Beam theory is applied to one fuel rod in order to calculate the resulting maximum bending moment and stresses (Ref. C.9-20) Thus, a maximum bending stress of 57.2 MPa is determined for one fuel rod. Comparing this value with an allowable bending stress of 348.2 MPa, it is concluded that the margin of safety is 5.1 and there is no failure in the fuel assembly due to a static load of a completely degraded WP.

The fuel rod flattening is also analyzed by using the equation of critical bending moment which is expressed in terms of the Young's Modulus, nominal radius, and thickness of the fuel rod. The results show that the moment required to cause a flattening of the rod is much higher than the moment calculated on a fuel rod due to the static weight above the fuel assembly. Therefore, it is also concluded that there is no flattening of the fuel rods because of this loading condition.

Based on the above analyses, the assumption of intact fuel assemblies is appropriate and conservative until significant corrosion of the fuel rods and spacer grids has occured. Efforts to estimate the amount of corrosion required for such failures are currently under way.

2.3. Effect of Rockfall on Basket Configuration

Rockfall onto a severely degraded WP also represents a potential mechanism for collapsing the basket structure. The 100 mm thick outer barrier provides the primary defense against damage from large rockfalls. The TSPA-95 general corrosion models for carbon steel (Eq. 1 & 2) were used to estimate the outer barrier thickness as a function of time for the purpose of showing how the rockfall mass required to plastically deform the WP outer barrier to the point of crack initiation changes with time. Use of the general corrosion rate for this purpose is based on the assumption that localized corrosion mechanisms such as pitting, which may have produced earlier penetrations of the barrier, will not significantly affect the structural capability of the barrier. This study was performed for the 83 MTU/acre, low infiltration, no backfill case only, as rockfall would not be expected to be a concern for the backfill case (most if not all of the space above the waste package would be filled with backfill, thus preventing the rock from contacting the WP). The outer barrier thickness was determined in two-year timesteps using Mathcad+ v5.0. At timestep t_i, the outer barrier thickness remaining is given by:

v5.0. At timestep t_i, the outer barrier thickness remaining is given by:

$$L_i = L_{i-1} - \frac{dD_g(t_i - t_0, RH_i, T_i)}{dt}(t_i - t_{i-1}) \quad (4)$$

where i indicates the timestep, L is the outer barrier thickness (μm), t is the time since emplacement (years), t_0 is the time of initial exposure, RH is the average relative humidity for the timestep, T is the average temperature for the timestep, and D_g is either Eq. 1 or 2 as indicated by the relative humidity and temperature rules discussed above. The results are shown in the figure below.

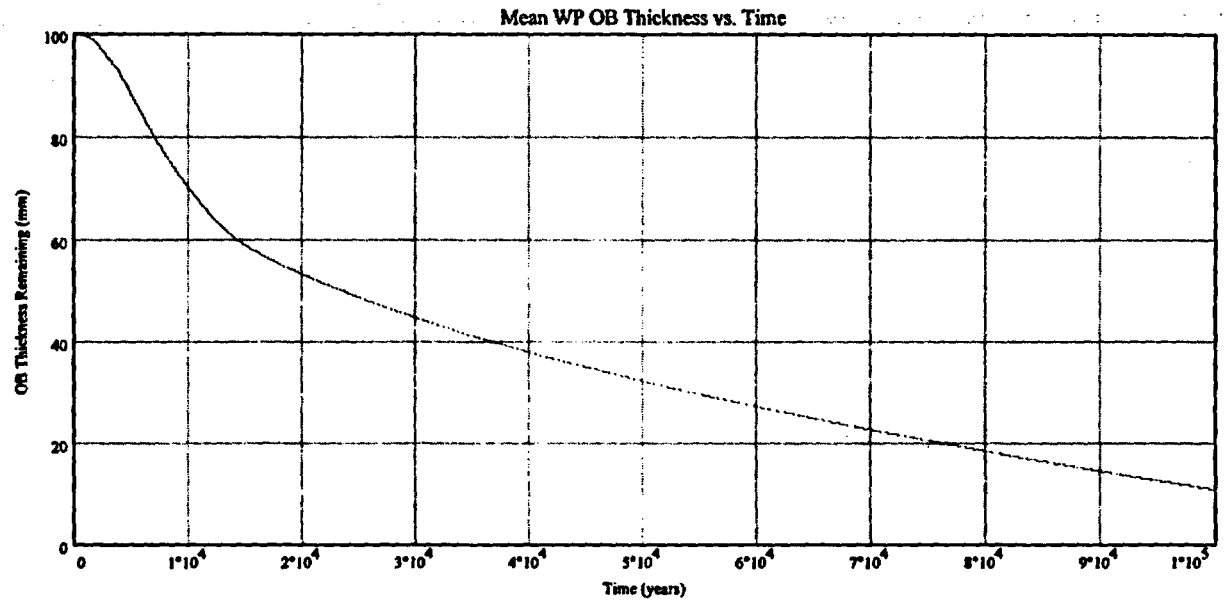

Figure 2-2. Mean WP Outer Barrier Thickness as a Function of Time

Using Figure 2-2 and the preliminary information on critical rockfall mass as a function of outer barrier thickness provided in Reference C.9-1, Table 2-5 has been generated. This table relates

collapse of the basket. This conclusion, however, is subject to future revision as more information on the distribution of potential rockfall masses is provided by the Repository Design Department.

Table 2-5. Critical Rock Mass With Respect to Time

Degradation Level	Time (years)	Critical Rock Mass (kg)
0% Outer Barrier Degradation	0	8000
50% Outer Barrier Degradation	23,000	2500
75% Outer Barrier Degradation	54,000	1000
100% Outer Barrier Degradation	>100,000	350

3. Simple Internal Configuration Bookkeeper

This section provides an example of a simple flooded WP configuration bookkeeper that was developed as part of the *Second Waste Package Probabilistic Criticality Analysis* (Ref. C.9-5). Section C.2 was primarily concerned with the physical structure of the WP interior as a function of time. The purpose of this initial configuration bookkeeper will be to examine the form of the WP basket materials and evaluate the time required to remove those materials important to criticality control from a WP which is assumed to be flooded.

The degradation of the waste package interior begins with corrosive attack from a humid and/or aqueous environment containing oxygen. As discussed in Section C.2, the waste package is sealed with an inert interior atmosphere, and the corrosion process cannot start until the waste package barriers have been breached. The time of breach depends on the rate of corrosion of the waste package barriers. This process has been modeled in other studies, with first penetration times ranging from 2,000 years to 10,000 years with very conservative models which have relatively rapid corrosion (Ref. C.9-2). This study will not include the value of this time explicitly, because it turns out to be much less than the times required to remove neutron absorbers from the package in sufficient quantity to permit a criticality.

3.1. Model Description

The waste package interior degradation model solves the coupled first order differential equations which connect the concentrations of iron and boron in the three phases: steel, oxide, and in solution. The model follows directly from the standard interpretation of chemical processes in terms of first order, time dependent linear differential equations.

Corrosion of borated stainless steel is assumed to release boron congruently, but a fraction, f, of the boron released thereby is assumed to be trapped in the solid iron oxide as it is being formed. This is a reasonable and conservative assumption since the boron in the stainless steel is in the form of a boride of iron, or other metal component of stainless steel, and such borides are generally found to be very stable and corrosion resistant. In this study a range of values will be used for f, all well under 0.1.

The model assumes that the water containing dissolved Fe, B, and oxygen is circulated (by convective cooling of the heat generating assembly) so that it passes in the vicinity of waste

package holes through which it can overflow or otherwise exchange with the water outside the waste package. The result of this circulatory exchange is the removal of the neutron absorbing corrosion products and the replenishing of the oxygen supply to support further corrosion. The principal processes, and the differential equations describing their time dependence and coupling, are as follows:

Carbon steel change:

$dm_{fec}/dt = -$ c_rate_cs; provided $m_{fec}>0$.

Stainless steel change:

$dm_{fes}/dt = -$ c_rate_ss*(1-alph); provided $m_{fes}>0$.

Iron oxide change:

dm_{feo}/dt = c_rate_ss + c_rate_cs - ex_rate*fe_sol;

in which the first and second terms on the right side are included if the mass of stainless steel and the mass of carbon steel are greater than zero, respectively.

Boron in stainless steel change:

dm_{bs}/dt= -c_rate_ss*alph; provided $m_{bs}>0$.

Boron trapped in the solid iron oxide change:

dm_{bot}/dt= f*c_rate_ss*alph - ex_rate*fe_sol*m_{bot}/m_{feo} ;

in which the last term on the right side represents the trapped boron released to solution as the iron oxide is permitted to go into solution to replace the amount which was exchanged.

Boron in solution change:

dm_{bosol}/dt = (1-f)*c_rate_ss*alph + ex_rate*fe_sol*m_{bot}/m_{feo} - ex_rate*m_{bosol} ;

in which the first term on the right side is included only if the mass of stainless steel is greater than 0, and the second term is the same as the second term of the previous equation but with opposite sign.

The following symbols have been used:

m_{fec} Mass of the remaining carbon steel (conservatively assumed to be 100% Fe, although actually only 99% iron, because most of the remainder is manganese which has a higher neutron absorption cross section than iron; the carbon content, from which the steel gets its name is only 0.2%, A516, Ref. C.9-23).

m_{fes} Mass of the metallic fraction of the remaining borated stainless steel (conservatively assumed to be all Fe, because most of the remainder is chromium, nickel, or manganese, all of which have higher neutron absorption cross section than iron, 316B6A, Ref. C.9-23).

m_{feo} Mass of iron as iron oxide not in solution (corrosion product of both the carbon steel and the stainless steel).

m_{bs} Mass of boron in the remaining stainless steel.

m_{bosol} Mass of boron oxide in solution.

m_{bot} Mass of boron trapped in the solid iron oxide.

c_rate_cs Corrosion rate of carbon steel (kg/yr).

c_rate_ss Corrosion rate of borated stainless steel (kg/yr).

ex_rate Exchange rate between the water in the waste package and the water in the immediate environment (per/yr).

f Fraction of the boron being trapped in the oxide of the stainless steel being oxidized.

alph Fraction of boron in stainless steel (used to compute the amount of boron going into solution as the stainless steel is oxidized).

fe_sol The amount of Fe ion in solution at any given time, approximated by a constant equal to the maximum permitted by the solubility limit (kg).

It will be noted that the five differential equations do not include specific accounting for the iron oxide in solution or the boron oxide not in solution. As indicated in the definition of fe_sol, above, the amount of Fe in solution is approximated by the maximum permitted by the solubility limit. This assumption (approximation) is justified by the fact that the iron oxide pool is still more than several thousand times the fe_sol at the time when the boron reaches very small values and the package reaches the criticality threshold, so that the solution remains saturated with iron, as will be shown in the discussion of calculation results, below.

The model is implemented by the simple program "deltasd.c", the annotated listing of which is given in Attachment I of Reference C.9-5. This implementation uses numerical integration of the differential equations with a time step of 10 years, which is assumed to be much shorter than the reciprocal of the exchange rate, so that the concentrations of absorber change little during the time step. The proper implementation of the algorithms is checked by MathCad. The model is intended to serve as a generator of configurations which represent the criticality potential of all the possible internally degraded states of the waste package.

In the exercises with this model the initial basket steel masses are fixed at the current design values, and the corrosion and exchange rates are varied over the range of likely values. For the current analyses, this variation has been performed manually. In the next version of the bookkeeper, currently planned for release in March 1997, this variation will be accomplished by Monte Carlo sampling of distributions for the value of each parameter.

3.2. Range of Input Parameters Values

This section provides the ranges of parameters input into the configuration bookkeeper, as well as a brief basis for each parameter. More detailed information and bases for the values presented is available in the *Second Waste Package Probabilistic Criticality Analysis* (Ref. C.9-5).

Carbon steel aqueous general corrosion rate:

- High value in medium oxygen water: 50 microns/yr (Ref. C.9-24)
- Low value in low oxygen water: 5 microns/yr

To convert to kg/yr multiply by :

- 7830 density of carbon steel in kg/m^3
- 178 surface area of carbon steel tubes in m^2 (Attachment VIII, Ref. C.9-5)
- 10^{-6} meters/micron

This process gives a high value of 69.7 kg/yr and a low value of 6.97 kg/yr. Since it has been shown in Reference C.9-5 that the maximum oxygen exchange rate for a flooded WP can oxidize no more than 1.65 kg of Fe per year, these estimates must be adjusted downward. As a conservative approximation, this study will use only the limiting value of 1.65 kg/yr.

Stainless steel aqueous general corrosion rate:

- High value measured near 100°C: 0.3 microns/yr (Ref. C.9-25, pg 24)
- Low value measured near 28°C: 0.1 microns/yr (Ref. C.9-4, pg 24)

To convert to kg/yr multiply by:

- 7770 density of stainless steel in kg/m^3
- 70 surface area of stainless steel plate in m^2 (Attachment VIII, Ref. C.9-5)
- 10^{-6} meters/micron

This process gives a high value of 0.163 kg/yr and a low value of 0.0544 kg/yr. Both are well below the 1.65 kg/yr upper limit supportable by the oxygen exchange rate, so they will be used for the calculations. This approximation is conservative, since the upper limit must be shared between the carbon steel and the stainless steel, so the actual rates should be lower.

Flush/exchange rate:

The water in the package will be flushed much faster if there are holes in the bottom. However, it is extremely unlikely that holes in the package bottom could be subsequently plugged to support filling the package with water, as is required for any criticality. Therefore, the flush rate is calculated under the assumption that the principal physical mechanism is exchange of water through holes near the top of the package. It is recognized that this is not conservative with respect to corrosion rates; however, with our present understanding of the effectiveness of hole plugging, it is the only mechanism for producing internal criticality.

Multiply the following:

- Drip rate (high 7.19 mm/yr, medium 0.53 mm/yr, low 0.03 mm/yr), based on the TSPA-95 abstraction discussed in Section C.1
- Efficiency of exchange through holes in the top of the package (high 0.1, medium 0.01, low 0.001); note that the exchange efficiency values are an order of magnitude smaller than the filling efficiency because even in the most favorable hole geometry (water flowing in one hole and out another) there will be some faster path for the entering water to leave than for some general parcel of water already in the package to be exchanged.
- Concentration factor (4)
- Waste package area projected on a horizontal plane of 6.63 m^2

Divide by:

- Waste package void volume of 4.84 m^3 (Attachment VIII, Ref. C.9-5)

The 4 possible combinations of the high and medium values of drip rate and exchange efficiency give the 4 exchange rate values 0.00394, 0.000291, 0.000394, 0.0000291. These are all used in the calculations of Section C.5, below, but they are tracked according to the individual drip rate and exchange efficiency values, so they will be presented that way in the input summary Table 3-1.

Upper limit of dissolved iron in the waste package filled with water:

- High value 0.00505 mole/liter, more acidic environment than is likely to be produced by radiolysis in the waste package,
- Low value 8.0×10^{-5} mole/liter, for neutral water

The calculation of the above solubility limits is given in Attachment IV of Ref. C.9-5. To convert to total kg in the waste package solution multiply by:

- 55.8 molecular weight of iron (gm/mole)
- 4.84 cubic meters of water in the waste package.

High result: 1.33 kg; Low result: 0.021 kg

Boron fraction trapped in solid iron oxide:

There has been virtually no quantitative investigation of this phenomenon, neither theoretical nor experimental. It is therefore appropriate to try a range of values to test the sensitivity to this parameter. It will be seen that the range 0.02 to 0.05 shows a large variation in the effect on earliest possible time of criticality, so these two values will represent the low and high values of the parameter f. Since f is the only parameter for which increasing values act to decrease k_{eff}, the value 0.02 will be referred to as the high value, and 0.05 will be considered the low value. Of course the actual values could turn out to be outside this rather narrow range after all. It is expected that current investigations into the solubility and corrosion rates of metal borides, and the corrosion behavior of borated stainless steels, will provide a basis for estimating this parameter, or provide a different model for the removal of boron.

Although the temperature and humidity dependence of the above parameters could have been explicitly modeled, as was done to some degree in Section C.2, a constant temperature approximation has been used for this analysis. This is justified because the temperature change is small over the period of interest and the resulting parameter changes would be smaller than the ranges covered above.

These input parameters are summarized in Table 3-1.

Table 3-1. Summary of Input Parameters

Parameter	High	Low
Dissolved Fe upper limit (kg)	1.33	0.021
Stainless steel corrosion rate (kg/yr)	0.163	0.0544
Trapped B fraction, f	0.02.	0.05
Exchange efficiency	0.1	0.01*
Drip rate (mm/yr)	7.19	0.53*

* These values correspond to the medium values given in the analysis above; they are given here because they are the ones which will be used as the basis for the variations used in the calculations of Section 3-5.

3.3. Sample Configuration Bookkeeper Output

The listing below provides the results of a sample run of the configuration bookkeeper. The input parameter used in this sample run are as follows:

Stainless steel corrosion rate:	0.0544	kg/yr
Carbon Steel corrosion rate:	1.65	kg/yr
Drip Rate onto WP:	0.53	mm/yr
Exchange Efficiency:	0.01	
Boron Trapping Fraction	0.02	
Dissolved Iron in flooded WP:	0.021	kg

The first column lists time in years following initial WP breach. The next three columns list the amounts of boron remaining (in kg) in the plates, trapped in the oxide corrosion products, and in solution, respectively. The fifth column lists the total amount of boron remaining in the WP in kg. Similarly, the sixth column lists the total amount of iron, in kg, remaining in the WP. The last three columns indicate the amounts, in kg, of this total iron inventory, in the carbon steel components, the stainless steel plates, and oxide corrosion products from both sources.

```
Output file
nus=0.054400  nuc=1.650000  dr=0.530000  ex=0.010000  f=0.020000  s=0.021000  tt=0
   Time    B Stl Tr B Ox    B sltn    Tot B  Tot Fe   Cs Fe   Ss Fe   Oxide
   1000    29.59 0.01755 8.5e-001   30.458  5372.0  1864.0  1804.5  1703.5
   2000    28.71 0.03511 1.7e+000   30.421  5372.0   214.0  1750.9  3407.0
   3000    27.84 0.05266 2.5e+000   30.361  5372.0     0.0  1697.4  3674.6
   4000    26.96 0.07022 3.2e+000   30.278  5372.0     0.0  1643.9  3728.1
   5000    26.08 0.08777 4.0e+000   30.173  5372.0     0.0  1590.4  3781.6
   6000    25.20 0.10533 4.7e+000   30.046  5372.0     0.0  1536.8  3835.1
   7000    24.33 0.12288 5.4e+000   29.898  5371.9     0.0  1483.3  3888.6
   8000    23.45 0.14044 6.1e+000   29.730  5371.9     0.0  1429.8  3942.1
   9000    22.57 0.15799 6.8e+000   29.542  5371.9     0.0  1376.2  3995.6
  10000    21.69 0.17555 7.5e+000   29.334  5371.9     0.0  1322.7  4049.2
  11000    20.81 0.19310 8.1e+000   29.108  5371.9     0.0  1269.2  4102.7
  12000    19.94 0.21066 8.7e+000   28.864  5371.9     0.0  1215.7  4156.2
  13000    19.06 0.22821 9.3e+000   28.602  5371.9     0.0  1162.1  4209.7
  14000    18.18 0.24577 9.9e+000   28.323  5371.9     0.0  1108.6  4263.2
  15000    17.30 0.26332 1.0e+001   28.028  5371.8     0.0  1055.1  4316.7
  16000    16.43 0.28087 1.1e+001   27.716  5371.8     0.0  1001.6  4370.3
  17000    15.55 0.29843 1.2e+001   27.389  5371.8     0.0   948.0  4423.8
  18000    14.67 0.31598 1.2e+001   27.046  5371.8     0.0   894.5  4477.3
  19000    13.79 0.33353 1.3e+001   26.689  5371.8     0.0   841.0  4530.8
  20000    12.91 0.35109 1.3e+001   26.317  5371.8     0.0   787.5  4584.3
  21000    12.04 0.36864 1.4e+001   25.931  5371.8     0.0   733.9  4637.8
  22000    11.16 0.38620 1.4e+001   25.531  5371.8     0.0   680.4  4691.3
  23000    10.28 0.40375 1.4e+001   25.119  5371.8     0.0   626.9  4744.9
  24000     9.40 0.42130 1.5e+001   24.693  5371.8     0.0   573.4  4798.4
```

25000	8.53	0.43886	1.5e+001	24.255	5371.8	0.0	519.9	4851.9
26000	7.65	0.45641	1.6e+001	23.805	5371.8	0.0	466.3	4905.4
27000	6.77	0.47396	1.6e+001	23.344	5371.8	0.0	412.8	4958.9
28000	5.89	0.49152	1.6e+001	22.871	5371.8	0.0	359.3	5012.4
29000	5.02	0.50907	1.7e+001	22.387	5371.8	0.0	305.8	5066.0
30000	4.14	0.52662	1.7e+001	21.892	5371.7	0.0	252.3	5119.5
31000	3.26	0.54418	1.8e+001	21.386	5371.7	0.0	198.7	5173.0
32000	2.38	0.56173	1.8e+001	20.871	5371.7	0.0	145.2	5226.5
33000	1.50	0.57928	1.8e+001	20.345	5371.7	0.0	91.7	5280.0
34000	0.63	0.59684	1.9e+001	19.810	5371.7	0.0	38.2	5333.5
35000	0.00	0.60393	1.9e+001	19.267	5371.7	0.0	0.0	5371.7
36000	0.00	0.60393	1.8e+001	18.733	5371.7	0.0	0.0	5371.7
37000	0.00	0.60393	1.8e+001	18.214	5371.7	0.0	0.0	5371.7
38000	0.00	0.60393	1.7e+001	17.710	5371.7	0.0	0.0	5371.7
39000	0.00	0.60393	1.7e+001	17.220	5371.7	0.0	0.0	5371.7
40000	0.00	0.60393	1.6e+001	16.744	5371.7	0.0	0.0	5371.7
41000	0.00	0.60393	1.6e+001	16.282	5371.7	0.0	0.0	5371.7
42000	0.00	0.60393	1.5e+001	15.834	5371.7	0.0	0.0	5371.7
43000	0.00	0.60393	1.5e+001	15.398	5371.7	0.0	0.0	5371.7
44000	0.00	0.60393	1.4e+001	14.974	5371.7	0.0	0.0	5371.7
45000	0.00	0.60393	1.4e+001	14.563	5371.7	0.0	0.0	5371.7
46000	0.00	0.60393	1.4e+001	14.163	5371.7	0.0	0.0	5371.7
47000	0.00	0.60393	1.3e+001	13.775	5371.7	0.0	0.0	5371.7
48000	0.00	0.60393	1.3e+001	13.398	5371.7	0.0	0.0	5371.7
49000	0.00	0.60393	1.2e+001	13.032	5371.7	0.0	0.0	5371.7
50000	0.00	0.60393	1.2e+001	12.676	5371.7	0.0	0.0	5371.7
51000	0.00	0.60393	1.2e+001	12.330	5371.7	0.0	0.0	5371.7
52000	0.00	0.60393	1.1e+001	11.995	5371.7	0.0	0.0	5371.7
53000	0.00	0.60393	1.1e+001	11.669	5371.7	0.0	0.0	5371.7
54000	0.00	0.60393	1.1e+001	11.352	5371.7	0.0	0.0	5371.7
55000	0.00	0.60393	1.0e+001	11.044	5371.7	0.0	0.0	5371.7
56000	0.00	0.60393	1.0e+001	10.745	5371.7	0.0	0.0	5371.7
57000	0.00	0.60393	9.9e+000	10.455	5371.7	0.0	0.0	5371.7
58000	0.00	0.60393	9.6e+000	10.173	5371.7	0.0	0.0	5371.7
59000	0.00	0.60393	9.3e+000	9.899	5371.7	0.0	0.0	5371.7
60000	0.00	0.60393	9.0e+000	9.633	5371.7	0.0	0.0	5371.7
61000	0.00	0.60393	8.8e+000	9.375	5371.7	0.0	0.0	5371.7
62000	0.00	0.60393	8.5e+000	9.124	5371.7	0.0	0.0	5371.7
63000	0.00	0.60393	8.3e+000	8.880	5371.7	0.0	0.0	5371.7
64000	0.00	0.60393	8.0e+000	8.643	5371.7	0.0	0.0	5371.7
65000	0.00	0.60393	7.8e+000	8.413	5371.7	0.0	0.0	5371.7
66000	0.00	0.60393	7.6e+000	8.189	5371.7	0.0	0.0	5371.7
67000	0.00	0.60393	7.4e+000	7.972	5371.7	0.0	0.0	5371.7
68000	0.00	0.60393	7.2e+000	7.761	5371.7	0.0	0.0	5371.7
69000	0.00	0.60393	7.0e+000	7.556	5371.7	0.0	0.0	5371.7
70000	0.00	0.60393	6.8e+000	7.357	5371.7	0.0	0.0	5371.7
71000	0.00	0.60393	6.6e+000	7.164	5371.7	0.0	0.0	5371.7
72000	0.00	0.60393	6.4e+000	6.976	5371.7	0.0	0.0	5371.7
73000	0.00	0.60393	6.2e+000	6.794	5371.7	0.0	0.0	5371.7
74000	0.00	0.60393	6.0e+000	6.617	5371.7	0.0	0.0	5371.7
75000	0.00	0.60393	5.8e+000	6.444	5371.7	0.0	0.0	5371.7
76000	0.00	0.60393	5.7e+000	6.277	5371.7	0.0	0.0	5371.7
77000	0.00	0.60393	5.5e+000	6.115	5371.7	0.0	0.0	5371.7
78000	0.00	0.60393	5.4e+000	5.957	5371.7	0.0	0.0	5371.7
79000	0.00	0.60393	5.2e+000	5.804	5371.7	0.0	0.0	5371.7
80000	0.00	0.60393	5.1e+000	5.655	5371.7	0.0	0.0	5371.7
81000	0.00	0.60393	4.9e+000	5.510	5371.7	0.0	0.0	5371.7
82000	0.00	0.60393	4.8e+000	5.370	5371.7	0.0	0.0	5371.7
83000	0.00	0.60393	4.6e+000	5.234	5371.7	0.0	0.0	5371.7

84000	0.00	0.60393	4.5e+000	5.101	5371.7	0.0	0.0	5371.7
85000	0.00	0.60393	4.4e+000	4.972	5371.7	0.0	0.0	5371.7
86000	0.00	0.60393	4.2e+000	4.847	5371.7	0.0	0.0	5371.7
87000	0.00	0.60393	4.1e+000	4.726	5371.7	0.0	0.0	5371.7
88000	0.00	0.60393	4.0e+000	4.608	5371.7	0.0	0.0	5371.7
89000	0.00	0.60393	3.9e+000	4.493	5371.7	0.0	0.0	5371.7
90000	0.00	0.60393	3.8e+000	4.382	5371.7	0.0	0.0	5371.7
91000	0.00	0.60393	3.7e+000	4.274	5371.7	0.0	0.0	5371.7
92000	0.00	0.60393	3.6e+000	4.169	5371.7	0.0	0.0	5371.7
93000	0.00	0.60393	3.5e+000	4.067	5371.7	0.0	0.0	5371.7
94000	0.00	0.60393	3.4e+000	3.968	5371.7	0.0	0.0	5371.7
95000	0.00	0.60393	3.3e+000	3.871	5371.7	0.0	0.0	5371.7
96000	0.00	0.60393	3.2e+000	3.778	5371.7	0.0	0.0	5371.7
97000	0.00	0.60393	3.1e+000	3.687	5371.7	0.0	0.0	5371.7
98000	0.00	0.60393	3.0e+000	3.599	5371.7	0.0	0.0	5371.7
99000	0.00	0.60393	2.9e+000	3.513	5371.7	0.0	0.0	5371.7
100000	0.00	0.60393	2.8e+000	3.430	5371.7	0.0	0.0	5371.7
101000	0.00	0.60393	2.7e+000	3.349	5371.7	0.0	0.0	5371.7
102000	0.00	0.60393	2.7e+000	3.270	5371.7	0.0	0.0	5371.7
103000	0.00	0.60393	2.6e+000	3.194	5371.7	0.0	0.0	5371.7
104000	0.00	0.60393	2.5e+000	3.120	5371.7	0.0	0.0	5371.7
105000	0.00	0.60393	2.4e+000	3.048	5371.7	0.0	0.0	5371.7
106000	0.00	0.60393	2.4e+000	2.978	5371.7	0.0	0.0	5371.7
107000	0.00	0.60393	2.3e+000	2.910	5371.7	0.0	0.0	5371.7
108000	0.00	0.60393	2.2e+000	2.844	5371.7	0.0	0.0	5371.7
109000	0.00	0.60393	2.2e+000	2.780	5371.7	0.0	0.0	5371.7
110000	0.00	0.60393	2.1e+000	2.717	5371.7	0.0	0.0	5371.7
111000	0.00	0.60393	2.1e+000	2.657	5371.7	0.0	0.0	5371.7
112000	0.00	0.60393	2.0e+000	2.598	5371.7	0.0	0.0	5371.7
113000	0.00	0.60393	1.9e+000	2.541	5371.7	0.0	0.0	5371.7
114000	0.00	0.60393	1.9e+000	2.486	5371.7	0.0	0.0	5371.7
115000	0.00	0.60393	1.8e+000	2.432	5371.7	0.0	0.0	5371.7
116000	0.00	0.60393	1.8e+000	2.379	5371.7	0.0	0.0	5371.7
117000	0.00	0.60393	1.7e+000	2.329	5371.7	0.0	0.0	5371.7
118000	0.00	0.60393	1.7e+000	2.279	5371.7	0.0	0.0	5371.7
119000	0.00	0.60393	1.6e+000	2.231	5371.7	0.0	0.0	5371.7
120000	0.00	0.60393	1.6e+000	2.185	5371.7	0.0	0.0	5371.7
121000	0.00	0.60393	1.5e+000	2.139	5371.7	0.0	0.0	5371.7
122000	0.00	0.60393	1.5e+000	2.095	5371.7	0.0	0.0	5371.7
123000	0.00	0.60393	1.4e+000	2.053	5371.7	0.0	0.0	5371.7
124000	0.00	0.60393	1.4e+000	2.011	5371.7	0.0	0.0	5371.7
125000	0.00	0.60393	1.4e+000	1.971	5371.7	0.0	0.0	5371.7
126000	0.00	0.60393	1.3e+000	1.932	5371.7	0.0	0.0	5371.7
127000	0.00	0.60393	1.3e+000	1.894	5371.7	0.0	0.0	5371.7
128000	0.00	0.60393	1.3e+000	1.857	5371.7	0.0	0.0	5371.7
129000	0.00	0.60393	1.2e+000	1.821	5371.7	0.0	0.0	5371.7
130000	0.00	0.60393	1.2e+000	1.786	5371.7	0.0	0.0	5371.7
131000	0.00	0.60393	1.1e+000	1.752	5371.7	0.0	0.0	5371.7
132000	0.00	0.60393	1.1e+000	1.720	5371.7	0.0	0.0	5371.7
133000	0.00	0.60393	1.1e+000	1.688	5371.7	0.0	0.0	5371.7
134000	0.00	0.60393	1.1e+000	1.657	5371.7	0.0	0.0	5371.7

A series similar runs based on various combinations of the parameters in Table 3-1. were performed. The results of these runs were used in combination with the information provided in Section C.2. to guide the criticality analyses summarized in Section C.4

4. Waste Package Criticality Analyses

4.1. MCNP Calculations For Degraded Configurations

Of the discrete degraded mode configurations discussed in Sections C.2 and C.3, two sets were found to be most relevant to the current level of study. The values of k_{eff} are given as a function of percentages which must be converted into mass of boron and iron to be useful in the present model. These conversions are given in Attachment VIII of Ref. C.9-5. The results are presented in the tables below.

(1) Partial Basket

The carbon steel tubes and guides have completely oxidized. The basket structure has collapsed, however, the fuel assemblies are still separated by the borated stainless steel plates between them. The borated stainless steel has partially corroded, with most of the borides conservatively assumed to quickly oxidize and immediately dissolve due to the high solubility of boron oxide. However, a small amount of boron remains trapped within the corrosion products. Although MCNP calculations did not explicitly model the trapped boron fraction, f, it is assumed that the results will be relatively insensitive to whether this small amount of boron is at the position initially occupied by the borated stainless steel plates or uniformly distributed throughout the package void space, as is assumed in the MCNP calculations. Table 4-1 below lists the results of the MCNP k_{eff} calculations for variations of this degraded configuration. In this table, the iron mass is the sum of the iron in the remaining uncorroded stainless steel plus the undissolved oxide, and the only boron is that remaining in the uncorroded stainless steel.

Table 4-1. Progressive Degradation of Borated Stainless Steel Control Panels

% SS-B Plate Thickness Remaining	% of WP Void Space Filled With Fe_2O_3	kg Fe	kg B	10,000 yr k_{eff}
50	0	929	15.24	0.917
50	10	2978	15.24	0.851
25	20	4608	7.618	0.857
25	15	3572	7.618	0.880
10	25	5399	3.05	0.887
10	20	4392	3.05	0.908
10	10	2271	3.05	0.944

(2) Assemblies Touching

The borated stainless steel is fully corroded, with large amounts of iron oxide remaining from corrosion of the carbon steel tubes and guides, and the stainless steel plates. With complete degradation of the stainless steel plates separating them, the fuel assemblies are assumed to have settled through the oxides and are now touching. Only small amounts of boron remain trapped within the mass of oxides, and are only released into solution as the oxide itself dissolves. The MCNP calculations modeled this configuration set with both the Fe and B uniformly distributed throughout the package void space. It is assumed that the k_{eff} calculated is a conservative approximation to the values which would be obtained by a more explicit model with some specific fraction of the Fe and B remaining in solid form at the initial location of the basket. Table 4-2 provides the results of the k_{eff} calculations for variations of this degraded configuration.

Table 4-2. Basket Structure Gone, Uniform Iron Oxide and Boron Concentration

% of WP Void Filled With Fe_2O_3	% of Original B-10 Remaining In WP	kg Fe	kg B	10,000 yr k_{eff}
30	0	6283	0.0	0.928
30	2	6283	0.6	0.913
30	5	6283	1.5	0.890

Table 4-2. Basket Structure Gone, Uniform Iron Oxide and Boron Concentration

% of WP Void Filled With Fe_2O_3	% of Original B-10 Remaining In WP	kg Fe	kg B	10,000 yr k_{eff}
20	0	4188	0.0	0.979
20	5	4188	1.5	0.941
20	10	4188	3.05	0.902
20	15	4188	4.57	0.872
10	10	2094	3.05	0.947
10	15	2094	4.57	0.909
10	20	2094	6.1	0.879

Both these sets also assumed that the carbon steel had already corroded by the time of the stated stainless steel corrosion, with the corrosion products contributing to the reservoir of iron oxide which is uniformly distributed throughout the water in the waste package.

4.2. Regression Analysis of the Data

The regression lines and goodness-of-fit for the two configurations are given by the following equations (where Fe is in metric tons and B is in kilograms):

Partial basket:

$$k_{eff} = 1.026 - 0.0242*Fe - 0.00645*B, \qquad R^2=0.91$$

Assemblies touching:

$$k_{eff} = 1.068 - 0.0221*Fe - 0.0236*B, \qquad R^2=0.99$$

Pooled data sets (17 data points):

$$k_{eff} = 0.989 - 0.0132*Fe - 0.00679*B, \qquad R^2=0.54.$$

It should be noted that the partial basket regression implicitly incorporates the effect of decreasing basket thickness, which is generally proportional to the explicitly decreasing amounts of boron and iron.

The fact that the pooled data set has such a small R^2 indicates that the two sets represent somewhat different physical processes, which is consistent with the fact that the partial basket variation incorporates the effect of varying assembly spacing, while the assemblies touching case does not. This distinction will be reflected in the calculations of earliest time to criticality performed in Section C.5. In those calculations the boron and iron concentrations are decreased at each time step to reflect the corrosion and removal process, and at each time step the k_{eff} is calculated as a function of the remaining boron and iron, using the partially basket regression while the stainless steel is still intact and the assemblies touching regression after the stainless steel has completely corroded.

Currently, these models also assume that the configuration occurs at the time of peak post-closure k_{eff} ($\approx$10,000 years). Future versions of these k_{eff} fits will also incorporate the effects of time, once sufficient MCNP runs have been performed to characterize this effect for each configuration.

5. Earliest Times To Internal WP Criticality

The final step in the process is to integrate the configuration dependent keff regressions with the configuration bookkeeper to allow an estimate of the flooded and degrading WP keff as a function of time. In the configuration bookkeeper, the boron and iron concentrations are decreased at each time step to reflect the corrosion and removal process. In this simple deterministic example, the five basic parameters affecting the corrosion of basket materials and the removal of boron and iron from the WP are varied between the high and low values discussed in Section C.3. The minimum amount of time required to remove sufficient boron and iron such that the flooded WP k_{eff} exceeds 0.91 (chosen as the deliminator for criticality based on the 10CFR60.131(b)(7) required 5% margin of safety and the estimated bias and uncertainty of the MCNP calculation) is estimated for various combinations of the five parameters. Future versions of the configuration bookkeeper will have probability distributions assigned to these parameters so that the probability of exceeding the defined criticality limit as a function of time can be estimated.

5.1. Calculation of Earliest Time to Criticality

The calculations generally show the greatest sensitivity to the corrosion rate of borated stainless steel, so all calculations are presented for both high and low values of this parameter. The dependence on the other four parameters is demonstrated with two combination sets. For the first combination set four configurations are generated by selecting one parameter at a time to have its high value with the other three parameters having their low values. The results are given in Table 5-1. For the second combination set, six configurations are generated by selecting two parameters at a time to have high values, with the other two parameters having low values. The results are given in Table 5-2. It should be noted that the trapped boron fraction, f, is the only parameter which is negatively correlated with criticality, so its lower numerical value is actually its high value, as was indicated in Table C-7.

The following observations on the results presented in Tables 5-1 and 5-2 are of interest:

- For all of the cases the remaining iron oxide is in excess of 5,300 kg, which is nearly all the iron in the intact basket. The boron remaining is less than 2 kg, which means that most of it has been removed. This is a consequence of the Fe solution limit, which keeps most of the iron in solid oxide, even at the high exchange rate.

- Under the worst case conditions: (1) waste package filling with water and remaining filled for tens of thousands of years, (2) a high value for both the drip rate (7.19 mm/yr, which is two orders of magnitude above the present value), and (3) a high value for the exchange rate, the smallest time to criticality can be, 12,000 years following penetration of the waste package barriers. The simultaneous occurrence of these three conditions should be considered extremely unlikely.

- Although not directly apparent, some significant effect of lowering the Fe solubility limit when the trapped boron fraction is large can be inferred by comparing the last 2 lines of Table 5-2 with the 2 lines immediately above. Comparing the times for the same stainless steel corrosion rates there is seen to be only a 50% decrease while increasing the drip rate by more than an order of magnitude. This limitation to a small decrease is due to the large decrease in the iron solubility limit (going from 1.33 kg to 0.021 kg) which keeps a significant amount of boron trapped in the oxide. This behavior is in contrast with the same change in parameters going from the first 2 lines of the table to the third and fourth lines. In this comparison the decrease is approximately an order of magnitude. The fundamental difference is that the trapped boron is very low so lowering the Fe solubility limit to slow the removal of the oxide has little effect. The influence of Fe solubility limit is more strongly demonstrated in the sensitivity study in the next Section.

Table 5-1. Times to earliest possible criticality with one parameter high

SS Corrosion rate (kg/yr)	Drip rate (mm/yr)	Exchange efficiency	f, Trapped boron fraction	Fe sol limit (kg)	High parameter	Earliest time to criticality (yr)
0.0544	0.53	0.01	0.02	0.021	f	1.35×10^5
0.163	0.53	0.01	0.02	0.021	f	1.22×10^5
0.0544	0.53	0.01	0.05	1.33	Fe sol	2.06×10^5
0.163	0.53	0.01	0.05	1.33	Fe sol	1.92×10^5
0.0544	7.19	0.01	0.05	0.021	Drip rate	4.21×10^4
0.163	7.19	0.01	0.05	0.021	Drip rate	2.16×10^4
0.0544	0.53	0.1	0.05	0.021	Exchg	4.58×10^4
0.163	0.53	0.1	0.05	0.021	Exchg	2.61×10^4

Table 5-2. Times to earliest possible criticality with two parameters high

SS Corrosion rate (kg/yr)	Drip rate (mm/yr)	Exchange efficiency	f, Trapped boron fraction	Fe sol limit (kg)	High parameters	Earliest time to criticality (yr)
0.0544	0.53	0.01	0.02	1.33	f, Fe sol	1.35×10^5
0.163	0.53	0.01	0.02	1.33	f, Fe sol	1.22×10^5
0.0544	7.19	0.01	0.02	0.021	f, Drip rate	3.67×10^4
0.163	7.19	0.01	0.02	0.021	f, Drip rate	1.62×10^4
0.0544	0.53	0.1	0.02	0.021	f, Exchg	3.84×10^4
0.163	0.53	0.1	0.02	0.021	f, Exchg	1.89×10^4
0.0544	7.19	0.01	0.05	1.33	Fe, Drip rate	4.16×10^4
0.163	7.19	0.01	0.05	1.33	Fe, Drip rate	2.14×10^4
0.0544	0.53	0.1	0.05	1.33	Fe, Exchg	4.53×10^4
0.163	0.53	0.1	0.05	1.33	Fe, Exchg	2.58×10^4
0.0544	7.19	0.1	0.05	0.021	Dr, Exchg	2.85×10^4
0.163	7.19	0.1	0.05	0.021	Dr, Exchg	1.20×10^4

5.2. Sensitivity Analysis: Extending the Range of the Trapped Boron Fraction

Increasing the value of trapped boron fraction only slightly above 0.05 will markedly increase the earliest time to criticality. With the same configuration selection scheme as was used for Tables 5-1 and 5-2, above, the range of values is changed to 0 to 0.055. The results are presented in Tables 5-3 and 5-4, below.

The following observations on the sensitivity results presented in Tables 5-3 and 5-4 are of interest:

- The earliest times to criticality for the f=0 cases show only a small decrease compared with the corresponding f=0.02 cases in Tables 5-1 and 5-2, indicating that f=0.02 does not trap enough boron in the oxide to prevent criticality.
- The last 4 lines of Table 5-3 show the striking effect of lowering the Fe solubility limit when the trapped boron fraction exceeds a threshold. This is in contrast with the first 2 lines of the table which also have the lower value of Fe solubility, but the trapped boron fraction is zero so there is little effect.
- Comparison of the last 2 lines in Table 5-4 with the 2 lines immediately above shows that only a slight change from f=0.050 to f=0.055 has reversed the relative dominance of drip rate and Fe solubility limit. Instead of a 50% decrease in earliest time to criticality when going from high Fe solubility limit and low drip rate to low Fe solubility limit and high drip rate, Table 5-4 shows nearly a 100% increase.

Table 5-3. Sensitivity to trapped boron fraction with one parameter high

SS Corrosion rate (kg/yr)	Drip rate (mm/yr)	Exchange efficiency	f, Trapped boron fraction	Fe sol limit (kg)	High parameter	Earliest time to criticality (yr)
0.0544	0.53	0.01	0	0.021	f	1.20×10^5
0.163	0.53	0.01	0	0.021	f	1.07×10^5
0.0544	0.53	0.01	0.055	1.33	Fe sol	6.61×10^5
0.163	0.53	0.01	0.055	1.33	Fe sol	5.64×10^5
0.0544	7.19	0.01	0.055	0.021	Drip rate	$>10^6$
0.163	7.19	0.01	0.055	0.021	Drip rate	$>10^6$
0.0544	0.53	0.1	0.055	0.021	Exchg	$>10^6$
0.163	0.53	0.1	0.055	0.021	Exchg	$>10^6$

Table 5-4. Sensitivity to trapped boron fraction with two parameters high

SS Corrosion rate (kg/yr)	Drip rate (mm/yr)	Exchange efficiency	f, Trapped boron fraction	Fe sol limit (kg)	High parameters	Earliest time to criticality (yr)
0.0544	0.53	0.01	0	1.33	f, Fe sol	1.19×10^5
0.163	0.53	0.01	0	1.33	f, Fe sol	1.07×10^5
0.0544	7.19	0.01	0	0.021	f, Drip rate	3.55×10^4
0.163	7.19	0.01	0	0.021	f, Drip rate	1.51×10^4
0.0544	0.53	0.1	0	0.021	f, Exchg	3.68×10^4
0.163	0.53	0.1	0	0.021	f, Exchg	1.73×10^4
0.0544	7.19	0.01	0.055	1.33	Fe, Drip rate	6.05×10^4
0.163	7.19	0.01	0.055	1.33	Fe, Drip rate	4.97×10^4
0.0544	0.53	0.1	0.055	1.33	Fe, Exchg	8.13×10^4
0.163	0.53	0.1	0.055	1.33	Fe, Exchg	6.73×10^4
0.0544	7.19	0.1	0.055	0.021	Dr, Exchg	3.18×10^5
0.163	7.19	0.1	0.055	0.021	Dr, Exchg	2.68×10^5

INTENTIONALLY LEFT BLANK

6. External Criticality Scenario Generation

6.1. Maximum uranium concentrations which could occur beneath Yucca Mountain

6.1.1 Applicability of other districts

In a study of radioactive mineral occurrences in Nevada, L.J.Garside has suggested (Ref C.9-26, p. 8) that, "charcoal carbonization of wood at the base of ash-flow tuffs [serves] as a precipitant for uranium." He also suggests that organic matter can serve as a food for anaerobic bacteria producing H_2S which is also an effective uranium reductant. However, there is no direct evidence of any uranium deposits in tuff resulting from this mechanism, and the same reference notes that the uranium deposits at Coaldale Prospect [a low-grade Tertiary occurrence in Miocene sedimentary rock some 200 km northwest of Yucca Mountain] are not replacement deposits.

Although oil occurs in Nevada, it is not likely to be a reductant for dissolved uranium at Yucca Mountain. Oil accumulations in Railroad Valley appear to have migrated from the Chainman Shale (Ref. C.9-27, p. 10), and are not likely to be duplicated at Yucca Mountain because the recent higher temperature history in that vicinity would have decomposed any oil (Grow et.al., Ref. C.9-28, p. 1298). Therefore, the identified Nevada oil accumulations are not analogous to any known conditions at Yucca Mountain.

With this evidence, it could be assumed that the organic deposits in Nevada are too weak to reduce uranium to concentrations found on the Colorado Plateau, let alone to the much higher concentrations found at Oklo. Nevertheless, since carbonaceous deposits of the log type do exist in Nevada at the base of ash-flow tuffs (Ref C.9-26, p. 8), and since a recognized geologic study has suggested that they could serve as a precipitant, it will be prudent to include the possibility in this analysis. For calculation purposes it will be assumed that logs could exist at the base of the tuff in Yucca Mountain (which is approximately 1 km below the repository) and in the concentration which appears on the Colorado Plateau. It is also assumed that any distribution of logs which did occur at the base of the tuff would not have a higher concentration than those found on the Colorado Plateau. It is not considered possible to have any significant organic accumulation within the tuff because the hot ash would have oxidized any organic material as it was deposited. The organic accumulations in tuff elsewhere in Nevada are attributable to carbonaceous material that occurs beneath the layers of tuff.

Although a reducing zone in the form of organic logs is conservatively assumed to be possible at the unconformity beneath the tuffs at Yucca Mountain, any significant roll-front deposition in tuff must be considered to be very unlikely, because fractures rather than interstitial porosity are thought to control fluid flow. In contrast, the interconnected porous grain structure of sandstone provides a more uniform permeability throughout the bulk of the rock.

6.1.2 Potential for uranium concentration within the tuff at Yucca Mountain

The maximum concentration of uranium which the zeolite clinoptilolite could accumulate by the ion-exchange mechanism from uranium-bearing groundwater at Yucca Mountain is most likely constrained by the maximum reported for natural deposits which have formed by this process. These maximum concentration occurrences include 0.5% at the Tono Mine in Japan (Ref. C.9-15, pp. 445,446, Figure 9 and Table I), or 0.7% at the more closely analogous Northern Reese River Valley (Ref. C.9-29), or just under 1%, the maximum observed in the laboratory using uranium saturated water (Ref. C.9-15, p. 448).

For a maximum theoretically possible value, it is possible to make a more conservative estimate under the assumption that the uranyl ion could replace all the Ca ion in the clinoptilolite. Using the chemical formula for clinoptilolite, $K_{0.6}Na_{0.2}Ca_3Al_{6.8}Si_{29.2}O_{72}\cdot 1.6H_2O$, and replacing 3 Ca with 3 UO_2, gives a uranium weight fraction of clinoptilolite of g_u=0.236. The following assumptions are used to convert this weight fraction of clinoptilolite to a weight fraction of rock: (1) both tuff and clinoptilolite have a density of approximately 2.52 g/cm^3, (2) the rock matrix is 70 vol% clinoptilolite and 30 vol% other mineral phases, and (3) the rock has 30 vol% porespace which is filled with water. These assumptions give the following volume fractions of the rock:

ordinary clinoptilolite	$v_{co} = .7*(1-.3) = 0.49$
tuff	$v_t = .3*(1-.3) = 0.21$
water	$v_w = 0.3$

If R is the ratio of the molecular weight of clinoptilolite with calcum replaced by uranium divided by the molecular weight of ordinary clinoptilolite (R=1.245), the overall density of the rock, with Ca replaced by UO_2 and including water, is

$$\rho_R = 2.52(Rv_{co}+v_t)+v_w = 2.37$$

The weight and volume fractions of UO_2 can then be computed from

$$w_{uo2} = g_u R \rho_{co} v_{co} / \rho_R = .149$$
$$v_{uo2} = w_{uo2} \rho_R / \rho_{uo2} = .032,$$

where ρ_{uo2} is the density of UO_2 =10.96 g/cm^3 and ρ_{co} is the density of clinoptilolite = 2.52 g/cm^3

Figure 6-5 shows that this volume fraction of UO_2 gives a k_∞ less than 0.88, so it is impossible to form a critical mass from zeolite in tuff, even if all the Ca is replaced by commercial SNF UO_2 from uranium bearing groundwater.

6.1.3 Potential uranium concentrations from reducing environments at the bottom of the tuff at Yucca Mountain

For purposes of estimating required critical mass (or radius) the nominal value of the uranium concentration which could be precipitated by an organic reducing zone beneath the repository could be conservatively estimated by the maximum concentration of uranium in the logs of the Colorado Plateau, which has been given in Section C.1.3 as 20%. However, as an extra measure of conservatism, the MCNP analyses will be conducted over a range of values from this maximum to the worldwide peak concentration observed at Oklo, 60%.

INTENTIONALLY LEFT BLANK

7. Far-Field Criticality Analysis

A set of 10 uranium/water concentrations in tuff was evaluated to determine the minimum critical mass/radius spheres. This set represented 3 SNF types, chosen to represent the 2%, 4%, and 13% most stressing fuel with respect to fissile content. For each of these fuel types, the analysis was a two step process. First the most critical volume % UO_2 (highest k_∞) was determined for a family of water concentrations calculating k_∞, using MCNP, for a range of UO_2 volume %. The k_∞ values for one fuel type (PWR, 3% initial enrichment, 20 GWd/MTU) are shown in Figure 6-5. [It should be noted that the water concentrations in this figure are expressed as a volume percent of the tuff water mixture without uranium (for convenience of analysis in Ref. C.9-30 from which the figure is taken), while the UO_2 concentrations are expressed as a volume percent of the total rock (including the UO_2).]

The second step is to calculate the k_{eff}, again using MCNP, for a range of radii, and interpolate to determine the critical radius, at which the value of k_{eff} is equal to the criticality threshold. The most appropriate value of criticality threshold k_{eff} was 1-(bias and uncertainty of the computational process) - (twice standard deviation of the specific Monte Carlo calculation). For these cases, the bias and uncertainty is lower than the usual value because it refers to the fissile content only. This is because we have made the *conservative assumption that none of the neutron absorbers from the SNF are in the uranium-bearing groundwater from the repository*, either having been removed from the SNF matrix much earlier than the fissile nuclides, or having remained in the matrix after removal of the fissile material. This process is illustrated in Figure 7-2, for the UO_2 concentration giving the highest peak k_∞ for the family of water concentrations in Figure 7-1. Both figures are from Ref. C.9-30.

The details of the calculations are given in Ref. C.9-30. The results are summarized in Table 7-1.

Table 7-1. Representative SNF/environment configurations and resulting spherical critical masses

SNF enrich & burnup (GWd/MTU)	Fissile % of SNF**	UO_2 vol % in rock*	H_2O vol % in rock*	UO_2 wt % in rock†	H_2O wt % in rock	Critical mass (MTU)*
3%, 20	1.94	18.5	38.3	58	11	1.6
3%, 20	1.94	8	43.2	35	17	10.1
3%, 20	1.94	17	33.2	54	9.6	2.50
3%, 20	1.94	8	36.8	33	14	10.1
3%, 20	1.94	15	25.5	48	7.5	6.5
3%, 20	1.94	10	27.0	37	9.1	7.4
3%, 20	1.94	8	27.6	32	10	18.0
3%, 20	1.94	11.6	17.7	39	5.5	55.2
3.5%, 30	1.87	14	25.8	46	7.8	11.1
4.0%, 40	1.82	15	25.5	48	7.5	30.9

* These values correspond to those given in Ref. C.9-30, Section 8.

** These values were derived under worst case reactor burn conditions, as contrasted with average reactor burn conditions used to develop the CDB data (Ref. C.9-6).

† The UO_2 wt % is computed from the volume percents by the formula $10.96U_{v\%}/(10.96U_{v\%}+W_{v\%}+2.52T_{v\%})$, and the water wt% in a similar manner, where $U_{v\%}$ is the volume percent of UO_2, $W_{v\%}$ is the volume percent of water and $T_{v\%}$ is the volume percent of tuff.

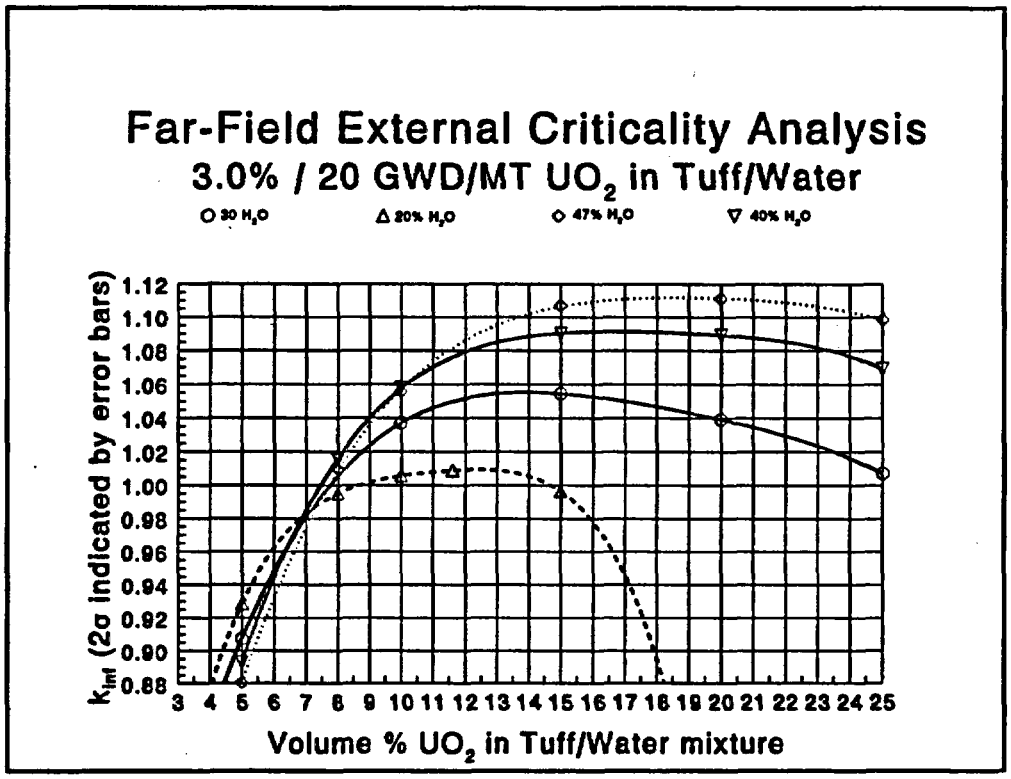

Figure 7-1.

Note:Error bars were not plotted if the 2σ value was smaller than the data point marker.

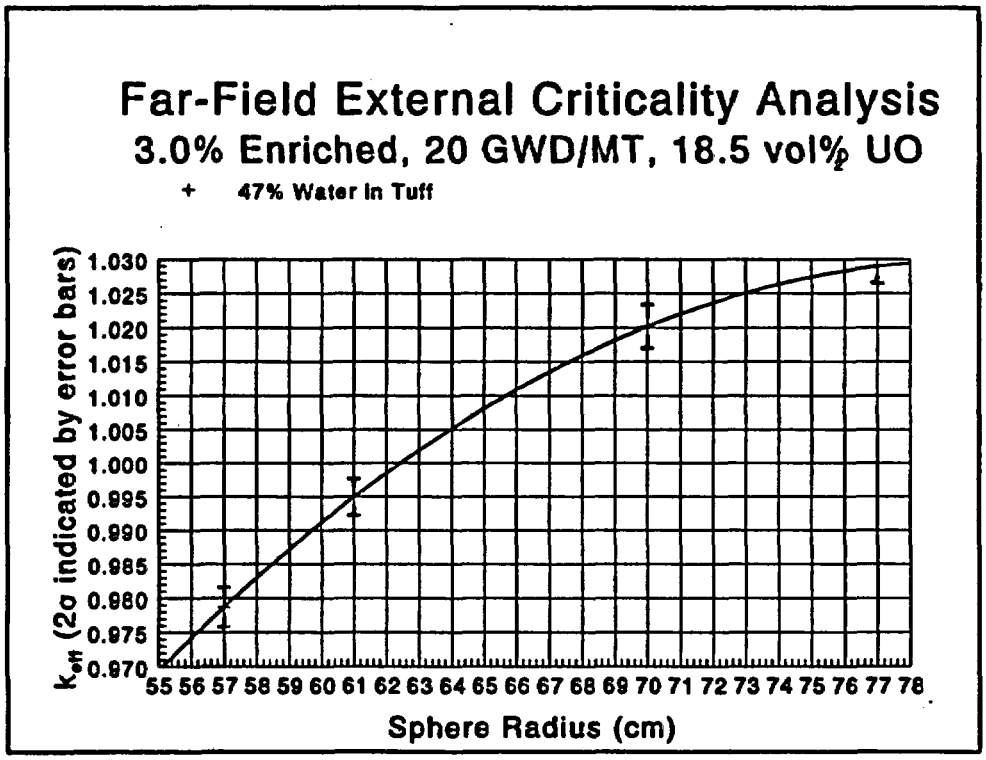

Figure 7-2.

INTENTIONALLY LEFT BLANK

8. Probability of Assembling a Far-Field Critical Mass

The methodology described in this section is based on the assumption that the mass provided by a single log will be insufficient for criticality. The validity of this assumption is demonstrated in Section C.8.2, below. Because of this insufficiency, any reducing zone capable of adsorbing a critical mass will have to be built from a juxtaposition of logs.

8.1. Methodology

The upper bound for the probability of the groundwater from a single waste package precipitating into a critical mass is determined by combining two independent probabilities, according to the following formula

$$Pr\{\text{critical precip per pkg}\} = Pr\{\text{log}\} * Pr\{\text{clusterllog}\},$$

where Pr{log} is the probability of the repository effluent encountering a carbonized log, and Pr{clusterllog} is the probability that the log is part of a cluster of sufficient size to precipitate a critical mass. The required cluster size, or mass, is inversely proportional to the fissile content of the fuel in the waste package which served as the source of the groundwater flow, and is also inversely proportional to the uranium and water concentrations, as indicated in the results of the previous section (Table 7-1).

The total probability of criticality is obtained by multiplying Pr{critical precip per pkg} by the number of waste packages having sufficient fissile percentage to produce a criticality with the cluster size associated with the corresponding Pr{clusterllog}.

The next two sections describe the computation of Pr{clusterllog} and of Pr{log}.

8.2. Probability of reducing material, Pr{clusterllog}

This section is a summary of the data analysis and calculations described in Attachment II of Reference C.9-6.

The concentrations of uranium required for criticality can be modeled by the juxtaposition of logs onto a circle through the cross section of the critical mass sphere, to achieve the specified critical

mass (upwards of 1 metric ton UO_2). The probability of such random juxtapositions is built from the probability distributions of log length and of uranium concentration within the log.

In this model, three log parameters are generated from specific distributions: log length, potential concentration of uranium, and log radius. For the distribution of log lengths, the analysis of Attachment III of Ref. C.9-6 shows a negative exponential distribution with a floor of 3.0 meters and a decay length of 4.6 meters.

Based on analysis of 3 data sources in Attachment II of Ref. C.9-6, a uniform distribution between 1% and 21.5% is used for potential uranium concentration

$$f_c(x) = 1/(x2-x1) \qquad \text{for } x1<x<x2$$

where x is expressed as a fraction (instead of a percent) to correspond to the actual mathematics of calculation used in the program listing below, and the constant values are x1=0.01, x2=0.215. This distribution gives an average ore grade (U_3O_8 concentration) of 11.25%.

It should be noted that for the highest concentration in this distribution, 21.5wt% (4.3 vol% assuming 47 vol% water in the remaining rock, or 4.6 vol% assuming 40 vol% water in the remaining rock), $k_\infty<0.9$, as can be seen from Figure 7-1, so there is no possibility of criticality of any size log of this concentration. It is still necessary, however, to consider the juxtaposition of logs as representing the possibility of higher concentrations, even though no single log could reach such high concentrations. The juxtaposition of material presumes the organic material in multiple logs is chemically concentrated. The concentration of organic material provides a concentrated reducing zone with the capability of producing uranium concentrations higher than possible with individual logs.

Although no geological analogs for such an organic reducing zone concentration process exist in the United States, it is thought that some highly concenrated organic reducing zone was responsible for the highest uranium concentrations observed at Oklo (up to 60%, Ref. C.9-9, p. 20). In the absence of a geochemical model of the transformations which would be required for such a concentration process, the probabilistic/analog analysis is offered as a very conservative estimate of the actual risk. The probabilities of occurrence of the actual physical and chemical processes are currently unknown. Because of the lack of direct observations of the actual occurrence of such processes, any associated probabilities are assumed to be quite small.

For the distribution of log radii, the smallest of 4 diameters cited by Hess (Ref C.9-17, pg 467), 16 inches, which translates into a radius of 20 cm, is used as the lower limit. The distribution is taken to be triangular with peak at this lower limit, based on anecdotal information from those who have seen the logs (e.g. Ref. C.9-31) and the assumption that only the few largest logs are of sufficient interest to be reported in the literature. Since the probability density of a triangular decreases to zero at the upper limit, this upper limit is taken to be well above radius corresponding to the maximum observed diameter, 4 feet (61 cm radius) given by Hess. This distribution is a conservative model because the Hess article is primarily interested in reporting the largest ore concentrations, which would correspond to the largest logs. This conservative designation for the model is also consistent with the Chenoweth (Ref. C.9-18, pg 166) statement cited above that the largest log diameter is 1 meter. The pdf for the resulting triangular distribution is

$$f_r(r) = 2(rl2-r)/(rl2-rl1)^2 \qquad \text{for } rl1<r<rl2$$

where rl1=0.20 meter, rl2=0.80 meter.

As a worst case, the potential for criticality of the largest log can be estimated under the further conservative approximation that it contain the maximum possible uranium concentration, 21.5 wt%. It was already shown, above, that $k_\infty<0.9$; however, it is of interest to evaluate k_{eff} for this case. For 4.6 vol% UO_2, with the remaining rock being 40 vol% water and 60 vol% tuff, k_{eff} = 0.79 (Ref. 5.43).

The methodology can now be summarized by an algorithm stated as follows: (1) Determine a critical mass - critical radius pair from the set generated in Ref. C.9-30, and apply the adjustment factors 0.325 and 0.686, respectively, as a measure of conservatism to account for the neutron contribution of the portions of the logs falling outside the critical sphere; (2) Select the three random parameters for a sample log from the appropriate distributions as described above (log length, log radius, uranium wt%); (3) Calculate the contributed mass for this log from Eq (2), above and accumulate the sum of the masses of overlapping logs thus far; (4) Multiply the accumulated probability by the value for this log as computed from Eq (1) of Attachment II, using the uncorrected sphere radius; (5) If the accumulated mass is greater than the required critical mass, end the calculation and report the remaining probability, otherwise repeat steps (2) through (5) for the next log. This algorithm is repeated, starting with step 1, for each critical mass - critical radius pair in the set generated in Ref. C.9-30.

Table 8-1 Upper bound of probabilities of log clusters which could be capable of precipitating a uranium concentration sufficient for criticality

Fissile %	UO_2 g/cm^3	H_2O g/cm^3 *	Critical radius (m)†	Critical mass (metric ton)†	Pr{clusterllog} ‡
1.94	2.03	0.383	0.394	0.520	1.58×10^{-4}
1.94	0.877	0.432	0.961	3.283	3.71×10^{-14}
1.94	1.86	0.332	0.470	0.813	9.63×10^{-7}
1.94	0.877	0.368	0.961	3.283	8.31×10^{-11}
1.94	1.64	0.255	0.673	2.112	1.52×10^{-11}
1.94	1.10	0.270	0.803	2.405	1.43×10^{-10}
1.94	0.877	0.276	1.167	5.850	1.52×10^{-21}
1.94	1.27	0.177	1.496	17.940	1.03×10^{-57}
1.87	1.53	0.258	0.824	3.608	4.7×10^{-18}
1.82	1.64	.255	1.133	10.042	7.18×10^{-46}

* This column is simply the vol% water of Table 7-1 divided by 100.

† These columns computed in Attachment II, Ref. C.9-6 as adjustments from the values in Ref. C.9-30. The critical mass is, therefore, adjusted from the values given in Table 7-1

‡ The arithmetic means from Attachment II, Ref. C.9-6 have been used for conservatism.

8.3. Probability of encountering a log, Pr{log}

The calculations of this section are based on the possible analogy between the planar distribution of logs observed on the Colorado Plateau and logs which could be distributed somewhere at the base of the tuff beneath Yucca Mountain.

Since there are no statistics on logs at the base of the ash-flow tuff of Yucca Mountain, there is no direct way to estimate Pr{log}. A very conservative upper bound can, however, be developed from statistics of the log occurrences on the Colorado Plateau, according to the formula

Pr{log} = (Area occupied by logs)/(Area of sample space),

where the sample space is the area which has been investigated for logs. The analysis starts with

the 84 logs counted in the 87,000 m^2 orebody described by Fischer (Ref. C.9-32). Using the triangular distribution of log radii given above, the average radius can be calculated as 40 cm so that the average diameter is 80 cm. Using the negative exponential distribution of log lengths given above, an average of 7.6 meters is calculated. The total cross-section area of 84 logs lying horizontally is 511 m^2. The question is what larger area (or sample space) this represents.

Chenoweth (Ref C.9-29) has estimated that the geologic formation of the Colorado Plateau in which the logs are found occupies 1100 square miles (2850 km^2). He has also estimated that there are 165 orebodies similar to the one mapped by Fischer in this area. Since these orebodies have not been mapped for log occurrences, the best estimate of the total log area in this 2850 km^2 sample space would be to simply multiply the 511 m^2 of the Fischer orebody by 165, giving a total log area of 84,000 m^2. This analysis is equivalent to the assumption that the sample space for the distribution of organic deposits (to be found at the base of the tuff under Yucca Mountain) is the entire geologic formation containing log deposits in orebodies on the Colorado Plateau.

An alternative, and more conservative, interpretation would be that the identified orebodies do not represent all the occurrences of logs, only those which would be mineralized. To be mineralized, the organic log must not only exist, it must also be contacted by a uranium-bearing groundwater. Since there is no way to estimate the number of unmineralized logs in the large sample space identified by Chenoweth, the alternative is to use a smaller sample space. This can be defined by examining a map of orebodies in a buried river channel given in Thamm et. al. (Ref C.9-31, p. 50) which shows the orebodies to be occupying approximately 7% of the riverbed. Since the entire river channel was probably exposed to the same uranium-bearing groundwater, all identified orebodies should represent all the organic matter present. Hence the area of this smaller, more conservative, sample space could be estimated by dividing the area of the orebody by .07. This analysis is equivalent to the assumption that the sample space for the distribution of organic deposits (to be found at the base of the tuff under Yucca Mountain) is a typical buried river channel found on the Colorado Plateau and diagrammed in Ref. C.9-31, and that such a buried river channel exists at the base of the tuff beneath Yucca Mountain.

The results for the two alternative interpretations are given in the following table.

Table 8-2 Alternative estimations of probability of encountering a log

Sample Space	Area of sample space (km^2)	Total log area in sample space (m^2)	Pr{log}
Underground river channel	1.24*	511	4.1×10^{-4}
Geologic formation	2850	84,000	2.9×10^{-5}

* Calculated from Ref C.9-31, figure 16.

8.4. Calculation of expected number of criticalities

The expected number of criticalities is the product of three factors:

- The number of waste packages with sufficient fissile content to provide a source for a reducing zone
- The probability of the stream from a single waste package encountering a reducing zone, Pr{log}
- The probability of the reducing being of sufficient size to remove a critical mass, Pr{clusterllog}

The number of waste packages for each criticality threshold is determined from the tabulation of percentiles of number of PWR assemblies having greater than a specified k_{inf} given in Ref. C.9-33, where the k_{inf} is calculated as a function of enrichment and burnup according to the procedure also given in that reference. The results are given in the following table.

Table 8-3 Percentile of SNF having less fissile % than stated value

% enrichment, burnup (GWd/MTU)	% Fissile	k_∞	Fissile content percentile
3.0%, 20	1.94	1.13	98
3.5%, 30	1.87	1.08	96
4.0%, 40	1.82	1.04	87

Using the expected total of 12,000 waste packages of commercial SNF (Ref. C.9-34), and making the conservative assumption that the packages are loaded homogeneously (so that all the high fissile fuel is grouped together), the number of packages having higher fissile content (or higher k_{inf}) than the indicated values can be estimated by multiplying the total number of waste packages by the complement of the percentile in the above table, and dividing by 100.

For Pr{log} the conservative alternative from Table 8-2, 4.1×10^{-4} is used. For Pr{clusterllog} the values from Table 8-1 are used, except that the cases which require a high volume % water should have the probabilities of Table 8-1 multiplied by the probability of finding such a high porosity in the saturated zone. From Table 7-1 it is seen that the first 4 cases all require more than 30 vol% water (which is equivalent to porosity in the saturated zone). From Table 8-1 it is seen that the first and third cases will be the only ones contributing significantly to total probability. These cases require 38.3 and 33.2 percent porosity, respectively. From Ref. C.9-6, Figure 4.1-1 it is seen that the probabilities of having such high porosities are .01 and .23, respectively. Multiplying by the corresponding probabilities in Table 8-1 and adding gives 1.8×10^{-6} for the porosity adjusted Pr{clusterllog}.

Although only the first and third cases of Table 8-1 can contribute significantly to the overall expected number of criticalities, it is still useful to present the results for the last 2 cases which represent different fuel characteristics, and a lower fissile content. These cases do not need to be porosity adjusted because they have porosities of less than 26%, which can be found in over 90% of the rock.

Table 8-4 Summary of upper bound for probability of criticality as a function of fissile content

% fissile	Number pkgs with more fissile	Pr{clusterllog}	Expected criticalities
1.94*	240	1.8×10^{-6} **	1.8×10^{-7}
1.87*	480	4.70×10^{-18} *	9.2×10^{-19}
1.82*	1560	7.18×10^{-46} *	4.6×10^{-46}

* From Table 8-1

** Porosity adjusted as described above

8.5. Adjustment for critical masses greater than a single waste package

For those cases with required critical mass significantly greater than 10 tons (the contents of 1 waste package) some focusing from 2 or more waste packages would be necessary. There are two mechanisms for such focusing: (1) Random fractures which accidentally happen to channel the flow in a concentrating direction, and (2) highly permeable rock which acts as an attractor for groundwater streamlines. This section provides a simplified analysis of the first mechanism. It should be noted that this section stands alone, and is for illustrative purposes only, so that if future investigations indicate a significant potential for the second mechanism, the validity of other sections of this document will not be affected, and the conclusions will remain unchanged.

which would decrease the probability by multiplying by a factor less than the ratio of the critical sphere cross section area divided by the repository area enclosing the required number of waste packages, which could be quite a small factor if the design basis waste packages are distributed throughout the repository. There are four cases in Table 7-1 which require significantly more than 10 tons of uranium, but this correction has not been applied because the initial calculation showed the probability to be incredibly small. It should be noted that groundwater focusing does occur naturally, but rarely, as the source of artesian springs being at the focus of a large catchment area.

It is, nevertheless, useful to estimate the per-package multiplicative factor. At 80 MTU/acre, the average area per waste package is 493 sq meters; a typical critical sphere radius from Table 8-1 is 1 meter, so the reduction factor would be $\pi/493 = 0.006$.

It should be noted that a realistic analysis of the groundwater flow in the saturated zone from a single waste package indicates a dilution of such magnitude that even the smallest critical mass requirements of Table 8-15 would require more than one package. The following simplified analysis indicates the magnitude of the dispersion.

It is conservatively assumed that the groundwater which has passed through a waste package flows vertically downward through the unsaturated zone with no lateral dispersion. In the saturated zone the flow follows the fluid potential gradient with a dispersion approximated by Equation 7.6-5 of Ref C.9-2 which gives the concentration as a function of vertical distance below the water table, z, distance from the plume centerline, y, and downstream distance, x,

$$C(x,y,z)=(2Q/u)\exp\{-y^2/[4D_y(x/u)]-z^2/[4D_z(x/u)]\}/[4\pi\phi(D_yD_z)^{.5}(x/u)],$$

where Q is the mass flux from a point source, u is the groundwater velocity, ϕ is the porosity, and D_y and D_z are the diffusion coefficients in the y and z directions and are modeled by

$$D_y = \beta_y xu, \quad D_z = \beta_z xu$$

Conservatively assuming y=0, the concentration will peak at a downstream distance of $x=z^*\mathrm{sqrt}(1/\beta_z)/2$.

The remaining parameters are modeled as follows:

$$\phi=V_{sat}/u, \quad Q=C_{uz}V_{uz}A,$$

where A is the waste package footprint, and the subscripts indicate the zone to which the parameters apply, which reduces the concentration formula to

$$C/C_{uz} = 4V_{uz}A\,\mathrm{sqrt}(\beta_z/\beta_y)\exp(-1)/[V_{sat}z^2]$$

Generally, $V_{uz}<V_{sat}$, $\beta_z/\beta_y<0.1$, and for any appreciable distance below the water table $A<<z^2$, so the concentration of uranium from a waste package will be diluted by at least a few orders of magnitude by the time it has moved a few hundred meters below the water table (top of the saturated zone).

Since the smallest critical mass found in this study is 16% of a waste package (1.6 tons required for the smallest critical mass out of approximately 10 tons uranium in the whole waste package), this dilution implies that the streams from a number of waste packages would have to be combined to deposit a single critical mass. Since the probabilities calculated without this correction are already very small, the correction was not quantified further or applied.

INTENTIONALLY LEFT BLANK

9. References

1. *Emplaced Waste Package Structural Capability Through Time Report*, DI# BBAA00000-01717-5705-00001 REV00, CRWMS M&O, June 14, 1996.

2. *Total System Performance Assessment 1995: An Evaluation of the Potential Yucca Mountain Repository*, B00000000-01717-2200-00136, Rev. 01, November 1995.

3. Van Konynenburg, R.A., Curtis, P.G., *Scoping Corrsoion Tests on Candidate Waste Package Basket Materials for The Yucca Mountain Project*, LLNL, Summary Acct. OL252 AJD, August 31, 1995.

4. *Progress Report on the Results of Testing advanced conceptual Design Metal Barrier Materials Under Relevant Environmental Conditions For A Tuff Repository*, LLNL, UCID-21044, December 1987.

5. *Second Waste Package Probabilistic Criticality Analysis: Generation and Evaluation of Internal Criticality Configurations*, DI# BBA-01717-2200-00005 REV00, CRWMS M&O, March 27, 1996.

6. *Probabilistic External Criticality Evaluation*, DI# BB0000000-01717-2200-00037 REV00, CRWMS M&O, May 31, 1996.

7. Brinck, J.W., *The Geologic Distribution of Uranium as a Primary Criterion for the Formation of Ore Deposits, in Formation of Uranium Ore Deposits*, IAEA-SM-183/19, International Atomic Energy Agency, 1974.

8. Finch, W.I., Butler, A.P.Jr., Armstrong, F.C., Weissenborn, A.E., Staatz, M.H., Olson, J.C., *Nuclear Fuels, from United States Mineral Resources*, Ed. Brobst, D.A., Pratt,W.P., United States Geologic Survey Prof. Paper 820, 1973

9. Smellie, J., *The Fossil Nuclear Reactors of Oklo, Gabon*, Radwaste Magazine, March 1995, pg 18-27.

10. Bish, D.L., Carey, J.W., Levy, S.S., Chipera, S.J., *Mineralogy-Petrology Contribution to the Near-Field Environment Report MILESTONE LA3668*, LA-EES-1-TIP-96-003, R1, March 1996.

11. Goodell, P.C., *Geology of the Pena Blance Uranium Deposits, Chihuahua, Mexico*, from Uranium in Volcanic and Volcaniclastic Rocks, AAPG Studies in Geology No. 13, 1981

12. George-Aniel, B., Leroy, J.L., Poty, B., *Volcanogenic Uranium Mineralizations in the Sierra Pena Blanca District, Chihuahua, Mexico: Three Genetic Models*, Economic Geology, 86, March-April 1991, pg 233-248.

13. Castor, S.B., Berry, M.R., *Geology of the Lakeview Uranium District, Oregon, from Uranium in Volcanic and Volcanoclastic Rocks,* AAPG Studies in Geology No. 13, 1982, pp. 55-62.

14. Schrader, E. *Relationships between Uranium and trace metal concentrations in volcanic rocks from Nevada*, Economic Geology, 72, p104-107, 1977

15. Katayama,N.,Kubo, K., Hirono,S., *Genesis of Uranium Deposits of the Tono Mine*, Japan, in Formation of Uranium Ore Deposits, IAEA-SM-183/19, International Atomic Energy Agency, 1974, pp. 437-452.

16. Breger, I.A., *The role of Organic Matter in the Accumulation of Uranium*, in Formation of Uranium Ore Deposits, IAEA-SM-183/19, International Atomic Energy Agency, 1974

17. Hess, F.L., *Uranium, Vanadium, Radium, Gold, Silver, and Molybdenum Sedimentary Deposits, in Ore Deposits of the Western States*, Lindgren Volume of The American Institute of Mining and Metallurgical Engineers, New York 1933.

18. Chenoweth, W.L. *The Uranium-Vanadium Deposits of the Uravan Mineral Belt and Adjacent Areas, Colorado and Utah*, New Mexico Geological Society Guideboook, 32nd Field Conference, Western Slope Colorado, 1981, pg 165-170.

19. Gascoyne, M., *Geochemistry of the Actinides and Their Daughters, in Uranium Series Disequilibrium: Applications to Environmental Problems*, ed M.Ivanovich and R.S.Harmon, Clarendon Press - Oxford, 1982

20. *Dynamic Impact Effects on Spent Fuel Assemblies,* Lawrence Livermore National Laboratory (LLNL), UCID-21246, October 1987.

21. *Static Structural Analyses of Waste Package in Degraded States*, DI#: BBAA00000-01717-0200-00014 REV 00, CRWMS M&O.

22. *Modeling of Gaseous CO_2 Release from Perforations in Spent Fuel Disposal Containers,* Brookhaven National Laboratory, BNL 52308, November 1991.

23. *Material Compositions and Number Densities for Neutronics Calculations*, DI#: BBA000000-01717-0200-00002 REV 00, CRWMS M&O

24. *Corrosion Rates for Carbon Steel*, Interoffice Correspondence LV.WP.JKM.03/96.060, J.K. McCoy, March 15, 1996, CRWMS M&O

25. *Electrochemical Determination of The Corrosion Behavior of Candidate Alloys Proposed for Containment Of High Level Nuclear Waste in Tuff*, Lawrence Livermore National Laboratory (LLNL), UCID-20174, Livermore, CA, June 1984

26. Garside, L.J., *Radioactive mineral occurrences in Nevada*, Nevada Bureau of Mines and Geology, Bulletin 81, 1973

27. French, D.E., *Origin of Oil in Railroad Valley*, Nye County, Nevada, The Wyoming Geological Association Earth Science Bulletin, 16, 1983 (pg 9-21)

28. Grow, J.A., Barker,C.E., Harris, A.G., *Oil and Gas Exploration Near Yucca Mountain*, Southern Nevada, High Level Radioactive Waste Management, Fifth Annual International Conference, ASCE & ANS, 1994, pg 1298-1315.

29. Gottlieb, P., *Estimate of mineralized areas*, Interoffice Correspondence, LV.WP.PG.05/96-120, CRWMS M&O, May 30, 1996.

30. Davis, J.W., *External Criticality Analysis*, Interoffice Correspondence, LV.WP.JWD.05/96.122, CRWMS M&O, May 30, 1996.

31. Thamm, J.K., Kovschak,A.A., Adams, S.S., Geology and Recognition Criteria for Sandstone Uranium Deposits of the Salt Wash Type, Colorado Plateau Province, Prepared for the U.S. Department of Energy, Grand Junction Office, Colorado, GJBX-6(81), January 1981.

32. Fischer, R.P., *Vanadium Deposits of Colorado and Utah*, Geological Survey Bulletin 936-P, 1942.

33. *Waste Package Design Basis Fuel Analysis*, DI#: BBA000000-01717-0200-000121 REV 00, 1994, CRWMS M&O

34. Davis, J., Fleming, M., King, J., *FY95 CDA Update OFF Waste Stream Data*, CRWMS M&O Contractor, Interoffice Correspondence SA.VA.JK.04/95.045, April 3, 1995.

APPENDIX D

Criticality Event Consequence Analysis Supporting Information

INTENTIONALLY LEFT BLANK

Table of Contents

INTENTIONALLY LEFT BLANK

Appendix D: Criticality Event Consequence Analysis Supporting Information

Introduction

The purpose of this appendix is to illustrate the estimation of the consequences of an internal criticality event, under the assumption that such an event does occur. For this illustration, it is assumed that such an internal criticality event occurs at 15,000 years following emplacement. Furthermore, in order to support the maintenance of a criticality internal to the WP for up to 10,000 years, it is necessary to assume that the highest possible infiltration rate (10 mm/yr) does occur and can have, at most, a 10,000 year duration. The basis for the first assumption is that it is the approximate time of the highest postclosure criticality potential for the PWR criticality design basis SNF (as has been demonstrated by many time-dependent k_{eff} calculations) and it is one of the earliest potential criticalities discussed in Appendix C. The basis for the second assumption is that it is the expected upper bound for the conditions supporting criticality (high infiltration, integrity of the lower part of the barrier, sufficient fissile material remaining). The consequences of such a criticality event will be discussed in terms of the heat generated and the change in the radionuclide inventory of the waste package. These calculations were performed in Reference D.4.8, the *Second Waste Package Probabilistic Criticality Analysis: Generation and Evaluation of Internal Criticality Configurations.*

INTENTIONALLY LEFT BLANK

1. Estimated Power and Duration of an Internal Criticality

The criticality scenarios discussed in the previous Sections detail a picture of a flooded waste package that is gradually approaching a critical condition (k_{eff}=1) as a result of positive reactivity insertions caused by a slow loss of boron and iron from the package interior. Once a WP reaches a k_{eff} of 1, continued small positive reactivity insertions will cause the power output of the WP to begin to slowly rise (i.e., a long reactor period). If the power exceeds a certain limit, the rate at which water is consequentially removed from the WP will exceed the rate of input, and the resulting water level drop will provide a negative reactivity insertion driving the WP back towards a subcritical condition. Conversely, if insufficient power is produced, the water level will be maintained and the exchange process discussed previously will continue to remove dissolved boron, thus providing a continued source of positive reactivity insertions until the point of equilibrium is achieved. The maximum steady state power can then be estimated by determining the power required to maintain the bulk WP water temperature at the point where water is removed at the same rate that it drips into the WP. The WP must produce sufficient power to raise the temperature of the incoming water to this equilibrium value, as well as account for heat losses to the environment by radiation and/or conduction.

It is conservatively assumed that airflow is stagnant in a drift at the 15,000 year-plus time frame under consideration, and evaporation can be modeled as diffusion of water vapor into air. The first step is to obtain the diffusion coefficient for water into air. The following expression obtained from Ref. D.4-7 provides an approximation for the diffusion coefficient as a function of temperature:

$$D(T) = [435.7 \cdot T^{3/2} \cdot (M_1^{-1} + M_2^{-1})^{1/2}] / (P_{atm} \cdot (V_1^{1/3} + V_2^{1/3}) \qquad \text{Eq. D-1}$$

where,
- $D(T)$ is the diffusion coefficient in cm^2/s at temperature T,
- T is the temperature in K,
- P_{atm} is the atmospheric pressure (1.0132×10^5 Pa),
- V_1, V_2 are the molecular volumes of substances 1 and 2 (in this case water, 18.8 cm^3/mole, and air, 29.9 cm^3/mole, respectively) and,
- M_1, M_2 are the molecular weights of substances 1 and 2 (water, 18.02 kg/kmol, and air, 28.97 kg/kmol).

An additional factor of 0.056 cm^2/s has been added to values calculated by Eq. D-1 to correspond with empirical measurements of the diffusion coefficient of water vapor into air at 8°C and 25°C.

With the diffusion coefficient determined, the volumetric flow rate of water out of the package due to evaporation is determined using the integrated form of Stefan's law (Ref. D.4-7):

$$V_{evap}(T) = [(D(T) \cdot P_{atm} \cdot M_1 \cdot A \cdot v(T)) / (R_0 \cdot T \cdot z)] \cdot \ln[(P_{atm} - p(T) \cdot RH) / (P_{atm} - p(T))] \qquad \text{Eq. D-2}$$

where,
- $V_{evap}(T)$ is the volumetric evaporation rate,
- $D(T)$ is the diffusion coefficient at temperature T,
- T is the temperature,
- P_{atm} is the atmospheric pressure,

$p(T)$	is the saturation pressure of water at temperature T,
R_0	is the Universal Gas Constant (8.315 kJ/kmol*K),
z	is the distance from the water surface to the bulk environment,
$v(T)$	is the specific volume of the water at temperature T,
A	is the surface area of the water in the WP,
RH	is the drift relative humidity, and
M_1	is the molecular weight of water.

The maximum rate of water dripping on a WP in TSPA-95 (Ref. D.4-2) was approximately 1.9×10^5 cm^3/yr, and was assumed (in TSPA-95) to occur 50,000 years after emplacement. Using Eq. D-2, the WP would have to produce sufficient power to maintain the water in the WP at a temperature of 57.4°C, as well as compensate for other mechanisms of heat loss, to match this drip rate. This indicates that evaporation alone will be sufficient to remove the incoming water, and bulk boiling will not occur.

It is assumed for this analysis that the WP configuration has a slightly negative moderator temperature coefficient, which also contributes to slowing rate of power increase such that a stable power level is gradually reached. This assumption is based on previous analyses of the ACD 21 PWR Uncanistered Fuel WP (Ref. D.4-7) which indicate that the first 5% reduction in moderator density from that used in the calculation (sat. liq. at 27°C) will result in a negative reactivity insertion of approximately 10^{-2} $\Delta k/k$ for the criticality design basis fuel (Ref. D.4-5). For comparison purposes, a 30°C increase results in only a 1% density reduction.

The amount of reactor heat dissipated by heating the incoming water, which is assumed to be at a temperature of 30°C, to a temperature of 57.4°C is given by the following expression:

$$q_{water} = [Cp(30°C) \cdot V_{drip} \cdot \Delta T]/v(30°C) \qquad \text{Eq. D-3}$$

where,

q_{water}	is the heat input required to raise the water temperature 27.4°C,
V_{drip}	is the rate of water dripping into the WP,
$Cp(30°C)$	is the specific heat of water at 30°C,
$v(30°C)$	is the specific gravity of water at 30°C, and
ΔT	is the temperature increase (27.4°C).

Using Equation D-3, only 0.677 W are required to raise the temperature of the water to the point where the evaporation rate equals the rate of influx.

Once at 57.4°C, the amount of power required to vaporize water at a rate of 1.9×10^5 cm^3/yr of water must also be accounted for. This is equal to the product of the heat of vaporization at 57.4°C, 2364.8 kJ/kg (linear interpolation from Ref. D.4-4, Table A-3), the volume of water to be evaporated, 1.9×10^5 cm^3/yr, and the density of water at 57.4°C, 984.4 kg/m^3. Multiplying the above three values and performing the appropriate unit conversions yields an additional 14 W.

As stated above, additional heat losses will also occur due to radiation and/or conduction heat transfer to the local environment. The actual configuration of the drift thousands of years after emplacement cannot be defined sufficiently to allow a detailed heat transfer estimate. It is highly

likely that a portion of the WP may be covered with rubble, possibly as a result of the gradual collapse of the drift, and both radiation and conduction mechanisms will be active. However, examination of ideal radiation-only and conduction-only systems should respectively provide an upper and lower bound on the heat loss from a WP with a bulk water temperature of 57.4°C. Heat losses due to radiation alone can be estimated by treating the WP and drift as a system of concentric cylinders, with the WP surface at 57.4°C, and the drift wall assumed to maintain a constant 30°C. The radiation heat transfer rate is then given by:

$$q_{rad} = [\sigma \cdot A_1 \cdot (T_1^4 - T_2^4)]/[\epsilon_1^{-1} + (A_1/A_2)(\epsilon_2^{-1} - 1)] \quad \text{(Ref. 5.14)} \qquad \text{Eq. D-4}$$

where,

q_{rad}	is the radiation heat transfer rate,
T_1	is the WP surface temperature,
T_2	is the drift wall temperature,
A_1	is the WP surface area,
A_2	is the drift surface area,
ϵ_1	is the emissivity of oxidized carbon steel, 0.80,
ϵ_2	is the emissivity of tuff rock, 0.85, and,
σ	is the Stephan-Boltzman constant (5.669×10^{-8} W/m^{2}K^4).

Using the above equation, radiation heat loss from a 57.4°C WP is estimated to be 3859 W. Again assuming the system of concentric cylinders and a drift wall temperature of 30°C, a WP entirely covered by crushed tuff would lose heat by conduction according to:

$$q_{cond} = [2\pi \cdot k \cdot L \cdot (T_1 - T_2)]/[\ln(d_2/d_1)] \quad \text{(Ref. 5.14)} \qquad \text{Eq. D-5}$$

where,

q_{cond}	is the conduction heat transfer rate,
k	is the average thermal conductivity of crushed tuff,
L	is the WP outer length less that of the skirts,
T_1	is the WP surface temperature,
T_2	is the drift wall temperature,
d_1	is the WP outer diameter; and,
d_2	is the drift diameter.

Solving the above equation for a WP surface temperature of 57.4°C indicates that 504 W will be lost if all heat transfer occurs by conduction through crushed tuff. Assuming the more likely configuration of a WP covered half-way with rubble, the heat loss may be approximated (i.e., not specifically accounting for the radiation heat transfer between the rubble and the drift wall) by taking the mean of the above two extremes, 2.182 kW. Since the power dissipated in heating the water dripping in to 57.4°C and vaporizing it at that temperature has been shown to total less than 15 W, it is not added in this approximation.

The above power represents a conservative ideal condition because, in reality, there will be a number of feedback mechanisms which will act to disrupt the equilibrium. Some of these mechanisms include the decreases in the infiltration rate resulting from climatic cycles, the production of neutron absorbing fission products, the depletion of fissile nuclides, changes in moderator density, corrosion of the cladding or spacer grids (leading to consolidation of the fuel

rods), and corrosion of the remainder of the WP barriers (leading to the formation of drainage holes). The combined effect of these mechanisms will likely limit any single WP criticality event to a relatively short duration, with criticality events reoccurring in the same WP in a cyclic pattern as long as the necessary conditions continue to recur. Therefore, use of a steady state power of 2.182 kW to estimate total burnup resulting from a long-term postclosure internal WP criticality should be a reasonable approximation to the cumulative effect of multiple pulses.

The overall duration of such a cyclic criticality is also dependent on some of the above-mentioned feedback mechanisms, primarily the continued availability of water, the ability of the WP to hold water, and the depletion of fissile nuclides. While the climate cycle period over the past 2 million years has been approximately 100,000 years, infiltration rates near the peak (which are required to maintain the steady state power level and water exchange rates discussed previously) may occur for only several thousand years (Ref. D.4-2). Based on this information, a range of 1,000 year to 10,000 year durations has been evaluated, for the purposes of estimating the effects of criticality on radionuclide inventory. A 10,000 year criticality at a steady state power level of 2.182 kW yields an additional burnup of 7965 MWd for the SNF in the WP (817 MWd/MTU). Such long periods of steady state power production are expected to be conservative because of the cyclic nature of the criticality itself, the duration of the peak infiltration rates, and the expectation that the WP will have a much lower probability of being able to hold water by the time the next peak in infiltration returns.

2. Effects of an Internal Criticality on the Radionuclide Inventory of the WP

To evaluate the effects of a criticality on the radionuclide inventory of a WP, the computer code ORIGEN-S was run using the criticality design basis fuel, and the steady state power of 2.182 kW discussed in Section 1 above. The criticality was assumed to occur after the fuel had aged/decayed for 15,000 years and was maintained at the above mentioned power for three durations: 1,000, 5,000 and 10,000 years. The output of these runs was the radionuclide inventory, in curies, at the times corresponding to the end of each criticality, and at fuel ages (time since reactor discharge) of 45,000 and 65,000 years. A fourth, decay-only case was run to determine the radionuclide inventories at the above times for fuel which did not experience a criticality event. The details of the ORIGEN-S calculations performed to obtain the radionuclide inventories for both decay-only and fission-plus-decay cases are reported in Ref. D.4-3.

To provide a comparison between a WP which experienced a criticality, and one only decayed, 36 of the 39 isotopes in the TSPA-95 radionuclide inventory list (Ref. D.4-2) were extracted from the ORIGEN-S output (Ref. D.4-3). Comparisons of the activities of ^{36}Cl, ^{59}Ni, and ^{63}Ni were not made because the present ORIGEN-S analysis has not yet been extended to activation products. Differences were reported in terms of the percentage change in the activity of each radionuclide at each time, and the percentage change The calculations performed to determine the difference in radionuclide activities between the decay-only and criticality cases were performed using Excel v5.0. The results are summarized in Tables 2-1, 2-2, and 2-3 for the 1,000 year, 5,000 year, and 10,000 year duration criticalities respectively.

Neutron activation of stable isotopes in the WP materials and water represents another potential source of radionuclides which may be produced during such a criticality. The ORIGEN-S output (Ref. D.4-3) indicated that the total average neutron flux in the 2.182 kW WP was $\approx 2.9 \times 10^8$ neutrons/cm^{2}s, and that 10.9% of this flux was in the thermal part of the spectrum. ^{14}C and ^{36}Cl are two radionuclides in the TSPA-95 radionuclide inventory which may be produced from activation of trace elements in the water. ^{14}C is primarily produced by the $^{14}N(n,p)$ reaction and the $^{17}O(n,\alpha)$ reaction, although much smaller quantities may also be produced by multiple neutron captures in ^{16}O ($^{16}O(n,\gamma) \rightarrow {}^{17}O(n,\alpha) \rightarrow {}^{14}C$). The number density for ^{14}N in 57.4°C water in equilibrium with air at atmospheric pressure is given by the following expression:

$$N_{NI4} = (A_{NI4} \cdot \rho_w \cdot v_N \cdot P_{atm} \cdot N_a \cdot 2)/(M_W \cdot H_N) \qquad \text{Eq. D-6}$$

where,

N_{NI4}	is the number density of ^{14}N
A_{NI4}	is the abundance of ^{14}N (99.63%),
ρ_w	is the density of water at 57.4°C,
v_N	is the volume fraction of N_2 in air (78.08%),
M_w	is the molecular weight of water,
P_{atm}	is the air pressure,
N_a	is Avogadro's Number (6.022×10^{23} atoms/mole), and,
H_N	is Henry's Law solubility of N_2 in water at 57.4°C in atm. N_2/(mole N_2/mole water).

This yields 4.35×10^{17} atoms of ^{14}N per cm^3 of water. The number density of ^{17}O in water is simply computed by:

$$N_{O17}=(A_{O17} \cdot \rho_w \cdot N_a)/M_w \qquad \text{Eq. D-7}$$

where,
- N_{O17} is the number density of ^{17}O,
- A_{O17} is the abundance of ^{17}O,
- ρ_w is the density of water at 57.4°C,
- M_w is the molecular weight of water, and,
- N_a is Avogadro's Number.

This yields 1.32×10^{19} ^{17}O atoms/cm^3. The amount of oxygen dissolved in the water is insignificant compared to that in the water itself, and has been neglected for this calculation.

Given the above flux and thermal fraction, and assuming that the number density of ^{14}N and ^{17}O remains constant, the production rate of ^{14}C can be calculated as follows:

$$^{14}C=\lambda_{C14} \cdot (N_{N14} \cdot \sigma_{pN14} + N_{O17} \cdot \sigma_{\alpha O17}) \cdot \phi \cdot f \cdot V_{WP} \qquad \text{Eq. D-8}$$

where, ^{14}C is the production rate of ^{14}C,
- λ_{C14} is the ^{14}C decay constant (ln2/half-life),
- N_{N14} is the number density of ^{14}N,
- N_{O17} is the number density of ^{17}O,
- $\sigma_{\alpha O17}$ is the microscopic thermal cross section for the $^{17}O(n,\alpha)$ reaction (0.24 barns),
- σ_{pN14} is the microscopic thermal cross section for the $^{14}N(n,p)$ reaction (1.81 barns),
- ϕ is the average total neutron flux,
- f is the fraction of the flux in the thermal part of the spectrum, and,
- V_{WP} is the volume of water in the fully flooded WP.

Using the parameters given in Section 4.1.7, this yields 1.98 µCi of ^{14}C/yr of WP criticality, which is not contained by the cladding and may be available for immediate release from the WP. However, this production rate is almost six orders of magnitude below the NRC release limits for the site of 0.796 Ci of ^{14}C/yr (Ref. D.4-2) and thus should have no impact on site performance.

Similarly, ^{36}Cl may be produced during the criticality by neutron activation of ^{35}Cl in the water. Chemical analyses of J-13 (Ref. D.4-1) well water have found it to nominally contain D µg Cl^- /mL. However, evaporation of water from the WP would be expected to increase this concentration. Corrosion tests involving boiling J-13 well water, tuff rock, and stainless steel specimens found that the stable concentration of Cl^- had increased to 161 µg/mL after 1 year (Ref. D.4-1). These values can be used to determine nominal and high ^{35}Cl number densities as follows:

$$N_{Cl35}=(C_{Cl}\cdot A_{Cl35}\cdot N_a)/M_{Cl} \qquad \text{Eq. D-9}$$

where,

N_{Cl35}	is the number density of ^{35}Cl,
A_{Cl35}	is the abundance of ^{35}Cl,
C_{Cl}	is the concentration of Cl^- in the water,
M_{Cl}	is the molecular weight of Cl, and,
N_a	is Avogadro's Number.

This yields a nominal value of 9.65×10^{16} atoms of $^{35}Cl/cm^3$ or a high value of 2.07×10^{18} ^{36}Cl atoms/cm^3 if the high concentration is used. The production rate of ^{36}Cl can then be calculated by:

$$^{36}C=\lambda_{Cl36}\cdot(N_{Cl35}\cdot\sigma_{\gamma Cl35})\cdot\phi\cdot f\cdot V_{WP} \qquad \text{Eq. D-10}$$

where,

^{36}Cl	is the production rate of ^{36}Cl,
λ_{Cl36}	is the ^{36}Cl decay constant (ln2/half-life),
N_{Cl35}	is the number density of ^{35}Cl,
$\sigma_{\gamma Cl35}$	is the microscopic thermal cross section for the $^{35}Cl(n,\gamma)$ reaction,
ϕ	is the average total neutron flux,
f	is the fraction of the flux in the thermal part of the spectrum, and,
V_{WP}	is the volume of water in the fully flooded WP.

This yields a nominal production rate of 0.04 μCi/yr of ^{36}Cl and a high rate of 0.86 μCi/yr. Both of these values are also several orders of magnitude below the NRC site release limits of 7.13 mCi/yr and should not impact site performance.

The overall effect of the criticality can be summarized by the percentage increase in the total curies for the 36 isotopes utilized in TSPA-95 immediately after the criticality ends and at later times. Table 2-4 below shows this comparison. The explicitly stated times are measured from emplacement. The duration of criticality times are relative to the start of criticality at 15,000 years, so the absolute (measured from emplacement) times at the end of criticality are determined by adding the duration of criticality to 15,000 years.

Table 2-1. Effects of 1,000 Year Criticality on the Radionuclide Inventory of a PWR Fuel Assembly

	16,000 yr				45,000 yr				65,000 yr			
	Act. (Ci) Critical	Act. (Ci) Decay Only	% Diff. Isotope	% Diff. Total	Act. (Ci) Critical	Act. (Ci) Decay Only	% Diff. Isotope	% Diff. Total	Act. (Ci) Critical	Act. (Ci) Decay Only	% Diff. Isotope	% Diff. Total
ac227	4.9e-003	4.3e-003	1.6e+001	4.9e-004	1.0e-002	1.0e-002	3.0e+000	5.6e-004	1.3e-002	1.3e-002	2.3e+000	9.3e-004
am241	2.6e+000	2.2e-003	1.2e+005	1.9e+000	2.0e-004	2.0e-004	-1.5e+000	-5.6e-006	3.9e-005	3.9e-005	-1.5e+000	-1.9e-006
am242m	2.0e-003	0.0e+000	N/A	1.4e-003	0.0e+000	0.0e+000	0.0e+000	0.0e+000	0.0e+000	0.0e+000	0.0e+000	0.0e+000
am243	4.8e-001	4.5e-001	7.2e+000	2.3e-002	3.1e-002	2.9e-002	7.2e+000	3.9e-003	4.8e-003	4.5e-003	7.2e+000	9.9e-004
c 14	4.9e-006	4.8e-006	2.5e+000	8.7e-008	1.5e-007	1.4e-007	2.8e+000	7.5e-009	1.3e-008	1.3e-008	2.3e+000	9.3e-010
cm244	1.7e-002	0.0e+000	N/A	1.2e-002	0.0e+000	0.0e+000	0.0e+000	0.0e+000	0.0e+000	0.0e+000	0.0e+000	0.0e+000
cm245	2.1e-003	2.1e-003	-1.4e+000	-2.2e-005	2.0e-004	2.0e-004	-1.5e+000	-5.6e-006	3.9e-005	3.9e-005	-1.5e+000	-1.9e-006
cm246	9.6e-005	8.8e-005	9.2e+000	5.8e-006	1.4e-006	1.3e-006	9.5e+000	2.3e-007	7.3e-008	6.7e-008	9.2e+000	1.9e-008
cs135	2.0e-001	2.0e-001	9.9e-001	1.4e-003	2.0e-001	2.0e-001	1.0e+000	3.8e-003	2.0e-001	2.0e-001	1.0e+000	6.2e-003
i129	8.8e-003	8.8e-003	4.5e-001	2.9e-005	8.8e-003	8.8e-003	4.5e-001	7.5e-005	8.8e-003	8.8e-003	3.4e-001	9.3e-005
nb 93m	3.5e-001	3.5e-001	5.8e-001	1.4e-003	3.4e-001	3.4e-001	2.9e-001	1.9e-003	3.4e-001	3.4e-001	2.9e-001	3.1e-003
nb 94	1.9e-005	1.4e-005	4.0e+001	4.0e-006	7.1e-006	5.0e-006	4.1e+001	3.9e-006	3.6e-006	2.5e-006	4.1e+001	3.2e-006
np237	3.8e-001	3.8e-001	2.6e-001	7.2e-004	3.8e-001	3.8e-001	2.6e-001	1.9e-003	3.8e-001	3.8e-001	2.7e-001	3.1e-003
pa231	4.9e-003	4.3e-003	1.6e+001	4.9e-004	1.0e-002	1.0e-002	3.0e+000	5.6e-004	1.3e-002	1.3e-002	1.6e+000	6.2e-004
pb210	8.0e-002	8.0e-002	0.0e+000	0.0e+000	2.1e-001	2.1e-001	4.7e-001	1.9e-003	2.8e-001	2.8e-001	7.1e-001	6.2e-003
pd107	2.6e-002	2.6e-002	3.8e-001	7.2e-005	2.6e-002	2.6e-002	3.8e-001	1.9e-004	2.6e-002	2.6e-002	7.7e-001	6.2e-004
pu238	2.9e+000	0.0e+000	N/A	2.1e+000	0.0e+000	0.0e+000	0.0e+000	0.0e+000	0.0e+000	0.0e+000	0.0e+000	0.0e+000
pu239	1.0e+002	1.0e+002	9.7e-001	7.2e-001	4.5e+001	4.5e+001	6.7e-001	5.6e-001	2.6e+001	2.5e+001	7.9e-001	6.2e-001
pu240	2.9e+001	2.8e+001	4.3e+000	8.7e-001	1.4e+000	1.3e+000	3.8e+000	9.4e-002	1.7e-001	1.6e-001	4.4e+000	2.2e-002
pu241	3.2e+000	2.1e-003	1.5e+005	2.3e+000	2.0e-004	2.0e-004	-1.5e+000	-5.6e-006	3.9e-005	3.9e-005	-1.5e+000	-1.9e-006
pu242	2.7e-001	2.7e-001	-3.7e-001	-7.2e-004	2.6e-001	2.6e-001	-3.9e-001	-1.9e-003	2.5e-001	2.5e-001	-4.0e-001	-3.1e-003
ra226	8.0e-002	8.0e-002	-1.3e-001	-7.2e-005	2.1e-001	2.1e-001	4.7e-001	1.9e-003	2.8e-001	2.8e-001	7.1e-001	6.2e-003
ra228	9.0e-008	9.0e-008	0.0e+000	0.0e+000	2.8e-007	2.8e-007	3.6e-001	1.9e-009	4.1e-007	4.1e-007	4.9e-001	6.2e-009
se 79	1.4e-001	1.4e-001	7.3e-001	7.2e-004	7.5e-002	7.5e-002	6.7e-001	9.4e-004	4.9e-002	4.9e-002	6.1e-001	9.3e-004
sm151	7.9e-001	0.0e+000	N/A	5.7e-001	0.0e+000	0.0e+000	0.0e+000	0.0e+000	0.0e+000	0.0e+000	0.0e+000	0.0e+000
sn126	1.3e-001	1.2e-001	8.1e-001	7.2e-004	1.0e-001	1.0e-001	0.0e+000	0.0e+000	8.9e-002	8.8e-002	4.5e-001	1.2e-003
tc 99	3.8e+000	3.7e+000	5.3e-001	1.4e-002	3.4e+000	3.4e+000	5.9e-001	3.8e-002	3.2e+000	3.2e+000	3.1e-001	3.1e-002
th229	1.1e-002	1.2e-002	-8.7e-001	-7.2e-005	5.1e-002	5.1e-002	0.0e+000	0.0e+000	7.8e-002	7.8e-002	0.0e+000	0.0e+000
th230	9.2e-002	9.2e-002	-2.2e-001	-1.4e-004	2.2e-001	2.2e-001	4.5e-001	1.9e-003	2.9e-001	2.9e-001	7.0e-001	6.2e-003
th232	9.0e-008	9.0e-008	0.0e+000	0.0e+000	2.8e-007	2.8e-007	3.6e-001	1.9e-009	4.1e-007	4.1e-007	4.9e-001	6.2e-009
u233	2.5e-002	2.5e-002	-8.0e-001	-1.4e-004	6.7e-002	6.7e-002	0.0e+000	0.0e+000	9.3e-002	9.3e-002	1.1e-001	3.1e-004
u234	6.7e-001	6.7e-001	9.0e-001	4.3e-003	6.3e-001	6.3e-001	9.6e-001	1.1e-002	6.1e-001	6.0e-001	1.0e+000	1.9e-002
u235	1.6e-002	1.6e-002	-6.4e-001	-7.2e-005	1.8e-002	1.8e-002	-5.6e-001	-1.9e-004	1.8e-002	1.8e-002	-5.4e-001	-3.1e-004
u236	1.3e-001	1.3e-001	7.9e-001	7.2e-004	1.3e-001	1.3e-001	0.0e+000	0.0e+000	1.4e-001	1.3e-001	7.5e-001	3.1e-003
u238	1.5e-001	1.5e-001	0.0e+000	0.0e+000	1.5e-001	1.5e-001	0.0e+000	0.0e+000	1.5e-001	1.5e-001	0.0e+000	0.0e+000
zr 93	3.5e-001	3.5e-001	5.8e-001	1.4e-003	3.4e-001	3.4e-001	2.9e-001	1.9e-003	3.4e-001	3.4e-001	2.9e-001	3.1e-003
36 Iso. Totals	1.5e+002	1.4e+002	8.5e+000	0.0e+000	5.4e+001	5.3e+001	7.3e-001	0.0e+000	3.3e+001	3.2e+001	7.3e-001	0.0e+000

Table 2-2. Effects of 5,000 Year Criticality on the Radionuclide Inventory of a PWR Fuel Assembly

	20,000 yr				45,000 yr				65,000 yr			
	Act. (Ci) Critical	Act. (Ci) Decay Only	% Diff. Isotope	% Diff. Total	Act. (Ci) Critical	Act. (Ci) Decay Only	% Diff. Isotope	% Diff. Total	Act. (Ci) Critical	Act. (Ci) Decay Only	% Diff. Isotope	% Diff. Total
Ac227	8.8e-003	5.2e-003	7.0e+001	3.1e-003	1.2e-002	1.0e-002	2.0e+001	3.8e-003	1.4e-002	1.3e-002	1.0e+001	4.0e-003
Am241	2.7e+000	1.6e-003	1.7e+005	2.3e+000	1.9e-004	2.0e-004	-7.5e+000	-2.8e-005	3.6e-005	3.9e-005	-7.4e+000	-9.0e-006
Am242m	2.4e-003	0.0e+000	N/A	2.0e-003	0.0e+000	0.0e+000	0.0e+000	0.0e+000	0.0e+000	0.0e+000	0.0e+000	0.0e+000
Am243	4.4e-001	3.1e-001	4.4e+001	1.1e-001	4.2e-002	2.9e-002	4.4e+001	2.4e-002	6.4e-003	4.5e-003	4.3e+001	6.0e-003
C 14	3.5e-006	3.0e-006	1.7e+001	4.3e-007	1.7e-007	1.4e-007	1.7e+001	4.5e-008	1.5e-008	1.3e-008	1.7e+001	6.8e-009
Cm244	1.6e-002	0.0e+000	N/A	1.3e-002	0.0e+000	0.0e+000	0.0e+000	0.0e+000	0.0e+000	0.0e+000	0.0e+000	0.0e+000
Cm245	1.4e-003	1.5e-003	-7.1e+000	-9.3e-005	1.9e-004	2.0e-004	-7.0e+000	-2.6e-005	3.6e-005	3.9e-005	-7.4e+000	-9.0e-006
Cm246	7.4e-005	4.9e-005	5.1e+001	2.1e-005	1.9e-006	1.3e-006	5.2e+001	1.2e-006	1.0e-007	6.7e-008	5.2e+001	1.1e-007
Cs135	2.1e-001	2.0e-001	4.4e+000	7.6e-003	2.1e-001	2.0e-001	4.5e+000	1.7e-002	2.1e-001	2.0e-001	4.5e+000	2.8e-002
I129	9.0e-003	8.8e-003	2.0e+000	1.5e-004	9.0e-003	8.8e-003	2.0e+000	3.4e-004	9.0e-003	8.8e-003	2.0e+000	5.6e-004
Nb 93m	3.5e-001	3.5e-001	2.0e+000	5.9e-003	3.5e-001	3.4e-001	2.0e+000	1.3e-002	3.5e-001	3.4e-001	2.1e+000	2.2e-002
Nb 94	4.1e-005	1.2e-005	2.5e+002	2.5e-005	1.8e-005	5.0e-006	2.5e+002	2.4e-005	8.9e-006	2.5e-006	2.5e+002	2.0e-005
Np237	3.8e-001	3.8e-001	1.0e+000	3.4e-003	3.8e-001	3.8e-001	1.1e+000	7.5e-003	3.8e-001	3.8e-001	1.3e+000	1.5e-002
Pa231	8.8e-003	5.2e-003	7.0e+001	3.1e-003	1.2e-002	1.0e-002	2.0e+001	3.8e-003	1.4e-002	1.3e-002	1.0e+001	4.0e-003
Pb210	1.0e-001	1.0e-001	-9.9e-001	-8.5e-004	2.2e-001	2.1e-001	2.3e+000	9.4e-003	2.9e-001	2.8e-001	3.6e+000	3.1e-002
Pd107	2.7e-002	2.6e-002	1.9e+000	4.2e-004	2.7e-002	2.6e-002	1.9e+000	9.4e-004	2.7e-002	2.6e-002	2.3e+000	1.9e-003
Pu238	3.0e+000	0.0e+000	N/A	2.5e+000	0.0e+000	0.0e+000	0.0e+000	0.0e+000	0.0e+000	0.0e+000	0.0e+000	0.0e+000
Pu239	9.6e+001	9.2e+001	3.6e+000	2.8e+000	4.7e+001	4.5e+001	3.8e+000	3.2e+000	2.6e+001	2.5e+001	4.0e+000	3.1e+000
Pu240	2.3e+001	1.9e+001	2.6e+001	4.1e+000	1.7e+000	1.3e+000	2.6e+001	6.4e-001	2.0e-001	1.6e-001	2.6e+001	1.3e-001
Pu241	2.6e+000	1.5e-003	1.7e+005	2.2e+000	1.9e-004	2.0e-004	-7.5e+000	-2.8e-005	3.6e-005	3.9e-005	-7.4e+000	-9.0e-006
Pu242	2.7e-001	2.7e-001	-1.1e+000	-2.5e-003	2.5e-001	2.6e-001	-1.2e+000	-5.6e-003	2.5e-001	2.5e-001	-1.6e+000	-1.2e-002
Ra226	1.0e-001	1.0e-001	-9.9e-001	-8.5e-004	2.2e-001	2.1e-001	2.8e+000	1.1e-002	2.9e-001	2.8e-001	3.9e+000	3.4e-002
Ra228	1.1e-007	1.1e-007	0.0e+000	0.0e+000	2.8e-007	2.8e-007	1.4e+000	7.5e-009	4.2e-007	4.1e-007	1.7e+000	2.2e-008
Se 79	1.3e-001	1.3e-001	3.2e+000	3.4e-003	7.7e-002	7.5e-002	3.1e+000	4.3e-003	5.1e-002	4.9e-002	3.1e+000	4.6e-003
Sm151	8.0e-001	0.0e+000	N/A	6.8e-001	0.0e+000	0.0e+000	0.0e+000	0.0e+000	0.0e+000	0.0e+000	0.0e+000	0.0e+000
Sn126	1.2e-001	1.2e-001	2.5e+000	2.5e-003	1.0e-001	1.0e-001	2.0e+000	3.8e-003	9.1e-002	8.8e-002	2.5e+000	6.8e-003
Tc 99	3.8e+000	3.7e+000	2.2e+000	6.8e-002	3.5e+000	3.4e+000	2.1e+000	1.3e-001	3.3e+000	3.2e+000	1.9e+000	1.9e-001
Th229	1.6e-002	1.6e-002	-6.1e-001	-8.5e-005	5.1e-002	5.1e-002	-3.9e-001	-3.8e-004	7.8e-002	7.8e-002	1.3e-001	3.1e-004
Th230	1.1e-001	1.1e-001	-8.8e-001	-8.5e-004	2.3e-001	2.2e-001	2.7e+000	1.1e-002	3.0e-001	2.9e-001	3.8e+000	3.4e-002
Th232	1.1e-007	1.1e-007	0.0e+000	0.0e+000	2.8e-007	2.8e-007	1.4e+000	7.5e-009	4.2e-007	4.1e-007	1.7e+000	2.2e-008
U233	3.1e-002	3.1e-002	-1.9e+000	-5.1e-004	6.7e-002	6.7e-002	-1.5e-001	-1.9e-004	9.3e-002	9.3e-002	3.2e-001	9.3e-004
U234	6.9e-001	6.6e-001	5.3e+000	3.0e-002	6.6e-001	6.3e-001	5.3e+000	6.2e-002	6.3e-001	6.0e-001	5.2e+000	9.6e-002
U235	1.6e-002	1.6e-002	-1.9e+000	-2.5e-004	1.8e-002	1.8e-002	-1.1e+000	-3.8e-004	1.8e-002	1.8e-002	-1.6e+000	-9.3e-004
U236	1.3e-001	1.3e-001	1.6e+000	1.7e-003	1.4e-001	1.3e-001	2.2e+000	5.6e-003	1.4e-001	1.3e-001	2.2e+000	9.3e-003
U238	1.5e-001	1.5e-001	0.0e+000	0.0e+000	1.5e-001	1.5e-001	0.0e+000	0.0e+000	1.5e-001	1.5e-001	0.0e+000	0.0e+000
Zr 93	3.5e-001	3.5e-001	2.0e+000	5.9e-003	3.5e-001	3.4e-001	2.0e+000	1.3e-002	3.5e-001	3.4e-001	2.1e+000	2.2e-002
36 Iso. Totals	1.4e+002	1.2e+002	1.5e+001	0.0e+000	5.5e+001	5.3e+001	4.2e+000	0.0e+000	3.3e+001	3.2e+001	3.7e+000	0.0e+000

Table 2-3. Effects of 10,000 Year Criticality on the Radionuclide Inventory of a PWR Fuel Assembly

	25,000 yr				45,000 yr				65,000 yr			
	Act. (Ci) Critical	Act. (Ci) Decay Only	% Diff. Isotope	% Diff. Total	Act. (Ci) Critical	Act. (Ci) Decay Only	% Diff. Isotope	% Diff. Total	Act. (Ci) Critical	Act. (Ci) Decay Only	% Diff. Isotope	% Diff. Total
Ac227	1.4e-002	6.3e-003	1.2e+002	8.0e-003	1.5e-002	1.0e-002	4.9e+001	9.2e-003	1.6e-002	1.3e-002	2.4e+001	9.6e-003
Am241	2.1e+000	1.1e-003	2.0e+005	2.2e+000	1.7e-004	2.0e-004	-1.4e+001	-5.5e-005	3.4e-005	3.9e-005	-1.5e+001	-1.8e-005
Am242m	1.9e-003	0.0e+000	N/A	2.0e-003	0.0e+000	0.0e+000	0.0e+000	0.0e+000	0.0e+000	0.0e+000	0.0e+000	0.0e+000
Am243	4.1e-001	1.9e-001	1.1e+002	2.2e-001	6.3e-002	2.9e-002	1.1e+002	6.3e-002	9.5e-003	4.5e-003	1.1e+002	1.6e-002
C14	2.4e-006	1.6e-006	4.8e+001	8.0e-007	2.1e-007	1.4e-007	4.9e+001	1.3e-007	1.9e-008	1.3e-008	4.8e+001	1.9e-008
Cm244	1.5e-002	0.0e+000	N/A	1.6e-002	0.0e+000	0.0e+000	0.0e+000	0.0e+000	0.0e+000	0.0e+000	0.0e+000	0.0e+000
Cm245	8.8e-004	1.0e-003	-1.4e+001	-1.5e-004	1.7e-004	2.0e-004	-1.4e+001	-5.5e-005	3.4e-005	3.9e-005	-1.5e+001	-1.8e-005
Cm246	5.2e-005	2.4e-005	1.2e+002	2.9e-005	2.8e-006	1.3e-006	1.2e+002	2.8e-006	1.5e-007	6.7e-008	1.2e+002	2.5e-007
Cs135	2.2e-001	2.0e-001	8.4e+000	1.7e-002	2.2e-001	2.0e-001	9.0e+000	3.4e-002	2.2e-001	2.0e-001	8.5e+000	5.3e-002
I129	9.2e-003	8.8e-003	4.1e+000	3.7e-004	9.2e-003	8.8e-003	4.1e+000	6.8e-004	9.2e-003	8.8e-003	4.0e+000	1.1e-003
Nb 93m	3.6e-001	3.4e-001	4.1e+000	1.4e-002	3.6e-001	3.4e-001	4.1e+000	2.6e-002	3.5e-001	3.4e-001	3.8e+000	4.0e-002
Nb 94	7.4e-005	1.0e-005	6.4e+002	6.5e-005	3.7e-005	5.0e-006	6.4e+002	6.1e-005	1.9e-005	2.5e-006	6.4e+002	5.0e-005
Np237	3.9e-001	3.8e-001	2.1e+000	8.2e-003	3.9e-001	3.8e-001	2.1e+000	1.5e-002	3.8e-001	3.8e-001	2.4e+000	2.8e-002
Pa231	1.4e-002	6.3e-003	1.2e+002	8.0e-003	1.5e-002	1.0e-002	4.9e+001	9.2e-003	1.6e-002	1.3e-002	2.4e+001	9.6e-003
Pb210	1.3e-001	1.3e-001	-7.9e-001	-1.0e-003	2.2e-001	2.1e-001	4.7e+000	1.9e-002	3.1e-001	2.8e-001	1.1e+001	9.9e-002
Pd107	2.7e-002	2.6e-002	3.8e+000	1.0e-003	2.7e-002	2.6e-002	3.8e+000	1.9e-003	2.7e-002	2.6e-002	4.2e+000	3.4e-003
Pu238	3.1e+000	0.0e+000	N/A	3.1e+000	0.0e+000	0.0e+000	0.0e+000	0.0e+000	0.0e+000	0.0e+000	0.0e+000	0.0e+000
Pu239	8.7e+001	8.0e+001	8.6e+000	7.0e+000	4.9e+001	4.5e+001	8.9e+000	7.5e+000	2.8e+001	2.5e+001	9.1e+000	7.1e+000
Pu240	1.8e+001	1.1e+001	6.9e+001	7.7e+000	2.2e+000	1.3e+000	6.8e+001	1.7e+000	2.7e-001	1.6e-001	6.9e+001	3.4e-001
Pu241	2.1e+000	1.0e-003	2.1e+005	2.2e+000	1.7e-004	2.0e-004	-1.4e+001	-5.5e-005	3.4e-005	3.9e-005	-1.5e+001	-1.8e-005
Pu242	2.6e-001	2.7e-001	-2.6e+000	-7.1e-003	2.5e-001	2.6e-001	-2.7e+000	-1.3e-002	2.4e-001	2.5e-001	-2.8e+000	-2.2e-002
Ra226	1.3e-001	1.3e-001	-7.9e-001	-1.0e-003	2.2e-001	2.1e-001	4.7e+000	1.9e-002	3.1e-001	2.8e-001	1.1e+001	9.9e-002
Ra228	1.5e-007	1.5e-007	6.8e-001	1.0e-009	2.8e-007	2.8e-007	2.2e+000	1.1e-008	4.2e-007	4.1e-007	2.9e+000	3.7e-008
Se 79	1.2e-001	1.1e-001	6.1e+000	7.1e-003	7.9e-002	7.5e-002	6.3e+000	8.8e-003	5.2e-002	4.9e-002	6.3e+000	9.6e-003
Sm151	8.1e-001	0.0e+000	N/A	8.2e-001	0.0e+000	0.0e+000	0.0e+000	0.0e+000	0.0e+000	0.0e+000	0.0e+000	0.0e+000
Sn126	1.2e-001	1.2e-001	5.1e+000	6.1e-003	1.1e-001	1.0e-001	4.9e+000	9.4e-003	9.3e-002	8.8e-002	5.0e+000	1.4e-002
Tc 99	3.8e+000	3.6e+000	4.1e+000	1.5e-001	3.5e+000	3.4e+000	4.1e+000	2.6e-001	3.3e+000	3.2e+000	3.8e+000	3.7e-001
Th229	2.3e-002	2.3e-002	-1.7e+000	-4.1e-004	5.1e-002	5.1e-002	-1.2e+000	-1.1e-003	7.8e-002	7.8e-002	-1.3e-001	-3.1e-004
Th230	1.4e-001	1.4e-001	0.0e+000	0.0e+000	2.3e-001	2.2e-001	5.0e+000	2.1e-002	3.1e-001	2.9e-001	7.3e+000	6.5e-002
Th232	1.5e-007	1.5e-007	6.8e-001	1.0e-009	2.8e-007	2.8e-007	2.2e+000	1.1e-008	4.2e-007	4.1e-007	2.9e+000	3.7e-008
U233	3.7e-002	3.9e-002	-3.1e+000	-1.2e-003	6.7e-002	6.7e-002	-6.0e-001	-7.5e-004	9.3e-002	9.3e-002	3.2e-001	9.3e-004
U234	7.2e-001	6.5e-001	1.1e+001	7.4e-002	6.9e-001	6.3e-001	1.1e+001	1.3e-001	6.6e-001	6.0e-001	1.1e+001	2.0e-001
U235	1.6e-002	1.6e-002	-3.6e+000	-6.1e-004	1.7e-002	1.8e-002	-2.8e+000	-9.4e-004	1.8e-002	1.8e-002	-2.7e+000	-1.5e-003
U236	1.4e-001	1.3e-001	3.1e+000	4.1e-003	1.4e-001	1.3e-001	4.5e+000	1.1e-002	1.4e-001	1.3e-001	4.5e+000	1.9e-002
U238	1.5e-001	1.5e-001	0.0e+000	0.0e+000	1.5e-001	1.5e-001	0.0e+000	0.0e+000	1.5e-001	1.5e-001	0.0e+000	0.0e+000
Zr 93	3.6e-001	3.4e-001	4.1e+000	1.4e-002	3.6e-001	3.4e-001	4.1e+000	2.6e-002	3.5e-001	3.4e-001	3.8e+000	4.0e-002
36 Iso. Total	1.2e+002	9.8e+001	2.4e+001	0.0e+000	5.8e+001	5.3e+001	9.9e+000	0.0e+000	3.5e+001	3.2e+001	8.5e+000	0.0e+000

Table 2-4. Percentage Increase in Total Curies of the 36 TSPA-95 Isotopes

Duration of Criticality	Percent Increase at End of Criticality	Percent Increase at 45,000 years	Percent Increase at 65,000 years
1,000 years	8.5% (16k yrs.)	0.73%	0.73%
5,000 years	15% (20k yrs.)	4.2%	3.7%
10,000 years	24% (25k yrs.)	9.9%	8.5%

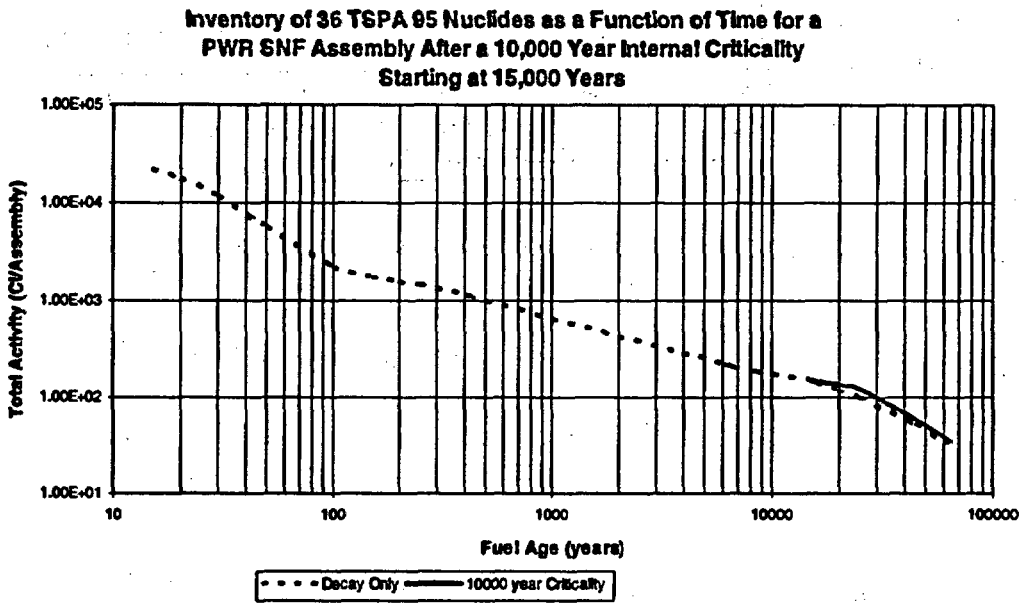

Figure 2-1

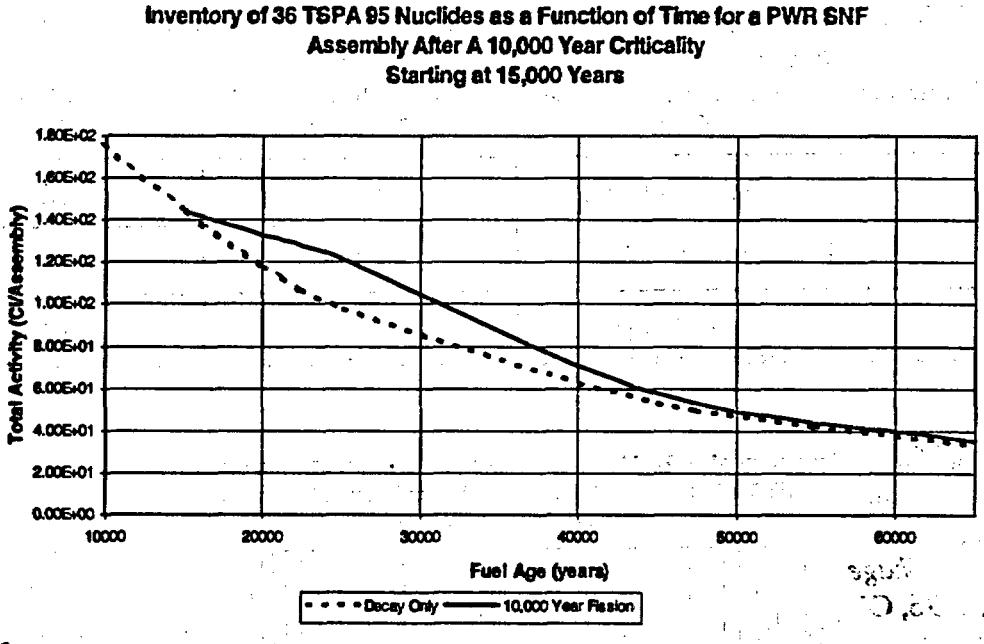
Inventory of 36 TSPA 95 Nuclides as a Function of Time for a PWR SNF Assembly After A 10,000 Year Criticality Starting at 15,000 Years
Total Activity (Ci/Assembly)
1.80E+02
1.60E+02
1.40E+02
1.20E+02
1.00E+02
8.00E+01
6.00E+01
4.00E+01
2.00E+01
0.00E+00
10000
20000
30000
40000
50000
60000
Fuel Age (years)
Decay Only
10,000 Year Fission

Figure 2-2

4. References

1. *Pitting, Galvanic, and Long-Term Corrosion Studies on Candidate Container Alloys for the Tuff Repository*, U.S. Nuclear Regulatory Commission, NUREG/CR-5709, January 1992

2. *Total System Performance Assessment - 1995: An Evaluation of the Potential Yucca Mountain Repository*, DI#: B00000000-01717-2200-00136 REV 00, CRWMS M&O

3. *AUCF Waste Package Criticality and SAS2H Evaluations*, Interoffice Correspondence LV.WP.DAT.03/96.070, Dan Thomas, March 26, 1996, CRWMS M&O

4. Moran, M.J., Shapiro, H.N., *Fundamentals of Engineering Thermodynamics*, John Wiley & Sons, 1988

5. *Waste Package Design Basis Fuel Analysis*, DI#: B00000000-01717-0200-000127 REV 00A, 1996, CRWMS M&O

6. *UCF Waste Package Criticality Analysis*, DI#: BBAA00000-01717-0200-00005 REV 00B, 1996, CRWMS M&O.

7. Holman, J.P., *Heat Transfer*, 7th Edition, McGraw-Hill Publishing Company, 1990

8. *Second Waste Package Probabilistic Criticality Analysis: Generation and Evaluation of Internal Criticality Configurations*, DI#: BBA000000-01717-2200-00005, 1996, CRWMS M&O

9. Smellie, J., *The Fossil Nuclear Reactors of Oklo, Gabon*, Radwaste Magazine, March 1995, pg 18-27.

10. *Second Waste Package Probabilistic Criticality Analysis: Generation and Evaluation of Internal Criticality Configurations*, DI#: BBA000000-01717-2200-00005 REV 00.

INTENTIONALLY LEFT BLANK